SHORT PAPERS IN—

Analytical methods
Economic geology
Evaporation
Geochemistry of water
Geochronology
Geohydrologic dating
Geomorphology
Geophysics
Glaciology
Ground water
Marine geology
Mineralogy and petrology
Paleomagnetism
Paleontology
Sedimentation
Stratigraphy
Streamflow studies
Structural geology

GEOLOGICAL SURVEY RESEARCH 1968

Chapter D

GEOLOGICAL SURVEY PROFESSIONAL PAPER 600-D

GEOLOGICAL SURVEY RESEARCH 1968

Chapter D

GEOLOGICAL SURVEY PROFESSIONAL PAPER 600–D

Scientific notes and summaries of investigations in geology, hydrology, and related fields

UNITED STATES GOVERNMENT PRINTING OFFICE, WASHINGTON: 1968

UNITED STATES DEPARTMENT OF THE INTERIOR

STEWART L. UDALL, Secretary

GEOLOGICAL SURVEY

William T. Pecora, Director

For sale by the Superintendent of Documents, U.S. Government Printing Office
Washington, D.C. 20402 – Price $3.25

CONTENTS

HYDROLOGIC STUDIES

GEOLOGIC STUDIES

GEOLOGICAL SURVEY RESEARCH 1968

This collection of 48 short papers is the third published chapter of "Geological Survey Research 1968." The papers report on scientific and economic results of current work by members of the Geologic and Water Resources Divisions of the U.S. Geological Survey.

Chapter A, to be published later in the year, will present a summary of significant results of work done during fiscal year 1968, together with lists of investigations in progress, reports published, cooperating agencies, and Geological Survey offices.

"Geological Survey Research 1968" is the ninth volume of the annual series Geological Survey Research. The eight volumes already published are listed below, with their series designations.

Geological Survey Research 1960—Prof. Paper 400
Geological Survey Research 1961—Prof. Paper 424
Geological Survey Research 1962—Prof. Paper 450
Geological Survey Research 1963—Prof. Paper 475
Geological Survey Research 1964—Prof. Paper 501
Geological Survey Research 1965—Prof. Paper 525
Geological Survey Research 1966—Prof. Paper 550
Geological Survey Research 1967—Prof. Paper 575

MOVEMENT OF MOISTURE IN THE UNSATURATED ZONE IN A DUNE AREA, SOUTHWESTERN KANSAS

By ROBERT C. PRILL, Garden City, Kans.

Work done in cooperation with the State Geological Survey of Kansas, the Environmental Health Services of the Kansas State Department of Health, and Kansas State Board of Agriculture

Abstract.—Moisture-content logs for the predominant vegetative conditions in the sand-dune area of southwestern Kansas depict the manner of moisture buildup and depletion, and illustrate conditions necessary for deep percolation. Even though the period of study included a year when precipitation was nearly the highest on record, built-up moisture under a sagebrush-grass community penetrated to a depth of only 14 feet, whereas the zone of evapotranspiration extended to at least 17 feet. Under a grass community where the zone of evapotranspiration extended to about 11 feet, a small amount of moisture (2 inches) moved as deep percolation. Under a barren area, where most of the loss by evaporation occurred in the upper 1 foot, large quantities of moisture moved as deep percolation.

The measurement of recharge from precipitation is a primary objective of current studies in dune-sand areas in southwestern Kansas. Moisture changes under different slopes and vegetation in the unsaturated zone in dune sand are measured by a nuclear meter. This report presents results that illustrate the requirements necessary for deep percolation under three types of vegetative conditions. Data for a barren area are presented to show moisture buildup during a period of high precipitation and moisture depletion during a subsequent period of low precipitation. Data for a sagebrush-grass community and a grass community are presented to show moisture buildup and depletion over a period from the fall of 1964 through 1966. This period depicts maximum moisture changes because 1965 was a year when precipitation was one of the highest on record and was preceded and succeeded by years when precipitation was below normal.

The study site is located in the extensive area of dune sand immediately south of the Arkansas River in southwestern Kansas (fig. 1). Smith (1940, p. 154) aptly described the dune forms as "a repetition of the basic alternation of hills and hollows, but with endless variations in shape and size. In some places there are smooth, well-rounded forms, but in other places there are abruptly varied shapes." The dune area has no external drainage, and rainfall either infiltrates directly into the dune sand or accumulates in innumerable interdune depressions.

At the present time, the dunes are mostly stabilized by grass and sagebrush vegetation. A few blowouts give evidence of recent wind activity. The predominant vegetation, identified by Prof. R. D. Waldorf, of the Garden City Community Junior College, Garden City, Kans., during the period of study consisted of sand sage (*Artemisia filifolia*), blowout grass (*Redfieldici flexuosa*), paspalum (*Paspalum pubesceas*), sand bluestem (*Andropogon squarroca*), stink grass (*Eragrostis cilianensis*), western ragweed (*Ambrosia psilostachya*), showy

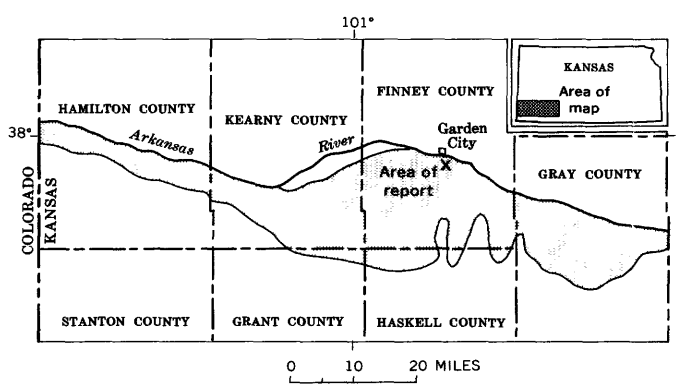

FIGURE 1.—Area of report in dune area (patterned) south of the Arkansas River in southwestern Kansas.

partridgepea (*Chamaecresta fasiculata*), and mat sandbur (*Cendhrus pauciflorus*).

Records of the Garden City Agricultural Experiment Station, 3½ miles northeast of Garden City, show an average annual precipitation (1908–66) of 17.92 inches. Approximately three-fourths of the precipitation occurs during the growing season from mid-April to mid-October. Table 1 shows a monthly summary of precipitation during the period of study (1964–66) compared to the average monthly values (1908–66). During the period from July 1965 through December 1966, data were obtained from a rain gage in the study area. The other data were obtained at the experiment station.

TABLE 1.—*Monthly and annual precipitation near Garden City, Kans.*

Month	Precipitation (inches)			
	1964	1965	1966	Average 1908–66
January	0	0.64	0.39	0.35
February	1.19	.60	1.29	.62
March	.34	.16	.07	.86
April	.22	.16	.55	1.64
May	4.76	6.20	.20	2.79
June	.90	6.80	1.44	3.01
July	.91	1.14	1.73	2.42
August	.32	5.39	3.09	2.21
September	1.41	3.63	1.50	1.64
October	.27	3.53	.85	1.29
November	1.42	0	.09	.65
December	.49	.82	.84	.44
Annual	12.23	29.07	12.04	17.92

Precipitation during the period of study was ideally distributed to demonstrate moisture buildup and depletion under different climatic conditions. In 1964, the total of 12.23 inches was considerably lower than the average annual precipitation. The 29.07 inches that occurred in 1965 was the fourth highest on record. In 1966, precipitation again was below normal with a total of 12.04 inches. There was no appreciable collection of runoff in 1964 and 1966. During several periods of high-intensity rainfall in 1965, water collected in the depressions. This runoff, however, probably represents only a small percentage of the total monthly precipitation.

DESCRIPTION OF SITES

Access holes for moisture-content logging by nuclear meter were drilled at 16 sites in the dune area: 6 under grass communities at different slope positions, 5 under sagebrush-grass communities at different slope positions, 2 under grass communities in interdune depressions, and 3 under barren areas in blowouts. This report presents moisture data collected at 3 of the 16 sites in the dune area (fig. 1). Although data are shown for only three sites, the general moisture relationships depicted by the moisture-content logs also were evident at other sites with similar vegetation but with different slope positions. The grass and sagebrush-grass sites are located in an area that is 2 miles south of Garden City; the barren site is in a blowout that is 3 miles south of Garden City. At each site, access holes containing 2-inch aluminum tubing were drilled through the dune sand into the underlying alluvial deposits. The water table in this area is about 30 feet below the top of the alluvial deposits.

The access holes for the grass and sage-grass sites are in an area of well-rounded dunes, as shown by the contours in figure 2. The sagebrush-grass site is adjacent to a large sage plant; the grass site is located 20 feet from the nearest sagebrush. The deposits underlying the sagebrush-grass site consist of dune sand from the surface to 18 feet, and alluvial sand and gravel from 18 to 20 feet. The deposits underlying the grass site consist of dune sand from the surface to 17 feet, alluvial loam from 17 to 18.5 feet, and alluvial sand and gravel from 18.5 to 20 feet.

The barren site is located in an almost circular blowout with a radius of 60 feet. There was very sparse vegetation, predominantly blowout grass, in the blowout during the study period. Vegetation was destroyed

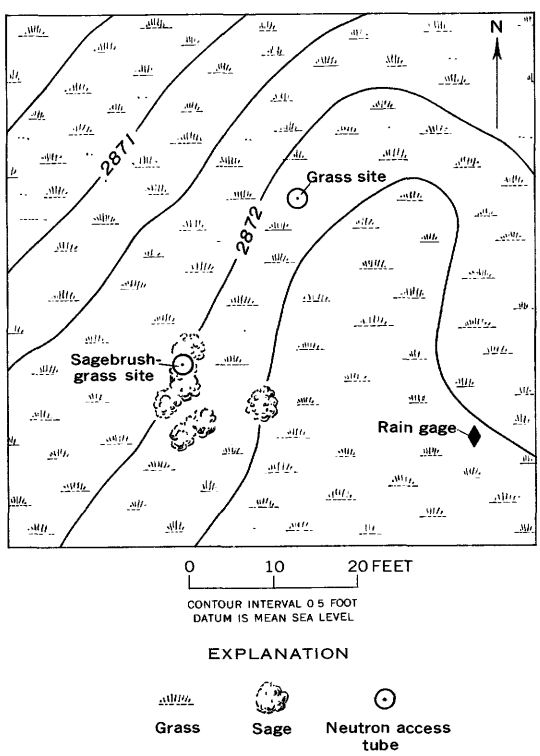

FIGURE 2.—Topographic map showing location of the rain gage and the grass and sagebrush-grass sites.

within a radius of 6 feet of the access hole. The deposits underlying the barren site consist of dune sand from the surface to 14 feet; eolian sandy loam from 14 to 15 feet; dune sand from 15 to 22.5 feet; stratified alluvial sand, silt, and sand and gravel from 22.5 to 26 feet; and sand and gravel from 26 to 32 feet.

Particle-size analysis of several dune-sand samples showed that most of the sand grains were in the 0.125–0.50 millimeter or predominantly fine- to medium-sand range. Dry unit weight for the dune sand ranged from 1.47 to 1.68 grams per cubic centimeter. Based on the average dry unit weight of 1.55 g/cc and a specific gravity of 2.65 g/cc, the calculated porosity is 41.5 percent.

MOISTURE MEASUREMENT

The moisture content at specified depths in the access hole was measured by a continuous-logging nuclear meter (Prill and Meyer, 1968). Selected logs are presented in this paper to illustrate moisture changes with time under different conditions of precipitation, vegetation, and plant growth. The logs show only data for dune sand with the exception of a 1-foot stratum of sandy loam at the barren site. Because of the difficulty in relating nuclear-meter readings to moisture values near the land surface, data for the upper 1 foot are not presented. When required for computational purposes, estimates of the amount of moisture contained in the upper 1 foot were made on the basis of gravimetric measurements.

Moisture values in this paper are expressed in both percentage and inches. The ratio of the volume of water in the soil to the total bulk volume of the soil (multiplied by 100) is expressed as the moisture content in percentage of volume. Both the amount of moisture contained in a depth interval and the amount of moisture change for a specified time period are expressed in inches. Other terms used in this paper are defined as follows: infiltration is the downward entry of water into the soil; deep percolation is moisture movement below the zone of evapotranspiration; water-holding capacity is the moisture content when further reduction by gravity drainage is very slow; and residual moisture is the minimum moisture content after the effects of gravity drainage and evapotranspiration become negligible.

BARREN AREA

The moisture-content logs shown in figure 3 were selected to illustrate the general characteristics of moisture movement as deep percolation under barren areas. The movement is illustrated best by the manner of moisture buildup from cumulative infiltration during a period of high precipitation and subsequent reduction of moisture during a period of low precipitation. The log for June 3, 1966, which reflects moisture content after 7 months of low precipitation, is referred to as the base log for comparative purposes. An examination of long-term precipitation records at Garden City shows that periods of such low rainfall are seldom of longer than 7 months duration. Because the base log reflects a long period of gravity drainage and is not affected by transpiration, the moisture values are approximately equal to water-holding capacity values. These values range from 8 to 16 percent, probably because of variations in the particle-size distribution or arrangement. The quantity of moisture contained in the 1- to 21.5-foot zone on the base log is calculated to be 29.25 inches.

The set of logs in figure 3 shows the manner of moisture buildup during a period of high rainfall (13 inches) in May and June of 1965 and the subsequent depletion of moisture during a period of low rainfall (1 inch) in July of 1965. A sequence of numerous logs run in May and June showed that the vertical penetration of the moisture from cumulative infiltration increased progressively with time. Below the depth of moisture

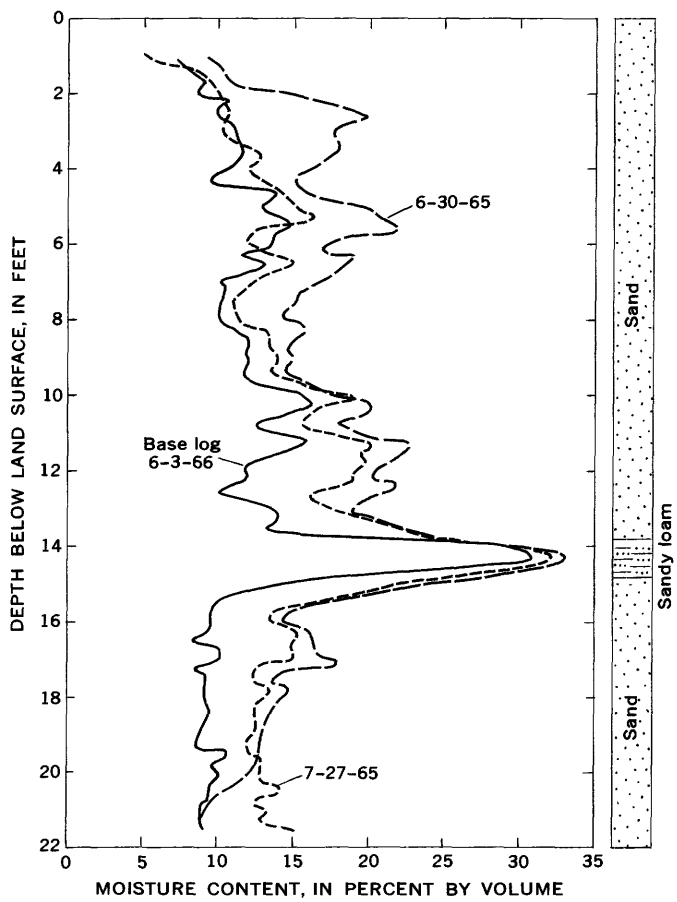

FIGURE 3.—Moisture-content logs for the barren area.

penetration, however, moisture content remained virtually equal to values on the base log.

By June 30 (fig. 3) the penetration of moisture from cumulative infiltration in May and June attained a depth of about 21 feet, and the moisture content ranged from 2 to 10 percent higher than the base log. The quantity of moisture contained in the 1- to 21.5-foot zone was calculated to be 41.75 inches (12.5 inches greater than for June 3, 1966). Thus, the moisture buildup in the profile on June 30 nearly equals the recorded precipitation of 13 inches in May and June.

The moisture depletion during the subsequent period of low precipitation is illustrated by the log run on July 27, as shown in figure 3. Most of the depletion occurred above the 8.5-foot depth. Moisture content above 3.5 feet nearly equaled values on the base log; moisture content from 3.5 feet to 8.5 feet was only 1 to 2 percent higher. Below 8.5 feet the moisture content was 1 to 2 percent less than the June 30 values but 3 to 5 percent higher than the base log values. Thus, the quantity of moisture in the 1- to 21.5-foot zone was reduced by 5.25 inches by July 27 but was still 7.25 inches more than for the base log.

Analysis of other logs run during the period of study further illustrated the manner of moisture depletion after sizable buildup from cumulative infiltration. Moisture was depleted rapidly in the upper part of the profile but less rapidly as depth increased. A period of several months was required before the moisture content at depths of 15 to 20 feet approximated water-holding capacity values. This time lag of moisture depletion with depth is attributed to slow drainage. Owing to the absence of vegetation most of the moisture depletion is by gravity drainage rather than by evapotranspiration.

The evaporation of water from sand is a complex process in which water may move as a vapor or a liquid. Generally the process is a combination of both heat and water transport. Although it is not possible to establish the effective depth of evaporation accurately from moisture data, moisture logs from the barren sites indicate that most of the added moisture moving below 1 foot continues to move downward and represents deep percolation losses.

The rapid development of a dry surface layer after a rain is effective in reducing evaporation losses in sand. The nature of this dry layer is illustrated by gravimetric moisture measurements made on July 27, 1965. Moisture content in the upper 3 inches was about 1 percent. Below 3 inches, moisture content rapidly increased to values consistent with water-holding capacity values at greater depth in the profile. Once the dry surface zone is developed, evaporation must move from the wet zone to the atmosphere by vapor transport, and evaporation is substantially retarded (Black, 1966; Hanks, 1967). During periods of high precipitation, most of the moisture penetrates the upper 1 foot and moves by gravity drainage to deep percolation. By contrast, periods of low precipitation are characterized by light showers that add only small amounts of moisture to the upper zone where the rate of evaporation is great.

Also illustrated in figure 3 is the moisture change in a 1-foot layer of sandy loam between 14 and 15 feet. The sequence of logs shows that the highest moisture buildup during this period increased only 2 percent over the water-holding capacity values and that there was little mounding of moisture above this layer. These observations show that the sandy loam layer was not a confining bed. Because of the low moisture buildup required to conduct the moisture through this zone, the advance of a moisture front should be more rapid in this zone than in the dune sand.

Moisture-content measurements in the underlying stratified material, though not shown in this paper, provided further information on the moisture changes with depth. Moisture changes in the 21.5- to 30-foot zone during 1965 were less in the beds containing mostly silt and clay than in the associated sandy beds. There was no evidence of restriction of the vertical movement of moisture through these finer textured beds. Measurements in the spring and summer of 1966 showed that virtually all the moisture added to this zone had moved through to depths below 30 feet. Because the stratified deposits from 30 to 60 feet are quite permeable, moisture added to this zone probably will reach the water table. Thus, movement as deep percolation should represent potential recharge to the ground-water reservoir.

SAGEBRUSH-GRASS COMMUNITY

The moisture-content logs shown in figure 4 were selected to illustrate the seasonal characteristics of moisture movement under a sagebrush-grass community. Three sets of logs are presented to illustrate the manner of moisture buildup and depletion during the 1965 growing season, the 1965–66 nongrowing season, and the 1966 growing season. A summary of moisture data from these logs as well as the log for May 6, 1965, is presented in table 2. The log for October 15, 1964, which reflects the lowest moisture value (5.9 inches) measured during the period of study, is used as the base log. Because this log probably approximates the maximum depletion by sagebrush-grass vegetation, the values are considered to represent the residual moisture values for this site. This moisture content, which ranges from 6 to 12 percent lower than the values under a

barren area, indicates the effectiveness of moisture removal by plant roots.

The first set of data in figure 4 illustrates the moisture buildup and depletion under a sagebrush-grass community during the 1965 growing season. A sequence of moisture-content logs showed a moisture buildup of 1.2 inches between October 15, 1964, and May 6, 1965. This buildup, which resulted from 4.0 inches of precipitation, accumulated in the upper 4 feet of the profile. By June 30, the log (fig. 4) showed a vertical penetration of moisture buildup to 9 feet, and an increase in moisture content of 6.3 inches over the May 6 log. Therefore, it is calculated that the 12.7 inches of precipitation from May 6 to June 30 contributed a net increase of 6.3 inches to the profile, and 6.4 inches were used by evapotranspiration.

From June 30 to August 30, 5.5 inches of precipitation were recorded. The log of August 30 showed that the moisture buildup had penetrated to a depth of 10.5 feet, or 1.5 feet lower than the depth shown on June 30. However, moisture content at a depth of 4.5 to 6 feet was reduced nearly to values on the base log. In the 6- to 9-foot depth interval, moisture content was reduced to about 7 percent, or 4 percent higher than the base log. On the basis of logs run during the 2-month period, it appears that the addition of moisture in July and August penetrated to a depth of only 4.5 feet. The net moisture loss in the profile during July and August was 3.4 inches. Considering that 5.5 inches of moisture were added from precipitation during the 2-month period, the total depletion by evapotranspiration is estimated to be 8.9 inches.

The second set of data in figure 4 illustrates the moisture change during the 1965–66 nongrowing season. Precipitation in September and October 1965 was much above average, whereas only a trace of precipitation was recorded during November. The log of December 7 shows that the vertical penetration of moisture buildup was about 11 feet (0.5 foot deeper than the penetration on August 30). The buildup from August 30 to December 7 was calculated to be 2.5 inches. Several logs run during that period indicate the moisture deficits caused by evapotranspiration prior to the cessation of plant growth were replaced by the additions of moisture in mid-October.

A comparison of logs for December 7, 1965, and April 19, 1966, shows the effect of 3.1 inches of precipitation, which occurred during that period. The moisture content in the 1- to 10.5-foot zone is similar, whereas, a moisture buildup occurred in the 10.5- to 13-foot zone. The moisture increase in the profile between these dates is calculated to be 1.3 inches, and the loss by evapotranspiration is estimated to be 1.8 inches. By April 19, some greening of plants gave evidence of growth. However, a comparison of the similarity of moisture content in both the March and April logs suggested that moisture use by evapotranspiration prior to April 19 was minimal.

The third set of data on figure 4 illustrates the moisture use during the 1966 growing season. The moisture-content log for July 29 was selected to show moisture conditions in the profile during midsummer, and the log for November 29 was selected to show conditions after the cessation of plant growth. Precipitation records at this site show that 3.4 inches were recorded from April 19 to July 29 and that 5.5 inches were recorded from July 29 to November 29.

An analysis of moisture-content logs run during the period from April 19 to July 29 shows a progressive decline in moisture values. Although precipitation in June and July added some moisture to the upper 4 feet of the profile, the net result was a depletion in the storage owing to the high rate of evapotranspiration. The log of July 29 shows that moisture content

TABLE 2.—*Precipitation and moisture data, in inches, for the sagebrush-grass and grass communities in a dune area of southwestern Kansas*

Date	Precipitation since previous date	Vegetation							
		Sagebrush-grass				Grass			
		0–16 foot depth interval		Moisture use by evapotranspiration since previous date	Moisture movement below 16 feet since previous date	0–16 foot depth interval		Moisture use by evapotranspiration since previous date	Moisture movement below 16 feet since previous date
		Amount of moisture in depth interval	Moisture change since previous date			Amount of moisture in depth interval	Moisture change since previous date		
Oct. 15, 1964		5.5				9.2			
May 6, 1965	4.0	6.7	+1.2	2.8	0	10.0	+0.8	3.2	0
June 30, 1965	12.7	13.0	+6.3	6.4	0	16.9	+6.9	5.8	0
Aug. 30, 1965	5.5	9.6	−3.4	8.9	0	14.4	−2.5	8.0	0
Dec. 7, 1965	8.1	12.1	+2.5	5.6	0	18.2	+3.8	4.3	0
April 19, 1966	3.1	13.4	+1.3	1.8	0	18.5	+0.3	1.8	1.0
July 29, 1966	3.4	7.7	−5.7	9.1	0	13.3	−5.2	8.0	0.6
Nov. 29, 1966	5.5	7.0	−0.7	6.2	0	11.8	−1.5	6.7	0.3

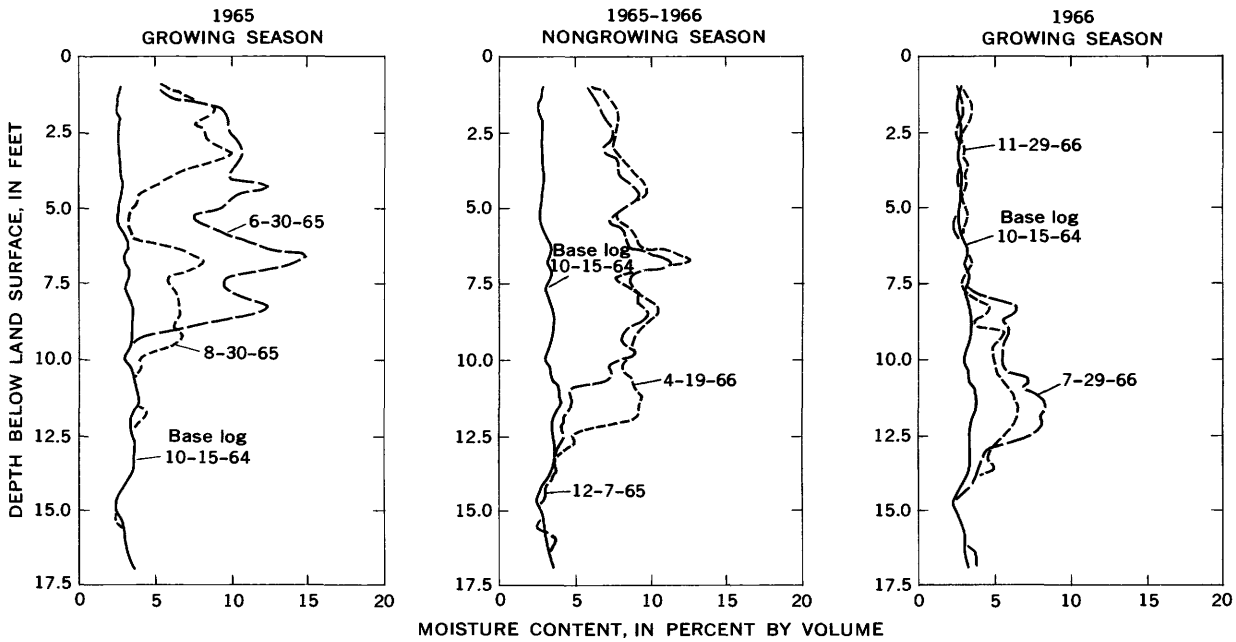

FIGURE 4.—Moisture-content logs for the sagebrush-grass community.

in the 1- to 7.5-foot zone was reduced nearly to values on the base log. In the 7.5- to 13-foot zone, the moisture content was reduced to within 3 to 5 percent of the values of the base log. Thus, evapotranspiration used all the moisture from precipitation during this period and an additional 5.7 inches from the profile.

During the period from July 29 to November 29, additions of moisture from precipitation were restricted to the upper 4 feet of the profile. However, the log of November 29 shows that all the moisture added to the profile in this period was used by evapotranspiration. Moisture content in the 1- to 7.5-foot zone approximates the values on the base log. Moisture content in the 7.5- to 13-foot zone was 1 to 2 percent lower than the values recorded on July 29 but was still slightly higher than the values on the base log. The net moisture loss during this period was calculated to be 6.2 inches.

During the 1966 growing season, the penetration of moisture buildup increased in depth from 13 to 14 feet. In this period, however, the moisture content in the profile was appreciably reduced. By November 29, the moisture contained in the profile was 7.4 inches (only 1.5 inches higher than the base log).

GRASS COMMUNITY

The moisture-content logs shown in figure 5 illustrate seasonal characteristics of moisture movement under a grass community. A summary of moisture data for these logs plus the log for May 6, 1965, is presented in table 2. For the purpose of comparison, the moisture-content logs at the grass sites are presented in three sets and for the same dates as those at the sagebrush-grass site. Consequently, much of the discussion in the following section parallels the discussion in the previous section, and frequent comparisons are made to the sagebrush-grass data.

The log for October 15, 1964, reflects the lowest moisture content measured during the period of study and is used as the base log in the three sets of data. As at the sagebrush-grass site, these values reflect maximum moisture depletion by plants and are considered to approximate residual moisture values. The moisture content in the 1- to 7.5-foot zone, which ranges from 2 to 3 percent, is similar to that observed on the base log at the sagebrush-grass site. Below 7.5 feet, however, the moisture content on the base log under grass is 3 to 6 percent higher than values on the base log under the sagebrush-grass. This marked change suggests a significant difference in the depth of plant feeding at the two sites.

The first set of data in figure 5 illustrates the moisture buildup and use under a grass community during the 1965 growing season. There was a moisture buildup of 0.8 inch in the upper 2.5 feet in the profile from October 15, 1964, to May 6, 1965. By June 30, the log (fig. 5) shows that moisture buildup from cumulative infiltration penetrated to a depth of 9 feet. It is calculated that the 12.7 inches of precipitation from May 6 to June 30 contributed a net increase of 6.9 inches of moisture to the profile, and 5.8 inches were used by

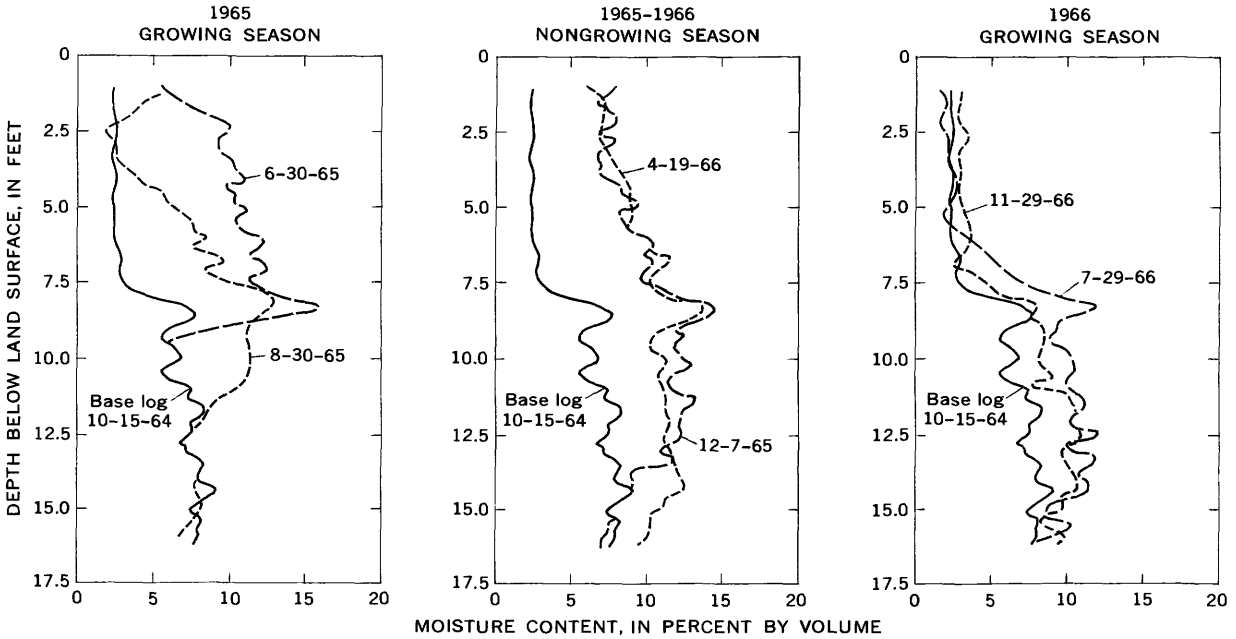

FIGURE 5.—Moisture-content logs for the grass community.

evapotranspiration. These values are comparable to those under a sagebrush-grass community where the depth of moisture penetration was 9 feet, the increase in moisture was 6.3 inches, and the use by evapotranspiration was 6.4 inches.

From June 30 to August 30 the penetration of moisture buildup moved to a depth of 12.5 feet (2 feet deeper than at the sagebrush-grass site). Precipitation during this period was 5.5 inches. The net reduction in moisture over the 2-month period is calculated to be 2.5 inches, and the moisture use by evapotranspiration is estimated to be 8.0 inches. These values may be compared to values under the sagebrush-grass community where the depth of penetration was 9.5 feet, net moisture reduction was 3.4 inches, and evapotranspiration use was 8.9 inches.

The second set of data in figure 5 illustrates the moisture buildup during the 1965–66 nongrowing season. The log of December 7, 1965, shows a penetration to a depth of 14 feet, an increase of 1.5 feet since August 30, 1965. The net increase in moisture was calculated to be 3.8 inches, and the moisture use by evapotranspiration was 4.3 inches. As under the sagebrush-grass community, the moisture deficits caused by evapotranspiration prior to the cessation of plant growth were eliminated by additions of moisture in mid-October. The moisture buildup at lower depths appears to be associated with infiltration from precipitation after the cessation of plant growth.

The log of April 19, 1966, shows that the penetration of moisture from cumulative infiltration during the nongrowing season reached a depth of 16 feet. The net increase in moisture was calculated to be 0.3 inch; use by evapotranspiration was 1.8 inches. Additional neutron measurements in the 16- to 20-foot zone, not shown in figure 5, indicate that slight increases of moisture also occurred in this zone. Thus, the moisture movement in the profile appears to have penetrated to a depth of at least 20 feet.

If it is assumed that the moisture buildup at the grass site was equal to the buildup at the sagebrush-grass site for the same period (December 7, 1965, to April 19, 1966), moisture movement below 16 feet may be determined. The moisture buildup, which penetrated to a depth of 13 feet, under the sagebrush-grass site was calculated to be 1.3 inches. Therefore, because the moisture buildup in the 0- to 16-foot zone under the grass site is calculated to be 0.3 inch, the remaining 1.0 inch of moisture moved below 16 feet.

The third set of data in figure 5 illustrates the moisture depletion under the grass site during the 1966 growing season. As at the sagebrush-grass site, additions of moisture to the profile from April 19 to November 29 were restricted to the upper 4 feet. The logs for July 29 and November 29 show values in the 1- to 5.5-foot zone that indicate the moisture content was rapidly reduced by evapotranspiration to values nearly equal to those shown on the base log. The rate of moisture reduction in the 5.5- to 8.5-foot zone was more gradual. Moisture content 2 to 5 percent higher than the base log was observed in the zone on July 29, but most of this excess was removed by November 29. In the 8.5- to 11-

foot zone the moisture content was substantially reduced but was still higher than the base log at the end of the growing season. There were slight reductions in moisture in the 11- to 16-foot zone with most of the reduction occurring between April 19 and July 29. The net depletion in the profile was calculated to be 5.2 inches by July 29 and 1.5 inches by November 29. The moisture use by evapotranspiration was calculated to be 8.0 inches from April 19 to July 29 and 6.7 inches from July 29 to November 29.

Moisture depletion during the 1966 growing season appears to be attributable mostly to evapotranspiration. The moisture changes above 11 feet, which are more pronounced than those below, principally reflect evapotranspiration. Because the moisture changes from 11 to 16 feet are slight, and because most of the changes occurred before July 29, a loss to deep percolation is suggested. Assuming that all the moisture below 11 feet is attributable to drainage, the amount of deep percolation below 16 feet from April 19 to November 29 would be about 1 inch.

It is estimated that moisture movement as deep percolation below 16 feet is 1.0 inch during the 1965–66 nongrowing season, and that an additional 1 inch of moisture moved below 16 feet as deep percolation during the 1966 growing season. The log of November 29, 1966 shows an estimated 1 inch of moisture in the 11- to 16-foot zone in excess of residual moisture. It is possible that some of this excess also may move downward as deep percolation.

SUMMARY AND CONCLUSIONS

Moisture-content logs for a barren area showed the characteristic manner of moisture buildup during a period of high precipitation and moisture reduction during a subsequent period of low precipitation. The moisture buildup, which varied markedly in the profile, ranged from 2 to 10 percent higher than the retained moisture content. These variations reflect differences in the water-transmitting properties of the dune sand at low flow rates. During the period of low precipitation, moisture was depleted rapidly in the upper part of the profile but more slowly with increasing depth. Moisture data at depths of 15 to 20 feet showed that a period of several months was required for the values to be reduced to the water-holding capacity values. Most of the moisture that infiltrated below the zone of high evaporation (1-foot depth) moved by gravity drainage to deep percolation. In the study area, the quantity of moisture that moves as deep percolation probably represents eventual recharge to the groundwater reservoir.

The manner of moisture buildup and reduction under sagebrush-grass and grass communities, shown by the moisture-content logs, indicated that moisture movement as deep percolation was slight. Even though the period of this study included a year when precipitation was nearly the highest on record, moisture buildup under the sagebrush-grass community penetrated to a depth of only 14 feet, whereas the zone of evapotranspiration extended to at least 17 feet. Under the grass community, where the zone of evapotranspiration was estimated to extend to 11 feet, a small amount of moisture (2 inches) moved as deep percolation.

The moisture content for logs for October 15, 1965, that were run during an extended dry period, was considered to represent residual moisture values. The values in the 1- to 7.5-foot zone (2 to 3 percent) were similar at the two sites. Below 7.5 feet the residual moisture values at the grass site were significantly higher than those at the sagebrush-grass site. The higher values evidently resulted from the absence of deep-feeding sagebrush roots.

Most of the moisture buildup at the grass and sagebrush-grass sites resulted from abnormally high precipitation (26.7 inches) from May 1965 to November 1965. Only small amounts of moisture were added from November 1965 to April 19, 1966. By April 19 a sufficient time had elapsed so that in the zone of evapotranspiration further movement by gravity drainage was negligible. Therefore, estimates of water-holding capacity were based on logs for this date. At the sagebrush-grass site, moisture had penetrated only slightly past 12 feet so the average moisture value (9 percent) in the 7.5- to 12-foot zone was used as an estimate of water-holding capacity below 12 feet. The water-holding capacity values ranged from 6 to 14 percent. Marked variations in these values observed over short depth intervals indicate differences in the particle size distribution or arrangement. Also, the lower values were associated with more intense root development.

The water-holding capacity values provided a basis for estimating the minimum moisture buildup needed in the zone of evapotranspiration for deep percolation. When the moisture content was at residual moisture values (October 15, 1964), the needed moisture buildup was calculated to be 7.5 inches for the grass site and 11.5 inches for the sagebrush-grass site (using 0 to 17 feet as the zone of evapotranspiration). Although precipitation in 1965 was high, most of the moisture added to the profiles either was used in the evapotranspiration process or was retained in the zone of evapotranspiration. At the start of the 1966 growing season, the additional moisture needed in the zone of evapotranspiration to bring the profile to water-holding capacity values

was estimated to be zero at the grass site and 3.5 inches at the sagebrush-grass site. Thus, conditions at this time were favorable for deep percolation. However, very little precipitation occurred during the early part of the growing season, and precipitation during the rest of the growing season was sporadic. Virtually all the moisture added to the profile during the 1966 growing season was used in the evapotranspiration process. Also, the moisture content in the zones of evapotranspiration was reduced to near the low values observed on October 15, 1964.

This report has illustrated the conditions necessary for deep percolation for the predominant vegetative conditions in the dune area. Although only three sites were discussed, the results were comparable at the other sites where vegetation was similar but the slope position was different. Also, comprehensive investigation of recharge in the dune area is being conducted. Moisture content from vegetated areas (exclusive of interdune depressions) is being related to long-term monthly precipitation records for estimated recharge. A similar approach is planned for the interdune depressions and barren areas. Early extrapolation, based on this approach, indicates that the average annual recharge in the vegetated areas is about half an inch. The periods when conditions are favorable for recharge are few. These periods usually occur when precipitation is considerably above average during the nongrowing season and the early part of the succeeding growing season. The high rate of evapotranspiration all but eliminates the possibility of recharge during the summer months.

REFERENCES

Black, C. A., 1966, Crop yields in relation to water supply and soil fertility, *in* Pierre, W. H., and others, Plant environment and efficient water use: Am. Soc. Agronomy and Soil Sci. Soc. America, Madison, Wis., p. 177–206.

Hanks, R. J., Gardner, H. R., and Fairbourn, M. L., 1967, Evaporation of water from soils as influenced by drying with wind or radiation: Soil Sci. Soc. America Proc., v. 31, p. 593–598.

Prill, R. C., and Meyer, W. R., 1968, Neutron moisture measurements by continuous- and point-logging procedures, *in* Geological Survey Research 1968: U.S. Geol. Survey Prof. Paper 600–B, p. B226–B230.

Smith, H. T. U., 1940, Geologic studies in southwestern Kansas: Kansas Geol. Survey Bull. 34, 212 p.

A SUGGESTED METHOD FOR ESTIMATING EVAPOTRANSPIRATION BY NATIVE PHREATOPHYTES

By S. E. RANTZ, Menlo Park, Calif.

Work done in cooperation with the California Department of Water Resources

Abstract.—A graph and table have been developed for selecting values of the coefficient K to be used in the Blaney-Criddle formula for estimating evapotranspiration by native phreatophytes. Values of K are dependent on the species of phreatophyte, the density of growth, and the depth to water table.

In reconnaissance studies of the hydrology of arid basins it is often desirable to make rough estimates of the average annual evapotranspiration by native phreatophytes. These plants usually draw the great bulk of their water from the underlying ground-water body, either directly or through the capillary fringe. The amount of water transpired depends not only on climatic factors, but also on plant species, thickness of the foliage canopy, density of cover (percentage of land area shaded by foliage), and depth to water table. Many researchers—for example, H. F. Blaney, W. D. Criddle, T. W. Robinson, and J. S. Gatewood—using a variety of methods have obtained and published data showing the effect of various factors on the water use by phreatophytes, but nowhere in the literature is there unified data showing the effect of all factors on the water use. In other words, no simple solution is available for the problem of estimating the use of water in a given locality (1) by a given species of phreatophyte, (2) for a given density of growth, and (3) for a given depth to water table. This paper attempts to provide a solution of sorts to that problem.

Acknowledgments.—The author acknowledges with thanks the helpful comments he received from T. W. Robinson, research hydrologist, U.S. Geological Survey, and from H. F. Blaney, consulting engineer and former irrigation engineer with the U.S. Agricultural Research Service.

BLANEY-CRIDDLE FORMULA

Of the several empirical formulas used for estimating evapotranspiration, the most popular is the Blaney-Criddle formula. One of the reasons for this popularity is the fact that the only climatic information required for application of the formula is mean monthly temperature which, if not available for a study site, may be inferred from records for the nearest U.S. Weather Bureau stations. In addition, the formula differentiates between vegetal species, a distinction that is not made by most of the other formulas.

The Blaney-Criddle method is based on the assumption that with ample moisture available, evapotranspiration is affected primarily by temperature, duration of daylight, and vegetal species. For a complete description of the method, the reader is referred to a report by Blaney and Criddle (1962). In brief, the Blaney-Criddle equation for evapotranspiration is

$$U = K\Sigma \frac{(T)\,(p)}{100},$$

where U is evapotranspiration during the growing period,

K is an empirical consumptive-use coefficient that is primarily dependent on the vegetal species,

p is the monthly percentage of total daytime hours in the year,

and

T is the mean monthly temperature, in degrees Fahrenheit.

Table 1 gives values of p for the various latitudes between 24° and 50° north. In using the equation, the monthly products of T and p are added for all months

TABLE 1.—*Monthly percentage of daytime hours of the year for latitudes 24° to 50° north of equator* [1]

[From Blaney and Criddle, 1962, p. 43]

Month	Latitude, in degrees north of equator													
	24	26	28	30	32	34	36	38	40	42	44	46	48	50
January	7. 58	7. 49	7. 40	7. 30	7. 20	7. 10	6. 99	6. 87	6. 73	6. 60	6. 45	6. 30	6. 13	5. 98
February	7. 17	7. 12	7. 07	7. 03	6. 97	6. 91	6. 87	6. 79	6. 73	6. 66	6. 59	6. 50	6. 42	6. 32
March	8. 40	8. 40	8. 39	8. 38	8. 37	8. 36	8. 35	8. 34	8. 30	8. 28	8. 25	8. 24	8. 22	8. 25
April	8. 60	8. 64	8. 68	8. 72	8. 75	8. 80	8. 85	8. 90	8. 92	8. 97	9. 04	9. 09	9. 15	9. 25
May	9. 30	9. 37	9. 46	9. 53	9. 63	9. 72	9. 81	9. 92	9. 99	10. 10	10. 22	10. 37	10. 50	10. 69
June	9. 19	9. 30	9. 38	9. 49	9. 60	9. 70	9. 83	9. 95	10. 08	10. 21	10. 38	10. 54	10. 72	10. 93
July	9. 41	9. 49	9. 58	9. 67	9. 77	9. 88	9. 99	10. 10	10. 24	10. 37	10. 50	10. 66	10. 83	10. 99
August	9. 05	9. 10	9. 16	9. 22	9. 28	9. 33	9. 40	9. 47	9. 56	9. 64	9. 73	9. 82	9. 92	10. 00
September	8. 31	8. 32	8. 32	8. 34	8. 34	8. 36	8. 36	8. 38	8. 41	8. 42	8. 43	8. 44	8. 45	8. 44
October	8. 10	8. 06	8. 02	7. 99	7. 93	7. 90	7. 85	7. 80	7. 78	7. 73	7. 67	7. 61	7. 56	7. 43
November	7. 43	7. 36	7. 27	7. 19	7. 11	7. 02	6. 92	6. 82	6. 73	6. 63	6. 51	6. 38	6. 24	6. 07
December	7. 46	7. 35	7. 27	7. 14	7. 05	6. 92	6. 79	6. 66	6. 53	6. 39	6. 23	6. 05	5. 86	5. 65
Total	100. 00	100. 00	100. 00	100. 00	100. 00	100. 00	100. 00	100. 00	100. 00	100. 00	100. 00	100. 00	100. 00	100. 00

[1] Computed from Smithsonian Meteorological tables (List, 1951, table 171).

in the growing period. Average monthly products of T and p for numerous locations in the western United States are tabulated in the report by Blaney and Criddle (1962, p. 44–49).

BLANEY-CRIDDLE COEFFICIENT

The only difficulty presented by the Blaney-Criddle formula is the selection of the proper value of the all-important coefficient, K. This coefficient, as implied earlier, depends not only on the vegetal species, but also on the depth to the water table and on the density of growth. In addition, K has a regional variation because mean monthly temperature is only an index to the many climatic factors that affect evapotranspiration. In those parts of the arid Southwest, however, where the use of water by native phreatophytes is a significant factor in the hydrologic budget, the variation in K attributable to climatic factors is less important than the variation attributable to vegetal species, density of growth, and depth to the water table. The literature was examined, therefore, to obtain a means of relating K to the latter three factors. Density of growth, as used in this paper, is a combination of two elements—thickness of foliage canopy and density of cover—and is expressed qualitatively as dense, medium, and light. No greater refinement in defining growth characteristics was warranted for this study.

From the welter of information on evapotranspiration by phreatophytes—much of it inconsistent—several reports were selected as being most useful for a generalized study of the coefficient, K. Even those selected reports contain some inconsistent data, and personal judgment was required in deciding what information to ignore and how to best manipulate the remaining data. The net result of this subjective process was figure 1, which is the end product of this paper.

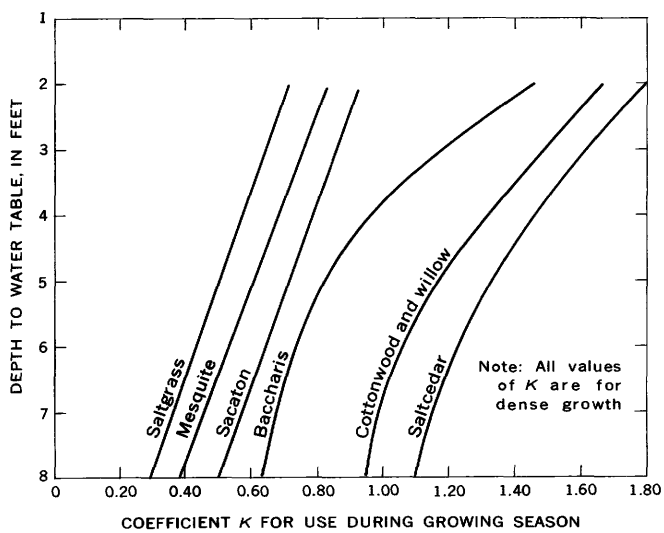

FIGURE 1.—Graph for estimating value of Blaney-Criddle coefficient K in determination of water use by phreatophytes in southwestern United States. (To be used only in the absence of quantitative data at a site.)

The graph in figure 1 gives values of K, for the growing season, for dense growths of various phreatophytes, and shows the variation of K with depth to water table. A K value of 1.30 is recommended for dense growths of hydrophytes, which are plants, such as tule and sedge, that live wholly or partly submerged in water or in saturated soil that is intermittently submerged. Factors for adjusting K values for the effect of density of growth of both phreatophytes and hydrophytes are given in the following tabulation. These factors were derived from a report by Blaney (1954, table 3).

Growth	*Factor by which to multiply K value for density of growth*
Dense	1. 00
Medium	. 85
Light	. 70

Figure 2 explains the derivation of the curves of figure 1. The three plotted values of K for saltgrass in figure 2 were obtained from an investigation in inland areas of southern California. A straight line was fitted to the points on the basis of the following statement by Muckel (1966, p. 29): "Several studies have been conducted in the arid Southwest that show a straight-line relationship between depth to ground water and water use by saltgrass." The two plotted values of K for sacaton were obtained from an investigation near Carlsbad, N. Mex. There was some question as to how to use the data for mesquite. The report by Blaney and Hanson (1965), from which the values for sacaton were obtained, gave K values of 0.65 and 0.75 for mesquite but did not indicate the corresponding depths to water table. For the purpose of this study the curve for mesquite was arbitrarily drawn midway between those for saltgrass and sacaton; the shaded area was added to the graph to show the range of K values given for mesquite.

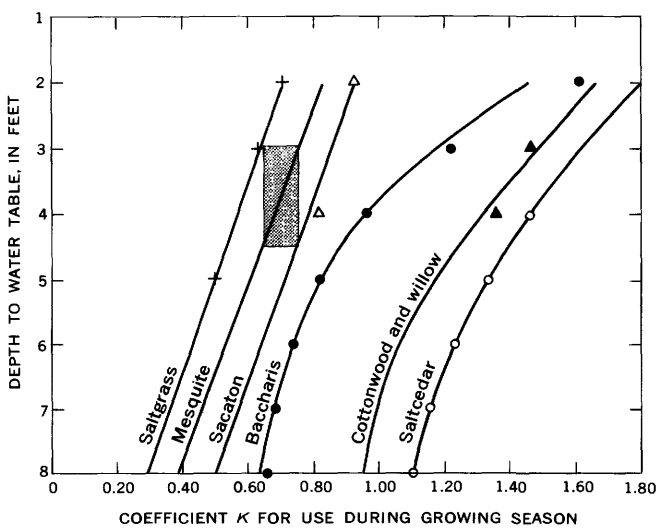

FIGURE 2.—Derivation of curves for relation of Blaney-Criddle coefficient K to depth to water table for various phreatophytes. Source of data: Saltgrass, Blaney and Muckel (1955, table 5, p. 818). Mesquite, Blaney and Hanson (1965, table 22). Sacaton, Blaney and Hanson (1965, table 20). Baccharis, Gatewood and others (1950, fig. 39) (inches converted to K values by use of $F=65$ for Safford, Ariz., and a tank coefficient of 0.85). Cottonwood and willow, Blaney and Hanson (1965, table 20). Saltcedar, Gatewood and others (1950, fig. 39) (inches converted to K values by use of $F=65$ for Safford, Ariz., and a tank coefficient of 0.85). The shaded area for mesquite was added to the graph to show the range of K values.

The data for baccharis were obtained from a study made by Gatewood and others in the Safford Valley, Ariz. In that study evapotranspiration was reported in inches of water. The absolute values of evapotranspiration were converted to corresponding K values by using a figure of $F=65$ in the Blaney-Criddle formula for Safford Valley, where $F=\Sigma(Tp)/100$. A tank coefficient of 0.85 was applied to the K values so derived, as suggested by data from Gatewood and others (1950, p. 194). In developing figure 2 considerable flexibility was used in fitting a curve to the plotted values of K for baccharis where depths to water table were less than 4 feet. The values of K used for cottonwood were obtained from a study made in southern California; those values were assumed to be appropriate also for willows. Values of K for saltcedar were determined from Safford Valley data by applying the same procedures used in the determination of K for baccharis.

SUMMARY

Figure 1, which provides values of the coefficient K for use in the Blaney-Criddle formula, was derived by applying somewhat subjective reasoning to selected data in an effort to obtain a practical method for making rough estimates of evapotranspiration by native phreatophytes in southwestern United States. The values of K from figure 1 should be used only in the absence of quantitative evapotranspiration data, at sites where the time and expense required for a quantitative study are not warranted.

REFERENCES

Blaney, H. F., 1954, Consumptive-use requirements for water: Agr. Eng., v. 35, no. 12, p. 870–873, 880.

Blaney, H. F., and Criddle, W. D., 1962, Determining consumptive use and irrigation water requirements: U.S. Agr. Research Service Tech. Bull. 1275, 59 p.

Blaney, H. F., and Hanson, E. G., 1965, Consumptive use and water requirements in New Mexico: New Mexico State Engineer Tech. Rept. 32, 82 p.

Blaney, H. F., and Muckel, D. C., 1955, Evaporation and evapotranspiration investigations in the San Francisco Bay area: Am. Geophys. Union Trans., v. 36, no. 5, p. 818.

Gatewood, J. S., Robinson, T. W., Colby, B. R., Hem, J. D., and Halpenny, L. C., 1950, Use of water by bottom-land vegetation in lower Safford Valley, Arizona: U.S. Geol. Survey Water-Supply Paper 1103, 210 p.

List, R. J., 1951, Smithsonian meteorological tables: Smithsonian Inst., Wasington, D.C., 527 p.

Muckel, D. C., 1966, Phreatophytes—water use and potential water savings: Am. Soc. Civil Engineers, Irrig. and Drainage Div. Jour., v. 92, no. IR4, p. 27–34.

ADSORPTION OF TRACES OF SILVER ON SAMPLE CONTAINERS

By T. T. CHAO, E. A. JENNE, and L. M. HEPPTING, Denver, Colo.

Abstract.—Special care is required to prevent container adsorption of significant parts of the trace amount of silver present in most natural waters. The use of strong acids appears to be the most effective means of retaining the silver in solution. Lowering the pH of the water samples to 1 with either hydrochloric or nitric acid reduced adsorption onto polyethylene containers to approximately 1 percent of the silver present. Silver adsorption after 30 days of contact time amounted to 4 and 10 percent, of the silver present, at pH 2 when adjusted with hydrochloric acid and nitric acid, respectively. Adjustment of the pH to 1 with either hydrochloric or nitric acid was effective in desorbing silver from polyethylene containers in the course of several days.

The prevention of the loss of silver from solution owing to adsorption on container walls during sample transport and storage is a critical problem in the determination of trace amounts of silver in natural waters. The removal of silver adsorbed by containers also presents a very formidable problem. The adsorption of silver by containers may be substantial and erratic; its magnitude varies with the concentration and composition of the dissolved salts, the pH, the type of container material, and the duration of contact.

Conventional laboratory cleansing methods such as soaking in dichromate solution, or the less conventional methods such as boiling in acidified saturated sodium chloride, are often ineffective for the removal of adsorbed silver from either glass or plastic containers (Chambers and others, 1953; Chambers and others, 1962; West and others, 1966). Coating glass containers with silicone was found to be relatively ineffective in preventing silver adsorption by containers (Dagnall and West, 1962; West and others, 1966; Dyck, 1968). Pretreatment of containers with silver solutions has been used to minimize loss of silver from solution in certain instances (Chambers and others, 1962), but is impractical for the determination of silver in natural waters because of variations in silver concentration, dissolved salts, and pH.

Various chemicals have been tested for their ability to prevent silver adsorption by containers. Non-complex-forming salts decrease the adsorption of trace metals (Eichholz and others, 1966) and silver (West and others, 1966; Dyck, 1968) but are ineffective in preventing it. The complex formers, sodium thiosulfate (0.1M) and EDTA (ethyl diamine tetraacetic acid) (0.1M), were found to be effective in holding container adsorption to less than 1 percent (West and others, 1966). In the presence of small chloride concentrations, it was necessary to increase the thiosulfate concentration to 1M to reduce container adsorption of silver to 1 percent of the amount present. EDTA began to lose its effectiveness after 2 to 10 or more days (West and others, 1967). Hence, its use is not reliable when several days to several weeks are necessarily involved in collecting, transporting, and storing of water samples before analysis for silver content.

Investigators have found a marked decrease in silver adsorption by containers as the pH is decreased (Chambers and Proctor, 1960; Hamester and Kahn, 1963; Dyck, 1968). Dyck (1968) has recently shown that silver adsorption by clear borosilicate glass decreased consistently as the pH of the solution was decreased from 8.0 to 4.0. Chambers and Proctor (1960) also found that silver adsorption onto containers was reduced with decreasing pH in the range pH 6.0 to 1.0. Hamester and Kahn (1963) observed that adsorption of silver onto glass containers decreased as the concentration of nitric acid was increased to 1M. Lai and Weiss (1962) found that pH adjustment with acetic acid to 3.5 to 4.0 was adequate to prevent the adsorption of silver from sea water onto polyethylene containers. The results of West, West, and Iddings (1966), showing that container sorption increased at pH 4.0 as compared to pH 7.0, are anomalous.

The relative effectiveness of various concentrations of hydrochloric, nitric, and acetic acids in preventing silver adsorption by polyethylene containers was studied as a function of time. Similar data were obtained for hydrochloric acid with glass containers.

EXPERIMENTAL METHOD

A test solution containing 60 milligrams per liter of Ca^{+2}, 20 mg/l of Mg^{+2}, 75 mg/l of Na^{+1}, 200 mg/l of HCO_3^{-1}, 20 mg/l of Cl^{-1}, and 195 mg/l of SO_4^{-2} was used to simulate natural conditions. New 1-liter polyethylene and Pyrex bottles were used as test containers. These were acid washed and thoroughly rinsed with distilled water before use. Each bottle was filled with 800 milliliters of the test solution. Sets of test solutions were adjusted to different pH values with hydrochloric, nitric, or acetic acid. The pH values of the test solutions were found to be within ± 0.1 of the designated values at all sampling times. The test solution contained 5 μg/l of silver labeled with Ag^{110m} as a tracer. Immediately after labeling and mixing, triplicate 1-ml aliquots were taken and transferred to tubes to serve as standards.

At intervals, usually 2 to 3 days or occasionally longer, triplicate 1-ml aliquots were taken from each bottle after the contents were mixed for 1 minute, and the gamma radiation was counted with a single-window gamma spectrometer. The spectrometer was set for the 0.65-million-electron-volt peak of Ag^{110m}. Samples were counted 10 minutes or longer to accumulate at least 10,000 counts.

The effectiveness of pH 1 hydrochloric and nitric acids in removing adsorbed silver from containers was determined by acidifying the pH 2, 3, and 6 hydrochloric acid and nitric acid series to pH 1 after these samples had been held 30 days or longer.

RESULTS AND DISCUSSION

Silver adsorption by polyethylene containers from the test solutions was markedly dependent upon pH. The pH effects were generally similar for adsorption onto polyethylene containers for both the hydrochloric acid and nitric acid series (figs. 1 and 2). Silver adsorption from the pH 6 sample increased almost linearly with contact time, and after 30 days more than two-thirds of the silver was retained by container surfaces. These data are in accord with the observation of Warburton (1965) that up to one-third of the silver from 0.01-μg/l solutions was adsorbed onto containers in 7 days.

At pH 3 in the hydrochloric acid series, there was an induction period of about 15 days with silver adsorption gradually increasing to about 5 percent of the total amount of silver in the solution, then increasing rapidly and linearly to about 45 percent at 30 days. In the pH 3 nitric acid series, the induction period was absent and silver adsorption was most rapid during the initial 8 days.

When the test solutions were acidified to pH 2 with hydrochloric or nitric acid, adsorption of silver onto containers was less then when the pH of the solutions was 3. In the hydrochloric acid series, adsorption of silver was less than 4 percent of that present during the first 30 days after the containers were filled. Duplicate runs (data not shown) confirm this fact. However, because the duplicate runs were not continued beyond 25 days it is not known if the increased adsorption at 35 days is real or spurious. In contrast to the pH 2 hydrochloric acid series, silver loss in the pH 2 nitric acid series increased gradually to about 10 percent during the initial contact time of 30 days.

Maintenance of water samples at pH 1 with either hydrochloric or nitric acid is most effective in keeping silver in solution in polyethylene containers. As shown in figures 1 and 2, these two acids were equally effective for this purpose. It may also be observed from these two figures that the amount of silver adsorbed by the polyethylene containers fluctuated around 1 to 2 percent for the entire 60-day period.

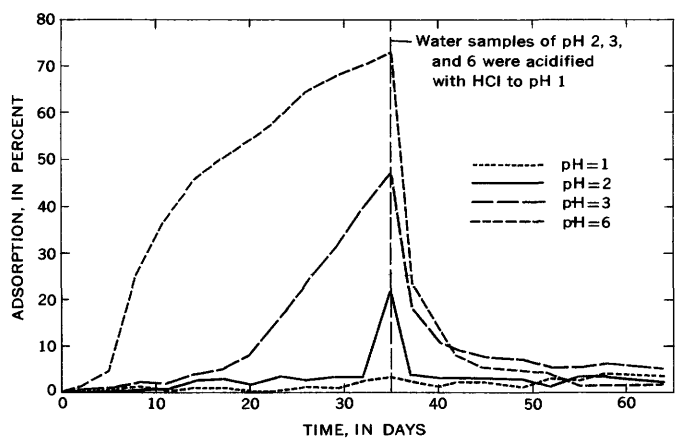

FIGURE 1.—Adsorption of silver onto polyethylene containers from test solutions (containing 5 μg/l of silver) adjusted to different pH values with hydrochloric acid.

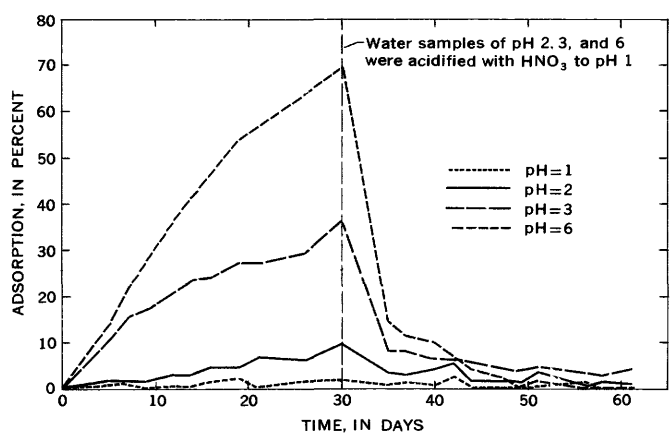

FIGURE 2.—Adsorption of silver onto polyethylene containers from test solutions (containing 5 μg/l of silver) adjusted to different pH values with nitric acid.

The effectiveness of pH 1 treatment in desorbing silver is comparable to its effectiveness in preventing adsorption (figs. 1 and 2). After increasing the acidity of samples with initial pH values of 2, 3, and 6 to pH 1, the amount of silver remaining adsorbed decreased within a few days to less than 10 percent of the total initially added. There was a further gradual decrease in silver adsorption which leveled off with time. Thus, an earlier report (Hensley and others, 1949) that 1*N* nitric acid was ineffective in removing adsorbed silver from soft glass can now be interpreted as being due to inadequate reaction time (4 hours).

The reduction in volume as a result of successive samplings for radioactive counting introduced a small error in calculating the percentage of adsorption during the desorption part of the experiment. This was especially true with test solutions of pH 6 and 3 because the silver adsorbed in the previous part of the experiment was desorbed into a smaller volume after acidification. This error does not affect values for test solutions of pH 1, for silver was held in solution throughout the experiment.

Similar experiments with polyethylene bottles, but using acetic acid to acidify test solutions, showed that a pH value of 1 was nearly as effective as pH 1 adjusted with hydrochloric or nitric acid in maintaining silver in solution up to 22 days, at which time the test was discontinued. However, such a large volume of glacial acetic acid is required to lower the pH to 1 (approximately 625 ml per liter of test solution) that it is hardly practical. There was little difference in the effectiveness of pH 2 and 3 adjusted with acetic acid; the percentage of adsorption increased gradually to 10–15 percent in the course of 20 days. The observation of Lai and Weiss (1962) that silver was not adsorbed from sea water on polyethylene bottles when acidified to pH 3.5 to 4.0 with acetic acid may be due to the formation of silver chloride complexes in the acidified sea water.

When test solutions contained in Pyrex bottles were acidified with hydrochloric acid to pH 1, 2, or 3, container adsorption of silver was kept below 2 percent of the amount of silver originally present for 30 days. The control test solution with a pH of 5.5 showed silver adsorption below 10 percent during the same period. Silver adsorption on glass surfaces is generally much lower than on polyethylene surfaces (West and others, 1966, 1967; Dyck, 1968). The observed greater affinity of silver for polyethylene than for glass surfaces is consistent with the findings of Eichholz, Galli, and Elston (1966) for fission products.

Although the adsorption of silver by polyethylene is generally greater than by glass, polyethylene sample containers are preferred for field sampling because they, unlike glass containers, do not break easily. The adjustment of pH to 1 with hydrochloric or nitric acids is equally effective in preventing silver adsorption by polyethylene surfaces. The use of these acids is preferable to EDTA because of the greater length of time for which the acids are effective.

Although most of the adsorbed silver may be removed from container surfaces simply by acidification to pH 1 with hydrochloric or nitric acid, there is uncertainty as to whether complete desorption can always be achieved. It is therefore advisable to establish proper acidity in the water sample when collected so that silver may be prevented from adsorbing onto container surfaces. To further reduce the possibility of cross contamination between samples, soaking the container in strong nitric or hydrochloric acid for some days is recommended before reuse.

REFERENCES

Chambers, C. W., Chambers, L. A., and Kabler, P. W., 1953, New colloidal silver disinfectant—Effect of environmental factors on bactericidal action: Indus. Eng. Chemistry, v. 45, p. 2569–2571.

Chambers, C. W., and Proctor, C. M., 1960, Bacteriological and chemical behavior of silver in low concentrations: U.S. Public Health Service, Tech. Rept. W 60–4, Taft Sanitary Engineering Center, Cincinnati, Ohio, 18 p.

Chambers, C. W., Proctor, C. M., and Kabler, P. W., 1962, Bactericidal effect of low concentrations of silver: Am. Water Works Assoc. Jour., v. 54, p. 208–216.

Dagnall, R. M., and West, P. W., 1962, Direct spectrophotometry of silver in a non-aqueous medium: Anal. Chim. Acta, v. 27, p. 9–14.

Dyck, Willy, 1968, Adsorption of silver on borosilicate glass—Effect of pH and time: Anal. Chemistry, v. 40, p. 454–455.

Eichholz, G. G., Galli, A. N., and Elston, L. W., 1966, Problems in trace element analysis in water: Water Resources Research, v. 2, p. 561–566.

Hamester, H. L., and Kahn, Milton, 1963, The adsorptive and radiocolloidal properties of carrier-free silver: U.S. Atomic Energy Comm. Rept. SCR–593, 46 p.

Hensley, J. W., Long, A. O., and Willard, J. E., 1949, Reactions of ions in aqueous solution with glass and metal surfaces—Studies with radioactive tracers: Indus. Eng. Chemistry, v. 41, p. 1415–1421.

Lai, M. G., and Weiss, H. V., 1962, Cocrystallization of ultramicro quantities of elements with thionalid—Determination of silver in seawater: Anal. Chemistry, v. 34, p. 1012–1015.

Warburton, J. A., 1965, The detection of silver in rainwater—Further developments of technique: Jour. Appl. Meterology, v. 4, p. 565–568.

West, F. K., West, P. W., and Iddings, F. A., 1966, Adsorption of traces of silver on container surfaces: Anal. Chemistry, v. 38, p. 1566–1570.

———1967, Adsorption characteristics of traces of silver on selected surfaces: Anal. Chim. Acta, v. 37, p. 112–121.

PREVENTION OF ADSORPTION OF TRACE AMOUNTS OF GOLD BY CONTAINERS

By T. T. CHAO, E. A. JENNE, and L. M. HEPPTING,
Denver, Colo.

Abstract.—Loss of significant parts of trace amounts of gold by adsorption on container walls, during sample transport and storage, poses a major problem in quantitative determinations of gold in natural water. Experiments using gold-198 as a tracer indicate that gold may be kept in solution for 21 days by (1) acidification of a test solution to pH 1 with hydrochloric acid and addition of between 5 to 50 mg/l of bromine, (2) acidification with hydrochloric acid to 1*N* without bromine, and (3) acidification with nitric acid to 2*N* or 3*N*. After 21 days, radioactive decay reduces gamma radiation of gold-198 beyond the limits of accuracy of available equipment and no information was obtained. Addition of 50 mg/l of bromine to a nonacidified test solution of pH 6 is almost as effective. In contrast to nonacidification, moderate acidification of the test solution to pH 2 or 3 with hydrochloric and acetic acids, as well as acidification to pH 1 with nitric acid, enhances gold adsorption. The pH 1 hydrochloric acid and 50 mg/l bromine combination is as effective in desorbing gold from container walls as it is in preventing gold adsorption.

The loss of gold from water samples by adsorption on container walls during sample transport and storage poses a major problem in the determination of trace amounts of gold in natural waters. Preliminary experiments with gold-198 demonstrated that detectable losses of gold from solution at nearly neutral reaction occurred within a few hours of contact with polyethylene or glass surfaces. Hence, analysis of gold in water without elimination of the problem of container adsorption might lead to erroneous results. The magnitude of loss of gold due to container adsorption may vary with the concentration and composition of dissolved salts of the water, its pH, the type and past usage of container, and duration of contact.

Only fragmentary information can be found in the literature concerning the adsorption mechanism, the extent of gold adsorption by containers, and the means used to prevent adsorption. Hummel (1957) reported that gold content of sea water stored for a 3-week interval in a polyethylene bottle decreased to less than a quarter of the amount collected directly in the irradiation tubes. Leutwein, as quoted by Beamish (1961), ascribed the loss of gold from dilute solution to base-exchange reactions with the glass container and to adsorption. Solutions containing 10 milligrams per liter of gold showed only 0.1 to 0.3 percent of the original strength after 230 days storage in Jena glass flasks. Brooks (1960) suggested the adjustment of the acidity of sea water to 0.1*N* with hydrochloric acid and the addition of 10 parts per million of bromine to lessen gold adsorption, whereas Weiss and Lai (1963) relied only on the acidification of sea water to pH 1 with hydrochloric acid to prevent gold adsorption on polyethylene containers.

Although trace amounts of gold can be kept in solution by the addition of large quantities of hydrochloric or nitric acid, it is inconvenient to handle the amounts of acids required to acidify the multiliter volume of water often needed for gold analysis. Also, gold present as an impurity in the large amounts of acid may necessitate the purification of acids before use. Still another problem is that the manipulation of solutions containing strong acids in large quantities imposes limitations in the selection of the analytical procedure for gold. Therefore, this study was undertaken to determine the optimum acidity required, as well as to compare the relative effectiveness of hydrochloric, nitric, and acetic acids, and bromine, as a function of contact time, in preventing gold adsorption by polyethylene containers.

EXPERIMENTAL METHOD

A test solution containing 60 mg/l of Ca^{+2}, 20 mg/l of Mg^{+2}, 75 mg/l of Na^{+1}, 200 mg/l of HCO^{-1}, 20 mg/l of Cl^{-1}, and 195 mg/l of SO_4^{-2} was used to simulate natural conditions. New 1-liter polyethylene bottles were used as test containers. These were washed with 3*N* hydrochloric acid and thoroughly rinsed with distilled water before use. Each bottle contained 800 milliliters of the test solution. Sets of test solutions

were adjusted to different pH values with hydrochloric, nitric, or acetic acid by using a pH meter, or to different normalities by adding calculated amounts of hydrochloric or nitric acid. The dilute hydrochloric acid series at pH 1 also received different amounts of bromine (5, 10, 25, and 50 mg/l). The pH values were checked occasionally and found to be within ± 0.1 of the designated values. Most of the container-adsorption experiments were carried out with 5-micrograms per liter gold solutions, although gold concentrations other than 5 μg/l were also used in some experiments. Gold solutions tagged with gold-198 as a tracer were used throughout this study. Immediately after labeling and mixing, triplicate 1-ml aliquots were transferred to counting tubes to serve as standards for the determination of fractions of gold remaining in solution as a function of contact time.

At 2- or 3-day intervals, triplicate 1-ml aliquots were taken from each bottle after swirling the contents for 1 minute, and the gamma radiation was counted with a single-window gamma spectrometer. The spectrometer was set to count the 0.41 million-electron-volt gold-198 peak. Samples were counted long enough to accumulate at least 10,000 counts for early samplings and 5,000 counts for later samplings

RESULTS AND DISCUSSION

Acidifying the water to 1*N* with hydrochloric acid prevented gold adsorption onto polyethylene surfaces throughout the test period of 21 days (fig. 1). After this time no information was obtained because, owing to decay, the gamma radiation of gold-198 was too low to be accurately counted by the available equipment. Lower acidities (pH 1, 2, or 3) were not effective in keeping gold in solution. In fact, there was an appreciable increase in gold adsorption with time of contact in all three treatments. This was especially true with the water acidified to pH 3, which showed the greatest loss in gold concentration. The amount of gold in a nonacidified test solution of pH 6 also showed a gradual decrease with contact time. The amount of gold adsorbed by containers from the nonacidified test solution (pH 6) was less than that from the pH 2 or 3 test solution. This is contrary to accepted concepts. The acidification of the test solution to pH 1 with hydrochloric acid, though causing some decrease in gold adsorption in comparison with that at pH 6, resulted in 30–40 percent adsorption in the later stage of the experiment. Weiss and Lai (1963) stated that at pH 1 with hydrochloric acid, gold was not adsorbed from sea water by walls of polyethylene containers. The apparent discrepancy between the data presented here and the above statement could be due to the high concentration of chloride ions in sea water.

The fact that bromination plus acidification of the test solution with hydrochloric acid is most effective in keeping gold from being adsorbed on container walls is indicated in figure 2. During the entire experiment adsorption of gold never amounted to greater than 1 percent when acidity of pH 1 and varied amounts of bromine were used. This is in line with the suggestion of Brooks (1960) regarding the maintenance of acidity of sea water at 0.1*N* with hydrochloric acid plus 10 mg/l of bromine to reduce gold adsorption on containers. Bromination of a pH 6 nonacidified test solution to a

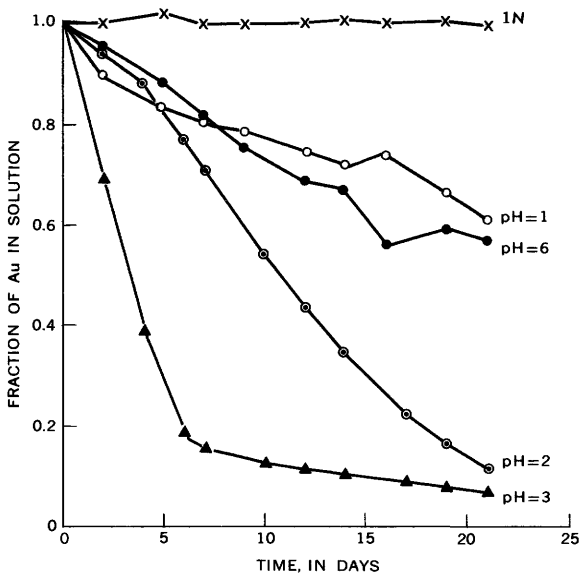

FIGURE 1.—Adsorption of gold from test solutions (containing 5 μg/l of gold) onto walls of polyethylene containers as influenced by different concentrations of hydrochloric acid. Adsorption of gold expressed as fraction of gold remaining in solution.

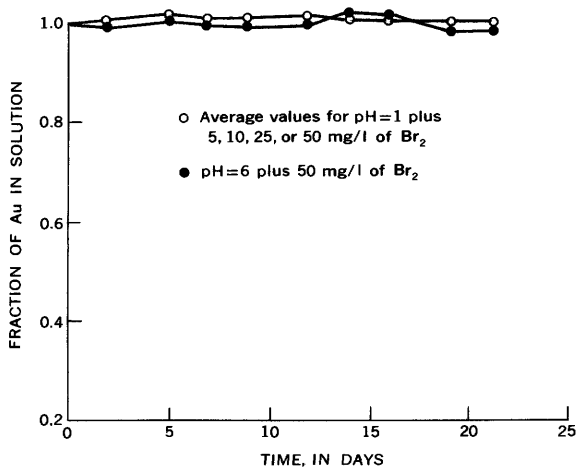

FIGURE 2.—The effectiveness of bromination with and without acidification (pH 1 with hydrochloric acid) in maintaining gold (5 μg/l) in solution in polyethylene containers.

50 mg/l bromine content was equally as effective as the pH 1 hydrochloric acid plus 50 mg/l of bromine treatment in preventing gold adsorption, with the exception of the last two samplings wherein about 2 percent of the gold was lost to the container walls. It is known that in the presence of free bromine a very stable gold(III) bromide complex is formed which does not appear to be adsorbed by the polyethylene container.

Nitric acid, though not as effective as hydrochloric acid at comparable concentrations, completely prevented gold adsorption at higher concentrations; that is, 2*N* or 3*N* (fig. 3). With 1*N* nitric acid there was an 11 percent loss of gold owing to container adsorption in 5 days of contact, after which the change of gold concentration in solution leveled off. A further decrease in nitric acid concentration to pH 1 resulted in an abrupt loss of 85 percent of the gold from solution and little change thereafter with time.

Acetic acid was not effective in preventing gold adsorption on container walls (fig. 4). The loss of gold from solution was appreciable in the first few days and then continued at slower rates. At the latter part of the experiment, the two curves indicating the degree of gold adsorption at pH 2 and 3 merged and more than 90 percent of the gold disappeared from the solution.

Additional work was done with the pH 1 hydrochloric acid plus 50 mg/l of bromine treatment. Water samples of different salt concentrations equivalent to 0.5, 1.0, 1.5, and 2.0 multiples of the salt content of the test solution and containing 0.5 μg/l and 1 mg/l of gold were also used. Gold remained in solution throughout the experiment. The above treatment was also applied to 15 liters of test solution in a large polyethylene container commonly used in the field for water sampling. Again gold remained in solution for more than 20 days with no loss by container adsorption.

The pH 1 hydrochloric acid plus 50 mg/l of bromine treatment was equally as effective in desorbing gold from container walls as in preventing adsorption. In a separate experiment, a test solution of pH 6 containing 5 μg/l of gold was allowed to stand for 10 days, after which time the test solution was acidified to pH 1 with hydrochloric acid and brominated with 50 mg/l of bromine. In 2 days the adsorbed gold was completely desorbed, and by the end of the experiment the gold had remained in solution for 16 days.

In developing a means to prevent gold adsorption on container walls, emphasis should be placed on compatibility with the method of analysis finally adopted for determining trace amounts of gold in waters. The pH 1 hydrochloric acid plus 50 mg/l of bromine treatment was tested for this requirement. When stabilized by the above treatment, known amounts of gold in the presence of other constituents commonly found in natural waters can be quantitatively collected by an ion-exchange resin column, eluted, and determined by atomic absorption spectrometry. By using the combined hydrochloric acid-bromine stabilization, an analytical procedure has been devised whereby 20 to 50 nanograms per liter of gold can be accurately determined using 10–25

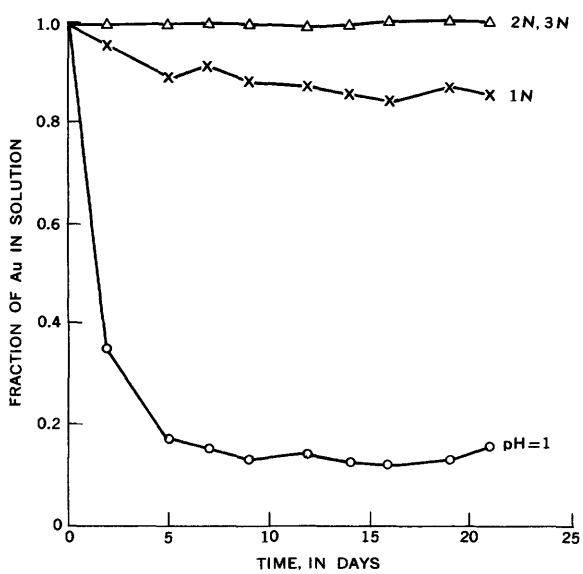

FIGURE 3.—Adsorption of gold from test solutions (containing 5μg/l of gold) onto walls of polyethylene containers as influenced by different concentrations of nitric acid. Adsorption of gold expressed as fraction of gold remaining in solution.

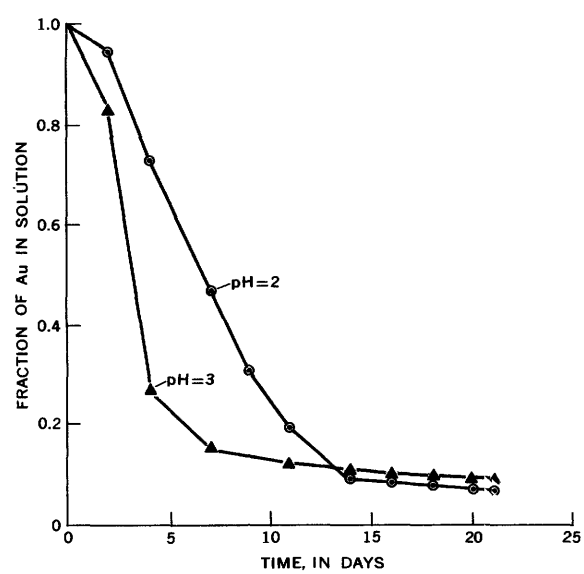

FIGURE 4.—Adsorption of gold from test solutions (containing 5μg/l of gold) onto walls of polyethylene containers as influenced by two concentrations of acetic acid. Adsorption of gold expressed as fraction of gold remaining in solution.

liters of water (larger volumes of water are required for lower gold concentrations).

Water samples collected for trace-metal analysis are frequently acidified to minimize the tendency of trace metals to adsorb onto containers, or to precipitate. The need to determine the optimum acidity required for each metal of interest is demonstrated by the results which were obtained with hydrochloric acid (fig. 1). An increase in acidity from pH 6 to 3 or 2 caused a marked decrease in the amount of gold remaining in solution. It is also noteworthy that in the presence of dilute nitric acid at pH 1 the gold remaining in solution decreased by about 40 percent as compared to gold in a pH 6 nonacidified test solution (figs. 1 and 3). Hence, indiscriminate acidification of water samples collected for trace-metal analysis may cause errors because of enhanced container adsorption. This is shown by the results of this study.

REFERENCES

Beamish, F. E., 1961, A critical review of colorimetric and spectrographic methods for gold: Anal. Chem., v. 8, p. 1059–1066.

Brooks, R. R., 1960, The use of ion-exchange enrichment in the determination of trace elements in sea water: Analyst, v. 85, p. 745–748.

Hummel, R. W., 1957, Determination of gold in sea water by radioactivation analysis: Analyst, v. 82, p. 483–488.

Weiss, H. V., and Lai, M. G., 1963, Cocrystallization of ultra micro quantities of elements with 2-mercaptobenzimidazole—Determination of gold in sea water: Anal. Chim. Acta, v. 28, p. 242–248.

NUCLEAR MAGNETIC RESONANCE STUDIES OF PHOSPHORUS(V) PESTICIDES—III, THE HYDROLYSIS OF ALIPHATIC PESTICIDES BY AQUEOUS SOLUTIONS

By MARVIN C. GOLDBERG, HARRY BABAD [1], DENNIS GROOTHIUS [2], and H. R. CHRISTIANSON, Denver, Colo., Muskegon, Mich., Denver, Colo.

Abstract.—Contrary to expectations, Cygon, Dyfonate, and Malathion hydrolyze slowly in treatment with stoichiometric amounts of water at ambient temperatures in the pH range of natural water. Nuclear magnetic resonance measurements showed the half life for the hydrolysis process to be greater than 2 weeks.

Much of the scientific literature accepts the supposition that various pesticides containing phosphorus(V) are lesser environmental pollutants than the chlorinated hydrocarbons. This reduced environmental longevity of pesticides containing phosphorus(V) is attributed to their ability to hydrolyze readily in aqueous solutions and form simple nontoxic materials such as phenols, alcohols and phosphoric acid in the non-sulphur-containing series, and easily oxidized thiols from the thio-derivatives. Little quantitative information exists, however, to support the supposition of reduced longevity of these materials, especially under the pH ranges of natural water at ambient temperatures.

To investigate these phenomena it was necessary to choose an analytical tool that allowed observation of the reaction conditions during the course of the reaction. It is clear that a wet analytical technique applied to the study of the kinetics of hydrolysis would be inappropriate since complete analysis of fractions would be tedious; and the desired accuracy for all components probably could not easily be achieved. Infrared analysis would involve the use of Irtran cells necessitating higher noise levels than sodium chloride or potassium bromide cells. The latter cells cannot be used with aqueous solutions. Owing to the severe overlapping of the group frequencies of the products and starting materials, it would be difficult to distinguish between all the absorption peaks sufficiently to allow analysis. Although the literature reports some progress (Suffet and others, 1967) in gas-liquid chromatography, analysis by this method would be difficult and would result in questionable data because many of the hydrolysis intermediates are both nonvolatile and thermally sensitive.

For these reasons the nuclear magnetic resonance (NMR) technique was applied, and studies were made of the kinetics of hydrolysis of some of the more common pesticides containing phosphorus(V). All the products were determined simultaneously without altering the composition of the samples. An advantage in using the technique of nuclear magnetic resonance spectroscopy is that increases in concentration of the hydrolysis products and decreases in concentration of the pesticide can be measured simultaneously with 3 ± 0.5 percent limit of detectability for each of the materials present. Changes of the chemical shifts of the protons in newly formed compounds and the state of collapse of coupled multiplets owing to bonding of substituents to phosphorus in the parent compound can both be observed.

Acknowledgments.—The authors thank Dr. Alvin L. Schalge, of the Marathon Oil Co.'s Denver Research Center, for allowing them to use Marathon's A–60 spectrometer. They also thank the Agricultural Division of the Stauffer Chemical Co., the Shell Chemical Co., the Agricultural Division of the American Cyanamid Co., and the Chemagro Corp. for supplying the pesticides used in this study.

DISCUSSION

The compounds selected for investigation had unique nuclear magnetic resonance spectra and were representative of the various classes of useful aliphatic pesticides. These componds include Bidrin (I), Cygon (II), Dipterex (III), Dyfonate (IV), and Malathion (V).

[1] Research Division, the Ott Chemical Co.
[2] Department of Chemistry, University of Denver.

Structural illustrations of organic hydrolysis products of these and related compounds discussed in the literature follow this paragraph. Details of their nuclear magnetic resonance spectra are listed in the experimental methods section. Because simple homologs probably react analogously, and the spectrum of a methyl derivative is simpler than that of the analogous ethyl compound, methyl rather than ethyl derivatives were used where possible.

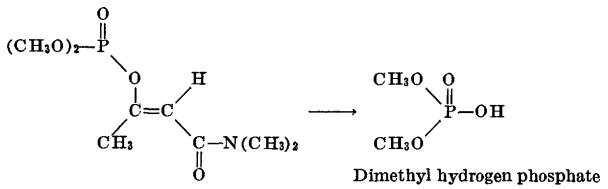

Dimethyl phosphate of 3-hydroxy-*N,N'*-dimethyl-*cis*-crotonamide

Bidrin (I)

Dimethyl hydrogen phosphate

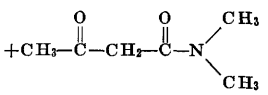

N,N-Dimethylacetoacetamide

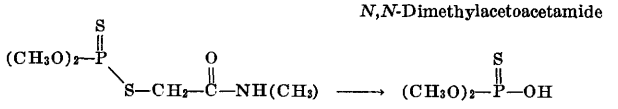

O,O-dimethyl S-*α*-mercapto-*N*-methylacetamido-dithiophosphate

Cygon (II)

Dimethyl hydrogen thiophosphate

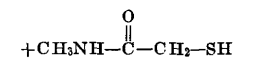

α-Mercapto-*N*-methylacetamide

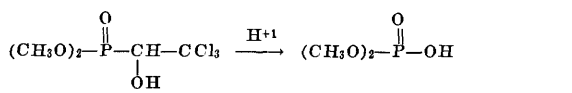

Dimethyl ester of 1-hydroxy-2,2,2-trichlorophosphonic acid

Dipterex (III)

Dimethyl hydrogen phosphate
+ CCl_3CH_2OH
2,2,2-trichloroethanol

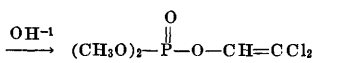

2,2-dichloroethenodimethoxy phosphinate

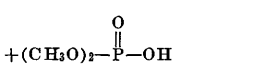

Dimethyl hydrogen phosphate
+ $Cl_2CH-CH=O$
Dichloroacetaldehyde

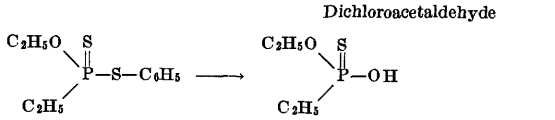

O-ethyl-S-phenyl-ethylphosphonodithioate

Dyfonate (IV)

Ethyl ethoxyphosphinic sulfide
+ C_6H_5SH
Phenyl mercaptan

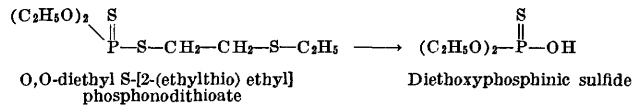

O,O-diethyl S-[2-(ethylthio) ethyl] phosphonodithioate

Dysyston

Diethoxyphosphinic sulfide
+ $C_2H_5S-CH_2CH_2-SH$
2-mercaptodiethyl sulfide

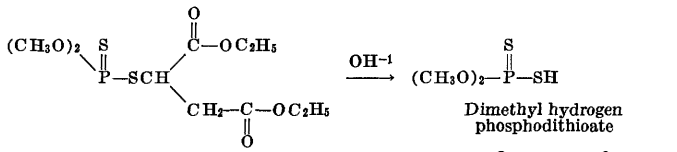

S-ester of O,O-dimethyl phosphorodithioate with diethyl *α*-mercapto succinate

Malathion (V)

Dimethyl hydrogen phosphodithioate
+ Diethyl fumarate
Dimethyl hydrogen phosphothioate
+ Diethyl-*α*-mercaptosuccinate

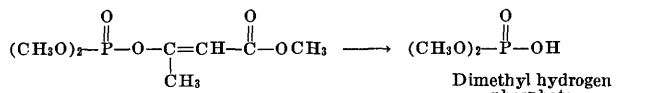

α-2-carbomethoxy-1-methylvinyl-O,O-dimethyl phosphate

Phosdrin (VI)

Dimethyl hydrogen phosphate
+ Methylacetoacetate

EXPERIMENTAL METHODS

Spectra were measured with a Varian A-60 NMR spectrometer calibrated with trimethylsilylpropionic acid (TMS) as zero parts per million in carbon tetrachloride solvent. Chemical shifts were measured in parts per million downfield from the internal TMS standard, and coupling constants were measured in cycles per second on expanded spectra taken at a sweep width of 100 cycles per second at a sweep rate of 250 seconds. The details of the spectra for the model compounds and their degradation products are listed as follows:

Bidrin (I)

Singlet (3H) at 2.9 ppm ($CH_3C{=}C$); Doublet (6H) at 2.97 ppm ($N{-}CH_3$) $\delta = 7$ cps; Doublet (6H) at 3.82 ppm (OCH_3), $J_{PH} = 12$ cps; Quartet (1H) at 6.08 ppm ($HC{=}C$). $J_{CH} = 1$ cps.

Dimethyl hydrogen phosphate (D_2O)

Doublet at 3.80 ppm (OCH_3), $J_{PH} = 12.5$ cps.

N,N-Dimethylacetoacetamide

Singlet (3H) at 2.17 ppm ($CH_3C{=}O$); Doublet (6H) at 3.00 ppm ($N{-}CH_3$) $\delta = 0$ cps; Singlet (2H) at 3.52 ppm (CH_2).

Cygon (II)

Doublet (3H) at 2.85 ppm (NCH_3), $J_{CH}=5$ cps; Doublet (2H) at 3.53 ppm (SCH_2CO), $J_{PH}=6$ cps; Doublet (6H) at 3.80 ppm (OCH_3), $J_{PH}=15$ cps.

Dimethyl hydrogen thiophosphate (D_2O)

Doublet at 3.80 ppm (OCH_3), $J_{PH}=15.5$ cps.

α-Mercapto-*N*-methylacetamide

Triplet (1H) at 1.90 ppm (SH), $J_{CH}=8$ cps; Doublet (3H) at 2.78 ppm (CH_3—N), $J_{CH}=6$ cps; Doublet (2H) at 3.73 ppm (CH_2S), $J_{CH}=8$ cps; Broad singlet (1H) at 5.16 ppm (N—H).

Dipterex (III)

Doublet (6H) at 3.9 ppm (OCH_3), $J_{PH}=11$ cps; Doublet (1H) at 4.55 ppm (OC—H), $J_{PH}=11$ cps; Singlet (1H) at 5.95 ppm (OH).

2,2,2-Trichloroethanol

Singlet (1H) at 3.40 ppm (OH); Singlet (2H) at 3.80 ppm (CH_2).

2,2-Dichloroethenodimethoxy phosphinate

Dichloroacetaldehyde

Doublet (1H) at 6.05 ppm (Cl_2CH), $J_{CH}=7$ cps; Doublet (1H) at 9.2 ppm (O=C—H), $J_{CH}=7$ cps.

Dyfonate (IV)

Multiplet (6H) at 0.8–1.5 ppm (CH_3); Sextet (2H) at 1.95 ppm (PCH_2), $J_{CH}=7$c ps; Multiplet (2H) at 3.9–4.5 ppm (OCH_2), $J_{PH}=9$ cps, peaks doubled due to hindered rotation; Singlet at 7.35 ppm (Ar—H).

O-Ethyl-ethylphosphonothioate (D_2O)

Multiplet (6H) at 0.9–1.6 ppm (CH_3); Sextet (2H) at 1.94 ppm (PCH_2), $J_{CH}=7$ cps, $J_{PH}=11$ cps; Octet (2H) at 4.23 ppm (OCH_2), $J_{CH}=7$ cps, $J_{PH}=11.5$ cps.

Thiophenol

Singlet (1H) at 3.32 ppm (SH); Singlet (5H) at 7.2 ppm (Ar—H).

Malathion (V)

Doublet triplet (6H) at 1.28 ppm (CH_3), $J_{CH}=7$ cps, $\delta=3$ cps; Unsymmetrical triplet (2H) at 2.85 ppm (CH_2C=O); Doublet (6.5H) at 3.78 ppm (OCH_3), $J_{PH}=15.5$ cps; Septet (4.5H) at 4.18 ppm (OCH_2), $J_{CH}=7$ cps, $\delta=4$ cps.

Diethyl fumarate

Triplet (6H) at 1.32 ppm (CH_3), $J_{CH}=7$ cps; Quartet (4H) at 4.27 ppm (OCH_2), $J_{CH}=7$ cps; Singlet (2H) at 6.83 ppm (C=C—H).

Diethyl α-mercaptosuccinate

Triplet (6H) at 1.25 ppm (CH_3), $J_{CH}=7$ cps; Doublet (1H) at 2.25 ppm (SH), $J_{CH}=8$ cps; Doublet (2H) at 2.62 ppm (CH_2C=O), $J_{CH}=7$ cps, Poorly resolved sextet (1H) at 3.62 ppm (S—CH); Quartet (4H) at 4.15 ppm.

GENERAL BULK-HYDROLYSIS PROCEDURES (ARTIFICIALLY INDUCED HYDROLYSIS)

A 0.1-mole sample of the appropriate pesticide (I–V) along with 500 milliliters of 1*N* hydrochloric acid or 1*N* sodium hydroxide solution was placed in separate 1-liter 3-necked flasks equipped with a stirrer and a reflux condenser. To this mixture was added 100 ml of reagent-grade toluene containing 0.1 moles of benzene as an internal standard. The reaction mixture was refluxed and stirred for 2 weeks, cooled, and the organic layer separated. The organic extract was vacuum distilled (0.5 millimeters at 70°) into a dry-ice-cooled trap, and the volatiles were analyzed by gas-liquid chromatography (GLC) at 110–130° C. An Aerograph A–90P chromatograph with a 30-foot by ¼-inch SE–30 [1] column (20 percent on 80-mesh Chromosorb P) was used in the analyses. The various components were collected by preparative chromatography and analyzed by infrared and NMR methods. The residue from the distillation was recrystallized from an appropriate solvent and was compared with standard known materials (the NMR spectra of these materials have been described in the preceding paragraphs). The aqueous phase was carefully neutralized and was reduced to a small volume in vacuo. The residue was dissolved in D_2O and was analyzed by NMR using the sodium salt of trimethylsilylpropionic acid (TMS) as an internal standard. Residues contained the major fraction of the phosphorus-containing products; products identical with known materials. Under the preceding reaction conditions, less than 5 percent of the original pesticide was detected in the organic and aqueous phases combined. All reaction products were recovered in concentrations containing more than 80 percent of the original material present.

KINETIC PROCEDURES (ATTEMPTED HYDROLYSIS UNDER ENVIRONMENTAL CONDITIONS)

The pesticides were dissolved in 100 ml of carbon tetrachloride in a 3-necked flask equipped with a stirrer, reflux condenser, and stopcock-protected no-air stopper; the solution was heated to reflux. Appropriate amounts of water, dilute acid, or dilute base were added, and the reaction mixtures were heated and stirred. At intervals, 1-ml fractions were removed from the reaction mixture. The fractions were dried over magnesium sulfate and were then analyzed by NMR. Under the reaction conditions described in table 1, less than 3 ± 0.5 percent of the pesticide in the mixture was hydrolyzed.

The pesticides in this study were at least 95 percent pure.

RESULTS

This study has demonstrated that the bulk hydrolysis of compounds I–V results in dialkoxy phosphates or thiophosphates, identical with those reported previously (Von Muhlmann and Schrader, 1957), and that the products of the hydrolysis of Dipterex and Malathion are particularly pH dependent. Dipterex hydrolyzes to 2,2 2-trichloroethyl alcohol under strongly acidic conditions (Arthur and Casida, 1957), but under neutral or slightly basic conditions a different path is followed. This reaction results in the formation of

[1] SE-30 is silicone gum rubber.

TABLE 1.—*Attempted hydrolysis of Cygon* (II), *Dyfonate* (IV), *and Malathion* (V)

[Reaction temperatures maintained at a constant 75° C]

Compound [1]	Reagent	Concentration [2] (equivalents)	Time (hours)
Cygon	H_2O	3	240
	0.01*N* HCl	6	240
	0.01*N* NaOH	6	240
Dyfonate	H_2O	3	280
	0.01*N* HCl	6	240
	0.01*N* NaOH	6	250
Malathion	H_2O	3	240
	0.01*N* HCl	6	260
	0.01*N* NaOH	6	260

[1] Pesticide solutions were prepared by diluting 0.1 mole of the compound to a volume of 100 ml in carbon tetrachloride.

[2] Each reagent was treated as if it were pure water, and 0.3-mole and 0.6-mole portions of the reagent were weighed and added to the reaction mixture. (No correction was made for weight of HCl.)

DDVP which upon further hydrolysis results in the formation of dichloroacetaldehyde (Lorenz and others, 1955; Barthel and others, 1955). Malathion hydrolyzes to diethyl fumarate in a strong alkaline medium by an elimination process (Gunther and Blinn, 1955) but to diethyl α-mercaptosuccinate in neutral or acidic media (Cowen, 1956). The intermediate dialkoxy phosphates are generally stable in the pH ranges studied. The hydrolysis of Bidrin was analogous to the known hydrolysis of Phosdrin (Von Muhlmann and Schrader, 1957; Casida and others, 1956), and produced the *N,N*-dimethylacetoacetamide in good yield. The hydrolysis of Cygon was found to be analogous to the known hydrolysis of Disyston (Von Muhlmann and Schrader, 1957; Gardner and Heath, 1953), and produced α-mercapto-*N*-methylacetamide in good yields. The hydrolysis of Dyfonate paralleled the known hydrolysis of esters of the alkyl substituted phosphonic acids in that a P–O, not a P–C, bond was broken to give O-ethyl-ethylphosphonothioate (Hudson and Keay, 1956).

The reaction of Cygon, Dyfonate, and Malathion with water under conditions amenable to obtaining the rates of reaction were then studied, and the conditions listed in table 1 were utilized for the study of the reaction kinetics.

CONCLUSIONS

Under the preceding reaction conditions, less than 3 ± 0.5 percent of the pesticide was hydrolyzed. This fact indicates that these materials are much more resistant to aqueous hydrolysis with stoichiometric amounts of water than is commonly believed. If materials of this nature are readily hydrolyzed in the environment, it may be due to enzymatic or catalytic mechanisms which were not operable under the experimental conditions employed in this study.

REFERENCES

Arthur, B. W., and Casida, J. E., 1957, Metabolism and selectivity of 0–0 dimethyl 2,2,2-trichloro-1-hydroxyethylphosphonate and its reaction products: Jour. Agr. Food Chemistry, v. 5, p. 186.

Babad, Harry, Herbert, Washington, and Goldberg, M. C., 1968 Nuclear magnetic resonance studies of phosphorus (V) pesticides—I, Chemical shifts of protons as a means of identification of pesticides: Anal. Chim. Acta, v. 41, p. 259–268.

Babad, Harry, Taylor T. N., and Goldberg, M. C., 1968 Nuclear magnetic resonance studies of phosphorus (V) pesticides—II, A rapid determination of the isomer ratio of Systox: Anal. Chim. Acta, v. 40, p. 387–392.

Barthel, W. F., Alexander, B. H., Giang, P. A., and Hall, S. A., 1955, Insecticidal phosphates obtained by a new rearrangement reaction: Jour. Am. Chem. Soc., v. 77, p. 2424.

Casida, J. E., Gatterdam, P. E., Getzkin, L. W., Jr., and Chapman, R. K., 1956, Residual properties of the systemic insecticide 0-0-dimethyl-1-carbomethoxy-1-propene-2-ylphosphate: Jour. Agr. Food Chemistry, v. 4, p. 236.

Cowen, F. M., 1956, Mercaptosuccinic acid: Am. Cyanamid Co., Jan. 3, 1956.

Gardner, Kenneth and Heath, D. F., 1953, Quantitative determination of isomers of *0-0*-diethyl ethylmercaptoethyl thiophosphate: Anal. Chem., v. 25, p. 1849–1853.

Gunther, F. A., and Blinn, R. C., 1955, Analysis of insecticides and acaricides: New York, Interscience Publishers, Inc., v. 6, p. 476.

Hudson, R. F., and Keay, L., 1956, Hydrolysis of diisopropyl methylphosphonodithiolate: Jour. Chem. Soc. [London], Chem. Soc. Jour., p. 3269–3271.

Lorenz, W., Henglein, A., and Schrader, G., 1955, Insecticide 0-0 dimethyl-2,2,2 trichloro-1-hydroxy-ethyl-phosphonate: Jour. Am. Chem. Soc., v. 77, p. 2554.

Suffet, I. H., Faust, S. D., and Carey, W. F., 1967, Gas liquid chromatographic separation of some organophosphate pesticides. Their hydrolysis products and oxons: Environ. Sci. Technology, v. 1, no. 8, p. 639.

Von Muhlmann, R., and Schrader, G., 1957, Hydrolyse der Insektiziden Phosphorsaureester: Zeitschrift. Naturforschung, v. 12, p. 196.

EVALUATION OF ORGANIC COLOR AND IRON IN NATURAL SURFACE WATERS

By WILLIAM L. LAMAR, Menlo Park, Calif.

Abstract.—Examination of organic color in natural surface waters revealed similarities in the complex color macromolecules extracted with *n*-butanol from stream waters in areas having pronounced differences in climatic conditions. The organic matter in the colored waters consists primarily of complex polymeric hydroxy carboxylic acids. Aromatic unsaturation also was observed. The infrared spectra of the predominant part of the organic matter were independent of the color intensity, pH, and mineral content of the water as well as the geographical location. Variable quantities of iron unrelated to the concentration and source of the organic matter are held in apparent solution by the complex organic acids. Preliminary results suggest that iron, probably as ferric hydroxide or oxide, forms colloidal sols with the organic matter. The sols vary considerably in particle size, and a relationship between particle size, pH, and iron concentration is indicated.

Natural waters containing organic matter that imparts a yellow to brown color occur in many places, particularly swampy areas. The principal part of the organic matter in naturally colored surface waters consists of many organic acids—volatile, nonvolatile, colored, colorless, simple, and complex. The volatile acids and those that can be made volatile for gas chromatographic analysis are present in low concentrations—generally less than several milligrams per liter of water. The concentrations of the complex polymeric acids cover a much wider range and in some highly colored surface waters these substances are the predominant constituents.

The designations most frequently used for fractions of the complex colored acids are fulvic, hymatomelanic, and humic. This nomenclature is based on separations by solubilities in water, mineral acid, and alcohol. Separations resulting from such solubilities are not specific and are related to concentration, the process used, and the physicochemical state of the solution. Adequate separation techniques have not been devised for these complex nonvolatile acids.

In 1786 Achard reported on the extraction of a brown substance from soil and peat. Since that time, difficulties have persisted in separating and in determining the molecular structure of the complex colored compounds extracted from soil, peat, coal, and water by many investigators. Black and Christman (1963) concluded that the fulvic acid fraction of the organic matter extracted from colored water consists of aromatic polyhydroxy methoxy carboxylic acids. Shapiro (1957, 1964) stated that the organic acids he obtained from large volumes of colored water are primarily aliphatic polyhydroxy carboxylic acids having molecular weights in the range of 180 to 426. Gjessing (1965) concentrated the organic substances present in a surface water from a moorland area and utilized Sephadex gel to estimate the molecular weights of the organic components. Using particle size as a measure, he observed at least two types of humic substances which differed considerably in molecular size. Apart from the precipitate formed during concentration, it was reported that the larger molecular fraction of the organic matter probably had a molecular weight between 100,000 and 200,000 and that the smaller was possibly below 10,000.

Lamar and Goerlitz (1966) extracted naturally colored surface waters and concentrates of the waters with *n*-butanol and found that the organic matter consists primarily of polymeric hydroxy carboxylic acids with aromatic and possibly olefinic unsaturation. Christman and Ghassemi (1966) subjected the organic material responsible for color to degradative chemical studies. They identified 7 phenolic degradation products and asserted that their results provide conclusive evidence for the presence of phenolic nuclei in the color macromolecule. In 1967 the Research Committee on Color Problems under the Committee on Research of the American Water Works Association Research Foundation published a "Report for 1966" that provided a comprehensive review and summary of organic color in water.

U.S. GEOL. SURVEY PROF. PAPER 600-D, PAGES D24-D29

INFRARED EXAMINATIONS

Samples of water were obtained from streams draining areas having widely different climatic conditions in the states of Alaska, California, Florida, Georgia, and Washington. Both humid and semiarid regions were included. The water was collected during periods of rainfall, periods of drought, and after the first rainfall following an extended period of drought. The color of the waters ranged from 7 to 250 units (platinum-cobalt scale).

The infrared analyses were made on a spectrophotometer equipped with sodium chloride optics. All the spectra were obtained by the use of potassium bromide pellets. The organic matter was extracted with *n*-butanol and infrared spectra were obtained for the total organic matter extracted, the organic acids, the esterified and acetylated derivatives of the acids, and the column chromatographic fractions of the acids from samples of slightly colored and highly colored waters.

The infrared examinations discussed cover a résumé of previous results obtained by Lamar and Goerlitz (1966) and also current results for samples collected from distant points. Figure 1 shows the infrared spectra of the total organic acids recovered from naturally colored waters from unpolluted streams in Alaska, Georgia-Florida, Washington, and California. The spectra of the total organic acids from these sources were practically identical. In figure 1, the band in the 3.1-μ (microns) region represents bonded hydroxyl and carboxyl absorption. It is not due to the nitrogen-hydrogen stretch, since nitrogen was absent in the elemental analysis. The band at 3.35μ is probably due to methyl and methylene groups. The most intense band at 5.8μ is in the region of carbonyl absorption. The band at 6.2μ is indicative of unsaturation. The broad absorption in the 8.3μ region is possibly due to carbon-oxygen bonding as with carboxyl or ester groups.

Figure 2 shows the infrared spectra of the organic acids, the esterified acids, and the acetylated acids. Figure 2*A* represents the usual spectrum observed for the total organic acids and figure 2*B* denotes the spectrum after the acids were esterified by use of sulfuric acid catalyzed butanol. Since esterification eliminates the carboxyl hydroxyl, the OH absorption observed after esterification indicates that there are alcoholic and probably phenolic hydroxy groups present. Because the esterification had no significant effect on the band at 6.2μ, the evidence of unsaturation is additionally supported. Increased band intensities in the region of aromaticity are revealed.

Figure 2*C* shows the spectrum for the acetylated acids after reaction with acetic anhydride. In this

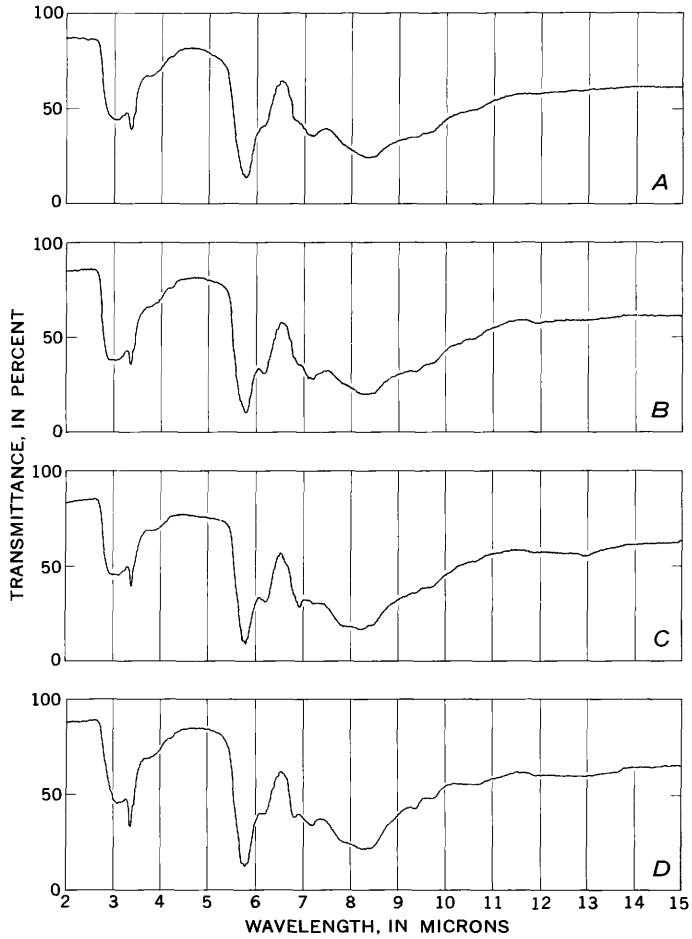

FIGURE 1.—Infrared spectra of natural organic acids from streams in several states. *A*, Alaska; *B*, Georgia-Florida; *C*, Washington; *D*, California.

spectrum, the hydroxy absorption is almost eliminated, thus further confirming the presence of hydroxy functional groups in the parent molecules. No free OH is present. The band at 6.2μ indicating unsaturation, remained. Absorption characteristics of anhydrides are evident.

Infrared spectra of the column chromatographic fractions of the total acids were obtained for selected samples. The spectra of the fractions from the highly colored water generally showed very little difference from fraction to fraction. However, pronounced variations were evident in the spectra of the chromatographic fractions from a lightly colored water that increased in color intensity after the sample was collected. Aromatic unsaturation was observed in some of the fractions and suspected in others.

The examinations show that the organic matter in naturally colored surface waters consists primarily of complex polymeric hydroxy carboxylic acids. Evidence of aromatic unsaturation was observed. The infrared

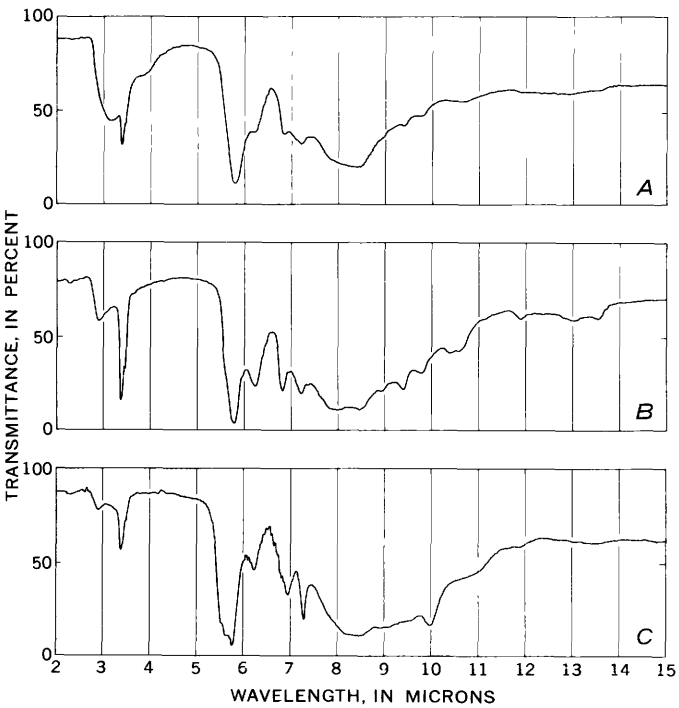

FIGURE 2.—Infrared spectra of natural organic acids and derivatives. *A*, organic acids; *B*, esterified acids; *C*, acetylated acids.

spectra of the predominant part of the organic matter were independent of the color intensity, pH, and mineral content of the water as well as the geographic location of the source of the water.

RETENTION OF IRON

Considerable study has been made on the retention of metals by organic matter extracted from soils, peat, lignin, and coal, while comparatively little examination of this mechanism has been devoted to the organic matter that occurs in naturally colored waters. This holding action has been variously referred to as chelation, complexing, sorption, bonding, and peptization.

In an investigation of metallo-organic interactions, Wright and Schnitzer (1963) leached, with a chelating agent, a calcareous parent material of a certain soil. They found that such leaching caused mobilization, transport, and redeposition of iron and aluminum. Fulvic acid was considered to be the dominant ligand affecting the translocation of these two metals in the podzolization process. Randhawa and Broadbent (1965) stated that humic acid has three or more types of sites capable of retaining zinc. At pH 5, zinc was observed to be more strongly bound on humic acid than was calcium, but less strongly than copper or ferrous iron. Levesque and Schnitzer (1967) reported on a relationship between phosphate and the metal content of the iron- and aluminum-fulvic acid complexes.

Shapiro (1964) studied the retention of several metals by the yellow organic acids that were obtained from surface water by freeze concentration and extraction with *n*-butanol. These acids were found to hold considerable iron in "solution" at high pH and Eh values. The behavior of cupric copper was reported to be qualitatively similar to that of ferric iron. On the basis of this study, he suggests that the large quantities of iron held in apparent solution by highly colored waters may be predominantly in the form of a protected colloid.

Relation of iron to organic color

Waters from streams draining two areas of widely different climatic conditions were used to study the relationship of iron and organic matter in naturally colored water. Table 1 gives the chemical analyses of samples collected from Hood Creek in Alaska and North Prong St. Marys River at the Georgia-Florida state line. These waters have rather widely different chemical and physical characteristics, but the infrared spectra of the organic matter extracted from them with *n*-butanol are practically identical.

The Alaska sample exhibited some turbidity and it contained a considerable amount of large flocculent agglomerates of organic matter associated with a relatively high concentration of iron. Because of the turbidity, the color of the Alaska water was not measurable without processing. This was done in two different

TABLE 1.—*Chemical analyses of naturally colored surface waters from Alaska and Georgia-Florida*

	Hood Creek, Alaska		North Prong St. Marys River, Georgia-Florida	
	mg/l	meq/l	mg/l	meq/l
Silica (SiO_2)			2.3	
Iron (Fe) unfiltered	4.5		.68	
Iron (Fe) filtered [1]	1.6		.52	
Manganese (Mn)	.0	0.00	.0	0.00
Calcium (Ca)	6.7	.33	1.3	.06
Magnesium (Mg)	2.5	.21	.7	.06
Sodium (Na)	2.3	.10	4.0	.17
Potassium (K)	.7	.02	.2	.01
Bicarbonate (HCO_3)	25	.41	0	.00
Carbonate (CO_3)	0	.00	0	.00
Sulfate (SO_4)	8.0	.17	.0	.00
Chloride (Cl)	2.1	.06	9.5	.27
Fluoride (F)			.2	.01
Nitrate (NO_3)	.6	.01	.5	.01
Dissolved solids	75		83	
Hardness as $CaCO_3$	27		6	
Specific conductance—micromhos at 25° C	67		61	
pH	6.4		4.4	
Color units (platinum-cobalt scale)	[2] 90		[3] 220	

[1] Filtered through fine sintered glass, nominal maximum porosity 4μ–5.5μ.
[2] Determined on filtrate from a fine sintered-glass filter and also on supernate after centrifugation.
[3] Determined on unfiltered sample promptly after collection and several days later on the unfiltered and fine sintered-glass filtered water.

ways—filtration through fine sintered glass, and centrifuging at 20,000 revolutions per minute. The Georgia-Florida sample had a clear brownish-yellow appearance and a small amount of brown flocculent organic matter associated with a slight amount of iron.

The Alaska sample had 4.5 milligrams per liter of iron before filtration and 1.6 mg/l of iron after passing through a sintered-glass filter. It had 25 mg/l of bicarbonate, a pH of 6.4, and a color of 90 units (platinum-cobalt scale). The Georgia-Florida sample had 0.68 mg/l of iron before filtration and 0.52 mg/l of iron after filtration. It had no bicarbonate, a pH of 4.4, and a color of 220 units (before and after filtration through fine sintered glass). Both waters were very high in organic matter, particularly the Georgia-Florida water which had over 60 mg/l of organic matter and only about 20 mg/l of dissolved minerals.

Table 2 provides data on iron and organic color upon centrifugation and at stages of filtration through filters of different porosity. Filtration of the Alaska sample through a medium sintered-glass filter (maximum nominal porosity 10μ–15μ) removed large agglomerates of organic matter associated with a relatively high concentration of iron. After this coarse filtration, the water was centrifuged at 20,000 rpm at 25°C for 2 hours and some brown particulate matter containing iron was removed. The color of the visually clear supernate was 90 units (platinum-cobalt scale). Additional centrifuging for 4½ hours removed a very small amount of brown particulate matter containing a trace of iron; however, the color of the recentrifuged water was not altered and remained at 90 units. When a portion of the original uncentrifuged water was filtered through a fine sintered-glass filter (nominal maximum porosity 4μ–5.5μ), a large amount of brown organic matter and nearly two-thirds of the total iron concentration were removed. The color of the visually clear filtrate also was 90 units.

TABLE 2.—*Effect of centrifuging and filtering iron and organic color*

	Hood Creek, Alaska		North Prong St. Marys River, Georgia-Florida	
	Iron (mg/l)	Color (units)[1]	Iron (mg/l)	Color (units)[1]
Total (unfiltered sample)	4.5	------	0.68	------
Supernate from centrifuging	1.5	90	-----	-----
Filtrate from fine sintered-glass filter [2]	1.6	90	.52	220
Filtrate from 0.1μ filter [3]	.80	75	.45	190
Retained on 0.1μ filter [3 4]	.64	------	.07	-----
Filtrate from 0.01μ filter [3]	.16	45	.35	145
Retained on 0.01μ filter [3 4]	1.3	------	.17	-----

[1] Platinum-cobalt scale.
[2] Nominal maximum porosity 4μ–5.5μ.
[3] Aliquots of the filtrate from the fine sintered-glass filter were used for these tests.
[4] Dissolved from filter and measured.

313-005 O—68——3

The color of the unfiltered Georgia-Florida water was measured as 220 units promptly after collection and several days later. When this water was filtered through fine sintered glass (nominal maximum porosity 4μ–5.5μ), very little particulate matter was removed and the color of the filtrate also was 220 units.

After filtration through fine sintered glass, both of the waters were subjected to further filtration through 0.1μ and 0.01μ Millipore filters. Separate aliquots were used for this filtration and progressively greater amounts of iron and organic color were removed as shown in table 2. Only 0.16 mg/l of the relatively large amount of iron in the Alaska water and 0.35 mg/l of the smaller amount of iron in the Georgia-Florida sample remained in the filtrate from the 0.01μ filter.

The final filtration removed much of the color from both samples. For the Alaska sample, 50 percent of the color intensity was due to components having particle sizes of less than 0.01μ, whereas for the Georgia-Florida water 66 percent of the color intensity was caused by the particle sizes of less than 0.01μ.

The results show a wide range in particle sizes and suggest that much of the iron is retained by coarse particles of organic matter as colloidal sols, probably in the form of ferric hydroxide or oxide, under natural conditions. Although agglomerates of organic matter and iron will precipitate under favorable conditions, it is observed that colored surface waters under natural conditions will carry varying amounts of iron (up to about 2 mg/l) in apparent solution. The iron in organically colored natural waters is not readily precipitated by aeration. In organic-free aerated waters whose pH is above about 5, ferric iron can be present in excess of 0.01 mg/l only as a suspension of oxide or hydroxide (Hem and Cropper, 1959). Thus, aerated waters that are not colored and that are not contaminated by acid mine drainage or wastes rarely contain more than a trace of iron in solution. The iron associated with organic color does not precipitate on the sides of the sample bottle, as will readily occur with other waters that contain appreciable iron, but instead it either remains in apparent solution or precipitates in agglomerates with the organic matter.

Variation of iron and organic color

Examination of a very large number of chemical analyses of highly colored surface waters (100 to more than 500 color units) from many sampling stations shows that there is no consistent direct relation between color intensity and concentration of iron in apparent solution, although some individual sources show some direct relationship. When the iron concentration exceeds 0.7 mg/l the pH is usually greater than 6.2.

The relationship of iron concentration to color intensity is shown in figure 3 for all surface water stations in the St. Marys river basin (Georgia-Florida) that were operated by the U.S. Geological Survey during the period March 1965–April 1967 (unpublished data furnished by D. A. Goolsby, U.S. Geol. Survey, Ocala, Fla., 1967). The scatter shown in this illustration may be due, at least in part, to the variable formation and precipitation of agglomerates of iron and organic matter as influenced by pH, availability of iron, concentration and composition of inorganic ions, period of contact, and possibly by competition among cations. Low dissolved oxygen or anerobic conditions resulting from decaying vegetation are favorable for the reduction of iron to the soluble ferrous species. This would provide a source of ferrous and ferric iron, as the ferrous species is readily oxidized by aeration. Inorganic iron unrelated to the concentration and source of the organic matter would be one of the factors in the scatter shown in figure 3.

DISCUSSION AND SUMMARY

The predominant part of the organic matter in naturally colored surface waters consists of complex polymeric acids. The infrared spectra obtained established a remarkably similar pattern for the complex acids extracted with *n*-butanol for a variety of surface waters from widespread geographical locations having pronounced differences in climatic conditions. This consistent pattern occurred for samples collected from the different sources and from the same source at different times during periods of rainfall, period of drought, and after the first rainfall following an extended period of drought. The spectra were independent of the color intensity, pH, and mineral content of the water. However, the mineral constituents in the water must be removed thoroughly; otherwise, variations and differences in the infrared spectra will occur.

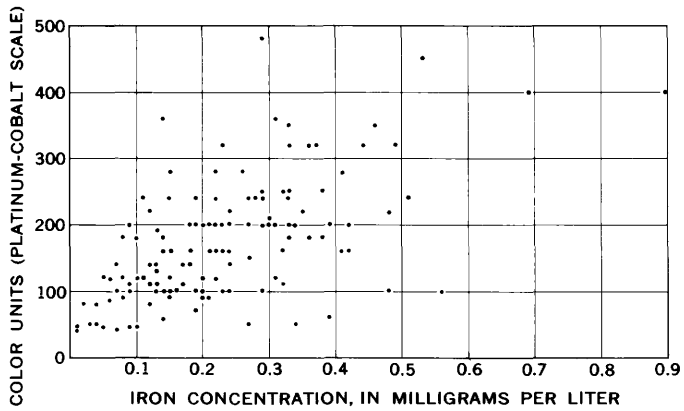

FIGURE 3.—Variation of iron with organic color intensity.

The infrared spectra of the column chromatographic fractions of the organic acids from the highly colored waters generally showed very little differences from fraction to fraction. However, pronounced variations were evident in the spectra of a lightly colored water that increased in color intensity after the sample was collected. Aromatic unsaturation was observed in some of the fractions and suspected in others. It seems probable that some of the complex acids may result from polymerization in aqueous solution.

The examinations indicate that the organic matter in naturally colored surface waters consists primarily of complex polymeric hydroxy carboxylic acids. Evidence of aromatic unsaturation was also observed.

Organically colored surface waters retain variable concentrations of iron (up to about 2 mg/l) in apparent solution under natural conditions. A relationship between particle size, pH, and iron concentration is indicated. There is no consistent direct relationship between color intensity and iron concentration, although some individual surface water sources show some direct relationship. Sources of iron unrelated to the concentration and source of the organic matter appear to be a factor in these variations.

Preliminary results suggest that the iron, probably as ferric hydroxide or oxide, forms colloidal sols with the organic matter under natural conditions. These sols vary considerably in particle size. They tend to be stable and hold the iron for long periods of time. Under changes in the environment the sols may precipitate, forming dark brown to black deposits in streams and swamps.

REFERENCES

Achard, F. K., 1786, Chemische Untersuchung des Torfs: Crell's Chem. Ann., v. 2, p. 391–403.

Black, A. P., and Christman, R. F., 1963, Chemical characteristics of fulvic acids: Am. Water Works Assoc. Jour., v. 5, no. 7, p. 897–912.

Christman, R. F., and Ghassemi, Masood, 1966, Chemical nature of organic color in water: Am. Water Works Assoc. Jour., v. 58, no. 6, p. 723–741.

Committee on Research of the American Water Works Association Research Foundation, 1967, Research Committee on Color Problems—Report for 1966: Am. Water Works Assoc. Jour., v. 59, no. 8, p. 1023–1035.

Gjessing, E. T., 1965, Use of "Sephadex" gel for the estimation of molecular weight of humic substances in natural water: Nature, v. 208, no. 5015, p. 1091–1092.

Hem, J. D., and Cropper, W. H., 1959, Survey of ferrous-ferric chemical equilibria and redox potentials: U.S. Geol. Survey Water-Supply Paper 1459–A, 30 p.

Lamar, W. L., and Goerlitz, D. F., 1966, Organic acids in naturally colored surface waters: U.S. Geol. Survey Water-Supply Paper 1817–A, 17 p.

Levesque, M., and Schnitzer, M., 1967, Organo-metallic interactions in soils—[6], Preparation and properties of fulvic acid-metal phosphates: Soil Sci., v. 103, no. 3, p. 183–190.

Randhawa, N. S., and Broadbent, F. E., 1965, Soil organic matter-metal complexes—[5], Reactions of zinc with model compounds and humic acid: Soil Sci., v. 99, no. 5, p. 295–300.

Shapiro, Joseph, 1957, Chemical and biological studies on the yellow organic acids of lake water: Limnology and Oceanography, v. 2, no. 3, p. 161–179.

——— 1964, Effect of yellow organic acids on iron and other metals in water: Am. Water Works Assoc. Jour., v. 56, no. 8, p. 1062–1082.

Wright, J. R., and Schnitzer, M., 1963, Metallo-organic interactions associated with podzolization: Soil Sci. Soc. America Proc., v. 27, no. 2, p. 171–176.

SODIUM AS A CLUE TO DIRECTION OF GROUND-WATER MOVEMENT, NEVADA TEST SITE

By STUART L. SCHOFF and JOHN E. MOORE,
Washington, D.C., Denver, Colo.

Work done in cooperation with the U.S. Atomic Energy Commission

Abstract.—Sodium dissolved in water generally stays in solution. It is the predominant cation in ground water in volcanic aquifers in the Nevada Test Site, but is nearly lacking in alluvial and carbonate-rock aquifers in southern Indian Spring valley south of the Nevada Test Site. The low content of sodium in the water of Indian Spring valley shows that the water has not migrated into the valley from the Nevada Test Site.

A determination of the origin and movement of ground water based on the chemical character of the water is often inconclusive. However, at the Nevada Test Site the chemical character provides a useful clue to the origin and movement of ground water. The most significant chemical characteristic is sodium, present in conspicuously large quantities in the ground water from certain aquifers and localities, and in noticeably small quantities in others. The location of the area studied is shown on figure 1.

Sodium compounds dissolved in water are likely to remain in solution and, hence, to travel with the water. Sodium may be dissolved directly from the minerals in the rocks through which the water passes. It may also be exchanged for calcium and (or) magnesium already dissolved in the water. The ion-exchange reaction may be reversed under circumstances of greater concentration of sodium in the water than has been found at or near the Nevada Test Site.

Sodium at the Nevada Test Site is related to volcanic rocks of Tertiary age, which consist principally of rhyolitic tuff, but also include flows of basalt, andesite, rhyodacite, and minor amounts of sedimentary rocks. Despite considerable variation in physical appearance these rocks act as a single unit in their effect on the chemical composition of the ground water. Zeolitized parts of the tuff seem to be especially important because the zeolites should facilitate ion-exchange reactions. The volcanic rocks underlie the land surface in most of the area northwest of a line running irregularly from the southwest corner of the map shown on figure 2 to Emigrant Valley in the northeast.

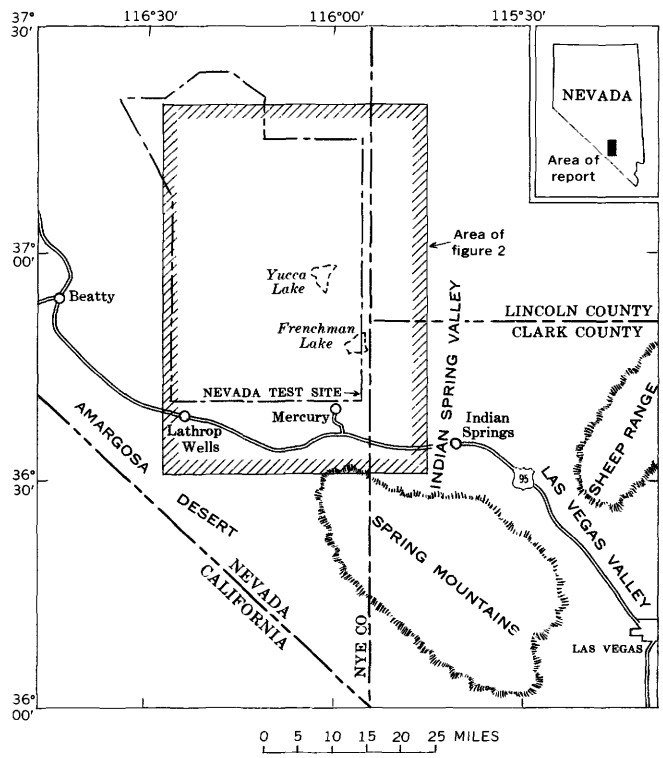

FIGURE 1.—Index map showing location of Nevada Test Site and areas mentioned in this report.

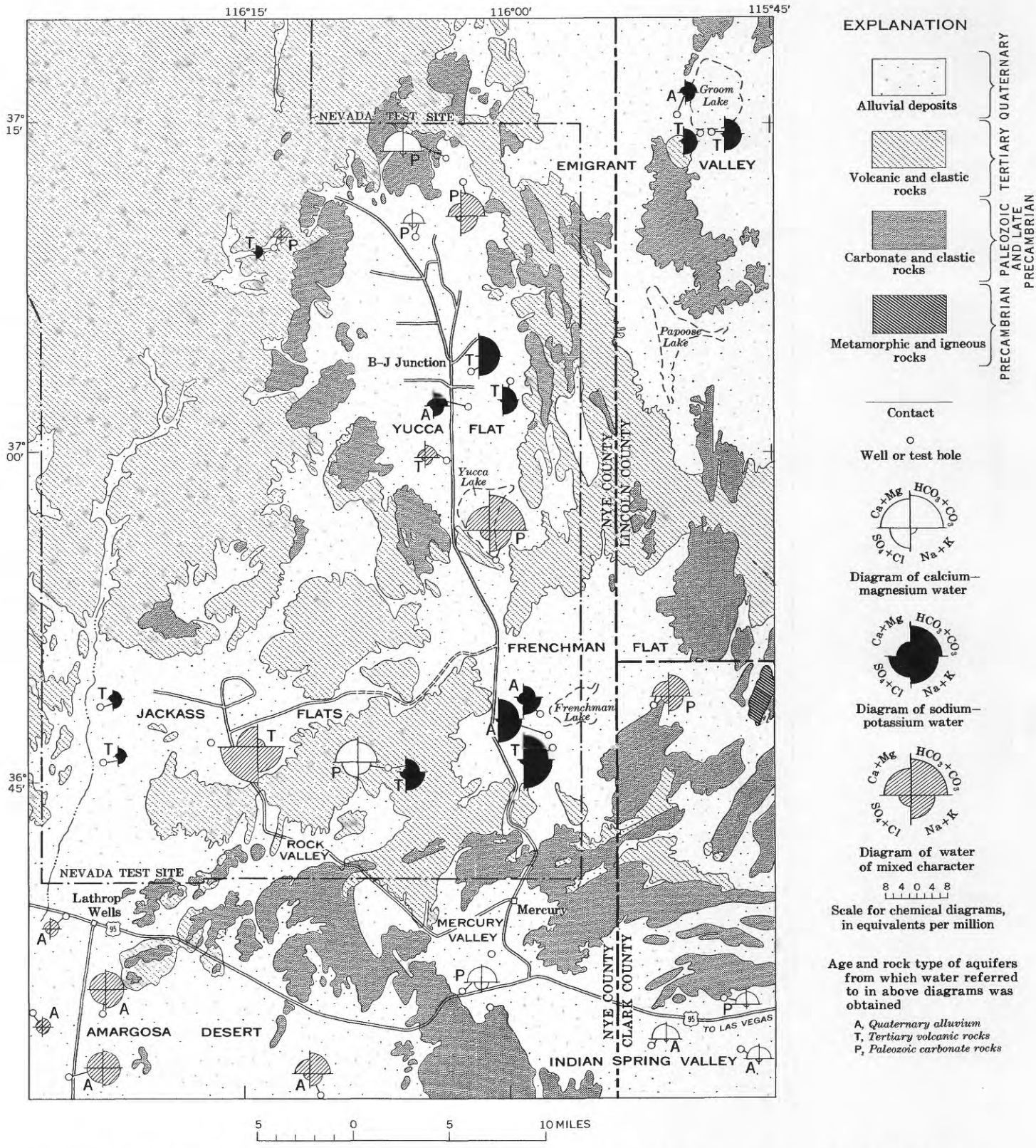

FIGURE 2.—Map of the Nevada Test Site and vicinity, showing principal rock types and chemical character of ground water.

CHEMICAL COMPOSITION OF THE GROUND WATER

Sodium was the predominant cation in most of the water samples taken from wells, springs, and mine drifts in the volcanic rocks—chiefly tuff—of the Nevada Test Site area. It was generally predominant, also, in water samples taken from alluvial aquifers containing abundant tuffaceous detritus. We found some contradictions to this generalization, but because we could account for most of them we still consider the association of sodium and volcanic rocks well substantiated.

In contrast, sodium was relatively less abundant—or simply absent—in waterfrom wells tapping carbonate bedrock or alluvium containing carbonate detritus. Carbonate rocks make up somewhat more than half of a late Precambrian and Paleozoic stratigraphic section totaling more than 35,000 feet. They crop out in the mountains east of the Nevada Test Site, and are notable in the Spring Mountains to the south. They also occur within the Nevada Test Site in the foothills of the mountains surrounding Yucca Flat, and have been penetrated in wells drilled through the volcanic rocks to depths of several thousand feet below the land surface (fig. 2). They are, by and large, much more productive aquifers than the volcanic rocks.

The predominant cations in the water samples from the carbonate rocks are calcium and magnesium. The amounts of sodium in these samples are so small as to imply that the water has not had much contact, if any, with volcanic rock. Water passing through volcanic rocks into carbonate rocks would carry with it, and retain, the sodium dissolved from the volcanic rocks. If the water went from carbonate rocks through volcanic rocks and back into carbonate rocks, it could, through ion exchange, lose calcium and magnesium dissolved from its first host and gain sodium. In neither case would the water be likely to lose any sodium; thus, the conclusion is that the typical water from carbonate rocks in the Nevada Test Site area has had little or no contact with volcanic rocks or volcanic detritus, and has undergone no great amount of mixing with water from such materials.

The relative abundance—or scarcity—of sodium in the ground water becomes important when regional relationships are shown by means of chemical diagrams, as in figure 2. The diagrams are placed adjacent to the symbol for the well that they represent, and the type of aquifer is shown by a letter symbol. If two water samples from different aquifers came from the same well, two chemical diagrams are shown.

The chemical diagrams are pie diagrams in four pieces, for convenience designated the northeast, southeast, southwest, and northwest quadrants. The principal ions are combined so as to emphasize the points important to this paper, and are arranged so that cations are opposite cations, anions opposite anions: sodium and potassium in the southeast quadrant, calcium and magnesium in the northwest, carbonate and bicarbonate in the northeast, and sulfate and chloride in the southwest. Plotted to a uniform scale of equivalents per million in all four directions, the wedges of the pie together give an impression of the dissolved-solids content of each water sample.

The water is classified into three types:

1. Sodium-potassium bicarbonate type. Sodium predominates, potassium is generally minor, and the two together are 60 percent or more of the total cations. They are approximately equaled by the carbonate and bicarbonate, with the result that the pie diagram is a semicircle in the east half of the diagram.

2. Calcium-magnesium bicarbonate type. Calcium and magnesium predominate and together are 60 percent or more of the total cations. With the anions carbonate and bicarbonate, they make a semicircle in the north half of the chemical diagram.

3. Mixed chemical type. The combined pairs of cations (1 and 2 above) do not exceed 60 percent of the total cations, neither pair individually exceeds 40 percent and either pair may predominate. This type generally has the largest wedge in the northeast quadrant of the pie (the bicarbonate), and smaller, more or less equal, wedges in the northwest (calcium and magnesium) and southeast (sodium and potassium). If significant amounts of sulfate and chloride are present, the diagram approaches a full circle. The term "mixed chemical type" means only that the water has features of the other two types of water shown by the diagrams. Water first moving through one type of rock and then another, with opportunity for dissolving two different mineral assemblages or a chance for ion exchange could become a mixed chemical type.

The chemical diagrams representing water from volcanic and alluvial aquifers in the Nevada Test Site—Emigrant Valley, and Yucca, Frenchman, and Jackass Flats—are the sodium-potassium bicarbonate type (fig. 2). Scattered among them are a few of the calcium-magnesium bicarbonate type, but these represent water from carbonate aquifers, not volcanic or alluvial aquifers. Also among them are a few of the mixed type, some of which require explanations too elaborate for this paper (see Schoff and Moore, 1964, p. 21, 25–34).

DIRECTION OF GROUND-WATER MOVEMENT

If the ground water in the tuff and alluvium within the Nevada Test Site were moving south into southern Indian Spring valley—whence it would seem that the

hydraulic gradient might carry it to Las Vegas—the ground water in Indian Spring valley should be rich in sodium, but it is not. It is a calcium-magnesium bicarbonate type.

Other evidence confirms our view that ground water does not move from volcanic and alluvial aquifers in the Nevada Test Site into aquifers in southern Indian Spring valley. Winograd (1962a, p. 8–9; 1962b, p. C110) has indicated that the water in the volcanic and alluvial aquifers in the Nevada Test Site moves down into the underlying carbonate-rock aquifer and then laterally. He has also shown by water-level contours that the ground water of a large area including the Nevada Test Site has a potential for movement toward the Amargosa Desert, that ground-water levels in southern Indian Spring valley are substantially higher than those within the Nevada Test Site (Winograd, 1963, fig. 2, p. 47), thus making movement from the Nevada Test Site an improbability. Eakin, Schoff, and Cohen (1963, p. 17–19), on the basis of regional recharge-discharge relations, hydraulic gradient, and chemical character of water, showed that the ground water in a large part of southern Nevada could be moving southward to the Amargosa Desert, if indeed there is regional movement, and that ground water within the Nevada Test Site cannot move into southern Indian Spring valley. The above studies indicate only that the potential for ground-water movement into southern Indian Spring valley is not present. The negligible amount of sodium in the ground water of southern Indian Spring valley shows more conclusively that this movement does not take place.

REFERENCES

Eakin, T. E., Schoff, S. L., and Cohen, Philip, 1963, Regional hydrology of a part of southern Nevada: U.S. Geol. Survey open-file rept. TEI–833, 40 p.

Schoff, S. L., and Moore, J. E., 1964, Chemistry and movement of ground water, Nevada Test Site: U.S. Geol. Survey open-file rept. TEI–838, 75 p.

Winograd, I. J., 1962a, Interbasin movement of ground water at the Nevada Test Site: U.S. Geol. Survey open-file rept. TEI–807, 12 p.

——— 1962b, Interbasin movement of ground water at the Nevada Test Site: Art. 104 *in* U.S. Geol. Survey Prof. Paper 450–C, p. C108–C111.

——— 1963, A summary of the ground-water hydrology of the area between the Las Vegas Valley and the Amargosa Desert, Nevada: U.S. Geol. Survey open-file rept. TEI–840, 79 p.

DECEMBER 1964, A 400-YEAR FLOOD IN NORTHERN CALIFORNIA

By EDWARD J. HELLEY and VALMORE C. LaMARCHE, JR.,
Menlo Park, Calif.

Abstract.—Twice in the past 13 years, recordbreaking floods have occurred over large areas of northern California. The true long-term recurrence intervals of these destructive floods is difficult to estimate by conventional flood-frequency analysis because prediction of a given flood discharge is based on historical records of flood peaks. Geomorphic and botanical evidence of a major prehistoric flood has been investigated on Blue Creek, a tributary to the Klamath River in northern California. Radiocarbon analysis, supplemented by tree-ring counts, established a date about 400 years ago of a flood event that had approximately the same order of magnitude as the devastating floods of December 1964.

In 1955 and again in 1964, unusually high floods and peak discharges were experienced in northern California. On many streams the peak discharges in both years were greater than any that had occurred during the period of record, and on some streams the 1964 peaks exceeded any that had previously occurred during the period of reasonably dependable observations by local residents; in some instances, more than 100 years. The occurrence of such extreme floods provides one reference point, sometimes a critical one, in the sampling of annual floods. Because the extreme floods sometimes seem to be outliers when viewed in company with data from other floods, the assignment of a reasonable probability of occurrence to such extreme floods is important and at the same time difficult. This difficulty requires an examination of all available hydrologic information that may help deduce the average length of time, or recurrence interval, between floods of similar magnitude.

To define the estimated frequency-magnitude relation, the annual discharges are arranged in order of magnitude. Each flood is assigned a recurrence interval T, by use of the arbitrary formula

$$T=\frac{n+1}{m}$$

where

T=the recurrence interval, in years,
n=the number of years of record, and
m=the rank of the event in the plotting array ($m=1$ for the maximum and $m=n$ for the minimum event).

Implicit in this method of flood-frequency analysis is the fact that the frequency of the highest observed flow is determined by the length of record. For example, the greatest flood in 100 years of record will be assigned a 101-year frequency interval. This leads to an unrealistic prediction of flood events like the high flows of December 1955 and December 1964 in northern California. Prior to 1964, the floods of December 1955 were the second highest reported since 1854 (Rantz, 1964, p. 55) and were the highest flows on record that were actually measured. The 1964 floods, which followed a scant 9 years later, proved to be the highest ever measured. The question then arose as to whether floods of a magnitude equal to those of December 1964 actually occur with a recurrence interval averaging 115 years or do they, in fact, have a longer recurrence interval, perhaps 200 years or more.

Geomorphic and botanical evidence may be useful in extending flood records and can perhaps yield a better estimate of the true long-term recurrence interval of large floods than can be obtained by conventional methods. Distinctive types of sedimentary deposits, for example, are direct evidence of past floods (Jahns, 1947; Stewart and LaMarche, 1967). These deposits may be dated by radiocarbon analysis of included organic material or they may be assigned minimum ages by dendrochronologic study of associated trees. Dating of other deposits that were undisturbed prior to erosion by recent floods can give a minimum date for the last previous flood of comparable magnitude. Tree-ring dating of flood damage to vegetation (Sigafoos,

U.S. GEOL. SURVEY PROF. PAPER 600-D, PAGES D34-D37

1964) is another promising source of information, particularly in areas where many trees reach ages of several hundred years.

Flood evidence of this type has already been described on Coffee Creek, a tributary to the Trinity River in northern California (Stewart and LaMarche, 1967). Radiocarbon dating of organic material buried in preflood deposits along the valley margin indicated that the flood of December 1964 exceeded any that had occurred in at least 200 years. That fact implies a recurrence interval much greater than that obtained from conventional methods of flood-frequency analysis.

In 1967, geomorphic and botanical evidence of a major prehistoric flood was investigated on Blue Creek, a tributary to the Klamath River (fig. 1). There, deposits of poorly sorted, obscurely bedded, coarse gravel underlie a high terrace. These old deposits were deeply eroded by the floods of December 1964 which just overtopped the terrace surface as is evidenced by flood debris and high-water marks. The flood erosion revealed stumps of redwoods, *Sequoia sempervirens* (D. Don) Engl., which had previously been buried in the terrace deposit to a depth of about 20 feet above the root crown (fig. 2). It was further established that the trees were dead and limbless snags when they were logged in 1958–59. The cutting of those snags at the then-existing ground level accounts for the fact that all the stumps now project to approximately the same height, about 21 feet above the present bed of Blue Creek (fig. 2). Tree-ring counts on six of the largest stumps indicated that the trees were 500–600 years old when they died.

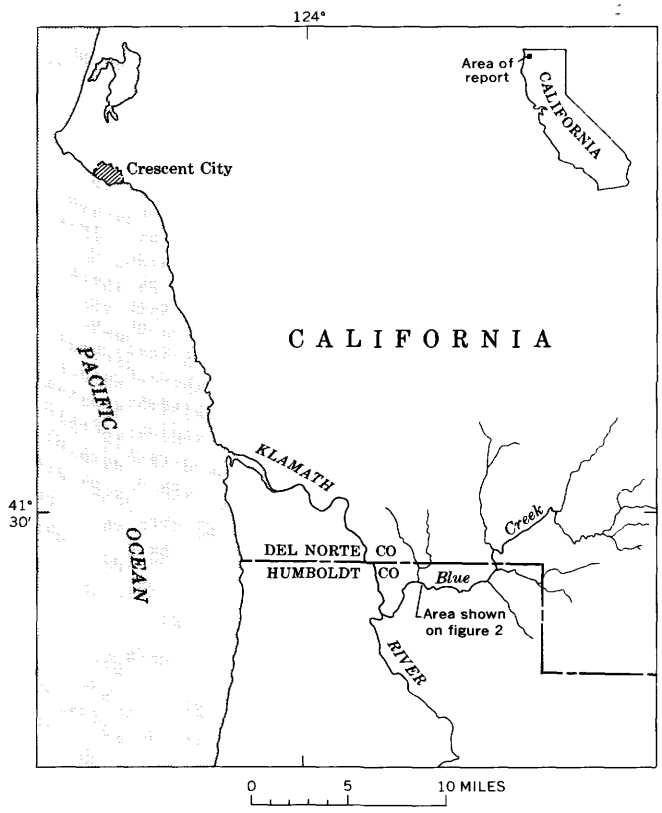

FIGURE 1.—Location of Blue Creek area, California.

The texture and structure of the deposits underlying the terrace indicate that the gravel may have been laid down in a single catastrophic flood. Similar deposits buried standing trees along Coffee Creek (Stewart and LaMarche, 1967) to depths of more than 5 feet in 1964. Another feature suggesting catastrophic burial of the older redwood trees is the simple pancake form of their root systems, some of which have been partly exposed by the 1964 erosion. Stone and Vasey (1968) showed that redwoods deeply buried by deposition of successive thin layers of sediment at long intervals develop new root systems at progressively higher levels from adventitious buds in the lower parts of their stems. The root system in the Blue Creek stand did not show such successive levels of root formation; this is strong evidence that the trees were killed as a consequence of rapid burial of their root system to a depth of 20 feet.

The terrace surface supports a mixed stand of redwoods and Douglas-fir (*Pseudotsuga menzieii* (Mirb.) Franco) whose maximum age does not exceed 90 years, as determined by tree-ring counts of increment cores from the 10 largest trees growing on the terrace surface near the buried trees. One of the redwood stumps displaying 560 rings and buried by the terrace deposit has been dated by radiocarbon analysis. The radiocarbon date of 850 ± 100 years before present was established on wood 100 rings from the center of the tree; hence, this established that the older trees began growth about A.D. 1000 and lived to about A.D. 1560 ± 100 years. If the older trees were killed by rapid deposition of flood deposits, then the floods responsible for their death must have occurred approximately 400 ± 100 years ago. Because the floods of December 1964 just overtopped the terrace deposit they are probably of the same order of magnitude as the event that deposited the terrace material. Thus, at least one or more floods equal to, or greater than, the flood of December 1964 have occurred in the past 400 years; that is, since A.D. 1560 ± 100 years.

A test of the acceptability of this hypothesis may be made by comparison with the results of conventional flood-frequency analysis. The Klamath River, to which Blue Creek is a tributary, has an unusually long record of flood events. Data on the major peak flows dating back to 1862 have been computed by Rantz (1964) on the basis of floodmarks and the hydraulic properties

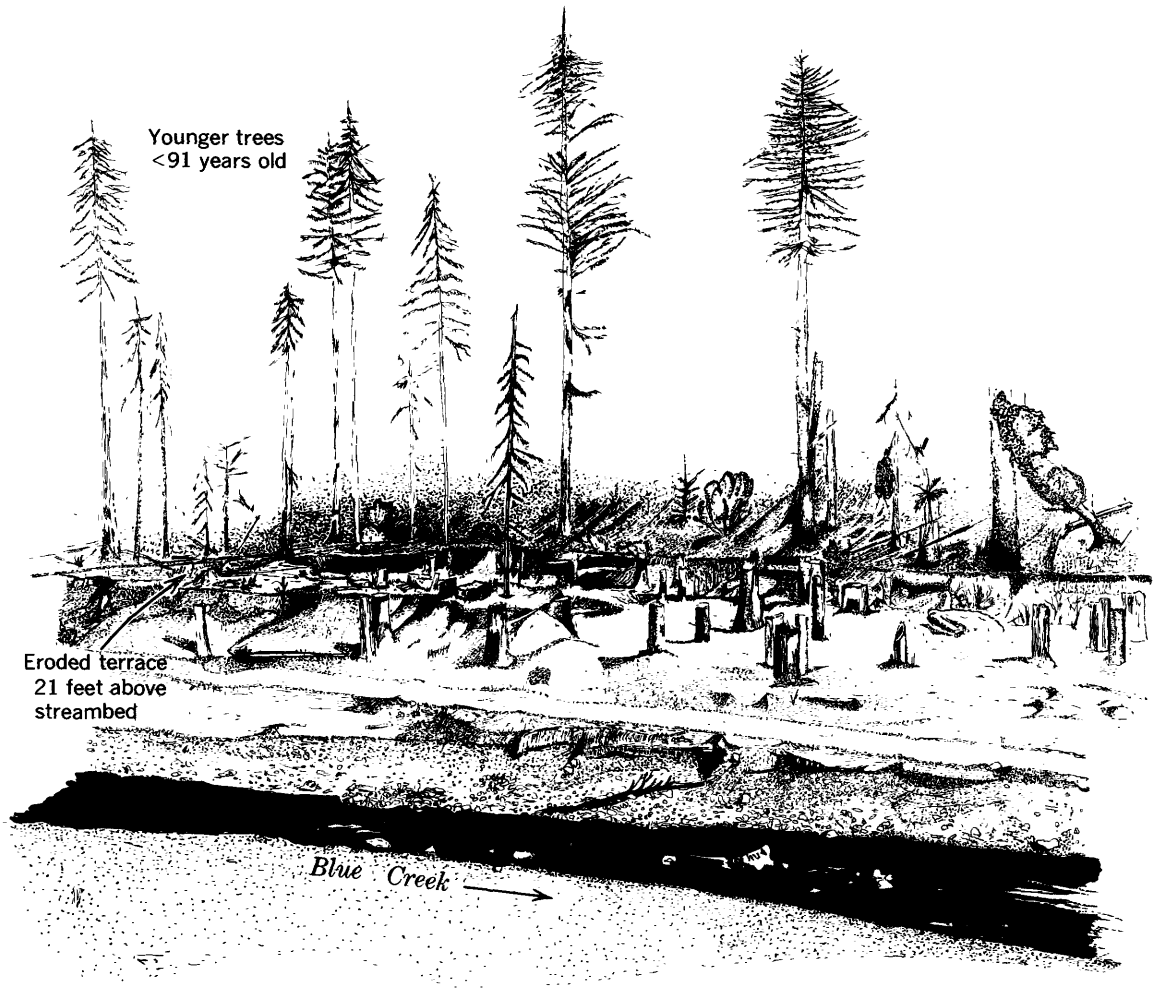

FIGURE 2.—Relation between younger and older trees in eroded terrace deposit along left (south) bank of Blue Creek.

of the channels. A major peak flow of unknown magnitude is also known to have occurred in the 1853 water year. Annual flood data for the period 1911–67 have been used to compute a frequency-magnitude relation based on a log Pearson type-3 distribution (fig. 3). Data for the historic floods of 1862, 1881, and 1890 are also shown in figure 3 at recurrence intervals based on knowledge of the relative magnitude of all major floods since 1854. The flood of December 1964 is shown by a dashed line. Extension of the flood-frequency curve from the base period and historic data would seem to support the hypothesis of an approximate 400-year recurrence interval for the flood of December 1964, although the agreement may be fortuitous.

Botanical and geomorphic evidence of past flood events can probably be useful in assigning a more meaningful recurrence interval to floods of large magnitude.

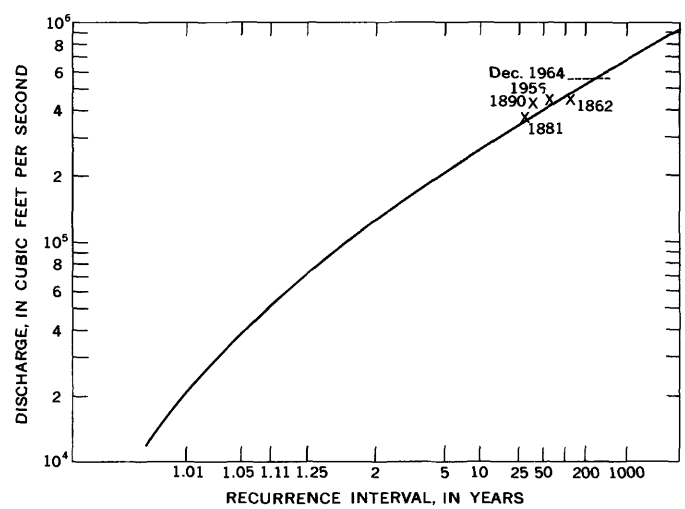

FIGURE 3.—Annual floods on the Klamath River at Klamath, Calif. plotted for base period 1911–67 by log Pearson type-3 method.

REFERENCES

Jahns, R. H., 1947, Geologic features of the Connecticut Valley as related to recent floods: U.S. Geol. Survey Water-Supply Paper 996, 158 p.

Rantz, S. E., 1964, Surface-water hydrology of coastal basins of northern California: U.S. Geol. Survey Water-Supply Paper 1758, 77 p.

Sigafoos, R. H., 1964, Botanical evidence of floods and flood-plain deposition: U.S. Geol. Survey Prof. Paper 485–A, 35 p.

Stewart, J. H., and LaMarche, V. C., Jr., 1967, Erosion and deposition produced by the flood of December 1964 on Coffee Creek, Trinity County, California: U.S. Geol. Survey Prof. Paper 422–K, 22 p.

Stone, E. C., and Vasey, R. B., 1968, Preservation of coast redwood on alluvial flats: Science, v. 159, p. 157–161.

SUBMERGENCE ALONG THE ATLANTIC COAST OF GEORGIA

By ROBERT L. WAIT, Richmond, Va.

Prepared in cooperation with the city of Brunswick, Glynn County, and the Georgia Department of Mines, Mining, and Geology

Abstract.—Cypress stumps recovered from river terrace material near Brunswick, Ga., may indicate submergence of the Atlantic coastal area during Holocene geologic time. The older material, found at a depth of from 9 to 17 feet below mean sea level, was dated by carbon-14 at 3,670 ±300 years (B.P., 1950); the younger, found 1 foot above mean sea level and buried in 3 feet of marsh silt and clay, was dated at 2,780 ±250 years B.P. Presence of the cypress stumps may indicate that fresh water once discharged from the Turtle River, now a drowned estuary.

Cypress stumps were recovered during dredging operations on the terrace alongside the Turtle River near Brunswick, Ga., in 1962, at the crossing of State Highway 303. Figure 1 shows the location of Brunswick, the Turtle River, and site of the find. Dredge cuts were made to depths ranging between 15 and 20 feet to remove silty clay and marsh material overlying a sand. The cuts were then filled with sand dredged from the river bottom to provide firm foundation for the approaches to the highway bridge. Figure 2 shows the section at the bridge site that was obtained from the State Highway Department resident engineer, Mr. McKinsey. Notations by the dredge operators give the depth and positions at which stumps were found during dredging.

The youngest stumps were found buried in marsh mud 1 foot above present-day sea level. A tide gage placed on the old bridge by the State Highway Department engineers was read at the time the stumps were collected and established their position with reference to sea level. The specimen (W–1223), number 1 on figure 2, was from a stump that was buried in about 3 feet of marsh mud. The tree stump was in place, in an upright position, and the specimen was sawed from the root of the stump.

The older stumps (W–1222), number 2 on figure 2' were found in a sand at depths ranging from about 12 to 20 feet below the surface of the marsh or 9 to 17 feet below mean sea level. The areas in which stumps were encountered by the dredge and noted by the operators are indicated by "S" on figure 2. Although the stumps were found at a depth range from 9 to 17 feet below sea level, all could be of the same age as determined by radiocarbon dating. The older stumps, found on both sides of the river, were buried in a medium to coarse sand on the west side and a fine sand and clay on the east side. Beneath the stumps on both sides was coarse sand.

Carbon-14 age determinations of the stumps were made in the radiocarbon laboratory by Meyer Rubin, of the U.S. Geological Survey. The results are given as follows:

Laboratory No.	*Site and material description*	*Age (years B.P., 1950)*
W–1223	Wood from stump at 1 foot above mean sea level, 3 feet below layer of marsh silt and clay, located southwest end of Turtle River Bridge, Georgia Highway 303, in excavation for new bridge. Collected September 26, 1962.	2, 780±250
W–1222	Wood fragments from assorted stumps hit by dredge, depth from 12 to 20 feet below mean sea level, located southwest end of Turtle River Bridge, Georgia Highway 303, in excavation for new bridge. Collected September 26, 1962.	3, 670±300

Fragments of wood were submitted to the U.S. Geological Survey's Paleontology and Stratigraphy Branch, Denver, Colo. and were identified as cypress by R. A. Scott. Scott reported (written commun., 1965), "The wood is cypress, *Taxodium* Sp. Identification of species of cypress is not possible on the basis of wood

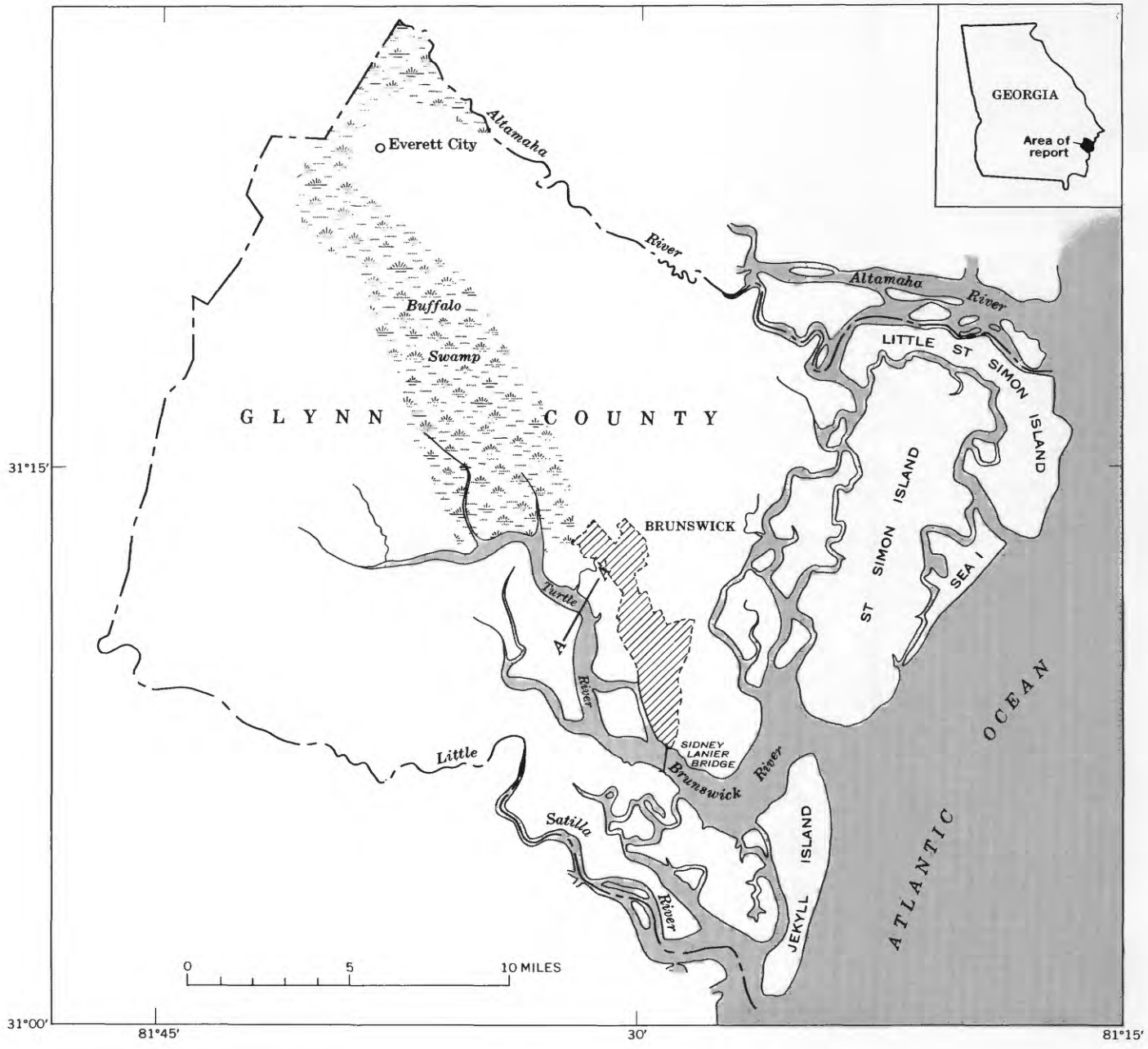

FIGURE 1.—Location of section *A–A'* at Georgia Highway 303 Turtle River bridge site at Brunswick.

alone, but based on its location, this is most probably *T. distichum*. This species is typically found in or near the margins of shallow, fresh-water swamps. The seeds require exposure to air for germination, hence depth of water imposes a limit on the distribution of swamp cypress."

Davis (1943) states, "* * * it is probable that all cypress forests occur only where water levels recede below the soil surface at times."

Scott also reports, "Cypress grows in some areas in Florida swamps where occasional invasion by brackish or marine waters must occur as a result of storms. Consequently, the plant must have a relatively high tolerance for salinity. However, it is typically limited to fresh-water habitats, and its occurrence *in situ* in the fossil state would be taken as good evidence for the former existence of fresh-water conditions at the site."

Thus the available evidence suggests that the trees

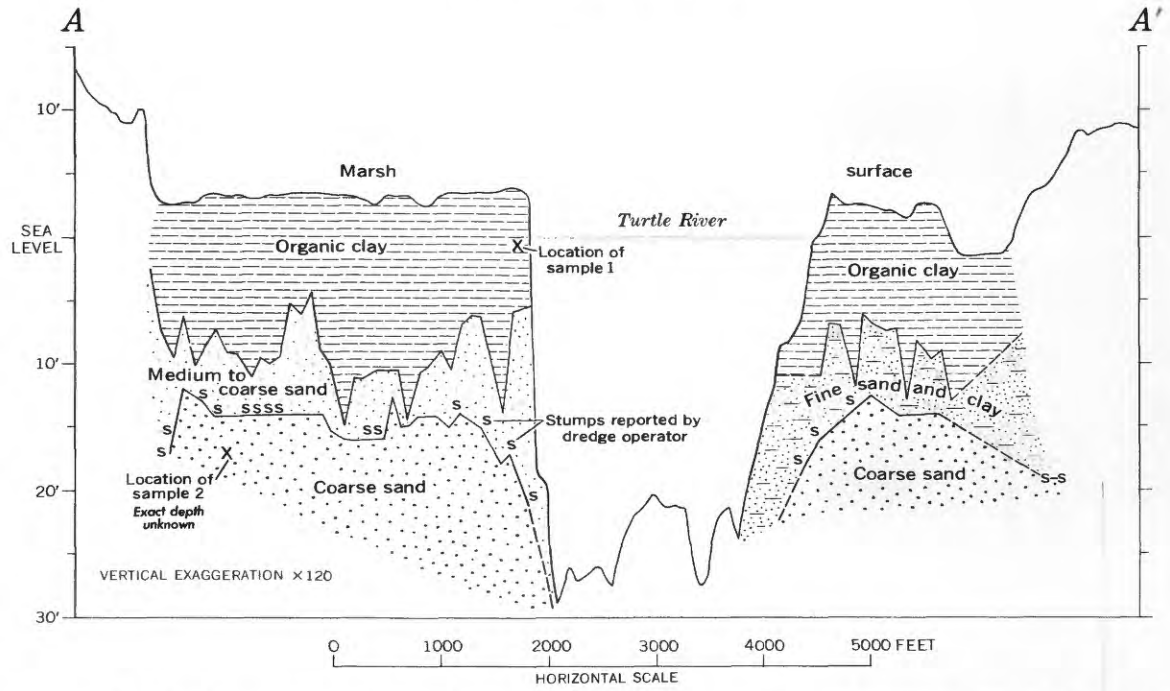

FIGURE 2.—Lithologic section showing location of two stumps sampled, and stumps reported by dredge operators.

which produced the stumps grew in or near a shallow, fluctuating fresh-water environment. Cypress trees do not presently grow on the terraces, which are flooded with salt water during high tides and especially during spring tides.

The Brunswick and Turtle Rivers now form a drowned estuary. The chloride content of water in the estuary is nearly that of sea water. The presence of such a large "river" into which almost no fresh water flows, except at rare times when the Altamaha River floods Buffalo Swamp in the western part of the county or when runoff caused by heavy rainfall is discharged from the swamp, poses a question as to its origin. The "river" is approximately 0.75 mile wide at the Sidney Lanier Bridge, near its mouth, and 0.5 mile wide at the site of the Highway 303 crossing; it is as much as 70 feet deep south of St. Simons Island, 50 feet deep at Sidney Lanier Bridge, and 30 feet deep at the Highway 303 crossing. Such a large river that discharges no fresh water at present suggests that it may once have been an outlet for a Coastal Plain stream. Possibly the Altamaha River may have once discharged (in part, at least) through this outlet. Aerial photographs of Glynn County show that the marsh and swamp adjacent to the Turtle River appear to be continuous with the Altamaha River in the northwest corner of Glynn County near Everett City.

Figure 3 compares the position of the two Brunswick carbon-14 dates with curves developed from New Jersey (Stuiver and Daddario, 1963) and from Boston, Mass. (Kaye and Barghoorn, 1964). Because of the uncertainty of the exact position of the oldest sample, it is shown at the range of depths from which it may have come.

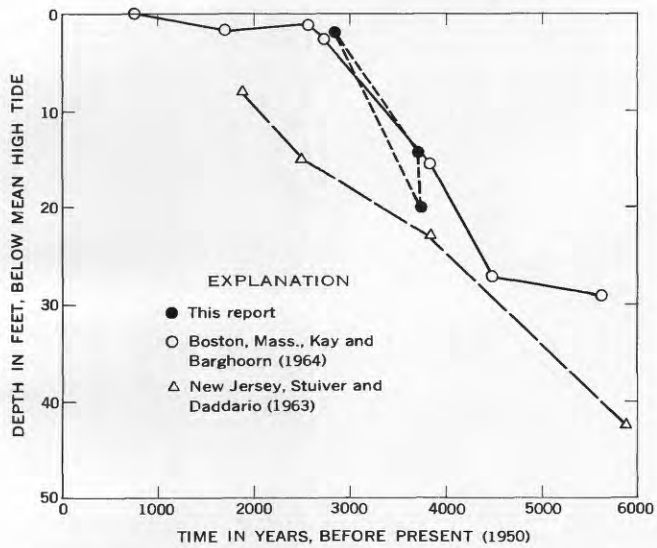

FIGURE 3.—Relative depths and ages of samples from Brunswick, Ga., Boston, Mass., and New Jersey.

The rate of subsidence appears to be nearly the same as that which occurred in the Boston area. Subsidence has also occurred at similar rates along the southwestern tip of the Florida peninsula as noted by Scholl and Stuiver (1967), and in Virginia as given by Harrison, Malloy, Rusnak, and Terasmae (1965).

REFERENCES

Davis, J. H., Jr., 1943, The natural features of southern Florida: Florida Geol. Survey Bull. 25, p. 178–185.

Harrison, W., Malloy, R. J., Rusnak, G. A., and Terasmae, J., 1965, Possible Late Pleistocene uplift, Chesapeake Bay entrance: Jour. Geology, v. 73, no. 2, p. 201–229.

Kaye, C. A., and Barghoorn, E. S., 1964, Late Quaternary sea level change and crustal rise at Boston, Massachusetts, with notes on the auto-compaction of peat: Geol. Soc. America Bull., v. 75, no. 2, p. 63–80.

Scholl, D. W., and Stuiver, Minze, 1967, Recent submergence of southern Florida: a comparison with adjacent coasts and other eustatic data: Geol. Soc. America Bull., v. 78, no. 4, p. 437–454.

Stuiver, Minze, and Daddario, J. J., 1963, Submergence of the New Jersey coast: Science, v. 143, p. 951.

COMPUTATION OF REAERATION COEFFICIENTS FOR A RIVER SYSTEM IN NORTHEASTERN NEW JERSEY

By THOMAS J. BUCHANAN, Trenton, N. J.

Work done in cooperation with the New Jersey State Department of Health

Abstract.—Based on an empirical relationship, reaeration coefficients are computed for 16.8 miles of a river system in northeastern New Jersey for three different duration points—50 percent, 80 percent, and 90 percent. The procedures used in obtaining the data and the results of the computations are shown. Discharges for the subreaches ranged from 16 cfs to 740 cfs, and the reaeration coefficients ranged from 3.1×10^{-3} per day to 9.78 per day. The method used has accuracy limitations, but as long as this limitation is recognized by the users, the method and procedures outlined are an inexpensive and rapid way to determine reaeration coefficients for a stream system.

The river system consisting of the Wanaque, Pequannock, Pompton and Passaic Rivers is located in northeastern New Jersey (fig. 1). Because of proposed inflow of new or additional sources of waste water into the system, the New Jersey State Department of Health was concerned with the effects of these new sources of waste water on the dissolved-oxygen concentration in the streams. However, before the oxygen sag could be computed, values for the reaeration coefficients were needed. Heretofore, reaeration coefficients were usually assumed on the basis of studies by others in the laboratory or in similar river basins. But for this study, the Health Department required a practical method to compute reaeration coefficients for the particular river system in question.

The reaches studied include the Wanaque River below Wanaque Reservoir, the Pequannock River below its confluence with the Wanaque River, the Pompton River, and the Passaic River from Two Bridges to the Passaic Valley Water Commission's water-supply treatment plant in Little Falls, a total stream distance of 16.8 miles. The drainage area at Wanaque Reservoir is 90.4 square miles, and the drainage area at Little Falls is 762 square miles. The length of each reach is as follows:

River	Length of reach studied (miles)
Wanaque	4.9
Pequannock	2.0
Pompton	6.4
Passaic	3.5

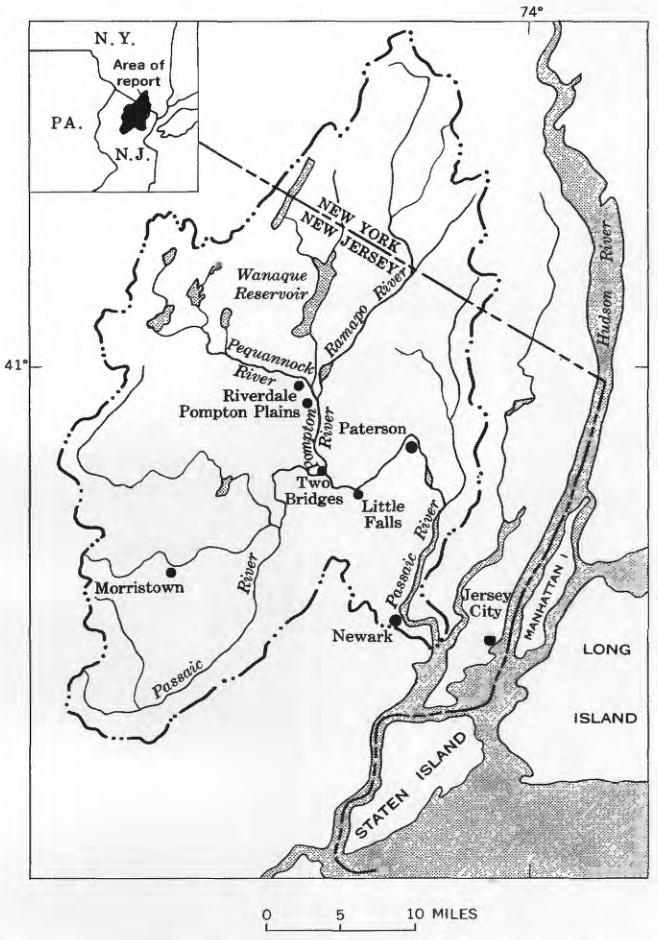

FIGURE 1.—The Passaic River basin in northeastern New Jersey.

The Wanaque River enters the Pequannock River at Riverdale, and the Pequannock and Ramapo Rivers meet to form the Pompton River at Pompton Plains. The Pompton River enters the Passaic River at Two Bridges (fig. 1).

METHOD

The method used to compute the reaeration coefficients in the study reaches was that proposed by Langbein and Durum (1967). They have taken several sets of laboratory and field data and have shown that a relation exists between velocity and depth in the stream, and the reaeration coefficient of the stream. This relation can be expressed as

$$k_2=\frac{3.3v}{H^{1.33}},$$

in which

k_2=the coefficient of reaeration (to the base 10), per day; the subscript 2 denotes this coefficient as the second coefficient in the Streeter and Phelps (1925) formulation for the deoxygenation (k_1) and reoxygenation (k_2) of streams,
v=mean velocity in feet per second, and
H=mean depth in feet.

Langbein and Durum (1967) recognized that factors other than depth and velocity are significant in determining the reaeration coefficients in streams. For example, the occurrence of pools and riffles and the extent of meandering of the stream also affect the rate of reaeration. Also, temperature, wind, aquatic vegetation, and other related factors must be considered. But the most significant hydraulic and geometric properties that affect reaeration coefficients are the depth and velocity, and because these two factors are so significant and are relatively easy to determine, they were used to compute the reaeration coefficients in this study.

PROCEDURE

The reaeration coefficients for the river system were computed for the 50-percent, 80-percent, and 90-percent points on the streamflow duration curves. The first step was to develop a discharge profile for the entire system for each of the duration points. Five gaging stations were available in the study area; in addition, two low-flow partial-record stations were on principal streams of the system, and two additional low-flow partial-record stations were available on tributaries. Data from these stations and some miscellaneous measurements made for another study were used to define the discharge profile for each of the duration points (fig. 2).

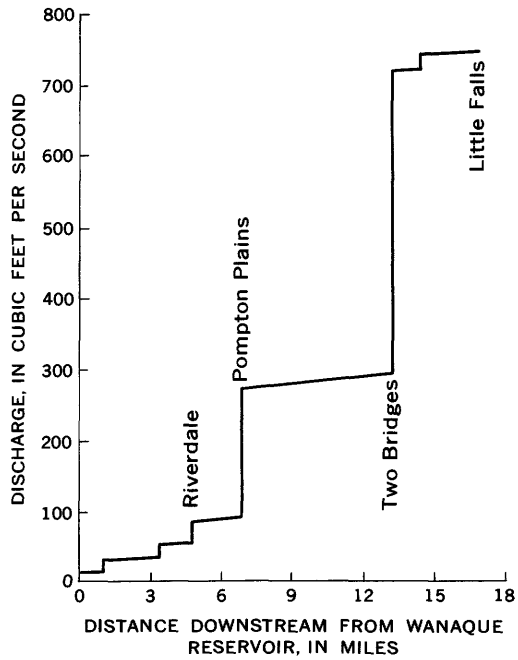

FIGURE 2.—Discharge profile for 50 percent duration point.

The next step was to decide how the 16.8 miles of river system should be broken down for the study. On the basis of map study and field reconnaissance, the system was broken down into 18 subreaches, which ranged in length from 0.5 to 2.2 miles. This subdivision was made so that each subreach had a constant discharge and a more or less constant cross-sectional area.

Fieldmen then measured the cross-sectional area of a typical section for each of the 18 subreaches. The cross sections were selected as being typical of a given subreach rather than being the type that might be selected for a discharge measurement. In general, the sections selected for discharge measurements are not typical because they are usually at contracted and shallow parts of the stream. In addition to measuring a cross-sectional area in each subreach, the fieldmen also determined the discharge duration point from the gaging station at the time they were collecting the data. Then the data for each measured cross-sectional area were adjusted to the cross-sectional areas that would be expected at the 50-percent, 80-percent, and 90-percent duration points. This was done by using the known or computed relationship between stage and discharge in each subreach and the duration point at which the cross-sectional area data were collected.

Using the discharge profile for each duration point and the cross-sectional area for each duration point for each subreach, the mean velocity in the subreach could then be computed. Using the width and cross-sectional

313-005 O—68——4

TABLE 1.—*Results of the computation of the oxygenation coefficients for three duration points*

[Symbols: L, length of subreach; H, mean depth; v, mean velocity; Q, discharge; k_2, coefficient of reaeration]

Subreach No.	L (miles)	Range of H (feet)	Range of v (ft/sec)	Duration point					
				50 percent		80 percent		90 percent	
				Q (cfs)	k_2 (day^{-1})	Q (cfs)	k_2 (day^{-1})	Q (cfs)	k_2 (day^{-1})
1	1.0	1.16	0.34	16	0.92	16	0.92	16	0.92
2	1.1	3.04–2.61	.11–.08	30	.083	21	.079	18	.074
3	1.2	6.33–6.00	.02–.01	34	.0057	23	.0045	20	.0031
4	.5	.80–.61	.63–.52	35	2.80	26	3.39	21	3.31
5	.5	1.48–.86	.62–.45	54	1.22	29	1.37	22	1.82
6	.6	1.40–.81	.40–.29	56	.85	30	.99	23	1.27
7	.5	.91–.56	1.83–1.18	89	6.86	44	9.78	35	8.44
8	1.1	.91–.56	.92–.59	91	3.45	45	4.92	37	4.22
9	.4	1.83–1.58	.94–.49	92	1.39	47	.91	40	.88
10	.7	2.22–1.63	1.33–.69	276	1.52	114	1.46	84	1.19
11	1.0	1.45–.93	1.36–.84	278	2.74	115	2.13	85	3.05
12	.4	2.18–1.48	.89–.42	280	1.04	116	.92	86	.83
13	1.0	1.81–1.11	.94–.49	282	1.41	117	1.50	86	1.40
14	1.3	5.72–5.37	.76–.26	286	.25	118	.12	87	.092
15	1.3	4.75–4.34	.48–.16	291	.20	119	.10	88	.075
16	.7	2.69–1.74	.65–.31	294	.58	121	.44	89	.49
17	1.3	3.87–3.60	.81–.21	726	.44	260	.18	175	.13
18	2.2	4.73–4.50	.60–.15	740	.25	270	.10	182	.067

area data, it was possible to compute the mean depth in each subreach. Knowing the mean velocity and the mean depth, the reaeration coefficient in each subreach was computed.

RESULTS

The results of the study are shown in table 1. This table gives the discharge and reaeration coefficient for all 3 duration points for each of the 18 subreaches. It also gives the length and the range in depth and velocity for each of the subreaches. The subreaches are numbered in consecutive order downstream from the beginning of the system.

For the 50-percent duration point, the discharge (Q) ranged from 16 to 740 cubic feet per second, and the reaeration coefficients ranged from 5.7×10^{-3} per day to 6.86 per day. For the 90-percent duration point, the discharge ranged from 16 cfs to 182 cfs and the reaeration coefficients ranged from 3.1×10^{-3} per day to 8.44 per day. The discharge for subreach 1 is the same for all duration points because this is the required release for conservation purposes from Wanaque Reservoir, and the only time the discharge is greater than 16 cfs is during periods of reservoir spillage, which is less than 10 percent of the time.

As might be expected, subreach 3, which is a deep slow pool caused by a dam across the Wanaque River, has the lowest reaeration coefficient, whereas subreach 7, which is a shallow relatively swift reach of stream, has the highest reaeration coefficient.

The results obtained are consistent with what might be expected in this stream system. Thus, the reaeration coefficients are being applied in determining the oxygen sag that would be caused by the addition of new waste-water discharges to the stream system.

Although the computation of these reaeration coefficients is based on an empirical relationship, the coefficients are better than those derived from laboratory studies or those computed for another river system, because in this case they were computed from actual field data from the river system to which they apply. At present (1968) there appears to be no better method to obtain these coefficients as readily and inexpensively.

REFERENCES

Langbein, W. B., and Durum, W. H., 1967, The aeration capacity of streams: U.S. Geol. Survey Circ. 542, 6 p.

Streeter, H. W., and Phelps, E. B., 1925, A study of the pollution and natural purification of the Ohio River: U.S. Public Health Service, Public Health Bull. 146, 75 p.

SLOPE-DISCHARGE RELATIONS FOR EIGHT RIVERS IN THE UNITED STATES

By CHARLES W. CARLSTON, Washington, D.C.

Abstract.—Graphs showing slope versus mean annual discharge have been prepared for eight rivers in the United States, and eye-fitted lines were constructed for those rivers showing acceptable statistical correlation of slope with discharge. Two alluvial-bed graded rivers, the Red River of Louisiana and Arkansas and the Arkansas River, showed a very close correlation of slope varying with discharge. A third river, the Missouri, showed a slope-discharge relation of $sQ \propto \frac{0}{m}^{0}$ for more than 1,800 miles upstream from its mouth. Two other rivers, the Tennessee-Holston and the Delaware, showed a good correlation of slope with discharge. The remaining three rivers—the Ohio, the Susquehanna, and the Alabama and its headwaters—showed no correlation of slope plotted against discharge.

In a paper published in 1964 on equilibrium states in channel morphology, W. B. Langbein and L. B. Leopold stated that in rivers the relation of slope (s) versus discharge (Q) generally lies within limits of $s \propto Q^{-0.5}$ and $s \propto Q^{-1.0}$ with an average near $s \propto Q^{-0.75}$ (Langbein and Leopold, 1964, p. 786). In a study of the slope characteristics of a number of rivers east of the Rocky Mountain front, described in the present report, I have attempted to distinguish between the slope characteristics of ungraded rivers and graded alluvial-bed rivers whose longitudinal profiles are unaffected (at even very great vertical exaggeration) by irregularities caused by the outcrop of resistant ledges of bedrock.

As a byproduct of the study it was decided to investigate the characters of the varied relations of the slope versus mean annual discharge of eight of these rivers by graphical plotting on logarithmic-type paper (slopes obtained from U.S. Corps of Engineers profiles). Longitudinal profiles and maps of three of these rivers indicated that they were graded rivers; these are the Red River of Louisiana and Arkansas, the Arkansas River, and the Missouri River. Two of the remaining rivers—the Ohio River and the Tennessee River and its Holston River tributary—are low in gradient and, despite showing some bedrock outcrop irregularities in their profiles, appear to be approaching grade in parts of their courses. The remaining three rivers, the Delaware, the Susquehanna, and the Alabama River and its headwaters, the Coosa, Oostanaula and Conasauga Rivers, drain the Atlantic and east Gulf slope of the Appalachians, where the rivers are largely ungraded.

Acknowledgments.—I am indebted to Dr. M. G. Wolman, Johns Hopkins University, and W. W. Emmett, U.S. Geological Survey, for their most helpful critical reviews of this manuscript.

GRAPHICAL CORRELATION OF THE EIGHT RIVERS

The Red River is considered to be in a graded condition throughout the range of mean annual discharge (Q_m) points that were graphed. For the Red River there is a close relation to an eye-fitted line. The trend of the line shows the relationship $s \propto Q_m^{-0.55}$ (see fig. 1).

Also shown on figure 1 is the graphical relation of slope to discharge for the Arkansas River. The nearly vertical arrangement of the first three points shows conditions in its ungraded mountain headwaters where slope is decreasing rapidly with little change in discharge. Shift of the points to the left shows the effects of diversion of water for irrigation at the foot of the mountains. The graphical slope of the points from here on to the end of the graph is highly correlated and indicates a relation of $s \propto Q_m^{-0.50}$ or very similar to that found on the Red River (see fig. 1).

The graph for the Missouri River begins with a steep slope representing the mountainous headwaters. After this, where the discharge of 7,500 cubic feet per second increases to 56,000 cfs, the slope of the Missouri varies only from 0.00015 to 0.00023. The higher slopes shown in the range of discharge from about 25,000 cfs to 35,000 cfs are the results of the loads carried into the river by the Niobrara and Platte Rivers. Slopes were obtained from a 1930 dated profile made before channel improvement and reservoir construction on

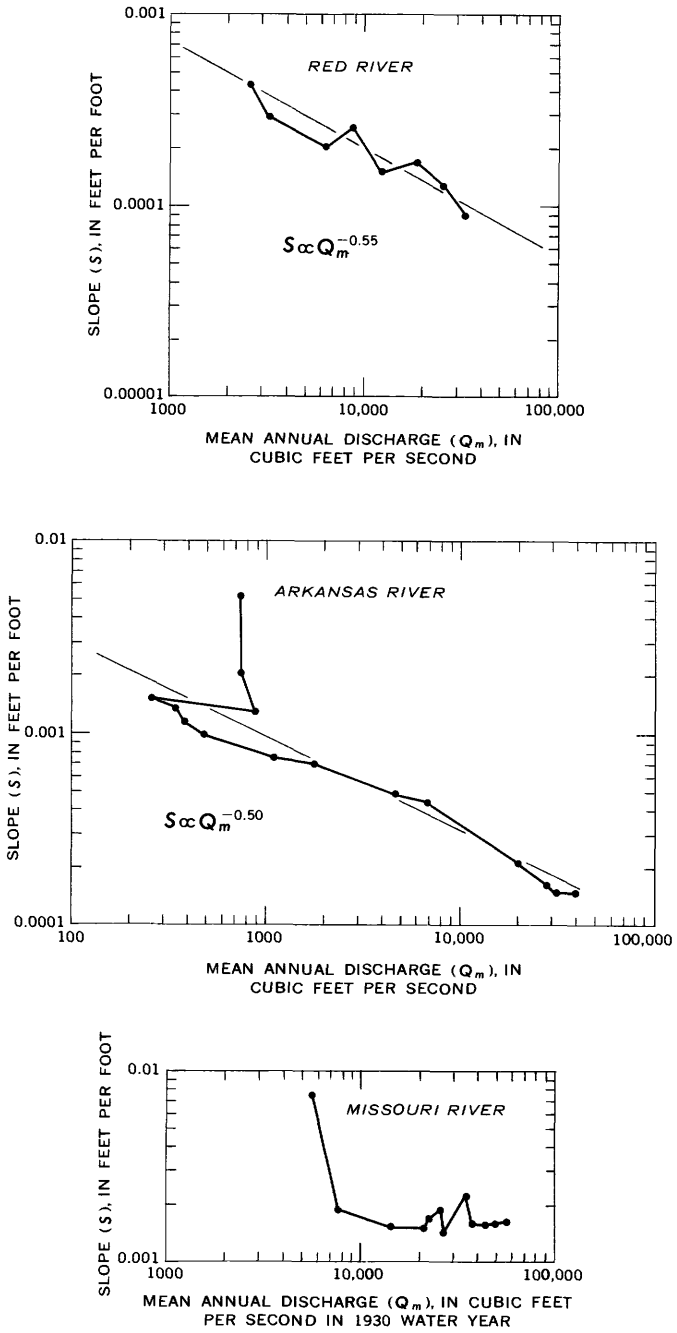

FIGURE 1.—Slope-discharge relations of the Red, Arkansas, and Missouri Rivers.

the river. For that reason, discharges given are also average discharges for the 1930 water year. For this section of the river the longitudinal slope indicates a graphical relation of $s \propto Q_m^{0.0}$ (see fig. 1).

A good graphical correlation can be made for the slope-discharge graph of the Tennessee River and its headwater, the Holston River. There are irregularities in its profile (such as Muscle Shoals and other bedrock outcrops) which indicate that the river is not yet in a fully graded condition, but the close alinement of the points in the central parts of the graph suggests that this part of the river's longitudinal profile is approaching a graded condition. The relation of slope to discharge for this river is $s \propto Q_m^{-0.62}$ (see fig. 2).

The lower part of the Ohio River below the Falls of the Ohio at Louisville, Ky., has a constant slope of only 0.000056 for a distance of 370 miles. This section of the river is shown by the three points of highest discharge. Upstream from Louisville the points on the graph for the Ohio are highly uncorrelated (see fig. 2).

Although there is a fairly high degree of irregularity of the points on the graph for the Delaware River (see fig. 3) they nevertheless show a good graphical alinement in the relation $s \propto Q_m^{-0.93}$.

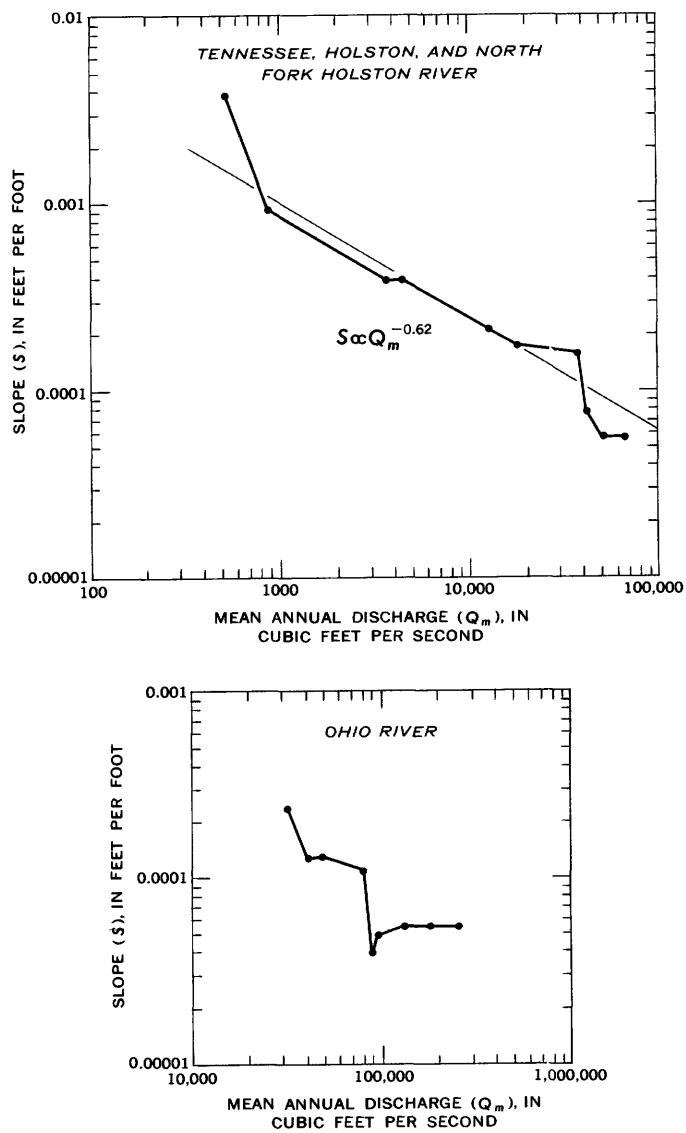

FIGURE 2.—Slope-discharge relations of the Tennessee, Holston, and Ohio Rivers.

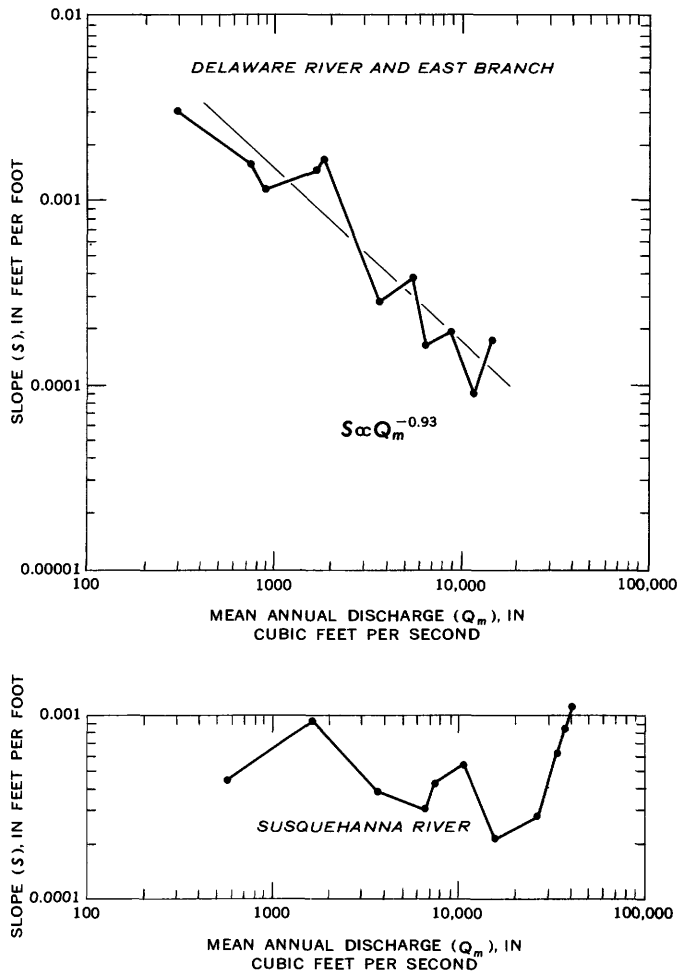

FIGURE 3.—Slope-discharge relations of the Delaware and Susquehanna Rivers.

The slope-discharge graph for the Susquehanna River is highly uncorrelated and represents an excellent portrayal of an ungraded river flowing across bedrock of highly varying degrees of resistance to erosion (see fig. 3).

The lower course of the Alabama River is at a very low gradient (0.000053) for 240 miles. Its constant slope in this region is shown by the two dots on figure 4 at the right end of the graph. The very high slope in the graph shows the Coosa River's course across the crystalline rocks of the Fall Zone. Two stretches of the river headwaters have constant slopes of 0.00012 and 0.00027, respectively, and they appear on the left part of the graph.

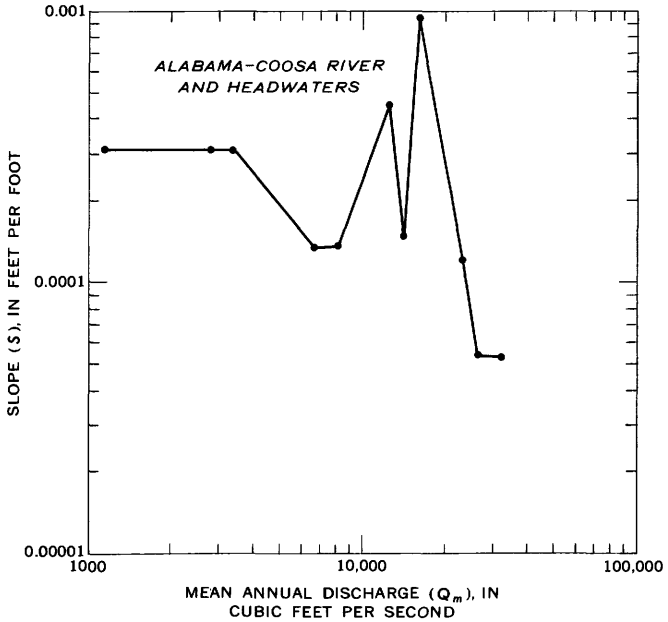

FIGURE 4.—Slope-discharge relation of the Alabama–Coosa River and headwaters.

CONCLUSIONS

In the graphical plotting of slope against discharge, close correlation was found for three graded alluvial-bed rivers west of the Mississippi. On the remaining five rivers east of the Mississippi, all ungraded at least in part, graphical correlations were not as successful, although eye-fitting lines could be constructed for the Tennessee River and the Delaware River. For the Red River, the Arkansas River, the Tennessee River, and the Delaware River, slope varies with discharge by powers ranging from -0.50 to -0.93 and averages -0.65. If the 0.0 exponent for the Missouri River is added to this listing, the average becomes $s \propto Q_m^{-0.52}$. Although this relationship between slope and discharge is empirical, it is a useful tool in showing the very close correlation between slope and discharge in an alluvial-bed graded river, or river segment, as well as showing the complete absence of correlation of slope with discharge in a typical ungraded stream such as the Susquehanna River.

REFERENCE

Langbein, W. B., and Leopold, L. B., 1964, Quasi-equilibrium states in channel morphology: Am. Jour. Sci., v. 262, p. 782–794.

THE USE OF PRECIPITATION RECORDS FOR PEAK STREAMFLOW SYNTHESIS

By ERNEST D. COBB, Washington, D.C.

Abstract.—A major problem in the extension of peak streamflow records by synthesis from precipitation records is to obtain a representative long-term precipitation record for the particular basin being studied. To help solve this problem a flood-frequency curve at a given site was developed using long-term precipitation records from surrounding areas and a relation with three climatic variables. This method was used on two Alabama streams and may be applicable to other similar areas. For a selected streamflow site, a set of frequency curves is synthesized from long-term precipitation records of surrounding areas. The flood of a given recurrence interval, T, for the stream site studied is then estimated from a relation between the T-year floods, obtained from the set of synthesized frequency curves, and a rainfall variable.

The U.S. Geological Survey is studying the discharge characteristics of small streams throughout much of the Nation. Most of the records on these small streams are short (5–10 years); hence the effectiveness of conventional methods of flood-frequency analysis is limited. Attempts are being made to use long-term precipitation records and runoff-rainfall models for the purpose of extending streamflow data by synthesis.

The areal distribution of long-term (about 50 years or more) continuously recorded precipitation records is generally inadequate for direct use of a long-term precipitation record at each gaging station site. For example, in some States only 3 to 5 long-term continuously recorded precipitation records are available, and the characteristics of these records are often significantly different. This paper describes a method for using long-term precipitation records to synthesize flood-peak data at stream sites which are remote from the precipitation stations.

DATA USED

Alabama was chosen as a study area for the following reasons: First, a runoff-rainfall model had been developed and calibrated for several streams in the area (Peirce, 1965); second, detailed long-term precipitation records have already been tabulated; and third, the area was not unduly complicated by large physiographic variations.

Annual precipitation in Alabama is heaviest near the Gulf of Mexico and generally decreases as one moves inland. In the northeast corner of the State, the Appalachian Mountains provide mechanical lifting of air masses; this produces some modification of precipitation in that area. The variation of mean-annual precipitation over the State is shown in figure 1.

The long-term hourly precipitation records used in this study are those for Mobile, Ala. (1906–53), Montgomery, Ala. (1897–1957), Birmingham, Ala. (1904–57), Meridian, Miss. (1901–57) and Chattanooga, Tenn. (1906–57). The locations of these stations are shown in figure 1.

Gages used in the collection of each of the above records have been moved one or more times during the periods of record. The consistency of each record of annual totals relative to the others was tested by the double-mass method. This test was not extended to totals for periods shorter than a year.

The double-mass curve for Montgomery, Ala., relative to the mean of six other precipitation stations, indicated a distinct change in slope corresponding to a gage location change on June 9, 1933. Similarly, the double-mass curve for Chattanooga showed a change in slope corresponding to a gage location change on October 1, 1909. Double-mass curves drawn for the other three records, however, did not reveal any inconsistencies.

Adjustment factors determined from double-mass curves of annual values are not necessarily applicable to precipitation durations shorter than 1 year. Hence, no adjustments were applied to the records. However, because of the inconsistencies in certain records, any techniques using these records are expected to be somewhat less reliable than if all the records were consistent.

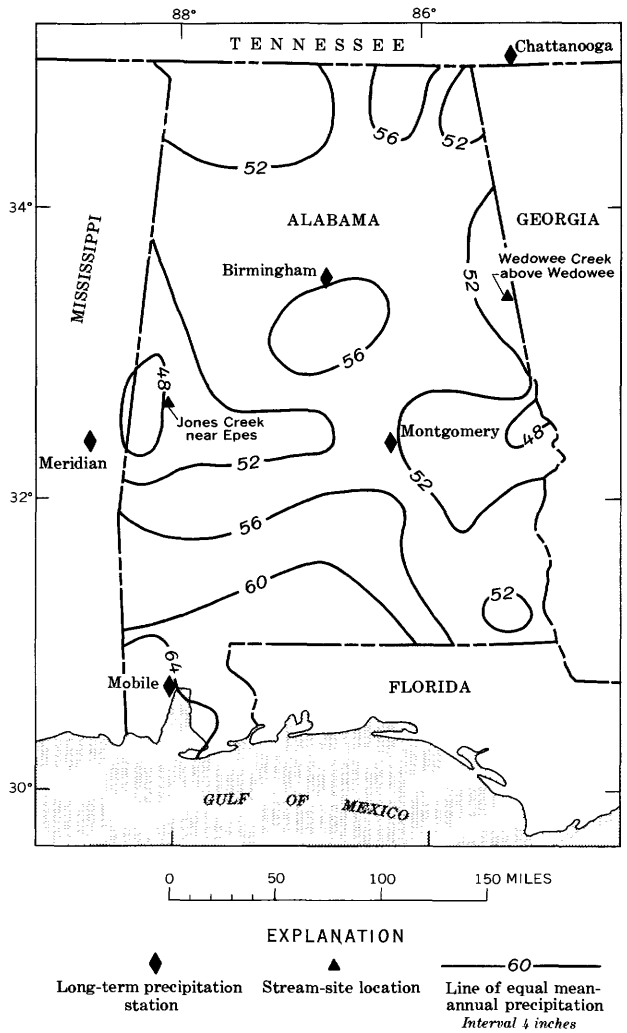

FIGURE 1.—Map of Alabama, showing mean-annual precipitation, locations of long-term recording precipitation gages, and locations of stream sites used in this study.

TECHNIQUE DEVELOPMENT

A method considered for the transference of precipitation records to intermediate sites for flood-peak data synthesis was to synthesize the precipitation data at each stream site studied. This could be accomplished by determining various distribution characteristics of the long-term precipitation records, such as the mean, variance, skew, and serial dependence of both hourly precipitation and periods of no rain (Pattison, 1965). Then the distribution characteristics could be simply interpolated between the long-term record sites or related to various precipitation characteristics, such as mean-annual or annual 3-hour maximum precipitations. Isograms of the distribution characteristics could then be drawn on a map of the area. Thereafter, for any selected location, the distribution characteristics for that site could be determined from the mapped characteristics and a precipitation record synthesized.

An advantage of synthesizing precipitation data is that it provides records of any length, but there is some question as to which precipitation characteristics are needed for flood-peak data synthesis and how accurately precipitation characteristics can be mapped. In the method described in this paper, only precipitation characteristics available from U.S. Weather Bureau maps were used to adjust for nonrepresentative precipitation at a selected site.

A runoff-rainfall model developed for Alabama streams by L. B. Peirce (1965) was used to obtain data for analysis. The Peirce model relates peak discharges to storm-precipitation depths, storm duration, antecedent conditions, and time of year. Graphical relations, needed for the Peirce model, have been developed for several small Alabama streams. Two streams were chosen for this study: Jones Creek, near Epes, which is on the Coastal Plain and drains an area of 11.7 square miles; and Wedowee Creek, above Wedowee, which is in the Piedmont and drains an area of 6.5 square miles (see fig. 1).

Each of the five long-term precipitation records shown in figure 1 were used with the runoff-rainfall model to synthesize flood peaks. Flood-frequency curves defined by each of the five sets of annual flood peaks are shown in figures 2 and 3.

The variables that accounted for the differences in the synthesized flood-frequency curves were empirically determined to be the mean-annual precipitation, $\bar{P}$, the 2-year–3-hour, and the 50-year–3-hour precipita-

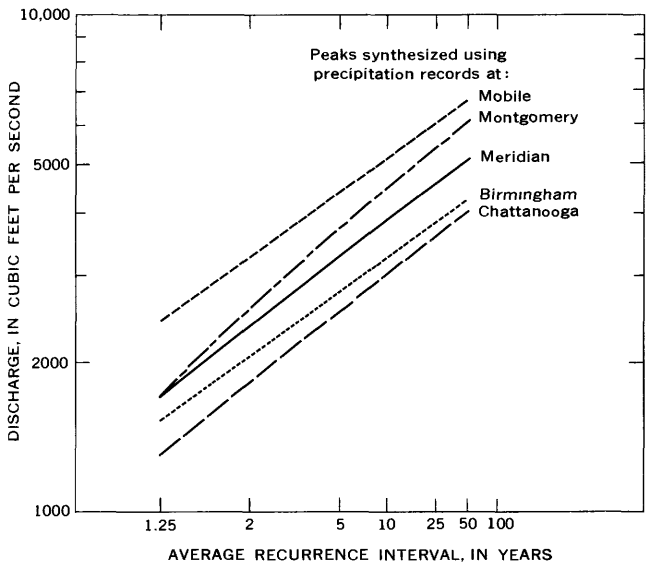

FIGURE 2.—Frequency curves for Jones Creek near Epes, Ala., for synthesized peaks using various long-term precipitation records.

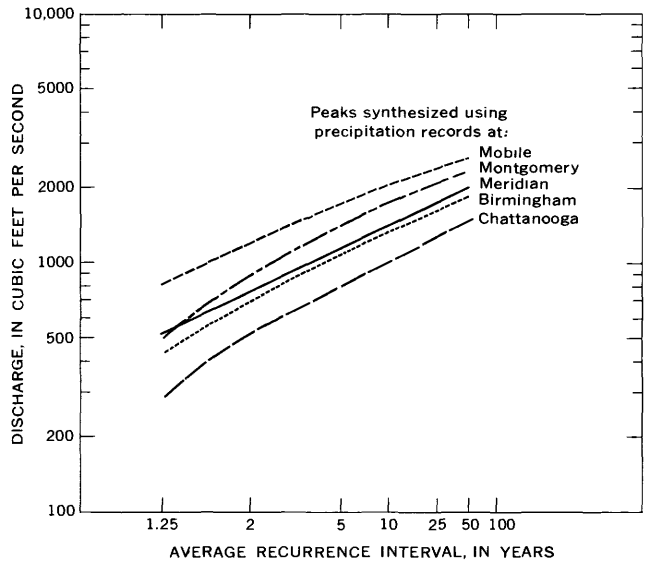

FIGURE 3.—Frequency curves for Wedowee Creek above Wedowee, Ala., for synthesized peaks using various long-term precipitation records.

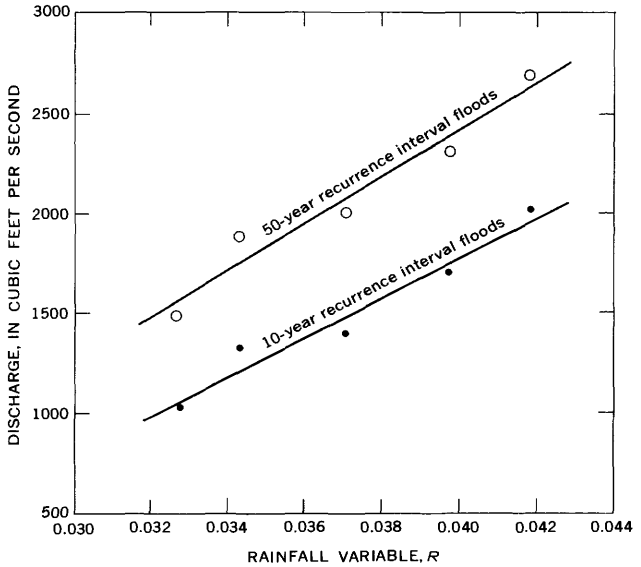

FIGURE 4.—Relation of the 10- and 50-year recurrence interval floods to the rainfall variable, R, for Wedowee Creek above Wedowee, Ala.

tions, P_2 and P_{50}, respectively. These variables were combined into a single rainfall variable, R, defined as

$$R=\frac{P_{50}-P_2}{\bar{P}} \quad (1)$$

The differences in the 10- and 50-year floods, from the curves of figure 3, are related to R in figure 4. These relations are of the form

$$Q_T=a+bR, \quad (2)$$

in which Q_T is the discharge corresponding to the recurrence interval T, and a and b are constants determined by the method of least-squares regression analysis. Values of P_{50} and P_2 can be obtained from U.S. Weather Bureau Technical Paper 40 (1961). Values for $\bar{P}$ can be determined from the U.S. Weather Bureau series, "Climates of the States" (U.S. Weather Bureau, 1959–60).

The specific relations developed for Jones Creek and Wedowee Creek along with the corresponding standard errors of estimate are given in table 1. The relations are all significant at the 0.05 significance level.

TABLE 1.—*Relations of* Q_T *versus* R *for* T=*10 and 50 years with corresponding standard errors of estimate, in cubic feet per second, for Jones Creek near Epes, Ala., and Wedowee Creek above Wedowee, Ala.*

Location	*Relations*	*Standard error of estimate (cfs)*
Jones Creek	$Q_{10}=227{,}400R-4{,}524$	124
	$Q_{50}=307{,}300R-6{,}140$	152
Wedowee Creek	$Q_{10}=97{,}550R-2{,}131$	101
	$Q_{50}=116{,}000R-2{,}239$	108

PROPOSED STEPS IN THE DETERMINATION OF A SYNTHESIZED FLOOD-FREQUENCY RELATION

Assuming that an adequate runoff-rainfall model is available, a synthesized flood-frequency relation can be determined by use of the technique described in this article. Below are the steps for determining the frequency relation.

1. Calibrate the runoff-rainfall model to be used in the extension of the peak-flow record with the observed at-site precipitation and streamflow records.
2. Compute synthesized peak runoff by using precipitation data from surrounding area long-term precipitation records. Peaks are synthesized by using the runoff-rainfall model and the calibration determined in step 1.
3. Determine the frequency curve for each set of peaks synthesized from each long-term precipitation record.
4. Obtain P_2 and P_{50} from U.S. Weather Bureau Technical Paper 40 (1961) and $\bar{P}$ from the U.S. Weather Bureau series "Climates of the States" (1959–60) for each long-term precipitation station.
5. Compute R from equation 1 for each long-term precipitation station.
6. Determine the selected T-year discharge, Q_T, from each of the computed frequency curves of step 3.
7. Determine the constants a and b of equation 2, by the method of least squares. These constants apply only to the selected recurrence interval. If the equation for a different recurrence interval is desired, a new set of constants must be determined.

8. Compute R by using values of P_2, P_{50}, and $\overline{P}$, as determined in step 4, for the stream basin under study.

9. Enter equation 2 by using the constants from step 7 and the R value from step 8, and compute Q_T for the basin studied.

10. Repeat steps 6, 7, and 9 for three or more values of T and plot the resulting Q_T versus T on probability or frequency paper. Determine a curve of best fit to obtain the desired synthesized flood-frequency relation.

A frequency curve computed in the above manner is shown in figure 5 for Wedowee Creek above Wedowee, Ala. Although eight annual flood peaks are not adequate to make a reliable comparison, the observed annual flood peaks for Wedowee Creek are plotted in figure 5 to show that no large discrepancy exists between observed and computed results.

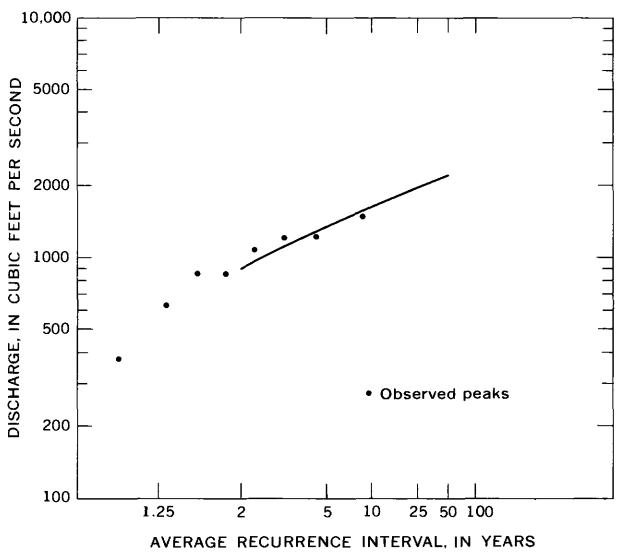

FIGURE 5.—Synthesized flood-frequency curve for Wedowee Creek above Wedowee, Ala., determined by the described techniques. Observed data shown for comparison.

DISCUSSION

The technique described in this paper may be applied most efficiently when a computerized runoff-rainfall model is used. With a graphical runoff-rainfall model, the procedure becomes time consuming because flood peaks for each stream site must be synthesized from three or more precipitation records. The synthesis of flows for several sites where several precipitation records per site are used often may require little more effort than the synthesis by an electronic computer of a single record per site.

Errors in a synthesized flood-frequency relation include those associated with the runoff-rainfall model and those resulting from the use of a nonrepresentative precipitation record. The methods described herein reduce the latter type of error. Their effectiveness in reducing the error is a function of the accuracy of the precipitation-characteristics maps and of the adequacy of the variables used.

At present, this method for determining flood-frequency curves by using long-term precipitation records has been investigated for only the two stream sites in the Alabama area. Thus, further work in synthesizing flood-frequency curves by using precipitation records is in order. However, the technique of adjusting flood-frequency relations instead of trying to adjust a precipitation record directly holds considerable promise, at least for areas similar to those of Alabama.

REFERENCES

Pattison, Allan, 1965, Synthesis of hourly rainfall data: Water Resources Research, v. 1, no. 4, p. 489–498.

Peirce, L. B., 1965, Flood-frequency synthesis for small streams, interim progress report: Alabama Highway Dept., Bur. of Research and Develop., HPR Rept. no. 11, 48 p.

U.S. Weather Bureau, 1959–1960, Climates of the States—Climatography of the United States: U.S. Weather Bureau series 60.

———1961, Rainfall frequency atlas of the United States: U.S. Weather Bureau Tech. Paper 40, 115 p.

FLOOD HEIGHT-FREQUENCY RELATIONS FOR THE PLAINS AREA IN MISSOURI

By E. EUGENE GANN, Rolla, Mo.

Work done in cooperation with the Missouri Division of Geological Survey and Water Resources and Missouri State Highway Commission

Abstract.—Regional relations are defined for estimating the heights of floods having recurrence intervals ranging from 1.2 to 50 years at natural flow sites in the plains area of Missouri. Drainage-area size is the only independent variable required. Average standard errors of the relations range from 21 percent for the 50- and 25-year floods to 35 percent for the 1.2-year flood. A method is presented for utilizing the relations at ungaged sites.

Regional flood height-frequency relations defined for the plains area of Missouri (fig. 1) can be used to estimate flood heights corresponding to selected frequencies at ungaged sites where natural floodflows and stream channels exist. These relations will be useful in the preliminary planning of proposed flood-plain developments.

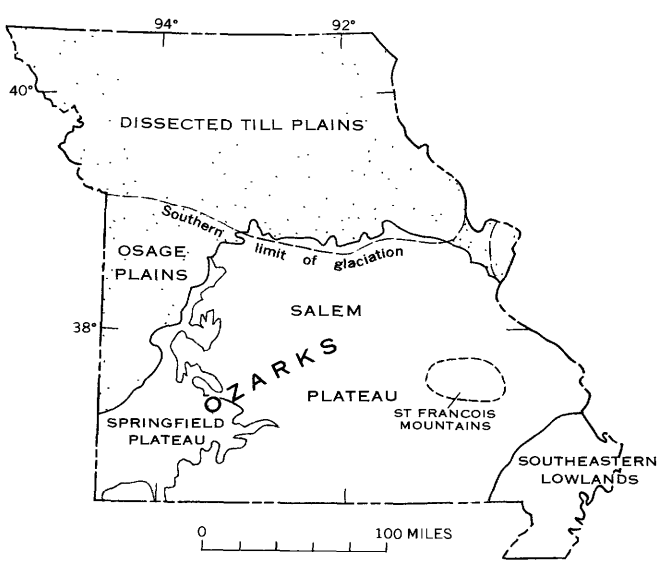

FIGURE 1.—Physiographic regions of Missouri. Area for which relations shown in figure 2 are applicable is shaded.

A study by Leopold and Maddock (1953) showed that for less than bankfull discharge a basin-wide relation exists between stream depth and discharge when discharge is of equal frequency of occurrence at all sites. They proposed a general equation of the form $d=cQ^f$, where d is the average cross-section depth, Q is the discharge of a given frequency at the section, and c and f are constants for a given frequency. Thomas (1964) found this type of relation applicable for greater than bankfull discharges in New Jersey, and for simplicity modified the equation to $h=cQ^f_{2.33}$, where h is the height of the water surface above the average channel bottom determined at time of median (50-percent duration) discharge, $Q_{2.33}$ is the mean annual flood discharge (recurrence interval of 2.33 years), and c and f are constants for a given frequency.

A further modification of Thomas' equation to $h=cA^f$, where A is the contributing drainage area, h is the height of the water surface above the elevation of the 50-percent duration discharge, and c and f are as previously defined, has been found to adequately describe the flood height–drainage area–frequency relation for the plains area in Missouri. These relations are presented graphically in figure 2.

The relations shown in figure 2 were defined from discharge-frequency and elevation-discharge curves at 81 stream-gaging stations. The higher frequency flood discharges were not defined for all 81 stations and only 42 and 47 stations were used to define, respectively, the 50- and 25-year flood relations.

Drainage areas for the stations used in defining the relations ranged from less than 1 square mile to 8,000 square miles. The 50-year flood discharge is not defined for drainage areas of less than 50 square miles in the plains area of Missouri; therefore, the extended 50-

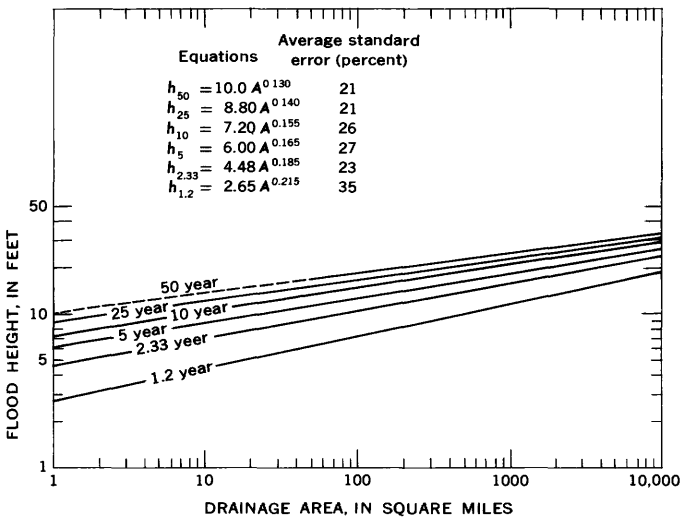

FIGURE 2.—Regional flood height–drainage area–frequency relations for the plains area in Missouri.

year relation is shown as a dashed line in figure 2 for drainage areas less than 50 square miles.

Values of the exponent f were found to range from 0.130 for the 50-year flood, to 0.215 for the 1.2-year flood, and values of the coefficient c ranged from 2.65 for the 1.2-year flood to 10.0 for the 50-year flood. Average standard errors, determined graphically, for the relations range from 21 percent for the 50- and 25-year floods to 35 percent for the 1.2-year flood.

The use of figure 2 requires knowledge of the elevation corresponding to the 50-percent duration discharge. This information must be estimated at an ungaged site. For most streams in the plains area of Missouri, the elevation of the 50-percent duration discharge is seldom found to exceed the elevation of zero flow by more than 1 foot. The elevation of zero flow corresponds to the lowest point at the upper end of the riffle just downstream from the point of interest, and it is suggested that the flood height be measured from the point of zero flow. When measuring flood height from the point of zero flow and for drainage areas larger than 100 square miles, add 1 foot to the values from figure 2 to adjust for the difference between the elevations of the 50-percent duration discharge and the point of zero flow.

The following examples will illustrate the use of figure 2.

Example 1: Assume that an estimate of the elevation of the 50-year flood is desired for a site on a stream draining 300 square miles in the plains area of Missouri.

Step 1: Determine the elevation of zero flow at the upper end of the first riffle downstream from the site. Assume an elevation of 600 feet above mean sea level for this example.

Step 2: Determine the flood height from figure 2 for a 300-square-mile drainage area and a 50-year flood to be 21 feet.

Step 3: Add 1 foot for drainage areas larger than 100 square miles. The desired elevation is therefore $600+21+1=622$ feet above mean sea level.

Example 2: Assume that a profile of the 50-year flood is desired for a 5-mile reach of the stream in example 1.

Step 1: Plot the low-water profile of the desired reach of stream from a topographic map.

Step 2: Determine the flood height for the desired frequency of flood from figure 2.

Step 3: Add flood height to low-water profile elevations to obtain the estimated flood profile for the desired frequency.

The relations described in this article are applicable only to sites where the floodflow and river channel are virtually natural. Less confidence may be placed in estimates from these relations than from estimates based upon computations using open-channel hydraulics formulas and detailed flood-peak estimating relations (Sandhaus and Skelton, 1968). Despite these limitations of use and accuracy, flood depths can be quickly and easily estimated from the presented relations and they should be useful for solving many common engineering and land-use planning problems.

REFERENCES

Leopold, L. B., and Maddock, Thomas, Jr., 1953, The hydraulic geometry of stream channels and some physiographic implications: U.S. Geol. Survey Prof. Paper 252, 57 p.

Sandhaus, E. H., and Skelton, John, 1968, Magnitude and frequency of Missouri floods: Missouri Div. Geol. Survey and Water Resources, Water Resources Report 23 [In press].

Thomas, D. M., 1964, Height-frequency relations for New Jersey floods: Art. 167 *in* U.S. Geol. Survey Prof. Paper 475–D, p. D202–D203.

AN EMPIRICAL FORMULA FOR DETERMINING THE AMOUNT OF DYE NEEDED FOR TIME-OF-TRAVEL MEASUREMENTS

By JAMES F. WILSON, JR., Cheyenne, Wyo.

Abstract.—Data from time-of-travel measurements in a wide variety of streams have been used empirically to relate the amount of rhodamine B dye required for slug injections to the volume of flowing water in a stream reach. The formula requires slight modification for low-flow or low-velocity measurements, or for use with Rhodamine WT, a newer dye for which sufficient field data are not yet available.

Since 1962 the U.S. Geological Survey has used fluorescent dyes routinely to measure time of travel and longitudinal dispersion of soluble materials in streams. Dilution gaging, the measurement of stream discharge, is a similar but separate activity. The only significant recurring problem in time-of-travel measurements has been determining the amount of dye required for a given situation. With little empirical data available, Buchanan (1964) and his colleagues developed the first rule-of-thumb formula for slug injections (continuous injections are rarely used), and it worked surprisingly well. By late 1965 a large number of time-of-travel measurements had been made with rhodamine B dye and its various solutions (such as DuPont Rhodamine BA) in a wide variety of streams. The writer has attempted to use those data to improve Buchanan's formula empirically. The result, although an improvement, is still not entirely satisfactory, but is reported here as the best available method to date for slug injections. Further improvements undoubtedly will be possible as more field data are collected.

Any dosage formula should be limited by safety at the high-concentration end of the scale and by the detectibility of the dye at the low-concentration end. To avoid any potential problems caused by imparting undesirable taste or discoloration to the water, and to maintain a high factor of safety, the U.S. Geological Survey has adopted 10 micrograms per liter as the maximum dye concentration, C_p, permitted at any water intake or similar critical feature along a stream (Wilson, 1968, p. 6). Field experience indicates that a minimum C_p of about 1 μg/l is necessary for adequate interpretation of the data, although less than 1 μg/l is sometimes acceptable. Within this range of 1–10 μg/l, economics is a factor—the use of more dye than necessary to produce a C_p of 1–2 μg/l at the lower end of a design reach is both wasteful and, for the larger streams, expensive.

A perfect dosage formula could be developed if it were possible to determine accurately in advance (1) the volume of flowing water in the reach, (2) the amount of dilution which will take place by the time the dye reaches the lower end of the reach, and (3) the amount of apparent loss of dye in the reach. Loss of dye, resulting either from a permanent decrease in fluorescence of the field samples or from a true loss of dye above the sampling site, is difficult to predict in advance. Losses depend on a variety of environmental conditions such as direct sunlight and water quality, which may destroy the dye or impair its ability to fluoresce; channel configuration, which may cause some of the dye to be held in storage; and aquatic vegetation and bed material, which attract and hold some of the dye by sorption.

Because of the difficulties in predicting dilution and dye loss, an empirical approach which ignored these two factors and was based on the volume of flowing water was attempted. Data from measurements on 49 reaches (most studies used more than one dose) are plotted in figure 1. Ordinates represent volume of dosage, V_d, in gallons of 40 percent rhodamine B (or DuPont Rhodamine BA) solution necessary to produce a C_p of exactly 1 μg/l at the lower end of the design reach. The amount of dye actually used was converted to equivalent gallons of 40-percent solution and divided by the observed C_p to obtain the plotting value. Con-

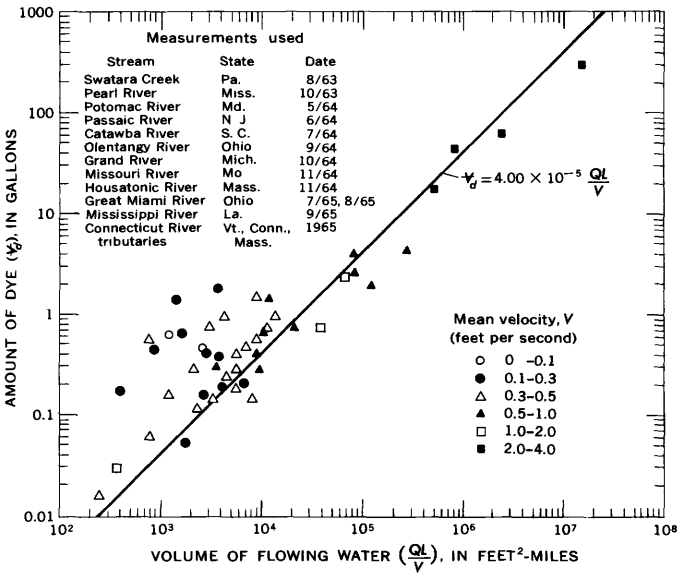

FIGURE 1.—Relationship of (1) the amount of 40-percent rhodamine B dye solution required to produce a peak concentration of 1 μg/l at lower end of reach to (2) the volume of flowing water in reach.

centrations usually are proportional to the amount of dye used. Abscissas represent the volume of flowing water in the design reach, defined as QL/V, where Q is the observed discharge in cubic feet per second, L is the reach length in miles, and V is the observed mean velocity of the dye in feet per second. For convenience the units are expressed as ft²-miles (derived from cfs×mile÷fps), to obtain a formula in terms of units normally used in the field. Cubic feet or gallons might have been used instead of ft²-miles, but with less convenience.

Variations in dispersion (primarily a function of velocity) and dye loss probably account for much of the scatter in figure 1. Human errors in data collection and analysis are probably much less significant. Rather than resorting to a least-squares method, the curve was placed by eye as a 45° line because a linear formula would be easier to use in the field and because such a curve, for the data used, is probably as meaningful as one defined mathematically. If only one curve is used, it must be conservative at the upper end because of the large amounts of dye involved. On the other hand, it is probably better to tend to overdose slightly, thus increasing the risk of wasted dye, than to underdose and risk wasting the time and effort put into the study by not being able to detect the dye adequately.

From the curve in figure 1, the following formula was derived for computing the amount, V_d, of 40-percent rhodamine B solution in gallons (regardless of specific gravity):

$$V_d = (4.00 \times 10^{-5}) \frac{QL}{V} C_p.$$

To use the formula for computing 40-percent rhodamine B in pounds, one should replace the coefficient 4.00×10^{-5} by 3.44×10^{-4}, for solutions with a specific gravity of 1.03 (DuPont Rhodamine BA, for example) and by 3.73×10^{-4}, for solutions with a specific gravity of 1.12 (common rhodamine B).

Discharge and reach length are usually known, whereas velocity must be estimated (the obvious weak point in any dosage formula). As a general rule, a C_p of 3 μg/l is recommended.

However, the distribution of the plotted points in figure 1 indicates that, unless modified, the above formula may cause slight overdosing on large fast streams, and serious underdosing on small slow streams. Hence, the value of C_p used in the formula may be modified by the user, on the basis of his experience and his evaluation of stream conditions.

For small slow streams, dye costs are not significant, and the user may increase C_p in the formula to 4–6 μg/l. Where long pools and very low velocities exist, a C_p as high as 9 or 10 μg/l should be used. Values greater than 10 μg/l should not be used. On larger streams with velocities greater than 2 fps, C_p may be reduced to as little as 1 μg/l for economy, with reasonable assurance of success. Data available to the writer for the October 1966 measurements on the Missouri River indicate that the formula calculated with a C_p of 1 μg/l would have produced observed values of C_p between 0.6 and 1.2 μg/l for the reaches in Missouri. The highest point in figure 1 represents a 125-mile reach of the Mississippi River in Louisiana at a discharge of 240,000 cfs. The lowest point represents a 2.8-mile reach of a tributary of the Connecticut River in Massachusetts at 38 cfs.

A newer dye, DuPont Rhodamine WT, available only in a 20-percent solution (specific gravity 1.19), exhibits better properties as a tracer than rhodamine B. Loss of Rhodamine WT in a given reach is usually smaller than that of rhodamine B. Because of its higher cost, Rhodamine WT has not until recently been used

for time-of-travel measurements, but its adoption for that purpose is growing. If the properties of the two dyes were the same, the coefficient in the above formula could simply be doubled to obtain the amount of 20-percent Rhodamine WT equivalent to 40-percent rhodamine B. However, it is reasonable to assume that comparatively less Rhodamine WT would be required because of its higher recovery potential. Empirical formulas for computing Rhodamine WT will not be possible until more measurements are made. In the meantime, increasing the coefficients in the above formula to 7.00×10^{-5} (for gallons) and 6.95×10^{-4} (for pounds) is, in the writer's opinion, a reasonable approach.

REFERENCES

Buchanan, T. J., 1964, Time of travel of soluble contaminants in streams: Am. Soc. Civil Engineers Proc., v. 90, no. SA 3, p. 1–12.

Wilson, J. F., 1968, Fluorometric procedures for dye tracing: U.S. Geol. Survey Techniques of Water-Resources Inv., Book 3, chap. A12, 31 p.

FLOOD-FLOW CHARACTERISTICS OF A RECTIFIED CHANNEL, JACKSON, MISSISSIPPI

By K. V. WILSON, Jackson, Miss.

Work done in cooperation with the city of Jackson

Abstract.—Extreme changes in velocity, stage, and Manning's roughness coefficient n were observed during the first year after construction of an earthen canal for Hanging Moss Creek at Jackson, Miss. The channel, constructed during the summer of 1963, had a 30-foot-wide bottom, 2:1 side slopes, and 12-foot depth. On March 2, 1964, velocities of 7.8 feet per second were observed at a 5½-foot depth in the clean channel and Manning's n was computed to be 0.025. By October 1964, velocities of 3.2 feet per second existed at a 5½-foot depth and Manning's n was computed to be 0.05 in the channel which was then lined with fairly thick vegetation consisting of small willows, weeds, and grasses. These observations indicate that the values of Manning's n commonly used in channel rectification are low, and that the carrying capacity of earthen channels may be reduced 100 percent as a result of only 1 year's growth of vegetation.

The Manning equation (1890, p. 161–207), one of the most commonly used open-channel flow formulas, is $Q=\frac{1.486}{n}AR^{2/3}S^{1/2}$, where Q is the discharge in cubic feet per second (cfs); n is a roughness coefficient, A is the cross-sectional area of the channel in square feet, R is the hydraulic radius in feet, and S is the energy gradient. All these factors are physical measurements with the exception of the roughness coefficient, which is estimated on the basis of values computed from known discharges. The n values shown herein for a newly constructed earthen channel are believed to be worthy of presentation. This appraisal of the flow-characteristics of a rectified channel of Hanging Moss Creek in Jackson, Miss., verifies the need for using high design friction values for earthen channels.

Values of Manning's n commonly used for designing earthen channels vary from 0.02 to 0.03. The carrying capacity of a channel is inversely related to this factor; therefore, if the n value is doubled, the carrying capacity is reduced 100 percent and damaging overflow may occur.

During the summer of 1963, the rectification of Hanging Moss Creek was extended 11,000 feet using the following design criteria:

1. 30-foot-wide-bottomed earthen channel with 2:1 side slopes approximately 12 feet deep.
2. Uniform grade of 0.0020 foot per foot for 2,500 feet downstream from U.S. Highway 51 and 0.0014 foot per foot for 2,500 feet upstream from U.S. Highway 51.
4. Discharge of 5,900 cfs in the vicinity of U.S. Highway 51, and
5. Roughness coefficient (Manning's n) of 0.045.

Elevations in this paper are referred to project datum, which is mean sea level, datum of 1929 with supplementary adjustment of 1941.

FLOOD-FLOW CHARACTERISTICS AT U.S. HIGHWAY 51

Flood data collected at the U.S. Highway 51 gage show an extreme variation in the characteristics of the new channel during the first year after canalization.

The design flow line of the new channel at the downstream side of U.S. Highway 51 was at an elevation of 269.91 feet which is the culvert flow line. Figure 1 shows the stage-velocity, stage-discharge, and stage-area relations as constructed, assuming Manning's n to be 0.045. Also shown on figure 1 are these same relations as measured in March 1964 and since October 1964. These relations reveal the following:

1. By March 2, 1964, the channel had degraded about half a foot and its cross-sectional area had increased considerably below an elevation of 272 feet. It had filled along its banks so that the total area of the channel between the elevations of 272 and 275 feet was about 10 percent less than the constructed area. The average velocity at the 275-foot stage was 7.8 feet per second, or

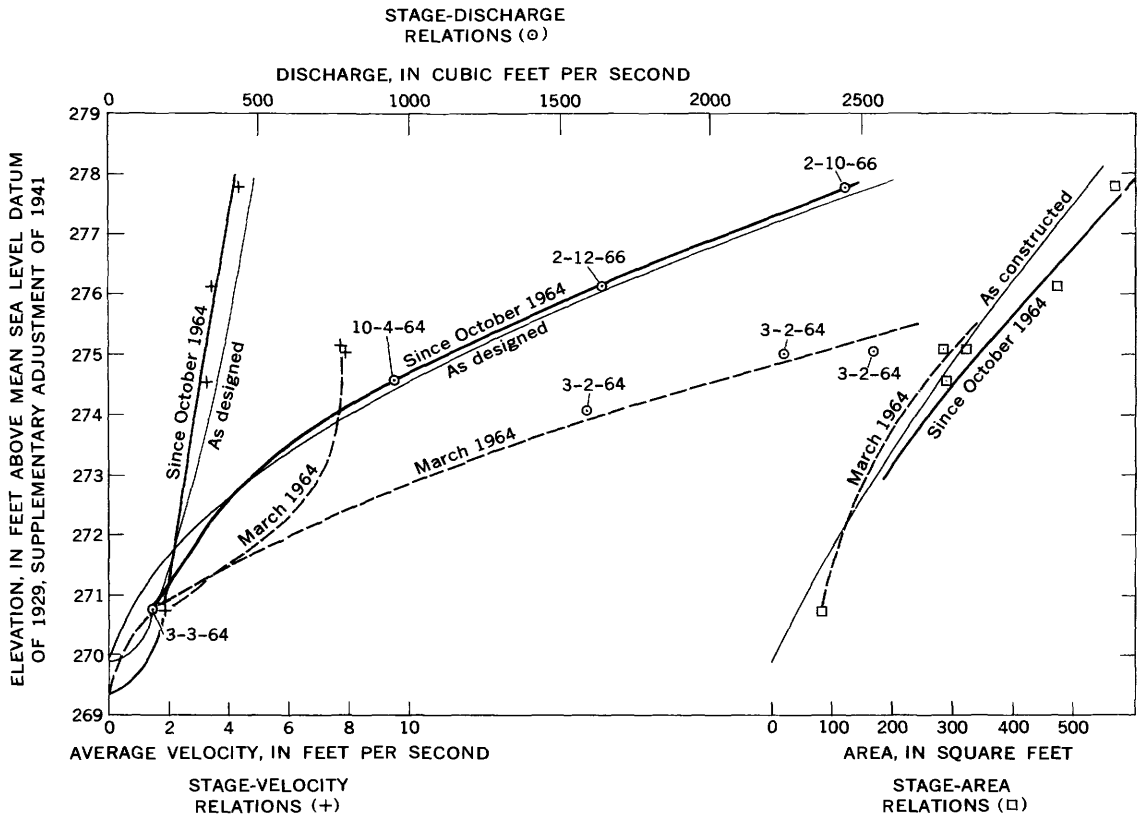

FIGURE 1.—Relation of stage to velocity, discharge, and area for an earthen canal constructed for Hanging Moss Creek at Jackson, Miss.

about double the design velocity. With this greatly increased velocity and slightly reduced area, the stage corresponding to the mean annual flood of 2,000 cfs was 274.5 feet, or 2.3 feet lower than the design stage of 276.8 feet.

2. By October 1964, moderately thick vegetation lined the new channel. The channel showed no further degrading, but erosion of the banks increased the channel area between elevations of 272 and 275 feet until it was, and presently is, about 10 percent larger than the constructed size. The average velocity at the 275-foot stage was reduced by the vegetation to only 3.2 feet per second which is less than the design velocity at that stage. With this slightly increased area but extremely reduced velocity, the stage-discharge relation shifted about 2 feet. The stage corresponding to the mean annual flood of 2,000 cfs was increased to 276.9 feet which is within 0.1 foot of the design stage of 276.8 feet.

Analysis of the above data indicates that the high velocity of March 1964 resulted from the newness of the channel whose friction value (Manning's n) was then computed to be only about 0.025. The low velocities since October 1964 resulted from the thick vegetation lining the channel, whose n value is now about 0.05.

Although the stages at U.S. Highway 51 are about as predicted, figure 1 shows that this is caused by channel erosion. If the channel had not eroded, the vegetation would have caused stages to be half a foot higher than those predicted. This condition exists at some points along the rectified channel of Hanging Moss Creek where less degrading or, perhaps, filling has taken place. One of these points is immediately downstream from Ridgewood Road.

FLOOD PROFILES OF FEBRUARY 10 AND MAY 21, 1966

Floods on Hanging Moss Creek on February 10 and May 21, 1966, had peak discharges of 2,500 and 2,400 cfs, respectively, at the gage at U.S. Highway 51. These peak discharges may be expected to be exceeded on the average of once in about 3 years. Profiles of these floods are shown on figure 2.

Moderately thick vegetation consisting of willows, weeds, and grasses presently line the channel. Effect of the vegetation on the flood profile is shown by an increase in stage downstream from Ridgewood Road.

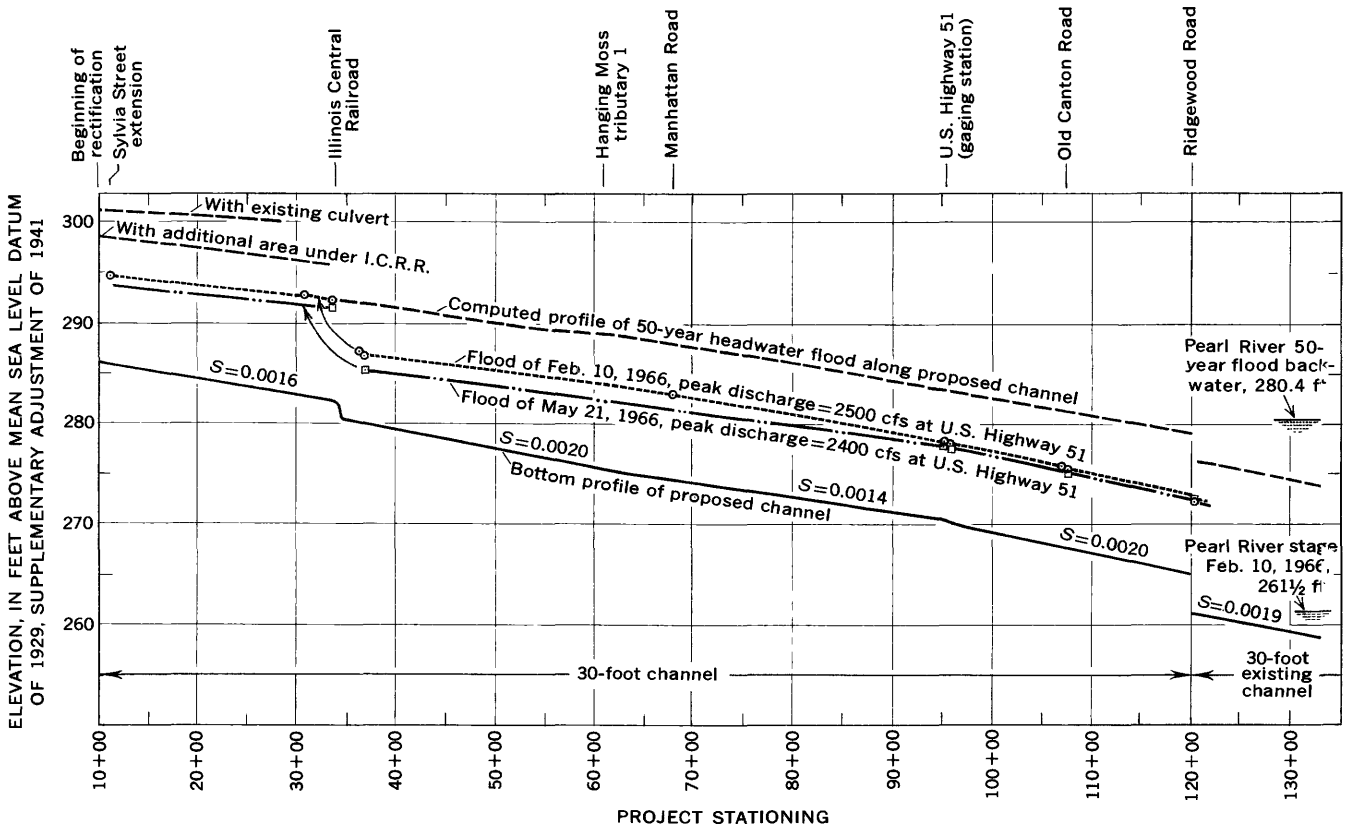

FIGURE 2.—Flood profiles of Hanging Moss Creek at Jackson, Miss.

The design depth for 2,500 cfs at that point is about 10 feet. The vegetation caused the depth on February 10 and May 21, 1966, to be increased to about 11 feet. This is the difference in the water surface elevation of 272 feet and the flowline of 261 feet (fig. 2).

In summary, values of Manning's n commonly used for designing earthen channels vary from 0.02 to 0.03. Observations presented herein indicate that these values are too low, and that the carrying capacity of earthen channels may be reduced 100 percent as a result of only 1 year's growth of vegetation.

REFERENCE

Manning, Robert, 1890, On the flow of water in open channels and pipes: Institution of Civil Engineers of Ireland [Dublin] Trans., v. 20, p. 161.

313-005 O—68——5

TEMPERATURE VARIATIONS OF DEEP FLOWING WELLS IN SOUTH DAKOTA

By D. G. ADOLPHSON and E. F. LeROUX, Rapid City, S. Dak., Huron, S. Dak.

Work done in cooperation with the South Dakota Water Resources Commission

Abstract.—Measurements from about 200 deep artesian wells in South Dakota indicate that temperature differences in water flowing from wells of similar construction are related to the depth of wells and volume of discharge. Geothermal gradients at wells in the Dakota Sandstone east of the Missouri River range from 0.7°C per 100 feet in the southeast and 1.1°C per 100 feet in the northeast to 1.6°C per 100 feet along the Missouri River. Immediately west of the river, geothermal gradients average 1.5°C per 100 feet. In a "hot water belt" farther west, average geothermal gradients of 2.2°C per 100 feet may be due to deep high-temperature recharge to the Dakota Sandstone. Relatively low geothermal gradients in pre-Cretaceous rocks in the Black Hills may be due, in part, to rapid downward movement of recharging water in very porous formations.

Artesian aquifers tapped by thousands of flowing and nonflowing wells underlie much of South Dakota. Wells have been developed in both the pre-Cretaceous and Cretaceous Systems.

Temperatures of water flowing from about 200 wells of similar construction have been found to be related to the depth of the well and the volume of discharge. For large volumes of discharge, the temperature of the water discharging at the surface is very nearly that of the water in the producing formation. For wells of low flow, the temperature of the discharging water has been cooled during the relatively slow movement of water up the casing and is not as representative of formation temperature. For example, in 1960 a well in western South Dakota, drilled to a depth of 2,225 feet in the Minnelusa Sandstone, flowed 75 gallons per minute at a temperature of 39°C (Celsius). By 1962 the flow had decreased to 24 gpm and the temperature to 36°C. In 1965 the flow was 7 gpm and the temperature 32°C, and in 1967 the flow was 3 gpm and the temperature 27°C.

The southeastern, northeastern, and western areas of the State, shown on figure 1, designate units within which water-temperature variations with depth and volume of discharge from flowing wells are characteristically similar. Temperature plots indicate that temperatures for flows of less than 20 gpm are not representative of formation temperatures. Lines in the graphs, computed by the least-squares method, show that most of the plots for small flows fall between 13° and 17°C, regardless of the depth of the well, whereas for wells flowing more than 20 gpm there is an increase in the temperature of water with increase in depth of wells.

SOUTHEASTERN AREA

Depth of well, temperature of water, and relative volume of discharge for 67 flowing wells that yield water from the Dakota Sandstone in the southeastern area are shown in figure 2. The measured temperatures of water discharged by flowing wells in the area ranged from 11°C for a well 200 feet deep, in Hutchinson County in the center of the area, to 24°C for a well

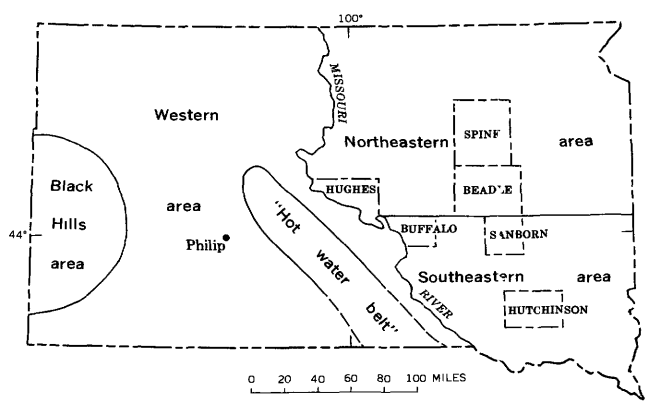

FIGURE 1.—Index map of South Dakota, showing approximate location of "hot water belt" and areas of similar geothermal gradients in the Dakota Sandstone.

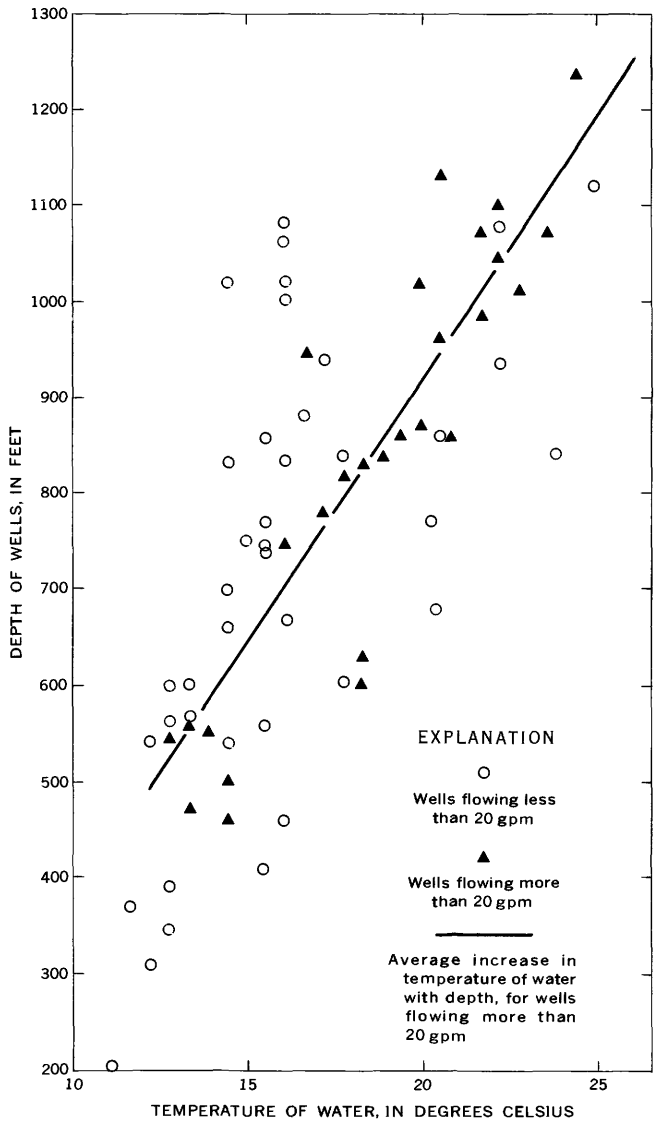

FIGURE 2.—Variations in water temperature with depth of well and volume of discharge for flowing wells in the Dakota Sandstone in southeastern South Dakota.

1,240 feet deep, in Buffalo County near the Missouri River. The average geothermal gradient in the southeastern area is 0.7°C per 100 feet.

NORTHEASTERN AREA

The 31 wells in the Dakota Sandstone represented by temperature and depth plots on figure 3 range in depth from 530 to 1,450 feet. Water temperatures range from 11° to 34°C. The water temperatures and geothermal gradients decrease eastward from the Missouri River. Temperatures as high as 34°C, and geothermal gradients of about 1.6°C per 100 feet are recorded for wells in Hughes and Buffalo Counties along the Missouri River. Farther east in Spink, Beadle, and Sanborn Counties, temperatures average about 20°C and geothermal gradients about 1.1°C per 100 feet.

WESTERN AREA

In the area immediately to the west of the Missouri River, known depths of wells flowing more than 20 gpm from the Dakota Sandstone range from 720 to 1,500 feet, and water temperatures range from 21° to 33°C (fig. 4, group *B*). Geothermal gradients at 22 wells average 1.5°C per 100 feet. Farther west there is a "hot water belt" (fig. 1) where well depths range from 1,180 to 1,830 feet and water temperatures from 36° to 54°C (fig. 4, group *A*). Geothermal gradients at 14 wells average 2.2°C per 100 ft. This "hot water belt" is in an area in which many of the deeper pre-Cretaceous formations are wedging out (Sandberg, 1962) and may be recharging the Dakota Sandstone (Hopkins and

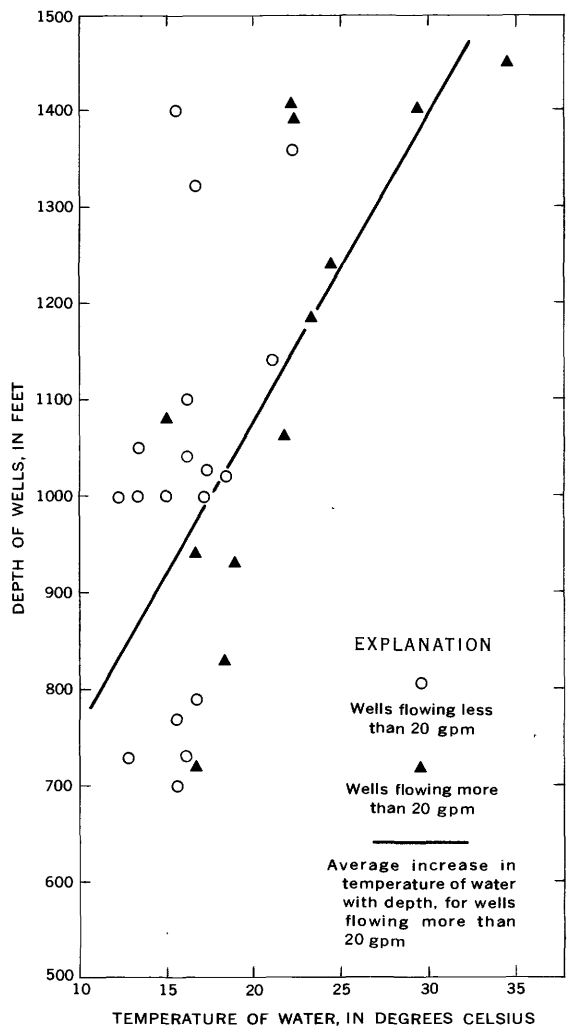

FIGURE 3.—Variations in water temperature with depth of well and volume of discharge for flowing wells in the Dakota Sandstone in northeastern South Dakota.

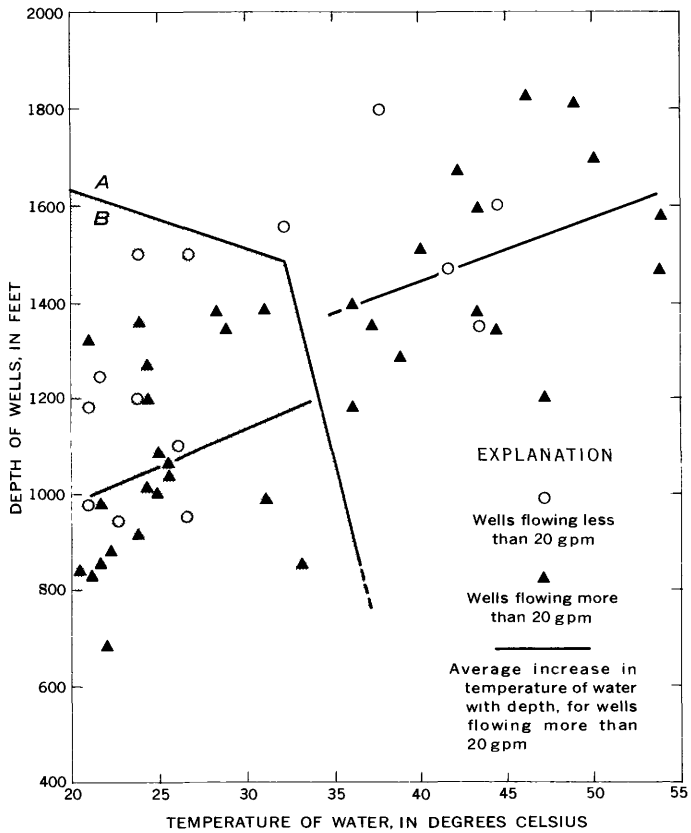

FIGURE 4.—Variations in water temperature with depth and volume of discharge for flowing wells in the Dakota Sandstone in western South Dakota. *A*, wells in "hot water belt;" *B* (shaded), other wells.

Petri, 1963) with high-temperature water. The municipal well at Philip, which is west of the "hot water belt," was drilled to a depth of 4,010 feet and produces 400 gpm from the pre-Cretaceous Madison Group at a temperature of 67°C.

BLACK HILLS AREA

Table 1 summarizes the water-temperature data for wells in the Black Hills area. The mean annual temperature in the area is about 8°C. Wells tap aquifers in the Pahasapa Limestone, Minnelusa Sandstone, Opeche Formation, Minnekahta Limestone, and the Spearfish Formation. Records are available for 42 wells ranging in depth from 300 feet near the outcrops to 4,900 feet 36 miles east of the outcrop area. Although the water temperatures range from 11° to 67°C, water temperatures of 26 wells ranging in depth from 300 to 1,300 feet are below 16°C.

The relatively low temperatures and geothermal gradients in the Black Hills area may be due to the rapid downward movement of recharging waters in very porous formations such as the Pahasapa Limestone. Or, it may be that, for many wells, a meaningful temperature gradient cannot be calculated because they are uncased holes which allow mixing of water from several aquifers (Cox, 1962).

TABLE 1.—*Summary of water-temperature data for wells in the Black Hills area, South Dakota*

Principal source	Well depth range (ft)	Temperature range (°C)	Average geothermal gradient (°C per 100 ft)
Spearfish Formation	400–560	11–17	1.3
Minnekahta Limestone	360–680	11–22	.9
Opeche Formation	640–1,310	12–16	.7
Minnelusa Formation	300–4,900	11–60	.7
Pahasapa Limestone	460–4,110	11–67	1.0
Average of 42 wells			0.9

CONCLUSIONS

Temperatures of water flowing from deep artesian wells are related to the depth of the well and the volume of discharge.

In South Dakota, temperatures and geothermal gradients at wells in the Dakota Sandstone generally decrease eastward from a "hot water belt" west of the Missouri River. The abnormally high geothermal gradients (Levorsen, 1958, p. 401) in the western area may be due to deep high-temperature recharge to the Dakota Sandstone. Throughout most of the eastern part of the State, where temperature gradients are more nearly normal, the Dakota Sandstone rests on crystalline basement rock and is not recharged from below.

The relatively low geothermal gradients computed for the Black Hills area may be due, in part, to rapid downward movement of recharging water in very porous formations.

REFERENCES

Cox, Earl, 1962, Preliminary report on the artesian water supplies from the Minnelusa and Pahasapa aquifers in the Spearfish-Belle Fourche area: South Dakota State Geol. Survey Spec. Rept. 19, p. 11.

Hopkins, W. B., and Petri, L. R., 1963, Geology and groundwater resources of the Lake Dakota plain area, South Dakota: U.S. Geol. Survey Water-Supply Paper 1539–T, p. 27–28.

Levorsen, A. I., 1958, Geology of petroleum: San Francisco, W. H. Freeman and Co., 703 p.

Sandberg, C. A., 1962, Geology of the Williston basin, North Dakota, Montana, and South Dakota, with reference to subsurface disposal of radioactive wastes: U.S. Geol. Survey Rept. TEI–809, open-file rept. 148 p.

THERMAL SPRINGS NEAR MIDWAY, UTAH

By C. H. BAKER, JR., Salt Lake City, Utah

Work done in cooperation with the
Utah Department of Natural Resources, Division of Water Rights

Abstract.—A group of thermal springs near Midway, Utah, is surrounded by a deposit of calcareous tufa that covers an area of about 4.5 square miles and locally is at least 70 feet thick. The springs include both flowing thermal springs and hot pots, which are small pools of warm water occupying shallow craters in the tops of conical or hemispherical mounds of tufa. Extinct hot pots (dry craters) and solid mounds of tufa as much as 10 feet high are also common. The water from the flowing springs and hot pots is not highly mineralized (the total dissolved solids rarely exceeds 2,000 mg/l), but it is saturated with respect to calcium carbonate. The spring water is of meteoric origin; it enters the carbonate bedrock in the nearby Wasatch Range and moves rapidly through fractures and solution openings. The geothermal gradient in the vicinity of Midway is abnormally high, but the reasons for the high heat flux are not known.

A group of thermal springs in western Wasatch County, Utah, presents some unusual geohydrologic features. The springs, known locally as the hot pots, are in secs. 26, 27, and 34, T. 3 S., R. 4 E., Salt Lake base line and meridian. The spring area surrounds the town of Midway on the west side of Heber Valley, one of a line of small valleys on the east flank of the Wasatch Range (fig. 1). The hot pots are surrounded by a deposit of calcareous tufa that covers an area of about 4.5 square miles and locally is at least 70 feet thick. The tufa deposit forms a low terrace that is underlain by alluvium; water apparently rises through the alluvium from a bedrock source.

The warm water and the unusual form of many of the springs attracted the attention of the earliest settlers in the area, and the water has been used by bathing resorts for many years. The fame of the hot pots is largely local, however, and no detailed hydrologic studies have been made in the area.

The hot pots were described briefly by Howell (1875, p. 256–257), who saw them in 1872. Emmons (Hague and Emmons, 1877, p. 317–319) called the hot pots "* * * a group of warm springs, the most important and considerable observed in this region * * *" and gave a general description of them, including a chemical analysis of a sample of tufa. Neither of these early observers offered any explanation of the source of the hot water. Heylmun (1966, p. 15) included the hot pots in a listing of thermal springs in Utah, and suggested that the source of the heat was "volcanic or tectonic." Milligan, Marsell, and Bagley (1966, p. 36)

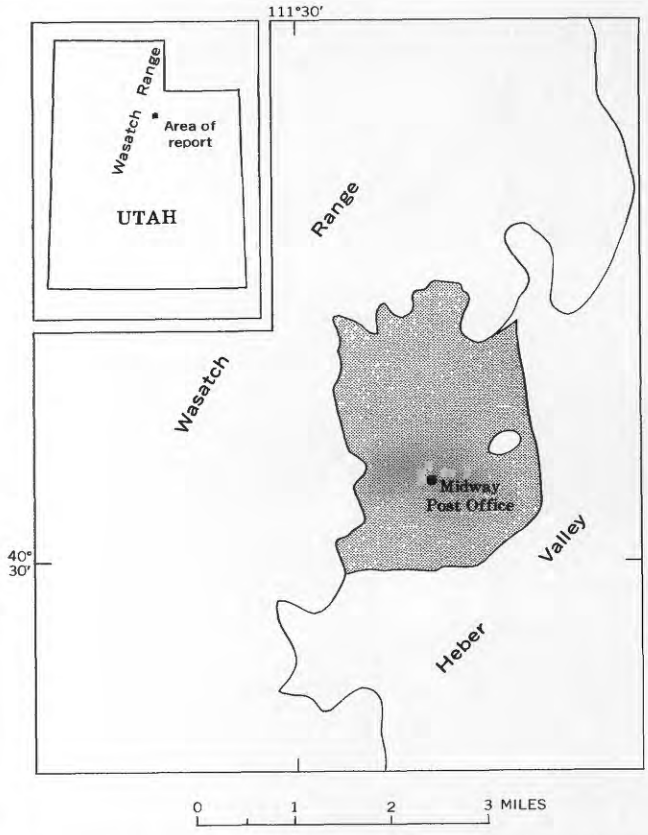

FIGURE 1.—Location of the area of thermal springs (shaded) near Midway, Utah.

described the hot pots briefly and speculated that their presence might indicate a zone of faulting beneath the alluvium from which they issue. The purpose of this report is to describe the hot pots as they presently exist and to offer some suggestions about their origin and history.

DESCRIPTION OF THE SPRINGS

Two kinds of thermal springs are found in the area—the typical hot pots, which generally do not flow, and a few warm springs which flow perenially. Chemical analyses of water from both types of spring indicate that it all comes from the same source. The typical hot pots are small pools that occupy craters in the tops of conical or hemispherical mounds of tufa (fig. 2). Most of the mounds are 10–25 feet in diameter and 3–10 feet high, but a few larger ones are as much as 50 feet in diameter and 15–20 feet high. One mound in the SW¼ sec. 27 is nearly 200 feet in diameter at the base and rises to a height of about 70 feet. The open craters do not extend to depths greater than 30–35 feet below the water surface; apparently the floors of the craters are built up by deposition of tufa only a little more slowly than are the sides. At the present time (1968), only two of these pots are known to overflow, and they discharge water only intermittently and in small quantity.

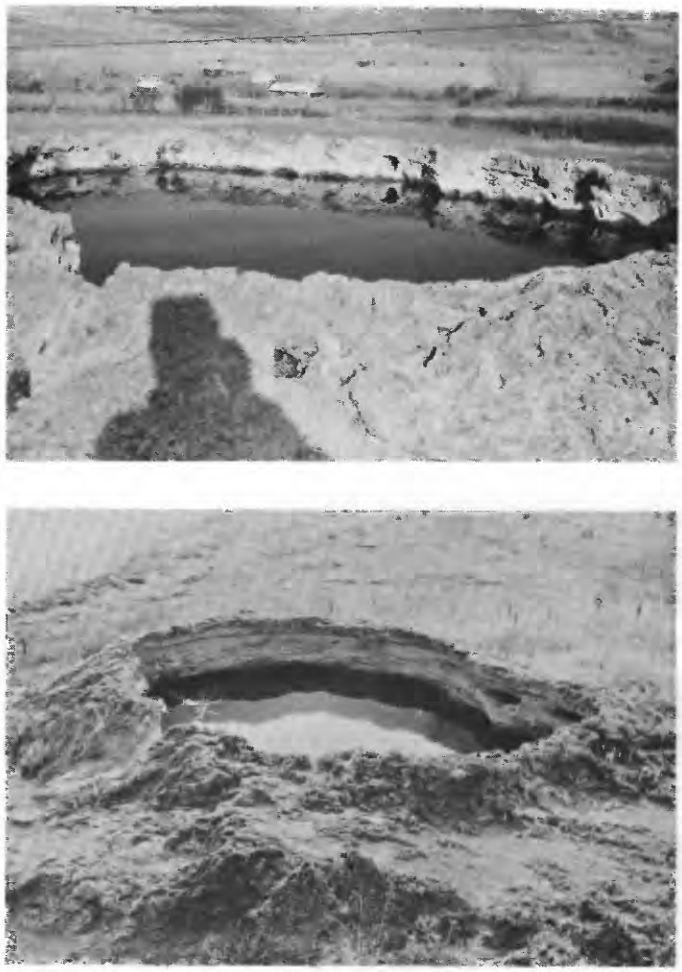

FIGURE 2.—Views of typical hot pots. Top, view northeastward across a water-filled crater. Opening is about 10 feet in diameter, and water level is 0.6 foot below rim. Bottom, view southeastward from point about 8 feet above the ground. Opening is 9 feet in diameter, and water level is 1.5 feet below rim; top of rim is about 5 feet above ground level on left side of photograph.

A few warm springs in the area, however, flow perennially. These springs issue from cracks in the tufa (fig. 3) or appear as seeps in areas where the tufa is covered with soil. None of the perennially flowing springs is surrounded by a mound of tufa. Seven such springs have been located in the area, and during 1967 they discharged a total of about 3,000 gallons per minute.

The typical hot pots are in two well-defined clusters. Each cluster includes some extinct pots identical in most respects with the typical hot pots, but with smooth dry floors a few feet below the rims of the craters. A third cluster of mounds contains no visible water; a few of the mounds have shallow dry craters, but most appear to consist of solid tufa (fig. 4). Each of the three clusters of mounds forms a broad, gently rounded shieldlike area, somewhat higher than the surrounding tufa. A fourth shieldlike area contains only a few low mounds and a single spring. The locations of the typical hot pots, flowing springs, and larger dry mounds are shown in figures 5 and 6.

Although most of the hot pots reportedly have not flowed for many years, circulation of warm water in the pots is sufficient to keep the temperature of the water well above the mean air temperature of the region

FIGURE 3.—Thermal spring flowing from an opening in a ledge of tufa. Stream is about 8 inches wide; discharge is about 200 gpm, and temperature is 46° C (≈114° F).

FIGURE 4.—Typical solid mound of tufa. Top is about 10 feet above ground level in foreground.

(about 6°C, or ≈43°F). The temperature of the water varies considerably from pot to pot, although within a single pot there is little variation from top to bottom. Water temperatures in the pots range from 12° to 40°C (≈54°–≈104°F), and pots a few tens of feet apart may have temperatures differing by as much as 17°C (≈30°F). The two pots that overflow have water temperatures of 32–34°C (≈89°–≈94°F) when they are flowing, but the temperatures drop as low as 30°C (≈86°F) during the periods of no flow. Water is withdrawn from four pots at bathing resorts; three of the pots have water temperatures of 40°C (≈104°F), the fourth has a temperature of 38°C (≈100°F). Water temperatures of the seven flowing springs range from 30° to 46°C (≈86°–≈114°F).

The altitude of the water surface, like the water temperature, is not uniform in the various pots, and some of the flowing springs are above some of the pots that do not flow (see figs. 5 and 6). Water levels within each cluster of pots are apparently independent of each other; one of the pots that occasionally overflows has a water surface as much as 8 feet above that of some of its nonflowing neighbors less than 100 feet away.

An automatic water-level recorder was installed on one of the nonflowing pots (location C–1, fig. 6*B*) in October 1966, and a thermograph was installed in May 1967. The thermograph was operated through October 1967 and the water-level recorder through September 1968. The record shows four kinds of water-level fluctuations. Slow seasonal changes of 2 or 3 feet undoubtedly represent changes in storage within the aquifer. The abrupt rises of 1 foot or more that occur during the spring and summer may result from pressure waves caused by addition of slugs of water (recharge) to the aquifer (see fig. 7). The small changes occurring during the autumn within a period of a few days correlate closely with changes in barometric pressure. Finally, the very small fluctuations, which occur daily and last for a few hours, seem to be related to circulation within the pot caused by cooling at the surface. No long-term temperature changes were recorded.

The hot pots support an abundant and varied biota. Algae, probably of several species, are plentiful in and around most of the hot pots and flowing thermal springs; and it is likely that some algae may be involved in the deposition of tufa. Numerous small (5–10 millimeters) crustaceans were collected by the author from many of the hot pots, and specimens were identified by Dr. S. B. Mulaik of the University of Utah as the amphipod *Hyalella azteca*, which is common in streams and ponds of the region. Microscopic life forms are also present, including probable diatoms and forms believed to be ostracods; but none of these was identified. The question of whether there are any life forms unique to the hot pots in this region would require detailed biologic study.

QUALITY OF THE WATER

Although the stagnant water in the nonflowing hot pots is opaque and murky green, brown, or black, water from the flowing springs, the occasional overflow from the two pots mentioned, and the water withdrawn from otherwise stagnant pots by the resorts are clear and colorless. Bubbles of odorless gas, possibly carbon dioxide, continually rise to the surface in most of the pots, and the gurgling noise from the flowing springs suggests that they too are giving off considerable quantities of gas.

Chemical analyses of water from several of the hot pots and flowing springs are shown in table 1. The water is not highly mineralized, but it is much more mineralized than other ground water in the area. The concentration of dissolved solids in six samples ranges from 1,710 to 2,040 milligrams per liter. The concentration of dissolved solids in water from wells and springs in the alluvium rarely exceeds 1,000 mg/l, and springs less than 1 mile from the hot pots yield cold water, from bedrock sources, having concentrations of dissolved solids of less than 500 mg/l.

Water from the hot pots and related thermal springs is unstable in the air at normal temperatures. When the water is exposed to the air, carbon dioxide escapes, the pH of the water increases, and calcium carbonate is precipitated. This fact is well illustrated by the changes that took place in a sample that was collected and stored. A sample of water was dipped from the surface in one of the hot pots (location C–3, fig. 6*B*) on October 17, 1967. The pH of the water was measured in the field, and the sample was filtered to remove any suspended sediment. An aliquot of the filtered sample was

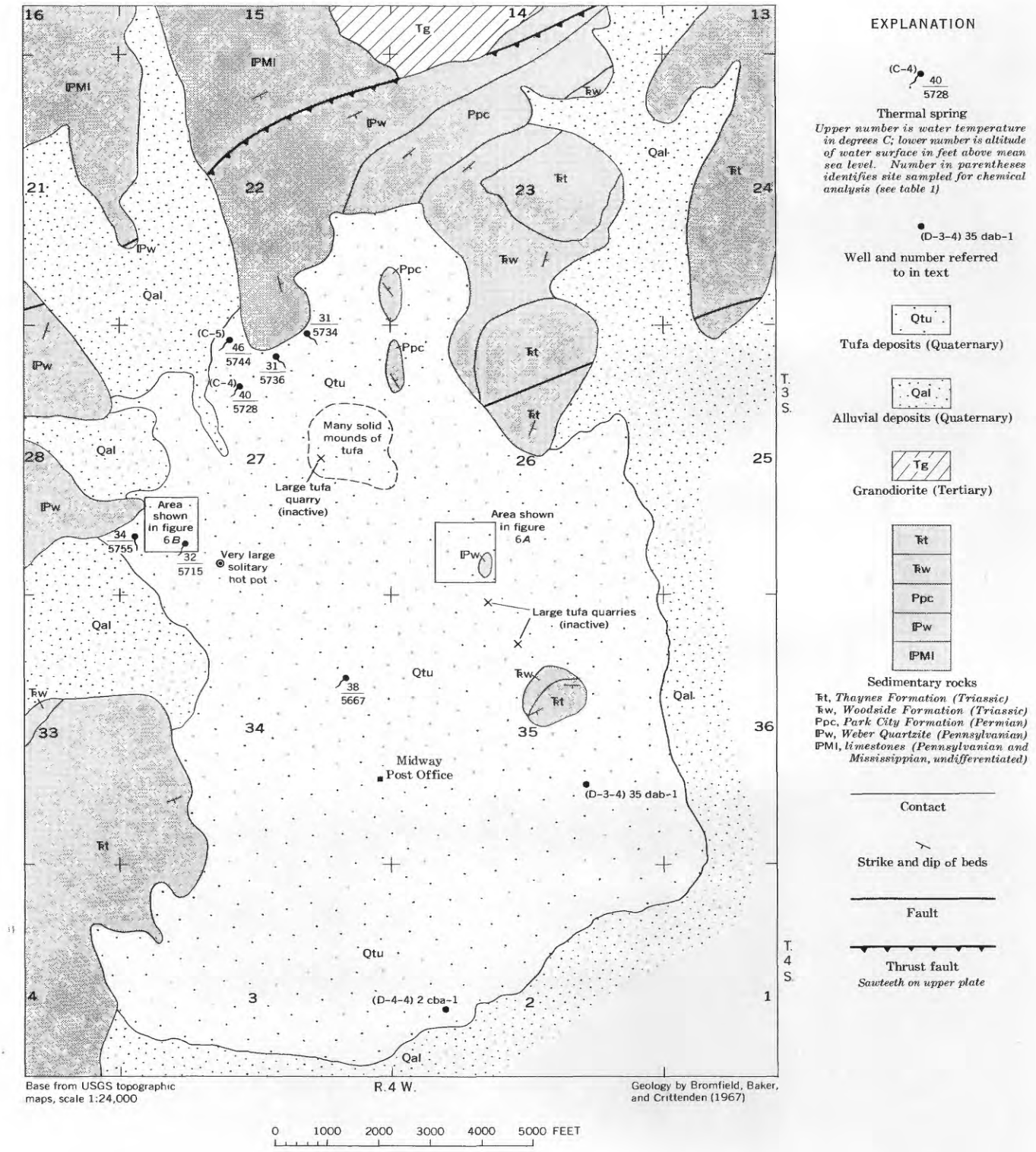

FIGURE 5.—Locations of flowing thermal springs and principal areas of hot pots and solid mounds of tufa. Location of map area shown on figure 1.

TABLE 1.—*Chemical analyses of water from hot pots and flowing thermal springs near Midway, Utah*

[Concentrations of dissolved constituents, dissolved solids, and hardness given in milligrams per liter. pH values in parentheses are calculated equilibrium values; see text for explanation]

Location number in figures 5 or 6	Date of collection	Temperature (° C)	Silica (SiO_2)	Calcium (Ca)	Magnesium (Mg)	Sodium (Na)	Potassium (K)	Bicarbonate (HCO_3)	Carbonate (CO_3)	Sulfate (SO_4)	Chloride (Cl)	Fluoride (F)	Nitrate (NO_3)	Boron (B)	Dissolved solids (residue on evaporation at 180°C)	Hardness as $CaCO_3$	Noncarbonate hardness as $CaCO_3$	Specific conductance (micromhos/cm at 25°C)	pH	Point of collection
Typical hot pot																				
C–1	9–28–66	29	21	353	72	125	28	716	0	702	115	2. 1	0. 1	0. 70	1, 840	1, 180	589	2, 330	7. 4 (6. 4)	Surface.
C–2	9–28–66	30	19	329	70	111	25	686	0	643	103	2. 2	. 1	. 64	1, 710	1, 110	545	2, 180	7. 7 (6. 5)	Do.
	[1] 10–17–67	34	------	315	68	----------		680	----------									2, 150	6. 8	Do.
	[1] 10–17–67	34	------	313	68	----------		676	----------									2, 150	6. 8	Depth of 20 ft.
C–3	5–15–67	28	21	329	88	163	33	584	0	805	150	2. 7	0	. 80	1, 980	1, 180	701	2, 610	7. 7 (6. 5)	Surface.
	[1] 10–17–67	32	------	394	76	----------		780	----------									2, 500	6. 8	Overflow.
	[1] 10–17–67	32	------	387	76	----------		770	----------									2, 600	6. 8	Depth of 23 ft.
C–6 [2]	9–28–66	40	23	331	68	114	25	674	0	661	108	2. 2	. 1	. 67	1, 730	1, 110	553	2, 200	7. 3 (6. 5)	End of pipe.
Flowing thermal spring																				
C–4 [3]	9–28–66	40	28	389	73	151	31	728	0	820	138	2. 5	0. 1	0. 79	2, 040	1, 270	673	2, 560	7. 3 (6. 4)	Discharge point.
C–5 [4]	9–13–67	46	27	345	83	148	16	644	0	742	132	2. 5	. 4	. 64	1, 910	1, 200	672	2, 410	7. 5 (6. 4)	Do.

[1] Determinations for bicarbonate, specific conductance, and pH are field determinations; calcium and magnesium concentrations were determined in the laboratory on samples acidified at the time of collection.
[2] Hot pot tapped by pipe driven into side of mound; discharge about 50 gpm.
[3] Discharge about 150 gpm.
[4] Discharge about 1,300 gpm.

titrated in the field to determine bicarbonate concentration, and another aliquot was acidified and sent to the laboratory for determination of calcium concentration. A clean 1-liter plastic bottle was filled with the filtered water, loosely capped, and stored. After 15 days the bottle was opened and the pH measured. A sample

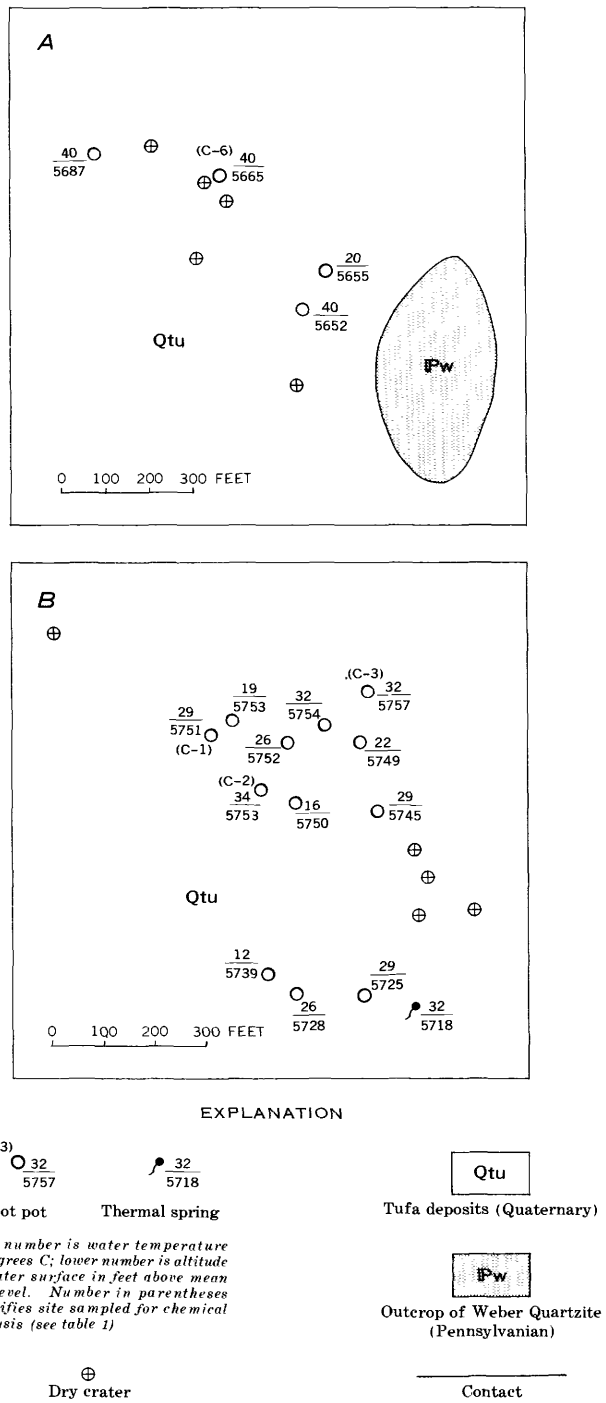

FIGURE 6.—Positions of hot pots and dry craters within the two principal clusters indicated in figure 5. *A*, eastern cluster; *B*, western cluster.

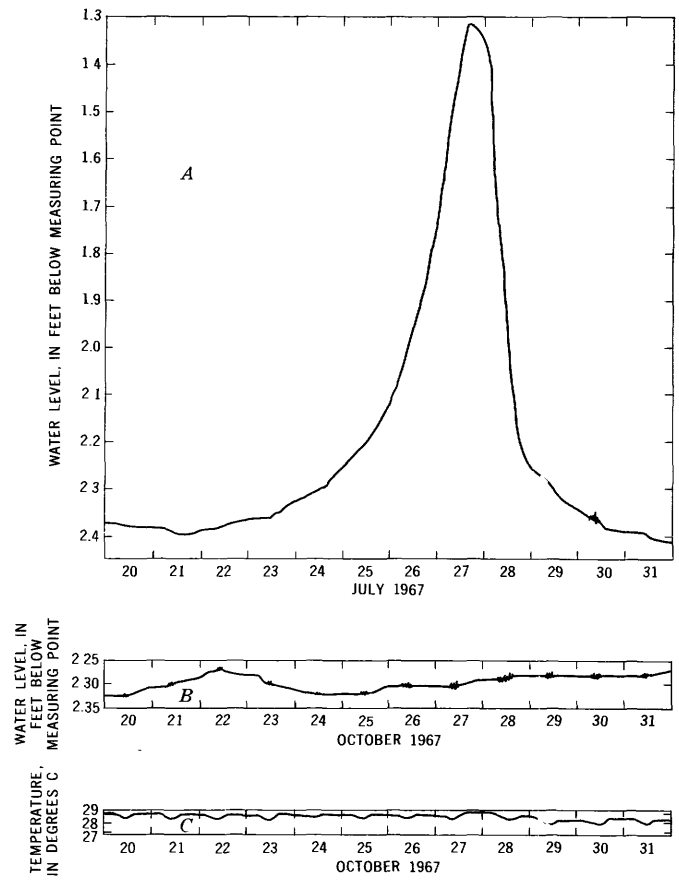

FIGURE 7.—Reproductions of charts from automatic recorders on hot pot at location C-1 (fig. 6*B*).
A, Hydrograph showing abrupt rise and fall of water level probably caused by slug of water (recharge) entering the aquifer.
B, Hydrograph showing small changes of water level caused by changes in barometric pressure and very small oscillations resulting from circulation of water within the pot due to cooling at the surface.
C, Thermograph record for the period covered by hydrograph *B*.

from the bottle was then filtered (a noticeable precipitate was present) and the concentrations of calcium and bicarbonate were determined in the laboratory. The procedure was repeated after 30 days and again after 45 days. The results are as follows:

	pH	Calcium (mg/l)	Bicarbonate (mg/l)
Field	6.8	[1] 394	780
15 days	7.3	335	644
30 days	7.5	208	276
45 days	7.7	164	122

[1] Acidified sample determined in the laboratory.

As a further comparison of the conditions existing in the laboratory and those prevailing in the aquifer, the pH required for the water samples to be in equi-

librium with calcite was calculated according to a method described by Hem (1961). The calculated equilibrium pH of all the samples was either 6.4 or 6.5 as compared to values of 7.3–7.7 measured in the laboratory and the value of 6.8 obtained in the field. The values for calculated pH at equilibrium with calcite are designated by footnote 1 in table 1.

From the foregoing, it can be seen that the hot pots, although not very active at present, are by no means extinct. Tufa is still being deposited around the orifices of the flowing springs and within the craters of the nonflowing hot pots.

TUFA DEPOSITS

The tufa that surrounds the spring area and forms the characteristic mounds around the typical hot pots is soft, porous, massive, buff to tan, and weathers to a dirty gray. When samples of the tufa were digested in dilute hydrochloric acid, 98 percent of the material was soluble. The insoluble residue consisted of about equal parts of silt-size quartz grains and organic material. The calcium-magnesium ratios of the tufa samples ranged from 106:1 to 140:1. The tufa is, therefore, nearly pure calcium carbonate, and has only traces of magnesium and a little insoluble debris. Fine concentric banding is visible on some polished surfaces of tufa; the shape of some of the banding and the presence of organic material in the residue suggest that algae may have been involved in at least some of the deposition.

Locally, at least, the tufa is moderately permeable; two shallow dug wells are known to obtain water from the tufa. The water from these wells is only weakly thermal; the temperature is about 12° C (≈53° F). A sample from one well contained 661 mg/l of dissolved solids—a much lower concentration than that of the thermal water.

Two drilled wells obtain water from gravel overlain by tufa. The locations of these two wells are shown in figure 5, and the drillers' logs of the wells are as follows:

Well (D–4–4)2cba–1

Material	Depth (feet)
Soil	2
Potrock (tufa)	38
Clay, sand, gravel, and boulders	78
Potrock (tufa)	84
Sand and gravel	87
Hardpan (tufa?)	98
Clay	105

Well (D–3–4)35dab–1

Material	Depth (feet)
Soil	5
Tufa	70
Gravel	86
Limestone (tufa?)	92
Sand and gravel	94

The fact that both these logs show a layer of tufa (potrock, limestone) at depth, overlain by alluvium, strongly suggests that the hot pots have been alternately active and dormant through at least two cycles of activity. Unfortunately, no information is available from greater depths to show whether other layers of tufa are also present.

GEOLOGIC RELATIONS

A geologic map of the area surrounding the hot pots (part of which is reproduced in fig. 5) was prepared by Bromfield, Baker, and Crittenden (1967). The geology of this part of the Wasatch Range is extremely complex, but the map does provide a basis for some speculation about the aquifer system that supplies water to the hot pots. Carbonate rocks of Mississippian and Pennsylvanian age crop out extensively in the high mountains north and west of Midway and are overlain by younger (Triassic) sedimentary rocks of low permeability. The sedimentary rocks dip steeply toward the valley. An intrusive body of Tertiary age crops out a short distance north of Midway, and the sedimentary rocks surrounding the intrusive are intensely fractured and faulted. According to C. S. Bromfield (oral commun., 1966), magnetic anomalies near Midway suggest that the intrusive body extends southeastward under the area of hot pots. If this is so, the fracturing of the sedimentary rocks in the vicinity of the intrusive body would provide the necessary break in the impermeable confining layers to permit water that is under artesian pressure in the carbonate rocks to escape to the surface.

The source of the heat is a more difficult question. The age of the intrusive body (30–35 million years according to Bromfield's data) seems to exclude it from consideration as a source of heat, and there is no evidence of more recent magmatic activity in the area. Mine operators a few miles north of Midway, however, report higher temperatures and flows of hot water in tunnels that approach or penetrate the intrusive rocks, indicating a higher-than-normal geothermal gradient. The causes of the abnormally high geothermal gradient are unknown.

INFERRED ORIGIN

The following theory of the origin and continued existence of the hot pots is proposed. Meteoric water enters the carbonate rocks in the Wasatch Range, descends along fractures and solution openings, and dissolves minerals from the rocks through which it passes. The mineralized water is heated at depth and, under artesian pressure, returns to the surface through fractures in the rocks. When the hot mineralized water nears the surface, the drop in confining pressure causes loss of dissolved carbon dioxide and resultant deposition of calcium carbonate (tufa). The velocity of the upwelling water maintains "pipes" (which may be no more than zones of higher permeability) through the

growing tufa deposit. Increased deposition around the point of emergence of each pipe would eventually form the characteristic mounds.

When the height of a mound reached the limit of the artesian head of the water, the spring would no longer flow. However, evaporation at the surface would maintain upwelling through the pipe, bringing fresh supplies of mineralized water to the surface. Tufa would under these conditions precipitate within the pipe, thus reducing upwelling and eventually blocking it entirely. At some point in the blocking process, upwelling would be unable to keep pace with evaporation; the temperature of the water within the pot would begin to decline; and the water level in the pot would respond more and more slowly to head changes in the aquifer. When the upwelling through the pipe was entirely blocked, water might be maintained in the mound by inflow of shallow (water-table) water; but if the closed floor of the crater is above the water table, it will eventually dry up. If the permeability of a pipe were very low, the spring might be only a seep; there would be no tendency to form an open crater, and the resulting mound would be nearly solid tufa, as are most of the mounds in one of the principal clusters.

Examples of each stage in the process described above are present in the area. At least seven thermal springs flow, but have no mounds surrounding them. Most of the mounds in the two principal clusters of hot pots contain water, but do not flow. Two of the pots do overflow occasionally, and the water temperature in these two mounds is higher than that of their nonflowing neighbors. Each cluster of mounds includes some extinct pots with dry craters, and one cluster contains mostly solid mounds. Finally, there is one recognizable crater in Midway that is nothing more than a wall of tufa less than 2 feet high enclosing a circular flat area a few feet in diameter.

Thus it appears that the formation of the hot pots is a continuing activity, which has been going on for many hundreds of years.

REFERENCES

Bromfield, C. S., Baker, A. A., and Crittenden, M. D., 1967, Geologic map of the Heber quadrangle, Wasatch and Summit Counties, Utah: U.S. Geol. Survey open-file rept., scale 1:24,000.

Hague, Arnold, and Emmons, S. F., 1877, Report of the United States geological exploration of the fortieth parallel, *in* U.S. Geological exploration of the fortieth parallel; v. 2, Descriptive geology: Prof. Papers of the Engineer Dept., U.S. Army, no. 18, 890 p.

Hem, J. D., 1961, Calculation and use of ion activity: U.S. Geol. Survey Water-Supply Paper 1535–C, 17 p.

Heylmun, E. B., 1966, Geothermal power potential in Utah: Utah Geol. and Mineralog. Survey Spec. Studies 14, 28 p.

Howell, E. E., 1875, Geology of portions of Utah, Nevada, Arizona, and New Mexico, explored and surveyed in 1872 and 1873, *in* Report upon geographical and geological explorations and surveys west of the one hundredth meridian; v. 3, Geology: Engineer Dept., U.S. Army, 681 p.

Milligan, J. H., Marsell, R. E., and Bagley, J. M., 1966, Mineralized springs in Utah and their effect on manageable water supplies: Utah Water Research Lab. Rept. WG23–6, Utah State Univ., 50 p.

GROUND-WATER DISCHARGE TOWARD GREAT SALT LAKE THROUGH VALLEY FILL IN THE JORDAN VALLEY, UTAH

By R. W. MOWER, Salt Lake City, Utah

Work done in cooperation with the
Utah Department of Natural Resources, Division of Water Rights

Abstract.—Ground water in the northern part of the Jordan Valley is principally under artesian conditions in valley fill of Quaternary age consisting of clay, silt, and sand. The water is moving generally toward the southeast shore of Great Salt Lake. The computed quantity of water discharging into Great Salt Lake from the valley fill in the northern part of the Jordan Valley is estimated to be a maximum of 7,000 acre-feet per year.

The amount of ground water that is moving toward Great Salt Lake in the northern part of the Jordan Valley was determined as a result of an investigation of the water resources of Salt Lake County, Utah. The amount of ground water could not be measured directly; but an estimate was made using Darcy's law, $Q = PIA$, where Q is the amount of water flowing through a selected cross section of the saturated aquifer, P is the average permeability of the saturated materials, I is the existing hydraulic gradient, and A is the area of the cross section.

The main aquifer in the northern part of the Jordan Valley is valley fill consisting of strata of clay, silt, and sand. The water in the valley fill is under artesian conditions, with the clay and silt acting as the confining beds. Because these confining beds themselves are slightly permeable, some water moves slowly upward, eventually arrives at the land surface, and is discharged by evapotranspiration. Most of the ground water, however, probably moves horizontally and is discharged to Great Salt Lake, although some water is pumped from wells near the west end of the Kennecott Copper Corp. tailings pond.

The section used was along a line about 15 miles long near the north end of the Jordan Valley (fig. 1). The section coincided in part with the line of a refraction seismic study that was reported by Arnow and Mattick (1968). On the basis of the seismic work and interpretation of the logs of several nearby wells, Arnow and Mattick suggested that the valley fill is divided into units of Tertiary and Quaternary age (fig. 2). They found, also, that the seismic velocities in the Tertiary unit are characteristic of semiconsolidated sediments and that seismic velocities in the Quaternary unit are characteristic of unconsolidated water-saturated sediments. The maximum thickness of the Quaternary valley fill, computed by Arnow and Mattick, is 2,480 feet at shotpoint 9, the eastern end of their line. However, the total thickness of the valley fill may be as great as 4,000 feet east of shotpoint 9 (R. E. Mattick, written commun., 1968), and much or all of it is of Quaternary age.

The east end of the section investigated by Arnow and Mattick was extended a distance of 2.2 miles eastward from shotpoint 9 to an outcrop of Maxfield Limestone of Cambrian age (Marsell and Threet, 1960) that marks the east edge of the valley. The extension was made on the basis of a determination of the depth to bedrock by R. E. Mattick (written commun., 1968) using gravity data obtained by Cook and Berg (1961). The valley fill reaches its maximum thickness at about the point where the extrapolated trace of the seismic profile crosses the Jordan River, and from there it thins eastward toward the limestone outcrop. It is assumed that all the valley fill east of shotpoint 9 is saturated, and that it is all or mostly of Quaternary age.

The west end of the section defined by Arnow and Mattick was first extended 0.4 mile south-southwestward to Kennecott Copper Corp. well 3 that penetrated limestone (according to the driller's log)—probably a unit of the Oquirrh Formation—at 185 feet, and then extended 0.2 mile southwestward to an outcrop of limestone of the Oquirrh Formation (Tooker and Roberts, 1961). It is assumed that all the valley fill south of shotpoint 1 is saturated, and that it is mostly

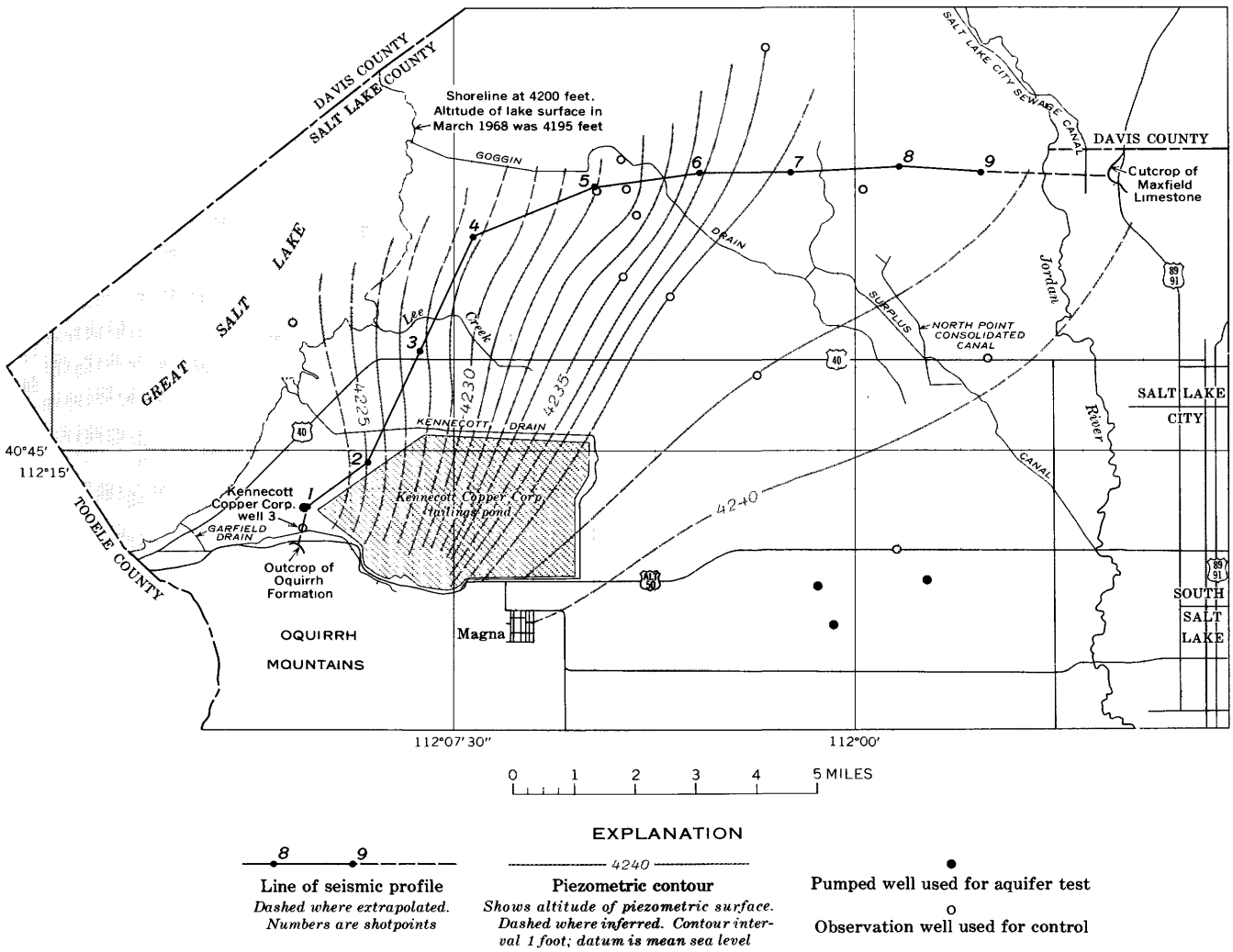

FIGURE 1.—Map of the northern part of the Jordan Valley, Utah, showing line of seismic profile, locations of observation wells, and piezometric contours, September 1967.

of Quaternary age. A small amount of water is discharged from valley fill of Tertiary age in this part of the section, where the upper part of the Tertiary fill may be as permeable as the Quaternary fill. The discharge from the Tertiary fill near the north end of the Oquirrh Mountains is lumped, in this report, with discharge from the Quaternary fill.

In order to determine the field coefficient of permeability (the amount of water in gallons per day that flows through a cross-sectional area of 1 square foot under a hydraulic gradient of 100 percent at the prevailing temperature) along the section of valley fill, aquifer tests were made by pumping four wells. The wells range in depth from 840 to 1,200 feet and tap from 400 to 600 feet of Quaternary deposits. The determined range of the coefficients of permeability is from 215 to 310 gallons per day per square foot, and the average is 260 gallons per day per square foot. Although the aquifer tests were made about 6 miles south of the central part of the section (fig. 1), a study of gamma-ray and lithologic logs of wells in the area between the section and the aquifer-test sites indicates that the texture of the Quaternary deposits is relatively uniform. Several beds can be correlated throughout most of the area, and only slight areal variation exists in the texture of the sediments. The average coefficient of permeability, therefore, which was determined for the aquifer tests, can be applied to the entire section with little error.

The hydraulic gradient across the section was determined from a map of the piezometric surface of water in a selected bed (fig. 1). The top of the bed, which was determined from gamma-ray logs, lies between 480 and 580 feet below the land surface, and

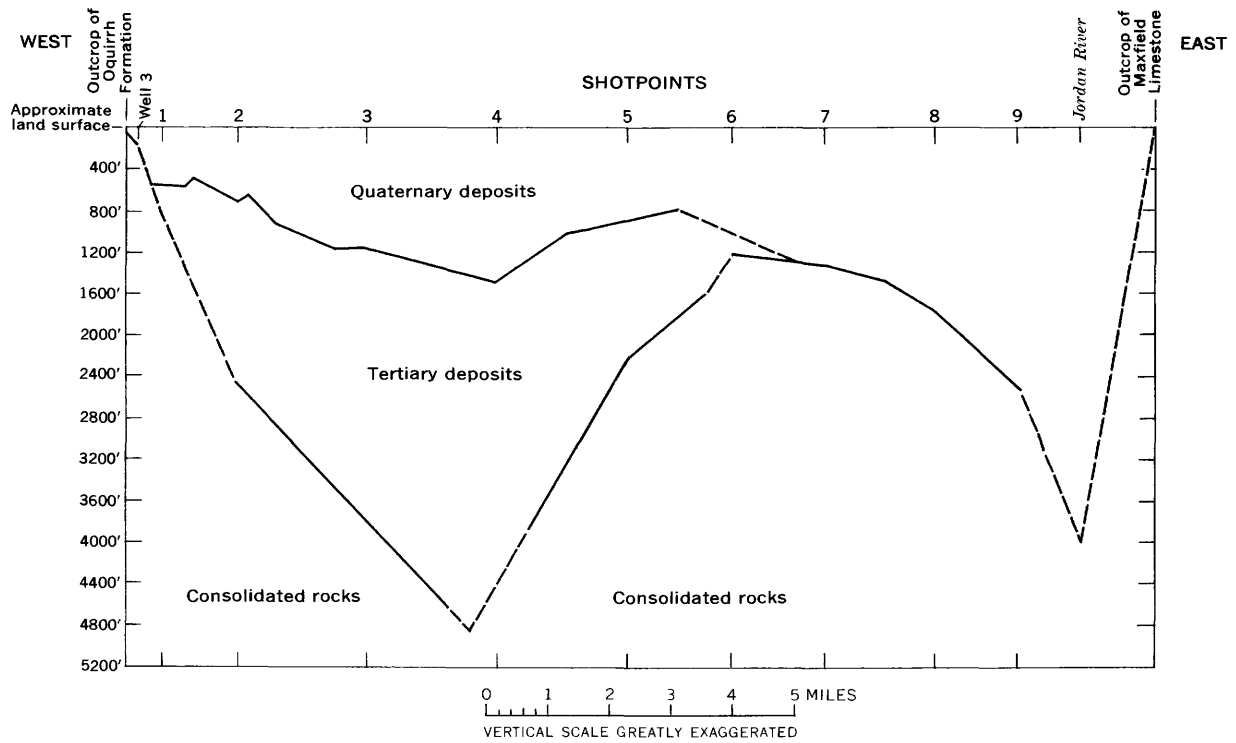

FIGURE 2.—Computed and extrapolated depth of three velocity layers along a seismic profile in the northern part of the Jordan Valley, Utah. (Section between shot points 1 and 9 after Arnow and Mattick, 1968, fig. 2.)

the bed is about 100 feet thick. The piezometric surface of the bed was from 10 to 15 feet higher than that for shallower beds, but the hydraulic gradient was about the same in all beds. The magnitude of the hydraulic gradient is independent of discharge by evapotranspiration, because evapotranspiration per unit area is similar south and north of the section.

In order to calculate the hydraulic gradient as accurately as possible, the section was divided into 10 segments. Each segment is the reach of the section between adjacent shotpoints on the seismic profile, and at the ends of the profile the segment is the reach between the end shotpoint and the nearest bedrock outcrop. The hydraulic gradient was not normal to the section for the full reach of any segment; therefore, it was necessary to compute the component of hydraulic gradient normal to the section at each segment (table 1). The component of hydraulic gradient normal to the section at individual segments ranges from 0.2 to 4.0 feet per mile, and averages 1.4 feet per mile.

Discharge was computed by applying Darcy's law to the various segments of the section and then totaling the results. As shown in table 1, the discharge across the section in the northern part of the Jordan Valley is estimated to be 8,000 acre-feet a year. Of this amount, about 1,000 acre-feet of water is flowing past the two westernmost segments; most of this water is being diverted toward a well field near the west end of the Kennecott Copper Corp. tailings pond. Some of the remaining 7,000 acre-feet of water is discharged by evapotranspiration, but most of the water is discharged as underflow into Great Salt Lake.

TABLE 1.—*Average saturated thickness, length, hydraulic gradient, and discharge by segment of a selected west-east profile across the northern part of the Jordan Valley*

Segment between—	Average saturated thickness of segment (feet)	Length of segment (miles)	Component of hydraulic gradient normal to cross section by segment (feet per mile)	Discharge (acre-feet per year)
West end and shotpoint 1.	400	0.6	4.0	280
Shotpoints 1 and 2	[1] 700	1.2	2.4	590
2 and 3	975	2.1	2.9	1,730
3 and 4	1,325	2.1	2.5	2,030
4 and 5	1,100	2.2	1.6	1,130
5 and 6	875	1.7	1.2	520
6 and 7	1,200	1.5	1.2	630
7 and 8	1,475	1.8	.3	230
8 and 9	2,100	1.3	.2	160
Shotpoint 9 and east end.	2,600	2.2	.2	330
Total (rounded)				8 000

[1] Includes the upper 125 feet of the Tertiary deposits.

REFERENCES

Arnow, Ted, and Mattick, R. E., 1968, Thickness of valley fill in the Jordan Valley east of Great Salt Lake, Utah, *in* Geological Survey Research 1968: U.S. Geol. Survey Prof. Paper 600–B, p. B79–B82.

Cook, K. L., and Berg, J. W., Jr., 1961, Regional gravity survey along the central and southern Wasatch Front, Utah: U.S. Geol. Survey Prof. Paper 316–E, p. 75–89.

Marsell, R. E., and Threet, R. L., 1960, Geologic map of Salt Lake County, Utah: Utah Geol. and Mineralog. Survey Map 15.

Tooker, E. W., and Roberts, R. J., 1961, Preliminary geologic map and sections of the north end of the Oquirrh Range (Mills Junction, Garfield, and Magna 7½-minute quadrangles), Tooele and Salt Lake Counties, Utah: U.S. Geol. Survey Mineral Inv. Map MF–240.

A WATER-BALANCE EQUATION FOR THE RATHDRUM PRAIRIE GROUND-WATER RESERVOIR, NEAR SPOKANE, WASHINGTON

By E. J. PLUHOWSKI and C. A. THOMAS,
Washington, D.C., Boise, Idaho

Abstract.—The highly permeable sand and gravel deposits which form the Rathdrum Prairie aquifer effectively store and transmit large quantities of ground water. From a water-balance equation for the ground-water reservoir, it is estimated that underflow from the aquifer to the Spokane Valley averages about 1,000 cubic feet per second, or about 650 million gallons a day. This water enters the Spokane River in the reach between Otis Orchards and Long Lake, Wash.

The Rathdrum Prairie, in western Idaho, near Spokane, Wash., is underlain chiefly by sand and gravel that overlie an impervious granitic rock floor. The highly permeable outwash deposits, commonly several hundred feet thick, constitute the Rathdrum Prairie aquifer, which has a capacity to store and transmit large quantities of ground water. Surrounding the prairie are highlands formed by granitic and metamorphic Precambrian rocks of low permeability.

As shown in figure 1, the regional flow of ground water is southwestward toward the head of the Spokane Valley. The coarse deposits beneath the Spokane Valley form a conduit that transmits an estimated 1,000 cfs (cubic feet per second) westward toward and beyond Spokane. Much of this ground water is discharged into the main stem of the Spokane River, although a significant part enters the Little Spokane River below Dartford, Wash. The well-sustained low-flow characteristics of both rivers are due, in large measure, to the outflow of water from the Rathdrum Prairie aquifer.

The principal sources of recharge to the aquifer are (a) direct infiltration of precipitation and irrigation water on the low-lying prairie region, (b) seepage from the numerous lakes along the perimeter of the prairie, (c) absorption of surface waters which originate in the surrounding uplands and flow onto but do not cross the prairie, and (d) seepage from the Spokane River. A quantitative assessment of the recharge contributed by each source must be made to evaluate ground-water outflow from the Rathdrum Prairie aquifer into the Spokane Valley conduit. The principal unknown factors in such an evaluation are (1) the quantity of recharge resulting from unconsumed precipitation falling directly on the sand and gravel deposits of the prairie, (2) the quantity of recharge derived from seepage from Coeur d'Alene Lake and the Spokane River, and (3) the volume of underflow from Pend Oreille Lake.

To simplify computations, the ground-water basin above the gaging station on the Spokane River near Otis Orchards was selected for study. The characteristics of the river change from those of an influent or "losing" stream above the station to those of an effluent of "gaining" stream downstream. Because of the strategic location of this gage, it is possible to ascribe much of the observed gain to streamflow immediately downstream to outflow from the aquifer and to attribute the loss of streamflow upstream to recharge of the aquifer by the river. A water-balance equation was prepared for the ground-water reservoir above Otis Orchards by equating recharge to discharge plus or minus any significant storage change. To insure data compatibility, the 50-year period (1911–60) was selected as a base period for all computations. The long base period minimizes the effect of storage fluctuations, which show no net change during the period, so that this factor may be eliminated from the water-balance equation. All short-term precipitation and streamflow records were extended to the base period by correlation with nearby long-term stations.

Recharge to the ground-water reservoir is defined as follows:

$$\text{Recharge}=P-E-SW_x+GW_1+I_r, \quad (1)$$

where

P=precipitation,
E=evapotranspiration,
SW_x=direct runoff,
GW_1=underflow into the basin, and
I_r=return flow from irrigation water.

U.S. GEOL. SURVEY PROF. PAPER 600-D, PAGES D75-D78

313-005 O—68——6

Discharge from the ground-water reservoir is defined as follows:

$$\text{Discharge} = GW_d + GW_u + GW_{et}, \quad (2)$$

where

GW_d=ground-water discharge to streams,
GW_u=underflow out of the basin, and
GW_{et}=ground-water evapotranspiration.

Owing to the fact that the water table is far below land surface in most of the basin, items GW_d and GW_{et} may be omitted from equation 2. Direct runoff (SW_x) may be omitted from equation 1 because the highly permeable sand and gravel in the valley absorb practically all surface flows. Equating equation 1 and 2 and eliminating negligible factors, we have

$$GW_u = P - E + GW_1 + I_r. \quad (3)$$

Under natural conditions, $P-E$ is equal to water yield or the unconsumed water which is available to become surface flow or ground water after all other demands on precipitation have been satisfied. Water yield was computed by a method developed by W. B. Langbein and outlined in the Raft River basin report (Nace and others, 1961, p. 36–47). Figure 2 shows the principal physiographic units of the Rathdrum Prairie basin and the computed water yield. Water yield ranges from about 3 inches at the head of the Spokane Valley to more than 25 inches at some of the higher elevations along the periphery of the basin. Total water yield generated within the basin itself is estimated to be 530 cfs, or 9.7 inches.

The principal sources of underflow (GW_1) to the Rathdrum Prairie aquifer system are Coeur d'Alene Lake, Pend Oreille Lake, and the Spokane River. A detailed water-budget analysis of Coeur d'Alene Lake shows that seepage from the lake and the reach of the Spokane River above Post Falls is about 250 cfs. From the long-term streamflow records on the Spokane River near Otis Orchards, Wash., and at Post Falls, Idaho, recharge along the reach between the gaging stations is estimated to be 120 cfs. Approximately 100 cfs is diverted from the river for irrigation purposes near

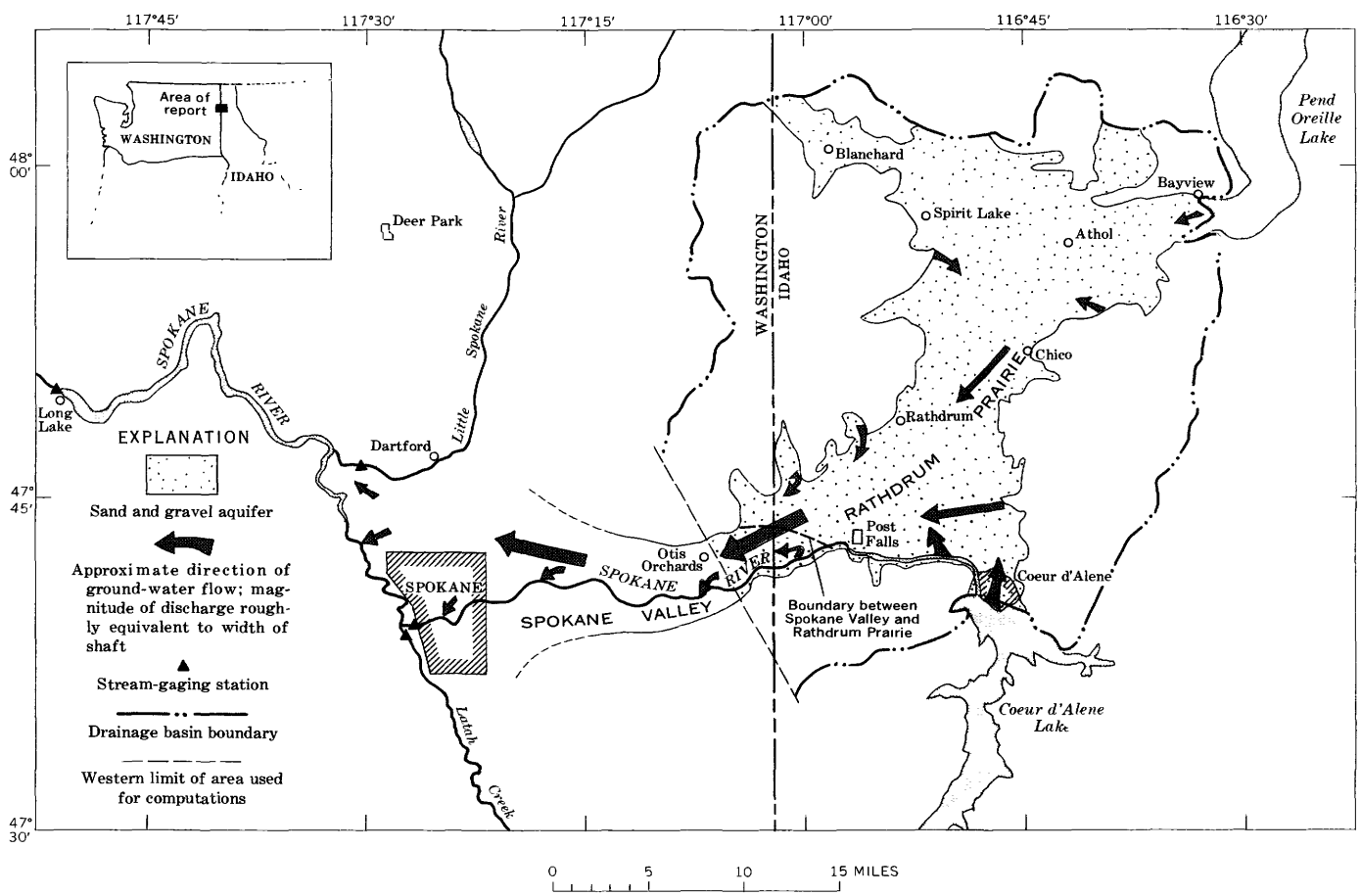

FIGURE 1.—Map of the Rathdrum Prairie basin, showing the regional pattern of ground-water flow.

Post Falls, and the assumption is made that half of this flow becomes recharge to the aquifer.

To estimate the water yield from the Rathdrum Prairie above Otis Orchards, a water budget was prepared for the Spokane River. Below the city of Spokane, Wash., the river flows on nearly impermeable basaltic bedrock, so that virtually the entire water yield of the Spokane River basin is measured at the Long Lake gage. The water yield generated in the intervening drainage area between the "at Long Lake" and "near Otis Orchards" stations is computed to be 720 cfs (column 2, table 1). This value was subtracted from the long-term streamflow "at Long Lake" (7,800 cfs), giving 7,080 cfs as an estimate of the water yield above Otis Orchards.

A second estimate of water yield at Otis Orchards was made by computing surface runoff and underflow past the station. The Spokane River is influent above Otis Orchards, so that all water entering the ground-water reservoir above this site is eventually discharged as underflow beneath the gaging station. Thus, water yield above Otis Orchards is equal to the observed streamflow at that point plus ground-water discharge under the gaging station (past the western limit of area used for computations, figs. 1 and 2). The necessary computations are shown in the right-hand part (columns 4–6) of table 1. Estimates of recharge to the Rathdrum Prairie aquifer from all sources except that received from Pend Oreille Lake are listed and summed (950 cfs) in column 5 of table 1. Adding this value to the gaged streamflow at Otis Orchards (6,080 cfs) yields 7,030 cfs, a figure which reflects water yield above Otis Orchards based on runoff from all upstream sources except that received from Pend Oreille Lake. Subtracting this esti-

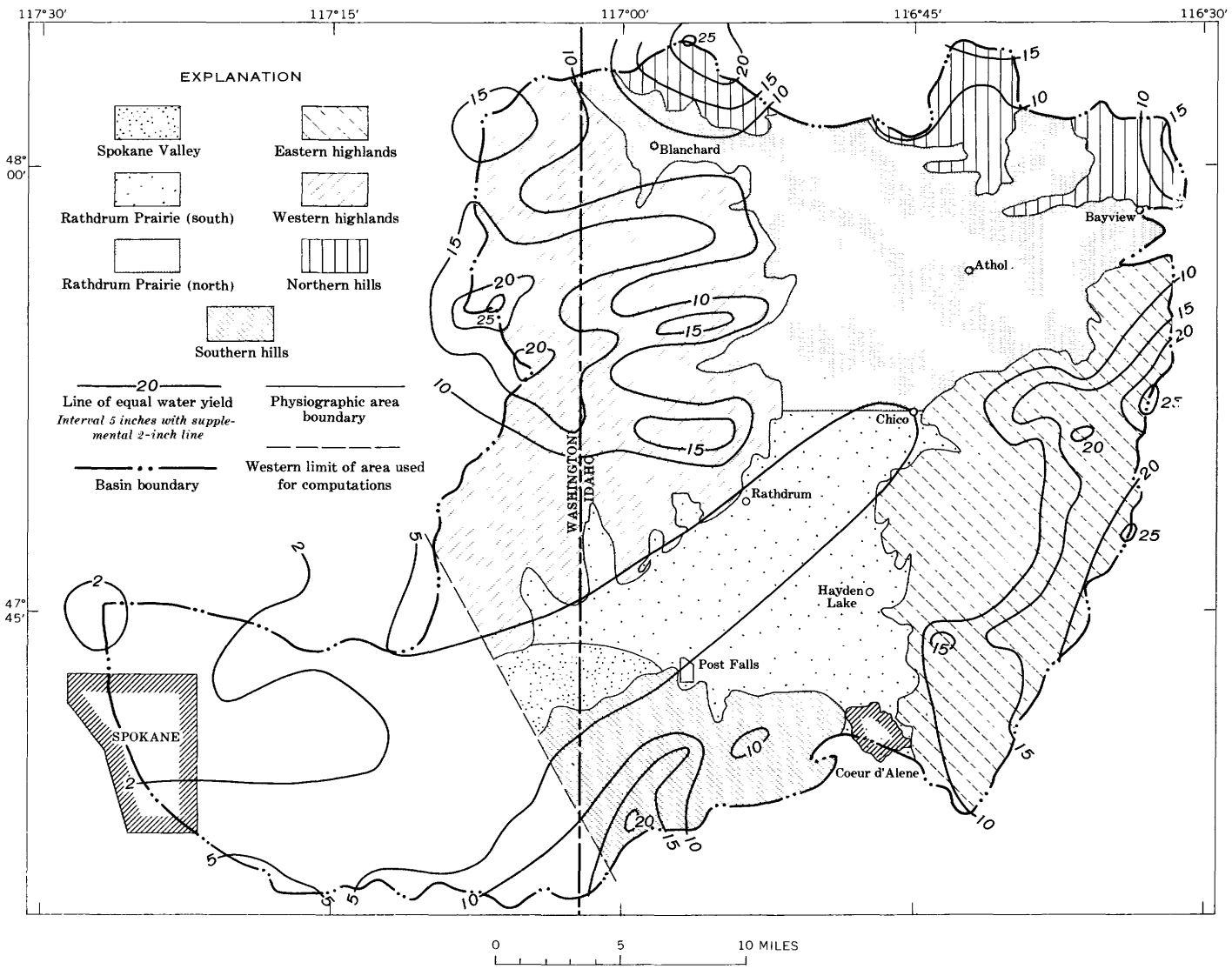

FIGURE 2.—Map showing the principal physiographic subdivisions and provisional water yield for the Rathdrum Prairie basin.

TABLE 1.—*Water budget for the Spokane River above Long Lake, Wash.*

Drainage unit	Discharge (cfs)		Drainage unit	Discharge (cfs)	
(1)	(2)	(3)	(4)	(5)	(6)
Water yield above station at Long Lake			**Water yield above station near Otis Orchards**		
Observed surface runoff:			Observed surface runoff:		
Spokane River at Long Lake		7,800	Spokane River near Otis Orchards		6,080
Observed or estimated runoff from intervening areas between Long Lake and Otis Orchards gaging stations:			Estimated accretions to the Rathdrum Prairie aquifer:		
Ungaged area between gages at Spokane and Long Lake.	70		Recharge from the Rathdrum Prairie Valley	530	
Little Spokane River at Dartford	360		Recharge from reach of Spokane River between Coeur d'Alene and Post Falls and from Coeur d'Alene Lake.	250	
Latah (Hangman) Creek at Spokane	240		Recharge from reach of Spokane River between Post Falls and Otis Orchards.	120	
Spokane Valley between Otis Orchards and gage at Spokane.	50		Return flow from irrigated areas	50	
Total runoff from intervening area	720		Total ground water from all sources except Pend Oreille Lake.	950	

mate of water yield from that previously computed (7,080 cfs) gives 50 cfs as an estimate of the underflow to the Rathdrum Prairie from Pend Oreille Lake. This quantity is very small when compared to the magnitude of the estimates used in the water budget and should, therefore, be considered to indicate an order of magnitude only. Because of complicated and poorly known subsurface flow conditions in parts of the prairie, particularly near Spirit Lake and Blanchard, the indicated water yield of 530 cfs to the Rathdrum Prairie aquifer system may be somewhat in error. When these factors are considered, the actual contribution to the aquifer from Pend Oreille Lake may be as much as 200 cfs. Accordingly, the actual total underflow to the aquifer, which reflects recharge from irrigated areas, the Spokane River, and Coeur d'Alene and Pend Oreille Lakes, is estimated to range from 370 to 570 cfs. For computation purposes, underflow is estimated to be 420 cfs, which is equal to the sum of the underflow from (a) Coeur d'Alene Lake and the Spokane River above Post Falls (250 cfs), (b) the reach of the Spokane River between Otis Orchards and Post Falls (120 cfs), and (c) Pend Oreille Lake (50 cfs).

Estimates of all factors required to solve equation 3 have now been made. Substituting back in equation 3, we obtain:

$$GW_u = 530 \text{ cfs} + 420 \text{ cfs} + 50 \text{ cfs} = 1{,}000 \text{ cfs}.$$

This estimate of average underflow from the Rathdrum Prairie basin is in agreement with estimates made by Piper and La Rocque (1944, p. 90) of at least 1,000 cfs, or about 650 million gallons per day. Approximately 80 to 90 percent of the underflow enters the main stem of the Spokane between Long Lake and Otis Orchards; the remainder enters the Little Spokane River, principally in the reach below Dartford, Wash.

REFERENCES

Nace, R. L., and others 1961, Water resources of the Raft River basin, Idaho-Utah: U.S. Geological Survey Water-Supply Paper 1587, 138 p.

Piper, A. M., and La Rocque, G. A., Jr., 1944, Water-table fluctuations in the Spokane Valley and contiguous area, Washington-Idaho: U.S. Geological Survey Water-Supply Paper 889-B, p. 83-139.

GLACIER OUTBURST FLOODS IN THE PACIFIC NORTHWEST

By DONALD RICHARDSON, Tacoma, Wash.

Abstract.—Glacier outburst floods, not uncommon in the Pacific Northwest in late summer or fall, are sometimes triggered by heavy rain but may occur even during a rainless period. Associated mudflows often compound the destruction downstream. Outburst floods are particularly hazardous at Mount Rainier, Wash., where debris flows are reported to occur at a rate of one in 3–10 years. Several floods witnessed at Mount Rainier were much larger than expected from direct storm runoff or release of water temporarily impounded by landslides. The principal source of those floods is believed to have been the large volumes of water that are stored at times within and beneath glaciers. At present there is no known way of predicting glacier outburst floods. Conceivably, their imminence might be indicated by measurements of englacial water pressure, and their potential size would be indicated by determinations of the volume of water stored in glaciers.

Glacier outburst floods, sometimes referred to by the Icelandic term "jökulhlaups," are a common occurrence at many places where there are active temperate glaciers. A jökulhlaup can be an awesome spectacle—an impressive display of powerful forces of nature. When a large amount of water is suddenly released at the head of a steep mountain valley containing loose alluvial and glacial deposits, the results can be very destructive. In this article some eyewitness accounts are given of floods that were affected by, or were the direct result of, glacier outbursts in the Pacific Northwest. Most of these floods were observed on the south side of Mount Rainier, Wash. (fig. 1). Crandell and Mullineaux (1967, p. 20) estimate that debris flows and floods not caused by volcanic activity probably have occurred at Mount Rainier at a rate of one in 3–10 years.

DESCRIPTION OF OUTBURST FLOODS

Nisqually River

In October 1926, a flood occurred on the upper Nisqually River during the first heavy rain at the end of the summer. The old Nisqually Glacier bridge was damaged so severely that it was temporarily closed. There is no record of the size of the flood, but on the basis of the reported damage to the bridge the flow must have been at least several thousand cubic feet per second (100–200 cubic meters per second). As the drainage area at the Nisqually Glacier bridge is only 6.2 square miles (16 square kilometers), the unit runoff during the peak flow was probably on the order of 1,000 cubic feet per second per square mile (11 m^3/sec/km^2). Direct storm runoff of such intensity is exceedingly rare in the Pacific Northwest (see later discussion of storm runoff), and it is suggested, therefore, that a glacier outburst was likely a contributing factor in the flood of October 1926. A concrete bridge, completed soon after the old bridge was damaged, was destroyed by an outburst flood in October 1932.

The Nisqually Glacier jökulhlaup of October 14, 1932, was the first of several that are known to have been witnessed in Mount Rainier National Park. The following description of the flood is from a monthly report of activities in the park, prepared by Park Superintendent O. A. Tomlinson:

> The outstanding occurrence of the month was the flood or "wash" from the Nisqually Glacier about noon, October 14 which destroyed the Nisqually River reinforced concrete bridge. Following several days' heavy rains a landslide above a series of three or four catch basins on the lateral moraine and on the glacier itself released large quantities of accumulated water which swept down over the glacier and down stream carrying away the bridge which was one-half mile below the end of the ice. The landslide occurred slightly more than a quarter mile above the snout of the glacier. Millions of gallons of water were suddenly released carrying rock and debris from the top and end of the glacier. By the time this moving mass reached the bridge it was approximately 25 feet high and 150 feet wide. The force of the impact carried away the entire center span which was of reinforced concrete 55 feet long and 27 feet wide with massive railings, a sidewalk, and heavy false arch curtains * * *. This heavy concrete structure was carried more than half a mile down stream before the force of the flood diminished sufficiently to permit it to settle on the river bar.
>
> A party of visitors were eating lunch on the parking area at the west end of the bridge when they heard the roar and saw the wall of water, mud, and rock moving toward them. Before they could start their automobile and escape the rushing water had covered the parking area and almost washed the car away. Three of the party were thoroughly wet to their knees and

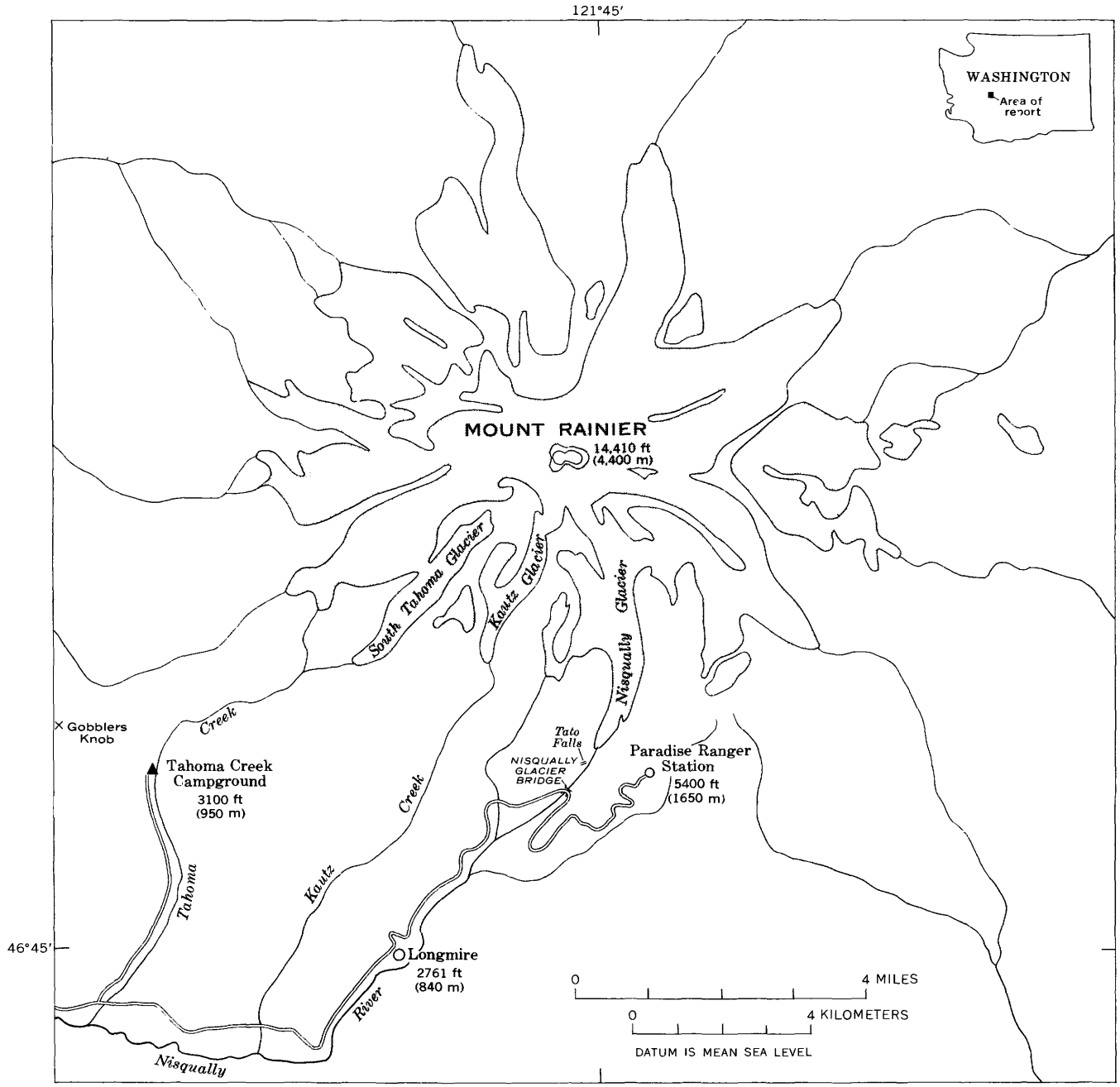

FIGURE 1.—Sketch map of Mount Rainier, Wash., showing the glaciers where outburst floods have been observed.

splashed with mud by the rushing torrent. Engineers Polk and Evanston of the Bureau of Public Roads were eye witnesses to the catastrophe. They saw the moving mass of water and rock coming over the end of the glacier and * * * described the material as similar to a huge mixture of concrete except that it was darker in color. They stated that the force was so great that immense boulders were thrown from ten to thirty feet into the air as the mass moved forward.

Three days after the flood, the lower part of Nisqually Glacier was inspected by Llewellyn Evans (Superintendent of Light, City of Tacoma Department of Public Utilities). In an unpublished report, Evans stated that the ice was swept clean along the west edge of the glacier and over the entire ice front. The flood also washed away debris for some 500 feet below the terminus, exposing ice on the valley floor.

Evans examined the west lateral moraine to a point beyond the first bend in the glacier. He came upon a break in the moraine and concluded that water had likely gathered in the open formation of the moraine and built up enough head to cause a sudden break,

which caused the flood by the outpouring of all the water stored in the loose material. This conclusion is probably incorrect. Even though recent moraines appear to be loosely compacted, they do not contain sufficient openings to store a large volume of water—certainly, not enough to result in a flood like that of October 1932. It is more likely that the large slide was a result rather than the direct cause of the 1932 flood. Such slides commonly occur during and soon after outburst floods because of excessive erosion near the base of unstable slopes on lateral moraines.

Another outburst flood occurred at Nisqually Glacier on October 24, 1934, after several days of continuous downpour. The following brief account appears in a monthly report of Park Superintendent O. A. Tomlinson

> On October 24 and 25 a series of floods having their source on the Nisqually Glacier destroyed the approaches and superstructure, and badly damaged the arch of Nisqually Glacier bridge. There were four distinct floods or surges caused by slides damming a valley or ravine between the lateral moraine and the glacier and impounding the water from melting snow and heavy rains. The first surge occurred during the night of October 24, carrying down a stream [of] huge boulders, mud, and other debris from the moraine. Thousands of tons of rock and debris crushed the railing and filled the comfort stations in the abutments. The second and subsequent surges, which occurred during the 25th, completely plugged the bridge and piled rock and debris fifteen feet deep on top of the arch. Approach roads on both sides of the bridge were washed out and some minor damage occurred to trucks and other equipment that were being used by repair crews trying to save the bridge.

As in 1932, the outburst flood of October 1934 was thought to be caused by slides on the lateral moraine of Nisqually Glacier. Only one surge was noted in 1932, whereas in 1934 there were three or four distinct surges, which caused only moderate damage to the bridge.

C. E. Erdmann and Arthur Johnson, U.S. Geological Survey (written commun., 1953), made the following observations based on records of precipitation at Paradise Ranger Station and records of Nisqually River discharge near Alder (drainage area, 249 sq mi, or 645 km^2) during the 1932 and 1934 floods:

> In 1932 there was no recorded rainfall at Paradise from September 25 to October 9. During October 10–14, rainfall totaled 8.70 inches and the discharge of the Nisqually River near Alder during this period rose from 297 to 761 second-feet. In 1934, during the period October 1–19, rainfall was recorded on seven days totalling 1.51 inches and during the period October 20–25, it totaled 9.92 inches. The discharge of the Nisqually River near Alder during this latter period rose from 682 to 12,000 second-feet. It is of interest to note that in 1934 with heavier rainfall the surges were less destructive than in 1932.

A new concrete bridge was constructed below Nisqually Glacier in 1936 (fig. 2). This was a massive concrete-arch structure with a clear span of 80 feet (24 m) and a width of 34 feet (10 m). In October 1947, at the time of the great Kautz Creek flood, the Nisqually Glacier bridge withstood a torrent of water that came from the glacier. The Nisqually River rose to flood stage on October 1, and a deep, V-shaped gorge was cut into the glacier by running water. The following day, the torrential rainfall reached its peak when 2.38 inches fell at Longmire and 5.89 inches at Paradise Ranger Station. A surge of high water damaged two trucks and a gasoline-powered shovel that had been working on the channel at the Nisqually Glacier bridge. The bulk of the flood water was undoubtedly

FIGURE 2.—Nisqually Glacier bridge before and after the flood of October 25, 1955. In the earlier view (above) the bridge is seen as it appeared soon after its construction in 1936. The terminus of Nisqually Glacier is visible in the background. After the 1955 flood all that remained of the bridge were the broken abutments and exposed reinforcing bars seen in the latter view (below). The large boulders on the far bank were left by the flood. Photographs by M. K. Potts, National Park Service.

storm runoff, but the peak flow may have been increased by a sudden release of water stored at the glacier.

Eight years later, on October 25, 1955, a spectacular jökulhlaup occurred at Nisqually Glacier. This is the best documented of any of the outburst floods on the Nisqually River, having been observed at an uncomfortably close range by Park Ranger Dwight L. Hamilton. Rain had begun falling at 4 a.m. on October 24, after 2 days of clear warm weather. At 4:30 p.m. on the 24th, the rainfall measured 1.72 inches (43.7 millimeters) at Paradise Ranger Station, and by 12:15 p.m. the following day an additional 3.79 inches (96.3 mm) had fallen. On the morning of October 25, Hamilton was watching the rising water at the Nisqually Glacier bridge while sitting in a panel truck that was parked about 90 feet (27 m) from the east bridge abutment. He later reported the following (written commun., 1955):

* * * [by 9:30 a.m.] water had been thrown around the [west] end of the bridge, washing boulders up to about 2 feet in diameter across and down the road. Several blocks of ice weighing about 20–30 pounds were seen.

* * * * *

For a time it looked as if the water level was dropping * * *. [Then] I glanced upstream in time to see water headed for me and the truck * * *. By the time I began backing up the road, I was engulfed by water, the motor stopped, and visibility was cut to zero by the muddy water. The truck was bounced around quite violently and pushed back another 10 yards. When things quieted down I looked out to see the bridge was gone * * *.

The following 45 minutes or so of watching are hard to describe. After the initial surge of water which took out the bridge, the water level would drop to a point where you could see the remains of the bridge abutments, then another surge which appeared to be at least 15–20 feet higher than the river level immediately in front of it would appear * * * and the abutments would again be hidden from sight. These surges probably came five or six times while I watched, each approximately the same size. The astounding thing was the size of the boulders and blocks of ice that the water carried. I would estimate some of them to be larger than an auto. They did not roll or turn but rode the surface of the water as a boat, the same end always down stream and the same surface out of the water. Occasionally large chunks of ice would collide with a rock and crumble, small pieces being thrown high into the air. The speed at which the rocks and ice traveled is hard to estimate but in comparing their speed with that of a car going by I would say between 30 and 40 miles per hour.

The figure 2 photograph shows the twisted steel reinforcing rods and broken concrete—all that remained of the Nisqually Glacier bridge after the 1955 flood. The flood wave that destroyed the concrete bridge also swept away a log bridge 1.8 miles (2.9 km) downstream. (This was witnessed by a group of miners at 10:15 a.m.). Some damage was also done at Longmire, where the Nisqually River was reported to be at a high stage from 11 a.m. to about 2 p.m.

An interesting feature of the 1955 flood observed by Hamilton was the repeated surges "each approximately the same size" that followed the initial outburst for a period of about 45 minutes. These secondary surges have been observed following other outbursts, and apparently are a characteristic feature of this type of flood. They might have been caused by the repeated plugging and unplugging of channels within the glacier, or temporary damming of the river by a series of slides from the unstable moraine.

On November 7, 1955, Park Ranger Aubrey L. Haines made a reconnaissance along the river from the site of the Nisqually Glacier bridge up to an altitude of about 6,000 feet (1,800 m) on the Nisqually Glacier. He reported (written commun., 1955) that at places the floodwater had been over the trail where it was 40 to 50 feet (12 to 15 m) above the river bottom. Upstream from Tato Falls, the trail was completely washed away as were the year dates that had been painted on large rocks to mark positions of the glacier as early as 1922. The streambed was cut by a wash 30 to 40 feet (9 to 12 m) deep and about 100 feet (30 m) wide near the old glacier terminus. Above the old terminus a canyon had been carved in the mass of stagnant ice that had remained under glacial debris after the glacier retreated some years before. This dead ice had been melting slowly even after the glacier's active terminus began to advance in 1953. Haines described in detail the channels that were formed in the stagnant ice and advanced the opinion that they were not entirely the result of the cutting action of flood waters, but were formed largely by "hydrostatic pressure blowing the roof from an existing water channel, or subglacial stream."

Above the upper, or active, ice face, a large gully had been formed for half a mile (0.8 km) along the west side of the glacier. It appeared to Haines to have been created by the removal of both morainal debris and glacial ice. Above the gully, the ice surface had a glossy, washed look as if a large quantity of water had flowed over it.

Two days after Haines' inspection of the lower part of Nisqually Glacier he assisted in a survey of the river channel near the site of the Nisqually Glacier bridge and found the cross-sectional area of the flooded channel to be 5,120 sq ft (476 m^2). He estimated that a velocity of 18 miles per hour (8 m/sec) would have been required to transport a large boulder (960 cu ft, or 27 m^3) that was deposited on the roadway during the flood. Assuming an average stream velocity of 20 mph (8.9 m/sec), he concluded that the peak discharge was about 150,000 cubic feet per second (4,250 m^3/sec). The estimate seems high. On the basis of the channel slope and roughness at the bridge, an average velocity of 20 feet per second (6.1 m/sec) seems more likely. If a sediment concentration of 30 percent by volume is

assumed, the estimated peak discharge of water would then be about 70,000 cfs (2,000 m^3/sec).

Since 1955, there have been no reports of any more outburst floods on the Nisqually River. Soon after the bridge was destroyed in 1955, it was replaced by a Bailey bridge that was used until the present span was completed in 1960. Compared with earlier bridges at the site the present structure is immense, having a clear height of 85 feet (26 m) above the river and a clear span of 300 feet (92 m) between the piers. With that much clearance the bridge is not so likely to be damaged by outburst floods. The river's discharge is now being recorded at a gaging station that was installed at the bridge on March 1, 1968.

Kautz Creek

According to Russell K. Grater, a former park naturalist at Mount Rainier, the destructive Kautz Creek flood of October 2, 1947, was one of the most spectacular events that has ever taken place in a National Park since the beginning of the Park Service. Grater, with a group of local residents, was watching the mudflow when it reached its final and climactic stage at the highway bridge 5.5 miles (8.8 km) below Kautz Glacier. In a written communication (1947) he described the scene as follows:

> A vast fan-shaped sea of rock and log debris was pouring down across the Nisqually Entrance Highway toward the Nisqually River. The force of the moving mass was terrific, with huge boulders being carried along like so much float material. One boulder was measured that reached approximately 13 feet in diameter. In many instances these boulders did not roll, but simply moved along buoyed up by the thick, cement-like material flowing across the region. Trees, even large ones with diameters in excess of three feet, were snapped off like sticks or else were uprooted. * * *. All of this activity was accompanied by a rumbling and earth shaking that was awesome in its magnitude.

After the flood, Grater inspected the Kautz Creek valley floor at the Kautz Glacier, where he saw the effects of the outburst near its source. His report continues:

> Evidence shows that approximately one mile in length of the Kautz Glacier was destroyed during the flood. Where the glacier once lay is now a deep canyon, ranging up to approximately 300 feet in depth and approximately 300 yards wide at the widest point. These figures are considered to be on the conservative side. Along the east side of the newly cut canyon is a large segment of the original glacier, now cut off and left stranded by itself. The segment is approximately 75 feet thick at the lower end of the ice mass. The canyon itself has been cut completely down to the original granite bedrock. * * *.
>
> At the box canyon of the Kautz, where it is believed the major surges developed through a damming up of the narrow channel, the canyon has been cut approximatly 60 feet in depth. Here an entirely new channel has been cut, with the old stream bed of the Kautz left high on the west side of the canyon.

Damming the box canyon compounded the destructiveness of the flood, for great masses of mud and debris were swept downstream in repeated surges that destroyed a large area of forest, as well as the Kautz Creek bridge, and covered part of the highway. The volume of material removed by the flood was estimated by the Park Service to be about 50 million cubic yards (38×10^6 m^3).

Some idea may be had of the discharge of water during the flood if it is assumed that the mudflow contained, on the average, about 40 percent water by volume. By further assuming that all the mudflow occurred in a 24-hour period, the average daily discharge of water required to transport the debris can be estimated as about 10,000 cfs (280 m^3/sec). The peak discharge was undoubtedly several times greater than the daily rate of flow and, in addition, there was probably more water flowing at times than was required to transport the material that was removed.

The Kautz mudflow of 1947 was the compound result of an abnormally intense downpour of rain and the release of additional water that was stored within the Kautz Glacier. The outburst of large amounts of water, combined with tremendous volumes of glacial sediment and rock debris that became temporarily trapped in the narrow box canyon, resulted in the spectacular mudflow in the lower Kautz Creek basin.

Previous debris flows on Kautz Creek are evidenced by older deposits that are exposed in cut banks (Crandell and Mullineaux, 1967, p. 18). The earlier debris flows go back at least 3,000 years and it is not known whether any of them resulted from an outburst flood.

On August 23, 1961, a flood was observed at the Kautz Creek bridge that was clearly the result of a jökulhlaup. No significant amount of rain had fallen in the area during the month, and the average temperature in August was the highest recorded since 1914 at Longmire. Park Superintendent Preston P. Macy reported that on August 23 Kautz Creek began a rampage with very muddy water and heavy surges taking place about every 2 hours. Later surveys at the bridge showed that the streambed was cut 7–10 feet below its previous level. Two trail bridges were destroyed on Kautz Creek during the flood.

Tahoma Creek

On August 31, 1967, during an exceptionally warm and dry summer, an outburst flood was observed on Tahoma Creek. Prior to August 31 no rain had fallen in the area for about 2 months, and the fire hazard was so severe that the Tahoma Creek campground was closed to the public on August 30. The closure turned out to be a fortunate circumstance, for on the next day part of the campground, which is 3.5 miles (5.6 km)

below South Tahoma Glacier, was swept over by a flood of water, mud, and debris.

Two days earlier, a short-lived outburst had destroyed a footbridge 1.2 miles (1.9 km) below the glacier, but the stream rose only about 1.5 feet (0.5 m) at the campground. On August 31, David Fluharty, fire control aid at the Gobblers Knob fire lookout about 5 miles (8 km) from South Tahoma Glacier, reported hearing a loud roaring noise coming from the Tahoma Creek valley at 8:40 p.m. He could see water flowing across the surface of the glacier, apparently breaking out at an altitude of about 7,500 feet (2,300 m). Between 9:00 and 9:30 p.m. James Erskine, a park ranger, found that the lower part of the campground was being buried by a slurry of mud and boulders. In the main stream, large boulders were being swept along by the torrent, and many smaller stones were being thrown into the air. Erskine noted that the mudflow had the appearance of fresh concrete, a resemblance that had been observed by others during outburst floods on Kautz Creek and Nisqually River. The rate of flow decreased rapidly downstream from the campground, and a later inspection by D. R. Crandell (U.S. Geological Survey) revealed that the deposits of mud and debris terminated within a mile (1.6 km) downstream. At the highway bridge 4.3 miles (6.9 km) below the campground, Park Service personnel observed that Tahoma Creek crested about 10:30 p.m. Later inspection of high-water marks by the writer revealed that the stage had risen only about a foot (0.3 m) at the bridge, and the peak discharge at that point was estimated to be about 100 cfs (3 m^3/sec).

On September 2, the writer inspected the upper reaches of Tahoma Creek and the lower part of South Tahoma Glacier. At the campground, where the channel slope averages about 10 percent, the cross-sectional area of the flooded channel was about 1,200 sq ft (110 m^2). An average velocity during the flood peak of 20 ft per sec (6 m/sec) seems reasonable, which would indicate a peak discharge of about 24,000 cfs (680 m^3/sec). If it is assumed that the flow contained about 50 percent water by volume, the maximum discharge of water must have been about 12,000 cfs (340 m^3/sec). It is remarkable that such a high discharge was almost entirely dissipated by channel storage and infiltration in a reach of only 4.3 miles (6.9 km) below the campground.

Between the campground and South Tahoma Glacier there was much evidence of a larger flood. Erosion of the channel was particularly evident in a half-mile (0.8 km) reach immediately below the glacier, where an estimated 50,000 cubic yards (38,000 m^3) of material was washed away by the flood of August 31. Below the active terminus, older, stagnant ice was found to be freshly exposed near the bottom of the channel.

The steep terminus of the glacier did not appear to have changed appreciably, on the basis of photographs taken in 1966. On September 2 the melt-water discharge was only about 30–40 cfs (0.8–1.1 m^3/sec), most of the flow being in a deeply eroded channel along the glacier's north margin. Aerial photographs revealed another large channel eroded by flood waters near the center of the glacier. As nearly as could be determined, the outburst of August 31 apparently reached the surface of the glacier at about the 7,500-foot (2,300 m) level, just as Fluharty reported. No firm evidence was found of geothermal activity that might have caused rapid melting.

Other outburst floods

Outburst floods are known to have occurred at other glaciers in the Pacific Northwest besides those at Mount Rainier. On August 15, 1963, a flood was observed below Chocolate Glacier (on Glacier Peak) by H. C. Chriswell, forest supervisor, while he was on a routine fire observation flight over the Mount Baker National Forest. In a written communication (1963), Chriswell reported:

> As we flew over Chocolate Creek a massive flow of what appeared to be muddy water had just started to move down Chocolate Creek from the snout of the Chocolate Glacier * * *. We circled for about ten minutes [and] in this time the flow moved the 2½ miles [to the Suiattle River]. The height of the frontal crest could have been anywhere between 20 and 40 feet high * * *. The flow was still continuing almost unabated from under the snout of the glacier when we left the area.
>
> The only downstream damage occurred when the flood carried away our Skyline Trail bridge above the mouth of Miners Creek [about 5 miles downstream from Chocolate Creek]. A tremendous amount of channel change and silt deposition occurred in the upper Suiattle. Heavy silt deposit was noted along the Sauk River [below the Suiattle].

It should be noted that there was no precipitation near Glacier Peak on August 15, 1963, and the Chocolate Creek flood that day was obviously the result of a true jökulhlaup. Chriswell also reported that from the condition of the channel and deposition on the upper Suiattle River, these flows have occurred back through the years. According to Austin Post, U.S. Geological Survey (oral commun., 1968), the source of most of the large mudflows in the upper Suiattle River valley was at Chocolate Glacier, a part of which has rapidly disintegrated. The deeply eroded canyon of Chocolate Creek is seen in the photograph of figure 3, which was taken 2 months after the 1963 outburst flood.

Outburst floods have also been reported at glaciers on Mount Hood, Oreg., and according to James R.

FIGURE 3.—Aerial view from the eastern side of Glacier Peak on October 16, 1963. Chocolate Glacier is above canyon in center of picture. Photograph by Austin Post, U.S. Geological Survey.

Craine, U.S. Forest Service (written commun., 1961) they generally are experienced during the first warm fall rains of the year.

INTERPRETATION

It seems significant that glacier outburst floods in the Pacific Northwest have been observed only during late summer and fall, and do not coincide with "normal" floods downstream. Most floods on the larger rivers occur in the winter and are associated with periods of heavy rain and general flooding throughout western Washington. On the lower Nisqually River, for instance, the largest known floods were those of November 1909, December 1917, December 1933, and November 1959. In contrast, jökulhlaups may occur at times when there is no rain at all.

During the floods that are described in this article, the peak flows were greater than might be expected from direct storm runoff. The magnitude and frequency of many floods resulting from storms in the Pacific Northwest have been analyzed by Bodhaine and Thomas (1964), and their analysis has been used to estimate the size of floods that could be expected to occur in the upper Nisqually River basin. In the following tabulation, estimates are given for peak flows expected at the three sites in the Nisqually basin where outburst floods are described:

	Drainage area		Mean annual flood		50-year flood	
	(sq mi)	(km²)	(cfs)	(m³/sec)	(cfs)	(m³/sec)
Nisqually River at Nisqually Glacier bridge	6.2	16.1	440	12	1,000	28
Kautz Creek at highway	13.5	35.0	750	21	1,700	48
Tahoma Creek at campground	6.3	16.3	400	11	920	26

The expected peak discharges may be compared with estimated flows experienced during outburst floods. At Nisqually Glacier bridge, the Nisqually Glacier outburst of October 25, 1955, resulted in an estimated peak discharge (adjusted for sediment concentration) of about 70,000 cfs (2,000 m^3/sec). The Kautz Creek flood peak of October 2, 1947, was probably on the order of 50,000 cfs (1,400 m^3/sec), and the Tahoma Creek flood of August 31, 1967, was estimated to peak at about 12,000 cfs (340 m^3/sec). In each of these events, the peak flows were many times greater than the expected magnitude of a "50-year" flood.

Some of the floods at Mount Rainier were obviously affected by landslides which temporarily blocked stream channels and stored some of the flow. The volume of water ponded behind such slides is limited, however, by the steep slope of channels near the mountain. (The glacier surfaces are also steep, excluding the possibility of much water storage over the ice.) To estimate the possible effect of a landslide at Nisqually Glacier, a rough computation can be made on the basis of average channel dimensions where slides were reported to have occurred. If it is assumed that a slide 30 feet (9 m) high blocked a rectangular channel 100 feet (30 m) wide where the slope is 15 percent, the volume of impounded water would have been 300,000 cu ft. (90,000 m^3). This is small in comparison to estimated volumes of as much as 50 million cu ft (1.4×10^6 m^3) which were probably discharged during outburst floods at Nisqually Glacier. It seems evident, therefore, that flood waters were released not only from behind landslides but also from within the glacier.

If there were a practicable way of determining the volume of water in a glacier at any particular time, the potential size of a jökulhlaup presumably could be estimated. The likelihood of an outburst might also be indicated by measurements of water pressures within glaciers. High water pressures in some glaciers have been evidenced by measurements during exploratory drilling. An example described by Mathews (1964) is at the South Leduc Glacier of British Columbia where an exploratory tunnel was driven in 1957. The mine tunnel made contact with the base of the glacier about 2 km above the terminus, where the ice was 150 m thick. Records of water levels in the mine, indicating water pressure in the upper part of the glacier, showed periods of moderately steady conditions (with slight diurnal fluctuations) interrupted by irregular and catastrophic surges, particularly during periods of rapid snowmelt and heavy rains.

Haefeli (1957, p. 27–29) has suggested that seasonal variations in water pressure at the base of a glacier may be responsible for seasonal variations in the rate of the glacier's movement, and Weertman (1962) has offered a theory that catastrophic advances of some glaciers are made possible by a basal layer of water. The relation of water pressure and rates of ice movement is not yet understood, however, and further study will be needed before the significance of these factors to glacier outbursts can be clearly shown. Some field measurements suggest that the flow of Nisqually Glacier normally decreases (suggesting perhaps lower water pressure) during August to October, which is the period when jökulhlaups occur. This seems to contradict the theory that outbursts are a result of sudden increases in water pressure. Conceivably, this apparent contradiction might be explained if it could be shown that water pressure may suddenly increase at times when there is not a noticeable increase in ice flow. Perhaps an increase in pressure occurs when decreasing melt-water flow fails to keep the plumbing open in late summer.

Mudflows are often associated with outburst floods, particularly at Mount Rainier where great quantities of loose glacial debris are readily available to streams. Beverage and Culbertson (1964) proposed a terminological limit for a mudflow, restricting the term to a flow having a sediment concentration of at least 80 percent by weight. (If a specific gravity of 2.65 is assumed for individual sediment particles, such a flow would contain about 40 percent water by volume.) Floods having sediment concentrations of 40–80 percent by weight are classified by Beverage and Culbertson as being "hyperconcentrated." On the basis of the high stream velocities described by witnesses during outburst floods on the Nisqually River and Tahoma Creek it would appear that those floods consisted, for the most part, of hyperconcentrated flows. As flood waves move downstream they sometimes degenerate into a mudflow because of insufficient slope and tributary inflow to overcome the loss of water by infiltration.

REFERENCES

Beverage, J. P., and Culbertson, J. K., 1964, Hyperconcentrations of suspended sediment: Jour. Hydraulics Div., Am. Soc. Civil Engineers Proc., v. 90, no. HY6, p. 117–128.

Bodhaine, G. L., and Thomas, D. M., 1964, Magnitude and frequency of floods in the United States, pt. 12, Pacific Slope basins in Washington and upper Columbia River basin: U.S. Geol. Survey Water-Supply Paper 1687, 337 p.

Crandell, D. R., and Mullineaux, D. R., 1967, Volcanic hazards at Mount Rainier, Washington: U.S. Geol. Survey Bull. 1238, 26 p.

Haefeli, R., 1957, Notes on the formation of ogives as pressure waves: Jour. Glaciology, v. 3, no. 21, p. 27–29.

Mathews, W. H., 1964, Water pressure under a glacier: Jour. Glaciology, v. 5, no. 38, p. 235–240.

Weertman, Johannes, 1962, Catastrophic glacier advances: Internat. Assoc. Sci. Hydrology, Obergurgl Symposium, Pub. 58, p. 31–39.

FIELD PROCEDURE FOR MEASURING SETTLING CHARACTERISTICS OF SEDIMENT SAMPLES

By G. L. FITZPATRICK [1] and N. J. KING, Denver, Colo.

Abstract.—In conjunction with morphologic studies of ephemeral stream channels, a simple field procedure requiring less than 20 minutes per sample has been developed for measuring the settling characteristics of selected sediment samples. Results are depicted graphically as sediment settling curves by plotting accumulated volume of sediment versus time. Parameters defining the settling characteristics of each sample tested are obtained by graphical solution of an equation fitting the settling curves. The form of this equation was obtained by comparing the sediment-water system with an analogous electrical system. Trial application of the procedure to selected samples from ephemeral stream deposits indicates that the values of the parameters thus obtained may provide an indirect method for determining flow conditions during the time of deposition.

Studies of ephemeral stream channels are seriously hampered by the unpredictable and transitory nature of runoff events, especially discharges that are of sufficient magnitude to influence channel morphology appreciably. For this reason measurement of semipermanent physical parameters of stream channels and channel deposits is needed to help discover relationships from which significant flow characteristics can be interpreted in lieu of actual flow measurements.

A significant contribution to this subject made by Leopold and Miller (1956) relates width, depth, slope, and suspended-sediment load to discharge of ephemeral streams. Schumm (1960, 1961) describes the effect of sediment type on channel shape. For the most part, however, attempts to relate sediment parameters of channel deposits to streamflow characteristics have not been very successful. Yet, even a cursory inspection of most channel deposits shows a pattern of deposition that must be related in some way to flow characteristics. The coarsest particles are almost invariably found in the lowest part of a channel where the depth of flow, and thus mean velocity and traction force for any given discharge, is greatest. Fine-grained particles usually accumulate in shallow reaches and backwater areas where velocity is least during high discharges. This general pattern of sediment size distribution is locally complicated, of course, by factors such as the transitory effects of eddy currents, peculiarities in the size and shape of particles available to the stream, and the deposition of fines on the channel bed during the period of diminishing flow near the end of a runoff event. Despite the above complications, a carefully selected point sample taken from the bed of an ephemeral stream channel might, under proper examination, reveal much about the prevailing flow conditions during the time of deposition. The individual particles constituting the selected sample would have come to rest farther upstream or been carried farther downstream before deposition if flow conditions, especially velocity distributions, had been significantly different.

Initially the writers considered the use of parameters obtained from mechanical size analyses as a means of interpreting flow conditions. They soon discovered, however, that size alone is not a reliable indicator of conditions of sediment transport. Other factors, such as shape and specific gravity of individual particles and the effective density and viscosity of the fluid media, also effect the movement of sediment by a stream. Moreover, mechanical analyses are comparatively laborious and time consuming to perform and are not easily adapted to field techniques. Twenhofel and Tyler (1941, p. 64) concluded after rigorous analyses of a large number of sediment samples that "One needs to be very cautious in expressing the value of any mechanical analysis so far as the sedimentational significance is concerned. Rigorous examination of the results of mechanical analyses has not as yet proved very fruitful." Furthermore, Rubey (1933, p. 331) concluded tentatively that "* * * the current required to move a particle along the bottom of a stream is approximately the same as the settling velocity of the same particle in still water." If such a relationship does exist, even though less direct than that suggested by Rubey,

[1] Denver Mining Research Center, U.S. Bureau of Mines.

U.S. GEOL. SURVEY PROF. PAPER 600-D, PAGES D87-D94

analyses of sediment settling curves of selected samples from channel deposits offers a promising aid in morphologic studies of ephemeral stream channels. Thus the writers have concentrated on analyses of settling characteristics of sediments rather than on mechanical analyses.

The objectives of this study are: (1) To develop a comparatively simple and rapid field procedure for measuring the settling characteristics of selected sediment samples, (2) to analyze the data thus obtained to determine which parameters appear to be most promising for use in morphologic studies of ephemeral stream channels, and (3) to apply the combined results to selected channel reaches to determine if the method warrants further research.

DESCRIPTION OF METHOD

Sampling procedure

At each sampling site a hole was spaded to a depth of 1 to 1½ feet to expose a shallow cross section of the deposit to be tested. At the same time the surface veneer of sediments was removed to eliminate the addition to the sample of any wind-blown particles or fines deposited during flow recessions. If the remainder of the deposit exposed in the side of the hole appeared to be uniform in particle size and composition, a channel sample was taken the full depth of the hole. If the section did not appear to be uniform, which was rarely the case, a channel sample was taken only from the uppermost uniform layer which appeared to have been deposited during the last significant runoff event.

Testing procedure

A dry sample weighing 50 grams is split from the original sample and placed to soak for 10 minutes in a 500-milliliter beaker containing locally available tap or stream water. No chemical dispersants are added to the sediment-water mixture. After the prescribed period of soaking, followed by gentle physical disaggregation with a rubber pestle, the sediment-water mixture is transferred to a standard 1-liter Imhoff cone, graduated from 0 to 40 ml, and sufficient water added to bring the contents to a volume of 1 liter at 25°C (or as close to that temperature as field conditions permit). The Imhoff cone is then capped and shaken vigorously by one person while another readies a stop watch and prepares to record the results of observations. As soon as the sample appears to be uniformly dispersed throughout the column of water, the Imhoff cone is turned upright and immediately placed in a stand. The stop watch is started on signal at the moment agitation ceases when the cone is turned upright. The volume (milliliters) of sediment accumulating on the graduated bottom part of the Imhoff cone per unit of time (seconds) is recorded at appropriate intervals over a period of 6 minutes. Equipment used in the field is shown in figures 1 and 2.

FIGURE 1.—Equipment used in the field to analyze sediment samples and measure channel parameters. *A*, Imhoff cones in stand; *B*, container for tapwater; *C*, plastic container for soaking sample prior to testing; *D*, steel tape for marking channel cross section; *E*, instrument for surveying cross section; *F*, shovel at sampling site.

FIGURE 2.—Imhoff cones in stand. Only one cone is needed, but two or three cones are often used to provide a visual comparison of a sample being tested with those previously run. The sediment-water mixture has been transferred to the cone in the foreground, and water is being added to bring the contents to a volume of 1 liter.

Occasionally, some fine-grained materials showed a poorly defined settling interface, which made it difficult to measure the accumulating volume of sediment in the bottom of the cone. When this happened, the writers found that with practice they could detect at any instant a level at which particle motion appeared to stop. This level was assumed to represent the settling interface, although no true interface, as such, was recognizable.

This testing procedure is not applicable, of course, to deposits made up of particles too large to be fitted into the cone or too small to be resolved by the eye.

ANALYSIS OF RESULTS

A graph of volume of sediment settled versus time for individual sediment samples (fig. 3) invariably yields a smooth Odén-type curve (Odén, 1925), indicating that the data can be approximated by a mathematical expression. The form of this expression was obtained by comparing the physical parameters of the sediment-water system with those of an analogous electrical system.

The capacity of the Imhoff cone used in the field technique remains virtually constant at its volume of 1 liter during the procedure. This rigid container with its fixed capacity can be compared to an electrical capacitor (condenser) having a fixed capacitance. The sediment sample represents a "sediment charge", which is analogous to electrical charge. The "sediment charge" experiences a resistance to settling through the fluid media which is analogous to electrical resistance. Finally, the "sediment charge" is subjected to a gravitational potential which is analogous to electrical potential. An electric analog model incorporating these elements can be represented by a simple circuit in which a charged capacitor is discharged into a resistor.

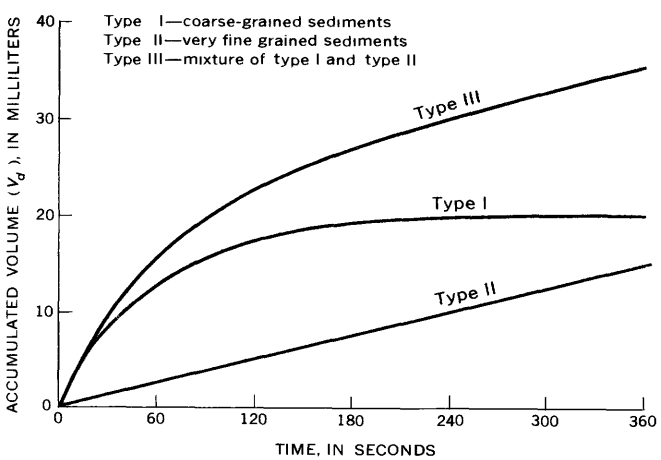

FIGURE 3.—General types of sediment settling curves obtained from analyses of ephemeral stream deposits.

The discharge of a charged capacitor into a resistor connected in series as shown in the following diagramed circuit is governed by the equation

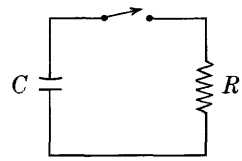

$$Q=Q_0e^{\frac{-t}{RC}}, \qquad (1)$$

where Q is the charge remaining on the capacitor at time t after the switch is closed, Q_0 is the initial charge, C is the capacitance, R is the resistance of the circuit, and e is the base of natural logarithms 2.7182. . . .

The charge Q_l lost by the capacitor in heating the resistor at any time t is equal to the difference between the initial charge Q_0 and the charge Q remaining on the capacitor at time t. This is shown by

$$Q_l=Q_0-Q. \qquad (2)$$

Substituting equation 1 in equation 2, the charge lost at time t is

$$Q_l=Q_0\left(1-e^{\frac{-t}{RC}}\right). \qquad (3)$$

Reasoning by analogy, equation 3 can be rewritten to describe the settling of a hypothetical sediment sample in water as

$$V_d=V_0\left(1-e^{\frac{-t}{R'C'}}\right), \qquad (4)$$

where V_d is the "sediment charge" (volume of sediment) accumulated on the bottom of the Imhoff cone at time t; V_0 is the initial "sediment charge" (total volume of sediment used); R' is a constant that represents a measure of the resistance to settling of a given bulk-sediment sample; and C' is a constant that represents a measure of the capacity of the Imhoff cone.

Examination of equation 4 shows that the volume of sediment dropped at any time, that is, the settling characteristics of the sediment, depends on the initial sediment concentration or "charge," V_0; the resistance to settling, R'; and the characteristics of the container, C'. By using the same sediment concentration or "charge" for all analyses, differences in settling characteristics between samples should be reflected only by differences in the value of $R'C'$, which has dimensions of seconds and is analogous to the time constant RC of the electric circuit defined by equation 3.

The foregoing analogy is not intended to imply that the electrical system is equivalent in detail to the sediment-water system described. This approach was used only because of the gross similarities of the two

systems and in the hope that such an analogy might reveal the mathematical form of the equation that would best fit the graphs (sediment settling curves) obtained by plotting volume of sediment settled versus time. Also, the reader should clearly understand that the intuitive reasoning that led to equation 4 is in no way a derivation. The fact that this equation seems to mathematically describe the settling characteristics of many of the samples analyzed by the writers is offered as its only justification for further consideration.

Hopefully, it will ultimately be possible to compare the results of this method with the work of others involving measurements of settling characteristics of sediments. The present paper, however, is more immediately concerned with the form of equation 4, the significance of the time constant in that equation as a parameter for showing differences in settling characteristics of ephemeral stream deposits, and the relevance of this general approach to morphologic studies of ephemeral stream channels.

It was previously stated that differences in the settling characteristics between sediment samples depend on differences in the value of the time constant $R'C'$ in equation 4, which in turn depends only on the resistance to settling R' and the characteristics of the container C'. As the same container (a 1-liter Imhoff cone) was used for all analyses in this study, it follows that C' can be regarded virtually as a constant. Therefore, differences in the value of the time constant in equation 4 from one sediment sample to another depend almost wholly on differences in the value of R'. Partly for this reason and partly for simplicity's sake, the writers suggest substituting the single symbol T for the time constant $R'C'$ in equation 4 such that

$$V_d=V_0\left(1-e^{\frac{-t}{T}}\right). \tag{5}$$

The value of the time constant T in equation 5 gives an indication of the time required for a sediment to settle. For example, coarse-grained sediments that settle rapidly have a small time constant. A graph of volume of sediment settled versus time for coarse-grained materials yields a settling curve similar to that of type I of figure 3. As sediments become progressively finer grained, they take longer and longer to settle and the value of T increases proportionately. The result is a progressive decrease in the slope of the settling curve until, eventually, very fine grained sediments exhibit a form that approximates a straight line (fig. 3, type II). The approximate linear form of this curve can be demonstrated by differentiating equation 5 with respect to time, to obtain the slope S of the settling curve, as follows:

$$S=\frac{d}{dt}(V_d)=\frac{d}{dt}[V_0(1-e^{\frac{-t}{T}})]$$

$$=\frac{V_0}{T}e^{\frac{-t}{T}}. \tag{6}$$

For very fine grained sediments where T is large, $e^{\frac{-t}{T}}\approx 1$ and

$$S\approx\frac{V_0}{T}. \tag{7}$$

Because V_0 and T are constants for a given sediment, the slope of the curve for large values of T is practically a constant, that is, the settling curve for fine-grained sediments is approximately linear and can be expressed by the equation

$$V_d=St, \text{ or}$$

$$V_d=\frac{V_0}{T}t. \tag{8}$$

The results of about 200 sediment analyses on samples collected under a wide range of conditions in Wyoming, Utah, and Arizona (see section "Testing Procedure"), showed that a number of coarse-grained channel samples exhibited a settling curve similar to that of type I (fig. 3). A few very fine grained flood-plain samples exhibited an approximately linear form such as that of type II (fig. 3). The great bulk of the samples, however, exhibited a form like that of type III (fig. 3), which appears to be composed of two parts, a coarse-grained fraction that settles like that depicted by type I, and a fine-grained fraction that settles as does that depicted by type II. This assumption was tested in the laboratory by sieving appropriate sediment samples into sand and silt plus clay fractions. The settling curve for each fraction was determined separately. Both fractions were then mixed and the settling curve determined for the whole sample. Results showed that for all practical purposes a type-III curve can be obtained by adding a type-II curve to a type-I curve. The equation of a type-III curve, therefore, can be expressed as the sum of equations 5 and 8 by

$$V_d=V_c\left(1-e^{\frac{-t}{T_c}}\right)+\frac{V_f}{T_f}t, \tag{9}$$

where V_d is the volume of sediment deposited on the bottom of the Imhoff cone at time t after settling has begun; V_c and V_f are the total volumes of the coarse- and fine-grained fractions, respectively; and T_c and T_f are the time constants for the coarse- and fine-grained fractions, respectively.

Values for V_c, V_f, T_c, and T_f in equation 9 can be obtained readily by the following method. A straight line that is drawn tangent to the sloping end of a type-III curve (see fig. 4) or to the horizontal end of a type-I curve has the same slope as the type-II curve representing the fine-grained fraction of the sediment. The point of intersection of this tangent line with the volume axis gives the total volume of the coarse fraction (V_c) directly (see fig. 4). The equation of the tangent line is

$$V=\frac{V_f}{T_f}t+V_c, \tag{10}$$

where V is the volume coordinate of the tangent line at time t; $\frac{V_f}{T_f}$ is nearly equal to the slope of the tangent line as shown by equation 7; and V_c is the total volume of the coarse fraction. The difference between equations 10 and 9 represents the vertical distance D (see fig. 4) between the tangent line and the settling curve at any time t as shown by the following equation:

$$D=V-V_d$$
$$=\left[\frac{V_f}{T_f}t+V_c\right]-\left[V_c\left(1-e^{\frac{-t}{T_c}}\right)+\frac{V_f}{T_f}t\right],$$

which reduces to $D=V_c e^{\frac{-t}{T_c}}$.

When the distance D between the tangent line and the settling curve has the value $\frac{V_c}{e}$, then $\frac{t}{T_c}=1$, and $t=T_c$. This last relationship enables one to obtain a simple graphical solution for T_c. The value $\frac{V_c}{e}$ can be obtained by dividing the volume intercept V_c of the tangent line by 2.7183. The value of T_c is then equal numerically to the abscissal time coordinate of the point on the settling curve that is the lower limit of the vertical distance $\frac{V_c}{e}$ below the tangent line (see fig. 4). V_f can be obtained approximately by subtracting V_c from the total volume of the sediment sample, which averages about 41 milliliters for a 50-gram sample. T_f can be obtained by measuring the slope of the tangent line and solving for T_f by use of the relationship $S\approx\frac{V_f}{T_f}$.

Equation 9 was tested by plotting theoretical curves for a number of sediment samples using values of V_c, V_f, T_c, and T_f obtained from actual settling curves by the method described above. In every plot the theoretical curve was found to superpose almost exactly on the actual settling curve, thereby supporting the tentative hypotheses that (1) naturally occurring sediments can be thought of as consisting of two parts, a coarse-grained fraction having a type-I settling curve and a fine-grained fraction having a type-II settling curve, and that (2) the settling characteristics of such sediments are adequately represented by equation 9.

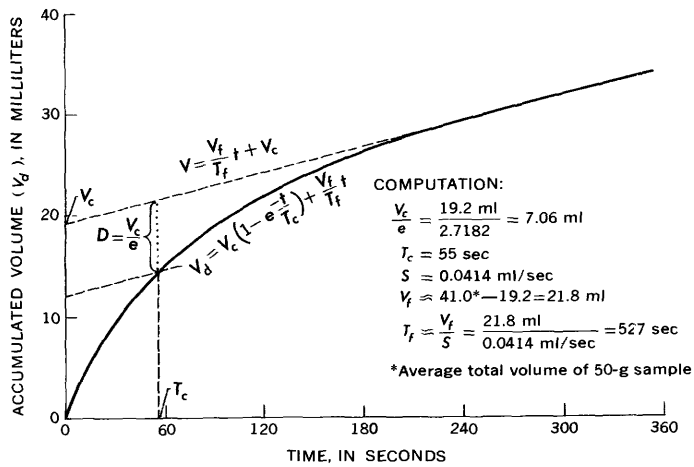

FIGURE 4.—Graphical solution of a type-III sediment settling curve.

Analyses completed by the writers show that values of T_c range from about 4 to about 100 seconds and values of T_f range from about 100 to about 1,000 seconds. These values of T correspond to average settling velocities ranging from about 0.3 to about 0.01 feet per second for the coarse-grained fraction and from about 0.01 to about 0.001 feet per second for the fine-grained fraction.

LIMITATIONS OF THE METHOD

The above method of analysis was developed primarily for use as a rapid field technique, with the full realization that accuracy was necessarily being sacrificed for speed and convenience. Several consequent limitations and sources of error inherent in the method are recognized.

The main limitations are that: (1) The sediment must be air dry before weighing out a 50-gram sample for analysis, (2) all analyses should be made with the sediment-water mixture at approximately 25°C to avoid necessitating adjustments for the effect of temperature on the viscosity of water (preliminary data show that sediment time constants decrease in value with increasing temperature and indicate that corrections are linear and of the magnitude of about 1 percent per degree Celsius), (3) coarse-grained sediments (>0.5 millimeter) settle so fast that it is difficult to stabilize the cone and read the rapidly moving sediment interface in the short period of time before all settling has ceased, and (4) sediments comprised largely of fine silt and clay usually exhibit a poorly defined settling interface that can be read only approximately and with considerable difficulty.

Perhaps the largest error is introduced by measuring sediment volume rather than sediment mass. Volume measurements depend on the packing of individual particles, which in turn depends largely on the size and shape of the particles settling at any time. Volume-weight relationships are relatively constant for coarse sediments, but they are subject to variations of up to 20 percent for sediments made up largely of silt and clay. This source of error could be eliminated by measuring sediment mass directly (Odén, 1925; U.S. Interagency Committee on Water Resources, 1943; Guy and others, 1966) and substituting mass for volume in equation 9, except that these techniques for measuring mass are not practical for use in the field.

The inclined sides of the Imhoff cone retard settling velocities slightly and thereby increase slightly the numerical value of time constants obtained. This effect can be disregarded if all analyses are made with an Imhoff cone and if the values of the parameters obtained are considered to be relative rather than absolute. The writers believe that the availability of Imhoff cones, the ease with which they can be transported in the field, and the increased accuracy of volume measurements afforded by their conical shape, far more than offset any disadvantages introduced by the inclined sides.

More rigorous disaggregation of the sample, coupled with chemical dispersion of the fine-grained particles, undoubtedly would affect the settling characteristics of a sediment. Although considerable disagreement exists as to the method of treatment that yields the most consistent results, the writers believe that sediment particles in transport are seldom completely disaggregated and (or) dispersed. Accordingly, treatment of the sample was purposely kept simple so that results would be more relevant than they would have been after elaborate artificial treatment. More work is needed to determine the effects of disaggregation and dispersion on the settling characteristics of sediments. The limited data available, however, indicate that the effects are comparatively small because of the short time duration of the analysis (6 minutes for a settling column of 27 to 38 centimeters, depending on the accumulation of sediment in the bottom of the cone).

Ideally, a longer settling tube should be used to minimize the effect of the change in height of the settling column due to accumulation of sediment in the bottom of the tube. In the Imhoff cone, for example, the height of the column decreases from 38 cm to about 27 cm, a change of almost 30 percent, during the average analysis. This source of error could be largely eliminated by using a 100-cm-long bottom-withdrawal tube (Guy and others, 1966) modified to serve as an accumulation tube. An elongate bottom-withdrawal tube, however, would be comparatively difficult to transport and use in the field.

After 6 minutes, the fine-grained particles remaining in suspension no longer settle at a constant rate as indicated by equation 9. This poses no problem to the present study because only the coarse fraction appears to be related to flow conditions in ephemeral stream channels. The fine-grained fraction appears to be important principally in the way it influences the settling characteristics of the coarse fraction. Once the coarse fraction has settled, the behavior of the fines remaining in suspension is relatively unimportant.

APPLICABILITY OF THE METHOD TO STUDIES OF EPHEMERAL STREAM CHANNELS

Analysis of about 200 sediment samples from selected locations in ephemeral stream channels in Arizona, Utah, and Wyoming, showed that virtually all channel deposits contained a coarse-grained (type I) fraction, and that most samples contained both a coarse-grained (type I) fraction and a fine-grained (type II) fraction. A few samples collected in quiescent backwater areas or on old flood plains showed only a fine-grained fraction.

It should be stressed here that the presence of both a coarse-grained (type I) fraction and fine-grained (type II) fraction does not mean that two separate phases of deposition occurred—one during high flow and another at a later time during the waning stages of flow. Rather, both sediment fractions seem to have been transported and deposited simultaneously as an integrated mixture. Available data suggest that the coarse-grained (type I) fraction is related in some way to flow conditions (probably velocity), whereas the fine-grained (type II) fraction reflects mainly sediment source and availability. The fine-grained fraction is important to this study mainly because it, in effect, increases the density and viscosity of the fluid media which, in turn, enhance the ability of the stream to transport the coarse fraction.

Results of analyses show that values of the time constant (T_c) were invariably lowest in the deepest part of a channel where velocity was inferred to be highest during any runoff event. As T_c is inversely proportional to average settling velocity of the coarse fraction, this is the same as saying that those particles that settle fastest were invariably found in the deepest part of the channel where the velocity was inferred to have been greatest. Without exception, values of T_c for samples collected across a given channel section increased with decreasing depth of flow and changed in the downstream direction consistent with changes in velocity as inferred

from channel geometry. For example, values of T_c increased in the downstream direction in expanding reaches through which stream velocity normally decreases and decreased in the downstream direction in contracting reaches through which stream velocity normally increases.

None of the ephemeral streams sampled during the course of this study was observed during a runoff event. The exact relationship of T_c to actual velocity distributions, therefore, remains unknown. It is significant to note, however, that attempts to correlate the single parameter T_c with corresponding channel parameters such as variations in apparent depth of flow across a channel width, revealed a greater scattering of points than might be expected from flow vagaries alone. As a result, the writers examined more closely other parameters in equation 9. As expected, values of the time constant for the fine-grained fraction (T_f) showed no apparent relationship to flow conditions. Values of V_c and V_f showed no obvious patterns in themselves, and yet simple comparison of these parameters with corresponding values of T_c for adjacent samples in a given reach showed that changes in T_c seemed to be compensated for in part by changes in the relative amount of the coarse materials deposited (V_c).

To test the significance of the parameters T_c and V_c as possible indicators of flow conditions, the writers collected samples at intervals of 10 feet along a line 1,000 feet in length up the center of a broad flood plain called Freeman Flat near Safford, Ariz. Prior to failure of a diversion dam, water diverted from Freeman Wash was artificially spread across the full width of this flood plain by a series of low V-mesh wire fences constructed along the contour and spaced at intervals of about 400 feet. Aggradation had occurred behind the fences, in effect, in a channel so wide that bank effects could be safely ignored. Presumably, flows moving across Freeman Flat experienced the same pattern of acceleration and deceleration and thus had the same tendency to degrade and aggrade as they passed through one permeable fence barrier after another. Although the system is no longer functional, the writers reasoned that the sediments that had accumulated behind the respective wire fence barriers should exhibit the same or very similar patterns of deposition; that is, if sediments are actually deposited in equilibrium with flow conditions. The writers were greatly encouraged to discover that such a pattern does in fact exist and can be shown graphically by plotting computed values of T_cV_c against distance on line.

SUMMARY AND CONCLUSIONS

The initial objectives of this study have been fulfilled. A simple field procedure requiring less than 20 minutes per sample was developed for measuring the settling characteristics of selected sediment samples. A novel approach was used to analyze results of the field procedure in that (1) graphs obtained by plotting accumulated volume of sediment versus time (sediment settling curves) were regarded as having a mathematical solution, (2) the form of the equation fitting a settling curve was obtained by comparing a sediment-water system with an analogous electrical system, and (3) sediments were regarded for the first time as being generally composed of a coarse-grained fraction which seems to be related to flow conditions during the time of deposition and a fine-grained fraction which influences transport of the coarse-grained fraction. Trial application of the method has yielded encouraging results at Freeman Flat near Safford, Ariz.

The next phase of the study involves (1) the collection of sediment samples during periods of streamflow when velocity distributions can be measured directly, and (2) the evaluation of the data in the light of past studies, particularly to determine what, if any, modifications should be made in the field procedure to yield the most meaningful and consistent results.

The applicability of this method of analysis to studies other than those pertaining to ephemeral stream deposits has not been determined. In theory, however, the method should be valid for all sediments deposited in a fluid media, provided only that they settle according to equation 9. Probably, however, the values of the parameters thus obtained would offer only a means of comparing one sample with another deposited in a similar environment. Present indications are that values are not absolute, but depend on a number of variables. For example, parameters determined by this method for eolian deposits should not be compared directly with those obtained from analyses of sediments deposited in water. The method need not be limited to studies of unconsolidated sediments if suitable disaggregation of lithified sedimentary rocks can be achieved.

REFERENCES

Guy, H. P., and others, 1966, Laboratory theory and methods: U.S. Geol. Survey open-file rept., 109 p.

Leopold, L. B., and Miller, J. P., 1956, Ephemeral streams—hydraulic factors and their relation to the drainage net: U.S. Geol. Survey Prof. Paper 282–A, 37 p.

Odén, Sven, 1925, The size distribution of particles in soils and the experimental methods of obtaining them: Soil Sci., v. 19, p. 1–35.

Rubey, W. W., 1933, Settling velocities of gravel, sand, and silt particles: Am. Jour. Sci., 5th ser., v. 25, no. 148, p. 325–338.

Schumm, S. A., 1960, The shape of alluvial channels in relation to sediment type: U.S. Geol. Survey Prof. Paper 352–B, p. 17–31.

——— 1961, Effect of sediment characteristics on erosion and deposition in ephemeral-stream channels: U.S. Geol. Survey Prof. Paper 352–C, p. 31–70.

Twenhofel, W. H., and Tyler, S. A., 1941, Methods of study of sediments: New York and London, McGraw-Hill Book Co., Inc., 183 p.

U.S. Inter-Agency Committee on Water Resources, 1943, A study of new methods for size analysis of suspended sediment samples, *in* A study of methods used in measurement and analysis of sediment loads in streams: U.S. Army Corps of Engineers, Iowa City, Iowa, Report 7, 102 p.

GEOLOGY OF A PART OF NORTH VICTORIA LAND, ANTARCTICA

By DWIGHT F. CROWDER, Menlo Park, Calif.

Abstract.—The extensive graywacke and siltstone sequence of the Robertson Bay Group is bounded on the west by the Bowers Group, of shallower water origin. Both groups are now low-grade semischists, phyllites, and slates with northwest-trending fold axes. The Bowers Group consists of the Camp Ridge Quartzite, and west of it the Sledgers Formation composed mostly of calcareous sedimentary rocks and some volcanic rocks. The extensive unit of medium-grade gneiss and schist that lies west of these various low-grade rocks may be their more highly metamorphosed equivalents. Posttectonic granodioritic plutons of possible late Paleozoic age intrude the Robertson Bay Group as discrete, equidimensional masses. Whether similar granodiorite plutons in the gneiss and schist terrane are of the same age is uncertain. Small outliers of flat-lying arkosic sandstone lie unconformably on the gneiss and schist and on the Sledgers Formation and are cut by dolerite sills. Locally, these Mesozoic Beacon and (or) Ferrar Group rocks are tilted or tightly folded.

In November 1964 a U.S. Geological Survey field party, consisting of the author and Warren Hamilton assisted by Donald A. Coates, made a helicopter reconnaissance of the rugged and high snow-shrouded mountain country making up the northern extremity of the Transantarctic Mountains. The area covered and all the geologic data mapped by us are shown in figure 1. Helicopters based at Hallett Station were used to reach approximately 100 landing spots in a 40,000-square kilometer study area. Plutons were delimited from the air by flying along their conspicuous contacts. The continuity of units was rapidly and firmly established by flying close to the most exposed ridges and cliffs while estimating attitudes (from the sun's position and the time) and observing characteristic color, cleavage, and bedding. Thirty man-days were spent in fieldwork. This reconnaissance rapidly tied together largely confirmed and slightly modified discoveries made during three sledging surveys in 1956–57 (Harrington and others, 1964, 1967), 1962–63 (Le Couteur and Leitch, 1964), and 1963–64 (Sturm and Carryer, 1968). As a result, the rock types and their distribution, as well as the general trend of foliation, bedding, cleavage, and fold axes in this part of north Victoria Land, are now well known by present Antarctic standards. Much more detailed surveys will be needed if further subdivisions are to be made, particularly of the extensive and uniform easternmost unit, the Robertson Bay Group. A recently compiled geologic map of the whole of north Victoria Land (Am. Geog. Soc., 1968) draws on all studies to date. This map should be referred to for the best locations of our data.

The present report, a supplement to that map, clarifies our contributions and discusses the important unsolved problems that are now recognized. The late Cenozoic volcanic rocks along the Ross Sea, which have been described briefly (Hamilton, 1967; Crowder and Hamilton, 1967), are not discussed here.

Acknowledgments.—Discussions with New Zealand geologists have been very helpful; we thank Simon Carryer for his excellent advice without which we would not have extended our explorations westward, beyond the uniform metasedimentary rocks near Hallett Station, to the more diverse rocks of the Bowers Group near the Rennick Glacier; George Grindley for his information concerning the stratigraphic relations of the Bowers Group; and Bryce Wood for discussions of the form of plutons near Hallett Station. Field logistical support was provided by the U.S. Navy; the U.S. Army provided the essential helicopter support. The study was made under the auspices and with the support of the Office of Antarctic Programs, U.S. National Science Foundation.

GENERAL GEOLOGY

West of the volcanic rocks along the Ross Sea, the Transantarctic Mountains are carved from slightly metamorphosed sedimentary rocks and a few granodiorite plutons. The metasedimentary rocks are folded about northwest-trending axes and are fairly well exposed (fig. 2) east of long 167° E. Three distinct lithologic units were mapped—the Robertson Bay Group on the east, and the two formations of the Bowers Group on the west (fig. 1). A terrane of distinctly higher grade metamorphic rocks—medium-grade gneiss

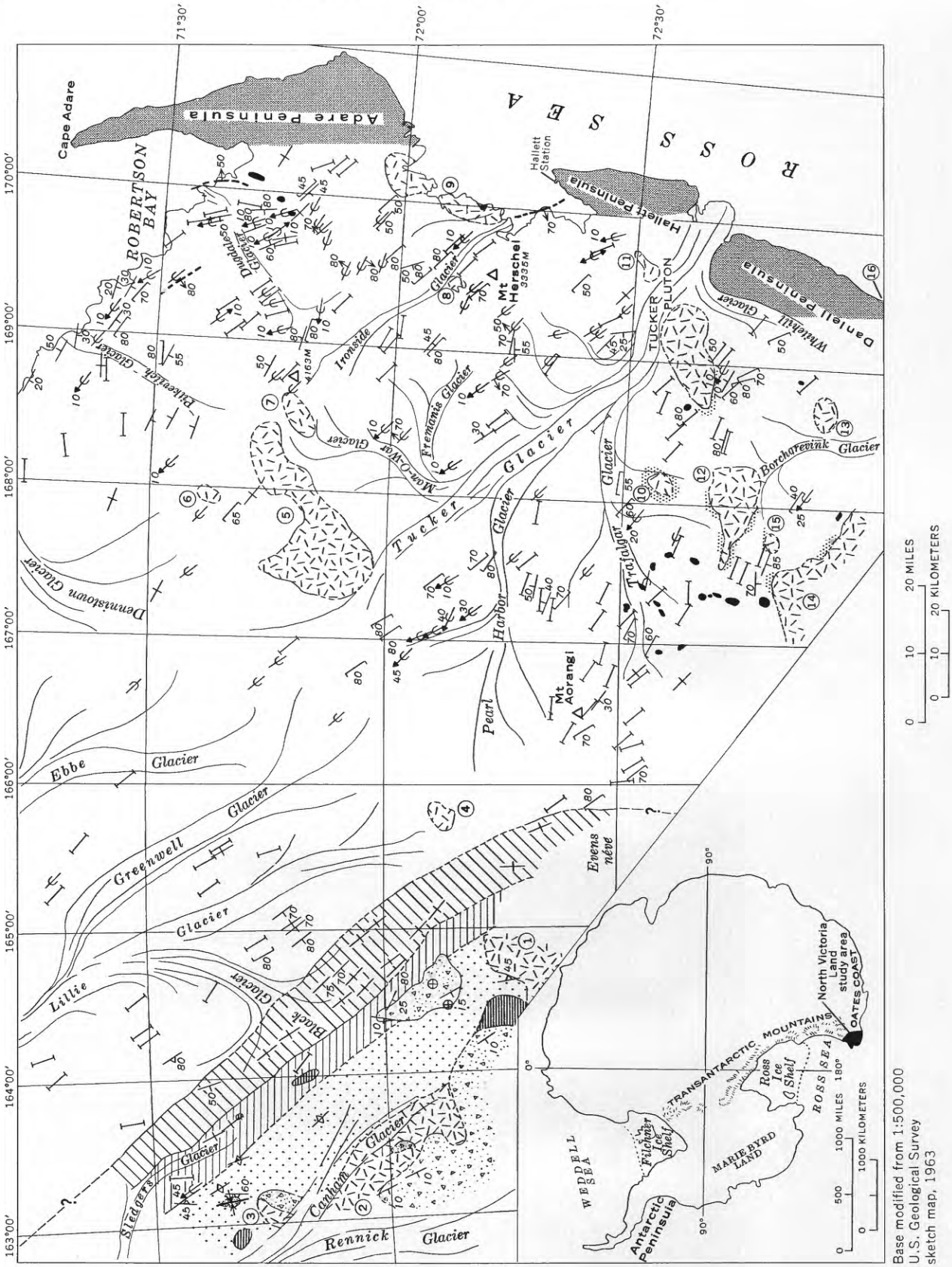

Base modified from 1:500,000
U.S. Geological Survey
sketch map, 1963

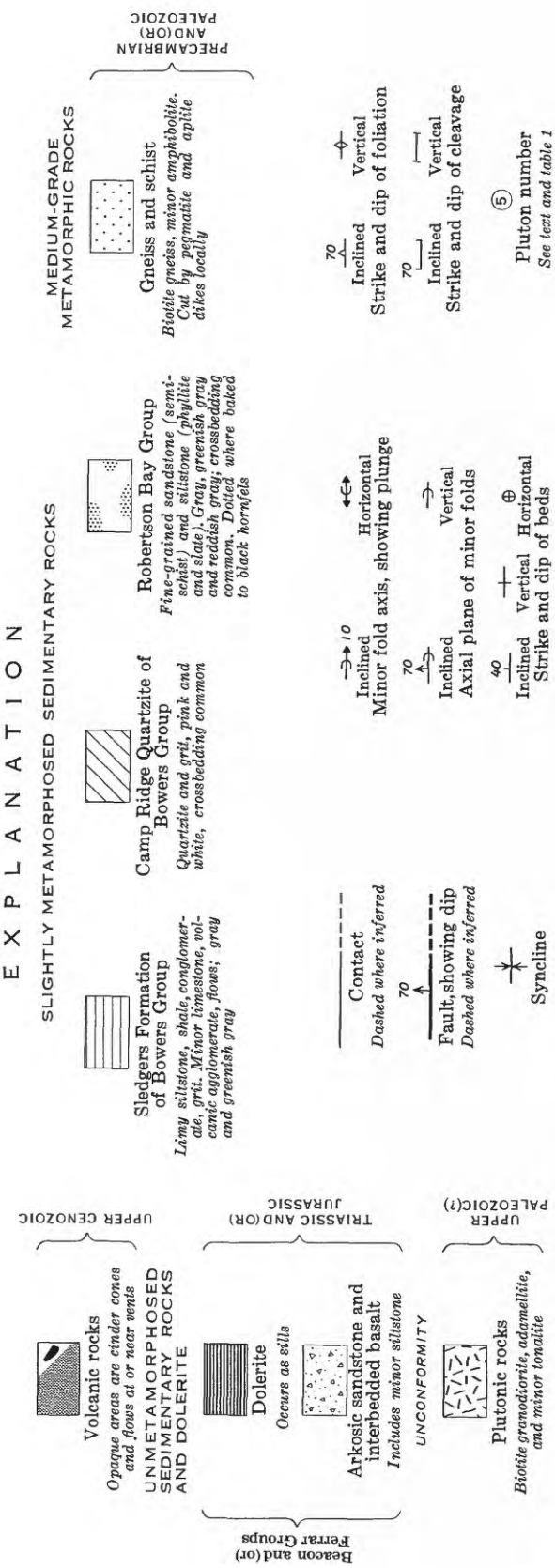

FIGURE 1.—Geologic map of a part of north Victoria Land, Antarctica.

and schist—occurs west of these metasedimentary rocks. Plutons also occur in this gneiss and schist terrane. Because the stratigraphic relations between the several low- and medium-grade unfossiliferous rocks are unknown, they are discussed geographically east to west.

Unmetamorphosed sandstones lie unconformably on the gneiss and schist, on some plutons, and on some of the low-grade sedimentary rocks, and are intruded by dolerite sills. The rocks are Triassic and (or) Jurassic phases of the Ferrar and (or) Beacon Groups.

SLIGHTLY METAMORPHOSED SEDIMENTARY ROCKS

Robertson Bay Group

The type localities for the Robertson Bay Group on Robertson Bay and near Hallett Station were designated by previous workers (Rastall and Priestley, 1921; Harrington and others, 1967, p. 21). These rocks are remarkably uniform, simply folded, and fairly thin bedded semischist, phyllite, and slate that were once argillaceous quartzose sandstone and siltstone (fig. 2). They were found to be virtually as described by previous workers (Harrington and others, 1967, p. 21–26; Le Couteur and Leitch, 1964, p. 230–232; Sturm and Carryer, 1968).

Lithology.—Dark- to light-gray, brownish-gray, and greenish-gray rocks, particularly fine-grained semischists, predominate. The term "graywacke" is commonly used in describing the Robertson Bay Group and refers to a dark, usually gray semischist or phyllite containing poorly sorted angular to subangular clasts, mostly quartz, in a sericitic and chloritic matrix of recrystallized argillaceous material (see p. D99). A volcanic detrital component has not been recognized. Le Couteur and Leitch (1964, p. 231) report that sills and flows of altered basic volcanic rocks occur locally in minor amounts. Small chips of argillite and round grains of granoblastic quartzite occur sparingly in some of the semischist. It is unlikely that these are intraformational clasts, hence the source terrane probably included sedimentary rocks. Calcareous rocks are rare, and calcite clasts were found in only one sandstone near Dennistoun Glacier (long 168° E., lat 71°15′ S.). Near the mouth of the Tucker Glacier, calcite occurs as "irregular grains" in calcareous biotite-bearing metagraywacke (Harrington and others, 1967, p. 31).

Depositional environment.—Harrington and others (1967, p. 25) found no slump structures, nor did we; but load casts occur (long 168°30′ E.; lat 72°45′ S.) and flute casts and flow casts have been reported (Le Couteur and Leitch, 1964, p. 230; Sturm and Carryer, 1968). The

FIGURE 2.—Slightly metamorphosed sedimentary rocks of the Robertson Bay Group on the north side of the upper Tucker Glacier. View is toward northwest along the regional strike of the vertical to steeply dipping axial planes, axial-plane cleavages, and the horizontal or nearly horizontal fold axes. Foreground ridge is about 300 meters high. The clearly visible beds extend for long distances and have a uniform thickness ranging generally from a few centimeters to a few meters. Laminations of millimeter scale occur in many places.

extensive and uniformly thick beds are commonly graded and crossbedded and were clearly deposited by currents in standing water. Both Le Couteur and Leitch (1964, p. 232) and Sturm and Carryer (1968) propose that the sediments were deposited in deep water, and the former suggest that they were deposited by marine turbidity currents though definitive features have not yet been reported.

Bowers group

Bounding the notably uniform Robertson Bay Group on the west is a northwest-trending belt of comparatively diverse sedimentary and volcanic rocks named the Bowers Group by Sturm and Carryer (1968); they believe that this group was deposited in shallower water than was the Robertson Bay Group. Two rock types can be delimited at reconnaissance scale: on the east is a belt of pink to white quartzite and quartz conglomerate named the Camp Ridge Quartzite by Le Couteur and Leitch (1964, p. 232–234), and on the west is a belt of sandstone, siltstone, and lesser amounts of conglomerate, all characteristically calcareous, and some volcanic rocks herein named the Sledgers Formation. Rocks of the Bowers Group, like those of the Robertson Bay Group, are mostly metamorphosed in the greenschist facies, as described below.

Camp Ridge Quartzite.—The light color of this formation, so distinctive from the air, enabled us to establish that the quartzite occurs in a uniformly narrow, elongate outcrop area 10–15 km wide—a belt that extends for about 140 km parallel to regional trends.

At the three outcrops visited, the rocks found were massive thick-bedded quartzites that are characteristically crossbedded, vary in color from white to pink including tan, and vary in grain size from fine to coarse. Some quartz-pebble conglomerate occurs. A few shale clasts were noted in addition to the well-rounded grains of quartzite and single quartz grains. Present between the larger clasts are sericite, iron oxide granules, and some small angular quartz grains. Overgrowths on quartz clasts were not seen, but some clasts have been

slightly to totally obliterated by recrystallization to granoblastic quartzite.

Sledgers Formation.—West of the Camp Ridge Quartzite lies a 10-km-wide belt of calcareous sandstone and siltstone including some limestone, grit, and conglomerate. A considerable amount of volcanic agglomerate and volcanic-derived argillite was seen, and some extrusives showing indistinct pillow structure were found in this belt by Sturm and Carryer (1968). Gray and greenish-gray rocks predominate. This belt of rocks is here named the Sledgers Formation for outcrops on either side of upper Sledgers Glacier. The sandstone and siltstone of the Sledgers Formation strongly resemble the Robertson Bay Group except that calcite clasts, instead of being rare, are ubiquitous.

Just north of the dolerite outlier at the head of Sledgers Glacier there is at least one bed of fissile limestone. West of upper Sledgers Glacier, conglomerate and grit contain clasts of marble and various calc-silicate granofelses that are clearly calcareous rocks (medium-grade metamorphic rocks as described below). Previous workers (Le Couteur and Leitch, 1964; Sturm and Carryer, 1968) noted calcite veins, calcareous agglomerates, and limestone. It is, therefore, safe to characterize the Sledgers Formation as calcareous.

Depositional environment.—The probability that the Bowers Group was deposited in relatively shallow water (Sturm and Carryer, 1968) is suggested by the presence of the limestone and coarse clastic rocks and by the dearth of argillaceous detritus in the quartzite. Le Couteur and Leitch (1964, p. 232–233), in contrast, class the whole sequence as "dominantly nonmarine" and interpret the quartz conglomerate and quartzite of Camp Ridge as deltaic and estuarine deposits and the pink quartzite as possible dune or flood-plain deposits because of the pink to red color.

Metamorphism

The regional metamorphism of the slightly metamorphosed sedimentary rocks, as typified by rocks of the Robertson Bay Group, is of the low-grade greenschist facies. This metamorphism has been ascribed to the prehnite-pumpellyite subfacies and possibly to some chlorite-2 facies metamorphism (Harrington and others, 1967, p. 27) or simply to the greenschist facies (Le Couteur and Leitch, 1964, p. 231; Sturm and Carryer, 1968). In our samples muscovite in parallel and subparallel flakes is the most common metamorphic mineral and occurs throughout the phyllite and slate and in the once argillaceous matrix of the semischist and phyllite. Chlorite occurs in the scattered flakes that are conspicuously larger but much less abundant than the muscovite grains. Crosscutting veinlets of quartz and calcite, felsic halos around pyrite, and saussuritized plagioclase occur, but such effects of late solutions are neither conspicuous nor pervasive.

Thermal metamorphism has locally produced hornfels around plutons as discussed below. Indeed, all rocks of the Robertson Bay Group described by Harrington and others (1967, p. 27–31) are considered as contact metamorphic rocks and contain biotite, plus hornblende or cordierite, in the inner parts of aureoles. There is, therefore, a possibility that the low-grade greenschist facies metamorphism, called regional above, is instead a pervasive low-grade contact metamorphism.

Folds and faults

The overall aspect of folds in the Robertson Bay and Bowers Groups as exemplified by the Robertson Bay Group is fairly simple; entire folds are visible in exposed mountainsides (fig. 2, this report; Sturm and Carryer, 1968; Harrington and others, 1967, p. 26; Le Couteur and Leitch, 1964, p. 231). Prevalent wavelengths and amplitudes extend a few hundred meters. Apical angles of the folds were found to range generally from 20° to 50° (fig. 2), and isoclinal folds are rare; thus the folds are fairly tight or chevron, as described by Le Couteur and Leitch. In relatively few places are the folds open, as described by Harrington and others (1967, p. 26). No significant difference in the general character of the folding was noted from place to place, even though this was looked for during the several areal traverses that were made of the whole area. Sizable domains of more nearly west-striking fold axes and cleavage occur south of Tucker Glacier and west of Robertson Bay. These do not appear to be due to shouldering aside by plutons.

The parallelism of the northwest-trending fold axes in the Robertson Bay and Bowers Groups suggests that both have been involved in the same period of deformation (Sturm and Carryer, 1968). Explorations to date have probably not been intensive enough to have revealed multiple periods of folding, if such occurred.

Close inspection of mountainsides and cliffs, where cross sections of folds can be seen, shows that locally faults and small shears have been directed along preexisting bedding planes and along axial-plane cleavages (figs. 3 and 4). These dislocations have complex relations to quartz veins of diverse age and have resulted in a peculiar reversed cleavage worthy of further study (fig. 3). Whether these faults and reversals occurred during the main period of folding or later is uncertain.

Age

Plutons of possible late Paleozoic age intrude the Robertson Bay Group, and Mesozoic sandstone and dolerite correlative with the Ferrar and (or) Beacon Groups overlie the Sledgers Formation of the Bowers

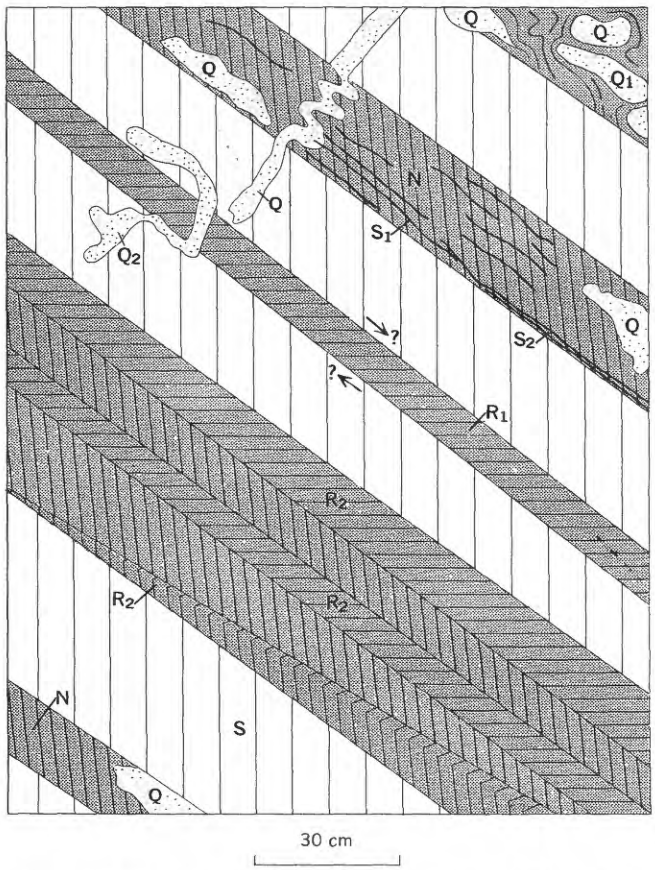

FIGURE 3.—A diagrammatic section perpendicular to the horizontal axis of a typical fold as seen in sea cliffs west of Hallett Station. Alternating semischist beds (unstippled) and phyllite beds (stippled). The vertical axial-plane fracture cleavage is better developed and more closely spaced in the phyllite than in the semischist. The cleavage is more nearly parallel to bedding in the normally cleaved phyllite layers (N) than it is in the semischist. In single anomalously cleaved phyllite layers (R_1), late differential movement(?) has reversed the cleavage beds. The cleavage also appears reversed in parts of other phyllite beds (R_2) without any sign of shearing. Late secondary cleavage parallel to bedding (S_1) and conspicuous at contacts (S_2) partly obliterates earlier axial-plane cleavage. Quartz veins and pods (Q) are concentrated in the phyllite and are contorted along with axial-plane cleavage in some layers (Q_1) but postdate its reversal in other places (Q_2).

Group. Deposition, metamorphism, and folding of the slightly metamorphosed sedimentary rocks must be pre-Mesozoic and possibly pre-late Paleozoic.

MEDIUM-GRADE METAMORPHIC ROCKS

Gneiss and schist

The medium-grade gneiss and schist of the study area were found west of the slightly metamorphosed (greenschist facies) sedimentary rocks in the Rennick Glacier area, except as noted below. The predominant rocks are composed of fine-grained biotite-plagioclase-quartz gneiss (minerals listed in order of increasing abundance) with a granoblastic texture. The plagioclase consists of oligoclase-andesine or, locally, albite. Mafic minerals are concentrated in millimeter- to centimeter-thick layers. Black to greenish schistose layers several meters thick and rich in hornblende are subordinate to the gneiss. In places clinozoisite-epidote, diopside, and hornblende are abundant. Microcline or muscovite are present locally.

Medium-grade metamorphism is suggested by the mineral assemblage (epidote-amphibolite or amphibolite facies). The foliation and layering, as measured at five of the six landing spots by us and by Sturm and Carryer (1968), trend north and northwest. In many outcrops in the study area the gneiss and schist are cut by numerous light-colored granitoid and pegmatite dikes and conformable lenses of quartz, but other features that might suggest very deep burial and ultrametamorphism such as felsic segregations, swirling, brecciation, or massive phases were not observed. Such features are conspicuous north and west of Rennick Glacier (Sturm and Carryer, 1968).

Origin.—These rocks may be of sedimentary origin, but the evidence is sparse. Angular quartz grains, scattered through granoblastic aggregates, may be relict clasts, and small-scale layering may be relict bedding. The abundance of clinozoisite-epidote, diopside, and quartz suggests an original siliceous and calcareous composition.

Correlation and age.—Neither the name Wilson Group nor Rennick Group previously applied to the gneiss and schist in the map area (Grindley and Warren, 1964; Sturm and Carryer, 1968; Am. Geog. Soc., 1968; Gair and others, 1965) has been used in this report. Because exposures are few and lithologic types are not distinctive, the gneiss and schist have not been traced (and possibly cannot be traced) successfully to type localities in the Wilson Hills or elsewhere. Furthermore, the rocks of the type area in the Wilson Hills appear to be more varied and are migmatized (Sturm and Carryer, 1968). I agree with McLeod's summary of the many uncertainties that concludes "at the present state of knowledge petrographic correlations are of doubtful value" (McLeod, 1964, p. 485). Like the slightly metamorphosed sedimentary rocks, the gneiss and schist lie under the Mesozoic arkosic sandstone and dolerite and thus are pre-Mesozoic in age.

Anomalies and contact relations.—One traverse was made up a well-exposed spur west of Sledgers Glacier (long 164° 15′ E.; lat 92°25′ S.) across about 1.5 km of the Sledgers Formation to its contact with the gneiss and schist unit. The Sledgers Formation here consists of alternating layers of calcareous or limy grit and conglomerate. These rocks were not observed elsewhere in this unit, though they have been seen at other places by Sturm and Carryer (1968). In the conglomerate, greenish-white to greenish-black clasts as much as

FIGURE 4.—Faults subparallel to bedding in an anticline of the Robertson Bay Group on Mount Aorangi (long 166°30′ E; lat 72°25′ S.). Note that the thin beds in the core of the fold are truncated (on the right) by the bedding-plane fault lying below the upper, more massive unit.

several inches in length and angular to lenticular in form occur in a dark-green to black matrix. Contacts between clasts and matrix vary from sharp to gradational. Some clasts are attentuated though cataclastic textures are absent. The clasts consist of marble, actinolite semischist, quartz-actinolite-hornblende rock, and sericitic quartzite and occur in a matrix of hornblende-epidote-calcite-plagioclase-quartz granofels. Ill-sorted sericitic quartz sandstone layers interbedded with the conglomerate contain some quartzite clasts and chlorite altered from biotite. At the abrupt contact with the gneiss, a 10-meter-thick layer of breccia occurs in which a matrix of epidote-hornblende-plagioclase-quartz granofels contains inclusions of similar but darker granofels notably rich in hornblende. The epidote-muscovite-biotite-plagioclase-quartz gneiss next to this breccia has a granofelsic texture and contains a considerable amount of chlorite, some of which is clearly derived from biotite. Mafic-rich layers in the gneiss are folded on centimeter scale and are cut by a later foliation marked by parallel biotite flakes. It is apparent that the limy conglomerates and grits of the Sledgers Formation near this contact are medium-grade rocks (epidote-amphibolite or amphibolite facies). They thus resemble in metamorphic grade the adjacent gneiss and schist and not the lower grade (greenschist facies) rocks to the northeast.

In the Robertson Bay Group there is an "island" of medium-grade gneiss located at long 164°10′ E., lat 71°28′ S. It is of unknown size and its relationship to the low-grade rocks nearby has not been determined. The foliation dips steeply west. It may be an area of contact-metamorphosed rocks overlying a pluton.

PLUTONIC ROCKS

Seventeen separate bodies of granitoid rock (plutons) were mapped in the study area. Fourteen of the plutons intrude and thermally metamorphose the folded rocks of the Robertson Bay Group and are clearly post-tectonic; because evidence to the contrary is lacking, these are all assumed to be contemporaneous. Harrington (Harrington and others, 1963, 1967) was convinced

that most of the plutons intruding the Robertson Bay Group are portions of a stratiform mass that he called the Tucker granodiorite. The existence of this stratiform mass was not confirmed. In this report (fig. 1) the informal name "Tucker pluton" is used for the pluton south of lower Tucker Glacier, and all other plutons are numbered.

Three plutons (fig. 1, Nos. 1, 2, 3), that could well be part of a single mass called the Freyberg batholith (Sturm and Carryer, 1968), occur in the gneiss and schist terrane. We found no evidence to suggest that these granitoid bodies differ in either character or age from the posttectonic plutons farther east. However, the contacts of these bodies with the adjacent gneiss and schist were not observed.

Lithology and internal variations

The prevalent rock of the plutons in the study area is a massive and hypidiomorphic granular biotite granodiorite containing orthoclase or microcline or both, oscillatory zoned plagioclase, and, locally, hornblende; biotite adamellite, biotite tonalite and biotite-hornblende tonalite also occur. The compositions (table 1, fig. 5) show a range compatible with crystal-liquid fractionation of a single magma.

In pluton 9 on a promontory at lat 72°4′ S., numerous melanocratic tonalite inclusions occur, sharply cut by dikes of lighter colored granodiorite. Both inclusions and dikes are cut by other varieties of granodiorite, including the prevalent biotite adamellite (table 1, sample 276). Farther south (on a promontory and island at lat 72°11′ S.) the prevalent hornblende biotite granodiorite (table 1, sample 353) contains numerous melanocratic granitoid inclusions and is locally splotched and streaked with indistinct wisps of darker granodiorite. A sheared hornblende-biotite tonalite containing inclusions of sandstone occurs a few kilometers to the north. The range in composition of granitoid rocks in pluton 9 (fig. 5) is considerable; this was also recognized by earlier workers (Harrington and others, 1967, p. 40), who aptly concluded that there were "a number of complexities in the emplacement of the granodiorite."

The same wide variation of rock types may exist in the Tucker pluton. At the north end of this mass a gray biotite granodiorite containing some hornblende (table 1, sample 310) is in sharp contact with a lighter colored, hornblende-free biotite adamellite (table 1, sample 311). The relative age of these two phases was not determined.

No significant differences were noted in either the appearance or the composition of plutons 1, 2, and 3 in the gneiss and schist (pluton 2, a large pink mass, was mapped from the air and was not visited). The biotite adamellite of pluton 3 (table 1, sample 424) lacks the oscillatory zoned plagioclase and is more altered to sericite and chlorite than are the other plutons. Pluton 1, a biotite-hornblende granodiorite (table 1, sample 391), is slightly gneissic and notably melanocratic at the one outcrop seen. The foliation may have formed during a late deformation that, at least locally, folded the overlying arkosic sandstone.

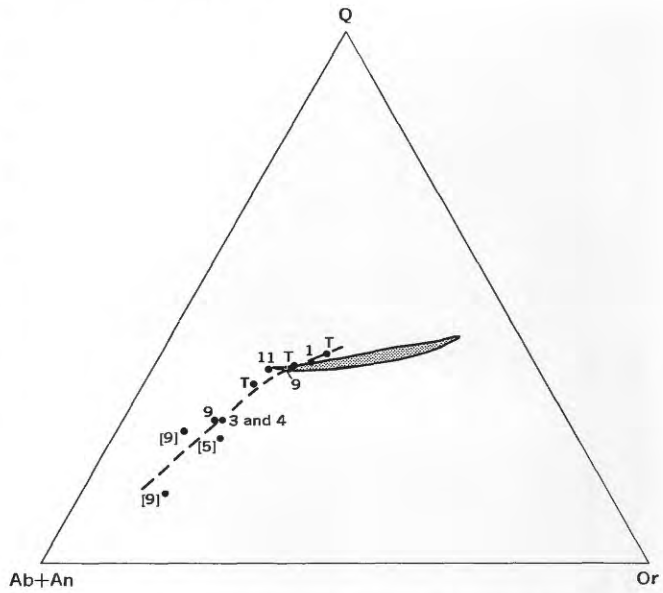

FIGURE 5.—Norms of plutons in north Victoria Land, Antarctica. Numbers correspond to numbers of plutons on figure 1; T corresponds to the Tucker pluton; data from table 1; bracketed pluton numbers are analyses of these plutons from Harrington and others (1967, p. 49). Outlined area is position of minimum melting trough at 1,000 atmospheres of water pressure (Bowen, 1954); the 760°C temperature contour is the line shown. Albite is the coordinate for the melting trough; error introduced is not appreciable because rocks that plot near the trough have plagioclase containing 80–90 percent albite. Compositions deviate little from the dashed line which trends toward the minimum melting trough; this suggests that the compositions were controlled by crystal-liquid fractionation of a single magma.

Inclusions

A few large inclusions of dark color and tabular form are revealed in cliffs of granodiorite facing the Tucker Glacier at long 169°15′ E. (Tucker pluton) and 167°30′ E. (pluton 5). These have been called "rafts" by Harrington and others (1963; 1964, p. 225; 1967, p. 40). Large dark inclusions are also numerous in pluton 16 on the coast, 3 km south of lat 73° S. The large inclusions and most of the small angular ones that we found in many other places are composed of muscovite-biotite-quartz-plagioclase hornfels and granofels. Some of them are slightly gneissic, and all are clearly fragments from the enveloping Robertson Bay host rocks.

Rounded, melanocratic hornblende-biotite tonalite inclusions occur at the north end of the Tucker pluton and are abundant in pluton 9. These plutons, as described above, consist of several types of granitoid

TABLE 1.—*Chemical composition and norms of plutons in part of north Victoria Land, Antarctica*

Name or No. of pluton	Tucker pluton			9		11	5	1	3
Sample No.	310	311	314	276	353	315	347	391	424
Chemical analyses [1]									
SiO_2	69.0	73.5	73.0	71.9	66.4	69.5	66.9	62.6	72.6
Al_2O_3	15.7	14.5	14.3	14.4	15.9	16.0	15.2	14.6	14.0
Fe_2O_3	.62	.37	.00	.33	.91	.13	.95	.74	.86
FeO	2.8	1.3	2.1	1.7	2.9	2.7	2.5	4.6	1.4
MgO	1.3	.6	.7	.9	2.4	1.4	2.6	5.1	1.0
CaO	3.1	1.4	1.9	2.3	4.3	3.0	4.0	5.6	1.8
Na_2O	3.2	2.9	3.2	3.1	3.5	2.8	3.6	2.1	3.1
K_2O	2.7	4.2	3.6	3.5	2.2	2.8	2.3	2.1	3.7
H_2O-	.26	.16	.13	.17	.13	.19	.15	.19	.18
H_2O+	.74	.58	.55	.62	.72	.75	.85	1.3	.82
TiO_2	.52	.22	.29	.32	.56	.49	.50	.60	.33
P_2O_5	.02	.23	.03	.25	.07	.11	.07	.15	.05
MnO	.07	.05	.06	.05	.08	.06	.08	.10	.03
CO_2	.05	.05	.05	.05	.05	.05	.05	.05	.05
Sum	100	100	100	100	100	100	100	100	100
Norms [2]									
Q	29.7	36.5	34.0	34.0	23.3	32.4	23.7	20.6	34.6
or	16.0	24.8	21.3	20.8	13.0	16.6	13.6	12.4	21.9
ab	27.1	24.5	27.1	26.4	29.6	23.7	30.6	17.8	26.3
an	15.2	5.4	9.2	9.8	20.9	14.2	18.6	24.3	8.6
C	1.9	3.2	----	2.0	.1	3.2	----	----	1.7
hl	----	----	----	----	----	----	----	----	----
wo	----	----	----	----	----	----	.4	1.1	----
en	2.3	1.5	1.7	2.3	6.0	3.5	6.5	12.7	2.5
fs	3.9	1.8	3.5	2.4	3.8	4.2	3.1	7.0	1.4
mt	.9	.5	----	.5	1.3	.2	1.4	1.1	1.2
hm	----	----	----	----	----	----	----	----	----
il	1.0	.4	.6	.6	1.1	.9	1.0	1.1	.6
ap	.1	.5	.1	.6	.2	.3	.2	.4	.1
fr	----	----	----	----	----	----	----	----	----
cc	----	----	----	----	----	----	----	----	----
Total	99.0	99.1	97.5	99.4	99.3	99.2	99.1	98.5	98.9
Total salic minerals	90.0	94.5	93.5	92.9	86.8	90.0	86.5	75.1	93.1
Total femic minerals	9.1	4.8	5.9	6.4	12.3	9.0	12.5	23.4	5.9
Semiquantitative spectrographic analyses [3]									
Ba	0.07	0.03	0.05	0.07	0.05	0.07	0.05	0.07	0.05
Be	.0002	.0002	.0003	.0002	.0001	.00015	.00015	.00015	.00015
Ce	.015	0	0	0	0	.015	0	0	0
Co	.001	.0003	.0005	.0007	.001	.001	.0015	.003	.0007
Cr	.0015	.001	.0007	.0015	.007	.003	.01	.03	.0015
Cu	.0015	.0005	.001	.001	.003	.0015	.003	.0015	.001
Ga	.0015	.0015	.0015	.0015	.0015	.0015	.0015	.0015	.001
La	.005	0	0	0	.005	.007	.003	.007	.003
Ni	.001	.0007	.0005	.0015	.005	.0015	.007	.01	.001
Pb	.003	.005	.005	.005	.003	.005	.003	0	.003
Sc	.0015	.0007	.0007	.0007	.0015	.001	.0015	.003	.0007
Sr	.02	.007	.01	.015	.03	.03	.02	.05	.015
V	.007	.005	.005	.005	.015	.01	.01	.02	.005
Y	.003	.002	.002	.002	.002	.002	.003	.003	.002
Yb	.0003	.0002	.0002	.0002	.0002	.0002	.0003	.0003	.0002
Zr	.03	.015	.01	.015	.015	.02	.015	.015	.015

310 Hornblende-biotite granodiorite; long 169°11′ E.; lat 72°36′ S.
311 Biotite adamellite; long 169°11′ E.; lat 72°36′ S.
314 Biotite adamellite; long 169°00′ E.; lat 72°37′ S.
276 Biotite adamellite; long 169°38′ E.; lat 72°08′ S.
353 Hornblende-biotite granodiorite; long 169°59′ E.; lat 72°13′ S.
315 Biotite granodiorite; long 169°41′ E.; lat 72°31′ S.
347 Hornblende-biotite granodiorite; long 168°10′ E.; lat 71°47′ S.
391 Biotite-hornblende granodiorite; long 163°08′ E.; lat 71°44′ S.
424 Biotite adamellite; long 164°51′ E.; lat 72°21′ S.

[1] By Lowell Artis, S. D. Botts, G. W. Chloe, P. L. D. Elmore, J. L. Glenn, H. Smith, D. E. Taylor.
[2] Norms calculated by computer.
[3] Semiquantitative spectrographic analysis by Chris Heropoulos. Looked for but not detected: Ag, As, Au, B, Bi, Cd, Ge, Hf, Hg, In, Li, Mo, Nb, Pd, Pt, Re, Sb, Sn, Ta, Fe, Th, Tl, U, W, Zn. 0 means looked for but not detected. Data have an overall accuracy of ±15 percent except that they are less accurate near 1 mits of detection, where only one digit is reported.

rocks, and the melanocratic granitoid inclusions may be cognate. The obvious effects of engulfment on these dark inclusions are: the late crosscutting veinlets of orthoclase, the mottled extinction of plagioclase and its conversion to epidote, and the reduction of the original large crystals of hornblende and biotite to aggregates of small grains.

Contact relations

The plutons that intrude the Robertson Bay Group are light colored and are easily distinguished from their dark host. All contacts are steep and sharp, and conspicuous dike offshoots are rare or absent. A complete areal circumnavigation of each mass was made (except Nos. 6, 4, 14, 16), and the shape and extent of each were thus well established. No evidence either for or against shouldering aside was found. There is no apparent pattern to the distribution of the plutons in the Robertson Bay terrane, though many plutons are somewhat elongate perpendicular to the regional fold axes and parallel to the elongate peninsulas of late Cenozoic volcanic rocks along the Ross Sea. Northeast-trending fractures may have guided the rising magmas. A northwest elongation of plutons in the gneiss and schist terrane is also recognized (Sturm and Carryer, 1968).

The dark-gray to black hornfels of the contact aureoles in rocks of the Robertson Bay Group was mapped from the air where well exposed. Detailed petrographic descriptions of various hornfelses, as given by Harrington and others (1967, p. 27–31), were confirmed; biotite is ubiquitous and characteristic, cordierite is common, and hornblende is rare. No biotite gneiss (Harrington and others, 1964, p. 225) was noted.

The contact on the south side of pluton 12 at long 167°30′ E. is knife sharp, and the evident width of the aureole is about 1.5 km, as judged from the extent of black rocks seen from the air. About a kilometer south of the pluton, biotite occurs in the argillaceous matrix of sandstone as irregular tiny grains. This matrix has recrystallized to a very fine grained granoblastic mosaic which surrounds large quartz grains whose original angular, clastic nature is still apparent. Closer to the pluton (a few hundred meters away), the grain size of the matrix is larger, cordierite is present, and the quartz clasts have been transformed to a granoblastic mosaic. The biotite, instead of occurring in the matrix in irregular grains as it does farther from the pluton, occurs throughout the whole rock in euhedral flakes. It is evident that a small-scale migration of K, Fe, Mg, and Al from the matrix into the quartz clasts has occurred.

Still closer to the pluton the black hornfels is cut by indistinct subparallel seams of slightly lighter colored hornfels and by definite and fairly sharply bounded dikes and sills of a dark-gray granofels. Angular inclusions of the darker hornfels are present in the dikes and sills. The lightest colored granofels, a fine-grained light-gray rock, is closest to the pluton. The gray granofels is identical to the nearby black hornfels in mineralogy and texture. It differs only in being somewhat coarser grained and in having biotite more fully segregated from the felsic minerals. The lighter color of the rock is caused by this difference in grain size and mineral distribution. Even though the gray granofels appears to be intrusive when it occurs in sharply bounded dikes and sills, it must be classed as a metamorphic rock formed by contact thermal metamorphism of sandstone. Perhaps the metamorphism has been catalyzed by solutions permeating the host along fractures. The only sign that the rocks have been mobilized in this process is a streakiness of some of the hornfels inclusions in the granofels. Despite the ultrametamorphic phenomena evident in the gray granofels, none of it contains hornblende.

Age

The Tucker granodiorite of Harrington (1967) has a Devonian whole-rock K-Ar age (Am. Geog. Soc., 1968); this is the only radiometric date within the study area proper and, being a single whole-rock age, is of questionable value. Potassium-argon age determinations on plutons (and metamorphic rocks) far removed from the study area (Ravich and Krylov, 1964; Webb and others, 1964) have been taken as indicating that some plutons intruding the Robertson Bay Group are of late Paleozoic age (Admiralty intrusives) and that others are early Paleozoic (Granite Harbor intrusives) or Precambrian (Campbell intrusives) (Grindley and Warren, 1964, p. 315, 320, 325–327; Sturm and Carryer, 1968; Webb and others, 1964, p. 599–600; Am. Geog. Soc., 1968). Local geologic relations neither support nor refute these age designations. The applicable radiometric work to date is of a reconnaissance nature and may be misleading. The K-Ar ages commonly vary more than the probable analytical error. These ages have not been tested by determinations on coexisting minerals, which are more retentive of argon than is biotite. Many ages were determined on whole rocks containing feldspar whose argon retention is poor and variable. Finally, the specimens are from regions of complex and little-understood geologic history.

UNMETAMORPHOSED SEDIMENTARY ROCKS AND DOLERITE

Flat-lying to gently dipping arkosic sandstones intruded by dolerite sills and interbedded with some basalt flows lie unconformably on the gneiss and schist, on the three plutons in the gneiss and schist terrane,

and on the Sledgers Formation. These relatively undeformed rocks have not been found overlying the Camp Ridge Quartzite or, with certainty, rocks of the Robertson Bay Group. On the top of an unvisited peak located at long 168°3′ E., lat 71°50′ S., a buff-colored rock, possibly sandstone if not a granitic rock, lies on folded sedimentary rocks of the Robertson Bay Group.

In the study area, dolerite is considerably less widespread than arkosic sandstone. The dolerite layers we observed were judged to be sills, not flows, because of dike offshoots and large conspicuous inclusions of sandstone that occur at the upper contact of one layer. Flows are reported in addition to sills, and basalt clasts and volcanic bombs occur in some of the interbedded sediments (Sturm and Carryer, 1968); thus, volcanism and sedimentation must have been contemporaneous. The sills would appear to be later rocks because their contacts are sharp and sandstone inclusions in them are angular. If the sills were the intrusive equivalents of the flows and had intruded the contemporaneous unconsolidated sediments, such features would not be expected.

Age and correlations

Probable correlatives of the arkosic sandstones, sills, and flows of the study area lie along the upper Rennick Glacier in a belt extending south of the study area for at least 250 km. Most of this belt to the south (Gair, 1967) is covered with flat-lying flows of Kirkpatrick Basalt of the Ferrar Group—flows having a thickness of at least 1,500 m and lying unconformably on basement terrane. Sills are not present, and interbedded sedimentary rocks are scarce. On Section Peak some 120 km to the south these interbeds, called Ferrar sediments, contain Early Jurassic fossils and volcanic clasts (Gair, 1967; Gair and others, 1965; Norris, 1965). On the basis of lithologic similarity and relative proximity, the sandstones and flows of the study area may be correlative.

One cannot dismiss the possibility that the sedimentary rocks and flows of the study area correlate instead with older Late Triassic sandstones 100 km farther south. On Timber Peak the fossiliferous sedimentary rocks referred to the Beacon Group are cut by a dolerite sill and underlain by dolerite that may be a sill or a flow (Gair and others, 1965; Norris, 1965).

What can be said with some certainty is that the arkosic sandstone and the flows and the sills of the lower Rennick Glacier area correlate with some of the youngest (Mesozoic) phases of that widespread suite of rocks referred to elsewhere as the Beacon and Ferrar Groups and, furthermore that in this area at the extremity of the Transantarctic Mountains volcanism was significant.

Deformation

The unconformity beneath the sandstone and dolerite is subhorizontal southwest and east of upper Canham Glacier and under the two small outliers of dolerite along upper Sledgers Glacier, but in two outliers north of lower Canham Glacier the unconfromity and the overlying sandstones are considerably deformed. (The structure of the third and westernmost outlier in this area was not observed.) Because in most places the sandstone and dolerite of the Beacon and Ferrar Groups are little deformed (Grindley and Warren, 1964, p. 327–328), the two deformed occurrences are anomalous. Sandstone beds and conformable layers of dolerite occur in the larger outlier adjacent to the lower Canham Glacier. These beds are parallel to the contact with the underlying tonalite and dip about 40° to the southwest. At the contact, a dolerite sill is present that contains tonalite xenoliths and from which small dikes branch into the tonalite. In the smaller outlier, overlying sandstone beds (and very minor amounts of shale) and the contact with the underlying gneiss form a tight syncline trending north. These outliers of deformed sandstone are assumed to be erosional remnants of a widespread sheet that was locally deformed. The folded sandstone beds might have been considered to be the Camp Ridge Quartzite were it not for their arkosic composition and their close association with dolerite. Not far to the west, Sturm and Carryer (1968) found similar rocks that are faulted and tilted.

STRATIGRAPHIC COMPLEXITIES AND STRUCTURE

Knowledge of the stratigraphy of the Robertson Bay Group, the Camp Ridge Quartzite, the Sledgers Formation, and the gneiss and schist, which also may be of sedimentary origin, is at present too vague, and the relations of the units too poorly known to interpret with confidence.

Relations between the Sledgers Formation and gneiss and schist

The only contact described by workers to date between any of these rocks is the one between the limy metaconglomerates and metagrits of the Sledgers Formation and the gneiss west of Sledgers Glacier as previously described. Nothing was seen that revealed their relative ages. The contact is not obviously a fault; however, shearing and visible offset of beds in cliffs along the eastern side of the Rennick Glacier have been noted (Sturm and Carryer, 1968). The elongate, stretched clasts in the conglomerate and the foliation that transects small folds in nearby gneiss attest to some differential movement parallel to the trace of the contact, but this movement has been healed by later

medium-grade metamorphism. The rocks at the contact show a transition from the calcareous conglomerate and grit of the Sledgers Formation on the east (now metaconglomerate and metagrit) to locally calcareous metasedimentary rocks(?) on the west (now gneiss and schist). The relation of either of these medium-grade rocks to the metasedimentary rocks of the greenschist facies, constituting the Bowen Group farther to the east, has not been observed. Neither has the relation been determined between the rock of the Robertson Bay Group and the gneiss "island" to the northeast. Sturm and Carryer (1968) have mapped rocks of the Robertson Bay Group within the Bowers Group. Unresolved complexities clearly lie in the Sledgers Glacier area.

The seeming absence of a fault and the continuity of medium-grade metamorphism across the contact with gneiss and schist in the Sledgers Glacier area support the possibility, voiced by others (McLeod, 1964; Sturm and Carryer, 1968), that the gneiss and schist may be more highly metamorphosed parts of the metasedimentary rocks that occur farther east. McLeod (1964; McLeod and Gregory, 1967, p. 8, 40) also makes this inference for "schists of the almandine-amphibolite facies" at Zykov Glacier on the Pacific Coast north of the study area (at long 164° E.) and separated from it by about 8,000 square kilometers of rugged and yet unvisited mountains.

Relations between the Bowers and Robertson Bay Groups

It has been suggested that the Bowers Group is younger than the Robertson Bay Group (Sturm and Carryer, 1968; Le Couteur and Leitch, 1964) and that the Camp Ridge Quartzite occurs as an infolded and downfaulted block (Le Couteur and Leitch, 1964, p. 232–233). However, it seems doubtful that downfaulting and downfolding of a younger Camp Ridge Quartzite would preserve a quartzite belt of such uniform width for more than 120 km along strike. Overall bedding attitudes (fig. 1) do not reveal a syncline in the quartzite but confirm the previous observations that most beds dip steeply and strike northwest along regional trends.

Sturm and Carryer (1968) state that owing to structural complexities and the reconnaissance nature of the work done, the stratigraphic sequence within the Bowers Group and its relation to the Robertson Bay Group are imperfectly known. Their subsequent speculation that the Bowers Group is the younger is based on their observation that it represents a different, shallower water facies and that it shows a different, lesser amount of deformation (we did not note a noticeably different amount of deformation). Differences in facies or in degree of deformation do not establish relative age. No definitive contact relations have been noted. Pebbles of quartzite in Bowers conglomerates have been noted by us west of Sledgers Glacier and by Sturm and Carryer (1968). These might be clasts of Camp Ridge Quartzite, but no clasts that are definitely known to have been derived from the Robertson Bay Group have been found. It seems best to conclude that the relative age of the Bowers Group is unknown.

REFERENCES

American Geographical Society, 1968, Geologic map of northern Victoria Land, Antarctica, *in* Bushnell, V. C., ed., Antarctic map folio series: Am. Geog. Soc., scale 1:1,000,000. [In press]

Bowen, N. L., 1954, Experiment as an aid to the understanding of the natural world: Acad. Nat. Sci. Philadelphia Proc., v. 106, p. 1–12.

Crowder, D. F., and Hamilton, W. B., 1966, Geology of northeastern Victoria Land, Antarctica [abs.], *in* Pacific Science Congress, 11th, Tokyo 1966, Proceedings, v. 3: Tokyo, Sci. Council Japan, Symposium 22, p. 11.

Gair, H. S., 1967, The geology from the upper Rennick Glacier to the coast, northern Victoria Land, Antarctica: New Zealand Jour. Geology and Geophysics, v. 10, no. 2, p. 309–344.

Gair, H. S., Norris, G., and Ricker, John, 1965, Early Mesozoic microfloras from Antarctica: New Zealand Jour. Geology and Geophysics, v. 8, no. 2, p. 231–235.

Grindley, G. W., and Warren, Guyon, 1964, Stratigraphic nomenclature and correlation in the western Ross Sea region, *in* Adie, R. J., ed., Antarctic geology: New York, John Wiley and Sons, Inc., p. 314–333.

Hamilton, W. B., 1967, The Hallett volcanic province: Antarctic Jour. United States, v. 2, no. 5, p. 177–178.

Harrington, H. J., Wood, B. L., McKellar, I. C., Lensen, G. J., 1963, Geological map of Ross Dependency, Tucker Glacier district: New Zealand Geol. Survey map, scale 1:250,000.

——— 1964, The geology of Cape Hallett–Tucker Glacier district, *in* Adie, R. J., ed., Antarctic geology: New York, John Wiley and Sons, Inc., p. 220–228.

——— 1967, Topography and geology of the Cape Hallett district, Victoria Land, Antarctica: New Zealand Geol. Survey Bull., n.s. 80, 99 p.

Le Couteur, P. C., and Leitch, E. C., 1964, Preliminary report on the geology of an area southwest of upper Tucker Glacier, northern Victoria Land, *in* Adie, R. J., ed., Antarctic geology: New York, John Wiley and Sons, Inc., p. 229–236.

McLeod, I. R., 1964, Geological observations in Oates Land, *in* Adie, R. J., ed., Antarctic geology: New York, John Wiley and Sons, Inc., p. 482–486.

McLeod, I. R., and Gregory, C. M., 1967, Geological investigations along the Antarctic Coast between longitudes 108° E. and 166° E.: Commonwealth of Australia Dept. Nat. Devel., Bur. Mineral Resources, Geology and Geophysics Rept. 78, 53 p.

Norris, G., 1965, Triassic and Jurassic microspores and acritarchs from the Beacon and Ferrar Groups, Victoria Land, Antarctica: New Zealand Jour. Geology and Geophysics, v. 8, no. 2, p. 236–278.

Rastall, R. H., and Priestley, R. E., 1921, The slate greywacke formation of Robertson Bay: British Museum, Nat. History Rept. (British Antarctic Terra Nova Expedition 1910–13), Geology, v. 1, no. 4, p. 121–129.

Ravich, M. G., and Krylov, A. J., 1964, Absolute ages of rocks from east Antarctica, *in* Adie, R. J., ed., Antarctic geology: New York, John Wiley and Sons, Inc., p. 579–589.

Sturm, A., and Carryer, S., 1968, Geology of the region between the Matusevich and Tucker Glaciers, North Victoria Land, Antarctica: New Zealand Jour. Geology and Geophysics. [In press]

U.S. Geological Survey, 1963, Northern Victoria Land, Antarctic sketch map, scale 1:500,000.

Webb, A. W., McDougall, I., and Cooper, J. A., 1964, Potassium-argon dates from Vincennes Bay region and Oates Land, *in* Adie, R. J., ed., Antarctic geology: New York, John Wiley and Sons, Inc., p. 597–600.

313-005 O—68——8

ISOCLINAL FOLDING INDICATED BY PRIMARY SEDIMENTARY STRUCTURES IN WESTERN MASSACHUSETTS

By NORMAN L. HATCH, JR., Beltsville, Md.

Work done in cooperation with the Massachusetts Department of Public Works

Abstract.—Regionally metamorphosed lower Paleozoic stratified rocks in the east limb of the Berkshire anticlinorium in western Massachusetts were affected by several stages of folding, one of which resulted in major isoclinal folds. The geometry of these isoclinal folds locally can be deduced from the map pattern of thin subunits and from abundant sedimentary structures that indicate tops of beds. Wavelengths of 200 to 1,000 feet are measured where the rocks involved are phyllites and schists; wavelengths of 2,000 feet are common where thicker bedded, more quartzose rocks are folded. Later folds, though widespread, are all small and apparently do not affect mapped contacts.

Minor isoclinal folds have long been recognized in outcrops of the metamorphic rocks in New England, and the existence of larger isoclinal folds has been inferred from various field data. Little information is available, however, on the number, size, and distribution of these isoclinal folds in most areas. In many places, this has led to great uncertainties in estimates of the thickness of map units.

Determinations of tops of beds from abundant primary sedimentary structures prove the existence of a set of major isoclinal folds in the well-bedded rocks of the Goshen Formation of Silurian and Devonian age in western Massachusetts. It is the purpose of this paper to present information on the form, size, and orientation of these folds.

Some of the mapping on which this paper is based was done with S. A. Norton, Department of Geological Sciences, Harvard University, with whom many of the ideas presented below were discussed. Able assistance in the field was provided by R. G. Clark, Jr., and S. F. Clark, Jr.

GEOLOGIC SETTING

The east limb of the Berkshire anticlinorium in western Massachusetts comprises a sequence of metamorphosed lower Paleozoic volcanic and sedimentary rocks (fig. 1). The regional metamorphic grade increases southward from garnet zone along the Massachusetts-Vermont border through staurolite and kyanite to sillimanite zone on the Massachusetts-Connecticut border.

The mapped units along the east limb of the Berkshire anticlinorium form north-trending steeply dipping parallel bands of rock that are offset only locally by mappable folds (Emerson, 1917, pl. 10; Chidester and others, 1967; Hatch and Hartshorn, 1968). Examination of individual outcrops, however, commonly shows very complex fold patterns with as many as three stages of superimposed folds. During the course of fieldwork in the Plainfield quadrangle (fig. 1) (P. H. Osberg, N. L. Hatch, Jr., and S. A. Norton, unpub. map), P. H. Osberg and the author worked out a structural history that involved four regionally significant stages of folding, as well as a fifth stage of minor folds that are localized around a small pluton (Hatch and others, 1967, p. 11–12). Briefly, in their inferred chronologic order, the four regionally significant stages are as follows:

1. A pre-Silurian, probably Taconic, deformation produced northwest-trending tight folds that are seen only in a few outcrops. This period of folding is in part inferred from the fact that the axes of the stage-2 folds generally are moderately to steeply plunging in the pre-Silurian rocks and gently plunging or horizontal in the Silurian and Devonian rocks.
2. A major deformation, probably Acadian, that affected both the pre-Silurian and the Silurian and Devonian rocks formed north- to northeast-trending isoclinal folds with generally steeply dipping axial surfaces. The dominant regional schistosity is parallel to the axial surfaces of these folds.

3. A geographically widespread but apparently less severe deformation (also probably Acadian in age) developed a conspicuous northeast-trending, northwest-dipping slip cleavage parallel to the axial surfaces of small open, commonly chevron, folds in both the bedding and the stage-2 schistosity. The slip cleavage is much more common than the related folds.
4. North-trending open folds with subvertical axial surfaces parallel to a well-developed axial-plane slip cleavage locally deform the stage-3 slip cleavage and are distinguished from the stage-3 folds largely on the basis of orientation.

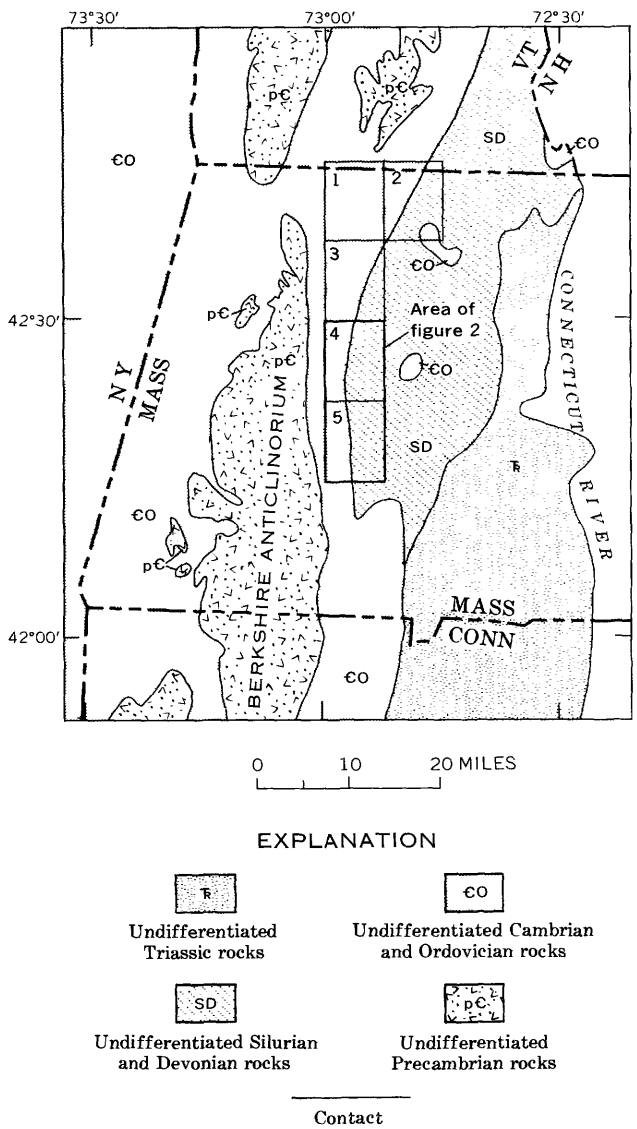

FIGURE 1.—Generalized geologic map of western Massachusetts and vicinity. Numbered 7½-minute quadrangles are (1) Rowe, (2) Heath, (3) Plainfield, (4) Worthington, and (5) Chester. Area of figure 2 outlined with heavy line.

The area of the present study consists of the eastern half of the Worthington and Chester 7½-minute quadrangles (quadrangles 4 and 5 of fig. 1) which are shown in figure 2. General descriptions of the stratigraphic units are available in Hatch and others (1967), Hatch (1967a, b), Chidester and others (1967), and Hatch and Hartshorn (1968). Only those aspects of the Goshen Formation that pertain to the present discussion are presented here.

The Goshen Formation of Silurian and Devonian age (Hatch, 1967b) underlies the eastern half of the Worthington and Chester quadrangles (fig. 2). It unconformably overlies the Middle Ordovician and older rocks that crop out in the western half of the quadrangles. The lower part of the Goshen, shown as the phyllite unit on figure 2, consists predominantly of gray to dark-gray quartz-muscovite-garnet-biotite-staurolite and locally kyanite phyllite and schist interbedded with light-gray, fine-grained quartz-mica schist or micaceous quartzite. These rocks form graded units generally 2 to 6 inches thick in which micaceous quartzite grades through quartz-mica-garnet schist into staurolite or staurolite-kyanite phyllite or schist. These rocks are metamorphosed cyclically graded sediments and probably represent an original gradation from slightly muddy fine sand or silt to silty mud. The upper part of the Goshen Formation, shown as the quartzite unit on figure 2, consists predominantly of light-brown to light-gray fine- to medium-grained quartzite, micaceous quartzite, calc-silicate schist and granulite, minor gray sandy garnet phyllite, and rare beds of punky-brown-weathering gray siliceous marble. Beds are generally 6 inches to 20 feet thick. A sequence of thin-bedded, generally graded bedded staurolite and staurolite-kyanite phyllite and quartzose schist, similar to the rocks in the lower unit of the formation, overlies the quartzite unit. This upper phyllite unit, which for reasons of scale is not distinguished on figure 2, is preserved in a few deeper synclines in the southern half of the area. The thickness of both the lower phyllite unit and the quartzite unit is probably about 1,000 feet. An estimated 500 feet of the upper phyllite unit is preserved locally.

The boundaries between these three Goshen units are gradational by interlamination of the characteristic lithologies for intervals of 50 to 100 feet. Staurolite- or kyanite-bearing phyllites are generally absent from the quartzose unit, whereas calcareous rocks and thick beds of quartzose rocks are generally absent from the phyllite unit. Local intertonguing of units in the Goshen is possible and even probable, but the continuity of the mapped units, the overall uniformity of their lithology, sequence, and thickness throughout the

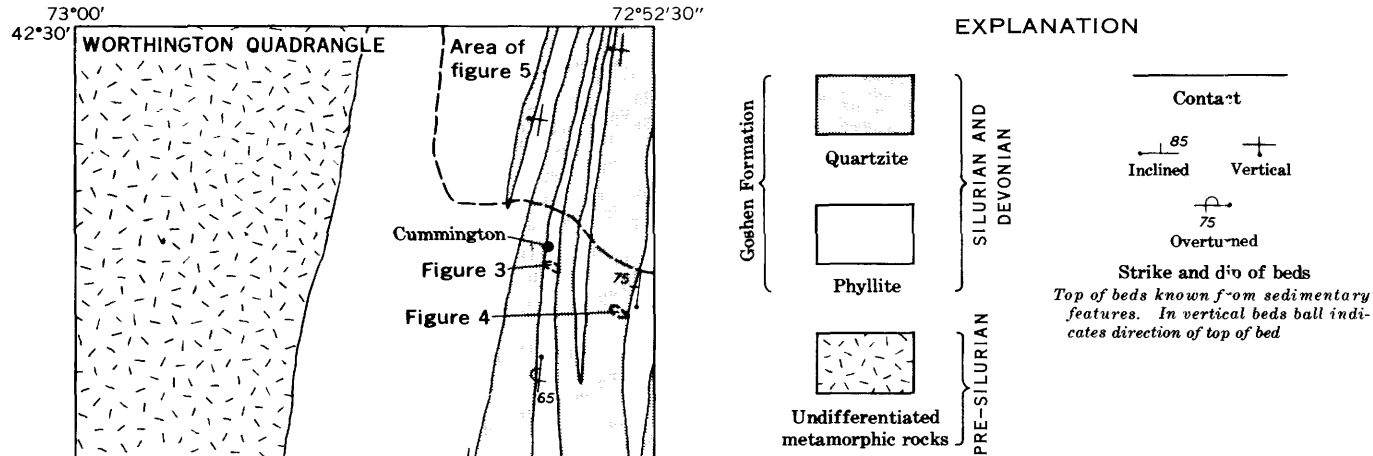

FIGURE 2.—Generalized geologic map of the Worthington and Chester quadrangles, Massachusetts, showing location of roadcuts illustrated in figures 3 and 4 and area of figure 5.

area, and the sedimentary tops data presented below, all indicate that such facies tongues are small or of very local extent.

EVIDENCE FOR AND SHAPE OF ISOCLINAL FOLDS

A fortunate combination of two factors makes it possible to work out, at least locally, the number, size, distribution, and orientation of isoclinal folds in these rocks. First is the abundance of primary sedimentary structures that indicate tops of beds, and second is the fact that the Goshen Formation can be subdivided into thin subunits. In addition to the graded bedding described above, channeling, crossbedding, and, rarely, intraformational breccias (Shrock, 1948, p. 277) have been used to determine tops of beds. Reliable determinations of tops have been recorded from about 75 percent of the exposures of the phyllite units and about 20 percent of the exposures of the quartzite unit.

In the eastern part of the area shown in figure 2, all beds dip steeply or vertically, and the regional schistosity is generally, though not everywhere, parallel to bedding. The only noticeable regional variation in the attitude of bedding (or schistosity) is a gradual change from steep east dips on the west to steep west dips on the east. The structure of the area was first interpreted as a homoclinal thick sequence of interlayered phyllite and quartzite bands. As mapping progressed, however, the sedimentary structures indicated that in nearly every case the quartzite unit overlay the phyllite unit. Thus, what was thought originally to be a thick

sequence of interbedded quartzite and phyllite was found to be a structurally complex but stratigraphically simple sequence of three fairly thin units. A sequence of tight isoclinal folds with generally vertical axial surfaces is indicated by (1) the abrupt and systematically distributed reversals of the direction of tops of beds, (2) the parallel strike and universally steep dips of all beds, regardless of top direction, and (3) the distribution of the quartzite and the phyllite lithologies.

The map pattern of the quartzite and the phyllite units is shown in figure 2. The overall continuity and parallelism of the major belts in figure 2 suggest that these folds, many of which are doubly plunging, plunge gently or horizontally; an inference supported by the few axes of isoclinal folds seen in the field. Unfortunately, no bedding cleavage or other lineation parallel to the axes of these folds was developed in the Goshen rocks to supplement the sparse field data on the local orientation of fold axes. Because of their gentle plunges, these folds can only be seen on large vertical or steeply inclined surfaces. Two such exposures, which have been described briefly elsewhere (stops 9 and 10 in Hatch and others, 1967) are here taken as examples.

Immediately south of the village of Cummington, on State Route 9, a large highway cut exposes a major isoclinal (stage-2) anticline (fig. 3). The rocks in the cut are predominantly thin-bedded phyllite and sandy schist typical of the lower phyllite unit of the Goshen. At the extreme west end of the cut, a few hundred feet west of the area shown in figure 3, thicker beds of micaceous quartzite and calcsilicate schist characteristic of the overlying quartzite unit are exposed. Excellent graded bedding in all parts of the outcrop proves that the fold (indicated by *A* on fig. 3) is a true anticline, the oldest rocks being in the core. The minor fold on the west limb of this anticline has the proper "sense" to be a drag fold related to the anticline, and the graded beds around it are compatible with this interpretation. Figure 2 shows the location of this roadcut. Although figure 2 does not, for reasons of scale, show fold axes, the map pattern indicates that this anticline has been traced across two quadrangles.

About 1 mile southeast of the exposure portrayed in figure 3 is another large roadcut that is shown in part in figure 4; its location is shown on figure 2. The rocks in this cut are micaceous and calcareous quartzites and schists in beds 6 inches to 3 feet thick and are typical of the quartzite unit of the Goshen Formation. They are folded into a broad open syncline. Graded beds and an intraformational breccia indicate that all the beds are right side up. Although the open and rounded form

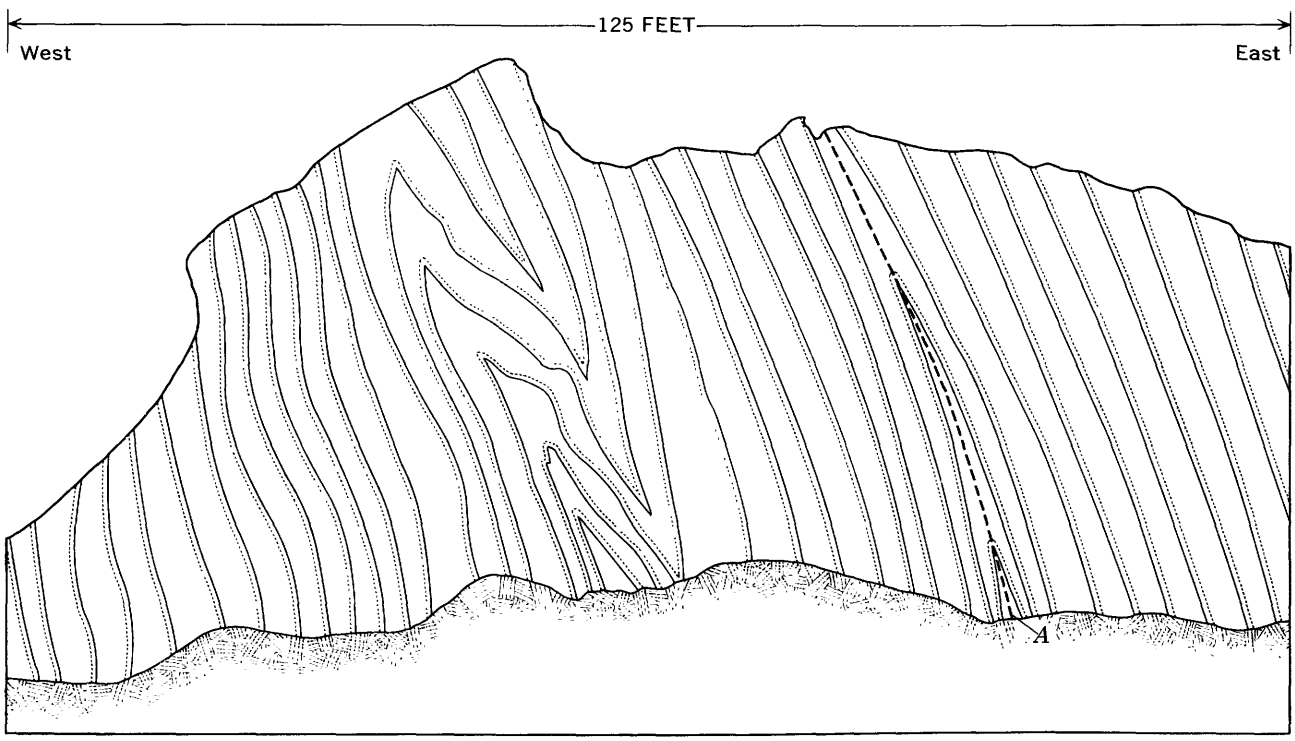

FIGURE 3.—Sketch of an isoclinal anticline in thin-bedded Goshen phyllite and sandy schist in roadcut immediately south of Cummington village (see fig. 2). Lines indicate form but not true thickness of beds. Dots are along bottom of graded beds and indicate that the major fold, *A*, is a true anticline. Dashed line is axial trace.

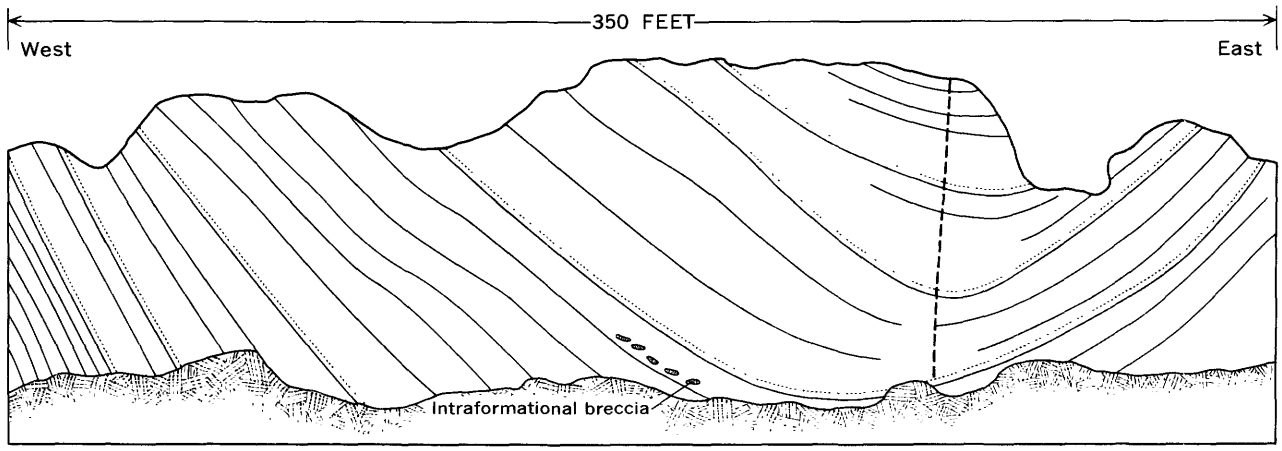

FIGURE 4.—Sketch of a syncline in micaceous and calcareous quartzites and schists of the Goshen Formation; roadcut southeast of Cummington village. Dots are along bottom of graded beds. Dashed line is approximate position of axial trace.

of this fold contrasts sharply with the tight fold shown in figure 3, examination of the ends of the roadcut shown in figure 4 and of nearby outcrops shows that within about 300 feet east and west of the axial trace of the fold, the two limbs are parallel; thus, the fold is indeed isoclinal. The openness of this syncline in the vicinity of its axis is presumably due to the greater competence of the thicker bedded, more granulose rocks of the quartzite unit relative to the thinner bedded, more micaceous rocks of the phyllite unit.

Minor folds related to the major isoclinal folds, though abundant in the pre-Silurian rocks, are scarce in the Goshen Formation. In fact, the one illustrated in figure 3 is the only one present in about 750 feet of across-strike exposure in this cut; none are present in a similar length of the cut, part of which is shown in figure 4. Only about 10 such minor stage-2 folds were seen in the whole area of this report. This scarcity of minor folds is entirely consistent with the smooth contacts along the limbs of the major folds (fig. 2).

DISTRIBUTION AND WAVELENGTH OF FOLDS

Axial traces of the isoclinal folds have been located primarily from reversals in the direction of tops of beds as indicated by sedimentary structures. These data, with few local exceptions, are compatible with the structure indicated by the distribution of map units. In the westernmost part of the area of the Goshen Formation, all the rocks are assigned to the lower phyllite unit, and the geometry of the isoclinal folds has been deduced entirely from tops of beds data. Unfortunately, bedrock exposures, and thus tops data, are irregularly distributed, so that the pattern of folding within the phyllite unit is well known in some areas and is virtually unknown in others. The distribution and wavelength of isoclinal folds in the phyllite are shown by the axial traces in the western part of the area shown in figure 5 (location shown on fig. 2) and by the interpretive section of the same area (fig. 6). The spacing of the axial traces in the phyllite area is typical of other fairly well-known areas that are underlain by phyllite (fig. 2). The axial traces are about 100 to 500 feet apart, meaning that the folds have wavelengths of 200 to 1,000 feet. In the eastern part of the area shown in figure 5, where the quartzite unit is involved in the folding, the wavelengths of the folds average nearly 2,000 feet. This difference in wavelengths is observed throughout the area and, like the difference in angularity between the folds in phyllite and the folds in quartzite, is believed to be simply a function of the relative competence of the rocks involved.

The pattern of axial traces in the eastern part of the area shown on figure 5 is consistent with about 95 percent of the field data on stratigraphic tops. The few anomalous readings could presumably be attributed to (1) local reversals resulting from minor folds similar to the one shown in figure 3, (2) misinterpretation or misreading of the sedimentary structures, (3) gross errors in interpreting the distribution of the major folds, or (4) failure to consider some other structural complication such as faulting or later refolding. Either or both of the first two possibilities probably explain the anomalous readings. Minor folds, though few, are known to exist, and many of the sedimentary structures, particularly in small or moss-covered outcrops, are ambiguous. Most of the available data fit the pattern of the axial traces in figure 5 too well to allow for any major errors in interpretation of the fold pattern, and evidence is lacking for either significant faulting or late mappable refolding in the area.

The preceding discussion is restricted to the isoclinal folds in the Goshen Formation of Silurian and Devonian

age. Small isoclinal folds are abundant in the pre-Silurian rocks of the area, and larger folds analogous to the folds in the Goshen Formation are assumed to exist. However, the scarcity of both stratigraphic tops data and continuous thin marker beds makes it impossible to map these larger folds. No attempt is made to explain or describe them here, except to note that in the pre-Silurian rocks the axes of small isoclinal folds, and, by inference, the larger ones also, generally plunge moderately to steeply and in any direction. Thus, the map pattern produced by large isoclinal folds in the pre-Silurian rocks would be markedly different from the pattern in the Goshen Formation. The difference in the orientation of isoclinal fold axes in the pre-Silurian and the Silurian and Devonian rocks is thought to result from the fact that at the time of the isoclinal folding (stage 2) the pre-Silurian rocks were already folded (in stage 1), whereas the Silurian and Devonian rocks were undeformed.

REGIONAL SETTING OF THE ISOCLINAL FOLDS

About 2 miles east of the Worthington quadrangle is a dome in which pre-Silurian rocks are brought to the surface (fig. 1). On the west flank of this dome, the basal beds of the Goshen dip from 25° to 40° W. Westward away from the basal contact, the dips of the Goshen beds become progressively steeper and are nearly vertical along the east edge of the Worthington quadrangle. A brief reconnaissance study of sedimentary structures in this area indicates that isoclinal folds in

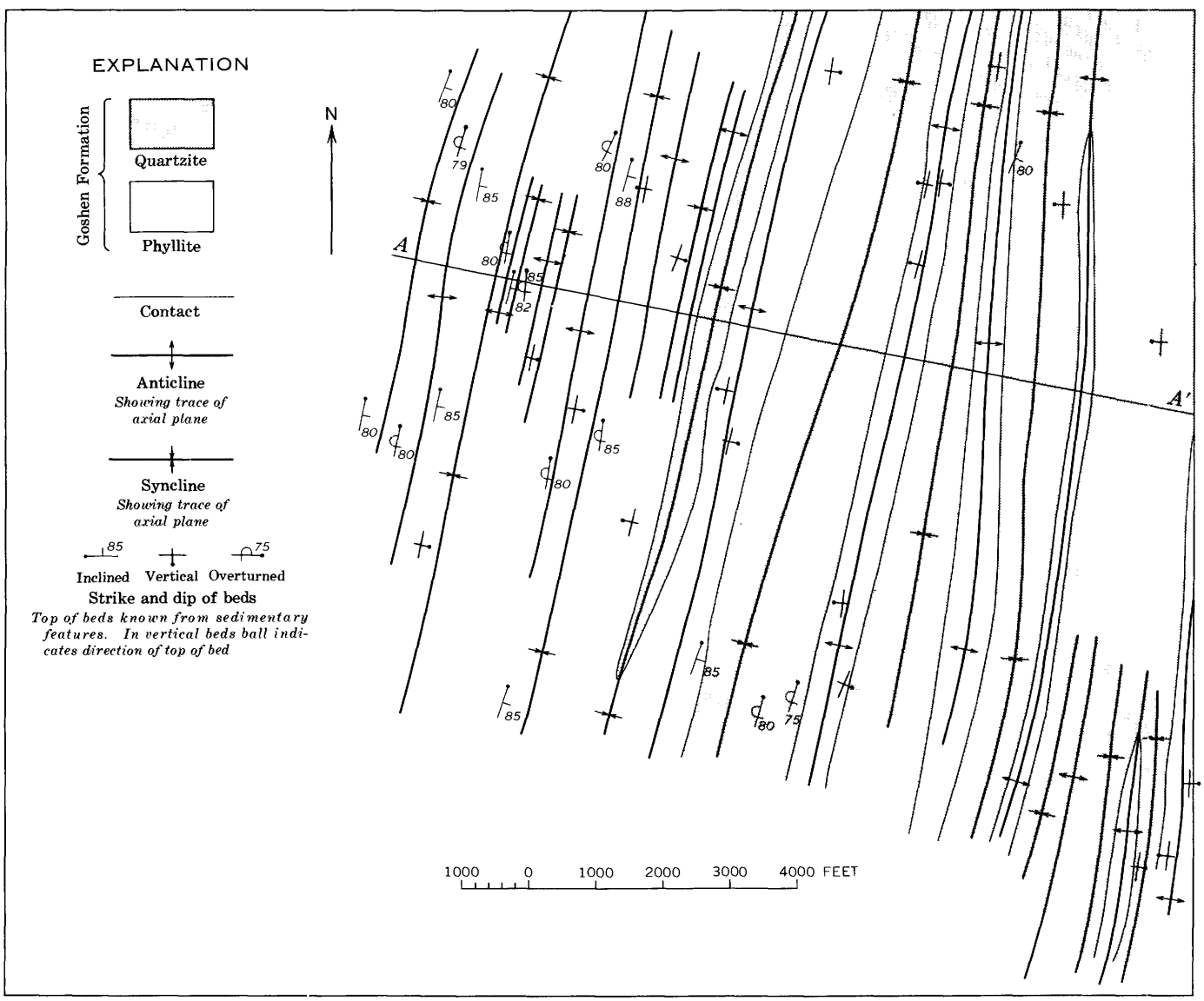

FIGURE 5.—Detailed geologic map of the northeast corner of the area shown in figure 2, showing axial traces of isoclinal folds. *A–A'*, line of geologic section (fig. 6).

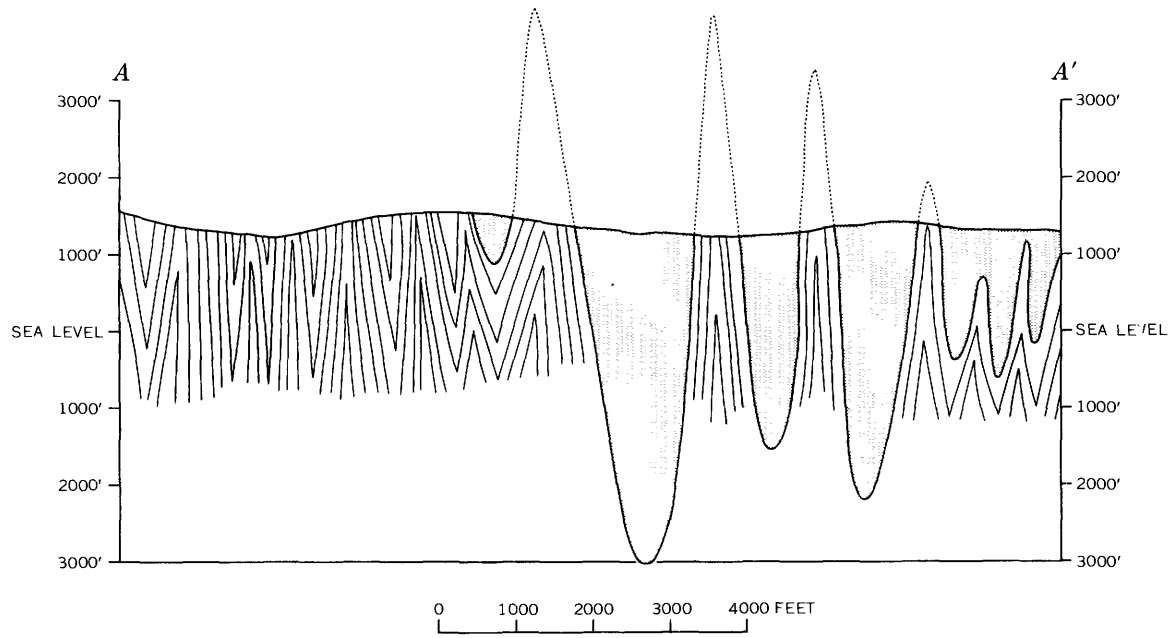

FIGURE 6.—Interpretive geologic section along line A–A' of figure 5. Horizontal scale same as vertical. Quartzite unit shaded. Folds within the phyllite unit are indicated by thinner lines.

the Goshen are strongly overturned over the dome. Thus, the major structure between the pre-Silurian rocks on the west and those in the dome is a complex open syncline composed of many isoclinal folds, the axial surfaces of which dip steeply east in the western part, moderately west in the eastern part, and vertically in the central part of the syncline.

A similar situation has been described from the Heath quadrangle (fig. 1), where the base of the Goshen is exposed around the Shelburne Falls dome (Hatch and Hartshorn, 1968). In the Heath quadrangle, however, neither the wealth of tops of beds data nor the mappable stratigraphy within the Goshen are present, and only the general pattern of the isoclinal folding can be inferred from the attitudes of beds and the overall relative ages of the formations.

LATER FOLDING

The Goshen Formation was affected by two later stages of folding. Although slip cleavage related to these later stages is present throughout the area shown in figure 2, the associated folds are small, having amplitudes of only a few inches to a foot. No late folds have been recognized that are large enough to deflect any of the contacts mapped in the area. Thus, of the three stages of deformation that affected the Silurian and Devonian rocks in this part of western Massachusetts, only one was intense enough to develop folds of sufficient magnitude to be mapped at a scale of 1:24,000.

REFERENCES

Chidester, A. H., Hatch, N. L., Jr., Osberg, P. H., Norton, S. A., and Hartshorn, J. H., 1967, Geologic map of the Rowe quadrangle, Massachusetts-Vermont: U.S. Geol. Survey Geol. Quad. Map GQ–642.

Emerson, B. K., 1917, Geology of Massachusetts and Rhode Island: U.S. Geol. Survey Bull. 597, 289 p.

Hatch, N. L., Jr., 1967a, Stratigraphy of the east limb of the Berkshire anticlinorium [abs.]: Geol. Soc. America, Northeast Sec., Ann. Mtg., Boston, Mass., 1967, Program, p. 33–34.

———1967b, Redefinition of the Hawley and Goshen Schists in western Massachusetts: U.S. Geol. Survey Bull. 1254–D, 16 p.

Hatch, N. L., Jr., and Hartshorn, J. H., 1968, Geologic map of the Heath quadrangle, Massachusetts-Vermont: U.S. Geol. Survey Geol. Quad. Map GQ–735.

Hatch, N. L., Jr., Osberg, P. H., and Norton, S. A., 1967, Stratigraphy and structure of the east limb of the Berkshire anticlinorium, *in* New England Intercollegiate Geol. Conf., 59th Ann. Mtg., Oct. 13, 14, 15, 1967, Guidebook for field trips in the Connecticut Valley of Massachusetts: Amherst, Mass., p. 7–16.

Shrock, R. R., 1948, Sequence in layered rocks: New York, McGraw-Hill Book Co., 507 p.

DEVONIAN PALEOTECTONICS IN EAST-CENTRAL IDAHO AND SOUTHWESTERN MONTANA

By WILLIAM J. MAPEL and CHARLES A. SANDBERG, Denver, Colo.

Abstract.—Post-Devonian low-angle thrust faults have greatly modified the original thicknesses of Devonian and some older Paleozoic rocks in a large area north of the Snake River Plain. Along the Idaho-Montana State line, extreme thinning of Devonian rocks, which previously had been cited as evidence for emergence of a Late Devonian Tendoy dome, is reinterpreted as partly due to faults. Slight thinning along the north side of the so-called Tendoy dome is interpreted to be the result of thinner deposition over the west end of an eastward-trending 300-mile-long ancestral Yellowstone Park uplift.

Devonian and older Paleozoic rocks north of the Snake River Plain are extensively cut by thrust and normal faults in an area about 80 miles wide. This area includes, from west to east, the southern parts of the Lost River and Lemhi Ranges, the southern part of the Beaverhead Mountains, and the Tendoy Range (fig. 1). Faults that originally were low-angle thrust type and normal type subparallel to the strike apparently thicken Devonian rocks by repeating parts of the sequence in some places and apparently thin Devonian and some older Paleozoic rocks by cutting out parts of the sequence in other places. In the Lost River Range south of Hawley Mountain and Lower Cedar Creek the Devonian sequence is doubled or tripled in apparent thickness for several miles along its strike. At the south end of the Lemhi Range, the Devonian rocks appear to be severely thinned by faulting and are interleaved with thin slivers of Ordovician and possibly some Silurian rocks. In the southern Beaverhead Mountains and locally in the Tendoy Range, the sequence of Devonian and underlying Paleozoic rocks also appears to be thinned and, at several places, is represented mainly by fault breccia in a zone below rocks of Mississippian age and above quartzites of Ordovician and (or) Precambrian age.

The structural complexities greatly hamper detailed stratigraphic analysis of Devonian rocks, although some general relations can be established. This paper reviews and reevaluates thickness data for Devonian rocks in light of these newly recognized faults and presents a tentative reconstruction of Devonian paleotectonics that differs markedly from the reconstructions of previous workers who explained anomalous thicknesses wholly by differences in sedimentation or erosion. Attention is focused on the stratigraphic and structural relations within the Devonian rocks, and between them and adjacent strata. However, in many of the areas studied local mechanics of faulting were not investigated.

Stratigraphic and structural relations described here were observed in 1965–67 during detailed mapping near Hawley Mountain and in adjacent areas of the Lost River Range, and in reconnaissance of selected localities in the Lost River, Lemhi, and Tendoy Ranges, and in the Beaverhead Mountains.

Paleotectonic interpretations along the east side of the isopach map (fig. 1) are based on sections measured by Benson (1966) and on our previous work in Montana and Wyoming. Interpretations for Idaho and extreme southwestern Montana, however, are based solely on our observations at the sections named in figure 1. Several other sections in Idaho and Montana that have been described by previous workers were visited but were not used because we believed the exposure to be inadequate or the structure too complex.

REGIONAL STRUCTURAL SETTING

The region discussed includes part of the Paleozoic miogeosyncline in Idaho and the bordering craton on the east in Montana (Scholten, 1957). Rocks of these two stratigraphic and tectonic provinces abut along an indefinitely located north- to northwest-trending line that follows roughly the east side of the Beaverhead Mountains. A complicated pattern of thrust and normal faults of Laramide and younger ages has been partly delineated along and near the margin of the miogeo-

U.S. GEOL. SURVEY PROF. PAPER 600-D, PAGES D115-D125

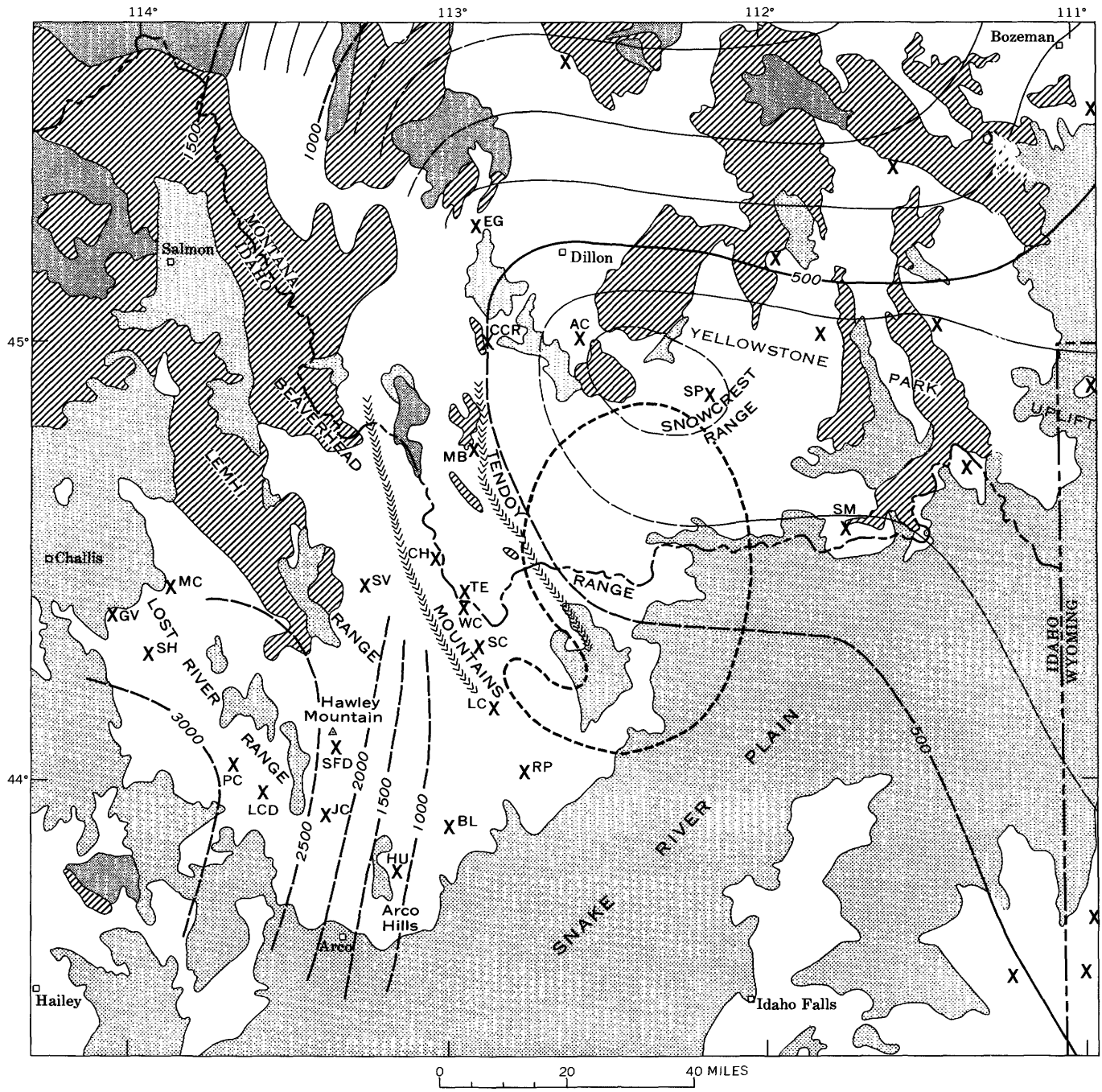

FIGURE 1.—Isopach map showing restored original thickness of Jefferson and Three Forks Formations and related rocks. Localities studied designated as follows: AC, Ashbough Canyon; BL, Black Canyon; CCR, Clarks Canyon Reservoir; CH, Chamberlain Creek; EG, Ermont Gulch; GV, Grand View Canyon; HU, Hurst Creek; JC, Jepson Canyon; LC, Long Creek; LCD, Lower Cedar Creek; MB, McBride Creek; MC, Meadow Creek; PC, Pete Creek; RP, Reno Point; SC, Scott Canyon; SFD, South Fork Deer Creek; SH, Sheep Creek; SM, Sheep Mountain; SP, Sunset Peak; SV, Silver Moon Gulch; TE, Tendoy Creek; WC, Willow Creek. Short-dashed line is zero isopach of Jefferson Formation as shown by Scholten and Hait (1962, fig. 2); it outlines the inferred Tendoy dome of Scholten (1957).

EXPLANATION

Volcanic rocks

Igneous rocks

Paleozoic and younger sedimentary rocks

Precambrian sedimentary and metamorphic rocks

Contact

—2000—

Isopachs

Dashed where approximately located. Interval 100 and 500 feet

>>>>>>>>>>>>>>>>>>>>>>>>>>

Approximate edge of area where Devonian rocks are largely fault breccia

X

Measured section or partial section of Devonian rocks

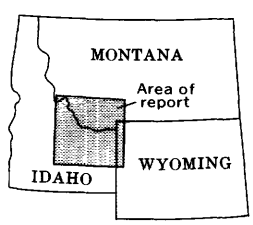

FIGURE 1.—Continued

syncline, mainly by Shenon (1928), Anderson (1948), Ross (1961), Smith (1961), and Hait (1965), in the Lemhi Range, Idaho, and by Scholten, Keenmon, and Kupsch (1955), Scholten (1960), and Ramspott (1962), in the southern Beaverhead Mountains and Tendoy Range, Idaho and Montana. In addition, a large number of dominantly right-lateral strike-slip faults were mapped or inferred by Ruppel (1964) in east-central Idaho.

Stratigraphic syntheses of Devonian rocks that give valuable information on the structural and stratigraphic patterns in Idaho have been presented by Scholten (1957), Churkin (1962), Scholten and Hait (1962), and Benson (1966). A synthesis for the Northern Rocky Mountains by Sandberg and Mapel (1967) was based partly on the stratigraphic and structural data presented here.

DEVONIAN STRATIGRAPHY

Devonian and adjacent stratigraphic units recognized in east-central Idaho are shown in table 1.

Devonian rocks at most places in the region comprise the Jefferson and Three Forks Formations, although in southwestern Montana they locally include the Maywood and Beartooth Butte Formations. Channel-fill and sinkhole deposits (Churkin, 1962, p. 583; Scholten and Hait, 1962, p. 19) locally underlie the Jefferson in east-central Idaho. Some of these, which are unnamed, are Middle Devonian; others, which are assigned to the Beartooth Butte Formation, are Early Devonian (Sandberg and Mapel, 1967). These basal Devonian deposits are limited in extent and do not affect the thickness trends shown by the isopach map (fig. 1).

The Grand View Dolomite, which is not shown on table 1, is considered here as a local facies of the upper half of the Jefferson Formation. The Grand View consists of light and dark-gray dolomite several hundred feet thick that has been mapped as a separate formation between the Jefferson and Three Forks Formations only at Grand View Canyon (fig. 1) and in the north end of the Lost River Range (Ross, 1937, 1947; Baldwin, 1951; Mapel and others, 1965). It is not used outside these areas, and it was not mapped in the southern part of the Lost River Range during the present work. Some geologists have treated the Grand View as a member of the Jefferson Formation (Sloss, 1954, fig. 1; Brooks and Andrichuk, 1953, fig. 3; Churkin, 1962, p. 583; Scholten and Hait, 1962, p. 14–15; Benson, 1966, p. 2589).

Jefferson Formation

The Jefferson Formation in the Lost River and Lemhi Ranges, Idaho, is very similar to the type Jefferson of southwestern Montana as described by Sandberg (1965, p. N4–N7) in its lithologic character, fossil content, and cyclical alternation of beds. In both southwestern Montana and east-central Idaho the formation can be divided into the Birdbear Member and an under-

TABLE 1.—*Generalized stratigraphic section of Devonian and adjacent rocks, east-central Idaho*

[Modified from Ross (1937, 1947, 1961, 1962), Sloss (1954), Scholten (1957), Scholten and Hait (1962), Churkin (1962), and Beutner and Scholten (1967)]

Age		Stratigraphic unit		Dominant rock	
Mississipian		Milligen Formation	Lodgepole Limestone	Grayish-black argillite	Thin-bedded shaly limestone
Devonian	Late	Trident Member of Three Forks Formation		Dark-gray limestone; yellowish-gray calcareous shale and shaly limestone	
		Birdbear Member of Jefferson Formation		Cliff-forming limestone and dolomite	
		Lower member of Jefferson Formation		Light- to dark-gray dolomite and quartzite	
	Middle	Local channel-fill deposits		Yellowish-gray silty dolomite	
	Early	Beartooth Butte Formation		Breccia and silty dolomite	
Silurian		Laketown Dolomite		Medium- to light-gray dolomite	
Ordovician		Saturday Mountain Formation	Fish Haven Dolomite	Dark-gray dolomite	
		Kinnikinic Quartzite		Light-gray quartzite	
Cambrian(?)				Dolomite and quartzite	
Precambrian		Belt Series		Quartzite, siltite, and argillite	

lying lower member. The Jefferson is much thinner, however, in southwestern Montana, where it is entirely early Late Devonian (Frasnian), than in Idaho, where it includes late Late Devonian (Famennian) beds at the top and late Middle Devonian (Givetian) beds at the base.

In Montana, the Jefferson is as little as 120 feet thick in a gently dipping, unfaulted section at Ashbough Canyon (NW¼NW¼NW¼ sec. 34, T. 9 S., R. 8 W., Beaverhead County) south of Dillon (fig. 1). It appears to be as thin or thinner nearby at Sunset Peak in the Snowcrest Range.

In Idaho, the Jefferson Formation is about 2,900 feet thick at Pete Creek (SW¼ sec. 12 and NW¼ sec. 13, unsurveyed, T. 8 N., R. 23 E., Custer County) on the west side of the Lost River Range. It is probably as thick or thicker at Grand View Canyon (fig. 1), but there the lower 600–800 feet is covered by Tertiary volcanic rocks. The moderately dipping and largely unfaulted Jefferson at these localities provides a standard for comparison to the folded and more complexly faulted Jefferson farther south in the Lost River Range.

Westward thickening of the Jefferson Formation in Idaho is due partly to addition of Middle Devonian beds in the basal part of the lower member, and partly to miogeosynclinal thickening of the overlying Upper Devonian beds (Scholten and Hait, 1962, p. 19, 20; Churkin, 1962, fig. 3, p. 585; Benson, 1966, fig. 12; Sandberg and Mapel, 1967).

The westward thickening of the upper part of the formation is illustrated by thickness changes in the Birdbear Member. The generally cliff-forming Birdbear Member, which caps the Jefferson Formation in Montana and Wyoming (Sandberg, 1965; Benson, 1966), is readily identified directly below the Three Forks Formation at least as far west as the central part of the Lost River Range in Idaho. In southwestern Montana the Birdbear commonly is 50–80 feet thick. In Idaho the Birdbear has the following thicknesses at our measured sections: about 105 feet in Black Canyon at the south end of the Lemhi Range; at least 120 feet at Silver Moon Gulch in the central part of the Lemhi Range; 140 feet at Hurst Creek in the Arco Hills; at least 300 feet 2 miles east of Hawley Mountain, on the east side of the Lost River Range; and 313 feet at Lower Cedar Creek (Sandberg and others, 1967) on the west side of the Lost River Range (fig. 1).

Three Forks Formation

The Three Forks Formation in the Lost River and Lemhi Ranges is faunally, lithologically, and sequentially like the Trident Member of the Three Forks Formation of southwestern Montana (Sandberg, 1965, p. N12–N14). Rocks equivalent in age to the Logan Gulch Member, which underlies the Trident Member in Montana, probably are represented by nonfossiliferous to sparsely fossiliferous yellow-weathering argillaceous limestone in the basal part of the Trident in Idaho. However, evaporite-solution breccias such as those that characterize the Logan Gulch in Montana as far west as Clarks Canyon Reservoir (fig. 1) were not observed in Idaho. The Sappington Member of the Three Forks, which overlies the Trident Member in Montana as far west as Ashbough Canyon (fig. 1), was not identified and apparently is absent in east-central Idaho.

Unlike the underlying Jefferson Formation, which thickens abruptly westward within the Cordilleran miogeosyncline in east-central Idaho, the Three Forks Formation maintains a remarkably uniform thickness across the region. It is a cratonic sequence both in Montana and in Idaho as far west as the western limit of its exposures near Grand View Canyon (fig. 1). In southwestern Montana, the Trident Member of the Three Forks commonly is 100–225 feet thick (McMannis, 1962; Sandberg, 1965, p. N13). In east-central Idaho, the maximum, unfaulted thickness of the Three Forks that we measured is 267 feet at Lower Cedar Creek in the Lost River Range. The minimum measured thickness is 40 feet at Black Canyon in the Lemhi Range; however, there the formation may be thinned by a normal fault. Ross (1947, p. 1111) reported lesser and greater thicknesses, ranging from 30 to 350 feet, in the Lost River Range, but where he reported less than 100 feet the Three Forks was found to be thinned by faults. A thickness greater than 267 feet was reported by Mapel, Read, and Smith (1965) in a section near Sheep Creek (fig. 1) in the northwestern part of the Lost River Range. On reexamination, however, we found that the upper part of the formation contains a fault; the thickness of Three Forks, adjusted for the fault, is 200–225 feet.

In the Lost River Range, the depositional contact of the Three Forks Formation with the overlying Lower Mississippian Milligen Formation is a disconformity along which dark-gray fossiliferous nodular limestone of the Three Forks is abruptly overlain by thin-bedded grayish-black argillite and tan-weathering siltstone of the Milligen. Locally the Three Forks is capped by a few inches of regolithic limonite-stained claystone or manganese-rich oolite and pisolite.

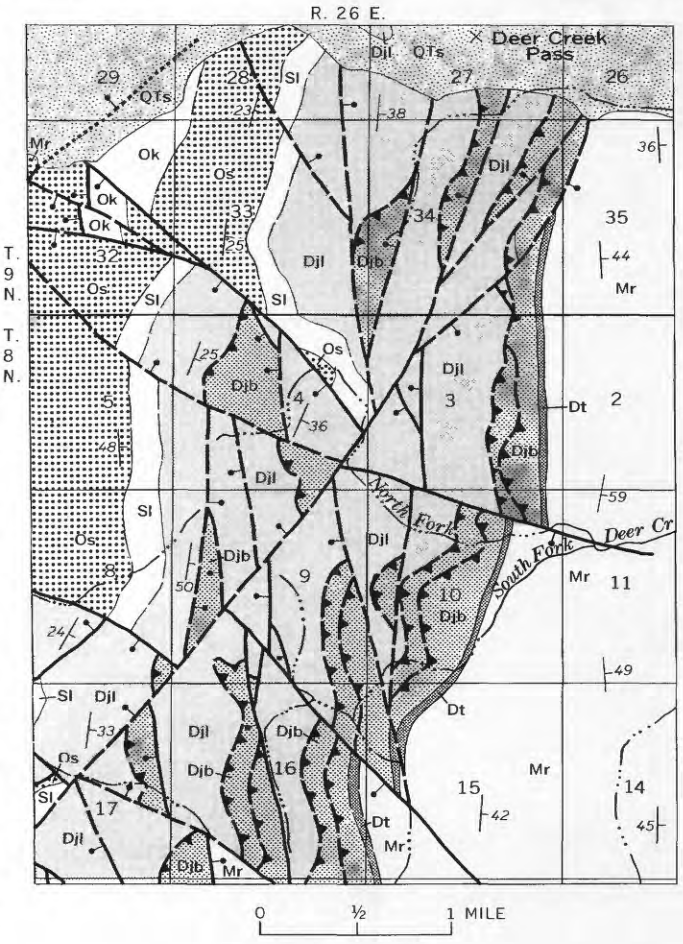

FIGURE 2.—Generalized geologic map showing fault systems in Devonian and adjacent rocks in vicinity of Deer Creek, Lost River Range, Idaho.

LOCAL STRATIGRAPHIC AND STRUCTURAL RELATIONS

Southern part of Lost River Range

Devonian and older Paleozoic rocks are well exposed in an almost continuous 20-mile-long belt extending southward across the Lost River Range from Hawley Mountain on the east to 12 miles north of Arco on the west (fig. 1). The same rocks crop out also in a belt about 3 miles long in the Arco Hills. A system of originally low-angle thrust faults at or near the base of the Birdbear Member cuts the Jefferson Formation along both outcrop belts. The faults are marked by anastomosing zones, commonly several feet thick, of intensely brecciated rock, generally subparallel to the bedding of the Jefferson. Because of later tilting, both the faults and beds now dip generally eastward 45°–60°. A complex pattern of normal faults is superimposed on the outcrop belt near Hawley Mountain and in the Arco Hills. Figure 2 shows the fault pattern about 2–6 miles south of Hawley Mountain, in the vicinity of Deer Creek. There faults have produced apparent stratigraphic thicknesses that are two or three times the originally deposited thickness of the Jefferson. Figure 3 illustrates intensely brecciated dolomite that characterizes the fault zones.

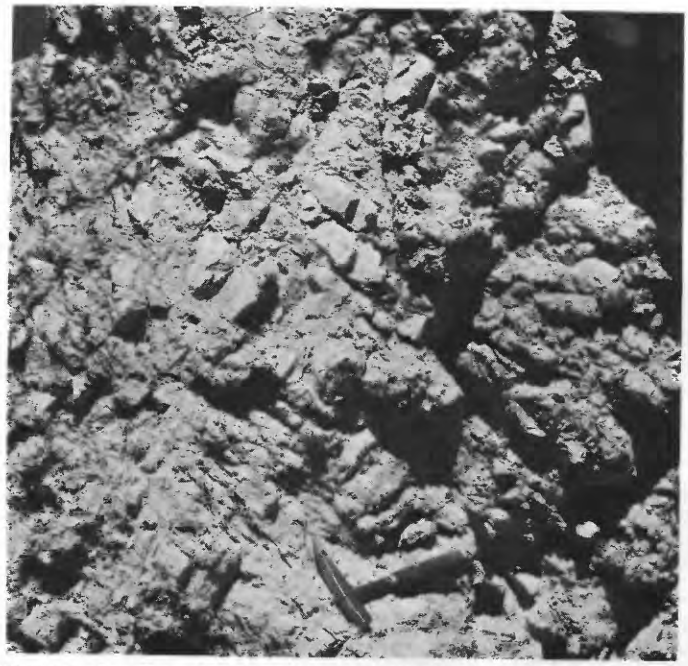

FIGURE 3.—Breccia along thrust fault in Jefferson Formation on North Fork Deer Creek, NW¼ sec. 10, T. 8 N., R. 26 E., Butte County, Idaho.

Faulting makes difficult any accurate measurement of the originally deposited thickness of the Jefferson at most places in the southern Lost River Range. A thickness of slightly more than 2,000 feet was reported for the Jefferson in a section in the Arco Hills (Churkin, 1962, p. 584). However, faults appear to repeat part of the Jefferson Formation on the hillside given as the location for his section. One mile north of Churkin's locality a section that contains the major subunits in a stratigraphic sequence comparable with that in the northern Lost River Range and at Grand View Canyon is about 1,200 feet thick, as described below:

Generalized composite section of Devonian rocks east of Hurst Creek in Arco Hills, NE¼ sec. 6, T. 5 N., R. 28 E., Butte County, Idaho

	Thickness (feet)
Three Forks Formation:	
Trident Member:	
7. Limestone, argillaceous, medium-dark-gray, thin-bedded, nonresistant; weathers grayish yellow. Upper one-third is dark-gray, fossiliferous, and less argillaceous limestone that weathers dark gray and forms ledges. Lower two-thirds forms partly covered slope that conceals several faults	150+
Jefferson Formation:	
Birdbear Member:	
6. Limestone and dolomitic limestone, medium-gray, pseudobrecciated. Bed 18 feet thick, 25 feet below top, is yellowish-gray-weathering silty dolomitic limestone that contains conodonts and abundant brachiopods and gastropods. Weathers to medium-gray rough, deeply pitted surface, and forms massive resistant cliff, except for 18-foot-thick fossiliferous bed which forms reentrant	140
Lower member:	
5. Dolomite, medium-gray, sucrosic. Weathers medium gray; weakly resistant; poorly exposed; forms scattered ledges in slope; possible thrust fault indicated by breccia zone 13 feet thick about 150 feet below top	300
4. Interbedded dolomite, cross-laminated quartzite, and sandy dolomite. Quartzite constitutes about 40 percent of interval. Dolomite is medium gray to medium dark gray; quartzite is light gray to brownish gray and fine to medium grained. Resistant; forms prominent ledges	225
3. Dolomite, dark-gray, finely crystalline. Interbedded with thin beds of light-gray fine to very fine grained quartzite. Local thin breccias along bedding-plane faults in basal and upper parts. Weathers medium dark gray; weakly resistant; forms partly covered slope	135
2. Dolarenite, grayish-black, medium-dark-gray, and medium-gray, fine- to medium-grained, locally sandy. In cyclically alternating beds; resistant; forms ledges and cliffs	265
1. Dolomite, medium-gray to medium-dark-gray, mostly finely crystalline. Thin interbeds of light-gray crossbedded quartzite. Weathers medium gray, medium light gray, and yellowish gray; thin to medium bedded; weakly resistant; forms slope	140
Total thickness of Jefferson Formation (rounded)	1, 200

South end of Lemhi Range

Devonian rocks are well exposed in Black Canyon near the south end of the Lemhi Range. Outcrops there were described by Sloss (1954) and Churkin (1962, fig. 7), and were mapped by Anderson (1948) and C. P. Ross (1961, pl. 7). Sloss (1954) pointed out that the Devonian and some older rocks at Black Canyon were extremely thin compared with corresponding sections in the northern Lost River Range. He explained the thinning as due to onlap of the Jefferson Formation on a postulated uplift, named the Lemhi arch, that was active and deeply eroded in Middle and Late Devonian time. Scholten (1957), who elaborated on this explanation, placed the center of the supposed uplift in the Tendoy Range and renamed it the Tendoy dome. Ross (1961, p. 206–207, 211) found that Devonian rocks, as well as the underlying Ordovician Saturday Mountain Formation, had wide ranges of thickness near Black Canyon, and that both were locally deformed and cut by faults.

Figures 4 and 5 show the lithologic sequence in a section measured on the east side of Black Canyon. Inversion and repetition of beds, discordance between adjacent beds or groups of beds, closely spaced breccia zones, and abrupt lateral termination of beds indicate that the entire sequence between the Kinnikinic Quartzite and the Milligen Formation is cut by originally low-angle thrust faults. Because of these faults, and because of the regularity of regional thickness trends and nearly uniform content of terrigenous sediment in Devonian rocks in surrounding areas, we conclude that the anomalous thinness of the Devonian and Ordovician sequence at Black Canyon is more reasonably explained by post-Devonian faulting than it is by uplifting and erosion of a dome during the Middle or Late Devonian.

In the Jefferson Formation at Black Canyon, Sloss (1954, p. 336) and Churkin (1961, p. A11–A12) noted zones of breccia that they considered to be evaporite-solution or intraformational sedimentary breccia. Breccias at many levels in the section (fig. 5) appear to be discontinuous pods commonly 1–2 feet thick bounded by curved surfaces roughly parallel to bedding. Some surfaces coalesce laterally and pass into unbrecciated rock. The lithologies and stratigraphic relations of these breccias are unlike those of evaporite-solution or sedimentary breccias in Devonian rocks of Montana and Wyoming (Sandberg, 1965, p. N11; 1967, p. 16–18). Rather, the breccias seem clearly due to shearing, as was suggested by Ross (1961, p. 205–206, 211).

In the measured section (fig. 5), quartzitic sandstone that alternates with dolomite in the intervals 27–77 and 139–161 feet above the Kinnikinic Quartzite is mostly medium to coarse grained, slightly limonitic, and locally dolomite cemented. Shearing and local brecciation along the contacts suggest that the sandstone is faulted against adjacent beds of dolomite. We agree somewhat with Sloss (1954) and Churkin (1962) in tentatively assigning most of the sandstone interbeds in these intervals to the Jefferson because the coarser grained parts resemble some quartzite and sandstone of the Jefferson Formation in the southern Lost River Range. However, we disagree with Sloss and Churkin in that we believe their basal Devonian contact to be tectonic rather than stratigraphic. Moreover, parts of a massive 20-foot-thick bed of quartzitic sandstone at the base of their Devonian also resemble the Kinnikinic Quartzite, and in the absence of fossils an alternative assignment of this bed to the Kinnikinic cannot be entirely discounted.

Dolomite in the interval 0–27 feet above the Kinnikinic Quartzite contains Late or Middle Ordovician brachiopods, according to R. J. Ross, Jr. (1959; oral commun., 1967). Dolomite in the interval 77–139 feet above the Kinnikinic yielded two collections of late Middle or Late Ordovician conodonts (R. J. Ross, Jr., L. A. Wilson, and J. W. Huddle, written communs., 1967, 1968). Therefore, both of these intervals, the upper of which lies within the Devonian of Sloss (1954) and Churkin (1962), are assigned unequivocally to the Saturday Mountain Formation.

We agree to some extent with C. P. Ross (1961) in that we recognize beds of the Saturday Mountain Formation to be present in the section (fig. 5) as high as 215 feet above the Kinnikinic Quartzite—approximately the same horizon where Ross placed his contact between the Saturday Mountain and the Devonian. However, we tentatively assign a few thin interleaves of light-gray dolomite in the intervals 139–161 and 191–215 feet above the Kinnikinic to the Silurian Laketown Dolomite on a lithologic basis. C. P. Ross (1961, p. 205) regarded the sandstone in the intervals 27–77 and 139–161 feet above the Kinnikinic as channel-fill deposits within the Saturday Mountain. This seems unlikely, however, as sandstone interbeds are unknown within the main body of the Saturday Mountain elsewhere in east-central Idaho.

On the restored isopach map (fig. 1), Devonian rocks at Black Canyon are assigned a prefaulting thickness of slightly more than 500 feet, or about twice their present thickness. The thickness allowed for the Jefferson Formation is based on a regionally recognized ratio between local thicknesses of the Birdbear Member and the entire formation.

FIGURE 4.—Devonian and associated rocks in fault system on east side of Black Canyon. Mm, Milligen Formation; Dt, Three Forks Formation; Djb, Birdbear Member, and Djl, lower member of Jefferson Formation; Djl(?), quartzitic sandstone tentatively assigned to Jefferson Formation; Sl(?), Laketown(?) Dolomite; Os, Saturday Mountain Formation; Ok, Kinnikinic Quartzite. Section shown on figure 5 was measured at right of symbols.

Southern parts of the Beaverhead Mountains and Tendoy Range

Devonian rocks have been mapped locally in the southern part of the Beaverhead Mountains (Ramspott, 1962), and they crop out at a few places in the Tendoy Range (Scholten and others, 1955). The Jefferson Formation was reported to range in thickness from 0 to about 300 feet, and the Three Forks Formation from 0 to about 160 feet in these areas (Scholten and Hait, 1962, figs. 2 and 5). The thinness and local absence of the Jefferson and Three Forks Formations were interpreted as depositional or erosional effects and were cited as the main evidence for a Late Devonian Tendoy dome along the Idaho-Montana State line by Scholten (1957), Scholten and Hait (1962), Churkin (1962), and Benson (1966). The characteristic basal unit of the Jefferson Formation in parts of the Beaverhead Mountains was described as an evaporite-solution breccia (Scholten and Hait, 1962, p. 15).

We find no compelling physical evidence for a Tendoy dome in the Beaverhead Mountains or Tendoy Range and interpret basal breccias of the Jefferson as fault breccias. At all sections visited, Mississippian rocks are faulted against the Jefferson Formation or pre-Devonian rocks, and the Three Forks is missing. Consequently, the possibilities of depositional thinning of the Three Forks, or of post-Three Forks erosion, are difficult to evaluate. The Jefferson Formation undoubtedly was thinned depositionally, largely as a result of the regional transgression of the sea from the miogeosyncline eastward onto the craton in late Middle or early Late Devonian time. Appreciable post-Devonian tectonic thinning of the Jefferson also may have occurred locally, however, as suggested by structural and stratigraphic relations at Long, Chamberlain, Tendoy, and McBride Creeks (fig. 1). Tectonic thinning apparently resulted from thrust faults similar to those at Black Canyon in the Lemhi Range.

In the southern Beaverhead Mountains, the only section where we found a large part of the Jefferson to be well exposed and unbrecciated is on the crests of ridges adjacent to Long Creek and some of its tributaries in secs. 26 and 35, T. 10 N., R. 30 E., Clark County, Idaho. Beds assigned to the Jefferson are about 120–140 feet thick in this area and consist mostly of cyclically interbedded medium-gray and medium-light-gray dolomite overlain at the top by a massive bed of lighter-colored dolomite 20–30 feet thick that resembles the Birdbear Member. The Jefferson is separated from underlying angularly discordant Precambrian quartzite by dolomite and quartzite breccia as much as 60 feet thick, which locally is intruded by a sill. The Milligen Formation, consisting of locally contorted dark-gray and brown

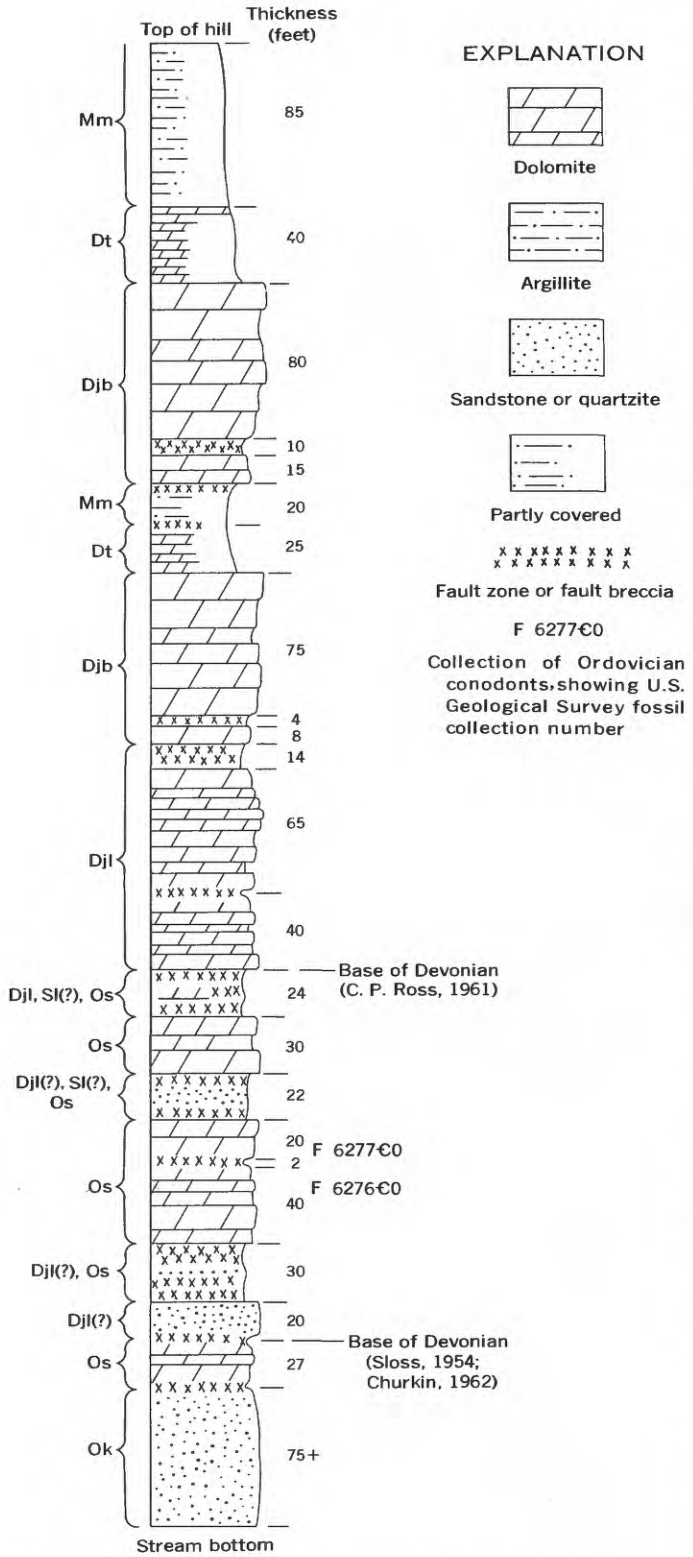

FIGURE 5.—Generalized section of Devonian and associated rocks at Black Canyon, SE¼ sec. 34, T. 7 N., R. 29 E., Butte County, Idaho. Base of Devonian, according to other writers, at right of column. Formation symbols identified on figure 4.

argillite, directly overlies the Jefferson in fault contact (fig. 6). The fault, which apparently cuts out the Three Forks Formation, parallels bedding of the Milligen and is slightly discordant to bedding of the Jefferson. The lithologies and sequence of units within the Jefferson at Long Creek indicate that the Late Devonian depositional environment there was the same as in adjacent areas of Idaho and Montana. Abnormal amounts of terrigenous sediment that would suggest nearby land are lacking.

FIGURE 6.—Fault contact between Jefferson (Dj) and Milligen (Mm) Formations on ridge north of Long Creek, sec. 35, T. 10 N., R. 30 E., Clark County, Idaho. d, pod of dolomite of Jefferson Formation incorporated in contorted beds of Milligen Formation.

Farther north in the Beaverhead Mountains, a section of Devonian and adjacent rocks that illustrates extreme brecciation, ascribed here to thrust faulting, can be seen on the high ridge south of Chamberlain Creek in the E½ sec. 31 (unsurveyed), T. 14 N., R. 29 E., Lemhi County, Idaho. Figure 7 is a generalized profile showing the main lithic units identified along the ridge at this locality. A partly covered

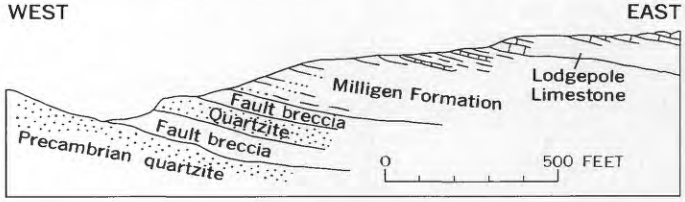

FIGURE 7.—Sketch showing stratigraphic sequence on ridge south of Chamberlain Creek, E½ sec. 31 (unsurveyed), T. 14 N., R. 29 E., Lemhi County, Idaho. Vertical exaggeration about × 2.

breccia zone immediately below the Milligen Formation contains a mixture of dolomite fragments from the Jefferson Formation and Fish Haven Dolomite, quartzite fragments from the Kinnikinic Quartzite and Precambrian rocks, and smaller fragments of argillite from the Milligen. The Three Forks Formation could not be identified. A locally well-exposed breccia zone at the base of this section consists mostly of thoroughly mixed fragments of Kinnikinic Quartzite and Fish Haven Dolomite. Discontinuous outcrops of quartzite questionably assigned to the Kinnikinic separate these two breccia zones.

Other localities visited at which Devonian rocks are represented mainly by fault breccia or are absent because of faulting are at Tendoy Creek (NE¼ NE¼NE¼ sec. 21, T. 16 N., R. 11 W., Beaverhead County, Mont.) in the Beaverhead Mountains, and at McBride Creek (SW¼NE¼ sec. 22, T. 12 S., R. 11 W., Beaverhead County, Mont.) (fig. 1) in the Tendoy Range. At Tendoy Creek, the Milligen Formation is faulted against the Kinnikinic Quartzite, and no rocks recognizable as Three Forks or Jefferson Formation were found. At McBride Creek, the interval between underlying outcrops of the Kinnikinic Quartzite and overlying outcrops of basal Mississippian rocks is partly covered, but it includes a breccia 75–150 feet thick of dolomite and limestone from the Jefferson and grayish-white quartzite probably from the Kinnikinic. Rock fragments from different formations heterogeneously mixed at different levels in this breccia seem clearly to indicate faulting.

Dolomite referred by Ramspott (1962) to the Jefferson Formation crops out along Willow Creek, secs. 1 and 2 (unsurveyed), T. 12 N., R. 11 W., Lemhi County, about 8 miles southeast of Chamberlain Creek, and 2 miles south of Tendoy Creek. The dolomite, which is about 150 feet thick in a partial exposure at this locality, is lithologically more like the Fish Haven Dolomite than the cyclically bedded Jefferson Formation at Long Creek, 17 miles to the south.

In an isolated outcrop at Reno Point (center of sec. 16, T. 8 N., R. 31 E., Clark County, Idaho) 9 miles southeast of Long Creek, rocks overlying the Kinnikinic were identified by Scholten and Hait (1962, p. 18, loc. 14) as the Jefferson and Three Forks Formations. We believe the unit identified as Jefferson is Fish Haven Dolomite, and the unit identified as Three Forks is the basal quartzite of the Jefferson Formation.

THICKNESS INTERPRETATIONS

Thicknesses of Devonian rocks, adjusted at places for post-Devonian faulting, are shown in figure 1. The isopachs are intended to suggest the form, orientation, and present location of the westward-thickening wedge of miogeosynclinal Devonian rocks. Palinspastic reconstruction was not attempted. We believe, however, that cratonic and miogeosynclinal Devonian rocks probably were once separated by a north-trending transitional zone, containing rocks of intermediate thicknesses, at or slightly west of the central part of the present Beaverhead Mountains. Post-Devonian thrusting has narrowed any such transitional zone and increased the apparent rate of thickening of the miogeosynclinal Jefferson Formation in Idaho.

An elongated southeast-trending Late Devonian uplift or arch, which was suggested by previous workers (Andrichuk, 1951, fig. 9; Benson, 1966, figs. 5 and 11), was more closely delineated and was named the ancestral Yellowstone Park uplift by Sandberg and Mapel (1967). This structural feature is indicated by thin Devonian rocks in a 300-mile-long area extending from just south of Dillon, Mont. (fig. 1) southeastward into the Bighorn Basin of northern Wyoming. Compelling evidence for this uplift in southwestern Montana is provided by a well-exposed unfaulted sequence of Devonian rocks at Ashbough Canyon (fig. 1) in the Blacktail Mountains. There the upper part of the lower member of the Jefferson unconformably overlies the Hasmark Dolomite of Cambrian age. Thin Devonian rocks at this section are explained by absence of the lower part of the lower member and by reduced thicknesses of individual beds in the upper part of the lower member. Overlying the lower member successively are the Birdbear Member of the Jefferson, and the Logan Gulch, Trident, and Sappington Members of the Three Forks Formation, all of which have thicknesses consistent with their regional thickness trends.

A small low dome at the west end of the ancestral Yellowstone Park uplift (fig. 1) partly coincides with the outline of the Tendoy dome as illustrated by Scholten and Hait (1962, fig. 2). The Yellowstone Park uplift, including the small dome at its west end, was emergent for a while during transgression of the sea from Idaho into Montana in early Late Devonian time, but subsided and was inundated during deposition of the upper part of the Jefferson Formation and the Three Forks Formation.

CONCLUSIONS

1. Devonian and some older Paleozoic rocks were cut by originally low-angle thrust faults, and subsequently by normal faults, in a large area of east-central Idaho. The structural complexity greatly hampers detailed stratigraphic analysis of the Devonian.

2. Measured thicknesses of Devonian rocks in much of east-central Idaho must be adjusted for the effects of thrust faulting in any reconstruction of Devonian paleotectonics.

3. Apparent anomalous thinning and local absence of Devonian rocks in the area of the supposed Lemhi arch or Tendoy dome actually resulted partly from post-Devonian tectonic thinning, and partly from uniform depositional thinning from the miogeosyncline eastward onto the craton and northward within the craton onto the Yellowstone Park uplift.

REFERENCES

Anderson, R. A., 1948, Reconnaissance survey of the geology and ore deposits of the southwestern portion of Lemhi Range, Idaho: Idaho Bur. Mines and Geology Pamph. 80, 18 p.

Andrichuk, J. M., 1951, Regional stratigraphic analysis of Devonian System in Wyoming, Montana, southern Saskatchewan, and Alberta: Am. Assoc. Petroleum Geologists Bull., v. 35, no. 11, p. 2368–2408.

Baldwin, E. M., 1951, Faulting in the Lost River Range area of Idaho: Am. Jour. Sci., v. 249, no. 12, p. 884–902.

Benson, A. L., 1966, Devonian stratigraphy of western Wyoming and adjacent areas: Am. Assoc. Petroleum Geologists Bull., v. 50, no. 12, p. 2566–2603.

Beutner, E. C., and Scholten, Robert, 1967, Probable Cambrian strata in east-central Idaho and their paleotectonic significance: Am. Assoc. Petroleum Geologists Bull., v. 51, no. 11, p. 2305–2309.

Brooks, J. E., and Andrichuk, J. M., 1953, Regional stratigraphy of the Devonian System in northeastern Utah, southeastern Idaho and western Wyoming, *in* Intermountain Assoc. Petroleum Geologists 4th Ann. Field Conf., Guide to the geology of northern Utah and southeastern Idaho, 1953: p. 28–31.

Churkin, Michael, Jr., 1961, Middle Paleozoic stratigraphy of central Idaho: Northwestern Univ. unpub. Ph. D. thesis, 44 p., app., p. A1–A70.

——— 1962, Facies across Paleozoic miogeosynclinal margin of central Idaho: Am. Assoc. Petroleum Geologists Bull., v. 46, no. 5, p. 569–591.

Hait, M. H., Jr., 1965, Structure of the Gilmore area, Lemhi Range, Idaho: Pennsylvania State Univ. unpub. Ph. D. thesis, 134 p.

McMannis, W. J., 1962, Devonian stratigraphy between Three Forks, Montana, and Yellowstone Park, *in* Three Forks–Belt Mountains area, *and* Symposium—The Devonian System of Montana and adjacent areas, Billings Geol. Soc. 13th Ann. Field Conf., 1962: p. 4–12.

Mapel, W. J., Read, W. H., and Smith, R. K., 1965, Geologic map and sections of the Doublespring quadrangle, Custer and Lemhi Counties, Idaho: U.S. Geol Survey Geol. Quad. Map GQ–464.

Ramspott, L. D., 1962, Geology of the Eighteenmile Peak area and petrology of the Beaverhead pluton, Idaho-Montana: Pennsylvania State Univ. unpub. Ph.D. thesis, 237 p.

Ross, C. P., 1937, Geology and ore deposits of the Bayhorse region, Custer County, Idaho: U.S. Geol. Survey Bull. 877, 161 p.

——— 1947, Geology of the Borah Peak quadrangle, Idaho: Geol. Soc. America Bull., v. 58, no. 12, p. 1085–1160.

——— 1961, Geology of the southern part of the Lemhi Range, Idaho: U.S. Geol. Survey Bull. 1081–F, p. 189–260.

——— 1962, Upper Paleozoic rocks in central Idaho: Am. Assoc. Petroleum Geologists Bull., v. 46, no. 3, p. 384–387.

Ross, R. J., Jr., 1959, Brachiopod fauna of Saturday Mountain formation, southern Lemhi Range, Idaho: U.S. Geol. Survey Prof. Paper 294–L, p. 441–461.

Ruppel, E. T., 1964, Strike-slip faulting and broken basin-ranges in east-central Idaho and adjacent Montana, *in* Geological Survey Research 1964: U.S. Geol. Survey Prof. Paper 501–C, p. C14–C18.

Sandberg, C. A., 1965, Nomenclature and correlation of lithologic subdivisions of the Jefferson and Three Forks Formations of southern Montana and northern Wyoming: U.S. Geol. Survey Bull. 1194–N, p. N1–N18.

——— 1967, Measured sections of Devonian rocks in northern Wyoming: Wyoming Geol. Survey Bull. 52, 93 p.

Sandberg, C. A., and Mapel, W. J., 1967, Devonian of the Northern Rocky Mountains and Plains, *in* Oswald, D. H., ed., International symposium on the Devonian System, Calgary, Alberta, Sept. 1967: Calgary, Alberta Soc. Petroleum Geologists, v. 1, p. 843–877.

Sandberg, C. A., Mapel, W. J., and Huddle, J. W., 1967, Age and regional significance of basal part of Milligen Formation, Lost River Range, Idaho, *in* Geological Survey Research 1967: U.S. Geol. Survey Prof. Paper 575–C, p. C127–C131.

Scholten, Robert, 1957, Paleozoic evolution of the geosynclinal margin north of the Snake River Plain, Idaho-Montana: Geol. Soc. America Bull., v. 68, no. 2, p. 151–170.

——— 1960, Sedimentation and tectonism in the thrust belt of southwestern Montana and east-central Idaho, *in* Wyoming Geol. Assoc. Guidebook 15th Ann. Field Conf., Overthrust belt of southwestern Wyoming and adjacent areas, 1960: p. 73–83.

Scholten, Robert, and Hait, M. H., Jr., 1962, Devonian System from shelf edge to geosyncline, southwestern Montana-central Idaho, *in* Three Forks–Belt Mountains area, *and* Symposium—The Devonian System of Montana and adjacent areas, Billings Geol. Soc. 13th Ann. Field Conf., 1962: p. 13–23.

Scholten, Robert, Keenmon, K. A., and Kupsch, W. O., 1955, Geology of the Lima region, southwestern Montana and adjacent Idaho: Geol. Soc. America Bull., v. 66, no. 4, p. 345–403.

Shenon, P. J., 1928, Geology and ore deposits of the Birch Creek district, Idaho: Idaho Bur. Mines and Geology Pamph. 27, 25 p.

Sloss, L. L., 1954, Lemhi arch, a mid-Paleozoic positive element in south-central Idaho: Geol. Soc. America Bull., v. 65, no. 4, p. 365–368.

Smith, J. G., 1961, Geology of the Clear Creek area, Montana-Idaho: Pennsylvania State Univ. unpub. M.A. thesis, 75 p.

THE BOUSE FORMATION (PLIOCENE) OF THE PARKER-BLYTHE-CIBOLA AREA, ARIZONA AND CALIFORNIA

By D. G. METZGER, Yuma, Ariz.

Abstract.—A marine to brackish-water deposit of Pliocene age, older than the Pliocene and Quaternary deposits of the Colorado River in the Parker-Blythe-Cibola area, Arizona and California, is here named the Bouse Formation. It is primarily a subsurface formation, and is composed of a basal limestone and interbedded clay, silt, and sand, and a tufa. The greatest known subsurface thickness is 767 feet, whereas the greatest exposed thickness is 215 feet. The Bouse Formation contains foraminifers, mollusks, ostracodes, charophytes, and barnacles, although the number of species is small. The Bouse Formation was deposited in an embayment of the Gulf of California; however, the limited faunas prevent a correlation of the Bouse with marine deposits of the Imperial Valley.

The Bouse Formation of Pliocene age, named herein for Bouse Wash, is a marine to brackish-water sequence that is older than Pliocene and Quaternary deposits of the Colorado River in the Parker-Blythe-Cibola area, Arizona and California (fig. 1). The Bouse Formation includes deposits that have been referred to informally as the "Cibola beds" (Wilson, 1962, p. 72) and the "lakebeds near Parker" (Ross, 1923, p. 25). The greatest exposed thickness is 9 miles south of Parker, Ariz. and about 3 miles south of Bouse (rhymes with house) Wash, an ephemeral stream that enters the Colorado River flood plain from the east, 6 miles south of Parker, Ariz.

The Bouse Formation is composed of three units: (1) a basal limestone, (2) an interbedded clay, silt, and sand, and (3) a distinctive tufa that formed at or near the water surface throughout the time of deposition of the other units. The Bouse Formation was deposited in an embayment of the Gulf of California in which were numerous islands, now the major mountains of the area. The Bouse Formation is mostly flat lying, or has only gentle dips. Locally, it is warped upward near the present-day mountains.

The Bouse Formation is principally a subsurface unit. Although exposures are numerous in the Parker-Blythe-Cibola area (fig. 1), these generally have a thickness of only tens of feet. The results obtained from the drilling of eight test wells during an investigation of the water resources of the Lower Colorado River, and data from other wells, indicate a greater thickness of this formation than is apparent from outcrops, and a continuity of the formation throughout the area (fig. 2). Table 1 shows the locations, total depths, and depths of the Bouse Formation in Geological Survey test wells.

The Bouse Formation rests unconformably on a fanglomerate of Miocene(?) age (Metzger, 1965) composed of cemented gravel and sand that are thought to have come from a nearby source, and on older Tertiary and pre-Tertiary rocks. In all the test wells that penetrated the Bouse Formation, the contact with the underlying and overlying units could be determined easily. The basal contact ranges in altitude from several hundred feet below sea level to as high as 1,050 feet above sea level.

The upper surface of the Bouse Formation is erosional. At least three degradations of the Colorado River have occurred since the unit was deposited, and each removed some of the Bouse Formation. Therefore, the original thickness of the Bouse may be very difficult, if not impossible, to determine.

PREVIOUS INVESTIGATIONS

Blanchard (1913, p. 24, 25, 38, 39) was the first to describe fossiliferous beds along Osborne Wash that now are referred to the Bouse Formation. However, he mistakenly identified a rhyolite tuff 5 to 50 feet thick near Osborne well, about 13 miles east of Parker, Ariz., as gradational into a fossiliferous calcareous tuff 44 inches thick farther west along Osborne Wash, and in addition, believed that the calcareous tuff was capped with basalt. These erroneous interpretations have been accepted by several later authors. Actually, both the tuff near Osborne Wash and the basalt are parts of a volcanic sequence that unconformably underlies the Bouse Formation; the "calcareous tuff" farther west is the basal limestone of the Bouse Formation.

U.S. GEOL. SURVEY PROF. PAPER 600-D, PAGES D126-D136

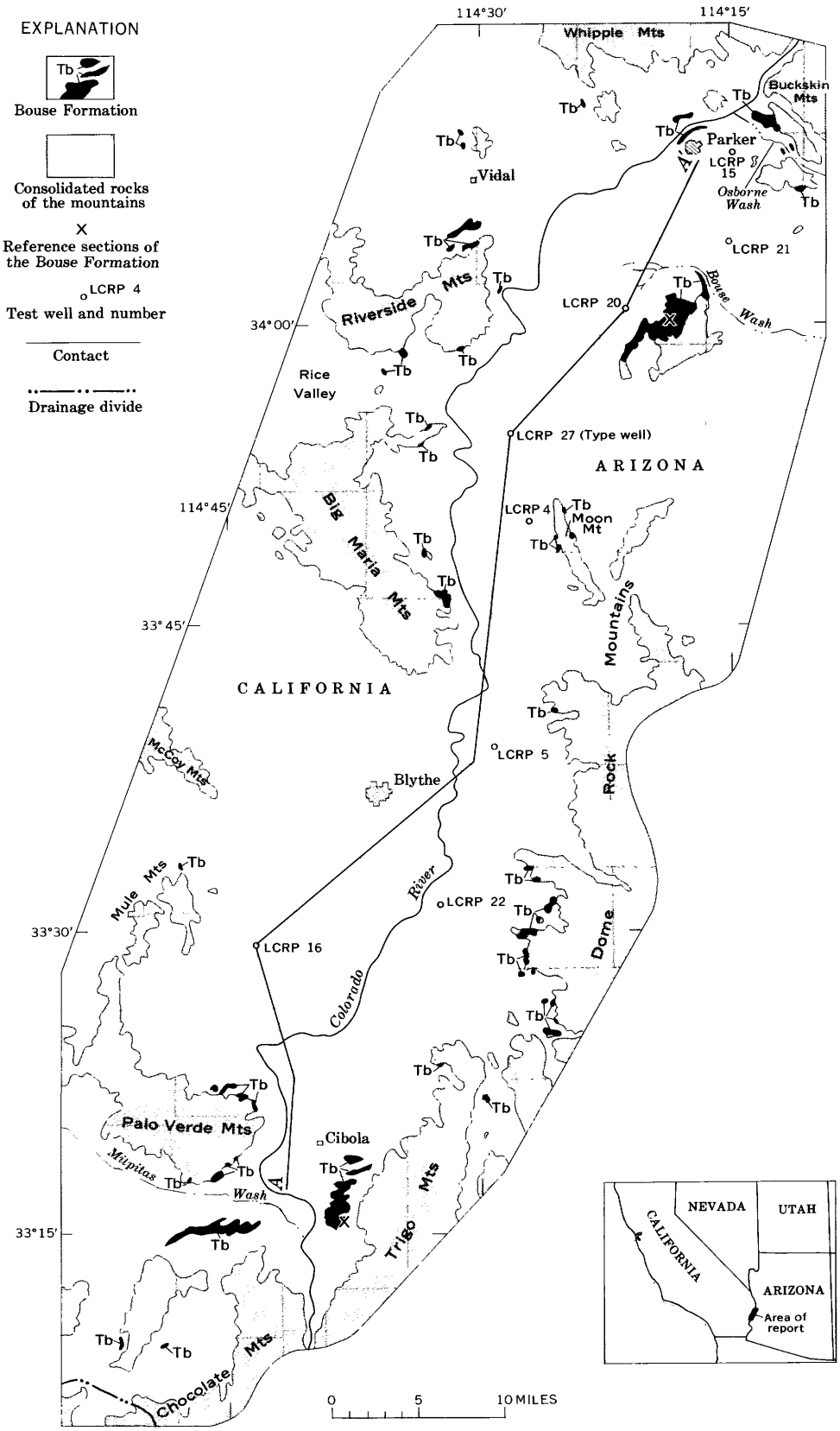

FIGURE 1.—Map of Parker-Blythe-Cibola area, Arizona and California, showing outcrops of the Bouse Formation, and U.S. Geological Survey test wells. *A*–*A*′, line of geologic section (fig. 2).

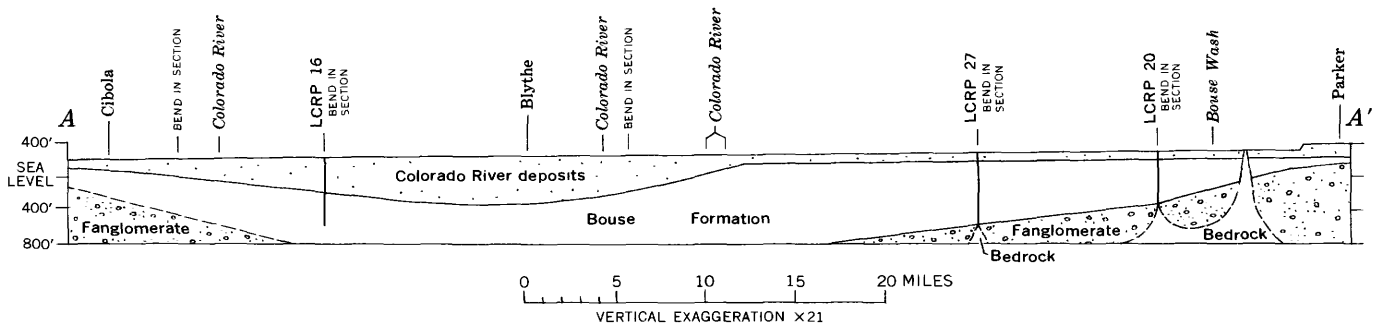

FIGURE 2.—Geologic section A–A' showing the continuity of the Bouse Formation, Parker-Blythe-Cibola area, Arizona and California. Location is shown on figure 1.

TABLE 1.—*Data from U.S. Geological Survey test wells along and near geologic section A–A' (fig. 2), Parker-Blythe-Cibola area, Arizona and California*

Well No. (fig. 1)	Location	Depth of well (feet below land surface)	Bouse Formation (feet below land surface)
	Arizona		
LCRP 4	SE¼SE¼SE¼ sec. 20, T. 6 N., R. 21 W.	585	130–585
5	NW¼NE¼NW¼ sec. 36, T. 4 N., R. 22 W.	471	----------
15	SE¼SE¼SE¼ sec. 5, T. 9 N., R. 19 W.	520	199–275
20	NE¼NE¼NW¼ sec. 29, T. 8 N., R. 20 W.	763	130–615
21	NE¼NW¼NW¼ sec. 5, T. 8 N., R. 19 W.	1,000	153–633
22	NE¼NW¼NW¼ sec. 16, T. 2 N., R. 22 W.	998	254–811
27	NE¼NE¼NE¼ sec. 31, T. 7 N., R. 21 W.	961	114–881
	California		
LCRP 16	SE¼SE¼NE¼ sec. 13, T. 8 S., R. 21 E.	800	445–800

Ross (1923, p. 23–25) in his study of the Lower Gila region, Arizona, discussed a thin-bedded limestone along Osborne Wash (basal limestone of the Bouse Formation in this paper and the "calcareous tuff" of Blanchard), and a green and yellow banded clay in the Colorado River Indian Reservation (interbedded clay, silt, and sand of the Bouse Formation). Ross (1923, p. 30, 31) was the first investigator to speculate that the calcareous sediments of the Lower Gila region (including the limestone along Osborne Wash) may have been deposited in an estuary of the Gulf of California.

Brown (1923, p. 46, 255) found small clams in a thin-bedded limestone (basal limestone of the Bouse Formation) on the south flanks of the Palo Verde Mountains, when he was making a survey similar to the one by Ross (1923). Brown suggested that if the fossils were marine, this would indicate an extension of the Gulf of California during Tertiary time.

Noble (1931, p. 55) described a clay deposit about 2 miles south of Vidal, Calif., which he believed to be lakebeds. These beds are now recognized as a part of the interbedded clay, silt, and sand of the Bouse Formation. A thin bed (½ inch thick) of limestone, found in this deposit during the present investigation, contained numerous barnacle plates and other fossils.

E. D. Wilson (1931) described sediments in the Cibola area and stated that they are marine, on the basis of barnacles found in the section. He tentatively correlated the sediments with marine beds of the Imperial Formation in the Imperial Valley. He described these beds as "well-stratified, weakly consolidated conglomerates, sandstones and marls, alternating with chalky and dense limestones to make up a total maximum apparent thickness of approximately 1,000 feet." In the present report these beds have been differentiated into a pre-Bouse fanglomerate and the basal limestone of the Bouse Formation. The fanglomerate may be as thick as 2,100 feet, and the basal limestone has a maximum thickness of about 100 feet.

Hamilton (1960) described sediments of salt-water origin on the flanks of the Big Maria Mountains referred to in this report as the tufa and interbedded clay, silt, and sand of the Bouse Formation. Hamilton postulated that the sediments represent deposition either in an extension of the Gulf of California or a huge saline lake.

Smith (1960) described fossil Foraminifera from the southeastern California deserts. The localities include cores from Panamint, Cadiz, and Danby Dry Lakes, and outcrop samples from along the Colorado River. The sediments along the Colorado River containing these fossils are a part of the Bouse Formation. The more recent work of Mrs. Smith, based on a study of the drill cuttings obtained during the drilling of the deep holes for this investigation, is discussed later in this report (p. D133).

Durham and Allison (1960, p. 61) reported the presence of planktonic Foraminifera from the Danby 1 hole at Danby Dry Lake, which they stated is an

indication of the accessibility of oceanic currents. They gave a map showing the extension of this invasion, and it included the Parker-Blythe-Cibola area. They suggested that the marine invasion occurred during the time of deposition of the Imperial Formation in the Imperial Valley, southwest of the Parker-Blythe-Cibola area.

TYPE AND REFERENCE SECTIONS

The type section for the Bouse Formation is the 767 feet of sediments penetrated in the U.S. Geological Survey test well LCRP 27 (table 2). This is the thickest known section for which subsurface data are available. In addition, two reference sections are designated: (1) Outcrops south of Bouse Wash and east of the Colorado River flood plain in T. 8 N., R. 20 W., Gila and Salt River base line and meridian, where 215 feet is exposed; and (2) outcrops in secs. 9 and 16, T. 2 S., R. 23 W.,

TABLE 2.—*Type section of the Bouse Formation from U.S. Geological Survey test well LCRP 27 located in the NE¼NE¼NE¼ sec. 31, T. 7 N., R. 21 W., Gila and Salt River base line and meridian, Arizona*

Description	Thickness (feet)	Depth (feet)
Colorado River deposits	114	114
Bouse Formation:		
Silt, yellowish-gray	4	118
Clay, light-brown, very pale-green streaked; contains fine to very fine yellowish-gray sand, and scattered small pebbles	11	129
Sand, chiefly very fine to medium; a few grains from medium to very coarse; few scattered small pebbles	36	165
Sand, chiefly very fine to medium; a few grains from medium to very coarse; contains numerous hard white and medium-orange-pink limestone balls as large as 3 inches across	26	191
Silt, pale-yellowish-brown and grayish-orange-pink; pale-olive and pale-reddish-brown clay	3	194
Sand, fine, yellowish-gray, dusky-yellow streaked	6	200
Sand, medium to fine, medium-greenish-yellow; scattered small rounded pebbles	8	208
Sand, coarse to fine, pale-olive and light-olive-gray; scattered pebbles of greenish-gray limestone	27	235
Gravel and sand, medium-gray; gravel subrounded to rounded, mostly pebble size, but some as much as 4 inches across; also armored balls composed of dense hard light-olive-gray limestone	15	250
Sand, coarse to fine, light-olive-gray; few granules	6	256
Sand, fine to very fine, light-olive-gray; few scattered small pebbles	4	260
Clay, greenish-gray; and light-gray silt	11	271
Sand, fine to medium, light-gray; contains scattered small pebbles and armored pebbles of dense hard light-olive-gray limestone	18	289
Bouse Formation—Continued		
Silt, sandy, light-olive-gray; contains greenish-gray clay, fragments of carbonized wood, and few scattered small pebbles	23	312
Sand, fine to very fine, light-olive-gray and very light gray; few small pebbles from 312–316-foot interval	14	326
Clay, silty, greenish-gray	2	328
Sand, very fine, light-olive-gray	10	338
Clay, greenish-gray; and fine to very fine sand interbedded with thin hard sandstone and hard limestone	5	343
Sand, fine, light-olive-gray	33	376
Sand, fine, light-olive-gray; light-olive-gray silt and clay	9	385
Clay and silt, greenish-gray and light-olive-gray; some siltstone and claystone; some fine yellowish-gray sand from 410–415-foot interval	30	415
Sand, fine, yellowish-gray; some thin beds of light-olive-gray clay, a 6-inch bed of light-olive-gray claystone at 455 feet	53	468
Clay, greenish-gray; some fine yellowish-gray sand and light-olive-gray claystone	5	473
Sand, fine, yellowish-gray	11	484
Clay, greenish-gray	1	485
Sand, fine, yellowish-gray	11	496
Clay and claystone, greenish-gray; fragments of carbonized wood	4	500
Sand, fine, yellowish-gray	3	503
Clay and claystone, greenish-gray	7	510
Sand, fine, yellowish-gray	6	516
Clay and claystone, light-olive-gray and greenish-gray	8	524
Sand, fine, yellowish-gray	9	533
Clay, greenish-gray; some light-olive-gray silt, and fine yellowish-gray sand	6	539
Sand, fine to medium, yellowish-gray	15	554
Clay, greenish-gray; and fine to very fine yellowish-gray silty sand	41	595
Claystone, light-olive-gray; thin streaks of siltstone and sandstone and fragments of carbonized wood	14	609
Sand, very fine to fine, light-olive-gray; some medium silty sand	45	654
Claystone, light-olive-gray; and fine silty light-olive-gray sand	16	670
Clay, greenish-gray; and fine silty light-olive-gray sand	23	693
Claystone and clay, light-olive-gray; and fine silty light-olive-gray sand; thin streaks of very hard greenish-gray limestone from 708–722-foot interval	29	722
Clay, greenish-gray; and fine to very fine light-olive-gray sand	40	762
Clay and claystone, greenish-gray; interbedded with fine light-olive-gray sand, and light-olive-gray silt	95	857
Marl, light-yellowish-gray, almost white	8	865
Marl, light-greenish-gray	5	870
Marl, yellowish-gray; contains granules and pea gravel	11	881
Pre-Bouse sedimentary rocks	80	961

southeast of Cibola, where 100 feet of the basal limestone is exposed.

LCRP 27 was drilled in the NE¼NE¼NE¼ sec. 31, T. 7 N., R. 21 W., Gila and Salt River base line and meridian (table 2). The well was drilled by the cable-tool method using a mud scow. During the drilling the casing was kept at the bottom of the hole, so that the samples are reliable as to depth. Also, the use of the mud scow facilitates the collection of excellent samples of the drilled materials. The cuttings are available for inspection at the office of the U.S. Geological Survey, Yuma, Ariz. Upon termination of the Lower Colorado River Project, the cuttings will be forwarded to the Arizona Bureau of Mines, Tucson, Ariz., for permanent storage in the well-sample library of that organization.

The reference section south of Bouse Wash and east of the flood plain is in the SW¼ sec. 26 and the SE¼ sec. 27, T. 8 N., R. 20 W., Gila and Salt River base line and meridian. At this locality the Bouse Formation is 215 feet thick and is composed of interbedded clay, silt, and sand. It is flat lying and rests on a fanglomerate which dips 5° westward.

The reference section southeast of Cibola is in secs. 9 and 16, T. 2 S., R. 23 W., Gila and Salt River base line and meridian. It has a composite thickness of 100 feet and is made up entirely of the basal limestone.

DISTRIBUTION AND THICKNESS

The Bouse Formation occurs in the subsurface throughout the Parker-Blythe-Cibola area (fig. 2). In the northern part of the Colorado River flood plain, the Bouse underlies Holocene alluvium at a depth no greater than about 130 feet. Near Blythe, the Bouse occurs at a depth of about 600 feet beneath Pliocene and Pleistocene Colorado River deposits. Near Cibola, the Bouse underlies Holocene alluvium at a shallow depth. Surface exposures of the Bouse Formation occur in the Cibola area, near Parker, and as scattered outcrops of small areal extent near the mountains throughout the rest of the area.

The thickest section known is the 767 feet in LCRP 27, where the Bouse Formation is overlain by Holocene alluvium. Assuming no structure between LCRP 20, 10 miles northeast of LCRP 27, and the outcrops to the east, an assumption which may or may not be valid, the thickness may be as much as 900 feet. The upper surface in the outcrops is an erosional unconformity like that at LCRP 27.

The basal limestone was found in all test wells that penetrated the Bouse Formation. The thickness of the limestone in the test well is as follows: LCRP 22, 5 feet; LCRP 27, 24 feet; LCRP 20, 7 feet; LCRP 21, 10 feet; and LCRP 15, 9 feet. The basal limestone is about 100 feet thick in the area south and southeast of Cibola, and in the lower part of the Milpitas Wash drainage basin. About 20 feet of the limestone, including one thin (about 4 inches thick) ashfall tuff, is exposed near the drainage divide between Milpitas Wash and Imperial Valley in sec. 4, T. 12 S., R. 20 E., San Bernardino base line and meridian. The limestone crops out to the north along Osborne Wash and the Colorado River near Parker, where it is generally less than 4 feet thick.

The interbedded unit occurs extensively in the subsurface in the Parker-Blythe-Cibola area. All but one of the test wells penetrated a part of the unit. In addition, the logs of many private wells indicate that the wells are bottomed in this interbedded sequence. This unit is by far the thickest unit in the Bouse Formation. As an example, this unit was 743 feet thick in LCRP 27, whereas the basal limestone was only 24 feet thick. The unit is exposed south of Bouse Wash along the terrace bordering the flood plain south to Moon Mountain, south of Vidal, and along Osborne Wash and the Colorado River near Parker. Small outcrops occur in the Cibola area, and on the flanks of the Big Maria and Riverside Mountains.

The tufa occurs on the lower slopes of most of the mountains in the area. The more extensive outcrops are in T. 2 N., R. 21 W., Gila and Salt River base line and meridian, and on Moon Mountain. It is less than one foot thick, but it effectively conceals the older rocks.

LITHOLOGY

The basal limestone of the Bouse Formation grades upward into the interbedded sequence. The tufa is distinct, and it was formed throughout the time of deposition of the other two units. There is always a sharp break between the tufa and the other two units, but it is not a significant time break.

Basal limestone

The basal limestone (fig. 3), at the reference section in secs. 9 and 16, T. 2 S., R. 23 W., about 4 miles south of Cibola, is composed of three subunits. The lower subunit is composed of thin-bedded marly white limestone containing one 5-foot bed of barnacle coquina, and it is about 50 feet thick. The middle subunit is a crossbedded light-tan, barnacle-coquina limestone about 20 feet thick. The upper subunit is a marly white limestone about 30 feet thick. These subunits vary laterally, to the extent that the subdivision was not recognized in the outcrops west of the Colorado River.

The dip of the limestone at the above-cited reference section is 2° in a N. 50° W. direction. The dip is re-

FIGURE 3.—The basal limestone of the Bouse Formation near Cibola, in the NW¼ sec. 16, T. 2 S., R. 23 W. The contact between a fanglomerate and the basal limestone is in the center of the picture (see arrow). The two white layers are thin-bedded marly limestone, each 15 feet thick. The dark layer between the white layers is a lens not more than 10 feet thick of subrounded to rounded gravel. The dark capping material is a barnacle coquina. About 60 feet of the basal limestone is exposed in this picture.

markably uniform except near the mountain front where the limestone has been warped upward.

During the drilling of the test wells, the top of the limestone was easily detected. The color of the drilling mud changed from the dark gray, that was characteristic of the interbedded clay, silt, and sand, to white. The limestone drilled easily and was generally reported by drillers as white clay. Marl was the most abundant type of material, and pebbles were present.

Along Osborne Wash and the Colorado River near Parker, the limestone is white, thin bedded, and marly. It contains one thin (about 1 inch thick) chert layer in the NE¼ sec. 34, T. 10 N., R. 19 W.

Gravel, a minor lithologic type in the basal limestone, occurs in lenses and as scattered rocks (up to boulder size). One gravel lens (fig. 3) ranges from 0 to 10 feet thick. This gravel is composed of metamorphic, igneous, and volcanic rocks, which suggests local derivation. The gravel is subrounded to rounded, and commonly the pebbles have an iron stain. Another gravel lens on the flanks of the Palo Verde Mountains is 9 feet thick and has cross beds that dip 30°; the cross beds are truncated sharply at top and bottom. Some cross beds are composed mostly of pebbles, 1 to 2 inches in diameter, and others mostly of pebbles ¼ to ½ inch in diameter. Thin limestones, both above and below this gravel, contain barnacle plates.

The other scattered gravel has the same dip as the limestone and grades basinward into limestone. A few pebbles of tufa of the Bouse Formation occur in some of this gravel, which indicates that tufa antedated some of the limestone.

The basal limestone is a unique deposit. Although the limestone grades upward into the interbedded sequence, there is no evidence, either subsurface or surface, of significant limestone deposition higher in the Bouse Formation; neither is there evidence of interfingering of the two units. This suggests a change in environmental conditions after the deposition of the limestone. In addition, the crossbedding, both in some of the limestone beds and in the gravel lenses, indicates strong current action. No gravel lenses, and only a minor amount of crossbedding in some sand, have been observed in the overlying interbedded sequence. The gravel lenses of the limestone are believed to be nearshore or offshore bars because individual lenses are underlain and overlain by beds of limestone.

Interbedded unit

The thickest and most extensive exposure of the interbedded unit occurs south of Bouse Wash and east of the Colorado River flood plain (fig. 4). Here, the

FIGURE 4.—Interbedded unit of the Bouse Formation near Bouse Wash in the SW¼ sec. 26, T. 8 N., R. 20 W. About 215 feet of clay, silt, and sand is exposed. The Bouse Formation rests on a fanglomerate (see arrow) which crops out in the wash in the foreground.

Bouse Formation is flat lying, rests on a fanglomerate which dips 5° to the west, and is overlain by locally derived gravel.

At this locality, the formation is about one-half clay, and is mostly thin bedded. Few of the beds are thicker than 10 feet, an exception being a bed of fine sand which is 25 feet thick. During deposition of this sand, a subaqueous channel evidently was scoured to a depth of 12 feet, then filled with crossbedded sand, after which an additional 13 feet of horizontal-bedded sand was deposited.

Some of the beds grade upward from sand at the base to silt to clay. The beds may be less than 1 foot to as much as 20 feet thick. Although the thinner ones appear "varve-like", most are too thick to be considered as varves, but instead represent cycles of much longer periods.

Most of the clay beds are pale olive to pale yellowish green. Others are red, yellow, or gray. A characteristic of the clay is that it swells when moistened, which may indicate that some of the clay is montmorillonite. Because of this characteristic, the outcrops are coated with an amorphous greenish mass.

The silt and fine-sand layers are commonly grayish orange, or very light gray to very light pink. Most of the sand is only weakly compacted or cemented; however, some thin sandstone layers are well cemented with calcium carbonate. Some of the light-gray sand layers contain numerous black minerals that result in a "salt and pepper" appearance.

Cuttings from wells of the interbedded unit have some characteristics different from those in outcrops. One of the most noticeable is the color. Cuttings of clay, when wet, are dark blue, dark gray, or dark green, and are generally referred to by drillers as "blue clay". When dried, the cuttings are a gray or green. The sand is all gray or dark gray; none of the lighter hues of the outcrops have been observed.

Another noticeable difference is in the induration of the sediments. Some of the clay cuttings are sufficiently indurated to be classed as claystones. In drilling, some of the claystones break up into cubes and others have a conchoidal fracture. As long as the clay and claystone are kept saturated, they remain solid and do not break down. However, if they become completely dry, and then are put in water, they swell and break down readily, similar to outcrop samples.

The drilling action in sand indicates that the sand is more compacted or cemented than would be suspected from inspection of outcrops. Some of the sand is well indurated, but it occurs as thin beds, or streaks as reported by well drillers.

Two minor constituents of the cuttings are microscopic pyrite crystals and small pebbles. The pyrite crystals occur as minute crystal groups, and some pyrite fills the tests of some of the microfossils.

Some of the cuttings contain small pebbles, for the most part enclosed by clay. Because the pebbles are "floating" in the clay, it is inferred that they were probably dropped into the body of water from rafts of vegetation. The pebbles are rounded to well rounded and composed of dense rocks, such as volcanic, granitic, and quartzitic rocks. The pebble assemblage is significantly different from that in the gravel deposits of the Colorado River.

No marker beds have been recognized in the interbedded sequence, possibly because of the limited subsurface data and the monotony of the sequence. Some thin beds (less than 1 inch thick) may eventually be shown to be marker beds. These beds are white limestone composed mostly of barnacle plates. One bed occurs in the section south of Bouse Wash and east of the flood plain, one is south of Vidal, Calif., and another is in the southwestern part of T. 2 S., R. 23 E. Not one of these beds has been recognized in test wells, but this is not surprising when one considers the limited thickness of the beds.

Three of the test wells penetrated a large amount of sand of the interbedded unit in the uppermost part of the drilled section. At LCRP 27, the upper 175 feet of the formation contained 146 feet of sand, and only 29 feet of silt and clay. At LCRP 4, the upper 310 feet was mostly sand. At LCRP 16, the upper 145 feet contained 141 feet of sand. In these wells, the remainder of the drilled section contained much more clay. Similar thicknesses of sand have not been observed in outcrops of the Bouse Formation.

Tufa

The tufa is a peculiar calcareous deposit that adheres to the pre-Bouse rocks of the area. It has many forms, and locally it is plastered to vertical cliffs. It was deposited on the slopes of small ridges and valleys in such a manner that the initial dips give the false impression that the limestone has been folded into small anticlines and synclines.

The tufa varies from a very hard and dense rock to a soft and porous rock, and from a white to a dark gray. It is for the most part, however, a resistant rock, and rather light in color.

The most notable characteristic of this thin deposit is the peculiar manner in which it adheres to the pre-Bouse rocks. Thin coatings have been observed that completely cover small hills. In other places, they may conceal the slopes of a hill, yet leave a small bald spot where the pre-Bouse rocks are exposed.

Another form of tufa is similar to cave stalactites. The stalactitic tufa is on nearly vertical cliffs, draping downward in large lobes.

Some of the outcrops, when viewed for the first time, and also where the outcrop is small, appear to be hot-spring deposits. However, the tufa is so widespread and in places forms such extensive exposures that little of it is likely to be of hot-spring origin. As an example, on Moon Mountain, it completely covers metamorphic rocks. It would be an unusual system of springs in metamorphic rocks that would produce such a deposit.

Locally, cavities have been found in the tufa. These cavities range from a few inches to about 2 feet in diameter and are lined with a dense finely laminated limestone that is botryoidal and smooth. Some of the laminae are dark, probably because of a manganese mineral.

PALEONTOLOGY

Fossils are common in the Bouse Formation, although the number of species is small. Some of the fossils are marine, but they are not helpful in determining the age of the Bouse Formation. The fossils include foraminifers, mollusks, ostracodes, charophytes, and barnacles. The tufa is believed by the author to be primarily the work of algae, but no paleontologic study has been made to verify this.

Cuttings obtained from the Bouse Formation during the drilling of the test wells were submitted to Mrs. P. B. Smith, U.S. Geological Survey. From a preliminary appraisal, Smith (written commun., 1967) reports eight species of marine Foraminifera. She concludes that the

> . . . fossils are more characteristic of a normal marine environment in the southern part of the area than near Parker. In the northern area samples tend to be monospecific, generally entirely composed of *Ammonia beccarii* (Linné). To the south more species appear and while the assemblage is not one that has been reported from any modern environment, the presence of the planktonic Globigerinas indicates a marine environment.

The Foraminifera as identified by Mrs. Smith are: *Ammonia beccarii* (Linné), *Eponidella palmerae* Bermudez, *Elphidium* cf. *E. gunteri* Cole, *Bolivina subexcavata* Cushman and Wickenden, *Rosalina columbiense* (Cushman), *Quinqueloculina* sp., *Globigerina* sp., and *Cibicides* sp. Most of these species were also found by Smith in cores from Danby and Cadiz Dry Lakes, west of Parker (Smith, unpub. data).

Marine clams from the Bouse Formation include *Halodakra*, *Diplodonta*, *Macoma*, and *Mulinia*? Marine snails include *Batillaria* and ?*Barleeia*. A brackish-water snail, *Tryonia*? also has been identified. Fresh-water snails include *Fontelicella*, *Physa*, and ?Hydrobiidae. Most of the mollusks were identified by D. W. Taylor (A. M. Keen, Stanford University identified *Halodakra*, *Diplodonta* and *Macoma*). Of particular interest is the marine snail *Batillaria*. Taylor (D. W. Taylor, written commun., 1967) states that "although the genus is living in warm-temperate to tropical waters of the Caribbean and East Asia, t is unknown on the Pacific Coast of North America as a native."

Ostracodes from the Bouse Formation were identified by I. G. Sohn. These include *Ilyocypris* or *Limnocythere*, *Candona*, *Cytheromorpha*?, *Candoniella*, and several species of *Cyprideis*. These fossils were both brackish- and fresh-water types.

The mollusks, by their limited collections and limited fauna, are indicative of an environment different from that of open marine waters (D. W. Taylor, written commun., 1967). According to Taylor, the presence of fresh-water types and the occurrence of *Chara* are significant in indicating a brackish-water environment. Also, although the salinity was sufficiently high at times to support the limited marine fauna, the water of the embayment was definitely more brackish than marine.

AGE

As discussed in the preceding section, a definitive age assignment for the Bouse Formation based on fossils is not possible at this time. However, a minimum age for the Bouse Formation is the time of entry of the Colorado River into the Basin and Range province because the Bouse is older than deposits of the Lower Colorado River. As will be explained below, the age of the Bouse Formation can be established broadly as Pliocene.

Gravel of the Colorado River that underlies lava about 10 miles west of the Grand Wash Cliffs at Sandy Point (fig. 5) indicates that the Colorado River at the time of outpouring of the lava had eroded older deposits until it was at a grade similar to that of the present. This lava has been dated as 2.6 ± 0.9 million years (Damon, 1965, p. 40). The erosion of the older deposits indicates a substantially earlier date for entry of the ancestral Colorado River into the Lake Mead area.

A thin tuff, which occurs in the basal limestone of the Bouse Formation near the drainage divide between Milpitas Wash and Imperial Valley in sec. 4, T. 12 S., R. 20 E., has been dated by the K–Ar method as equal to or greater than 3.02 ± 1.15 m.y. (P. E. Damon, written commun., 1967). This age is considered a minimum because of partial devitrification of the glass.

The outcrops of the Bouse Formation near the drainage divide between Milpitas Wash and the Imperial Valley indicate a marine connection between the two areas during the time of deposition of the Bouse. Therefore, a correlation between the Bouse Formation and some of the marine sediments of the Imperial Valley undoubtedly exists. However, the

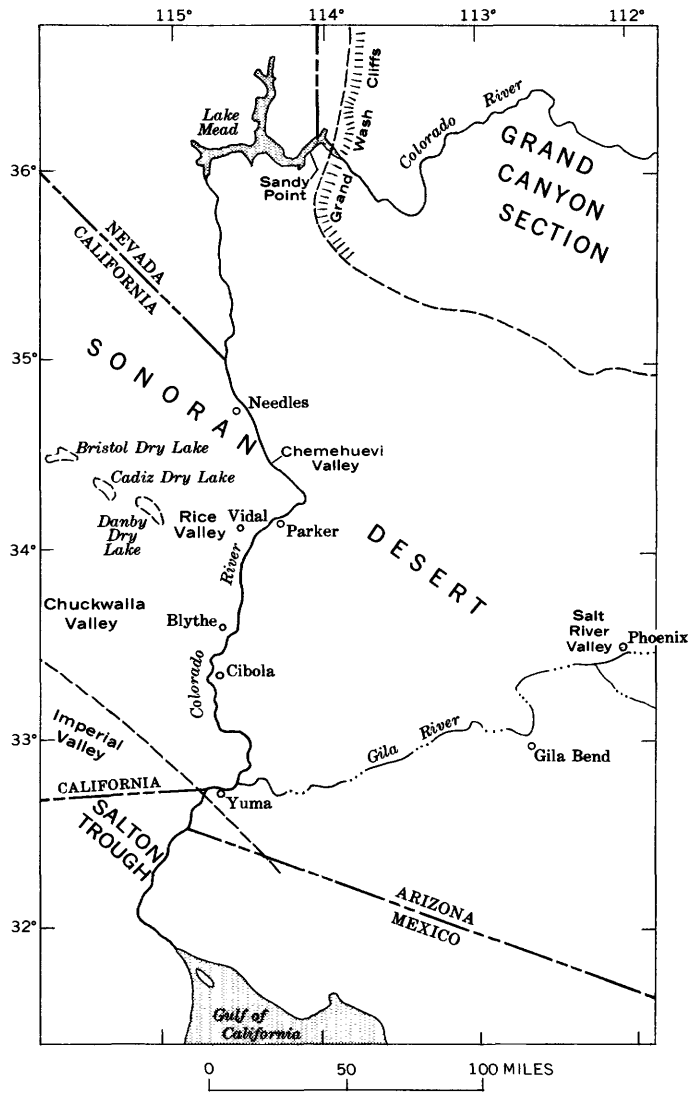

FIGURE 5.—Index map of Sonoran Desert area.

limited collections and the limited fauna of the Bouse Formation prevent a paleontological correlation with rocks in the Imperial Valley at this time (D. W. Taylor, written commun., 1967, and P. B. Smith, written commun., 1967). Further, controversy exists on the ages of the rocks of the Imperial Valley (Allison, 1964).

The above discussion indicates that a definitive age assignment within the Pliocene for the Bouse Formation is impossible at this time. The earliest deposits of the Lower Colorado River are at least late Pliocene in age and perhaps older. The oldest marine formation of the Imperial Valley with which the Bouse Formation may be tentatively correlated is the Imperial Formation of late Miocene or early Pliocene age. The youngest marine formation would be that beneath deltaic sediments that could be demonstrated to have been transported by the Colorado River, a topic not covered in the literature. Thus, the Bouse Formation could be as old as early Pliocene or as young as late Pliocene. Because of the uncertainty of assigning an age within the Pliocene, the Bouse Formation is referred to as Pliocene with the understanding that some of the Lower Colorado River deposits are also Pliocene.

CORRELATION WITH OTHER AREAS IN THE SONORAN DESERT

As was mentioned previously, the Bouse Formation is principally a subsurface unit. Because most of the basins adjacent to the Lower Colorado River are mantled by Pleistocene deposits, the extent of the Bouse Formation can be determined only from subsurface data. A common subdivision in many basins of the Sonoran Desert based on well logs is threefold: a lower cemented "basin fill", a middle fine-grained unit, and a younger "basin fill." In the Parker-Blythe-Cibola area, the middle unit is the Bouse Formation, but how far this interpretation of well data can be extended into the Sonoran Desert is speculative because unequivocal data are not available.

Outcrops of the Bouse Formation near the drainage divide between Blythe and Chuckwalla Valley indicate that the embayment extended into Chuckwalla Valley. Outcrops between the Riverside and Big Maria Mountains indicate an extension into Rice Valley, and probably Cadiz and Danby Dry Lakes (fig. 5). Bassett, Kupfer, and Barstow (1959) give core logs for holes drilled in Bristol, Cadiz, and Danby Dry Lakes. The logs for Cadiz and Danby Dry Lakes indicate fossiliferous sediments similar to the Bouse Formation.

Noble (1931) described sediments along the Colorado River near Needles, Calif., in Chemehuevi Valley, and near Vidal, Calif. He noted a similarity of the deposits in the three areas, and he referred to them as lake deposits. Most of his description is of the sediments in Chemehuevi Valley (fig. 5) in T. 4 N., Rs. 24 and 25 E., San Bernardino base line and meridian. Noble (1931, p. 41–42) recognized four units, of which the basal layer is a conglomerate composed of local rocks. This is overlain by a white chalky shale from 15 to 50 feet thick, which he interpreted in the field as being a very fine volcanic ash; a later chemical analysis proved the deposit to be largely calcium carbonate, a calcareous marl, or chalk. Overlying the marl are 25 to 50 feet of green clay, and 175 feet of buff clay containing a few sandy beds.

The Needles area of Noble (1931, p. 55) is about 10 miles southeast of Needles in secs. 1 and 12, T. 7 N., R. 23 E., San Bernardino base line and meridian. Noble does not describe the sediments other than to

say that they are similar to those in Chemehuevi Valley. However, about 100 feet of limestone overlain by interbedded clay and sand is exposed. The limestone is as much as 4 feet thick. The interbedded sequence is made up of tan sand and green clay.

As mentioned previously, the rocks of the Vidal area of Noble (1931, p. 55) are a part of the Bouse Formation. The other two areas may be of the same age as the Bouse Formation because of the similarities of their deposits and their relation to the Colorado River deposits. The logs of wells in the Needles area indicate that "blue clay" underlies Colorado River deposits, which also is true for the logs of wells drilled in the Parker-Blythe-Cibola area. However, the absence of the brackish-water fossils (other than ostracodes) casts some doubts on the extension of an embayment of the Gulf of California as far north as Needles.

Marine deposits, correlative with the Bouse Formation and older than Colorado River deposits, have been recognized from subsurface studies in the Yuma, Ariz., area (Olmsted and McDonald, 1967). The marine deposits range in depth from about 200 feet below land surface in a locality 10 miles northeast of Yuma to more than 3,000 feet in an area 20 miles southwest of Yuma. These deposits contain marine and brackish-water foraminiferal faunas, some of which are identical with those of the Bouse Formation (P. B. Smith, written commun., 1967).

Subsurface clays along the lower Gila River from Yuma to Gila Bend, Ariz. (fig. 5) were first described by Ross (1923, p. 90). He postulated that they may be lacustrine or estuarine, probably estuarine. Some of these probably were deposited in the Bouse embayment. Also, there is a possibility that the 600 feet of clay reported in well logs for an area west of Phoenix in the Salt River Valley may also be contemporaneous with the Bouse Formation. The similarity of electric logs of wells that are known to penetrate the Bouse Formation and of those for wells that penetrate the clay near Phoenix is unmistakable.

GEOLOGIC HISTORY

The Bouse Formation is underlain by locally derived gravel, and is overlain by Colorado River deposits containing the distinctive well-rounded gravels that could have come only from many miles upstream. The Bouse was deposited in an embayment of the Gulf of California that extended not only into the Parker-Blythe-Cibola area, but probably as far north as Needles, and both east and west of the present Colorado River into adjacent desert basins. The limited marine faunas indicate that the embayment was not a normal marine environment. The apparent absence of marine fauna north of the present Whipple Mountains suggests a freshening of the water, possibly by the ancestral Colorado River.

The outlines of the mountains of the Parker-Blythe-Cibola area and adjacent desert areas were present prior to the invasion of the waters of the embayment, as evidenced by the outcrops of the Bouse that were deposited against the mountains. The structure and erosion that produced the mountains occurred prior to the Bouse, and possibly the locally derived pre-Bouse gravels represent erosion following the latter stages of the structure. During the time of the embayment some mountains were buried and others were islands in this vast body of water.

After the deposition of the Bouse Formation, the Colorado River began to flow through the Parker-Blythe-Cibola area to the Gulf of California. Soon thereafter, the mountains began to rise relative to the basins. The Bouse Formation was eroded easily and, in the localities of the present canyons, the Colorado River eroded to bedrock. The uplift was sufficiently slow that the Colorado River became entrenched, and the canyons of the Lower Colorado River began to form. The differential movement between the basins and ranges has resulted in the present occurrence of the Bouse at altitudes as low as several hundred feet below sea level, and as high as 1,050 feet above sea level.

REFERENCES

Allison, E. C., 1964, Geology of areas bordering Gulf of California, *in* Marine geology of the Gulf of California—a symposium: Am. Assoc. Petroleum Geologists Mem. 3, p. 3–29.

Bassett, A. M., Kupfer, D. H., and Barstow, F. C., 1959, Core logs from Bristol, Cadiz, and Danby Dry Lakes, San Bernardino County, California: U.S. Geol. Survey Bull. 1045–D, p. 97–138.

Blanchard, R. C., 1913, The geology of the western Buckskin Mountains, Yuma County, Arizona: Columbia Univ. Contrib. Geol. Dept., v. 26, no. 1, p. 1–80.

Brown, J. S., 1923, The Salton Sea region, California; a geographic, geologic, and hydrologic reconnaissance, with a guide to desert watering places: U.S. Geol. Survey Water-Supply Paper 497, 292 p.

Damon, P. E., 1965, Correlation and chronology of ore deposits and volcanic rocks: Univ. Ariz., Geochronology Lab., Ann. prog. rept. C00–689–50, 60 p.

Durham, J. W., and Allison, E. C., 1960, The geologic history of Baja California [Mexico] and its marine faunas, *in* symposium—The biogeography of Baja California and adjacent seas—pt. 1, Geologic history: Systematic Zoology, v. 9, no. 2, p. 47–91.

Hamilton, Warren, 1960, Pliocene(?) sediments of salt water origin near Blythe, southeastern California: Art. 125 *in* U.S. Geol. Survey Prof. Paper 400–B, p. B276–B277.

Metzger, D. G., 1965, A Miocene(?) aquifer in the Parker-Blythe-Cibola area, Arizona and California, *in* U.S. Geological Survey Research 1965: U.S. Geol. Survey Prof. Paper 525–C, p. C203–C205.

Noble, L. F., 1931, Nitrate deposits in southeastern California, with notes on deposits in southeastern Arizona and southwestern New Mexico: U.S. Geol. Survey Bull. 820, 108 p.

Olmsted, F. H., and McDonald, C. C., 1967, Hydrologic studies of the Lower Colorado River region: Am. Water Resources Assoc., v. 3, no. 1, p. 45–58.

Ross, C. P., 1923, The Lower Gila region, Arizona; a geographic, geologic, and hydrologic reconnaissance, with a guide to desert watering places: U.S. Geol. Survey Water Supply Paper 498, 237 p.

Smith, P. B., 1960, Fossil Foraminifera from the southeastern California deserts: Art. 127 *in* U.S. Geol. Survey Prof. Paper 400–B, p. B278–B279.

Wilson, E. D., 1931, Marine Tertiary in Arizona: Science, v. 74, p. 567–568.

——— 1962, A résumé of the geology of Arizona: Ariz. Bur. Mines, Bull. 171, 140 p.

PROVENANCE OF IGNEOUS ROCKS IN CRETACEOUS CONGLOMERATES IN NORTHWESTERN MONTANA

By MELVILLE R. MUDGE and RICHARD A. SHEPPARD, Denver, Colo.

Abstract.—Igneous pebbles and cobbles are in conglomerates of four Cretaceous units in and near the Sun River area in northwestern Montana. These conglomerates occur in the Kootenai Formation (Aptian), Vaughn Member of the Blackleaf Formation (upper Albian), Two Medicine Formation (middle Campanian), and in the Horsethief Sandstone (upper Campanian). Both plutonic and volcanic rocks are in the Kootenai, whereas only volcanic rocks are in the younger conglomerates. Study of these sedimentary deposits indicates that, except for the Kootenai, volcanism was contemporaneous with deposition of each formation. The igneous rocks in the Kootenai conglomerates are probably very late Jurassic in age. The source of the igneous rocks in the Lower Cretaceous rocks was west of the Sun River area. The source for some of the Upper Cretaceous igneous-pebble conglomerates was south of the Sun River area, whereas for other conglomerates it was west of the area.

Igneous pebbles in conglomerates occur in four Cretaceous units in and near the Sun River area in northwestern Montana (fig. 1). These units are the Kootenai Formation (Aptian), the Vaughn Member of the Blackleaf Formation (upper Albian), the lower part of the Two Medicine Formation (middle Campanian), and the Horsethief Sandstone (upper Campanian). Study of the conglomerates indicates that volcanism occurred in northwestern Montana during a heretofore unrecognized very early Cretaceous episode as well as during the well-known later Cretaceous episodes.

In Alberta, Canada, igneous rocks in conglomerates of late Early Cretaceous age were noted as early as 1917 (Rose, 1917, p. 110). These are in the McDougall-Segur Conglomerate of the nonmarine Blairmore Group, and have been described and dated by Norris, Stevens, and Wanless (1965).

In northwestern Montana, igneous pebbles in Cretaceous conglomerates were collected by the writers during 1958 to 1966 while conducting geologic investigations in the Sun River area. Pebbles in the Kootenai were previously recognized in the Willow Creek area to the south (Merrill, 1965, p. 35). Igneous pebbles in the Two Medicine Formation, north of the Sun River area, were described by W. T. Pecora (*in* Cobban, 1955, p. 116). Similar pebbles, also from the latter formation, have been described in the Dearborn River-Wolf Creek area by Viele (1960), Schmidt (1963), Schmidt, Swanson, and Zubovic (1964), and Viele and Harris (1965). Igneous pebbles in the Horsethief Sandstone were observed in some exposures by Cobban (1955, p. 118). East and south of Augusta, Mont., igneous pebbles were recognized in this unit by Viele and Harris (1965, p. 405) and by J. F. Murphy (oral commun., 1967).

Volcanics and intrusions of very late Cretaceous age, called the Adel Mountain Volcanics, rest unconformably on the lower beds of the St. Mary River Formation in the Wolf Creek area to the south (Lyons, 1944; Schmidt and others, 1964).

STRATIGRAPHY

Cretaceous strata in northwestern Montana are mainly shale, siltstone, claystone, and sandstone (fig. 2). These rocks, about 8,000 feet thick, were deposited on a shelf that alternated between nonmarine and marine environments (Cobban, 1955, p. 107). Only those units containing conglomerates with igneous pebbles are discussed in this report.

Many of the marine sandstones, especially in the Lower Cretaceous, contain grains derived from altered lavas and tuffs as well as from metamorphic, plutonic, and sedimentary rocks. The pebbles in all these formations have a roundness of 7 to 9 on the Krumbein (1941, pl. 1) scale.

Kootenai Formation

The nonmarine Kootenai Formation is the oldest Cretaceous unit (Aptian) in northwestern Montana (Cobban, 1955, p. 108). In the Sun River area it ranges in thickness from 650 to 800 feet, and consists mainly of grayish-green and dull-reddish-brown siltstone and sandy siltstone with local thin gray, olive-drab, yellowish-gray, and purple beds of siltstone. Lenses of fine- to medium-grained, locally crossbedded sandstone occur

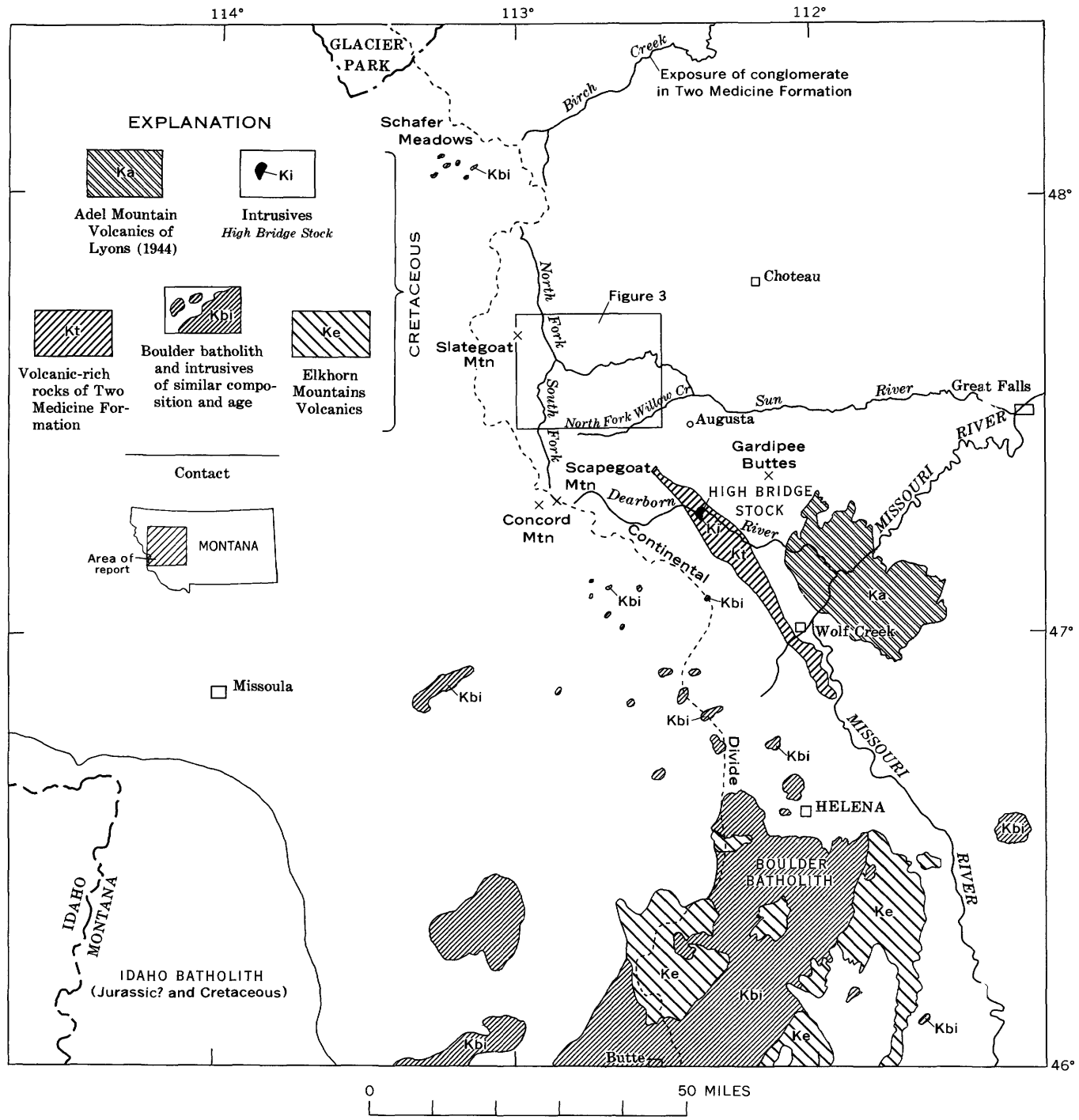

FIGURE 1.—Igneous rocks in part of northwestern Montana in relation to the Sun River area (fig. 3).

at various horizons in the formation. They consist mostly of well-rounded to subangular grains of quartz and chert that impart a "salt and pepper" appearance to the rock. Magnetite is a common constituent and locally it is abundant in a widespread sandstone unit about 50 feet above the base of the formation.

Sandstone beds are thicker and more widespread in the upper and lower parts of the formation than in the middle part; locally they fill small channels. Conglomerates are at the base of or within the channel sandstones. Locally, however, at locations shown on figure 3, conglomerates compose most of the channel fill and they range in thickness from about 1 foot to at least 50 feet. The thickest conglomerate is along No Business Creek,

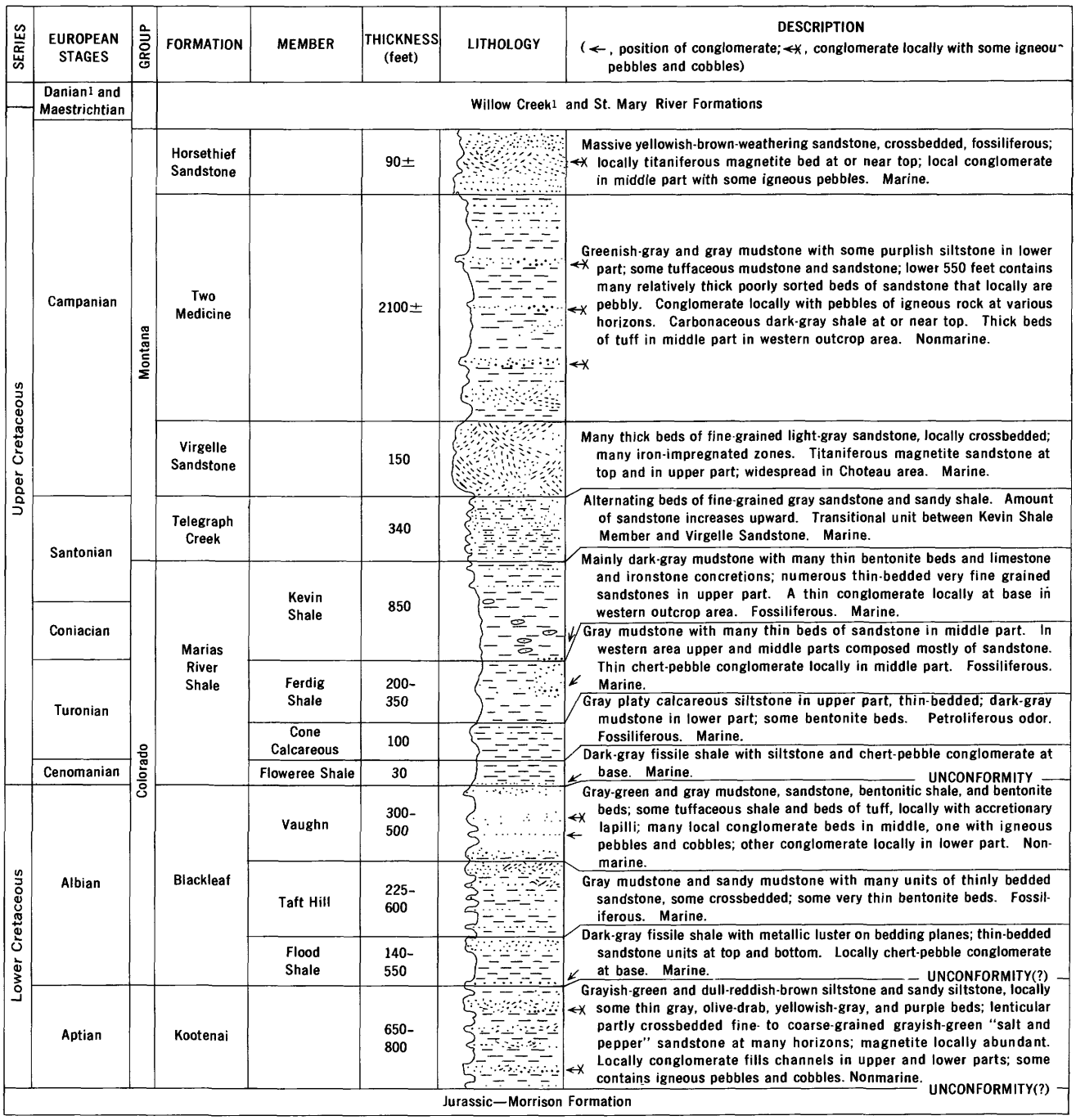

[1]Upper part of Willow Creek Formation is Paleocene (Danian).

FIGURE 2.—Cretaceous rocks in the Sun River area, Montana.

and it contains the largest fragments and greatest variety of igneous rocks.

The conglomerate at the base of the lower sandstone unit of the Kootenai is exposed locally in the southern part of the Sun River area. It consists of rounded to subrounded pebbles (as much as 3 inches across) and smaller fragments of quartzite, quartz, chert, and igneous rock. Along Benchmark Creek the crossbedding indicates a northeasterly direction of transport. Here the conglomerate is about 30 feet thick and of unknown width.

A poorly sorted conglomerate, with interbedded sandstone, fills a channel that is 600 feet wide and about 50 feet deep at a base of the upper sandstone of the

313-005 O—68——10

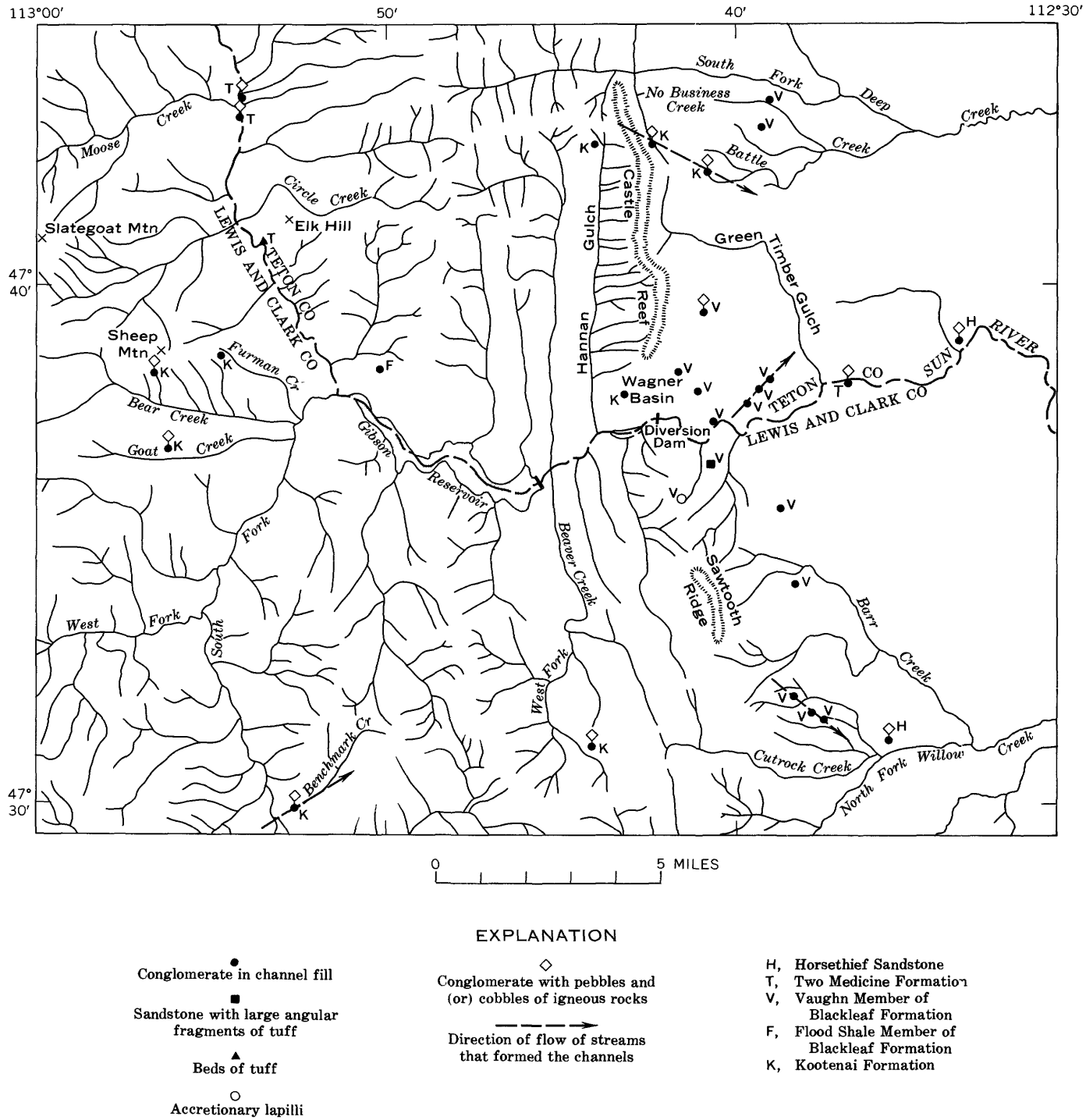

FIGURE 3.—Location of some conglomerates and volcanic-rich strata in Cretaceous rocks in the Sun River area, Montana.

Kootenai along No Business Creek (fig. 4). The sides of the channel trend N. 70° W., and some of the crossbeds indicate an easterly to southeasterly current direction. This channel trend is substantiated by the plot of a second exposure of this conglomerate in the next fault block to the east (fig. 3). The unconformity at the base of the channel fill is very irregular on sandy mudstone which has numerous quartz-filled fractures. The lower part of the channel fill has limonite and hematite stains along fractures. Coarse-grained arkosic sandstone occurs as interbedded lenses as much as 3 feet thick in the conglomerate. The sandstones are composed chiefly

FIGURE 4.—Helicopter view of the channel filled with conglomerate and sandstone in the Kootenai Formation along the west side of the upper reaches of No Business Creek. The channel fill is about 50 feet thick and 600 feet wide.

of angular to subangular grains of quartz, chert, and feldspar; wood and coal fragments are also common.

The conglomerate contains many well-rounded pebbles ½ to 1½ inches across and some cobbles as much as 6½ inches across. The fragments are chiefly extrusive and shallow intrusive igneous rocks, but also include chert, quartz, quartzite, and silicified carbonates. All the larger fragments are of igneous rock.

Most of the igneous pebbles and cobbles are quartz rich and include granite, quartz monzonite, granodiorite, and quartz diorite as well as silicic lavas and tuff. Quartz monzonite is most common, and quartz diorite is least common.

The plutonic rocks are medium to coarse grained and typically hypidiomorphic granular. Sodic plagioclase (An_{10-34}) grains commonly are larger than the other constituents and are as much as 5 millimeters in size. Plagioclase shows normal and oscillatory zoning, although the latter is rare. Most plagioclase is altered to sericite. Alkali feldspar occurs as anhedral grains, micrographic intergrowths, and, rarely, as mantles around plagioclase. The alkali feldspar is generally pale brown in transmitted light owing to kaolinitic(?) alternation. Quartz generally makes up 15 to 30 percent of the rocks and occurs as anhedral grains and micrographic intergrowths. Much of the quartz shows undulatory extinction. Pseudomorphs after mafic minerals constitute 5 to 20 percent of the rocks and consist of epidote, chlorite, sphene, and (or) a yellowish-green highly birefringent layered silicate mineral tentatively identified as saponite. Some pseudomorphs originally were biotite and hornblende; remnants of biotite are preserved in some pseudomorphs. Epidote also occurs as aggregates of anhedral grains and as veinlets. Irregular patches of calcite are rare. Accessory minerals are magnetite, zircon, and apatite.

The volcanic rocks are chiefly porphyritic rhyolite, rhyodacite, and dacite consisting of phenocrysts of sodic plagioclase (An_{12-34}), quartz, pseudomorphs after mafic minerals, and, rarely sanidine, set in a groundmass of quartz and alkali feldspar.[1] The groundmass of one pebble is locally spherulitic, and the groundmass of another contains abundant plagioclase microlites. Glomeroporphyritic clots are common and consist of plagioclase with or without quartz and pseudomorphs after biotite. Quartz and plagioclase phenocrysts are commonly resorbed. Magnetite and apatite microphenocrysts are common. Most of these rocks appear to have come from lava flows.

The feldspars show the same kind of alteration as that described for the plutonic rocks. The mafic phenocrysts originally were biotite and hornblende. Unaltered remnants of these minerals occur in some specimens, but most mafic minerals are replaced by epidote, chlorite, and saponite(?). These secondary minerals also occur disseminated in the groundmass and in veinlets.

A pebble of rhyolitic welded tuff was collected from the conglomerate in the upper part of the formation along No Business Creek. The tuff consists of about 10 percent quartz and plagioclase phenocrysts in a finely crystalline groundmass of quartz, alkali feldspar, chlorite, and saponite(?). Vague outlines of squashed shards and pumice are evident, although no glass was observed.

The abundance of epidote distinguishes the igneous pebbles in the Kootenai from those in the younger Cretaceous formations; epidote is absent or is only a minor constituent in the pebbles from the younger formations. Plutonic and volcanic rocks in the Kootenai conglomerates seem to have been affected by the same kind and degree of low-grade metamorphism prior to incorporation in the Lower Cretaceous deposit.

Vaughn Member of the Blackleaf Formation

The nonmarine Vaughn Member of the Blackleaf Formation is late Albian in age (Cobban and others, 1959, p. 2790–2792). In the Sun River area it is the uppermost Lower Cretaceous unit (fig. 2), and correlates with at least the upper part of the Crowsnest Volcanics of the Blairmore Group in the southwest foothills of Alberta, and with the Newcastle Sandstone and possibly the Mowry Shale of the Black Hills, Wyo. (Cobban, and others, 1959, p. 2792). The Vaughn in the Sun River area probably is also correlative with the

[1] Volcanic rocks are named in this paper on the basis of their content of modal quartz and their relative proportion of alkali feldspar and plagioclase, utilizing the classification of Williams, Turner, and Gilbert (1954, p. 35, 36, 93, 121).

nonmarine Vaughn and overlying marine Bootlegger Member of the Blackleaf Formation in the Sweetgrass arch area of Montana.

The Vaughn is a sequence of alternating sandstone and gray to olive-drab tuffaceous mudstone, bentonitic mudstone, and thin bentonite. Sandstone beds are thicker and more numerous in the middle and lower parts of the member than in the upper, and many of these beds locally contain conglomerate lenses. These sandstones are composed mainly of medium- to coarse-grained feldspar, rock fragments, and quartz. The rock fragments are of metasedimentary rocks, lava and tuff, and sedimentary rocks. One bed contains subrounded to angular fragments of tuff as much as ½ inch across (fig. 3). Some beds in the upper part of the Vaughn are altered ash deposits and porcellanite. One bed, a fine-grained stratified tuff, contains abundant accretionary lapilli (fig. 3). The lapilli are oblate spheroids 5 mm long and 3 mm high, like those described by Moore and Peck (1962, p. 184–191).

Locally, beds of conglomerate with interbedded sandstone fill small channels in the lower and middle parts of the Vaughn (figs. 3 and 5). These conglomerates range in thickness from 6 inches to 20 feet, and are composed of well-rounded pebbles and cobbles of quartz, chert, quartzite, and silicified carbonate (fig. 5). The average pebble size is 1 to 2 inches across, even though some cobbles are as much as 6 inches across. The width of the channel fill generally cannot be determined, but where measurable it ranges from 150 feet to about 3,000 feet. All the channels trend easterly. Three exposures of channel-fill deposits north of the Sun River are in separate fault blocks, but plot northeasterly (fig. 3), and three others, farther south, plot southeasterly.

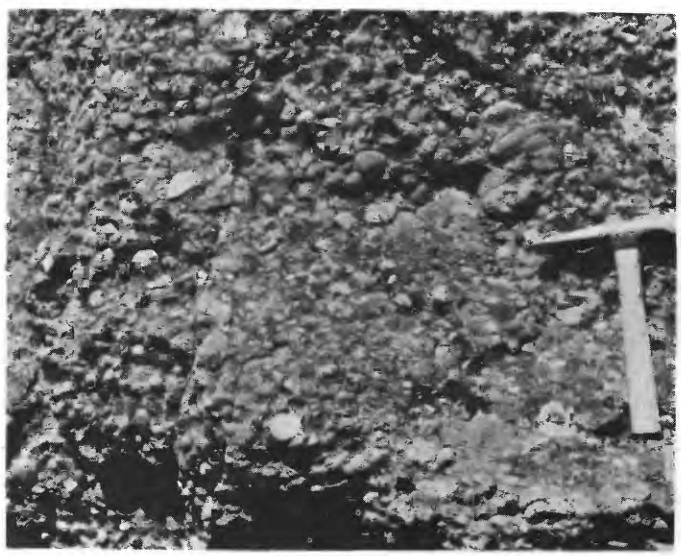

FIGURE 5.—Conglomerate at the base of a sandstone unit in the middle part of the Vaughn Member of the Blackleaf Formation exposed north of the Sun River, about 1½ miles east of Diversion Dam. The largest pebble, above the hammer, is about 5 inches long.

The only conglomerate in the Vaughn observed to contain fragments of igneous rock is south of the upper reaches of Green Timber Gulch (fig. 3). This channel is 20 feet thick and not more than 3,000 feet wide. The pebbles are well rounded, and have an average width of about 2 inches and a maximum of about 6 inches. The larger pebbles and cobbles are mostly igneous rock, but they constitute only a small percentage of the conglomerate. The fact that just this one channel contains igneous rocks indicates that its stream headed in a terrane of volcanic and sedimentary rocks, whereas all the other streams headed in terranes of sedimentary rock.

All the igneous pebbles from the Vaughn appear to be volcanic, chiefly rhyolitic welded tuffs and dacite lavas. Unlike the pebbles in the Kootenai Formation, no granitic varieties have been recognized.

The welded tuff consists of 5 to 10 percent phenocrysts of quartz, sodic plagioclase, and sparse partly altered biotite in a finely crystalline or spherulitic groundmass of quartz and alkali feldspar. Quartz and plagioclase phenocrysts are commonly resorbed. Abundant veinlets of calcite cut the rock. Although no glass remains, the squashed shards are made evident by outlines of irresolvable brownish material.

The dacite lavas consist of about 20 percent phenocrysts of sericitic sodic plagioclase, quartz, and pseudomorphs after hornblende in a groundmass of anhedral quartz and alkali feldspar. The pseudomorphs after hornblende are mainly chlorite and saponite(?) with minor epidote and sphene. Zircon, apatite, and magnetite are accessory minerals. Calcite is common as veinlets and irregular patches.

Two Medicine Formation

The nonmarine Two Medicine Formation, about 2,100 feet thick, is Late Cretaceous in age (Campanian). It is mainly grayish-green and gray mudstone with some relatively thick sandstone units, especially in the lower part (Cobban, 1955, p. 116). Volcanic-rich mudstone and sandstone are common. Two relatively thick beds of tuff, containing phenocrysts of oligoclase, occur in the middle part of this formation along the North Fork of the Sun River (fig. 3). The lower and middle parts of the formation in both the eastern and western outcrop areas (fig. 3) locally contain conglomerates with igneous pebbles.

The conglomerates are composed of well-rounded to subrounded pebbles (as much as 1½ inches across) of sandstone, red quartzite, carbonate, chert, and volcanic rocks. In most places the conglomerate occurs as lenses as much as 2 feet thick in coarse-grained sandstone.

Igneous pebbles in the Two Medicine of the Sun River area are entirely volcanic and consist chiefly of dacite and andesite lavas. The dacite contains phenocrysts of sodic plagioclase, quartz, and pseudomorphs of mafic minerals in a finely crystalline groundmass of anhedral quartz and alkali feldspar. The groundmass of some dacite is spherulitic. Magnetite and apatite are common accessory minerals. The pseudomorphs consist chiefly of chlorite and saponite(?), although minor epidote was also identified. Some pseudomorphs originally were hornblende, but others may have been pyroxene.

Andesite detritus occurs in the conglomerates as well as in coarse-grained sandstone. The andesite consists of phenocrysts of plagioclase (An_{20-35}) and chlorite pseudomorphs of mafic minerals in a groundmass of sodic plagioclase microlites, chlorite, and magnetite. Plagioclase microlites commonly show a conspicuous preferred orientation. The shape of the chlorite pseudomorphs suggests that most originally were pyroxenes. Veinlets and irregular patches of calcite are common in both andesite and dacite.

The composition of the conglomerates described above differs from that of the conglomerate that occurs about 800 feet beneath the top of the Two Medicine in Birch Creek, as described by W. T. Pecora (*in* Cobban, 1955, p. 116). That conglomerate is composed of pebbles of quartzite, hornfels, welded tuff, and quartz diorite to quartz monzonite.

Horsethief Sandstone

The Horsethief Sandstone is exposed in many places east of the Rocky Mountains in northwestern Montana. This formation, about 30 to 40 feet thick, is gray, fine- to coarse-grained, mostly crossbedded marine sandstone that is iron-stained dark brown (Cobban, 1955, p. 118). Locally, lenses of titaniferous magnetite sandstone occur at and near the top of the formation. As noted by Cobban (1955, p. 118), some exposures of the Horsethief contain pebbles of igneous rocks. In addition to the two localities shown on figure 3, volcanic pebbles and cobbles have been observed at Merrill Hill, about 3 miles east of Augusta (J. F. Murphy, oral commun., 1967) and at Gardipee Buttes (Viele and Harris, 1965, p. 405). At Gardipee Buttes (fig. 1), Viele and Harris (1965, p. 405) reported that the conglomerate contains angular to well-rounded boulders, as much as 2½ feet in diameter, of vitrophyre and ash-flow tuff that range in composition from andesite to quartz latite. They further note that this deposit thins to the northwest.

In the Sun River area the conglomerates occur as thin lenses of pebbles and locally as cobbles of volcanic rock and chert at various horizons in the middle and upper parts of the Horsethief. The coarser fragments are more numerous in the southern exposure at Willow Creek (fig. 3). The volcanic pebbles are porphyritic trachyandesite and andesite.

The trachyandesite contains about 20 percent phenocrysts of sodic plagioclase and mafic minerals in a finely crystalline groundmass of anhedral alkali feldspar and minor quartz. Apatite and magnetite are common accessory minerals. The mafic minerals are unaltered brown biotite and pseudomorphs of chlorite and saponite(?) after hornblende. Abundant calcite occurs as irregular patches in the groundmass and as replacements of plagioclase phenocrysts.

Andesite contains 10 to 20 percent phenocrysts of sodic plagioclase and mafic minerals in a felty groundmass of plagioclase microlites and chlorite. Much of the plagioclase is altered to sericite and calcite; some plagioclase phenocrysts are nearly replaced by calcite. The mafic minerals are rare unaltered brown biotite and common pseudomorphs of chlorite and saponite(?) after pyroxene. Magnetite and apatite are common accessory minerals.

SOURCE AND AGES OF THE PEBBLES AND COBBLES

During Cretaceous time, great amounts of detritus were shed eastward from highlands in westernmost Montana and adjacent Idaho (Reeside, 1957, p. 510–511). Most of the nonigneous constituents in the conglomerates described in the foregoing pages can be readily identified from older sedimentary formations that were presumably uplifted and eroded from these highlands. Evidence regarding the sources of the igneous rocks, on the other hand, is not as clear cut. The relationships suggest that four episodes of volcanism might possibly have taken place near the Sun River area during the deposition of the Cretaceous sediments, but the exact locations of the centers of activity are problematic. Data pertaining to possible sources of the igneous rocks are discussed in the following paragraphs.

Igneous pebbles in the Lower Cretaceous

The pebbles in the Kootenai and Vaughn conglomerates appear to have been derived from a similar source area, although certain stratigraphic data indicate that there were at least two periods of volcanism. An age of very Late Jurassic would be appropriate for the igneous pebbles in the Kootenai, thus suggesting that the uplift of the source area occurred during very early Kootenai time. Igneous pebbles in the Vaughn conglomerate, however, may be as young as late Albian, as shown by the presence of widespread bentonites and bentonitic and tuffaceous shales and by local beds of tuff and accretionary lapilli.

The size of the igneous cobbles in the conglomerates of the Sun River area suggests a moderately short distance of transport. A plot of the size of the largest cobble (6½ inches) on the graphs compiled by Pettijohn (1957, pp. 529–530) indicates a distance of travel of not more than 20 miles. A similar distance is inferred from the average size of pebbles (½ to 1½ inches). In the Sun River area, outwash gravels, whose roundness, size, and composition (including diorite and trachyandesite) are similar to the Cretaceous conglomerates, were transported not more than 30 miles. Pre-Wisconsin gravels of comparable size in the nearby plains areas may have been transported a maximum distance of 50 miles. Furthermore, the nonigneous rock fragments in the Cretaceous conglomerates came from nearby areas to the west. Also, of the many conglomerates in the Vaughn only one contains igneous pebbles, and these pebbles can be reconciled more easily with a local source than with a distant one.

The presence of accretionary lapilli and angular fragments of tuff in the Vaughn indicates that there was nearby volcanism during its deposition. The accretionary lapilli appear to be the best indicators of distance from the volcanic source. Moore and Peck (1962, p. 184–191), in their review of accretionary lapilli, stated: "The eruptive vent from which the volcanic ash of the lapilli was derived was very likely within 100 miles or so of the deposit, and probably was within about 10 miles." They further indicated that most occurrences of accretionary lapilli that have a known source are within a few miles of the vent. The angular fragments of tuff (up to ½ inch) in a sandstone bed of the Vaughn also suggest a relatively short distance of transport.

The above data suggest (1) a relatively close westerly source for the igneous pebbles and cobbles in the Kootenai and Vaughn, and (2) an association of the pebbles in the Vaughn with a contemporaneous volcanic episode. If the conclusions are valid, then the Idaho and Nelson batholithic areas and Libby area are too distant to have been the sources. The Idaho batholith is about 110 miles southwest of the Sun River area, the Libby area is about 150 miles west, and the Nelson batholith is about 200 to 250 miles northwest.

The source areas of the Kootenai and Vaughn igneous pebbles probably are buried by one or more of the thrust plates in the Lewis and Clark Range. Aeromagnetic and gravity data compiled by Mudge, Erickson, and Kleinkopf (1968) show two large anomalies just northwest and southwest of the Sun River area. These anomalies indicate plutons with a susceptibility contrast of quartz monzonite, now covered by thrust plates containing Precambrian and Paleozoic rocks. One possible buried pluton lies to the northwest beneath the continental divide and trends northwest from Slategoat Mountain (fig. 1). The computed depth is 9,500 ± 1,100 feet below the surface (Mudge and others, 1968). The other mass, southwest of the Sun River area, underlies the Concord and Scapegoat Mountains area (fig. 1). The depth of burial beneath the ground surface computed for this mass is 10,500 ± 1,200 feet (Mudge and others, 1968).

The age of these buried masses is unknown. The closest exposed quartz monzonite intrusives are the Boulder batholith and related stocks, southeast of the Sun River area, and the Schafer Meadows intrusions, northwest of the area (fig. 1). The Boulder batholith has been dated as Late Cretaceous by Klepper, Weeks and Ruppel (1957), Knopf (1964), and G. D. Robinson, M. R. Klepper, and J. D. Obradovich (written commun., 1968). The Boulder batholith was emplaced during much of the Campanian and part of the Maestrichtian (82–71 million years ago) according to Robinson, Klepper, and Obradovich (written commun., 1968). A Late Cretaceous or early Eocene age has been assigned to the Schafer Meadows intrusions by Largton (1931).

Other outcropping intrusives that may be Late Jurassic or very early Cretaceous in age are the stocks in the Libby area and the Idaho batholithic area, which lie southwest and west of the Sun River area. Ross (1936, p. 369–385) considered the age of the Idaho batholith to be either Jurassic or Cretaceous. Subsequent radiometric age determinations, ranging from 51 to 100 m.y., were made by Chapman, Gottfried, and Waring (1955, p. 609), who believe that the bulk of the batholith is probably mid-Cretaceous, although it may contain plutonic rocks of different ages. The age of the quartz monzonite, granite, and diorite stocks in the Libby area, Montana, has been postulated by Gibson (1948, p. 38) to be the same as that of the Idaho and Nelson batholiths.

The igneous pebbles in the Kootenai and Vaughn are lithologically similar to those in the McDougall-Segur Conglomerate in the Southern Rocky Mountains of Canada, which were dated (K–Ar method) by Norris, Stevens, and Wanless (1965, p. 5–6) as ranging from 113 to 174 m.y. Several of the pebbles are closely grouped between 142 and 158 m.y., which would be Middle and Late Jurassic, according to the Holmes (1959, p. 204) and Kulp (1961, p. 1111) time scales. The McDougall-Segur pebbles were very likely derived from the Nelson batholith area of the Purcell and Selkirk Mountains as proposed by Warren (1938, p. 66), Anderson (1951, p. 41), and Norris, Stevens, and Wanless (1965, p. 9). The Nelson batholith was dated by Baadsgaard, Folinsbee, and Lipson (1961, p. 693) as 96 m.y., but subsequent data by Rudkin (1964, p. 158) show earlier igneous phases dated as 100, 127, and 131 m.y. in the northeastern part of the Nelson and Cassiar-

Omineca batholiths. The Nelson, therefore, had Late Jurassic and mid-Cretaceous intrusive phases.

Igneous rocks in the Upper Cretaceous

The composition and areal distribution of the igneous-bearing conglomerates in the Two Medicine Formation indicate multiple sources for the igneous rock. In the eastern part of the Sun River area the igneous rock fragments in the Two Medicine and Horsethief were possibly derived from a southerly, principally volcanic source. The plutonic, volcanic, and contact-metamorphic pebbles in the conglomerate in the Two Medicine on Birch Creek reported by Cobban (1955, p. 116) were very likely derived from the west, possibly the Schafer Meadows area. Igneous-pebble conglomerates and tuff in this formation in the western part of the Sun River area, along the North Fork, may have a source either in the Schafer Meadows area (fig. 1) or from a buried pluton in the Slategoat Mountain–Continental Divide area just northwest of the Sun River area.

The most southerly source for the igneous rocks in the Upper Cretaceous conglomerates in the eastern part of the Sun River area is very likely in the area that extends from Wolf Creek northwest to the Dearborn River. Much of the lower part of the Two Medicine Formation in this area contains volcanic rocks and volcanic-rich sediments (Viele, 1960; Viele and Harris, 1965; Schmidt, 1963; and Schmidt and others, 1964), and some of these rocks extend northward to the Sun River. In the Dearborn River area, Viele and Harris (1965, p. 413) correlate these sediments with the Elkhorn Mountains Volcanics of the Boulder batholith area, which are dated as 79 to 77 m.y. by G. D. Robinson, M. R. Klepper, and J. D. Obradovich (written commun., 1968). In the Wolf Creek area these rocks occur mostly as flows, clastic volcanic rocks, tuffs, and volcanic conglomerates, according to Schmidt (1963), who also lists quartz latite sills and dikes and calcic rhyodacite sills that are the same composition as some of the volcanics. It is possible that other instrusives in this area are buried by the volcanics or by the thrust fault plates to the west.

The Schafer Meadows area may have been the source of the igneous rocks and hornfels in the Two Medicine conglomerates in Birch Creek, and of the beds of tuff and igneous-pebble conglomerate in the Two Medicine exposed on the North Fork of the Sun River. Numerous intrusives crop out in the Schafer Meadows area, but volcanics have not been recorded. This area is about 10 miles west of the present headwaters of Birch Creek and about 40 miles west of the exposed conglomerate containing igneous pebbles (fig. 1). Schafer Meadows is about 5 miles northwest of the head of the North Fork of the Sun River and about 25 miles northwest of the conglomerate and tuff beds exposed in the Two Medicine along that river.

The Schafer Meadows instusives are described by Langton (1931, p. 22) as monzonite chonoliths, probably of Late Cretaceous or early Eocene age. He (1931, p, 25) believed that they intruded the Precambrian Belt strata during the time of Laramide deformation, but prior to the translation of the large thrust fault in the area. The sequence of events is analogous to the Boulder batholith area, where Robinson, Klepper, and Obradovich (written commun., 1968) and Klepper, Weeks, and Ruppel (1957) concluded that (1) folding near the site of the batholith began in post-middle Campanian to pre-middle Eocene time, (2) volcanism began in late Coniacian or early Santonian time and culminated in late Campanian time (73 m.y.), (3) the bulk of the batholith was emplaced during the Campanian (82–71 m.y.), and (4) major thrusting began no earlier than middle Campanian and ended before late Eocene.

The igneous pebbles and tuff in the Two Medicine on the North Fork of the Sun River, however, may have had a more westerly source than the Schafer Meadows area. These conglomerates and beds of tuff are near but east of a possible source area for similar pebbles in the Lower Cretaceous rocks.

The igneous pebble conglomerates in the Horsethief could be as young as late Campanian, possibly from the Two Medicine episode of volcanism. Although thin pebble conglomerate occurs in the upper part of the Horsethief, Viele and Harris (1965, p. 411) believe, "It implies continuation of volcanism past the time of transgression of sea water, and the similarity of volcanic cobbles in the upper Horsethief to the pipe breccia of the High Bridge stock supports this hypothesis." The High Bridge stock (fig. 1) is a trachyandesitic pipe located along the Dearborn River (Viele and Harris, 1965, p. 405). The increase in size of the volcanic rock fragments in the Horsethief toward the south and southwest suggests a source from these directions, possibly the High Bridge stock.

REFERENCES

Anderson, F. D., 1951, The McDougall-Segur Conglomerate (Lower Cretaceous): McGill Univ. Master's thesis.

Baadsgaard, Halfdan, Folinsbee, R. E., and Lipson, J. I., 1961, Potassium-argon dates of biotites from Cordilleran granites: Geol. Soc. America Bull., v. 72, no. 5, p. 689–701.

Chapman, R. W., Gottfried, David, and Waring, C. L., 1955, Age determinations on some rocks from the Boulder batholith and other batholiths of western Montana: Geol. Soc. America Bull., v. 66, no. 5, p. 607–609.

Cobban, W. A., 1955, Cretaceous rocks of northwestern Montana, *in* Billings Geol. Soc. Guidebook 6th Ann. Field Conf., 1955: p. 107–119.

Cobban, W. A., Erdmann, C. E., Lemke, R. W., and Maughn, E. K., 1959, Revision of Colorado group on Sweetgrass arch, Montana: Am. Assoc. Petroleum Geologists Bull., v. 43, no. 12, p. 2786–2796.

Gibson, Russell, 1948, Geology and ore deposits of the Libby quadrangle, Montana, *with sections on* Pleistocene glaciation, by W. C. Alden, *and* Physiography, by J. T. Pardee: U.S. Geol. Survey Bull. 956, 131 p.

Holmes, Arthur, 1959, A revised geological time-scale: Edinburgh Geol. Soc. Trans., v. 17, pt. 3, p. 183–216.

Klepper, M. R., Weeks, R. A., and Ruppel, E. T., 1957, Geology of the southern Elkhorn Mountains, Jefferson and Broadwater Counties, Montana: U.S. Geol. Survey Prof. Paper 292, 82 p. [1958].

Knopf, Adolph, 1964, Time required to emplace the Boulder bathylith, Montana—A first approximation: Am. Jour. Sci., v. 262, no. 10, p. 1207–1211.

Krumbein, W. C., 1941, Measurement and geological significance of shape and roundness of sedimentary particles: Jour Sed. Petrology, v. 11, no. 2, p. 64–72.

Kulp, J. L., 1961, Geologic time scale: Science, v. 133, no. 3459, p. 1105–1114.

Langton, C. M., 1931, Geology along the Lewis thrust in the Schafer Meadows district, Montana: Cornell Univ. unpub. Master's thesis, 41 p.

Lyons, J. B., 1944, Igneous rocks of the northern Big Belt Range, Montana: Geol. Soc. America Bull., v. 55, no. 4, p. 445–472.

Merrill, R. D., 1965, Geology of the southern terminus of the Sawtooth Range, northwestern Montana: Massachusetts Univ. Master's thesis, 72 p.

Moore, J. G., and Peck, D. L., 1962, Accretionary lapilli in volcanic rocks of the western continental United States: Jour. Geology, v. 70, no. 2, p. 182–193.

Mudge, M. R., Erickson, R. L., and Kleinkopf, M. D., 1968, Reconnaissance geologic, geochemical, and geophysical studies of the southeastern part of the Lewis and Clark Range, Montana: U.S. Geol. Survey Bull. 1252–E [In press].

Norris, D. K., Stevens, R. D., and Wanless, R. K., 1965, K–Ar age of igneous pebbles in the McDougall-Segur conglomerate, southeastern Canadian Cordillera: Canada Geol. Survey Paper 65–26, 11 p.

Pettijohn, F. J., 1957, Sedimentary rocks, 2d ed.: New York, Harper and Brothers, 718 p.

Reeside, J. B., Jr., 1957, Paleoecology of the Cretaceous seas of the western interior of the United States, chap. 18 *of* Ladd, H. S., ed., Paleoecology: Geol. Soc. America Mem. 67, p. 505–541.

Rose, B., 1917, Crowsnest coal field, Alberta: Canada Geol. Survey Summ. Rept., 1916, p. 107–114.

Ross, C. P., 1936, Some features of the Idaho batholith [with discussion]: Internat. Geol. Cong., 16th, Washington, D.C., 1933, Rept., v. 1, p. 369–385.

Rudkin, R. A., 1964, Lower Cretaceous, chap. 11 *of* Geological history of Western Canada: Alberta Soc. Petroleum Geologists, p. 156–168.

Schmidt, R. G., 1963, Preliminary geologic map and sections of the Hogan 4 Southeast quadrangle, Lewis and Clark County, Montana: U.S. Geol. Survey Misc. Geol. Inv. Map I–379.

Schmidt, R. G., Swanson, D. A., and Zubovic, Peter, 1964, Preliminary geologic map and sections of the Hogan 4 Northeast quadrangle, Lewis and Clark and Cascade Counties, Montana: U.S. Geol. Survey Misc. Geol. Inv. Map I–409.

Viele, G. W., 1960, The geology of the Flat Creek area, Lewis and Clark County, Montana: Utah Univ. Ph. D. thesis, 212 p.

Viele, G. W., and Harris, F. G., III, 1965, Montana Group stratigraphy, Lewis and Clark County, Montana: Am. Assoc. Petroleum Geologists Bull., v. 49, no. 4, p. 379–417.

Warren, P. S., 1938, Age of the Selkirk and Rocky Mountain uplifts in Canada: Am. Jour. Sci., 5th ser., v. 36, no. 211, p. 66–71.

Williams, Howel, Turner, F. J., and Gilbert, C. M., 1954, Petrography—An introduction to the study of rocks in thin sections: San Francisco, W. H. Freeman and Co., 406 p.

THE KALTAG FAULT, WEST-CENTRAL ALASKA

By WILLIAM W. PATTON, JR., and JOSEPH M. HOARE,
Menlo Park, Calif.

Abstract.—The Kaltag fault has been traced for 275 miles across west-central Alaska from Norton Sound to Tanana. Reconnaissance geologic mapping along the fault indicates that between 40 and 80 miles of right-lateral offset may have occurred since Cretaceous time. Study of aerial photographs along the fault reveals evidence of recent activity over nearly its entire length, and of local drainage offset of as much as 1.5 miles. The remarkably straight trend of the fault, its parallelism with known and suspected strike-slip faults of southwestern Alaska, and the evidence of major lateral dislocation suggest that the Kaltag is a major strike-slip fault.

Reconnaissance geological and geophysical investigations in west-central Alaska during the past decade have provided evidence of a major fault extending from Norton Sound at least as far east as Tanana on the Yukon River, a distance of 275 miles. It has been suggested (Gates and Gryc, 1963; Patton, 1964; Grantz, 1966) that this fault, which has been given the name Kaltag, may be a major strike-slip fault because of its remarkably straight trend and because it is nearly parallel to the Denali, Iditarod-Nixon Fork, and Castle Mountain faults (St. Amand, 1957; Grantz, 1966) (fig. 1). The apparent large-scale lateral separation of the eastern boundary of the Yukon-Koyukuk Cretaceous basin has been cited as possible evidence of major strike-slip movement.

The purpose of this report is to describe briefly the physiographic features along the Kaltag fault and to summarize the evidence for lateral displacement.

PHYSIOGRAPHIC FEATURES

Norton Sound to Kaltag.—From the eastern shore of Norton Sound, at the village of Unalakleet, the Kaltag fault trends northeastward for a distance of 60 miles along a broad alluvial-floored trench occupied by the Unalakleet River. Evidence of recent movement on the fault can be seen in the alluvium and bedrock along the north side of the trench from a point about 15 miles east of the village to the upper end of the trench. Surface traces of the fault are clearly marked in aerial photographs by diverted streams, offset spurs, fault-bounded bedrock slivers, and sharply delineated changes in fine drainage and vegetation patterns. Most of the streams that flow southeasterly across the fault into the trench are bent or offset to the right; the total offset of some drainage lines appears to be as much as 0.5 mile.

About 15 miles southwest of the village of Kaltag the fault leaves the broad open trench and for the next 10 miles passes through narrow fault-line valleys. Two southeast-flowing tributaries of the Kaltag River which cross this segment of the fault appear to have been

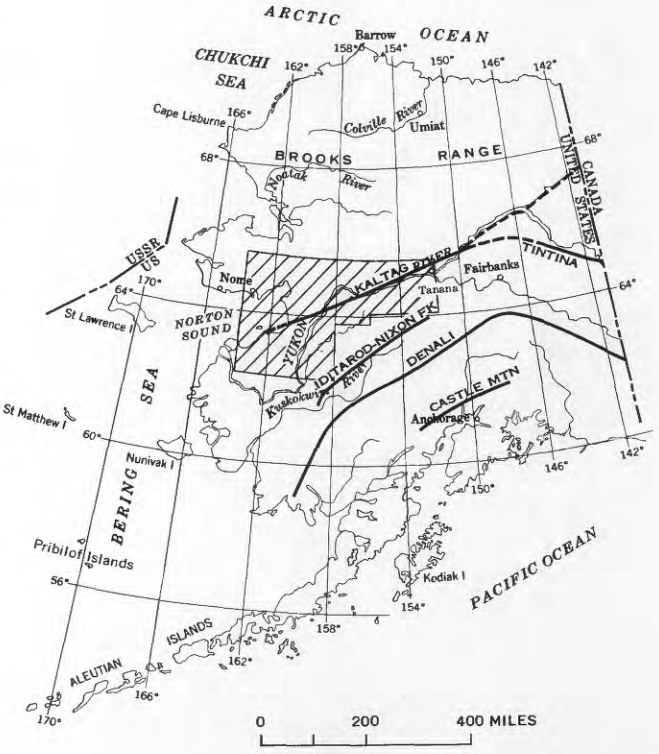

FIGURE 1.—Index map of Alaska, showing location of Kaltag and other suspected strike-slip faults and area (shaded) discussed in this report.

completely beheaded by right-lateral offset (figs. 2 and 3). Matching former drainage lines of the beheaded tributaries suggest a total offset of 0.6 mile for one and possibly as much as 1.5 miles for the other.

The fault emerges from a fault-line valley 5 miles west of the village of Kaltag and from this point to the Yukon River traverses the alluviated lowlands of the Kaltag River. The course of the fault, only faintly discernible as surface traces in the alluvial deposits, gradually curves 10° to the east and intersects the Yukon River about 1 mile north of the village.

Kaltag to Louden.—From the Yukon River the fault appears to strike east-northeast across the Koyukuk Flats. This part of its course must be largely inferred, as only a few faint surface traces can be detected in the Pleistocene and Recent alluvial silt deposits that mantle the flats. East of the Khotol River the fault crosses a markedly depressed area of countless coalescing thaw lakes and ponded drainages, possibly the result of recent settlement along the fault zone.

About 40 miles northeast of Kaltag the fault swings to a slightly more northerly course and for the next 25 miles follows along the base of the Kaiyuh Mountains. Here the surface trace is clearly marked by a thin line of heavy vegetation, scarplets of alluvium and colluvium, and up-faulted slivers of bedrock (fig. 4). Although numerous breaks in the surficial deposits attest to the recency of movement along this segment, no consistent pattern of stream offset is evident in aerial photographs.

Louden to Tanana.—The fault leaves the Kaiyuh Mountains and enters the Yukon valley at a sharp bend in the Yukon River near the abandoned village of Louden. For the next 130 miles its course lies along—and undoubtedly has guided—the straight reach of the Yukon River between Louden and Tanana. Surface traces of the fault can be seen along the steep north bank of the river on the delta of the Melozitna River and along a narrow terrace that extends 20 miles upriver from Kokrines.

The Kaltag fault probably extends east of Tanana, but its precise course cannot be determined owing to the absence of basic geologic data in this part of Alaska. Two possible courses (fig. 1) are suggested by gross physiographic trends: (1) the fault continues northeastward from Tanana along the alined courses of the Yukon and Porcupine Rivers, or (2) the fault continues northeastward from Tanana up the Yukon River valley as far as the Yukon Flats, where it swings an arcuate course across the southern edge of the flats and joins the southeast-trending Tintina fault along the upper Yukon River valley. The latter possibility is par-

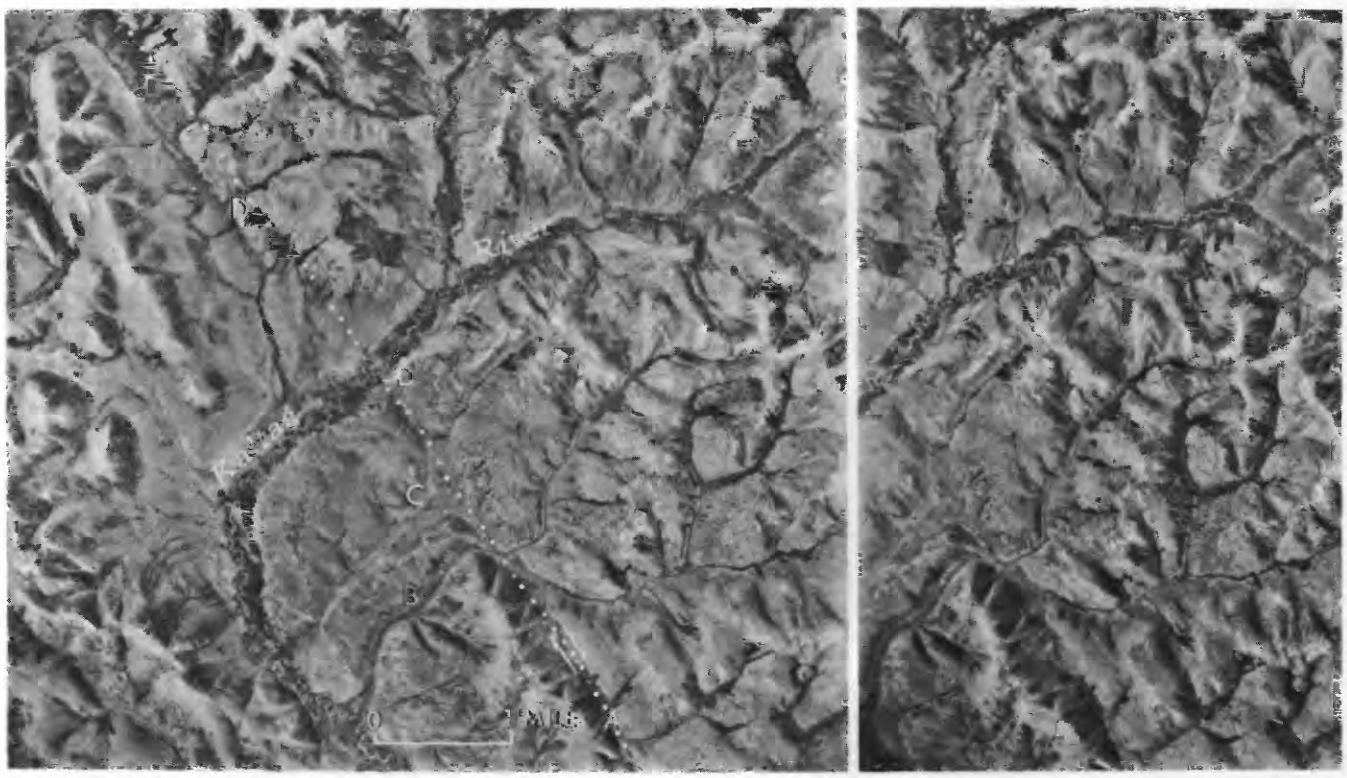

FIGURE 2.—Stereoscopic pair of aerial photographs showing beheaded drainage along Kaltag fault, 9 miles southwest of the village of Kaltag. *A*, trace of fault. *B*, present stream course. *C*, probable former stream course now occupied by underfit stream. *D*, sharp changes in vegetation and fine drainage patterns marking surface trace of fault. North is to the right.

ticularly attractive not only because the course thus defined parallels the arcuate trends of the Denali fault and Alaska Range but also because it ties the Kaltag to the Tintina fault where evidence has been found recently for as much as 260 miles of right-lateral offset (Roddick, 1967).

GEOLOGIC SETTING

Between Tanana and Norton Sound the Kaltag fault transects two major geologic provinces (figs. 5 and 6): (1) on the east, a structurally positive complex of Paleozoic and early Mesozoic metamorphic, volcanic, and plutonic rocks, and (2) on the west, the Yukon-Koyukuk basin, a structural depression composed largely of unmetamorphosed but highly deformed Cretaceous rocks. A metamorphic complex, chiefly of Paleozoic age, bounds the Yukon-Koyukuk basin on the west on the Seward Peninsula and presumably extends southward beneath Norton Sound and the Yukon delta.

No lithologic or structural trends can be traced across the Kaltag fault, and several conspicuous regional discontinuities are evident at the fault even on small-scale maps (fig. 5). Between Ruby and Kaltag, sedimentary rocks of mid-Cretaceous age (Albian and Cenomanian) trending into the fault at an acute angle on the north side are opposed on the south side by Paleozoic and early Mesozoic(?) metasedimentary rocks of the Kaiyuh Mountains. Farther west, between Kaltag and Norton Sound, a north-trending belt of Mesozoic volcanic and plutonic rocks south of the fault is truncated by the fault and opposed on the north side by mid-Cretaceous sedimentary rocks.

EVIDENCE FOR RIGHT-LATERAL STRIKE-SLIP DISPLACEMENT

Large-scale strike-slip displacement along the Kaltag fault is suggested by: (1) lateral separation of the eastern margin of the Yukon-Koyukuk basin; (2) suspected lateral separation of the western margin; (3) offset of gross geologic trends within the basin; and (4) possible regional drag north of the fault in the western part of the basin.

All this evidence should be considered speculative owing to the reconnaissance nature of the mapping. Conclusive proof that these apparent structural anomalies along the fault do, in fact, result from large-scale right-slip movement must await detailed mapping and stratigraphic studies.

At the eastern margin of the basin the geologic map (figs. 5 and 6) clearly shows a lateral separation of approximately 80 miles. At the western margin the

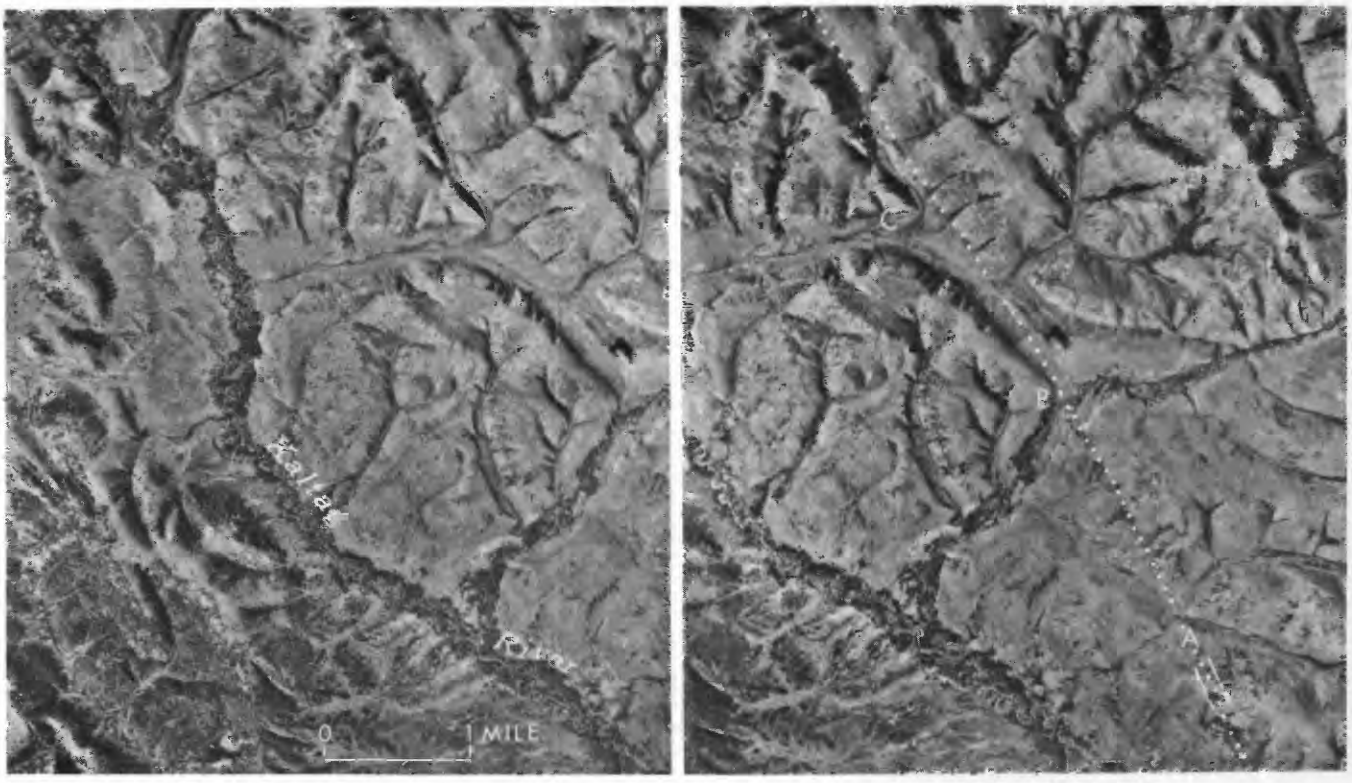

FIGURE 3.—Stereoscopic pair of aerial photographs showing beheaded drainage along Kaltag fault, 6 miles southwest of the village of Kaltag. *A*, trace of fault. *B*, present stream course across fault, showing evidence of recent downcutting. *C*, former stream course now occupied by conspicuously underfit stream. *D*, offset spur along fault trace. North is to the right.

FIGURE 4.—Stereoscopic pair of aerial photographs showing surface trace of Kaltag fault in alluvial deposits along northwest side of Kaiyuh Mountains. *A*, fault trace marked by line of heavy vegetation, scarplets, and slice ridges of bedrock. Kaiyuh Mountains on southeast side of fault composed of Paleozoic metasedimentary rocks. Thermokarst alluvial deposits of Koyukuk Flats on northwest side of fault composed chiefly of Pleistocene silts. *B*, ridges of Cretaceous sedimentary rocks trending into fault at acute angle. North is to the bottom of the photographs.

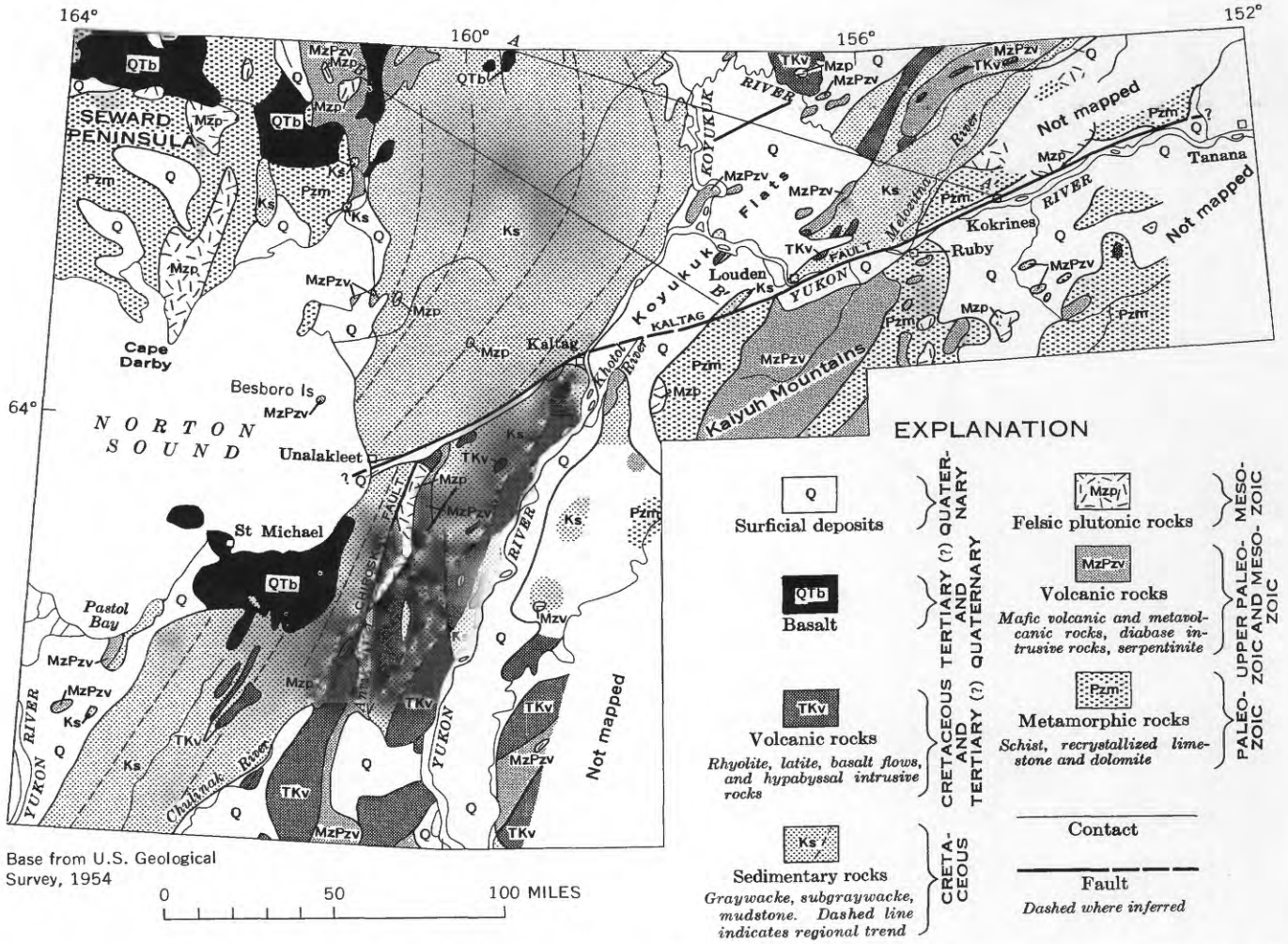

FIGURE 5.—Generalized geologic map along Kaltag fault, west-central Alaska. *A–A′* and *B–B′*, flight lines of aeromagnetic profiles (fig. 7).

evidence for lateral separation is highly speculative, but, if the land-mapped margins north and south of the fault are extended across Norton Sound to the westward projection of the fault, about 40 miles of offset is suggested (fig. 6).

Admittedly these offset margins could be the result of a vertical component of movement on the fault. However, both east and west margins of the basin appear to constitute gross facies and structural trend lines whose lateral offset for scores of miles can be reasonably explained only by a large component of horizontal movement. Both margins are believed to coincide roughly with the margins of the original depositional basin and, over much of their extent, are characterized by massive conglomerates that grade abruptly basinward into finer clastics. The margins seem to lie along major tectonic hinge lines which served to delimit the depositional basin and along which these marginal conglomerates accumulated in great thicknesses.

Offset of gross trends within the Yukon-Koyukuk basin.—As indicated in figure 6, the Yukon-Koyukuk basin is divided into two separate and distinct belts. The western belt consists of a thick sedimentary prism which is generally free of pre-late Cenozoic volcanic and plutonic rocks. The eastern belt consists of a much thinner sedimentary section which is intercalated with and overlain by widespread Late Cretaceous and early Tertiary volcanics and infolded with Jurassic and Early Cretaceous volcanic and plutonic rocks. The fundamental difference in the two belts is clearly shown in a series of aeromagnetic profiles that traverse the northern part of the basin (fig. 7) (Dempsey and others, 1957a, b; Zietz and others, 1959). Over the western belt the profiles are generally smooth and free of large-amplitude anomalies reflecting the nonmagnetic character of the thick sedimentary prism. Over the eastern belt they are typified by steep-gradient and high-amplitude anomalies reflecting a mixed terrane of volcanic, plutonic, and sedimentary rocks.

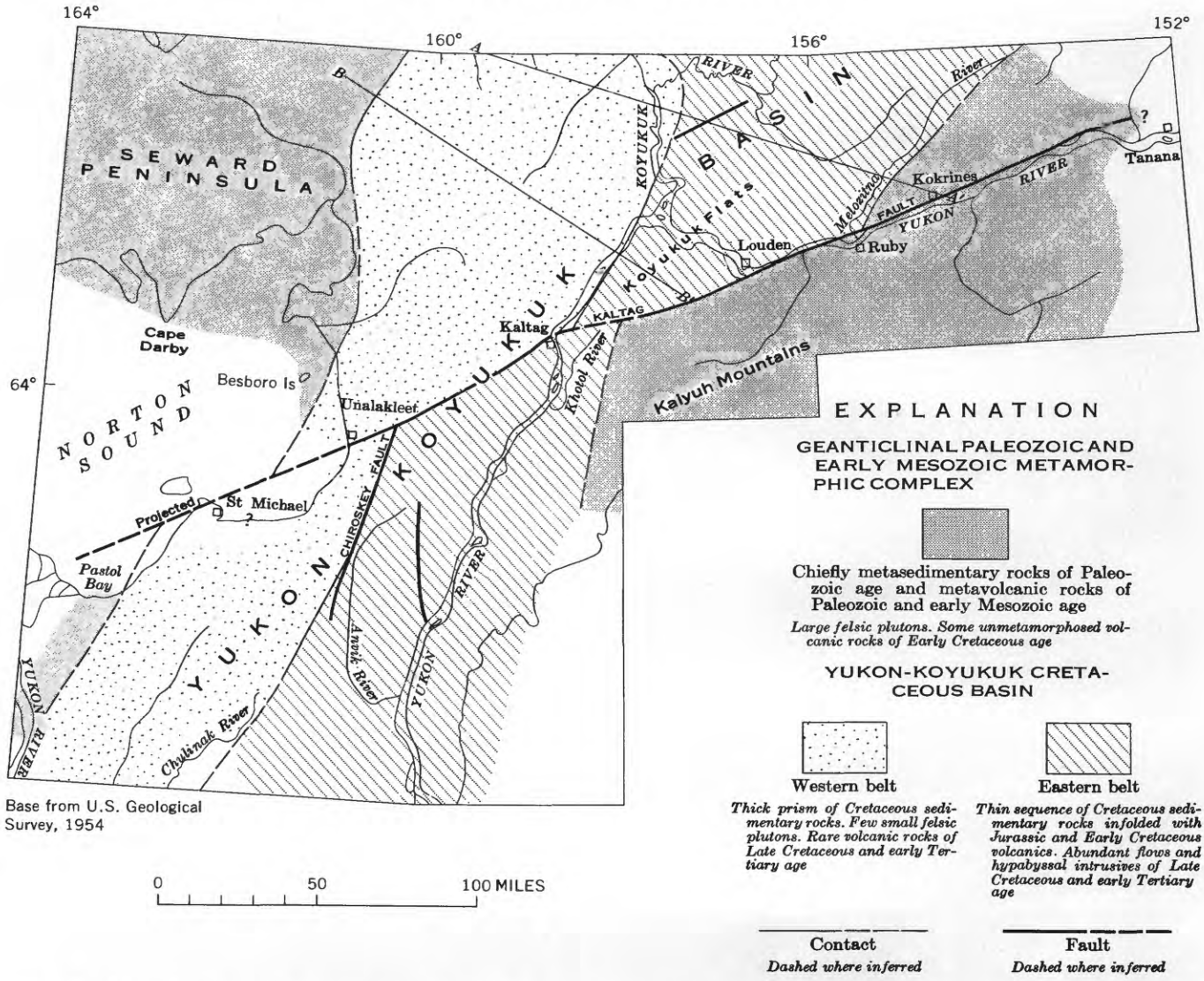

FIGURE 6.—Map of west-central Alaska, showing major geologic elements and their apparent lateral offset along the Kaltag fault.

Reconnaissance mapping and aeromagnetic data suggest that these two belts are offset right laterally between 60 and 80 miles along the Kaltag fault (fig. 6). South of the fault the boundary between the two belts is marked by the northeast-trending Chiroskey fault and by a structural high of Lower Cretaceous volcanic and plutonic rocks which extends from the Kaltag fault southwestward at least as far as the Chulinak River. North of the Kaltag fault the boundary between the two belts is believed to lie along the Yukon and Koyukuk Rivers at the western edge of the Koyukuk Flats. Although largely obscured by surficial deposits, its presence here is suggested by an abrupt change in character of the aeromagnetic profiles (fig. 7) and by the occurrence of scattered exposures of volcanic rocks near the mouth of the Koyukuk River.

Possible regional drag.—Structural trends in the western part of the Yukon-Koyukuk basin north of the Kaltag fault make a conspicuous bend to the southwest and intersect the fault at a small angle. This southwestward swing is accompanied by a marked increase in the intensity of deformation of the basin sediments and may represent large-scale fault drag.

AGE OF FAULTING

Presently available data do not permit close dating of the major transverse movement in the Kaltag fault. Clearly it postdates deposition of the mid-Cretaceous sediments of the Yukon-Koyukuk basin, and probably it postdates extrusion of the Late Cretaceous and early Tertiary(?) volcanic rocks in the eastern part of the basin.

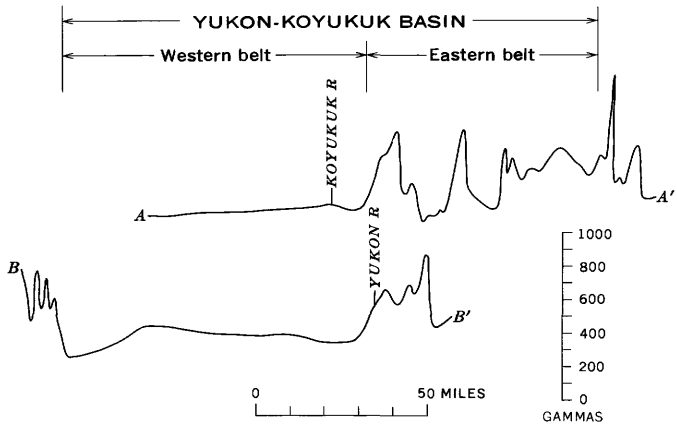

FIGURE 7.—Characteristic aeromagnetic profiles across Yukon-Koyukuk basin along flight lines A–A' and B–B' (figs. 5 and 6). Arbitrary datum; flight lines are approximately parallel to contours of earth's magnetic field (U.S. Coast and Geod. Survey, 1965). Aeromagnetic profiles from Dempsey, Meuschke, and Andreasen (1957a, b).

At least two small patches of middle to late Tertiary coal-bearing deposits (too small to be shown in fig. 5) are preserved in or near the fault zone but, because of their limited extent, furnish little definitive information on the age limits of the principal movement. One of the deposits, located near Unalakleet, is so badly slumped that virtually nothing can be determined of its structure. The other deposit, located on the Yukon River between Kokrines and Tanana, is reported by Eardley (1938) to be steeply dipping and overlain unconformably by Pleistocene alluvial deposits, possibly indicating activity on the fault in latest Tertiary.

Pliocene and Pleistocene basalt flows near St. Michael appear to straddle the westward extension of the fault (fig. 5) but show no significant lateral dislocation.

In summary, the major lateral displacement of Mesozoic tectonic elements appears to have occurred in early and middle Tertiary time. Physiographic evidence, however, provides evidence that some movement has continued to the present.

CONCLUSIONS

We regard the Kaltag as a probable strike-slip fault for the following reasons:

1. Its remarkably straight course over a distance of at least 275 miles.
2. Its parallelism with the major strike-slip or suspected strike-slip faults of southwestern Alaska.
3. Geologic evidence of 40 to 80 miles of right-lateral separation of major Mesozoic geologic elements in west-central Alaska.
4. Possible regional drag in the Yukon-Koyukuk basin north of the fault.
5. Presence along recent surface traces of the fault of offset drainage, rift structures, ridges and depressions, and other features commonly recognized along such well-known strike-slip faults as the San Andreas in California.

REFERENCES

Dempsey, W. J., Meuschke, J. L., and Andreasen, G. E., 1957a, Total intensity aeromagnetic profiles of Koyukuk, Alaska: U.S. Geol. Survey open-file rept., June 10, 1957, 2 sheets.

——— 1957b, Total intensity aeromagnetic profiles of West Hogatza, Alaska: U.S. Geol. Survey open-file rept., June 10, 1957, 1 sheet.

Eardley, A. J., 1938, Unconsolidated sediments and topographic features of the lower Yukon valley: Geol. Soc. America Bull., v. 49, no. 2, p. 303–341.

Gates, G. O., and Gryc, George, 1963, Structure and tectonic history of Alaska, *in* The backbone of the Americas—Tectonic history from pole to pole, a symposium: Am. Assoc. Petroleum Geologists Mem. 2, p. 264–277.

Grantz, Arthur, 1966, Strike-slip faults in Alaska: U.S. Geol. Survey open-file rept., Sept. 2, 1966, 82 p.

Patton, W. W., Jr., 1964, Mineral fuel resources—Northern and interior Alaska, *in* Mineral and water resources of Alaska: U.S. 88th Cong., 2d sess., Comm. Print, 31–068, p. 62–75.

Roddick, J. A., 1967, Tintina trench: Jour. Geology, v. 75, no. 1, p. 23–32.

St. Amand, Pierre, 1957, Geological and geophysical synthesis of the tectonics of portions of British Columbia, the Yukon Territory, and Alaska: Geol. Soc. America Bull., v. 68, no. 10, p. 1343–1370.

U.S. Coast and Geodetic Survey, 1965, Total intensity chart of the United States, 1965.0—Lines of equal magnetic total intensity and equal annual change (United States 3077f): U.S. Dept. Commerce, scale 1 : 5,000,000.

Zietz, Isidore, Patton, W. W., Jr., and Dempsey, W. J., 1959, Preliminary interpretation of total-intensity aeromagnetic profiles of the Koyukuk area, Alaska: U.S. Geol. Survey open-file rept., Nov. 12, 1959, 7 p.

BASE OF THE JOHN DAY FORMATION IN AND NEAR THE HORSE HEAVEN MINING DISTRICT, NORTH-CENTRAL OREGON

By DONALD A. SWANSON and PAUL T. ROBINSON,[1]
Hawaiian Volcano Observatory, Hawaii, Corvallis, Oreg.

Abstract.—The distinctive porphyritic welded tuff that forms the base of the John Day Formation from near Grizzly to 8 miles east of Clarno, a distance of about 45 miles, has been found in scattered outcrops in the Horse Heaven mining district, where it unconformably overlies rocks formerly thought to be in the John Day Formation. This welded tuff is widespread and easily recognized, represents a nearly instantaneous time interval, and initiated a lengthy period of silicic volcanism. Hence, the welded tuff is logically taken as the base of the John Day Formation in the Horse Heaven district, as it is elsewhere in its outcrop area. Rocks beneath the welded tuff and above a saprolite-mantled unconformity, which once was considered to mark the top of the Clarno Formation in the Horse Heaven district, are herein tentatively reassigned to the Clarno. A potassium-argon age of 41.0 ± 1.2 m.y. (late Eocene) for a rhyolite flow above the saprolite-mantled unconformity supports its assignment to the Clarno Formation.

Geologic studies in central Oregon north of the Ochoco Mountains have long been hampered by the difficulty in distinguishing between the Clarno and John Day Formations and in accurately locating the contact between them. This difficulty stems largely from the varied and, in part, comparable lithologies of the two formations and from the lack of precise age control.

The Clarno Formation was defined by Merriam (1901) from exposures in the John Day River drainage 5–30 miles north and east of Horse Heaven mine (fig. 1). It is a heterogeneous unit composed principally of andesite flows and breccias derived from numerous stratovolcanoes, shield volcanoes, and cinder cones; tuffs and tuffaceous sedimentary rocks locally overlap and intertongue with the lavas. The flows are typically pyroxene andesite containing abundant phenocrysts of andesine, augite, hypersthene, and, commonly, hornblende (Calkins, 1902; Waters and others, 1951). Many of the rocks underwent deuteric or hydrothermal alteration and later weathering, and contain secondary zeolites, carbonate minerals, chlorite, and clay minerals. The Clarno Formation has been assigned an Eocene age on the basis of fossil plants (Knowlton, 1902, p. 102–103; Arnold, 1952, p. 68–70; Scott, 1954), but Hergert (1961) and Wolfe and Hopkins (1967) suggested that part of the formation may be of Oligocene age. Potassium-argon dates (table 1) from the upper part of the formation indicate that the formation extends into the lower Oligocene, using the time scales of Holmes (1959, p. 204), Kulp (1961, p. 1111), and Harland and others (1964).

The John Day Formation was named and described by Marsh (1875) and Merriam (1901) from scattered exposures along John Day River between Clarno and Picture Gorge, 50 miles southeast of Clarno. East of lower John Day River and Bridge Creek, the John Day consists chiefly of varicolored tuff and tuffaceous claystone of rhyolitic, dacitic, and andesitic composition which was deposited as ash falls with or without subsequent reworking (Calkins, 1902; Merriam, 1901; Hay, 1962, 1963; Fisher and Wilcox, 1960; Fisher, 1966). West of lower John Day River, lava flows and welded ash-flow tuffs are also abundant (Waters, 1954; Peck, 1961, 1964; Robinson, 1966). The tuffs and welded tuffs were erupted from vents near or west of the 121st meridian and spread eastward for many miles into the John Day basin; the lava flows, however, had local vents. Most of the lava flows and welded tuffs are rhyolitic in composition, but flows of trachyandesite and basalt are common in the lower and middle parts of the formation and are easily confused with flows of the Clarno Formation. The John Day Formation has been considered to be late Oligocene and early Miocene in age on the basis of paleontologic evidence, but previously published potassium-argon dates (table 1) and reconsideration of the fossil floras (Wolfe and Hopkins, 1967) indicate that the lower part of the formation is as old as middle Oligocene (Harland and others, 1964). The basal welded tuff of the formation

[1] Department of Geology, Oregon State University.

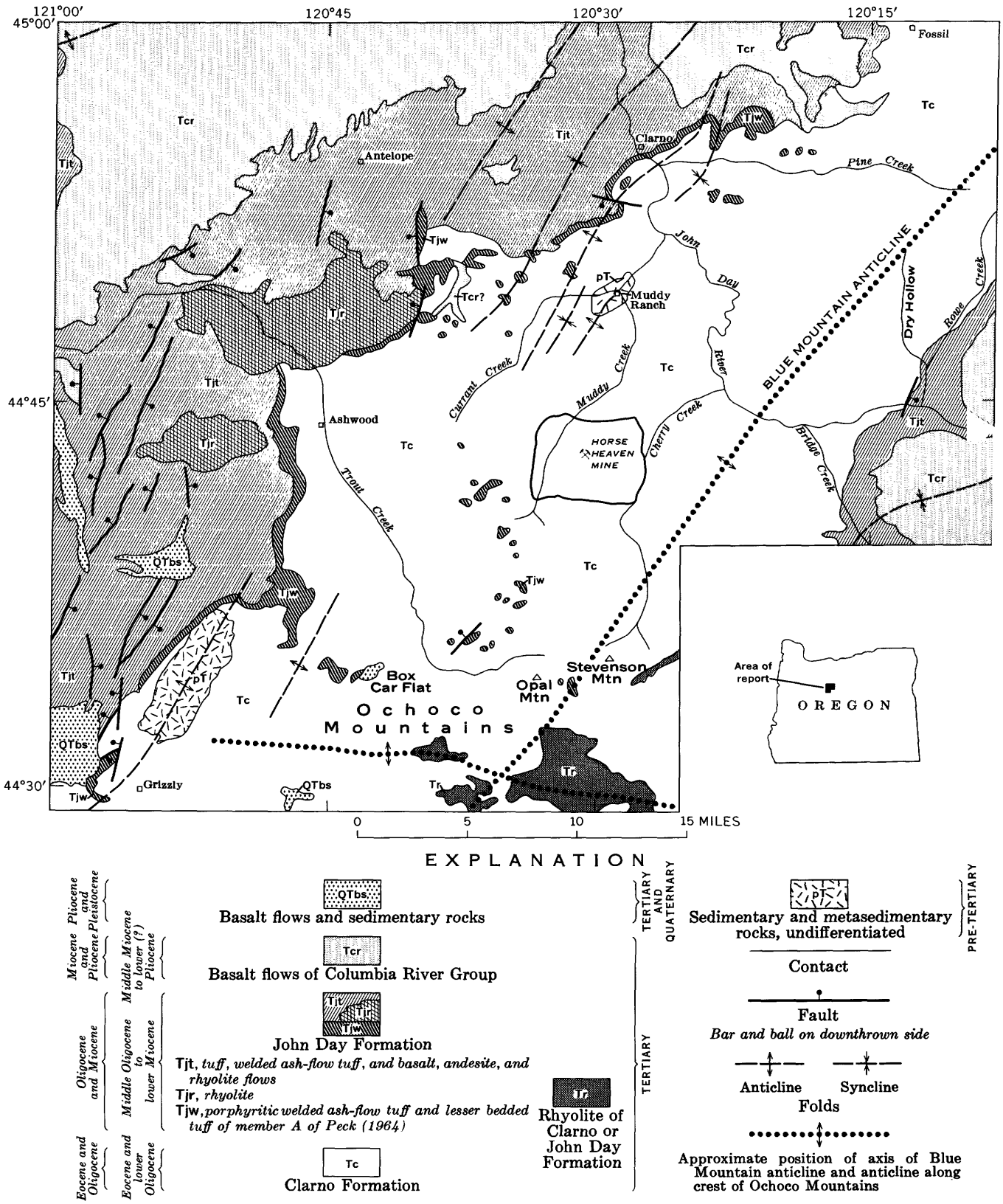

FIGURE 1.—Geologic map of northeastern part of Bend quadrangle (1:250,000 series), Oregon, generalized from Swanson (unpublished map). Outlined area centering on Horse Heaven mine was mapped and described by Waters and others (1951).

813-005 O—68——11

TABLE 1.—*Potassium-argon ages of Clarno and John Day Formations*

Formation and age (m.y.)	Stratigraphy	References
John Day Formation:		
24.9	1,550 feet above base of formation	Evernden and others (1964).
25.3	1,100–1,135 feet above base of formation	Do.
31.1	165 feet above base of formation	Do.
31.5	115 feet above the base of formation	Do.
[1] 32.0	Bentonite below basal ash-flow tuff	Evernden and James (1964).
[1] [2] 36.4±1.1	Basal ash-flow tuff	Present report.
Clarno Formation:		
[1] 34.2	Clarno "nutbed," top of formation	Evernden and James (1964).
36.5±0.9	Bentonite below 400-foot sequence of andesite flows, top of formation	Evernden and others (1964).
37.5	400-foot sequence of andesite flows, top of formation	Do.
[3] 41.0±1.2	Porphyritic rhyolite flow, "post-Clarno rocks" near Horse Heaven mine	Present report.

[1] The 32.0- and 34.2-m.y. dates were obtained from soda sanidine and plagioclase phenocrysts, respectively, in bedded bentonitic tuffs beneath the lower welded tuff of member A, one mile east of Clarno, and hence should be older than the lower welded tuff (36.4±1.1 m.y.). The feldspars in the bedded tuffs were subjected to intense weathering during alteration of the enclosing ash to bentonite, and they could have lost argon, giving rise to younger ages. For these reasons, the 36.4±1.1-m.y. age may be the more nearly correct.

[2] New date. Soda sanidine phenocrysts from lower welded tuff of member A. From roadcut along county road 2.2 miles southwest of Ashwood (NE¼NE¼ sec. 10, T. 10 S., R. 16 E.). Analyzed in 1967 in U.S. Geological Survey laboratories by Joan Engels, J. C. Von Essen, and Lois Schlocker.

[3] New date. Sanidine phenocrysts from porphyritic rhyolite flow overlying saprolite-mantled unconformity 1 mile north-northeast of Horse Heaven mine (NE¼NW¼ sec. 6, T. 10 S., R. 19 E.). Shown separately on geologic map of Waters and others (1951). Analyzed in 1968 in U.S. Geological Survey laboratories by Joan Engels, J. C. Von Essen, and Lois Schlocker.

may be as old as early Oligocene if the newly obtained potassium-argon date of 36.4±1.1 million years (table 1) can be substantiated.

The top of the Clarno Formation was mapped by Waters and others (1951) in the Horse Heaven mining district, an area bounded approximately by Trout, Currant, and Cherry Creeks and Opal Mountain (fig. 1). They recognized a saprolite-mantled angular unconformity separating "northward-tilted Clarno rocks from a younger series of flows and pyroclastic rocks" (p. 118) that they called the "post-Clarno rocks" and believed might be "approximately contemporaneous with the John Day Formation." Since then, many workers have included the rocks above this unconformity in the John Day Formation (Hay, 1963; Fisher, 1967). Red saprolites similar to the one along the unconformity at Horse Heaven have been recognized in many places in north-central Oregon and have commonly been interpreted as marking the top of the Clarno Formation (Waters, 1954; Hay, 1962, p. 196).

Peck (1964) defined a distinctive porphyritic welded tuff as the base of the oldest member (member A) of the John Day Formation in the Antelope-Ashwood area a few miles west of Horse Heaven mine (fig. 1). The porphyritic welded tuff rests unconformably on a thin layer of saprolite that overlies volcanic rocks assigned by Peck to the Clarno Formation.

The purpose of this paper is to show that this porphyritic welded tuff, which unconformably overlies the "post-Clarno rocks" south and west of Horse Heaven mine and can easily be recognized between Grizzly and the middle part of Pine Creek (fig. 1), is a good basis for defining the base of the John Day Formation in the area of figure 1 northwest of the Blue Mountain anticline. A new potassium-argon age of 41.0±1.2 m.y. from the "post-Clarno rocks" suggests that they should be reassigned to the Clarno Formation.

GEOLOGY NEAR HORSE HEAVEN MINE

The oldest rocks near Horse Heaven mine are andesite flows, tuffs, and tuffaceous sedimentary rocks belonging to the Clarno Formation. These rocks have a total thickness of approximately 5,800 feet and have been divided into four mappable units by Waters and others (1951):

Unit 1. A basal unit, about 600 feet thick, composed of andesite flows and interbedded layers of clay.

Unit 2. Approximately 1,350 feet of interbedded tuffs, tuffaceous clay, and volcanic mudflow deposits with a few thin andesite flows.

Unit 3. Tuffaceous clay, about 1,750 feet thick, containing beds of coarse tuff and a few andesite flows.

Unit 4. At least 2,100 feet of white coarse-grained rhyolitic and andesitic tuff.

Numerous small dikes and plugs of andesite and rhyolite intrude these rocks, and nearly all the rocks have been somewhat altered by either hydrothermal activity or weathering. The bedded rocks dip a few degrees northward in most of the area, but are gently folded along northeast-trending axes a few miles north of Horse Heaven mine.

A younger sequence of andesite flows and rhyolite tuffs, flows, and domes termed the "post-Clarno rocks" by Waters and others (1951) unconformably overlies the more steeply dipping andesite tuffs and flows. The younger rocks are nearly flat lying and are separated from the older rocks by a layer of red clayey saprolite that mantles the surface of unconformity. The thickness of the saprolite layer is generally 10 to 20 feet but varies from a few inches to at least 100 feet. Scattered lenses of sand and gravel in the saprolite mark stream channels on the old weathering surface, which had an

original relief of several hundred feet (Waters and others, 1951, p. 118).

The oldest rocks above the unconformity are dark-gray basaltic andesite flows. These rocks contain numerous phenocyrsts of altered ferromagnesian minerals and a few quartz xenocrysts but, unlike the older andesites, generally lack plagioclase phenocrysts. After extrusion of the basaltic andesites, flows and domes of rhyolite and sheets of pumice lapilli tuff and tuff breccia, largely of nuée ardente origin, were erupted from vents near Horse Heaven mine and upper Muddy Creek (fig. 1). These vents are now marked by steep-sided plugs of pinkish-gray flow-banded rhyolite containing sparse phenocrysts of quartz, alkali feldspar, oligoclase, and biotite. Most of the well-known quicksilver deposits of the district are closely related to these rhyolite plugs. The youngest rocks in the area mapped by Waters and others (1951) are nearly flat-lying augite andesites that disconformably overlie the rhyolite tuffs and flows. The augite andesites are generally fresh and contain phenocrysts of zoned plagioclase and augite and scattered xenocrysts of quartz.

Waters and others (1951) considered the rocks above the saprolite-mantled unconformity to be post-Clarno in age and thought that they "may be approximately contemporaneous with the John Day Formation" (p. 126). They carefully acknowledged, however, that this assignment was based on "inconclusive evidence" and realized that their "post-Clarno rocks" might also be late Clarno in age.

A potassium-argon age of 41.0 ± 1.2 m.y. was obtained from sanidine phenocrysts in a porphyritic rhyolite flow that overlies the "post-Clarno" basaltic andesite flows (table 1). This rhyolite flow may be considerably older than the other "post-Clarno" rhyolites, according to Waters and others (1951, p. 124), but it nevertheless dates at least the lower part of the "post-Clarno rocks" as of late Eocene or older age. On this basis, at least the lower part of the "post-Clarno rocks" belongs to the Clarno, not the John Day Formation (table 1). Correlation of John Day welded tuffs, described in following sections, supports this conclusion (fig. 2).

WELDED TUFF IN THE HORSE HEAVEN DISTRICT

Mapping in adjacent areas has shown that the youngest augite andesites of the Horse Heaven district are overlain by a distinctive porphyritic welded tuff. This tuff occurs in numerous erosional outliers along the ridges between Trout Creek and Cherry Creek; outcrops occur from as far south as Opal Mountain, 11 miles south of Horse Heaven mine, to as far north as 2.5 miles west of Muddy Ranch, a distance of nearly 20 miles (fig. 1). The porphyritic welded tuff unconformably overlies all older rocks and locally is separated from them by a thin saprolite. Along Currant Creek, west and southwest of Muddy Ranch (fig. 1), the tuff rests unconformably on more steeply dipping andesite flows which in turn overlie a sequence of rhyolitic pumice flows, slurry-flood deposits, and tuffs similar to the nuée ardente deposits erupted from the rhyolite-plugged vents near Horse Heaven mine (Waters and others, 1951). Localities where these relationships can best be seen are in sections 26, 27, 28, and 33, T. 8 S., R. 18 E and in sec. 9, T. 9 S., R. 18 E. The pumice flows and slurry-flood deposits can be traced almost continuously into the Horse Heaven area, and they contain abundant fragments of flow-banded rhyolite like that of the Horse Heaven plugs; most likely they are downslope equivalents of the nuée ardente deposits. The pumice flows, slurry-flood deposits, and overlying andesites have been folded into several shallow northeast-trending anticlines and synclines (fig. 1). The overlying porphyritic welded tuff is also gently folded, though not as strongly as the unconformably underlying rocks (a relationship best seen in sec. 26, T. 8 S., R. 18 E.). Farther south, near the head of Muddy Creek (fig. 1), the porphyritic ash-flow tuff rests with erosional unconformity on fresh andesites that are continuously trace-

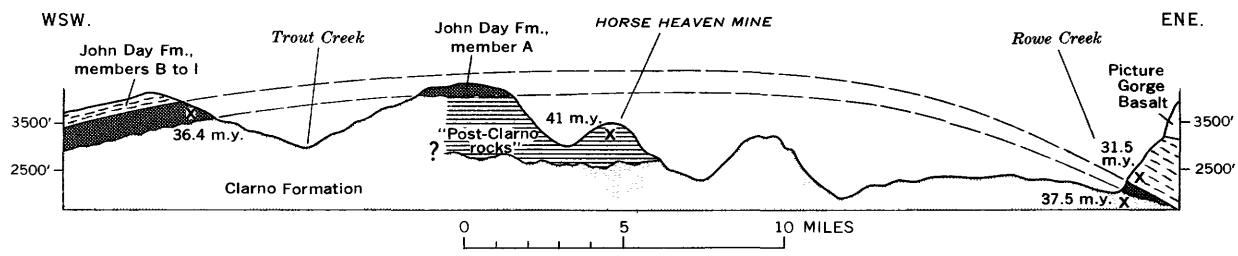

FIGURE 2.—Schematic cross section showing stratigraphic interpretations put forth in this paper. Dashed lines connect areas of welded tuff that is correlated with member A of John Day Formation. Most significant potassium-argon ages given in table 1 are located in approximate stratigraphic positions. Ages shown along Rowe Creek were obtained from rocks that crop out along strike about 8 miles to southwest (Evernden and others, 1964). The "post-Clarno rocks" (Waters and others, 1951) could not be mapped separately from the Clarno Formation in most places; they are tentatively assigned to the Clarno in this paper.

able into the "augite andesites"—the youngest "post-Clarno rocks"—of the Horse Heaven district. The best localities for observing these relationships are in sec. 17, T. 10 S., R. 18 E., and sec. 29, T. 10 S., R. 18 E., which are most easily reached by roads leading northwest from Stevenson Mountain.

The porphyritic welded tuff is as thick as 50 feet but averages about 30 feet. It is light gray, stony, and contains sparse lithophysae. The upper few feet of the tuff are commonly oxidized reddish brown. It has a well-defined eutaxitic structure, and flattened pumice fragments are as long as 2 feet. Phenocrysts of quartz and feldspar make up 5 to 10 percent of typical specimens (table 2, columns 12–22); hornblende is commonly present in trace amounts, and rock fragments (mostly andesite and rhyolite) make up 0.5 to 2 percent of most specimens. The feldspar, determined by universal-stage methods, is sodium-rich sanidine ($2V_x$=38°–48°) and oligoclase (An_{25}); in most specimens the sanidine is slightly more abundant (table 2). A chemical analysis (table 3, col. 2) of a sample of the welded tuff collected 2 miles east-southeast of Opal Mountain (fig. 1) shows that the tuff is of rhyolitic composition.

At several localities (5–6 miles west-southwest of Horse Heaven mine and 3–5 miles west-northwest of Muddy Ranch), the porphyritic welded tuff is overlain by 20–30 feet of white or red tuff capped by a fine-grained, densely welded ash-flow tuff. This fine-grained welded tuff is light gray to pinkish gray, stony, and typically contains less than 2 percent phenocrysts (table 4, col. 4–7). Lithophysae are generally absent, and the tuff lacks a megascopic eutaxitic structure. Oligoclase (An_{25}) makes up the bulk of the phenocrysts, but most specimens also contain small amounts of quartz (table 4).

TABLE 2.—*Modes of lower welded tuff of member A of the John Day Formation and its proposed correlative in the Horse Heaven mining district*

[Columns 1-11 represent specimens of lower welded tuff of member A, and columns 12-22 represent specimens of lower welded tuff in vicinity of Horse Heaven mining district. 1,000 points counted except as indicated. Abbreviation: tr., trace]

	1	2	3	4	5	6	7	8	9	10	11	Average 1-11
Groundmass	91.3	92.2	95.0	91.1	95.7	96.6	89.4	96.9	94.9	95.6	95.1	94.0
Quartz phenocrysts	1.6	4.5	3.5	4.3	3.0	1.6	5.8	1.3	3.1	3.4	3.0	3.2
Sanidine phenocrysts	1.1	1.8	.4	1.5	.9	.6	2.0	.9	1.3	.9	1.0	1.1
Plagioclase phenocrysts	4.3	.4	tr.	1.1	tr.	.7	1.2	.2	.2	.1	------	.8
Hornblende phenocrysts	------	------	------	------	------	------	.1	.1	------	------	------	tr.
Opaque phenocrysts	.2	------	tr.	tr.	tr.	tr.	tr.	------	------	------	------	tr.
Rock fragments	.5	1.1	1.1	2.0	.4	.5	1.5	.6	.5	------	.9	.9

	12	13	14	15	16	17	18	19	20	21	22	Average 12-22
Groundmass	94.2	92.7	95.1	92.2	94.1	92.8	94.5	95.2	95.2	93.9	96.3	94.2
Quartz phenocrysts	1.3	3.8	2.2	5.2	2.8	1.8	3.0	2.9	3.4	2.8	2.4	2.9
Sanidine phenocrysts	.7	.9	1.5	1.0	1.1	1.3	1.0	.7	1.3	1.4	.8	1.1
Plagioclase phenocrysts	1.8	1.0	1.2	.2	.1	2.0	.7	.6	------	1.1	.4	.8
Hornblende phenocrysts	tr.	------	------	------	------	tr.	------	------	------	------	------	tr.
Opaque phenocrysts	tr.	------	------	------	------	.1	.1	.1	------	------	------	tr.
Rock fragments	2.0	1.6	------	1.4	1.9	2.0	.7	.5	.1	.8	.1	1.0

1. R648–1a. Vitric base, 2 miles southwest of Ashwood, NE¼NE¼ sec. 10, T. 10 S., R. 16 E.
2. R648–1b. Upper crystallized part, 2 miles southwest of Ashwood, NE¼NE¼ sec. 10, T. 10 S., R. 16 E.
3. R648–13. 6.5 miles south-southwest of Ashwood, sec. 3, T. 11 S., R. 16 E.
4. R648–15. 8 miles south of Ashwood, sec. 12, T. 11 S., R. 16 E.
5. R648–17. 4.5 miles southwest of Ashwood, sec. 26, T. 10 S., R. 16 E.
6. R648–149. 3.5 miles southwest of Clarno, sec. 13, T. 8 S., R. 18 E.
7. R648–395. 1 mile east of Clarno, sec. 33, T. 7 S., R. 19 E.
8. DAS67–111. 5 miles east-northeast of Clarno, NE¼ sec. 25, T. 7 S., R. 19 E.
9. DAS66–106 and DAS66–208. 2 miles southwest of Ashwood, NE¼NE¼ sec. 10, T. 10 S., R. 16 E. (2,000 points total).
10. DAS66–142. 6 miles southeast of Antelope, SW¼ sec. 26, T. 8 S., R. 17 E.
11. DAS66–166. 2 miles west of Grizzly, NE¼ sec. 32, T. 12 S., R. 15 E.
12. R648–142. 4.5 miles west of Muddy Ranch, sec. 33, T. 8 S., R. 18 E.
13. DAS67–75. 4.25 miles northwest of Muddy Ranch, border of NE edge of sec. 28 and NW edge of sec. 27, T. 8 S., R. 18 E.
14. DAS66–132. 2 miles west of Muddy Ranch, sec. 26, T. 8 S., R. 18 E.
15. DAS67–77. 5 miles west-southwest of Muddy Ranch, sec. 9, T. 9 S., R. 18 E.
16. DAS66–195. 5 miles southwest of Horse Heaven mine, sec. 17, T. 10 S., R. 18 E.
17. DAS67–197. 5 miles southwest of Horse Heaven mine, sec. 17, T. 10 S., R. 18 E.
18. DAS66–105 and DAS67–192. Head of Muddy Creek, sec. 29, T. 10 S., R. 18 E. (2,000 points total).
19. DAS67–199. 3.5 miles north-northwest of Opal Mountain, N½ sec. 16, T. 11 S., R. 18 E.
20. DAS67–200. 2.5 miles north-northwest of Opal Mountain, NW¼ sec. 21, T. 11 S., R. 18 E.
21. DAS66–102. 4 miles northwest of Opal Mountain, sec. 19, T. 11 S., R. 18 E.
22. DAS66–90 and DAS67–191. East side of Opal Mountain, NW¼ sec. 36, T. 11 S., R. 18 E. (2,000 points total).

TABLE 3.—*Chemical analyses of welded tuffs of member A of John Day Formation and porphyritic welded tuff in Horse Heaven mining district*

[Analysts for columns 1 and 2: Paul Elmore, G. W. Chloe, Lowell Artis, H. Smith, S. D. Botts, James Kelsey, and John Glenn]

Constituent oxides	1	2	3
SiO_2	76.8	72.9	71.8
Al_2O_3	12.1	13.4	13.0
Fe_2O_3	.20	1.0	1.3
FeO	.04	.24	.26
MgO	.12	.20	.12
CaO	.57	1.0	.87
Na_2O	2.5	2.5	2.3
K_2O	5.4	5.5	5.0
H_2O-	.31	.86	5.4
H_2O+	.50	.84	
TiO_2	.20	.52	.16
P_2O_5	.06	.12	.01
MnO	.00	.06	.03
CO_2	.05	.05	.05
Total	98.85	99.19	100.30

1. DAS66–208. Porphyritic welded tuff, member A, roadcut along county road 2.2 miles southwest of Ashwood (NE¼NE¼ sec. 10, T. 10 S., R. 16 E.).
2. DAS66–90. Porphyritic welded tuff, east side of Opal Mountain, SW¼NW¼ sec. 36, T. 11 S., R. 18 E.
3. DLP–58–42. Welded tuff from vitric base of upper ash-flow sheet of member A in NE¼NE¼ sec. 10, T. 10 S., R. 16 E., 1.9 miles S. 62° W. of Ashwood. Quoted from Peck (1964).

The porphyritic welded tuff and the overlying fine-grained welded tuff are mineralogically, lithologically, and structurally similar to the welded tuffs in the basal member of the John Day Formation west and south of Ashwood as defined by Peck (1964).

MEMBER A OF THE JOHN DAY FORMATION

The base of the John Day Formation, as mapped by Peck (1964) in the Antelope-Ashwood area, is marked by a distinctive porphyritic welded tuff (basal welded tuff of member A) that unconformably overlies andesites and basalts of the Clarno Formation in the Antelope-Ashwood area west and north of the Horse Heaven district. We have traced this tuff in nearly continuous exposures from Pine Creek Canyon southwest of Fossil to Grizzly, a distance of approximately 45 air miles (fig. 1). A thin saprolite occurs locally at the base of the welded tuff, but in many places the tuff rests directly on relatively fresh andesites and basalts.

The porphyritic welded tuff of member A closely resembles the one in the Horse Heaven district. It is 50–100 feet thick and is light gray and stony. A layer of light-gray glass occurs locally at the base of the sheet, and the upper few feet are commonly reddish brown owing to oxidation. Most rocks have well-developed eutaxitic structure, defined by large flattened pumice fragments, and some are sparsely lithophysal. Typical specimens contain 5–10 percent phenocrysts, mostly sanidine, quartz, and oligoclase (table 2, col. 1–11); biotite and hornblende are rare. According to

TABLE 4.—*Modes of upper welded tuff of member A of the John Day Formation and its proposed correlative in the Horse Heaven mining district*

[Columns 1-3 represent specimens of upper welded tuff of member A, and columns 4-7 represent specimens of upper welded tuff in the vicinity of Horse Heaven mining district. 1,000 points counted except as indicated. Abbreviation: tr., trace]

	1	2	3	4	5	6	7
Groundmass	98.7	96.8	98.0	97.9	97.9	96.7	98.7
Quartz phenocrysts	tr.	.2	------	.1	------	.1	------
Sanidine phenocrysts	----------	----------	----------	----------	----------	----------	----------
Plagioclase phenocrysts	.3	.4	.2	.1	2.1	.9	.8
Hornblende phenocrysts	----------	----------	tr.	----------	----------	----------	----------
Pyroxene phenocrysts	----------	tr.	----------	----------	----------	----------	----------
Rock fragments	1.0	2.6	1.8	1.9	------	2.3	.5

1. R648–3. 2.3 miles southwest of Ashwood, NE¼NE¼ sec. 10, T. 10 S., R. 16 E.
2. DAS66–138. 6.5 miles northeast of Ashwood, near corner of sec. 11, 12, 13, and 14, T. 9S., R. 17 E.
3. DAS67–100. Box Car Flat north of Foley Butte, NW¼ sec. 32, T. 11 S., R. 17 E.
4. DAS67–76. 4.25 miles northwest of Muddy Ranch, border of NE edge of sec. 28 and NW edge of sec. 27, T. 8 S., R. 18 E.
5. DAS66–133. 2 miles west of Muddy Ranch, sec. 26, T. 8 S., R. 18 E.
6. DAS67–196. Head of Muddy Creek about 5 miles southwest of Horse Heaven mine, sec. 17, T. 10 S., R. 18 E.
7. DAS66–115 and DAS67–194. Head of Muddy Creek about 5 miles southwest of Horse Heaven mine, sec. 17, T. 10 S., R. 18 E. (2,000 points total).

Peck (1964, p. D8), the sanidine is optically monoclinic sodium-rich sanidine with a $2V_x$ of 42° to 48°. A chemical analysis of a sample of this tuff is given in table 3 (col. 1).

Peck (1964) found that the basal ash-flow tuff of member A is overlain by about 100 feet of white vitric tuff and pumice lapilli tuff which, in turn, are overlain in most places by a strongly welded, fine-grained ash-flow sheet that forms the upper part of Peck's member A. The upper welded tuff, as thick as 200 feet, is light gray, stony, and contains about 2 percent phenocrysts and a few lithophysae (table 4, col. 1–3). A layer of vitrophyre as thick as 40 feet occurs at the base of the sheet in many places. Phenocrysts in the welded tuff are dominantly oligoclase (An_{25}), but most specimens also contain small amounts of quartz (table 4, col. 1–3). A chemical analysis of the basal vitrophyre of this tuff was published by Peck (1964) and is listed in table 3 (col. 3).

CORRELATION OF WELDED TUFF AND "POST-CLARNO ROCKS"

The welded tuffs of the Horse Heaven mining district are mineralogically, lithologically, and modally similar to the two ash-flow sheets of member A of the John Day Formation (tables 2 and 4), and a correlation is highly

probable. The tuffs crop out at altitudes consistent with eastward projections of the ash-flow sheets of member A west of Ashwood (fig. 2). In addition, scattered outcrops connect the porphyritic welded tuff in the Horse Heaven district with the basal welded tuff of member A between Ashwood and Clarno (fig. 1). Chemical analyses of samples of this tuff from two different localities (table 3, col. 1 and 2) are not identical, but the differences are within the range of variation that is commonly found in a single ash-flow sheet (see, for example, Lipman and others, 1966). The presence of both the porphyritic and fine-grained welded tuffs in the Horse Heaven area, in the same sequence in which they occur in member A, strongly supports the correlation.

The lower welded tuff of member A is a widespread unit that marks the base of the John Day Formation for about 45 miles between Clarno and Grizzly. Apparently it once extended far eastward across the crest of the Blue Mountain anticline, judging from present outcrops (fig. 1) and Hay's (1963, p. 204–205) discovery of a similar welded tuff at the junction of Dry Hollow and Rowe Creek (fig. 1). This relationship, portrayed in figure 2, suggests that significant uplift of the southern part of the anticline did not take place until after member A time, a conclusion different from that reached by Fisher (1967), working farther northeast.

Correlation of the porphyritic welded tuff in the Horse Heaven district with Peck's basal member A of the John Day Formation forces reconsideration of the "post-Clarno rocks." Are they of Clarno, John Day, or an intermediate age? We believe there are good reasons for omitting them from the John Day Formation. The potassium-argon age of 41.0 ± 1.2 m.y. obtained from the "post-Clarno rocks" is about 5 m.y. older than the oldest rocks which can definitely be assigned to the John Day (table 1). Furthermore, the "post-Clarno rocks" are overlain, with erosional and angular unconformity, by the porphyritic welded tuff that is the base of the John Day Formation everywhere that Peck (1964) and we have mapped it outside of the Horse Heaven district (fig. 2). Thus on stratigraphic and radiometric grounds the "post-Clarno rocks" are older than the John Day Formation, as recognized by Peck (1964), in the area of figure 1. This does not, of course, imply anything about the age relationships of the "post-Clarno rocks" to the John Day Formation near Picture Gorge, though we are unaware of any evidence that the John Day near Picture Gorge is as old as late Eocene.

The question of whether the "post-Clarno rocks" should be assigned to the Clarno Formation or should be given a separate formational name cannot yet be resolved satisfactorily, but the potassium-argon date of 41.0 ± 1.2 m.y. suggests correlation with the Clarno. The "post-Clarno rocks", however, are separated from the Clarno Formation by a saprolite-mantled angular unconformity. The question arises: Is this unconformity a good criterion for defining the top of the Clarno?

A saprolite-mantled angular unconformity occurs at the top of the Clarno Formation in many places (Waters, 1954). Examples can be seen on Bridge and Rowe Creeks (Hay, 1963); between Prineville Dam and Eagle Rock, 35 miles south of Horse Heaven mine; near Ashwood (Peck, 1964); and at several other places (Waters, 1954; Fisher, 1964). In the Horse Heaven mining district, however, there are *two* saprolite-covered unconformities. One is at the base of the "post-Clarno rocks", and the other separates, at least locally, the "post-Clarno rocks" from the overlying porphyritic welded tuff of Peck's member A of the John Day Formation. From this relationship, it is clear that a saprolite-mantled angular unconformity is an unreliable criterion with which to define the top of the Clarno Formation in the Horse Heaven district. Support for its unreliability elsewhere is shown by the fact that many discontinuous saprolite layers, some of which cap erosional and angular unconformities, occur within the Clarno Formation in the Ochoco Mountains, as recognized by Waters and others (1951) and Peck (1964), and they cannot be distinguished lithologically from each other or from the layer of saprolite that caps the formation in places. To add further confusion, a saprolite-mantled angular unconformity is missing at the top of the Clarno over large areas, such as in much of the Post quadrangle (Waters, 1968), the Grizzly area, and at many places in and near the Horse Heaven mining district.

We believe, therefore, that it is most realistic to reassign the "post-Clarno rocks" to the Clarno Formation because of the potassium-argon age of 41.0 ± 1.2 m.y. and because of the unreliability in using unconformities, such as the one that the "post-Clarno rocks" overlie, to define the top of the Clarno.

CONCLUSIONS

The lower welded tuff of Peck's member A of the John Day Formation and its correlative in the Horse Heaven district can be recognized over a wide area of north-central Oregon (figs. 1 and 2). It is easily recognized and represents a nearly instantaneous time interval of deposition. It overlies andesites and basalts of the Clarno Formation with erosional and, in places, angular unconformity, laps against and across constructional highs formed by thick flows and mounds of near-vent lava, and is locally separated from the older rocks by a thin layer of saprolite. Most of the rocks below the porphyritic welded tuff are mafic lava flows and breccias; most above it are silicic bedded tuffs and

welded tuffs. For these reasons, the porphyritic welded tuff is well suited as the base of the John Day Formation in the Horse Heaven mining district, where it overlies "post-Clarno rocks" that have yielded a potassium-argon age of 41.0±1.2 m.y. (late Eocene). The "post-Clarno rocks" are reassigned tentatively to the Clarno Formation on the basis of the potassium-argon age. The saprolite-covered angular unconformity at the base of the "post-Clarno rocks" is not considered to be a reliable criterion for separating them from the Clarno Formation because of the large number of such saprolite layers and unconformities elsewhere within the Clarno.

Potassium-argon ages suggest that little time elapsed between eruption of the youngest Clarno lava flows and deposition of the basal John Day welded tuff (table 1). A short time interval is also suggested by the absence of a thick cover of saprolite at the contact in the Horse Heaven district. In fact, this interval may have been shorter than many of those represented by thick weathering zones within the Clarno Formation, but it was nonetheless more significant, for it ended with eruption of an ash-flow tuff that spread over wide portions of north-central Oregon and initiated a long period of predominantly rhyolitic and dacitic volcanism.

REFERENCES

Arnold, C. A., 1952, Fossil Osmundaceae from the Eocene of Oregon: Palaeontographica, [Stuttgart, Germany] v. 92, pt. B, p. 63–78.

Calkins, F. C., 1902, A contribution to the petrography of the John Day Basin [Oregon]: California Univ. Pubs., Dept. Geology Bull., v. 3, p. 109–172.

Evernden, J. F., and James, G. T., 1964, Potassium-argon dates and the Tertiary floras of North America: Am. Jour. Sci., v. 262, no. 8, p. 945–974.

Evernden, J. F., Savage, D. E., Curtis, G. H., and James, G. T., 1964, Potassium-argon dates and the Cenozoic mammalian chronology of North America: Am. Jour Sci., v. 262, no. 2, p. 145–198.

Fisher, R. V., 1964, Resurrected Oligocene hills, eastern Oregon: Am. Jour. Sci., v. 262, no. 6, p. 713–725.

——— 1966, Textural comparison of John Day volcanic siltstone with loess and volcanic ash: Jour. Sed. Petrology, v. 36, no. 3, p. 706–718.

——— 1967, Early Tertiary deformation in north-central Oregon: Am. Assoc. Petroleum Geologists Bull., v. 51, no. 1, p. 111–123.

Fisher, R. V., and Wilcox, R. E., 1960, The John Day Formation in the Monument quadrangle, Oregon: Art. 140 *in* U.S. Geol. Survey Prof. Paper 400–B, p. B302–B304.

Harland, W. B., Smith, A. G., and Wilcock, Bruce, eds., 1964, The Phanerozoic time-scale—A symposium dedicated to Professor Arthur Holmes: Geol. Soc. London Quart. Jour., supp., v. 120s, 458 p.

Hay, R. L., 1962, Origin and diagenetic alteration of the lower part of the John Day Formation near Mitchell, Oregon *in* Petrologic studies: Geol. Soc. America, Buddington Volume, p. 191–216.

——— 1963, Stratigraphy and zeolitic diagenesis of the John Day Formation of Oregon: California Univ. Pubs. Geol. Sci., v. 42, no. 5, p. 199–261.

Hergert, H. L., 1961, Plant fossils in the Clarno formation, Oregon: Ore Bin, v. 23, no. 6, p. 55–62.

Holmes, Arthur, 1959, A revised geological time scale: Edinburgh Geol. Soc. Trans., v. 17, pt. 3, p. 183–216.

Knowlton, F. H., 1902, Fossil flora of the John Day Basin, Oregon: U.S. Geol. Survey Bull. 204, 153 p.

Kulp, J. L., 1961, Geologic time scale: Science, v. 133, no. 3459, p. 1105–1114.

Lipman, P. W., Christiansen, R. L., and O'Connor, J. T., 1966, A compositionally zoned ash-flow sheet in southern Nevada: U.S. Geol. Survey Prof. Paper 524–F, p. F1–F47.

Marsh, O. C., 1875, Ancient lake basins of the Rocky Mountain region: Am. Jour. Sci., ser. 3, v. 9, p. 45–52.

Merriam, J. C., 1901, A contribution to the geology of the John Day Basin [Oregon]: California Univ. Pubs., Dept. Geology Bull., v. 2, no. 9, p. 269–314.

Peck, D. L., 1961, John Day formation near Ashwood, north-central Oregon: Art. 343 *in* U.S. Geol. Survey Prof. Paper 424–D, p. D153–D156.

——— 1964, Geologic reconnaissance of the Antelope-Ashwood area, north-central Oregon, with emphasis on the John Day Formation of late Oligocene and early Miocene age: U.S. Geol. Survey Bull. 1161–D, p. D1–D26.

Robinson, P. T., 1966, Facies changes in John Day Formation, Oregon [abs.]: Geol. Soc. America, Rocky Mountain Sec., Ann. Mtg., Las Vegas, Nev., Program, p. 49.

Scott, R. A., 1954, Fossil fruits and seeds from the Eocene Clarno formation of Oregon: Palaeontographica, [Stuttgart, Germany], v. 96, pt. B, no. 3–6, p. 66–97.

Waters, A. C., 1954, John Day formation west of its type locality [Oregon] [abs.]: Geol. Soc. America Bull., v. 65, no. 12, pt. 2, p. 1320.

——— 1968, Reconnaissance geologic map of the Post quadrangle, Crook County, Oregon: U.S. Geol. Survey Misc. Geol. Inv. Map I–542, scale 1:62,500.

Waters, A. C., Brown, R. E., Compton, R. R., Staples, L. W., Walker, G. W., and Williams, Howel, 1951, Quicksilver deposits of the Horse Heaven mining district, Oregon: U.S. Geol. Survey Bull. 969–E, p. 105–149.

Wolfe, J. A., and Hopkins, D. M., 1967, Climatic changes recorded by Teritary land floras in northwestern North America, *in* Tertiary correlations and climatic changes in the Pacific—Pacific Sci. Cong., 11th, Tokyo, 1966, Symposium 25: Tokyo, Sci. Council Japan, p. 67–76.

LITHOFACIES OF UPPER ORDOVICIAN ROCKS EXPOSED BETWEEN MAYSVILLE AND STANFORD, KENTUCKY

By GORDON W. WEIR and JOHN H. PECK, Berea, Ky., Flemingsburg, Ky.

Work done in cooperation with the Kentucky Geological Survey

Abstract.—Upper Ordovician strata overlying the Garrard Siltstone and the Kope Formation in east-central Kentucky are divided into nine lithofacies based on differences in composition, texture, bedding, and fossil content. Strata in southeast-central Kentucky are dominantly unfossiliferous dolomitic mudstone lithofacies which mostly pinch out near Owingsville, east-central Kentucky. Equivalent strata in northeast-central Kentucky are made up chiefly of very fossiliferous limestone and mudstone lithofacies. The lithofacies were deposited on a shelf in an inland sea that toward the south was generally shallower and closer to a source of terrigenous material.

Upper Ordovician strata in east-central Kentucky (fig. 1) consist of limestone, mudstone, and dolomite. These major rock types intergrade and vary in texture, bedding, and fossil content. The strata may be divided into lithofacies, rock units that have distinctive lithologic features by which they may be separated from adjacent units. (See Weller, 1958, p. 633.) The purpose of this report is to outline the relations of the chief lithofacies in Upper Ordovician strata exposed along the curving line of outcrop between Stanford and Maysville, Ky. (See fig. 2.)

This preliminary report is based on mapping of Ordovician outcrops between Maysville and Flemingsburg, Ky., and between Stanford and Richmond, Ky., and on reconnaissance of sections between Flemingsburg and Richmond. Of special help was the information contributed by E. R. Cressman, R. C. Greene, F. A. Schilling, Jr., and G. C. Simmons, all of the U.S. Geological Survey.

DESCRIPTION OF LITHOFACIES

Between Stanford and Owingsville the stratigraphic interval studied is bounded at the base by the Garrard Siltstone (Weir and others, 1965). North of Owingsville the Garrard is not present and the interval is bounded below by the Kope Formation (Weiss and Sweet, 1964). The upper boundary is the top of the Ordovician section. In most of the area the Ordovician rocks are overlain by dolomite, limestone, and shale of the Brassfield Formation of Early Silurian age. The rock units within the interval studied make up the Maysville and Richmond Groups of Palmquist and Hall (1961).

Details of stratigraphic nomenclature are excluded from this report. Weiss and Sweet (1964), Weir and others (1965), and Peck (1966) have reviewed some of the nomenclatural problems and have proposed several

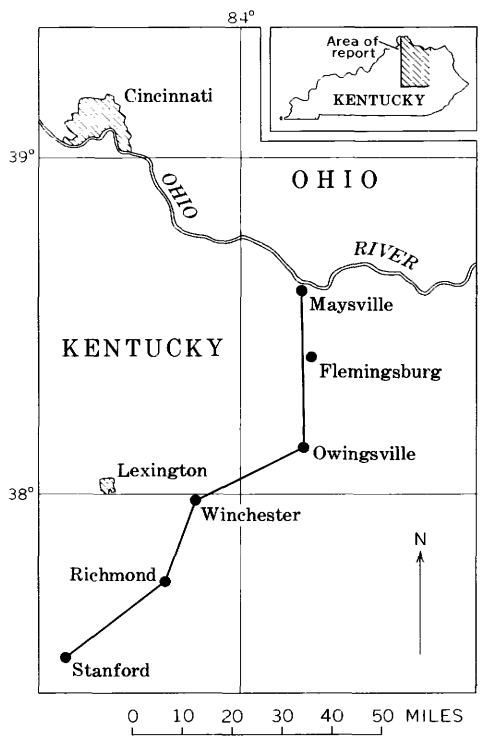

FIGURE 1.—Index map of part of central Kentucky, showing location of line of section of figure 2.

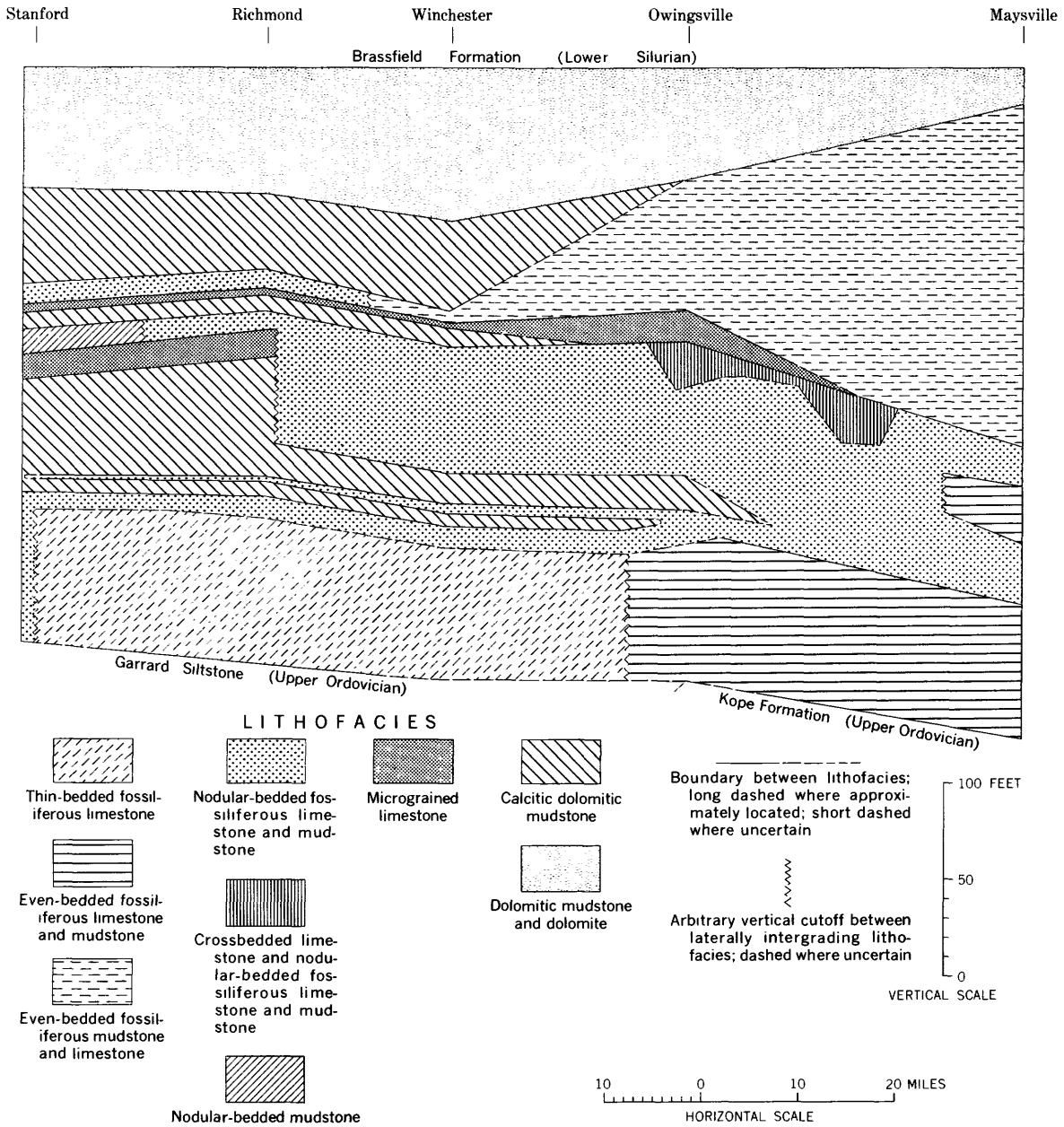

FIGURE 2.—Diagram of lithofacies in Upper Ordovician strata exposed along the line of outcrop between Stanford and Maysville, Ky.

new names for Upper Ordovician rock units in east-central Kentucky.

For the purpose of this report the Upper Ordovician strata in the region studied are divided into nine lithofacies, which are described in table 1 and illustrated in figures 3, 4, and 5. The lithofacies are generalized intergrading rock units that are differentiated by bulk composition, grain size, bedding character, and relative abundance of fossils. Vertical gradations range from a few inches to a few tens of feet. Lateral gradations are obscure and take place in a distance of several miles. The defining limits of the intergrading characters of the lithofacies listed in table 1 and the placing of cutoffs of laterally intergrading lithofacies in figure 2 are based on our experience in mapping these units. Most of the lithofacies could be further subdivided; those shown are known to have a broad extent.

The lithofacies described in table 1 are assembled into four groups. Within each group the lithofacies are more alike than different and more difficult to separate from one another than from lithofacies of another group. The first group is characterized by various proportions of planar beds of fossiliferous, fine- and medium-grained limestone and mudstone.

TABLE 1.—*Description of lithofacies*

Composition (in percent)	Texture	Bedding	Fossils	Outcrop
Planar-bedded fossiliferous limestone and mudstone lithofacies				
Thin-bedded fossiliferous limestone (fig. 3*A*):				
Limestone (70–80).	Fine to medium grained, fossil fragmental; fairly sorted.	Thin beds (1–4 in.), laterally continuous and fairly uniform in thickness.	Abundant brachiopods and bryozoans.	Moderately resistant. Forms rough, ledgy slopes.
Mudstone (15–25).	Silty to clayey.	Crude laminae in sets 1–6 in. thick and as partings.		
Siltstone (5).	Fine to coarse silt.	Smooth-surfaced thin beds (1–4 in.), laterally continuous and fairly uniform.	Sparse brachiopods.	
Even-bedded fossiliferous limestone and mudstone (fig. 3*B*):				
Limestone (45–65).	Very fine, and medium to coarse grained, fossil fragmental; fairly sorted.	Thin to medium beds (1–10 in.), laterally continuous and slightly variable.	Abundant brachiopods and bryozoans.	Moderately resistant. Forms rough, ledgy slopes.
Mudstone (35–50).	Silty to clayey.	Crude laminae in sets 1–6 in. thick and as partings.		
Siltstone (5–10).	Fine silt.	Smooth-surfaced thin to thick beds (1–18 in.), laterally discontinuous and variable in thickness; some beds contorted, ball-and-pillow structure common.	Sparse brachiopods.	
Even-bedded fossiliferous mudstone and limestone (fig. 3*C*):				
Mudstone (30–70).	Clayey to silty.	Crude laminae in sets 1–36 in. thick.	Common to very abundant. Chiefly brachiopods, bryozoans and corals. Locally gastropods, pelecypods, trilobites, and crinoid stems.	Poorly to moderately resistant. Forms slopes littered with fossil and limestone fragments.
Limestone (30–70).	Micrograined to coarse grained, chiefly very fine grained, silty, fossil fragmental; poorly sorted.	Thin beds (1–4 in.), laterally continuous and variable in thickness; also as lenticles and partings in mudstone.		
Nodular-bedded fossiliferous limestone and mudstone lithofacies				
Nodular-bedded fossiliferous limestone and mudstone (fig. 4*A*):				
Limestone (65–90) Mudstone (10–35).	Micrograined to fine grained, muddy; fossil fragmental. Intermixed and intergrading with clayey to silty mudstone.	Obscure to ill-defined thin beds (1–4 in.) made up of closely packed nodular lenticles grading to irregularly wavy thin lenses; in part laterally discontinuous and variable in thickness.	Abundant brachiopods and bryozoans; pelecypods locally common	Slightly to moderately resistant. Forms rubbly slopes and smooth, rounded ledges.
Crossbedded limestone and nodular-bedded fossiliferous limestone and mudstone (fig. 4B):				
Limestone (70–90)	Micrograined to fine grained, and medium to coarse grained (mostly in crossbedded units), muddy; fossil fragmental.	Similar to lithofacies described above, but contains conspicuous planar sets, commonly 1–3 ft. thick, of wavy low-angle crossbeds. Partly in crude laminae in thin lenses (1–4 in. thick); partly intermixed with limestone.	Abundant brachiopods and bryozoans. Stromatoporoids locally abundant.	Moderately resistant. Coarse-grained, partly crossbedded limestone units form ledges on rubbly slopes.
Mudstone (10–30).	Clayey to silty.			

TABLE 1.—*Description of lithofacies*—Continued

Composition (in percent)	Texture	Bedding	Fossils	Outcrop
Nodular-bedded fossiliferous limestone and mudstone lithofacies—Continued				
Nodular-bedded fossiliferous mudstone (fig. 4*C*):				
Mudstone (70–80).	Clayey to silty and clayey.	Crude laminae in obscure sets, several feet thick, containing abundant nodular lenticles 0.5–2 in. in diameter of calcitic mudstone and muddy limestone.	Abundant brachiopods and bryozoans. Gastropods, pelecypods, ostracods and fragments of trilobites and crinoid stems locally common to abundant.	Nonresistant. Forms rubbly, fossil-strewn slopes.
Limestone (20–30).	Micrograined to fine grained, muddy; fossil fragmental.	Thin beds (1–4 in.), laterally discontinuous and variable in thickness, and as lenticles scattered through mudstone.		
Planar to wavy-bedded micrograined limestone lithofacies				
Micrograined limestone (fig. 5*A*):				
Limestone (60–90).	Aphanitic to medium grained, but chiefly micrograined. Well sorted.	Thin beds (1–4 in.), planar to wavy, laterally continuous and uniform to slightly variable in thickness.	Sparse to abundant ostracodes. Locally brachiopods, gastropods and stromatoporoids, sparse to common. Scolithoid markings locally common.	Resistant. Forms conspicuous ledges.
Mudstone (10–40).	Clayey.	Crude laminae in thin sets 1–2 in. thick and as partings.		
Dolomitic mudstone lithofacies				
Calcitic dolomitic mudstone (figs. 5*A*, 5*B*):				
Calcitic to dolomitic mudstone locally grading to muddy dolomite and to muddy dolomitic limestone.	Mostly silty. Locally micrograined.	Laminae and very thin beds (less than 1 in.), laterally continuous and uniform in thickness, in sets a few inches to few feet thick.	Absent to very sparse, chiefly bryozoans.	Nonresistant. Forms slope. Yields platy fragments.
Dolomitic mudstone and dolomite (fig. 5*B*):				
Calcitic dolomitic mudstone locally grading to muddy dolomite (75–90).	Probably mostly silty. Locally micrograined.	Laminae, in part crude or obscure, and very thin beds (less than 1 in.), laterally continuous and uniform in thickness, in sets a few inches to a few feet thick.	Generally absent, sparse bryozoans.	Mostly nonresistant. Forms slope with few ledges of dolomite and limestone.
Dolomite grading to dolomitic limestone (10–25).	Very fine to medium grained; muddy.	Thin to medium beds (1–8 in.), laterally continuous and fairly uniform, irregularly interstratified in unit as single beds and grouped in sets as much as 4 feet thick.	Bryozoans sparse to abundant; brachiopods generally sparse. Colonial corals and brachiopods locally common to abundant in limestone.	

A

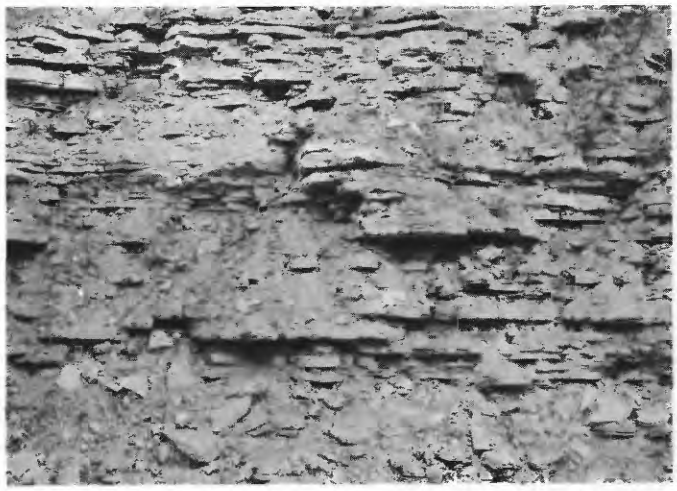

B

C

FIGURE 3.—Planar-bedded fossiliferous limestone and mudstone lithofacies. *A*, thin-bedded fossiliferous limestone lithofacies. Interstate Highway 75, about 6 miles north of Richmond, Ky. *B*, even-bedded fossiliferous limestone and mudstone lithofacies. Kentucky State Highway 1449, about 2 miles southeast of Maysville, Ky. Exposure about 15 feet high. *C*, even-bedded fossiliferous mudstone and limestone lithofacies. Louisville and Nashville Railroad cut about 3 miles south of Maysville, Ky. Exposure about 20 feet high.

The second group is characterized by nodular beds of fossiliferous limestone or mudstone. A third group includes a single transitional lithofacies of micrograined limestone in planar and wavy beds. The fourth group is characterized by dolomitic mudstone. The term used to designate each lithofacies is based on the more detailed descriptions given in table 1.

The diagram (fig. 2) shows that along the curving line of section controlled by outcrop data the lithofacies intertongue broadly as well as intergrade and that several lithofacies recur at different stratigraphic levels. In southeast-central Kentucky the intercalation of representatives from all four groups of lithofacies makes it easy to recognize many relatively thin rock-stratigraphic units. The dolomitic mudstone lithofacies thin northward and mostly pinch out near Owingsville, Ky. In northeast-central Kentucky fossiliferous limestone and mudstone lithofacies are dominant. These lithofacies are more readily divisible into biostratigraphic units than are equivalent less fossiliferous rocks cropping out farther south.

Not apparent from the diagram are minor differences in bulk composition and some significant differences in

A

B

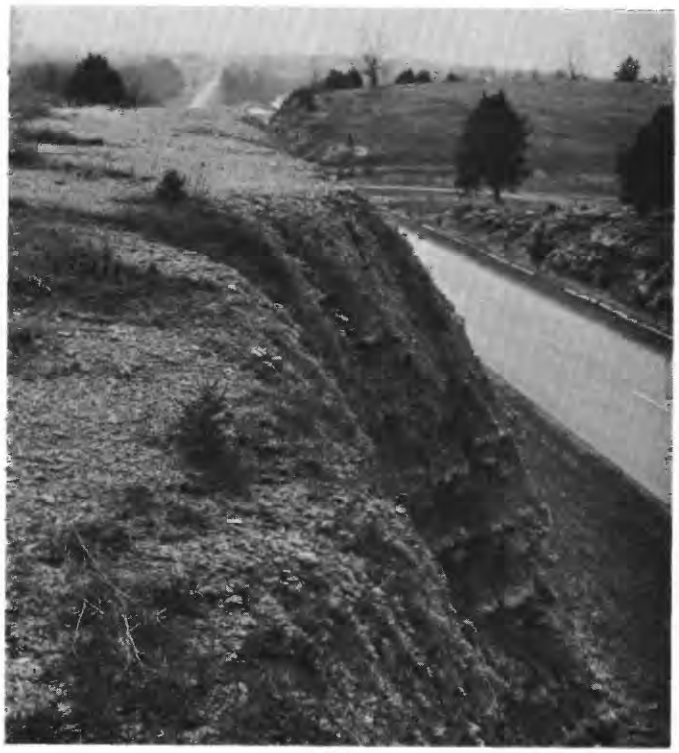

C

FIGURE 4.—Nodular-bedded fossiliferous limestone and mudstone lithofacies. *A*, nodular-bedded fossiliferous limestone and mudstone lithofacies. Brunton compass near bottom of photograph gives scale. Kentucky Highway 1449 about 2 miles southeast of Maysville, Ky. *B*, crossbedded limestone and nodular-bedded fossiliferous limestone and mudstone lithofacies. Roadcut on Oakley-Pebble road about 9 miles north of Owingsville, Ky. *C*, nodular-bedded fossiliferous mudstone lithofacies. Roadcut on U.S. Highway 27 about 4½ miles north of Stanford, Ky.

sedimentary structures. For example, the dolomitic mudstone lithofacies seem to be less muddy and more dolomitic in the south than in the north. Reddish tints occur sporadically in dolomitic mudstone lithofacies near Maysville, Ky. Ripple marks, especially large-scale ripple marks, and thin lenses of gently crossbedded limestone are more frequent north than south of Owingsville, Ky. Mudcracks have been found only in the dolomitic mudstone lithofacies and the micrograined limestone lithofacies.

DEPOSITIONAL HISTORY

The lithofacies shown diagrammatically on figure 2 were deposited on a shelf in an inland sea that, in the south, was shallower and was closer to a source of the

A

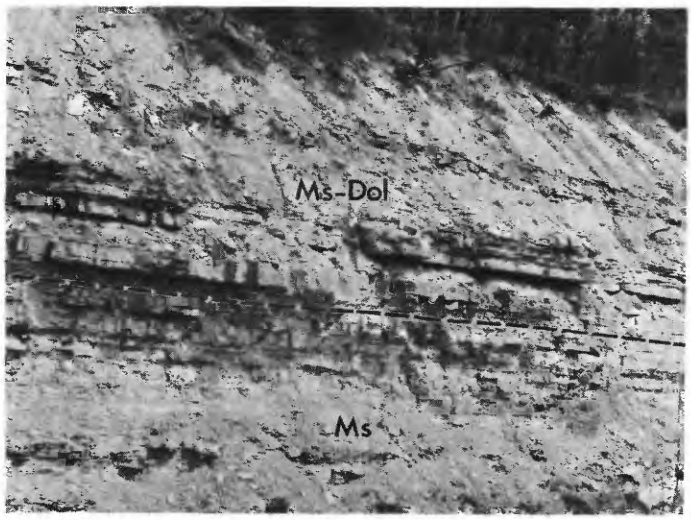

B

FIGURE 5.—Micrograined limestone lithofacies (Ls), calcitic dolomitic mudstone lithofacies (Ms), and dolomitic mudstone and dolomite lithofacies (Ms-Dol). *A*, U.S. Highway 27, about 4 miles north of Stanford, Ky. *B*, Louisville and Nashville Railroad cut near Agawam, about 4 miles southeast of Winchester, Ky. Ledge near middle of photo is about 1.2 feet thick.

admixed clay and silt. The dolomitic mudstone lithofacies are interpreted as very shallow quiet-water deposits, probably laid down on extensive flats. The micrograined limestone lithofacies was laid down in a similar environment, probably tide-level lagoons, relatively free of terrigenous material. The bedding and abundant abraded fossils of nodular-bedded limestone and mudstone lithofacies reflect a higher energy environment, possible wave-agitated shoals on the sloping shelf. The more regular bedding and abundant fossils of the planar-bedded limestone and mudstone lithofacies are probably indicative of intermittently wave-disturbed sediments deposited in more protected, perhaps deeper water.

The line of section of the diagram roughly parallels the line of outcrop and seems to be nearly perpendicular to the regional strike of the Upper Ordovician sedimentary basin. A regional picture of the rock relations is needed to work out the depositional history of the basin, but a few preliminary inferences can be made. Several lithofacies pinch out near Owingsville, Ky., suggesting that this area was a narrow zone of transition and that to the south the shelf was more shallow. Interlayering of contrasting lithofacies indicates that during the Late Ordovician there were at least two significant transgressions and regressions of the sea in the southern part of the region.

REFERENCES

Palmquist, W. N., Jr., and Hall, F. R., 1961, Reconnaissance of ground-water resources in the Blue Grass region, Kentucky: U.S. Geol. Survey Water-Supply Paper 1533, 39 p.

Peck, J. H., 1966, Upper Ordovician formations in the Maysville area, Kentucky: U.S. Geol. Survey Bull. 1244–B, 30 p.

Weir, G. W., Greene, R. C., and Simmons, G. C., 1965, Calloway Creek Limestone, Ashlock and Drakes Formations (Upper Ordovician) in south-central Kentucky: U.S. Geol. Survey Bull. 1224–D, 38 p.

Weiss, M. P., and Sweet, W. C., 1964, Kope Formation (Upper Ordovician), Ohio and Kentucky: Science, v. 145, p. 1296–1302.

Weller, J. M., 1958, Stratigraphic facies differentiation and nomenclature: Am. Assoc. Petroleum Geologists Bull., v. 42, p. 609–639.

LATE PLIOCENE LAGOMORPHS OF THE SAN PEDRO VALLEY, ARIZONA

By JOE S. DOWNEY, Grand Forks, N. Dak.

Abstract.—The Benson local fauna from the San Pedro valley of Arizona contains fossil rabbit material assignable to the genera *Hypolagus, Notolagus, Nekrolagus?*, and a new genus, *Aluralagus*, which appears to be related to the genus *Pratilepus* from the Pliocene Rexroad fauna of Kansas. *Sylvilagus? bensonensis* Gazin is reassigned to the new genus *Aluralagus*. A late Pliocene age is suggested for the Benson local fauna.

For many years the Pliocene and Pleistocene nonmarine sedimentary deposits in the San Pedro valley of southern Arizona have been attractive as a collecting area to workers in the field of vertebrate paleontology. Specimens belonging to many different orders have been recovered by field parties of several institutions throughout the United States. During the past few years the deposits have yielded a quantity of fossil material to collectors from the University of Arizona at Tucson.

Recent work by Gray (1967) in the San Pedro valley indicates that the deposits are a continuous succession of lacustrine sediments composed mainly of silt, clay, fine sand, and freshwater limestone with minor interbedded pyroclastic units. The fine-grained sediments constitute a distinct lithologic unit and the name St. David Formation was proposed by Gray. His work also indicated that the fossil localities in the San Pedro valley are near the top of the sedimentary sequence, and it is possible that additional exploration in the area may uncover pre-late Pliocene fossil assemblages.

Two general areas, both near the south end of the valley, have been particularly productive of fossil material, and the one near the town of Benson, Ariz. (fig. 1) is the source of the material described in this report.

This area, termed the Benson locality in Gazin's paper (1942), but referred to as the Post Ranch locality by Gray, is on the west side of the valley and approximately 1.8 miles south of the town of Benson (SE¼ sec. 21, T. 17 S., R. 20 E., Gila and Salt River base line and meridian). Several sites within the area yield fossil material, and most of these sites have been worked in the past (Gidley, 1922; Gazin, 1942). The other fossil-producing area in the valley is approximately 11 miles south of the town of Benson and 3 miles east of the town of St. David (NW¼ sec. 25, T. 18 S., R. 21 E.) and is referred to as the Curtis Ranch locality (Gazin, 1942; Lance, 1960). This area also has produced a large quantity of fossil material in the past. The fossil rabbit material that has been recovered recently from the Curtis Ranch locality will be the subject of a later report.

FIGURE 1.—Index map of Arizona, showing fossil lagomorph localities in the San Pedro valley.

A full description of both fossil localities, as well as photographs of the Curtis Ranch site, is given by Gazin (1942). Additional information and a brief description of both localities, as well as data concerning the geology of the area, are given in Gray's work.

The University of Arizona has assigned numbers 25 and 47 to the Curtis Ranch and Benson fossil localities, respectively. A full description and the location, keyed to the locality numbers, of each known fossil-producing site in the San Pedro valley are given in the paleontological record of the University of Arizona.

Four genera of fossil rabbits are tentatively recognized in this new material from the Benson locality, one of which is referred to the new genus *Aluralagus*. In general, the material consists of isolated teeth and fragmentary maxillary specimens. The material is well preserved and easily cleaned for study.

The fossil rabbit specimens from the San Pedro valley show an interesting variation in color, which helps in determining the locality of origin for some of the older specimens or material collected by local amateur collectors. Specimens from the Benson locality are usually a buff or ivory, whereas the specimens from the Curtis Ranch area are dark, almost black, with small surface cracks filled with calcareous material.

All material, except as noted, referred to in this report is a part of the paleontological collection of the University of Arizona at Tucson. Drawings of the fossil material described are shown in figure 2 and the dimensions are given in table 1.

Acknowledgments.—I am deeply indebted to Dr. John F. Lance, of the Department of Geology, University of Arizona, for the loan of the fossil rabbit material (contribution 167 in the program in geochronology of the Geochronology Laboratory, University of Arizona) described in this report, and for his help and encouragement with my study of fossil rabbits. I would also like to thank Dr. Claude W. Hibbard, of the Museum of

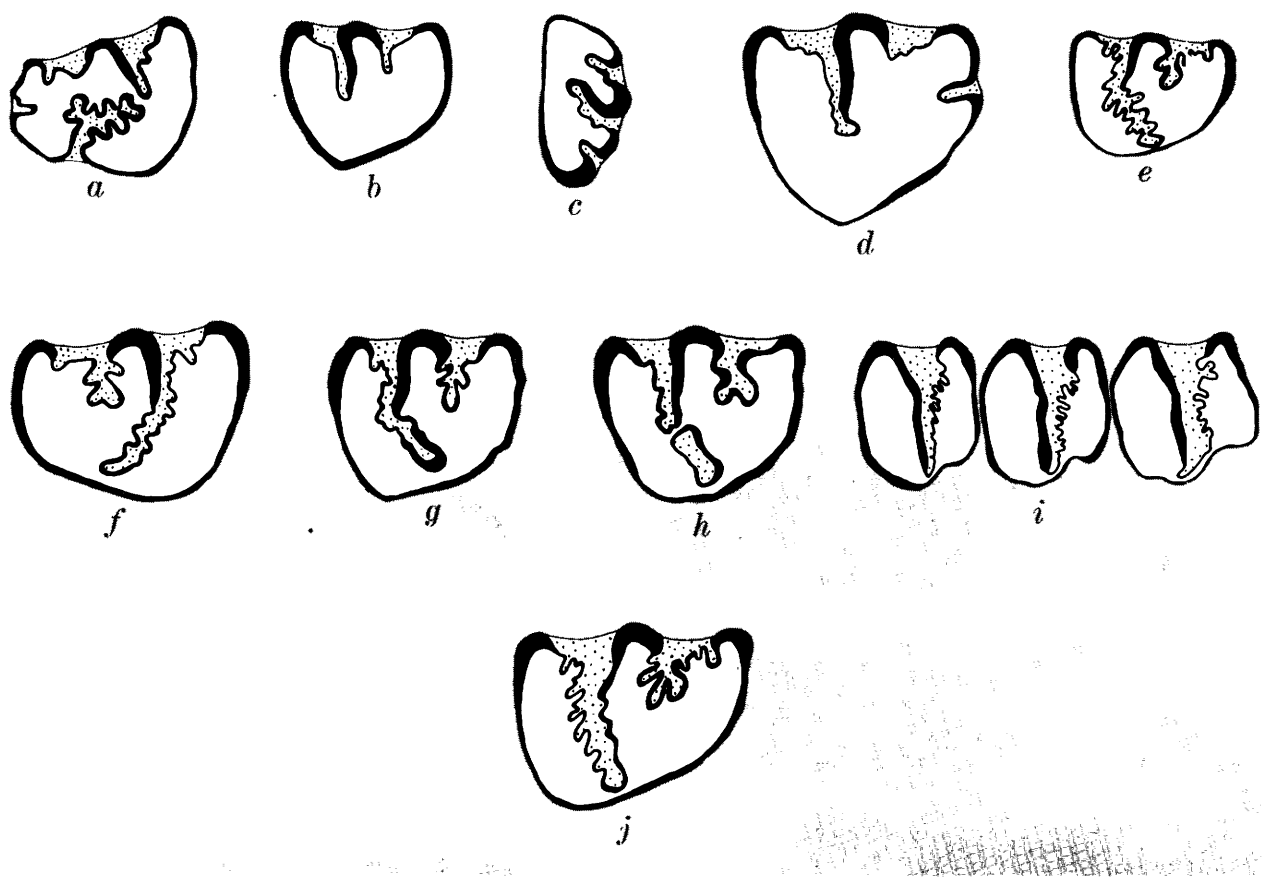

FIGURE 2.—Enamel patterns of the cheek teeth of the various genera of lagomorphs from the Benson local fauna. *a*, *Notolagus* cf. *N. velox*, RP_3, University of Arizona specimen 1434; *b*, *Hypolagus* near *H. limnetus*, LP_3, UA 1458; *c*, *Aluralagus bensonensis*, RP^2, UA 1432; *d*, *Nekrolagus?* sp., LP_3, UA 1504; *e*, *Aluralagus bensonensis*, RP_3, UA 1457, enamel pattern at base of tooth; *f*, *Aluralagus bensonensis*, RP_3, UA 1454; *g*, *Aluralagus bensonensis*, RP_3, UA 2575, enamel pattern at base of tooth; *h*, *Aluralagus bensonensis*, RP_3, UA 2576, enamel pattern at base of tooth; *i*, *Aluralagus bensonensis*, RP_4 to RM_2, UA 1456; *j*, *Aluralagus bensonensis*, RP_3, UA 1456, enamel pattern at base of tooth. Patterns *a*, *e*, and *f* are approximately ×11; patterns *b*, *c*, *d*, *g*, *h*, and *j* are approximately ×10; and pattern *i* is approximately ×7.

TABLE 1.—*Dimensions of cheek teeth of fossil lagomorphs from the Benson local fauna, San Pedro valley, Arizona*

	Specimen [1] and tooth type	Dimensions (millimeters)	
		Anteroposterior	Transverse
1432	RP^2 [2]	1. 22	2. 16
1434	RP_3	2. 31	2. 21
1454	RP_3	2. 90	2. 50
1456	RP_3	3. 05	2. 50
	RP_4	2. 31	2. 82
	RM_1	2. 40	2. 70
	RM_2	2. 52	2. 61
1457	RP_3	1. 95	1. 39
	[2] RP_3	2. 34	1. 78
1458	LP_3	2. 39	2. 28
1504	LP_3	3. 31	3. 06
2574	RP_3	2. 70	2. 50
2575	RP_3	2. 50	2. 40
2576	[2] RP_3	2. 70	2. 20

[1] University of Arizona specimen numbers.
[2] Measurement at base of tooth.

Paleontology, University of Michigan, and Dr. George Lammers, of the Department of Geology, University of Arizona, for their suggestions and help during the course of this study.

SYSTEMATIC DESCRIPTIONS

Order LAGOMORPHA Brandt, 1855
Family LEPORIDAE Gray, 1821
Subfamily LEPORINAE Trouessart, 1880

Genus *ALURALAGUS*, n. gen.

Type species.—*Aluralagus bensonensis* (Gazin). An incomplete left lower jaw with P_3 to M_1. U.S. National Museum 16595.

Generic characters.—Anterior and posterior external enamel reentrants of P_3 deep and complex. Posterior enamel walls of the posterior external reentrant of P_3 crenulated. Posterior external enamel reentrant on P_3 crosses almost the entire occlusal surface of the tooth. Anterior external enamel reentrant of P_3 crosses over one-fourth of the occlusal surface of the tooth and consists of a series of deep folds. Anterior enamel reentrant absent on the anterior face of P_3. Upper P^2 with three anterior folds on the anterior face. Posterior enamel walls of P_4 to M_1 crenulated. Size near that of *Pratilepus kansasensis* Hibbard.

Aluralagus bensonesis (Gazin)

Figure 2*c*, *e–j*

1942. *Sylvilagus*? *bensonensis* Gazin. U.S. Natl. Mus., Proc., v. 92, no. 3155, p. 492.

Holotype.—Incomplete left lower jaw with P_3 to M_1, USNM 16595.

Topotypes.—Incomplete right lower jaw with P_3 to M_2, UA 1456; incomplete right lower jaw with P_3 and P_4, UA 1454; right P_3, UA 1457; all from locality 47–1. Right P_3, UA 2574; right P_3, UA 2575 and right P_3, UA 2576; right P^2, UA 1432; all from locality 47.

313-005 O—68——12

Geologic age and distribution.—Benson local fauna. Late Pliocene of south-central Arizona.

Specific characters.—Anterior and posterior external enamel re-entrants of lower P_3 deep and complex. Posterior enamel walls of the posterior external reentrant of lower P_3 crenulated. P^2 with three enamel folds on the anterior face (fig. 2*c*). Posterior enamel walls of lower P_4 to M_2 crenulated (fig. 2*i*). Posterior external reentrant of lower P_3 crosses almost the entire occlusal surface of the tooth. The anterior external enamel reentrant of lower P_3 crosses over one-fourth of the occlusal surface and consists of a series of complex folds (fig. 2*j*). Size near that of *Pratilepus kansasensis* Hibbard (1939).

Comparison.—*Aluralagus bensonensis* differs from the species of *Lepus* and *Sylvilagus* in that the lower P_3 of *A. bensonensis* does not display the anterior reentrant on lower P_3 that is characteristic of the lower P_3 of these genera. Besides, the posterior external enamel reentrant is directed in most P_3's more anteriorly. In addition, the anterior external enamel reentrant on lower P_3 of *A. bensonensis* is deeper and more complex than that found on the same tooth in *Sylvilagus* and *Lepus*.

Aluralagus bensonensis differs from *Pratilepus kansasensis* Hibbard of the Pliocene Rexford fauna (Hibbard, 1939; 1941) by rarely showing on lower P_3 an internal enamel lake or fold (fig. 2*h*). However, the deep complex posterior external reentrant on lower P_3 is considered to be a feature resulting from the union of the posterior external enamel reentrant with an internal enamel fold. *A. bensonensis* is similar in most characters to *P. kansasensis* except that the posterior external reentrant on the lower P_3 of *A. bensonensis* nearly crosses the occlusal surface of the tooth and is more complex than what is found on the lower P_3 of *P. kansasensis* (fig. 2*j*).

Discussion.—At the time of the original description, which was based on only one specimen, *Aluralagus bensonensis* was questionably assigned to the genus *Sylvilagus* by Gazin. However, he pointed out in his paper that the one specimen of *A. bensonensis* may represent a form generically distinct from *Sylvilagus*. Later, Dawson (1958) suggested, in her work on fossil rabbits, that *A. bensonensis* may be an aberrant individual from a population of *Pratilepus kansasensis*. Other workers have avoided the question of the correct generic assignment in regard to *A. bensonensis* because of lack of material.

The enamel pattern displayed on the occlusal surface of the lower P_3 of *A. bensonensis* shows several major features that are not found on the same tooth in *Sylvilagus;* features such as the deep, crenulated anterior and posterior external reentrants. In addition, the lower P_3

of *Sylvilagus* shows an anterior enamel reentrant that is not present on any of the specimens assigned to *A. bensonensis*. The presence or absence of an anterior enamel fold on lower P_3 appears to be a valid taxonomic character in Pliocene and Pleistocene rabbits and may be used to differentiate fossil specimens of *Sylvilagus*, *Lepus*, and *Nekrolagus* from the genera *Pratilepus* and *Aluralagus*.

Aluralagus bensonensis is considered to be an advanced form of *Pratilepus kansasensis*, a fossil rabbit found in the Pliocene Rexroad fauna of Kansas (Hibbard, 1939; 1941). The differences between the two genera are similar to those that have been noted to have occurred in the *Nekrolagus–Lepus* line of descent (Hibbard, 1963); namely, the joining of the posterior external reentrant on lower P_3 with an internal enamel lake or fold, thus forming a deep enamel reentrant that crosses nearly the entire occlusal surface of the tooth. The deep posterior external reentrant on the lower P_3 of *A. bensonensis* appears to have developed by a similar but independent (Hibbard, 1963, p. 12) process, being derived from the union of the posterior external enamel reentrant and the internal enamel lake on the lower P_3 of *P. kansasensis*. This union must have occurred in the ancestral population of *A. bensonensis* during the time of the Rexroad fauna (Hibbard, 1963, figs. 2*d* and 2*e*). Apparently, the gene combination producing the deep posterior external enamel reentrant was well established in the rabbit population at the time of the Benson local fauna because specimens showing the internal enamel lake or fold on lower P_3 are rare.

Genus *NEKROLAGUS* Hibbard, 1939

Nekrolagus? sp.

Figure 2*d*

One isolated lower P_3, UA 1504, from the Benson local fauna is tentatively assigned to the genus *Nekrolagus*. This assignment is based mainly on the presence of an anterior enamel fold on the anterior face of lower P_3 (fig. 2*d*). The presence of an anterior enamel fold on the anterior face of lower P_3 appears to be a characteristic of the genera *Nekrolagus*, *Sylvilagus*, *Caprolagus*, *Oryctolagus*, and *Lepus* (Hibbard, 1963).

It is possible that this specimen represents a group of rabbits, which were a fringe population of the genus *Nekrolagus*, that became isolated in the San Pedro valley of Arizona during the late Pliocene before the gene combination producing the typical *Lepus* pattern could become firmly fixed in the population.

Additional material of this form is required in order to make a more definite assignment.

Subfamily ARCHAEOLAGINAE Dice, 1929
Genus *HYPOLAGUS* Dice, 1917

Hypolagus near *Hypolagus limnetus* Gazin

Figure 2*b*

One specimen, a lower P_3, UA 1458, from the Benson local fauna probably represents a small rabbit similar to *Hypolagus limnetus* Gazin (1934) from the Hagerman fauna of southern Idaho. The tooth is roughly triangular in outline and slightly smaller than the same tooth in *H. limnetus;* however, the enamel patterns displayed by both forms are similar.

Both the Benson specimen and *H. limnetus* display a relatively deep posterior external enamel reentrant on lower P_3 that crosses nearly half the occlusal surface of the tooth. The anterior external enamel reentrant of lower P_3 of both forms is deeper transversally than the reentrants normally displayed by specimens assigned to the genus *Hypolagus*.

Hypolagus arizonensis Downey (1962) of the Tusker fauna (Wood, 1963) from near Safford, Ariz., displays features on lower P_3 that are similar to features found on this specimen from the Benson local fauna, such as the deep anterior external reentrant and the deeper posterior external reentrant. The Tusker fauna is considered to be middle Pleistocene in age, and it is quite possible that this specimen represents a population of rabbits living in the San Pedro valley that were ancestral to *H. arizonensis*.

The genus *Hypolagus* was reported to occur in the Benson fauna by Gazin (1942), but limited and fragmentary material prevented specific assignment of the specimens.

Genus *NOTOLAGUS* Wilson, 1937

Notolagus cf. *N. velox* Wilson

Figure 2*a*

A lower P_3, UA 1434, collected in the Benson area from locality 47–8, appears to be very similar to specimens assigned to the genus *Notolagus*. *Notolagus* is reported to occur in the Yepomera local fauna from Mexico (Wilson, 1937) and the Rexroad fauna of Kansas (Hibbard, 1939). The Benson specimen displays a somewhat more complex enamel pattern on the occlusal surface of P_3 than that found in *Notolagus lepusculus* (Hibbard) and is more like *N. velox* Wilson. In addition, the specimen shows an anterior enamel reentrant on the anterior face of P_3 that is not reported to occur in other specimens assigned to the genus *Notolagus*. This is considered as a variation. The assignment of this specimen to the genus *Notolagus* is based mainly on the complex anterior internal enamel reentrant shown on the occlusal surface of lower P_3 and on the general elongation of the tooth.

REFERENCES

Dawson, M. R., 1958, Later Teritiary Leporidae of North America: Univ. Kansas Paleont Contr., Vertebrata, art. 6, p. 1–75.

Downey, J. S., 1962, Leporidae of the Tusker local fauna from southeastern Arizona: Jour. Paleontology, v. 36, no. 5, p. 1112–1115.

Gazin, C. L., 1934, Fossil hares from the late Pliocene of southern Idaho: U.S. Natl. Mus. Proc., v. 83, no. 2976, p. 111–121.

——— 1942, The late Cenozoic vertebrate faunas from the San Pedro valley, Arizona: U.S. Natl. Mus. Proc., v. 92, no. 3155, p. 475–517.

Gidley, J. W., 1922, Preliminary report on fossil vertebrates of the San Pedro valley, Arizona, with descriptions of new species of Rodentia and Lagomorpha: U.S. Geol. Survey Prof. Paper 131–E, p. 119–131.

Gray, R. S., 1967, Petrography of the upper Cenozoic nonmarine sediments in the San Pedro valley, Arizona: Jour. Sed. Petrology, v. 37, no. 3, p. 774–789.

Hibbard, C. L., 1939, Four new rabbits from the upper Pliocene of Kansas: Am. Midland Naturalist, v. 21, no. 2, p. 506–513.

——— 1941, Mammals of the Rexroad fauna from the upper Pliocene of southwestern Kansas: Kansas Acad. Sci. Trans., v. 44, p. 265–313.

——— 1963, The origin of the P_3 pattern of Sylvilagus, Caprolagus, Oryctolagus, and Lepus: Jour. Mammalogy, v. 44, no. 1, p. 1–15.

Lance, J. F., 1960, Stratigraphic and structural position of Cenozoic fossil localities in Arizona: Ariz. Geol. Soc. Digest, v. 3, p. 155–159.

Wilson, R. W., 1937, A new genus of Lagomorph from the Pliocene of Mexico: Southern Calif. Acad. Sci. Bull., v. 36, pt. 3, p. 98–104.

Wood, P. A. 1963, Pleistocene fauna from the 111 Ranch area, Graham County, Arizona: Univ. of Arizona, unpub. Ph. D. thesis, 121 p.

RESIDUAL ENRICHMENT AND SUPERGENE MIGRATION OF GOLD, SOUTHEASTERN UNITED STATES

By ARTHUR R. KINKEL, JR., and FRANK G. LESURE,
Washington, D.C.

Abstract.—Recent study of some gold deposits in the southeastern United States indicates that both near-surface residual enrichment and supergene migration of gold occur in addition to normal placer formation. Residual surface enrichment results where soil particles are removed by surface wasting on gentle slopes. Thick colluvial material or recently farmed land may not show such surface enrichment. Appreciable amounts of gold in limonite deposited by ground water in many mine areas indicate the solution and migration of gold in ground waters, especially in the presence of oxidizing sulfides. Both residual surface enrichment and the supergene transport of gold should be considered in planning a program of geochemical sampling.

Gold placers have been thoroughly studied and reported on, but examples of residual surface enrichment are sparse in the literature of gold deposits. Although geologists and chemists have found gold to be soluble in several types of naturally occurring solutions, few examples of chemically transported gold have been recognized or described. The heavy metals program of the U.S. Geological Survey has made possible the collection of a large number of samples and has provided the sensitive analytical methods necessary to accumulate some data on gold enrichment and migration. A preliminary report on these phenomena as noted in several mines in North Carolina, South Carolina, and Georgia is presented here because of the possible application to geochemical prospecting. All samples were assayed in the Geological Survey laboratories by atomic absorption techniques that detect parts per million values as low as 0.02 of gold.

RESIDUAL ENRICHMENT

Gold is residually enriched at the De Kalb prospect, 10 miles south of Kershaw in Kershaw County, S.C. The country rocks, which are exposed only in roadcuts and in a few streams, are weakly sheared rhyolite tuff and tuffaceous mudstone, rhyolitic pyroclastic rock, and rhyolite flows(?). These rocks are cut by many quartz veins and are locally altered to sericite; some contain sulfides. All the rocks have been weathered to saprolite and are less than 150 feet below the former base of the eroded coastal plain sediments (fig. 1). They were exposed to weathering before deposition of the coastal plain sediments, and also since removal of the cover of coastal plain sediments. Relief in the prospect area is generally less than 25 feet, and interfluves are rounded. The typical soil profile comprises 0 to 1 foot of gray soil and plant debris (A zone) underlain by 2 to 5 feet of red clayey soil (B zone) which grades into saprolite (C zone). In parts of the area, however, the red clayey soil is transported material, and a thin layer of angular quartz chips and a few rounded pebbles occur between the red soil and the saprolite. This coarse detrital material appears to represent local channels on saprolite, but it is not clear whether these are related to the first or second erosion cycle. Both the top gray soil (A zone) and the red soil (B zone) contain fine-grained gold, but the richest concentrations, as much as 4.4 ppm of gold, are in the discontinuous layer of quartz chips and pebbles at the base of the B zone. The source of the gold is not known with certainty. It may be from disintegration of the numerous quartz veins, as free gold was seen in two fragments of vein quartz. Most of the gold is fine grained, ragged, and unworn, and appears to be corroded. Gold from the soil and from the pebble layer is concentrated along present streams.

Over much of the prospect area, samples were taken at the top of the B zone at a depth of about 8 inches, and in the same locations power-auger samples were taken at depths of 8 inches to 2½ feet and 2½ feet to 5½ feet. Samples were taken along logging roads at 100-foot intervals. The results of one series of 13 samples show a marked concentration of gold in the near-surface zone (table 1).

U.S. GEOL. SURVEY PROF. PAPER 600-D, PAGES D174-D178

TABLE 1.—*Gold, in parts per million, in samples collected at 100-foot intervals, DeKalb prospect, Kershaw County, S.C.*

Depth	Sample													Average
	1	2	3	4	5	6	7	8	9	10	11	12	13	
0 to 8 in	0.52	0.27	0.08	0.13	0.10	0.13	0.09	0.63	0.33	0.80	0.13	0.12	0.15	0.27
8 in. to 2 ft, 6 in	.04	.15	.04	.08	.13	[1].19	.19	.18	.09	.06	.18	.12	.06	.12
2 ft, 6 in. to 5 ft, 6 in	.08	.02	.08	.11	.02	.17	.03	.24	.05	.08	04	.14	.03	.08

[1] Sample with high, erratic gold content (10.5 ppm) reduced to average.

In a nearby area, 6 localities 10 feet apart along a line were sampled at depths of 0 to ½ inch and ½ inch to 8 inches (table 2).

These samples show lower values, but again the surface material contains the most gold. A pit 12 feet deep was dug in the central part of the prospect area. Samples from the pit show that gold values generally decrease with depth (table 3).

The samples shown in tables 1 and 2 were taken in an area that apparently had not been farmed. To study the effect of farming on surficial enrichment, samples were taken along a logging road in a flat area, which had been farmed, about ¼ mile west of the first sample locations. Here, A and B soil zones were not clearly differentiated, but a pit showed that a channel with quartz chips and

TABLE 2.—*Gold, in parts per million, in samples collected at 10-foot intervals, DeKalb prospect, Kershaw County, S.C.*

Depth (inches)	Sample						Average
	1	2	3	4	5	6	
0–½	0.02	0.06	0.07	0.05	0.13	0.02	0.06
½–8	.02	.04	.02	.02	.08	.03	.03

TABLE 3.—*Samples from pit dug in central part of DeKalb prospect, Kershaw County, S.C.*

Soil zone	Depth (feet)	Gold (ppm)
A	0–1	0.23
B	1–3	.09
Saprolite	3–5	.14
	5–7	.07
	7–9	.05
	9–12	.03

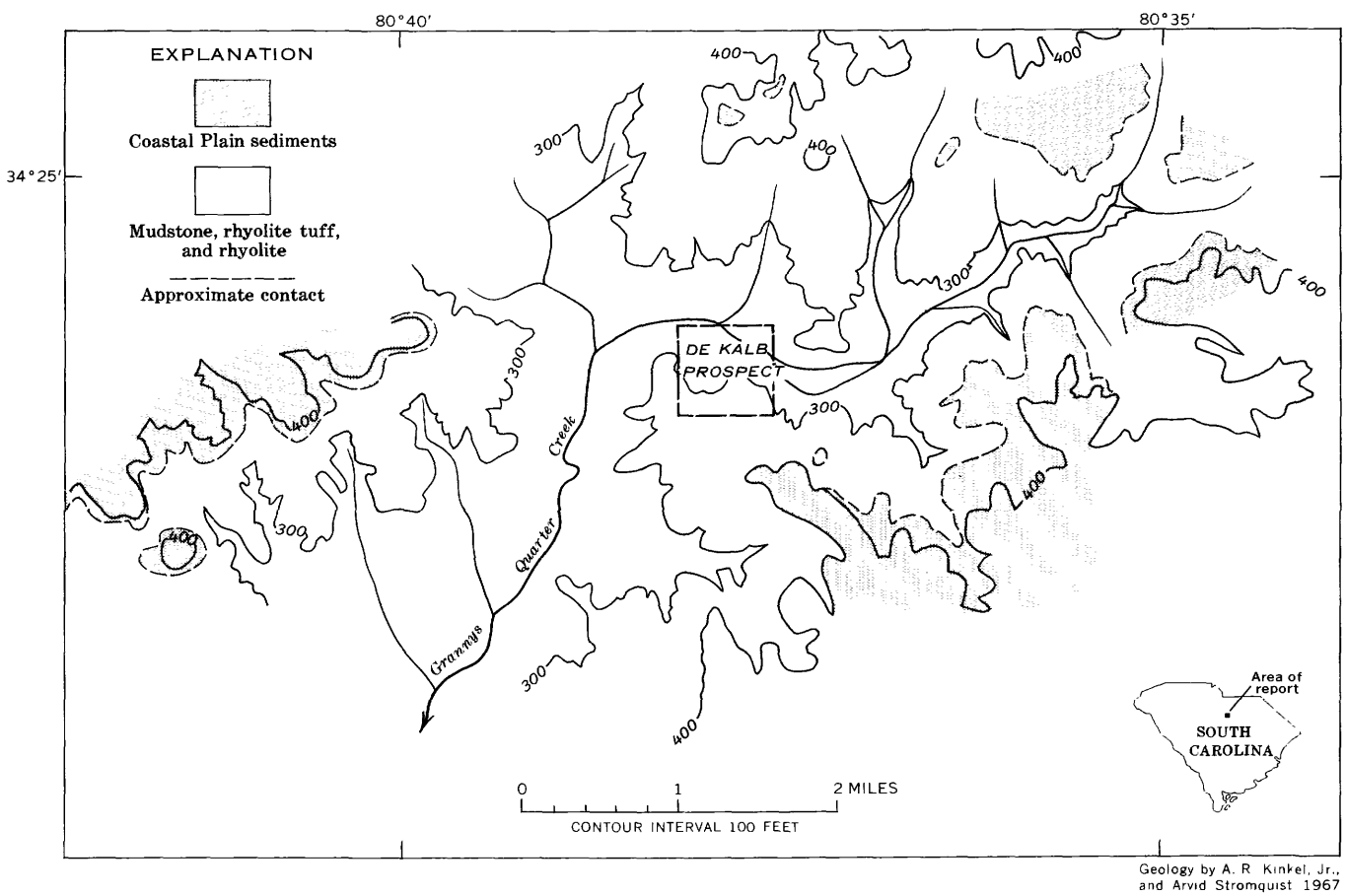

FIGURE 1.—Generalized geologic map of the De Kalb gold prospect area, Kershaw County, S.C. Base from Camden quadrangle, South Carolina, 1935 (15 min.).

pebbles, and gold, occurs on top of saprolite. In this area samples at 0 to 8 inches contained less gold than those from 8 inches to 2½ feet (table 4). Disturbance of the soil profile during farming apparently lowered the gold values in the uppermost soil zone and probably resulted in enrichment of the 8-inch to 2½-foot zone.

Analyses for copper and arsenic were made on all samples in the prospect area. No correlation between these metals and gold or depth was found.

Not all areas show residual enrichment at the surface. A section of colluvial material about 17 feet thick was sampled in a roadcut on Georgia State Highway 9E about 200 feet downslope from the Whim Hill gold mine near Auraria, Lumpkin County, Ga. The original topographic surface above the roadcut is moderately steep. The colluvium is a poorly sorted mixture of clay, sand, and pebbles derived from mica and hornblende schist saprolite and vein quartz. Most of the coarse gravel is concentrated in the lower 2 feet. Samples taken at 0 to 1, 1 to 2, 5 to 6, 10 to 11, 15 to 16, and 16 to 17 feet below the surface were washed to remove clay and fine silt size material. The coarse silt to medium sand size material was panned. Gold was found as ¼- to 1-mm flakes or irregular pieces in all samples except in the uppermost sample. In several samples small bits of amalgam were found which probably originated as a result of the widespread use of mercury in the early days of mining. A sample of hornblende schist saprolite below the colluvial material also contained a flake of gold and some amalgam. The colluvial section appears undisturbed, and the presence of amalgam in some of the samples indicates downward movement of mercury since mining began in the nineteenth century. The lack of gold in the surface sample may be the result of solifluction of colluvial material on a steeper slope.

Along the so-called gold belts of the southeastern United States, quite large but shallow opencuts were mined for gold. With a few exceptions these were largely in soil and extended only a few feet into the solid saprolite. In most places mining consisted of washing gold out of the soil cover and uppermost layer of soft saprolite, commonly by hydraulic methods. Samples from some of these pits show that they contain very low values in the walls and bottom and that the material remaining could not be mined profitably under the most favorable conditions. It seems probable that in the pit areas gold released during weathering of quartz veinlets and sulfides was concentrated in near-surface soil. In the Morganton district, North Carolina, for example, rich stream placers developed below these zones of widely spaced thin quartz veinlets, and large shallow pits were also mined in residual soil on hillsides. Most of the quartz veinlets that furnished the gold are too small and widely spaced to constitute ore without concentration by weathering processes.

TABLE 4.—*Gold, in parts per million, in samples collected at 100-foot intervals along a logging road in a previously farmed area*

Depth	Sample							Average
	1	2	3	4	5	6	7	
0 to 8 in	0.08	0.05	0.06	<0.02	<0.02	0.25	<0.02	0.06
8 in. to 2 ft, 6 in	.05	.38	.23	.22	.15	.05	.01	.17
2 ft, 6 in. to 5 ft, 6 in	.02	.02	.03	.03	.04	.05	<.02	.03

SUPERGENE ENRICHMENT

Gold is soluble in several types of naturally occurring solutions, especially in the presence of oxidizing sulfides (Brokaw, 1910; Cloke and Kelly, 1964). During the oxidation of pyrite and other iron-bearing sulfides, some iron remains to form limonite pseudomorphs or boxworks, but some migrates in ground water. Where iron-rich solutions move into open channels or spaces, hydrous iron oxides collect and form massive, laminated, or botryoidal vein fillings, surface coatings, or even stalactites. Gold associated with pyrite in quartz veins is freed during oxidation. Some remains as free gold particles in the iron-stained quartz, but some may be removed either in solution or as a colloid in the iron-rich ground water.

This supergene solubility and movement of gold is illustrated at the Calhoun mine, Lumpkin County, Ga. Fresh limonite mud forms a coating on the wall of a 500-foot adit driven 50 feet below an old stope sometime in the late 1930's or early 1940's. The limonite mud assayed 2.9 ppm of gold; the wallrock under the limonite is a quartz-biotite-muscovite schist containing about 0.1 percent pyrite and no detectable gold. Solutions depositing limonite are oozing out of fractures in the wallrock opened during mining. The area of limonite accumulation in the adit is below the old stope; joints in the vicinity of the limonite possibly intersect the stope (fig. 2).

The footwall of the stope near the northeast face is also coated with fresh limonite that assays 0.14 ppm of gold. However, samples of the country rock and of the main quartz vein in the face contain no detectable gold. A sample of the same quartz vein in a pillar in the stope to the southwest assayed 0.38 ppm, and a sample of possibly the same vein in the opencut above the stope assayed 0.60 ppm of gold.

Fresh pyrite is present in the unweathered schist and quartz veins in the lower part of the stope, but no sulfides are present in saprolite of the opencut or upper levels of the stoped area. Gold is apparently being taken into solution during the oxidation of pyrite in the stope area and is being transported and redeposited

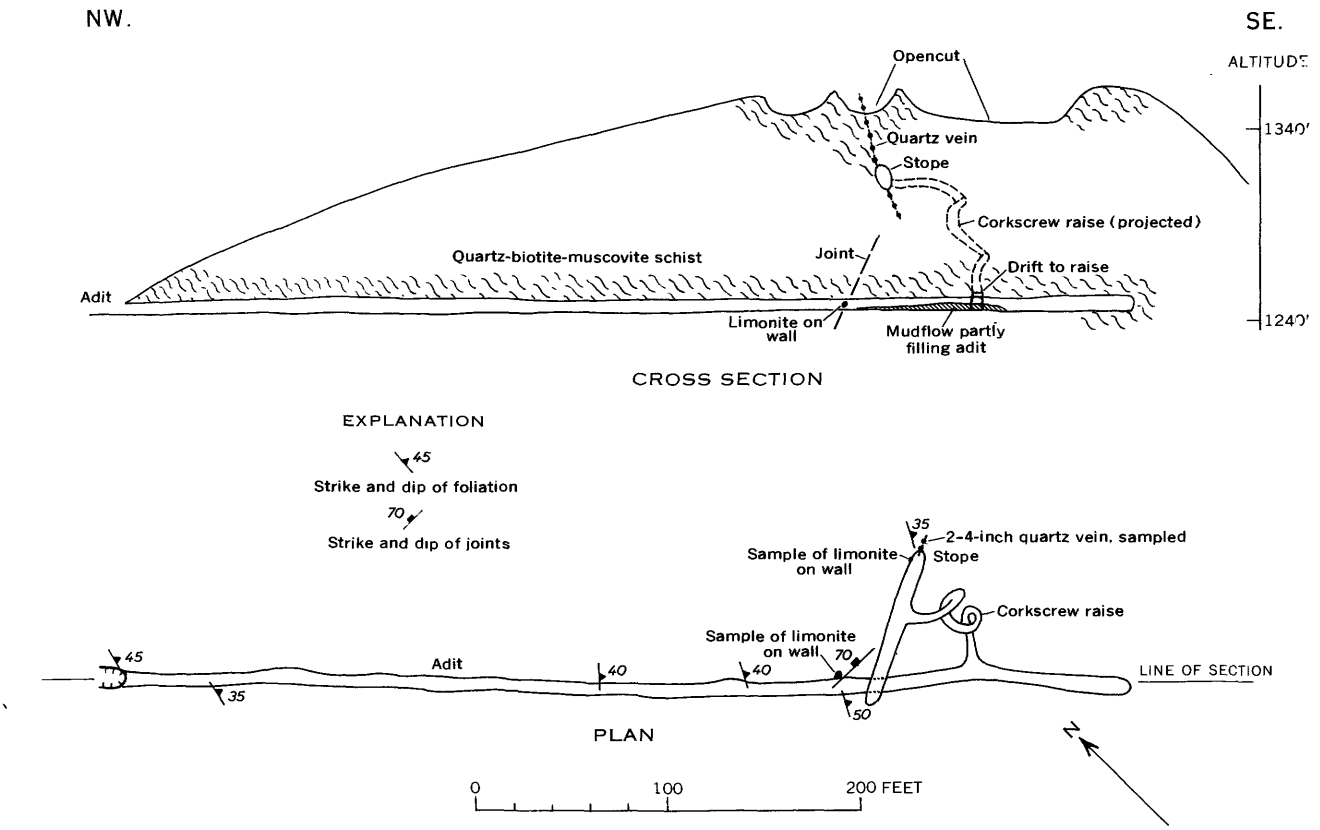

FIGURE 2.—Geologic plan and cross section of lower adit and stope, Calhoun mine, Lumpkin County, Ga. Mapped by F. G. Lesure and J. W. Whitlow, 1967.

with fresh limonite where the iron-rich ground water is exposed to air in the adit below the stope.

The following examples from other mines indicate that this process is not uncommon:

At the Jones Keystone mine, Randolph County, N.C., gold occurs in silicified sheared rhyolite which is cut by numerous veinlets of transported limonite. Two of these supergene limonite seams assayed 1.4 and 0.9 ppm of gold, respectively.

The Russell mine in Montgomery County, N.C., contains gold in strongly silicified, pyritized, thin-bedded tuffaceous(?) sediments. The sediments, which dip steeply, are cut by flat joints containing transported limonite and limonite-manganese veinlets. A limonite seam 2 inches thick contains 2.4 ppm of gold. A limonite and clay seam 4 inches thick contains 2.0 ppm of gold. A veinlet of manganese oxide and limonite 4 inches thick contains 0.4 ppm of gold.

The Haile mine, Lancaster County, S.C., is highly silicified, sheared, thin-bedded rhyolite tuff and pyroclastic rhyolite. Ore is of two types; highly silicified pyritized rock and massive pyrite ore replacing rhyolite. The massive pyrite ore is exposed in the walls of a large opencut, and is cut by large, irregular, generally sharp walled veins of supergene limonite. The limonite is banded and botryoidal, and the veins appear to die out about 50 feet below the land surface. The massive sulfide ore in the area of limonite veins averages 0.7 ppm of gold, whereas the limonite veins average 2.1 ppm of gold.

CONCLUSIONS

Both the residual surface concentration and the supergene movement of gold are important in any exploration program for gold in the southeastern United States. Gold is concentrated in the upper layers of the soil profile by removal of soil particles during surface runoff. Because of this enrichment, samples from the top few inches of soil give a better contrast between anomalous and background gold values than deeper samples. Halos of gold in soil can be outlined during reconnaissance from surface samples in areas where the soil profile has not been disturbed by solifluction or farming.

The gold contained in crosscutting banded and botryoidal transported limonite seams, and in the recent limonite mud at the Calhoun mine, indicates that there is transportation of gold in the zone of weathering. All the samples of limonite that contain gold are from areas

where oxidizing sulfides are plentiful. Limonite veins outside of zones of mineralization are barren, but this may only reflect the primary absence of gold in the rock. In most roadcut samples, if the rocks contain any detectable gold, the limonite veins contain more gold than the host rock. Samples from veins of transported limonite, therefore, offer a better chance of finding an area of gold mineralization than samples from quartz veins, as mineralization in most quartz veins in the gold belts of the southeast is spotty.

REFERENCES

Brokaw, A. D., 1910, The solution of gold in the surface alterations of ore bodies: Jour. Geology, v. 18, p. 321–326.

Cloke, P. L. and Kelly, W. C., 1964, Solubility of gold under inorganic supergene conditions: Econ. Geology, v. 59, no. 2, p. 259–270.

OPAQUE MINERALS IN DRILL CUTTINGS FROM METEOR CRATER, ARIZONA

By ROBIN BRETT, Washington, D.C.

Abstract.—In the early years of this century, 25 holes were drilled in the floor of Meteor Crater, Ariz., to depths of 550–650 feet. Recently obtained deep cuttings from three of these drill holes contain nickel-iron fragments; nickel-iron spherules surrounded by glass; iron fragments; iron plus hematite and iron plus goethite intergrowths cementing sandstone grains; and magnetite and fayalite plus glass, and wüstite plus fayalite, in eutecticlike intergrowths. Electron microprobe analyses indicated that most of the metal fragments were drill steel, the rest were from the Canyon Diablo meteorite. Impact metamorphism was apparently intense to depths of 650 feet below the present crater floor.

Cuttings from 3 of 25 churn-drill holes made in the floor of Meteor Crater, Ariz., by the Standard Iron Co. in the early years of this century (Barringer, 1910) were recently obtained by E. M. Shoemaker, of the U.S. Geological Survey, from the Barringer Crater Co. One sample is from a depth of 550 feet below the crater floor (hole 17), and two are from depths of 600–650 feet (holes 20 and 22).

Polished sections prepared from the cuttings show that most of the fragments consist of quartz with minor amounts of albitic plagioclase. Both the mineralogy and the depths of the samples indicate that the samples are from the Permian Coconino Sandstone. In some samples the quartz, but not the plagioclase, has been vitrified by shock.

Grains which were either dark or were attracted to a hand magnet were examined in detail. The opaque minerals were studied by reflected-light microscopy, by X-ray diffraction methods, and by electron microprobe. The iron-nickel standards were those used by Goldstein and Ogilvie (1965). Troilite, iron-rich pyroxenes, fayalite, and chromite were used as additional microprobe standards.

Acknowledgments.—I am grateful to Frank Wood of the Goddard Space Flight Center, National Aeronautics and Space Administration, Greenbelt, Md., for help in the analytical work, and to J. I. Goldstein and Louis Walter of the same center for lending the microprobe standards.

DESCRIPTION OF OPAQUE MINERALS

The following opaque minerals were noted:

1. Apparently homogeneous iron splinters as much as 3 millimeters long and 1 mm wide. The electron microprobe showed that the metal contained no nickel, but significant amounts (as much as a few weight percent) of chromium, tungsten, and manganese. As such a composition is completely foreign to meteorites but is typical of drill steel, it seems reasonable to conclude that these splinters were abraded from the drill bit.

2. Nickel-iron splinters as much as 1.5 mm long and 0.5 mm wide. These particles, 5–10 microns in size, contain as much as 10 percent by volume of troilite, uniformly disseminated throughout the metal. The texture strongly resembles that formed by rapid solidification of a melt. In the two fragments analyzed, the nickel content of the metal is 16 weight percent. Locally, the metal contains a considerable amount of phosphorus, which seems to be unrelated to any inclusions. Some metal fragments are surrounded by nickeliferous magnetite rims containing 10 ± 5 weight percent of nickel. Small remnants of nickel-iron within these rims contain 40–70 weight percent of nickel. Apparently, this nickel enrichment is due to oxidation (Brett, 1967) caused by percolating ground water at a low temperature (oxides formed at a high temperature contain very little nickel, Brett, 1967). The metal-troilite intergrowths were presumably formed from impact-produced melts. If it is assumed that the total sulfur content is about 2 weight percent, impact temperatures must have reached at least 1,480° C—a temperature estimate based on Hansen and Anderko's (1958) data on the system iron-sulfur. In the iron-rich portion of the iron-sulfur system, the effect of pressure on the melting relations is not large (Brett and P. M. Bell, unpub. data). The splinterlike

shapes of the metal grains are similar to those of the drill-steel fragments and were caused by the drilling operation; but these grains are only about one-fifth as abundant as the splinters of drill steel.

3. Angular to semirounded quartz grains cemented by hematite or less commonly by goethite. In these fragments the amount of hematite and quartz are approximately equal. Rarely, the quartz grains are cemented by drill steel. The quartz must have become embedded in the bit, fragments later became detached, oxidation occurred, and most of the metal was converted to hematite.

4. Spherules (as much as 0.01 mm in diameter) and fragments (as much as 0.2 mm in maximum dimension) of nickel-iron in impact glass. The glass around the metal is dark and rich in iron; the glass away from the spherules is colorless. The iron in the glass is derived from the oxidized skin of the meteoritic metal spherules and entered it while the glass was liquid (Brett, 1967).

5. Rare fine-grained, somewhat dendritic intergrowths of magnetite and fayalite plus glass, and wüstite and fayalite. The iron in the glass ranges from 45 to 60 weight percent. The glass, fayalite, and oxide contain no detectable nickel, phosphorus, or sulfur.

6. One anhedral pyrite grain about 1 mm across. This grain was presumably present in the sandstone before the impact.

CONCLUSIONS

The following conclusions may be drawn from the study of the churn-drill cuttings:

1. The magnetite and fayalite plus glass and wüstite plus fayalite assemblages are products of meteoritic impact—impact products that have not previously been described. As neither the oxide nor the glass contains detectable nickel, the oxide was presumably derived from the virtually nickel-free oxidized material of the Canyon Diablo meteorite. This material formed a liquid with the silica of the sandstone upon impact and cooled rapidly to produce the unusual intergrowth.

2. Vitrification, oxidation, and presence of meteoritic debris in the drill-hole cuttings indicate that impact metamorphism was intense at depths as of much as 650 feet below the crater floor. Significant amounts of meteoritic material were introduced into the Coconino Sandstone at this depth.

3. Investigators should use great care to distinguish meteoritic metal from drill steel when studying drill cuttings from impact craters.

REFERENCES

Barringer, D. M., 1910, Meteor crater (formerly called Coon Mountain or Coon Butte) in northern central Arizona: Paper read before the National Academy of Sciences, Nov. 16, 1909, 24 p. [privately published 1910?]

Brett, Robin, 1967, Metallic spherules in impactite and tektite glasses: Am. Mineralogist, v. 52, nos. 5–6, p. 721–733.

Goldstein, J. I., and Ogilvie, R. E., 1965, A re-evaluation of the iron-rich portions of the Fe-Ni system: Am. Inst. Mining Metall. Engineers Trans., v. 233, no. 12, p. 2083–2087.

Hansen, Max, and Anderko, K. P., 1958, Constitution of binary alloys, 2d ed.: New York, McGraw-Hill Book Co., 1305 p.

THE UPDIP TERMINATION OF A LARGE DIKE OF WESTERLY GRANITE AND THE REGIONAL DISTRIBUTION OF THE WESTERLY AND NARRAGANSETT PIER GRANITES IN RHODE ISLAND AND CONNECTICUT

By TOMAS FEININGER, Medellín, Colombia

Work done in cooperation with the State of Connecticut Geological and Natural History Survey and the State of Rhode Island Development Council

Abstract.—The updip termination of a large dike (thickness 67 feet) of Westerly Granite in Narragansett Pier Granite is well exposed near Westerly, R.I. Observations at the updip termination suggest that the Westerly magma was initially intruded along a preexisting fracture to the site of the updip termination. Continued intrusion of magma thickened the dike, but did not extend it farther updip. Effects of deformation in the host Narragansett Pier Granite, confined to a zone around the apex of the dike, are recrystallization to pegmatite and disharmonious plastic deformation of predike platy flow structure. The fracture followed by the dike was probably a cross joint in the Narragansett Pier Granite. These observations, and the fact that the Westerly has no chilled contact, are interpreted as direct evidence that Westerly Granite is an aplitic phase of Narragansett Pier Granite. The abundance of dikes of Westerly Granite cutting the metamorphic rocks of southeastern Connecticut suggests that the Narragansett Pier Granite may extend westward at depth and have batholithic dimensions.

The co-occurrence of the Westerly and Narragansett Pier Granites, the near identity of their modal compositions, and the overlapping of their radiometric ages have suggested to some geologists that the granites are genetically related. Observations made at the updip termination of a large dike of Westerly Granite in Narragansett Pier Granite near Westerly, R.I., support this view and lead to conclusions concerning the petrogenesis of Westerly Granite and the mechanism of intrusion of the dike. Inferences are drawn from the regional distribution of the two granites as to their probable subsurface extension.

WESTERLY AND NARRAGANSETT PIER GRANITE

The Westerly and Narragansett Pier Granites are Late Pennsylvanian or younger and intrude Pennsylvanian and older metamorphic and igneous rocks.

The granites occur in an east-west belt along the south shore of Rhode Island and Connecticut from Narragansett Bay nearly to the mouth of the Connecticut River (fig. 1). The distribution of the two granites within this belt, however, is not uniform. In the east, from Narragansett Bay to the Connecticut border, Narragansett Pier Granite forms a large stock. The westernmost known extent of the Narragansett Pier is only 1.5 miles west of the Rhode Island border. The Westerly Granite, on the other hand, forms extensive dikes in Connecticut from about 4 miles east of the mouth of the Connecticut River, eastward into Rhode Island to about 6 miles east of the Connecticut border. Farther east, the Westerly is virtually absent.

Westerly Granite is a fine-grained equigranular light-gray massive rock with a subsaccharoidal texture. It is composed of light-gray to pinkish-gray anhedral feldspar, pale smoky quartz, and black biotite and is exceptionally uniform, a fact which led to its choice as the felsic rock standard G–1 (Fairbairn and others, 1951). A composite mode of the Westerly is given in table 1.

Westerly Granite occurs exclusively as dikes in southwestern Rhode Island and southeastern Connecticut. Many of these dikes strike east and dip gently south (fig.1).

Narragansett Pier Granite is medium-grained, equigranular, weakly foliated to massive, and bright pink. It is composed of subhedral crystals of pink and white feldspar, dark smoky quartz, and black biotite. Some modes of the Narragansett Pier are given in table 1. Weak foliation visible in many outcrops is a primary platy flow structure.

The Narragansett Pier Granite is largely confined to an extensive east-west stock along the Rhode Island coast. The south contact of this stock is not exposed (fig. 1).

REDSTONE RIDGE DIKE

Geologic setting and description

One of the largest dikes of Westerly Granite crops out on the hills, locally known as Redstone Ridge, northeast of the town of Westerly, R.I. Detailed mapping showed that this dike (here referred to as the Redstone Ridge dike) is not continuous on the surface, but consists of two segments separated by a section of host rock about 100 feet long. Exposures in an abandoned quarry at the east end of the west segment indicate that the two segments of the dike are continuous just beneath the surface. The updip termination of this dike, elsewhere removed by erosion, is here preserved and is well exposed in the quarry (fig. 2).

The Redstone Ridge dike strikes east and is 1.6 miles long. Near the updip termination it is 67 feet thick. The dike is well exposed, partly owing to numerous quarries that are now nearly all abandoned.

Both upper and lower contacts of the dike are exposed in several places. The contacts are broadly smooth, though in detail they are locally irregular. Their dips range from 15° to 42° S., though most are less than 25°.

The headwall of the abandoned quarry at the east end of the west segment of the Redstone Ridge dike is normal to the strike of the dike and affords a spectacular exposure of its updip termination. In the photograph of this quarry (fig. 2) a white line, painted on the rock face, follows the contact between the host Narragansett Pier Granite (above and to the left) and the Westerly Granite. The horizontal segment of the contact at the right (the apparent inclination in the photograph is an effect of perspective) is the normal upper contact and its compass direction is the strike of the dike.

TABLE 1.—*Modes of Westerly and Narragansett Pier Granites*

[Volume percent]

	1	2	3	4
Quartz	23.6	29.2	27.0	27.5
Microcline	32.6	27.9	30.0	35.4
Plagioclase (oligoclase)	37.0	34.7	35.0	31.4
Muscovite	1.0	-------	0.5	1.3
Biotite	5.2	5.9	5.5	3.2
Opaque accessories	0.6	2.4	1.0	0.8
Other accessories			-----	0.4
Total	100.0	100.1	99.0	100.0

1. Narragansett Pier Granite, Kingston quadrangle (Moore, 1964, p. E5).
2. Narragansett Pier Granite, Quonochontaug quadrangle (Moore, 1959).
3. Narragansett Pier Granite, Ashaway quadrangle (Feininger, 1964).
4. Westerly Granite, average of 16 thin sections, Carolina quadrangle (Chayes *in* Fairbairn and others, 1951, p. 61).

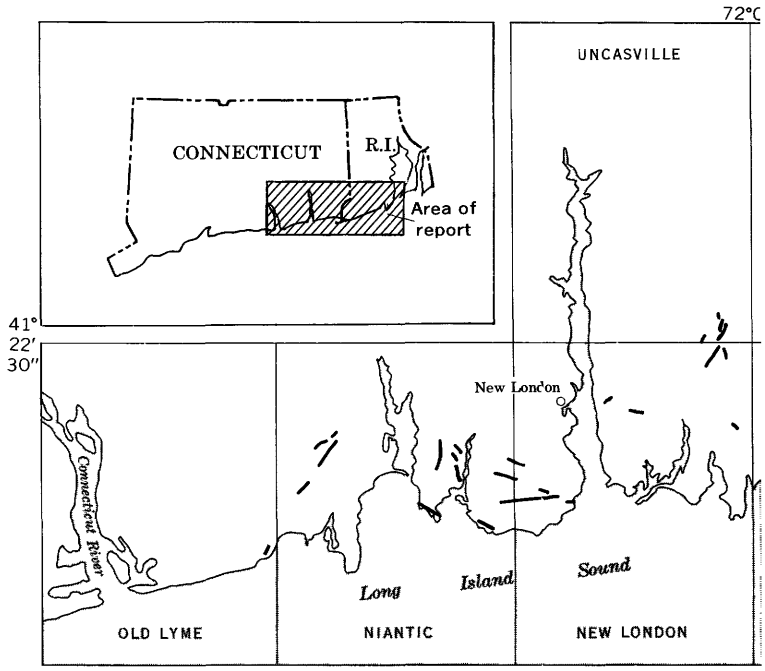

FIGURE 1.—Regional distribution of Westerly and Narragansett Pier Granites, Rhode Island and Connecticut.

The contact of the dike in this quarry differs conspicuously from the contact elsewhere along the same dike; here it is markedly more amoeboid, and apophyses, which are generally scarce and inconspicuous, are both numerous and prominent. The Westerly Granite in this quarry has no chilled border phase and no flow structure, not even at the contact. Here the Westerly is a little finer grained, but otherwise does not differ from the granite exposed in adjacent quarries in the same dike.

Deformation in the host Narragansett Pier Granite that was produced by intrusion of the dike is restricted to a small zone around the apex of the dike. Toward this zone, the Narragansett Pier Granite grades subtly into coarse bright-pink pegmatite. This pegmatite, found nowhere else along the contact, is judged to have formed by the recrystallization of the Narragansett Pier Granite, induced by deformation at the apex of the dike during intrusion of the Westerly magma. The sharp contact between the pegmatite and the dike shows

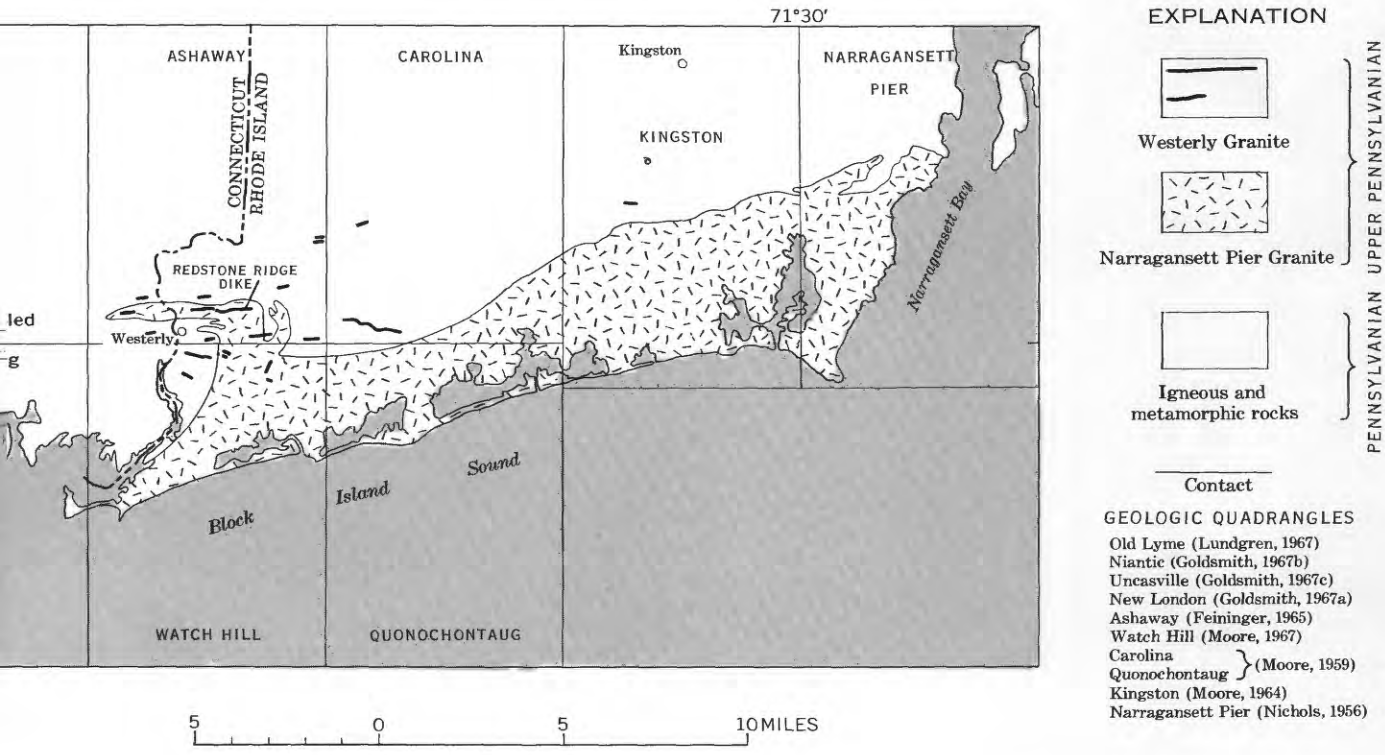

that the pegmatite formed slightly in advance of the arrival of the Westerly magma at any given point in the apical zone. Deformation in a somewhat wider zone around the apex of the dike has disturbed the weak platy flow structure of the Narragansett Pier. On Redstone Ridge this flow structure strikes east and dips uniformly 70° N. However, above the apex of the dike, adjacent to the large apophyses (fig. 3*C*), the platy flow structure is vertical. Farther north in the same exposure the flow structure dips steeply south. Under the apex (figs 3*C* and 2, lower left corner) it dips north, but more gently (35° to 40°) than the regional dip.

Mechanics of intrusion

The observations on the Redstone Ridge dike and its updip termination suggest the mechanism of intrusion schematically shown in figure 3. The initial intrusion of Westerly magma followed a planar fracture and reached the site of the updip termination as a thin sheet (fig. 3*A*). Continued intrusion of magma served to thicken the dike but did not extend it farther updip (fig. 3*B*, *C*). During intrusion the walls of the dike were forcibly pushed apart, but as integral units. Deformation was thus confined to a rather small zone around the apex of the thickening dike.

During intrusion, magma deep within the fracture, away from the termination, moved updip and largely parallel to the walls. At and near the apex, however, further updip movement of magma was not possible owing to the abrupt termination of the fracture; here, the magma moved at high angles to the walls, roughly parallel to the direction of wall dilation. Evidence of such movement could not be found in the Redstone Ridge dike, but in adjacent dikes of Westerly Granite, Balk (1937, p. 53, fig. 18) noted both platy and linear flow structures at high angles to the dike walls ("disconformable flow structures"). The updip terminations of those dikes were probably not far above the present level of exposure.

WESTERLY GRANITE AS AN APLITIC PHASE OF NARRAGANSETT PIER GRANITE

The view that the Westerly and Narragansett Pier Granites may be genetically related has, in the past, been based on such indirect evidence as their similar modal compositions (table 1), their co-occurrence (fig. 1), and the broad overlapping of their radiometric ages (Quinn and others, 1957). Relationships at the exposure of the updip termination of the Redstone Ridge dike, however, offer the first direct evidence of this. From my observations at this exposure I can further argue that the Westerly is an aplitic phase of the Narragansett Pier and was intruded immediately following the emplacement and crystallization of the Narragansett Pier magma.

FIGURE 2.—Updip termination of a dike of Westerly Granite. White line, painted on rock face, separates Westerly Granite (below) from host Narragansett Pier Granite and pegmatite. View looking east. Headwall exposure about 80 feet long. Abandoned quarry at east end of west segment of Redstone Ridge dike, Westerly, R.I.

Westerly Granite has a fine-grained equigranular subsaccharoidal texture and is poor in mafic minerals (4, table 1). It resembles aplite, and, like most aplite, it is a dike rock. The fracture along which the Redstone Ridge dike was intruded is normal to platy flow structure in the host Narragansett Pier Granite and is probably a cross joint, although absence of linear flow structure in the Narragansett Pier prevents confirmation (Balk, 1937, p. 27). Cross joints in plutons commonly are filled by late consanguinous aplites (Balk, 1937, p. 30). Even more pertinent, however, the absence of a chilled border in the Westerly, the recrystallization of the Narragansett Pier to pegmatite, and the disharmonious plastic deformation of the Narragansett Pier Granite's platy flow structure around the apex of the dike during dike thickening show that the Narragansett Pier, although completely crystallized, was still hot enough to yield plastically and to recrystallize readily in response to stresses imposed by the intrusion of the dike. It had not yet cooled enough to chill on contact the incoming Westerly magma. The Westerly by itself could not have provided the heat necessary to produce these deformational effects in the Narragansett Pier Granite. Had the Narragansett Pier long predated and been fully cooled at the time of intrusion of the Westerly, fracture effects would have governed deformation of the Narragansett Pier at the updip termination of the dike, rather than the plastic flowage and recrystallization that clearly prevailed.

The Westerly and Narragansett Pier Granites are comagmatic, and their magmas had virtually identical compositions. The Westerly magma probably was tapped from deep still-molten zones in the Narragansett Pier Granite and intruded upward to fill cross joints in the already crystallized higher portions of the Narragansett Pier and in other host rocks.

SUBSURFACE EXTENT OF NARRAGANSETT PIER GRANITE INFERRED FROM THE REGIONAL DISTRIBUTION OF WESTERLY GRANITE

Dikes of Westerly Granite are common in southeastern Connecticut and southwestern Rhode Island to about 6 miles east of the Connecticut border (fig. 1).

As an aplitic phase of Narragansett Pier Granite, the Westerly is probably restricted to high levels in the Narragansett Pier and to adjacent and overlying roof rocks. The near absence of Westerly Granite near Narragansett Bay suggests that the level of exposure there is a deeper one than that toward the Connecticut border where the two granites occur together. The abundance of dikes of Westerly Granite farther west in Connecticut suggests that Narragansett Pier Granite, not unroofed by erosion, extends westward at depth and may have batholithic dimensions. Possible effects of such a body on radiometric ages in eastern Connecticut were noted by Zartman and others (1965, p. D6).

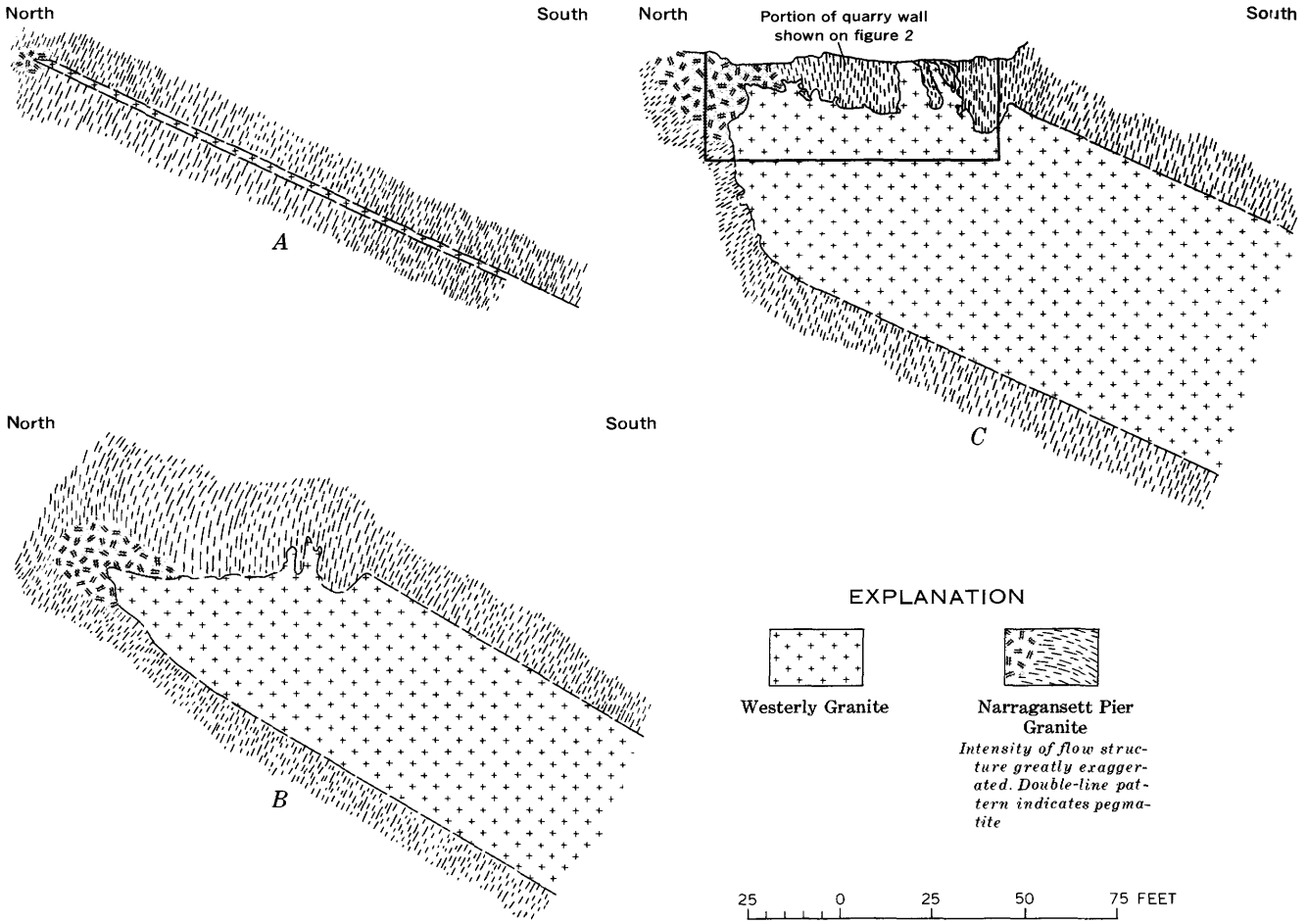

FIGURE 3.—Sections showing reconstruction of the stages of intrusion of the Redstone Ridge dike. *A*, Initial injection of Westerly magma along a preexisting fracture. *B*, Thickening of the dike by continued intrusion of magma. *C*, Present configuration of the dike. In *C*, the heavy line shows extent of the headwall exposure in the abandoned quarry at the east end of the west segment of the dike (fig. 2). Solid contacts are those exposed on the headwall or elsewhere in the same quarry; dashed contacts are those exposed in adjacent quarries or inferred.

REFERENCES

Balk, Robert, 1937, Structural behavior of igneous rocks: Geol. Soc. America Mem. 5, 177 p.

Fairbairn, H. W., Schlecht, W. G., Stevens, R. E., Dennen, W. H., Ahrens, L. H., and Chayes, F., 1951, A cooperative investigation of precision and accuracy in chemical, spectrochemical, and modal analysis of silicate rocks: U.S. Geol. Survey Bull. 980, 71 p.

Feininger, Tomas, 1964, Petrology of the Ashaway and Voluntown quadrangles, Connecticut-Rhode Island: U.S. Geol. Survey open-file report, 219 p.

——— 1965, Bedrock geologic map of the Ashaway quadrangle, Connecticut-Rhode Island: U.S. Geol. Survey Geol. Quad. Map GQ-403.

Goldsmith, Richard, 1967a, Bedrock geologic map of the New London quadrangle in Connecticut: U.S. Geol. Survey Geol. Quad. Map GQ-574.

——— 1967b, Bedrock geologic map of the Niantic quadrangle, New London County, Connecticut: U.S. Geol. Survey Geol. Quad. Map GQ-575.

——— 1967c, Bedrock geologic map of the Uncasville quadrangle, New London County, Connecticut: U.S. Geol. Survey Geol. Quad. Map GQ-576.

Lundgren, L. W., 1967, The bedrock geology of the Old Lyme quadrangle, with map: Connecticut Geol. Nat. History Survey Quad. Rept. 21, 30 p.

Moore, G. E., Jr., 1959, Bedrock geology of the Carolina and Quonochontaug quadrangles, Rhode Island: U.S. Geol. Survey Geol. Quad. Map GQ-117.

——— 1964, Bedrock geology of the Kingston quadrangle, Rhode Island: U.S. Geol. Survey Bull. 1158-E, 21 p.

——— 1967, Bedrock geologic map of the Watch Hill quadrangle, Rhode Island-Connecticut: U.S. Geol. Survey Geol. Quad. Map GQ-655.

Nichols, D. R., 1956, Bedrock geology of the Narragansett Pier quadrangle, Rhode Island: U.S. Geol. Survey Geol. Quad. Map GQ-91.

Quinn, A. W. Jaffe, H. W., Smith, W. L., and Waring, C. L., 1957, Lead-alpha ages of Rhode Island granitic rocks compared to their geologic ages: Am. Jour. Sci., v. 255, p. 547-560.

Zartman, Robert, Snyder, George, Stern, T. W., Marvin, P. F., and Bucknam, R. C., 1965, Implications of new radiometric ages in eastern Connecticut and Massachusetts, *in* Geological Survey Research 1965: U.S. Geol. Survey Prof. Paper 525-D, p. D1-D10.

PALMER GNEISS—AN EXAMPLE OF RETROGRADE METAMORPHISM ALONG AN UNCONFORMITY

By JACOB E. GAIR and GEORGE C. SIMMONS, Marquette, Mich., Denver, Colo.

Work done in cooperation with the Michigan Department of Conservation, Geological Survey Division

Abstract.—Van Hise and Bayley concluded, in 1895, that the Palmer Gneiss in the Marquette district, Michigan, was formed by the deformation and alteration of Archean granitic and amphibolitic gneiss, but since then this interpretation has been challenged many times. Field, petrographic, and chemical data recently assembled by us, however, support Van Hise and Bayley. We similarly attribute the origin of the gneiss to folding and shearing and to later alteration by solutions of probable metamorphic origin that passed along the unconformity between lower Precambrian gneiss and middle Precambrian metasedimentary rocks. Thin sections and mapping reveal gradations from slightly altered gneiss to the extensively sericitized, chloritized, carbonatized, and silicified rocks of the Palmer Gneiss. Chemical analyses of dolomite-chlorite (dark) and quartz-sericite (light) varieties of the Palmer Gneiss indicate similarities to amphibolitic and felsic parts of the basement gneiss.

PROBLEM OF THE PALMER GNEISS

The Palmer Gneiss was named by Van Hise and Bayley (1895, p. 514; 1897, p. 211–218) for schistose and gneissic rocks near Palmer, Mich., that occur in relatively narrow belts along the south side of the Marquette synclinorium between lower Precambrian (Archean) granitic and amphibolitic basement gneiss and middle Precambrian (Huronian) metasedimentary rocks (figs. 1 and 2). Pods of granitic rock and dolomite are common in the Palmer Gneiss, and in places the schist passes into fine-grained quartzose rock. The name Palmer Gneiss has been used commonly by some geologists for all the gneissic rocks within several miles south and southeast of Palmer, but such usage clearly was not the intent of Van Hise and Bayley.

Van Hise and Bayley presented much evidence to support their interpretation that the Palmer Gneiss is a comminuted, sericitized, and partly silicified phase of the lower Precambrian gneiss. However, they experienced difficulty in distinguishing the Palmer Gneiss—probably the silicified variety—from the similar-appearing juxtaposed Ajibik Quartzite that has also been somewhat altered. Thus they excluded middle Precambrian rocks from the Palmer Gneiss by definition, but the distinction was (and has remained) difficult to apply everywhere in the field. Van Hise and Bayley also distinguished the Palmer Gneiss from unmodified lower Precambrian gneiss conceptually, but intergradations exist and some of these rocks were inadvertently lumped together during mapping.

Van Hise and Leith (1911, p. 255–256) evidently recognized the practical difficulty of separating some quartzite and altered gneiss and decided that the Palmer Gneiss properly included both metasedimentary rocks and altered granitic and pegmatitic rocks; that is, rocks of both early and middle Precambrian age.

Lamey (1935) concluded that the quartzose and dolomitic parts of the Palmer Gneiss were remnants of middle Precambrian sedimentary formations (see fig. 2), two of which, the Mesnard Quartzite and Kona Dolomite, he extended from the northeast into the area southeast of Palmer where they had not previously been recognized. These formations, he believed, had been altered and partly replaced by post-middle Precambrian (post-Huronian) granite. The Palmer Gneiss thus was eliminated as a distinct unit. Lamey's interpretation was in part an outgrowth of his earlier idea (1931, 1933, 1934) that virtually all the granitic rock bordering the south side of the Marquette iron range is of post-Huronian age.

Tyler and others (1940, p. 1436, 1455, 1461) followed Lamey's interpretation. However, the quartzose rock and dolomite in the Palmer Gneiss do not resemble the typical Mesnard Quartzite and Kona Dolomite, so doubt has persisted about correlation of the Palmer Gneiss with middle Precambrian formations. Davis (1965, p. 87) followed Van Hise and Bayley in considering the Palmer Gneiss to be altered granitic and gneissic

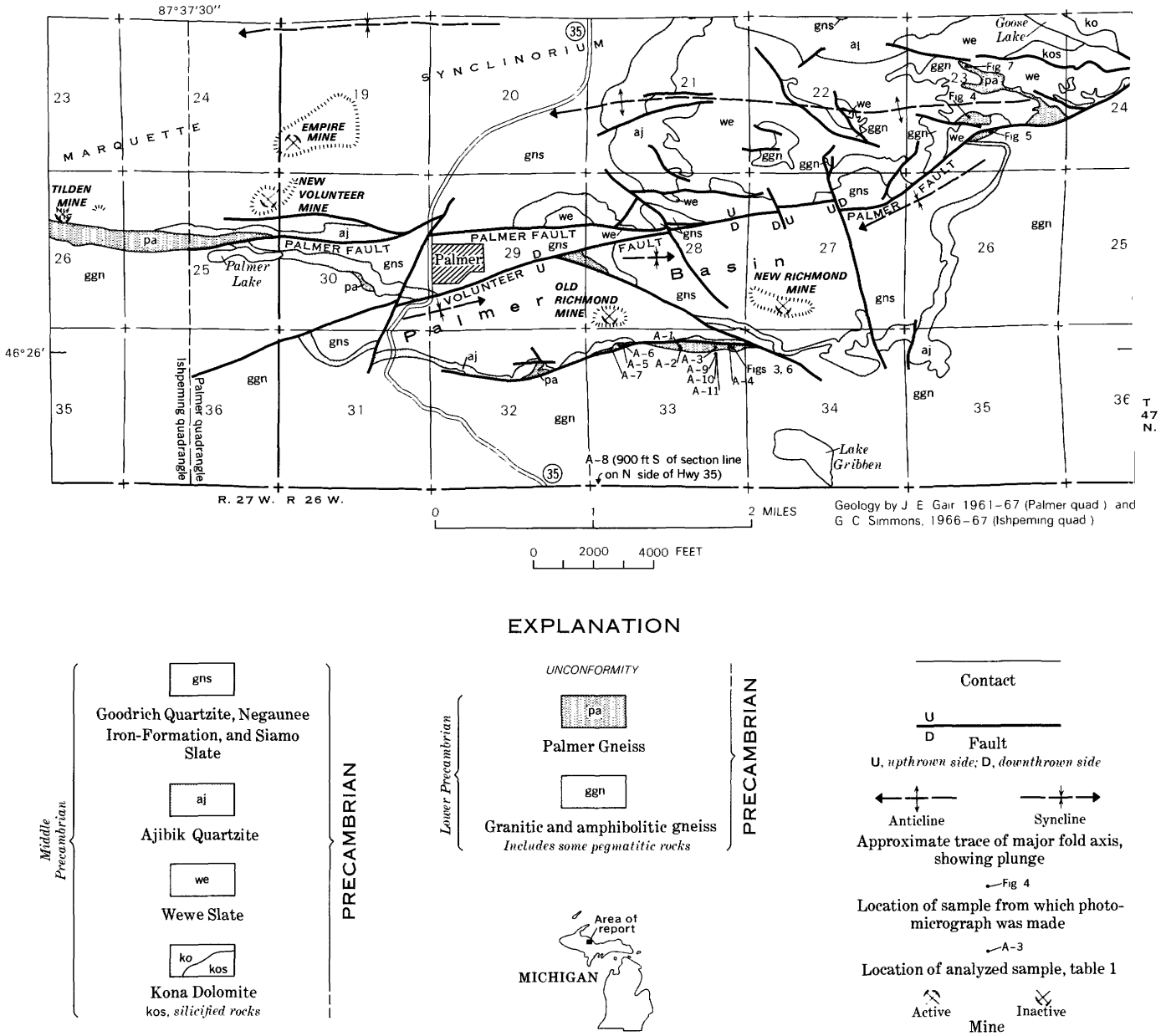

FIGURE 1.—Distribution of the Palmer Gneiss and bordering rocks, Ishpeming and Palmer 7½-minute quadrangles, Michigan.

rock. He specifically recognized the effects of retrogressive metamorphism, which he related to late middle Precambrian regional metamorphism, and suggested that the term phyllonite was applicable to the rocks.

Recent mapping in the Ishpeming and Palmer 7½-minute quadrangles and the study of about 90 thin sections of highly altered lower Precambrian gneissic-granitic rocks and adjacent middle Precambrian metasedimentary rocks indicate to us that Van Hise and Bayley (1895) and Davis (1965) were substantially correct in their views about the origin of the Palmer Gneiss. Most of the rocks originally called Palmer Gneiss are now recognized as being either altered granitic and amphibolitic rock—modifications of lower Precambrian rocks such as occur south of Palmer—or part of the middle Precambrian Ajibik Quartzite.

As used in this report, the definition of the Palmer Gneiss is restricted so that it again generally follows the original definition of Van Hise and Bayley (1895). In our mapping, we have thus endeavored to separate the Palmer Gneiss from unaltered lower Precambrian gneiss, and from the Ajibik Quartzite, regardless of how greatly the quartzite may have been modified by shearing and recrystallization. Accordingly, several

313-005 O—68——13

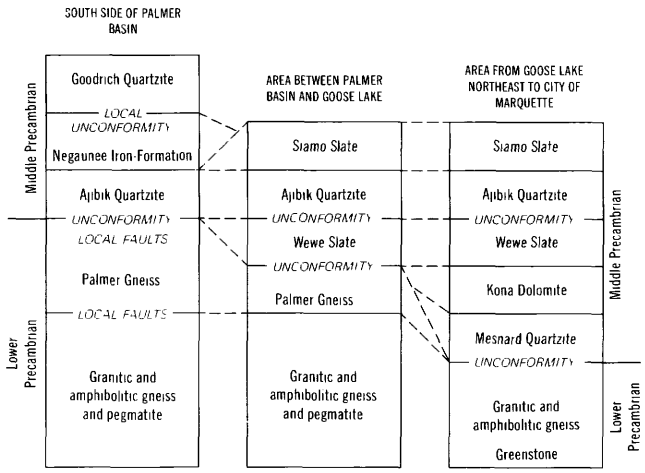

FIGURE 2.—Formations in eastern part of Marquette iron range.

isolated areas inadvertently mapped by Van Hise and Bayley as Palmer Gneiss are excluded from the Palmer Gneiss and are classified here as lower Precambrian granitic and amphibolitic gneiss, or as such rock bordered by Palmer Gneiss, as for example in sec. 23, T. 47 N., R. 26 W. Schistose to massive sericitic quartzite mapped partly as the Palmer Gneiss and partly as Ajibik Quartzite by Van Hise and Bayley in the NE¼ sec. 35, T. 47 N., R. 26 W., is now considered to be entirely Ajibik Quartzite. The sericitic quartzite is distinct from other rocks in the areas originally mapped as Palmer Gneiss in that it contains abundant quartz grains of clastic aspect, and generally contains more than 60 percent quartz. Quartz grains in this rock generally are coarser and have a much more regular or consistent distribution with respect to the sericite matrix than do quartz grains in the altered granitoid rocks. These rocks also contain pebbles in a few places. At other places, especially in the NE¼ sec. 31, chloritoid is abundant in the sericitic quartzite, as it is in several other occurrences of aluminous metasedimentary rock in the area.

GENERAL GEOLOGY

A major unconformity separates lower Precambrian gneiss and greenstone from middle Precambrian metasedimentary formations in the Marquette district. Within the area shown on figure 1, the lower Precambrian rock is the Palmer Gneiss, granitic and amphibolitic gneiss, and pegmatite, and the middle Precambrian metasedimentary formations are, in upward sequence, the Kona Dolomite, Wewe Slate, Ajibik Quartzite, Siamo Slate, Negaunee Iron-Formation, and Goodrich Quartzite (fig. 2). The basal middle Precambrian formation in contact with basement gneiss in the northeastern part of the area is the Wewe Slate, but the Ajibik Quartzite overlaps onto the basement gneiss to the south and southwest.

Orogeny culminating at the end of middle Precambrian time produced the Marquette synclinorium and, along the Palmer fault (fig. 1), downdropped a synclinal block containing the Ajibik Quartzite and younger middle Precambrian rocks to form the Palmer basin south of the main part of the synclinorium. Shearing and faulting related to the orogeny occurred along the unconformity between lower and middle Precambrian rocks on the south side of the Palmer basin and west of the basin for at least 1½ miles. In that area, the Palmer Gneiss occupies a belt as much as 1,000 feet wide along the unconformity and its spatially associated system of shears and faults and is exposed in several places within 200 feet of recognizable granitic-amphibolitic gneiss to the south. Faulting probably accounts for some of the variation in width of the Palmer Gneiss and Ajibik Quartzite along the margin of the Palmer basin and for the apparent absence of the Palmer Gneiss in places. And in the NE¼ sec. 32, T. 47 N., R. 26 W., the juxtaposition of granitic gneiss and metasedimentary rocks and the occurrence of a reentrant of the Palmer Gneiss on trend with the main belt of the Ajibik Quartzite are attributed to faulting (fig. 1).

A relatively broad area of lower Precambrian granitic gneiss and the adjacent Palmer Gneiss is exposed north of the Palmer fault in sec. 23, T. 47 N., R. 26 W., in the core of a large anticline within the Marquette synclinorium. The Palmer Gneiss in parts of that area is highly altered granitic gneiss, but is only slightly deformed and may represent a regolith developed on the granitic gneiss during early middle Precambrian time. The undeformed nature of the altered rock suggests that the margins of the relatively broad uplifts of lower Precambrian granitic gneiss within the Marquette synclinorium did not generally undergo the strong deformation that the gneiss did along the south margin of the Palmer basin and the Marquette synclinorium proper.

Along the south side of the synclinorium, several miles east of the area in figure 1, rocks resembling parts of the Palmer Gneiss are found locally in granitic gneiss within a few hundred feet south of (below) the contact between lower and middle Precambrian rocks (Gair and Thaden, 1968).

The granitic and amphibolitic gneiss south and west of the Palmer basin contains abundant salmon- and flesh-colored granitoid rock and well-layered amphibolite and other dark chloritized metaigneous rock that may once have been amphibolite. A few dark layers contain much quartz and may be metagraywacke, although their interlocking feldspar grains, irregularly shaped quartz blebs, and patchy distribution of quartz

relative to aggregates of feldspar and chlorite suggest that secondary quartz was introduced into amphibolite or other dark metaigneous rock during alteration. There seem to be more dark layers in the gneiss within half a mile south of the Palmer basin than there are farther south. Possibly this zone of abundant dark layered rock was relatively incompetent and thereby localized fault zones along the south side of the Palmer basin, as well as along the Marquette synclinorium 1–2 miles to the west. The granitoid rock commonly occurs in thick, slightly foliated or nonfoliated tabular masses conformable with the dark layered rock, but in many places it cuts across the dark layers. Most of the granitoid rock is medium grained, but locally it grades into or is sharply cut by pegmatite. Whether the pegmatite is a late phase of the granitoid rocks, markedly younger, or of several ages is unknown. The absence of pegmatitic rock in metasedimentary rocks of definite middle Precambrian age suggests that it is of early Precambrian age.

LITHOLOGY

The Palmer Gneiss consists chiefly of green, gray, and tan schist that in places is associated with massive quartz-sericite rock of pale olive green or tan color. Parts of the schist do not have a conspicuous foliation; other parts are well foliated, and because of their probable origin by the comminution of once-coarser-grained rocks, could be termed phyllonite (Knopf, 1931, p. 14–19). Locally the schist—generally the lighter colored varieties—contains pods as much as several feet thick and stringers of feldspar-rich granitoid rock or feldspar-chlorite gneiss. The pods and stringers are generally conformable with foliation of the enclosing schist and are extremely irregular in distribution. In a few places, small granitic or pegmatitic blobs or stringers, less than a foot long and less than an inch thick, cut the foliation of the schist.

The schist consists mainly of sericite, aluminous chlorite, fine-grained quartz, and dolomite in highly variable proportions.[1] The proportions of these minerals undoubtedly reflect original compositional variations in the parent rock of the schist. Davis (1965, p. 13–14) found that extensively altered lower Precambrian feldspathic rock drilled about 300 feet south of the west quarter corner of sec. 28, T. 47 N., R. 26 W., contains mixed-layer muscovite, 1M and 2M muscovites, and montmorillonite, all derived from feldspar. Magnetite and finely granular hematite or leucoxene are minor constituents in some parts of the Palmer Gneiss. In many places along the south margin of the Palmer basin, beds and lenses of schist have been replaced by fine-grained quartz. Locally in the NW¼ sec. 25, T. 47 N., R. 27 W., tourmaline is an accessory mineral in fine-grained quartz mosaics. In the NE¼ sec. 33, T. 47 N., R. 26 W., carbonate-chlorite schist is abundant and veins of quartz or dolomite are especially common; grain sizes in these veins range from about 0.01 millimeter to 1 centimeter in irregularly arranged patches. Large brown-weathering podlike masses of coarse dolomite or dolomite and quartz are also especially common in this area; these pods clearly transect and wedge into the foliation of the schist, and thus are of later origin than the foliation. The largest pods are about 20 feet long and 3 feet wide.

ORIGIN OF THE PALMER GNEISS

The external appearance of the schist in no way identifies the rock from which it was derived. The schist is distinctly layered at several places along the south edge of the Palmer basin and in the belt to the west, but the layering is of uncertain origin; it could represent (1) beds of lower Precambrian amphibolite or other metaigneous rock, such as that well exposed in the gneiss along Michigan Highway 35, within ½-1 mile south of the village of Palmer, (2) the characteristic fluxion structure of mylonitized rock (Lapworth, 1885), or (3) middle Precambrian sedimentary features. There are no definitely microclastic textures in the schist. Cataclastic texture that resembles clastic (wacke) fabric occurs in a few places, both in narrow shear-breccia zones and in zones bordering some pods of granitoid rock. The cataclastic fabric adjacent to pods may form a transition from unsheared to completely comminuted granitoid rock. Observable field relations, however, do not clarify whether most pods and other bodies of granitoid and gneissic rock enclosed by schist are relatively unsheared feldspar-rich remnants of lower Precambrian granitic-amphibolitic gneiss (compare Becke, 1909) or igneous rocks intruded during or after the late middle Precambrian deformation. The few small stringers and blobs of granitoid rock crosscutting the schist may be either material mobilized during deformation or postdeformation igneous intrusions. The absence of similar igneous rock in adjacent middle Precambrian metasedimentary rocks, however, seems to preclude middle Precambrian or post-middle Precambrian (postdeformation) intrusion, and so supports the idea that these igneous-appearing rocks are unsheared lenses or locally remobilized parts of the lower Precambrian granitic rock.

The least equivocal indication of the origin of the schist and associated massive quartz-sericite rock is

[1] X-ray identification of 2M muscovite, aluminous chlorite, and dolomite by L. C. Schultz, U.S. Geological Survey. The general chlorite half-cell formula is $(Mg_{6-(x+y)}{}^{+z}Fe_yAl_x)(Si_{4-x}Al_x)O_{10}(OH)_8$ where $x=1.5$-2.0 and $y=1.0$-1.5 (out of 6 positions).

their gradation into partly sericitized feldspathic granitoid and pegmatitic rocks in many places and into hornblende gneiss in sec. 26, T. 47 N., R. 27 W. (figs. 3, 4, 5). These gradations, however, are virtually impossible to detect except in thin section. Conclusions based on the examination of thin sections certainly are not infallible where sericitization of feldspar is complete, but the similarity of interlocking sericite aggregates and quartz (fig. 6) and partly sericitized sodic plagioclase and quartz (fig. 3) identify much of the massive and moderately schistose quartz-sericite rock as altered granitoid rock.

Quartz-sericite rock of the Palmer Gneiss characteristically contains rudely blocky or less well defined areas of very fine grained, nearly pure sericite separated by knots or subparallel ribbons of coarse-grained quartz (fig. 6). The knots stand out on weathered surfaces and are easily mistaken for detrital grains, but in thin section are seen to be irregular in outline, to lack detrital form, and to be interconnected by roughly subparallel thin quartz veins. The quartz knots are probably analogous to the lenses and nests of recrystallized quartz that Knopf (1931, p. 18–19) considered to be "particularly characteristic of phyllonites."

Partly altered gneiss cropping out in the east-central part of sec. 26, T. 47 N., R. 27 W., between chlorite-quartz-carbonate schist of the Palmer Gneiss to the north and amphibolitic gneiss to the south, contains partly chloritized biotite and partly carbonatized feldspar. These features suggest retrograde alteration of the amphibolitic gneiss to the chlorite-quartz-carbonate schist. The ancestry of the carbonate-chlorite schist is not readily determined east of the Ishpeming quadrangle; in a few thin sections, however, carbonate grades into remnants of feldspar, suggesting that carbonatization of feldspar played an important

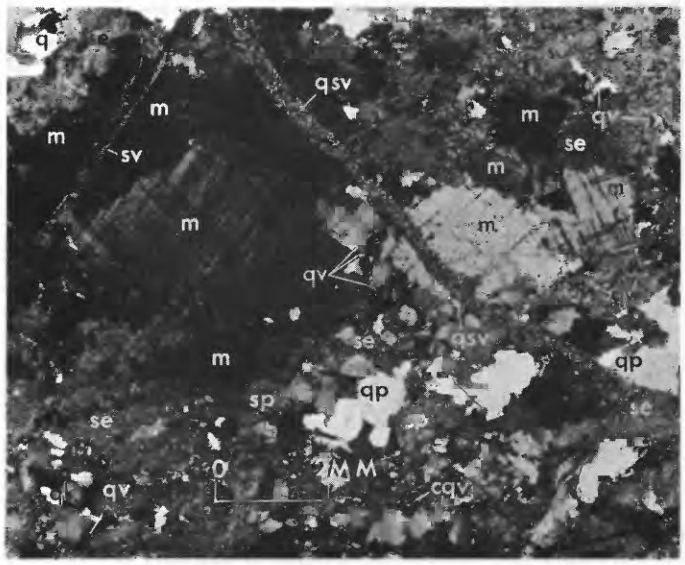

FIGURE 4.—Photomicrograph of partly sericitized and silicified granite gneiss. Original plagioclase completely converted to sericite (se) or sericite plus quartz. Sericite pseudomorphs of plagioclase (sp) are common. Microcline (m) is unaltered but locally fractured. Embayments of sericite into microcline represent original plagioclase-microcline relationships. Quartz (q) forms pods (qp), knots (qk), and veinlets (qv). Other veinlets contain quartz and sericite (qsv), cherty quartz (cqv), or sericite. Location: 1,650 feet N., 2,020 feet E. of SW cor., sec 23, T. 47 N., R. 26 W. Crossed nicols.

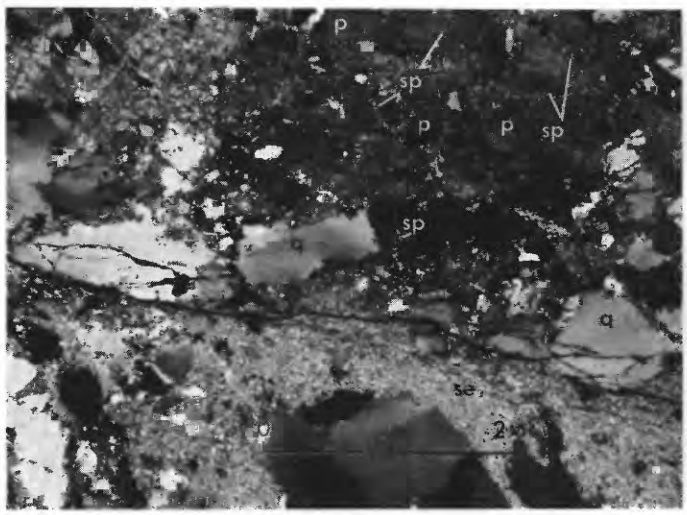

FIGURE 3.—Photomicrograph of brecciated, sericitized quartz-feldspar gneiss. Zones containing concentrations of sericite (se) are irregularly distributed between areas of brecciated quartz (q) and plagioclase (p) in which sericitization of plagioclase (sp) occurs along fractures. Location: 4,500 feet N., 4,550 feet E. of SW cor., sec. 33, T. 47 N., R. 26 W. Crossed nicols.

FIGURE 5.—Photomicrograph of extensively sericitized and silicified granitic gneiss. Fragments of unaltered microcline (m) surrounded by cherty quartz (cq) and sericite (se). Recrystallized quartz (q) forms irregular pods and knots. Rock laced by veinlets of cherty quartz (cqv). Location: 1,350 feet N., 2,480 feet E. of SW cor., sec. 23, T. 47 N., R. 26 W. Crossed nicols.

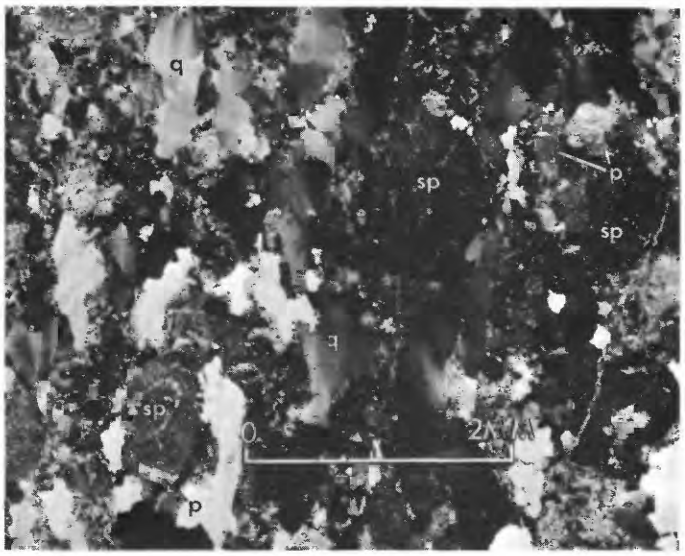

FIGURE 6.—Photomicrograph of sericitized quartz-plagioclase gneiss. Plagioclase (p) almost completely converted to sericite (sp). Tabular sericitized pseudomorphs of plagioclase are common. Recrystallized elongated quartz (q) in early stage of development of subparallel "ribbons." Location: 4,500 feet N., 4,550 feet E. of SW cor., sec. 33, T. 47 N., R. 26 W. Crossed nicols.

FIGURE 7.—Photomicrograph of sheared, sericitized, partly silicified granitic gneiss. Plagioclase completely converted to sericite (se). Silica redistributed mainly as lenses of quartz (ql). Secondary iron oxide (io) rims quartz (q) grains and lenses, and is intergrown with quartz (q+io) in concretionary pods. Location: 3,500 feet N., 1,950 feet E. of SW. cor., sec. 23, T. 47 N., R. 26 W. Crossed nicols.

part in the formation of that type of schist. Some thin sections show an increasing rearrangement of quartz into elongated grains and ribbons as shown in figure 6, with increasing sericitization of sodic plagioclase. Microcline occurs in some of the samples collected, and appears to be fresh, even where plagioclase has been completely replaced, (figs. 4, 5). The fresh microcline might be interpreted as having been emplaced in the rock after alteration of the plagioclase, except that its presence in granitic rock containing even slightly clouded plagioclase indicates that it is prealteration in age and was relatively immune to change even during the complete destruction of plagioclase.

Subparallel ribbons of recrystallized quartz (figs. 6, 7) and well-alined mica and chlorite indicate that the schist in general has been strongly sheared. Stringers and pods of granitoid rock and mottled salmon-green feldspar-chlorite gneiss, conformable within the schist, are interpreted here as gross remnants of unsheared or less sheared parent granitic rock, analogous to those described by Becke (1909). In some places, though, especially in sec. 23, T. 47 N., R. 26 W., the altered rock contains completely sericitized, but undeformed, large tabular crystals of feldspar, which suggests that sericitization of some zones or areas in the Palmer Gneiss, although a product of retrograde metamorphism, must not have been related to shearing. Such material is texturally similar to residual soil formed over granite in the Blind River area, Ontario (Collins, 1925, p. 39) and may represent a lower Precambrian or lower middle Precambr an regolith.

The brown-weathering pods of dolomite or dolomite and quartz that cut the schist along the south margin of the Palmer basin and west of Palmer closely resemble carbonate-quartz pods found in a few places in the lower Precambrian gneiss south of the Palmer basin. The pods are as much as several feet thick and 20 feet long. Widely ranging grain size, flamboyant and comb structures in irregular areas of quartz, and abundant veinlets within the pods suggest an origin for the most part as vein deposits. The pods of dolomite and dolomite-quartz seem to be related to alteration of the granitoid and gneissic rocks. The CaO, MgO, and SiO_2 could have been supplied entirely from the surrounding rocks.

CHEMICAL CHARACTERISTICS

Seven chemical analyses reveal a wide range in composition within the Palmer Gneiss (table 1). Analyses 1–3 represent greenish dolomite-chlorite-sericite-quartz ("dark") schist; these samples have a narrow compositional range. Analyses 4–7, on the other hand, represent massive quartz-plagioclase ("light") granitoid rocks that have undergone varying degrees of sericitization, plus some chloritization (analysis 4) and carbonatization (analyses 5 and 6); these rocks have a rather wide compositional range, especially for SiO_2, FeO, MgO, and CaO. The analyses are compared with

analyses of possibly related types of rock, including several adjacent varieties of the basement gneiss (table 1, analyses 8–11) and rocks from other places of types present in the granitic-amphibolitic gneiss south of Palmer (fig. 8). Analyses 1–3 are averaged in the figure.

The dark schist of the Palmer Gneiss is chemically similar (fig. 8A) to mafic metaigneous rock in the granitic-amphibolitic gneiss in section 33. Two analyzed layers of such rock—possibly chloritized amphibolite—(table 1, Nos. 10 and 11) are surrounded by orange leucocratic tonalite, 200–300 feet south of the dark schist. One of the layers in particular (table 1, analysis 11; fig. 8A) is chemically much like the averaged analysis of dark schist except for Al_2O_3, which is about 2¼ percent less. The dark schist is also generally similar to amphibolitic rocks from other areas (fig. 8A, lettered analyses), but to a lesser degree than to the sample for analysis 11 of table 1. Except for alumina, the chemical components of the dark schist appear to fall within the probable composition range of dark phases of the granitic-amphibolitic gneiss. Chemical differences between the analyzed samples probably reflect pre-Palmer Gneiss variations from layer to layer of amphibolitic basement gneiss, and possibly also minor effects of metasomatism.

Light-colored phases of the Palmer Gneiss have a wide range in chemical composition (table 1, Nos. 4–7). Field and petrographic evidence indicates that these rocks are derived from felsic (granitic) gneiss, and the chemical data are broadly consistent with this conclusion. Although most felsic gneiss a short distance south of the Palmer basin is tonalitic or granodioritic, the Palmer Gneiss appears chemically not only to encompass these types, but to include a variety of other compositions (fig. 8*B*, Palmer Gneiss and nearby tonalite shown by lines; other analyses shown by letters). Arkose, shale, and pelitic rock, rock types from which the granitic-amphibolitic gneiss may have been derived, also fall generally within the compositional range of the Palmer Gneiss. The wide compositional range probably reflects variations in pre-Palmer Gneiss basement rock, plus superimposed additive or subtractive effects of metasomatism. Metasomatism seems to be suggested, particularly in samples 5 and 6, by high MgO content; in sample 5 by high CaO content; and in all four samples of Palmer Gneiss by low Na_2O content relative to that in the other rocks represented in figure 8*B*.

TABLE 1.—*Chemical analyses, in weight percent, of the Palmer Gneiss and nearby granitic-amphibolitic gneiss*

[Rapid rock analyses by P. L. D. Elmore, S. D. Botts, G. W. Chloe, J. L. Glenn, Lowell Artis, Hezekiah Smith, and James Kelsey. Analyses of Cu, Pb, and Zn by Harry Bastron, J. Calkins and W. G. Schlecht, using single-solution method. Location of analyzed samples shown on figure 1 as "A1," "A2," "A3," and so forth]

	Palmer Gneiss							Nearby granitic-amphibolitic gneiss			
	1	2	3	4	5	6	7	8	9	10	11
SiO_2	44.2	46.9	47.8	75.9	56.0	60.6	69.4	74.3	79.2	44.3	43.8
Al_2O_3	15.0	13.6	15.6	11.6	13.0	11.5	13.3	13.0	12.2	12.6	12.2
Fe_2O_3	1.5	.75	.62	.70	.6	.64	1.2	.85	.47	1.2	2.7
FeO	9.6	8.5	10.8	4.0	.36	5.1	1.7	1.5	.48	7.2	10.2
MgO	8.4	9.0	7.0	1.5	5.0	5.5	2.9	1.2	.32	7.1	8.9
CaO	5.4	5.6	4.1	.20	7.1	4.7	3.2	1.1	.30	11.7	5.5
Na_2O	.20	.37	.33	1.2	.23	.15	1.1	2.7	5.3	1.9	1.1
K_2O	1.7	2.0	1.3	1.8	2.6	1.8	1.0	2.3	.81	.78	2.9
H_2O-	.08	.10	.11	.13	.07	.07	.11	.04	.02	.02	.15
H_2O+	3.6	4.2	4.9	2.3	1.1	2.0	1.1	.84	.56	3.3	3.2
TiO_2	1.3	.76	1.0	.32	.10	.62	.30	.36	.11	.75	1.0
P_2O_5	.29	.15	.20	.16	.11	.16	.16	.12	.02	.05	.13
MnO	.24	.25	.08	.08	.12	.09	.05	.05	.03	.18	.23
CO_2	7.7	8.0	5.8	.05	10.5	6.9	4.2	.76	.09	9.0	7.4
Cu	.030	.0007	.017	.0049	.0005	.0005	.0004				
Pb	.0022		.0024	.0023							
Zn	.019	.011	.014	.0045	.0022	.0038	.0017				

	Field No.	*Lab. No.*	*Description*	*Location*
1.	JG–33–66	W166958	Dolomite-chlorite-chert-sericite schist	2,960 ft E., 4,700 ft N. of SW. cor., sec. 33, T. 47 N., R. 26 W.
2.	JG–34–66	W166959	Dolomite-chlorite-plagioclase schist	2,900E–4,460N SW cor. 33–47–26.
3.	JG–36–66	W166960	Dolomite-chlorite-chert-sericite schist	4,220E–4,680N SW cor. 33–47–26.
4.	JG–25–66	W166957	Partly sericitized and chloritized plagioclase-quartz rock.	1,400W–3,900N SE cor. 32–47–26.
5.	JG–37–66	W166961	Quartz-sericite rock	1,150E–4,870N SW cor. 33–47–26.
6.	JG–38–66	W166962	Chert-sericite-chlorite-dolomite rock	1,150E–4,870N SW cor. 33–47–26.
7.	JG–43–66	W166964	Quartz-sericite-dolomite rock	900E–4,600N SW cor. 33–47–26.
8.	JG–20–67	W169264	Feldspar-quartz tonalite	500E–900S NW cor. 4–46–26.
9.	JG–40–67	W169265	Dark plagioclase-chlorite rock	900W–850S NE cor. 33–47–26.
10.	JG–40A–67	W169266	Quartz-plagioclase tonalite	1000W–900S NE cor. 33–47–26.
11.	JG–40B–67	W169267	Dark plagioclase-chlorite rock	1000W–930S NE cor. 33–47–26.

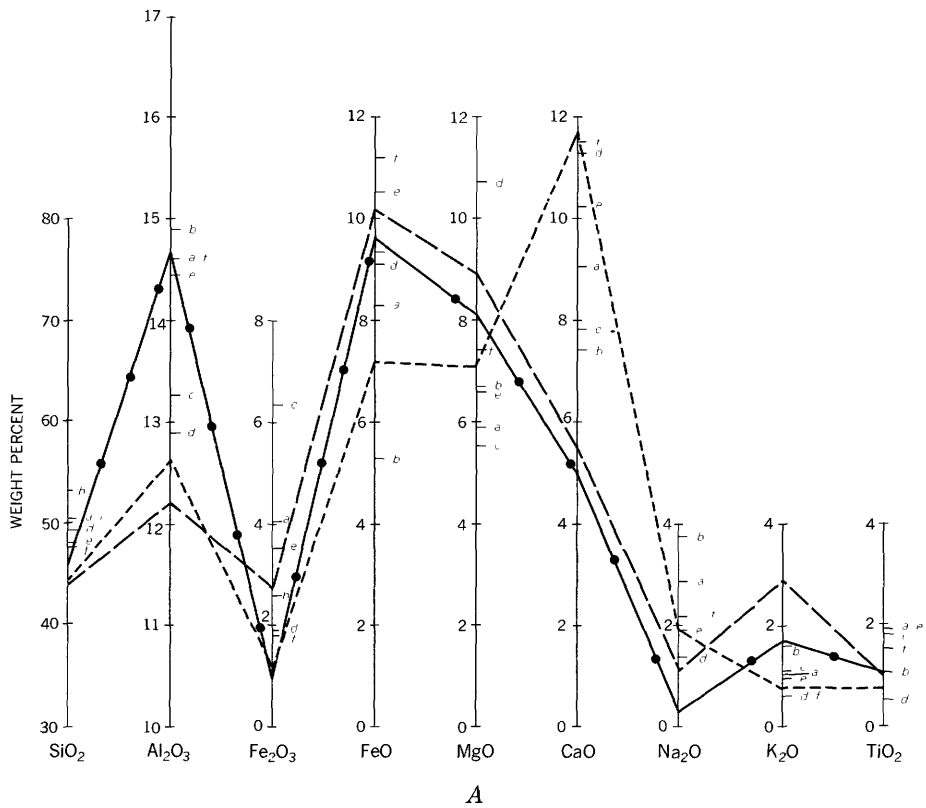

EXPLANATION

Average, 3 analyses of chlorite-dolomite-quartz-sericite schist, Palmer Gneiss, table 1, Nos 1–3

Dark metaigneous rock in lower Precambrian gneiss, south of Palmer basin, table 1, No. 11

Dark metaigneous rock in lower Precambrian gneiss, south of Palmer basin, table 1, No. 10

a Average, 3 analyses of amphibolite (Clarke, 1920, p. 595, A, B, C)

b Average, 2 analyses of amphibolite, lower Precambrian gneiss north of Marquette iron range (Gair and Thaden, 1968, table 8)

c Amphibolite, lower Precambrian gneiss, Dickinson County, Mich. (Bayley and others, 1966, table 20, No. 1)

d Amphibolite, lower Precambrian gneiss, Dickinson County, Mich. (Bayley and others, 1966, table 20, No. 2)

e Average amphibolite in paragneiss, Emeryville area, New York (Engel and Engel, 1962, table 7, No. 1)

f Average amphibolite in paragneiss, Colton area, New York (Engel and Engel, 1962, table 7, No. 2)

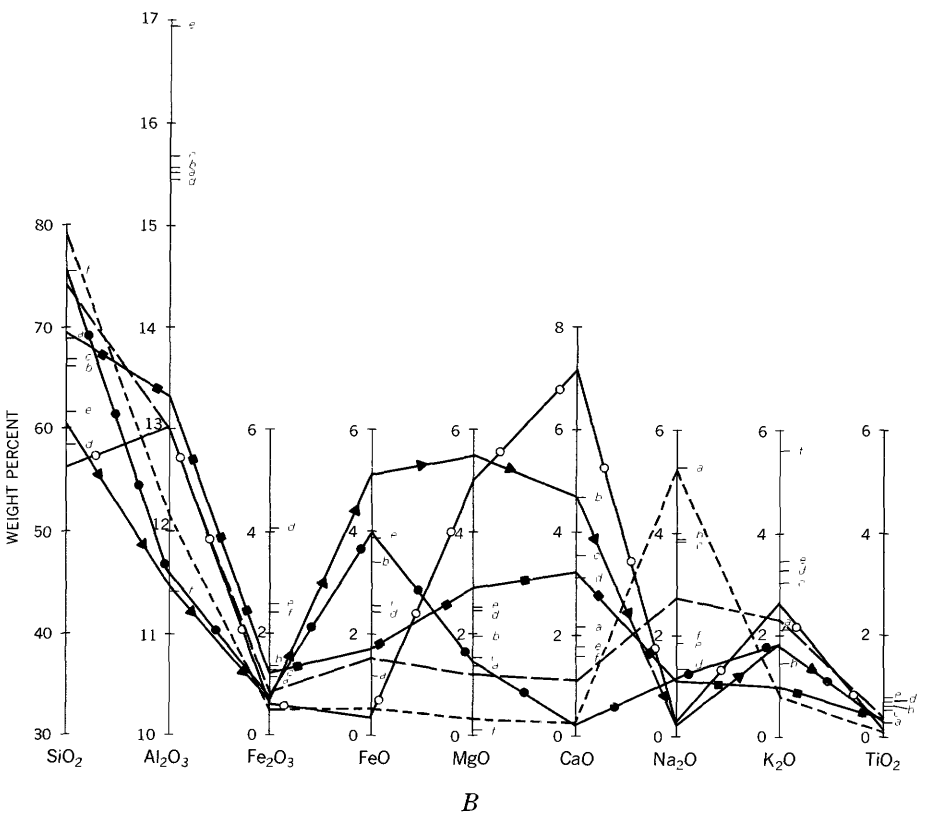

EXPLANATION

No. 4

No. 5

No. 6

No. 7
Light-colored phases of Palmer Gneiss, table 1, Nos. 4–7

Tonalite
Lower Precambrian gneiss south of Palmer basin, table 1, No. 8

Leucocratic tonalite
Lower Precambrian gneiss south of Palmer basin, table 1, No. 9

a Average, 4 analyses of tonalite gneiss, lower Precambrian area north of Marquette iron range (Gair and Thaden, 1968, table 8)

b Average tonalite (Nockolds, 1954, table 2, p. 1015)

c Average granodiorite (Nockolds, 1954, table 2, p. 101)

d Average, 78 shales (Clarke, 1924)

e Average, 155 pelitic rocks (Shaw, 1956, table 10, p. 928)

f Average, 3 arkoses No values for FeO and TiO_2 (Pettijohn, 1949, table 68, D, p. 259)

FIGURE 8.—Chemical analyses of the Palmer Gneiss compared with analyses of possible related types of rock. *A*, dark rocks; *B*, light-colored rocks.

CONCLUSION

The restriction of the highly altered granitoid and gneissic rock to narrow belts adjacent to the contact between lower and middle Precambrian rocks, and the strong schistosity of the altered rock in most places, suggest one or a combination of the following modes of origin:

1. Shearing and alteration during faulting of middle Precambrian rocks against lower Precambrian rocks at the close of middle Precambrian time.
2. Passage of aqueous solutions along the contact between lower and middle Precambrian rocks.
3. Alteration of a regolith, with or without shearing, during folding at the close of middle Precambrian time.

REFERENCES

Bayley R. W., Dutton, C. E., and Lamey, C. A., 1966, Geology of the Menominee iron-bearing district, Dickinson County, Michigan, and Florence and Marinette Counties, Wisconsin: U.S. Geol. Survey Prof. Paper 513, 96 p.

Becke, F., 1909, Ueber diaphthorite: Mineral. Petrog. Mitt., v. 27, p. 369–375.

Clarke, F. W., 1920, The data of geochemistry 4th ed.: U.S. Geol Survey Bull. 695, 832 p.

——— 1924, The data of geochemistry, 5th ed.: U.S. Geol. Survey Bull. 770, 841 p.

Collins, W. H., 1925, North shore of Lake Huron: Canada Geol. Survey Mem. 143, 160 p.

Davis, J. F., 1965, A petrologic examination of iron-formation and associated graywackes and pyroclastic breccias within the Negaunee formation of the Palmer area, Marquette district, Michigan: Wisconsin Univ., Ph. D. thesis, 205 p.

Engel, A. E. J., and Engel, C. G., 1962, Progressive metamorphism of amphibolite, northwest Adirondack Mountains, New York, *in* Petrologic studies: Geol. Soc. America, Buddington Volume, p. 37–82.

Gair, J. E., and Thaden, R. E., 1968, Geology of the Marquette and Sands quadrangles, Marquette County, Michigan: U.S. Geol. Survey Prof. Paper 397 [in press].

Knopf, E. B., 1931, Retrogressive metamorphism and phyllonitization: Am. Jour. Sci., 5th ser., v. 21, no. 121, p. 1–27.

Lamey, C. A., 1931, Granite intrusions in the Huronian formations of northern Michigan: Jour. Geology, v. 39, no. 3, p. 288–295.

——— 1933, The intrusive relations of the Republic granite: Jour. Geology, v. 41, no. 5, p. 487–500.

——— 1934, Some metamorphic effects of the Republic granite: Jour. Geology, v. 42, no. 3, p. 248–263.

——— 1935, The Palmer gneiss: Geol. Soc. America Bull., v. 46, no. 7, p. 1137–1162.

Lapworth, Charles, 1885, The highland controversy in British geology: Nature, v. 32, p. 558–559.

Nockolds, S. R., 1954, Average chemical compositions of some igneous rocks: Geol. Soc. America Bull., v. 65, no. 10, p. 1007–1032.

Pettijohn, F. J., 1949, Sedimentary rocks, 1st ed.: New York, Harper and Bros., 526 p.

Shaw, D. M., 1956, Geochemistry of pelitic rocks. pt. 3, Major elements and general geochemistry: Geol. Soc. America Bull., v. 67, no. 7, p. 919–934.

Tyler, S. A., Marsden, R. W., Grout, F. F., and Thiel, G. A., 1940, Studies of the Lake Superior Pre-Cambrian by accessory-mineral methods: Geol. Soc. America Bull., v. 51, p. 1429–1538.

Van Hise, C. R., and Bayley, W. S., 1895, Preliminary report on the Marquette iron-bearing district of Michigan: U.S. Geol. Survey 15th Ann. Rept., p. 485–650.

——— 1897, The Marquette iron-bearing district of Michigan: U.S. Geol. Survey Mon. 28, 608 p. and atlas.

Van Hise, C. R., and Leith, C. K., 1911, Geology of the Lake Superior region: U.S. Geol. Survey Mon. 52, 641 p.

SERPENTINITE AND RODINGITE IN HUNTING HILL QUARRY, MONTGOMERY COUNTY, MARYLAND—A SUMMARY

By DAVID M. LARRABEE, Washington, D.C.

Abstract.—A serpentinized dunite pluton 4 miles west of Rockville, Md., contains dikes of metasomatized gabbro—now rodingite. Forty-four minerals have been identified from the large active open quarry in which the rocks are well exposed. Rodingite intrusive bodies are as much as 1,500 feet long and 100 feet wide, and are composed of a mixture of bright-green diopside, cinnamon to pink grossularite, white diopside, zoisite, prehnite, and other minerals. These rocks are an important source of crushed stone in the Washington, D.C., area.

The Hunting Hill pluton, consisting of serpentinized dunite cut by gabbro dikes converted to rodingite, is best exposed in the active quarry of Rockville Crushed Stone, Inc., 4 miles west of Rockville, Montgomery County, Md. This quarry, opened in 1955, had in 1966 become about 2,600 feet long, 850 feet wide, and 210 feet deep. It was mapped by planetable methods in 1966 (Larrabee, 1966b). The quarry is centered within the ultramafite and trends about N. 45° E. Forty-four minerals have been identified from the quarry.

The pluton, about 1 mile wide and 4 miles long (Cloos and Cooke, 1953), is of probable Ordovician age and was intruded into quartz-mica schist of the Wissahickon Formation of late Precambrian age. The pluton trends about N. 22° E., parallel to schistosity of wallrock, and dips vertically or steeply southeast. The serpentinite ranges from dull green through gray to black, on fresh fracture, and is largely antigorite with subordinate magnetite. Minute roughly parallel gash veins of chrysotile occur in the serpentinite.

Serpentinite constitutes 80 to 90 percent of the rock exposed in the quarry, the remainder being chiefly rodingite. The prevailing dark color results from magnetite in two principal forms: (1) fine dust scattered throughout the rock or concentrated around the margins of original olivine and along cleavage planes of possible olivine pseudomorphs, and (2) larger plates and irregular masses generally between coarser antigorite blades. Much serpentinite is spotted, having magnetite-rich areas ¼ inch in diameter surrounded by lighter green antigorite that is generally free of magnetite. Banding in serpentinite is well developed at only one place—on a presently active bench at the southwest end of the quarry.

Five stages or ages of serpentine minerals have been identified: two of antigorite, and one each of chrysotile, clinochrysotile, and deweylite, the last two minerals being the latest formed. Two stages or ages of tremolite and talc are involved in the serpentinization, alternating with the antigorite. Serpentinization plainly took place over a long period, surges of higher temperature fluids from time to time alternating with the general decrease in temperature. The rodingitization presumably took place in surges also, for the rodingite and the associated tremolite were formed as a part of the overall serpentinization process.

The rodingite ranges in shape and size from lenslike bodies a few feet long to highly irregular branching dikelike masses as much as 1,500 feet long and 100 feet wide. Dikes of pegmatitic hornblende diorite cut the serpentinite northeast and southwest of the quarry but are not exposed therein. Neither the rodingite of this deposit nor any other rodingite between Alabama and New Jersey seems to have been described previously, though the rock is not necessarily as uncommon as this circumstance might imply (Larrabee, 1966a). No such brightly colored rodingite has been described elsewhere in the United States.

The rodingite is composed of bright-green chromian aluminous diopside, cinnamon to pink grossularite, white diopside, zoisite, prehnite, and other minerals. The dikelike intrusive bodies provide striking contrast with the host ultramafite, are approximately parallel to each other—strike N. 50°–65° E.—and most of them dip steeply or vertically. The diopside is a still brighter green, reflecting the higher chromium content, and grossularite is more abundant in the northeast end of the open pit than in the active benches of the southwest end. Well-defined compositional layering characterizes

U.S. GEOL. SURVEY PROF. PAPER 600-D, PAGES D195-D196

some of the smaller rodingites, the layers paralleling the walls of the dikes. Most contacts of the rodingite and serpentinite are slightly sheared, with chlorite, picrolite, or calcite and dolomite along the shear planes. The presence of tremolite of two apparent ages or stages in adjacent serpentinite indicates that calcium escaped from the gabbro during more than one stage of its metasomatism to rodingite. Strong narrow shear zones alternate with hard fresh rock in the southeast part of the quarry. In places the dikes have been offset a few feet by faulting.

Small veins include chrysotile and clinochrysotile, tremolite, talc, chlorite, calcite-dolomite, aragonite, deweylite, magnesite (and rarely hydromagnesite), anthophyllite, penninite, coalingite, tourmaline with clinozoisite-epidote, grossularite, hyalite, and chalcedony.

The major geologic factors affecting the use and economics of this important source of crushed stone are the fibrous nature of the antigorite, the attached minute but heavier particles of magnetite, the presence of very hard and heavy rodingite, and the shear planes and joints. The interlocking fibers add toughness to the crushed rock, and a mesh texture when the fine particles are used as asphalt binder. The attached minute magnetite particles increase the rate of settling of fibers from the air and thus reduce loss by wind dispersion. The rodingite improves the overall hardness of the various sized aggregates, but it adds to costs of drilling, blasting, the use of dropball, crushing, and screening. Shear planes contribute to back-break, thus increasing quarry costs in places and providing planes of weakness for rockfalls and slides. Where shear zones are present, as along the southeast side of the quarry, the rock is more deeply weathered and is discarded. Close joints are beneficial in that they lower blasting and crushing costs. The quarry is the principal source of crushed rock in northwestern Washington, D.C., and nearby parts of Montgomery County, Md. It therefore is an important economic factor in the expansion of building and highway construction in the Washington area.

REFERENCES

Cloos, Ernst, and Cooke, C. W., 1953, Geologic map of Montgomery County and the District of Columbia: Maryland Dept. Geology, Mines, and Water Resources, scale 1:62,500.

Larrabee, D. M., 1966a, Map showing distribution of ultramafic and intrusive mafic rocks from northern New Jersey to eastern Alabama: U.S. Geol. Survey Misc. Geol. Inv. Map I–476, scale 1:500,000.

——— 1966b, Serpentinite quarry at Hunting Hi", Montgomery County, Maryland: U.S. Geol. Survey open-file map, scale 1:1,200.

ACCESSORY ZIRCON FROM GRANITOID ROCKS OF THE MOUNT WHEELER MINE AREA, NEVADA

By DONALD E. LEE,[1] T. W. STERN,[2] R. E. MAYS,[3] and R. E. VAN LOENEN,[1]
[1] Denver, Colo., [2] Washington, D.C., [3] Menlo Park, Calif.

Abstract.—Twenty-five accessory zircon fractions recovered from granitoid rocks exposed just north of the Mount Wheeler mine area, Nevada, have been studied. Minor-element contents are listed for all; physical properties and radiometric age data are given for a few. Results support the conclusion reached from previous work on other minerals and indicate that the large compositional range and systematic chemical gradients found in the intrusive rocks result more from assimilation of sedimentary rocks than from differentiation of magma. Uranium-thorium-lead isotope ages given by one zircon concentrate date the time of crystallization as Middle Jurassic. Pb/α determinations on three zircon fractions recovered from small xenoliths gave mid-Tertiary ages, and these low ages appear to result from loss of lead.

The Mount Wheeler mine area is in the southern part of the Snake Range, about 50 miles southeast of Ely, Nev. The granitoid rocks studied intrude lower Paleozoic sedimentary rocks and are exposed in a westward-trending band 1–3 miles wide (Drewes, 1958; Whitebread and others, 1962). Within an outcrop area of about 20 square miles, the intrusive rock ranges in composition from granodiorite with a CaO content of 4.5 percent to quartz monzonite with a CaO content of 0.5 percent. The higher CaO values are found where the igneous rock is in contact with Middle Cambrian Pole Canyon Limestone, the lower CaO values where it is in contact with Lower Cambrian Prospect Mountain Quartzite, indicating that CaO values reflect assimilation of the country rock.

Mineralogical differences that are related to variations in composition of the intrusive rock include variations in types of accessory minerals (Lee and Dodge, 1964) and in rare-earth contents of accessory allanite and monazite (Lee and Bastron, 1967). This paper describes the zircon types present in the intrusive rock. Minor-element contents have been determined for 25 zircon fractions, physical properties and lead-alpha age data for a few, and isotopic ages for one. Variations in some of these properties can be related to CaO content of the intrusive rock.

Acknowledgments.—We gratefully acknowledge the use of a 12-inch solid-source mass spectrometer in the Analytical Mass Spectrometric Section, National Bureau of Standards, Washington, D.C. (W. R. Shields, section chief).

ACCESSORY ZIRCON

After the preliminary concentration according to the method described by Lee and Dodge (1964), the zircon fractions were purified by centrifuging in methylene iodide and by use of the Frantz isodynamic separator. Clerici solution was not used. As the final step in the cleaning, each zircon fraction was subjected to ultrasonic vibration in distilled water for about an hour.

As noted by Lee and Dodge (1964, fig. 4), the zircon content of the intrusive rocks shows a fairly regular increase with an increase of CaO. The present study shows (fig. 1) that the zircon content of the more CaO-

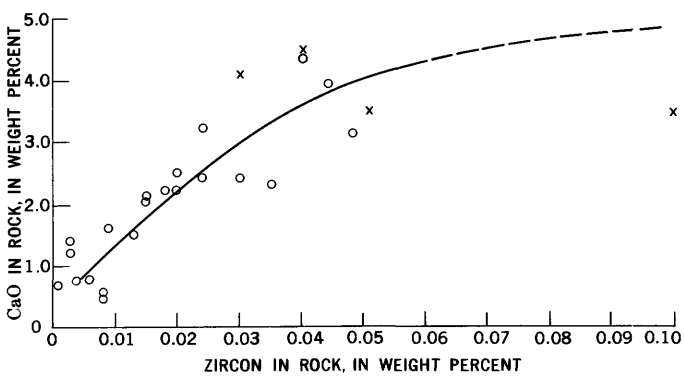

FIGURE 1.—Relation between amounts of CaO and zircon in 25 rocks on which this study is based. o, sample from main intrusive phase; x, xenolith.

rich rocks is 5–50 times as great as that of the CaO-poor rocks. Recovery of more than about 25 milligrams of clean zircon from rocks with a CaO content of less than about 1.5 percent was difficult, and so in general less information was obtained on the physical properties of zircons from such rocks.

Physical properties

The granitoid rocks in the Mount Wheeler mine area, Nevada, contain zircons having a rather wide range in size and elongation ratio (figs. 2, 3). The CaO-rich rocks contain acicular zircons, with elongation ratios in some grains reaching the extreme value of 20. The elongation ratios of the zircons show a rather large range; nevertheless, zircons recovered from the more mafic (CaO-rich) rocks are very similar in appearance from grain to grain, largely because of the simplicity of crystal habits and the clean, well-defined appearance of the grains (fig. 2). Many of the acicular zircons are completely free of inclusions. What inclusions are present are nearly always colorless, have indices of refraction much smaller than those of zircon, and are likely to be systematically oriented. Some of these inclusions may be apatite. The acicular zircons are almost devoid of zoning. Zoning, where present, is concentric, and indicates that the first-formed portions of the crystals also were elongated. This zoning is not pronounced; the difference between indices of refraction of adjacent zones is estimated to be less than 0.003 where observed. The outer zones may have either a higher or a lower index of refraction than the interior ones.

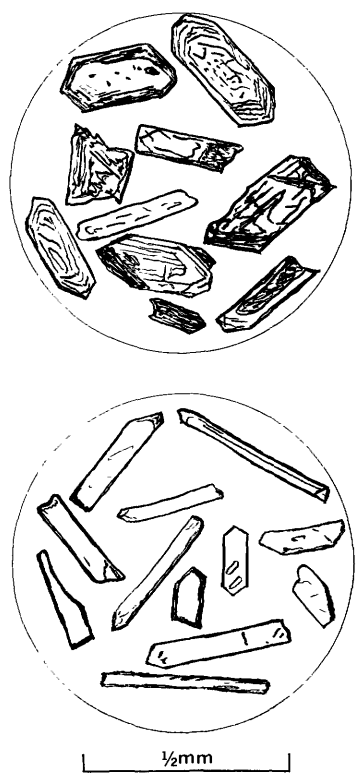

FIGURE 2.—Representative zircon concentrates recovered during this study. Top, zircons recovered from sample 63–MW–60, part of the main intrusive phase having a CaO content of 0.55 percent. Note the relatively clean grain near the center of the field. The number and clarity of those grains increase gradually with CaO content of the rock until an assemblage like the one below results. Bottom, zircons recovered from sample 40B–MW–60, a xenolith with a CaO content of 3.5 percent. This assemblage is typical of those recovered from rocks with a CaO content of 2.2 percent or more.

Zircons from CaO-poor rocks rarely have an elongation ratio greater than 6. The grains differ much more in appearance. Most grains contain many tiny inclusions that have haphazard orientation. Repeated zoning is common, with indices of refraction of adjacent zones estimated to differ by 0.005 or more.

According to the findings by Poldervaart (1956), such differences are not usually evident in zircons from a single pluton. The acicular zircon from the CaO-rich rocks of the Mount Wheeler mine area is much like the mineral described by Wyatt (1954), who studied the Monadhliath granite in Scotland and concluded (1954, p. 988) that "* * * the evidence indicates that very elongated zircon is produced only in granite which has been contaminated * * *." Taubeneck (1957) and Huang (1958) emphasized the greater elongation ratio of zircon from hybrid rocks. In the Mount Wheeler mine area the greatly elongated zircon is found where the country rock is limestone or shale; that contamination occurred is indicated both by the increased CaO content of the intrusive and by the presence of many xenoliths of Pioche Shale (Lee and Bastron, 1962, p. 1328).

Though differing in abundance, size, and elongation, the zircons from CaO-poor and CaO-rich rocks do not differ appreciably in optical properties (table 1). Indices of refraction of zircons recovered from a single hand specimen show about as great a range as do those from CaO-rich to CaO-poor rocks. Values are in the upper part of the range expectable for zircon, indicating relatively fresh, nonmetamict material (Deer and others, 1962, p. 59–66).

Unit-cell parameters (table 1) were calculated for several of the zircons by least-squares refinement of powder diffractometer data, using an internal standard of CaF_2 and a self-indexing computer program developed by Evans, Appleman, and Handwerker (1963). Results agree rather closely and these, too, typify relatively fresh, nonmetamict material (Deer and others, 1962, p. 59–66). Compared to the other zircons listed in table 1, however, samples 49–DL–61 and 63–MW–60 appear to have undergone incipient metamictization, as is indicated by their slightly expanded cell parameters and their less sharp diffractometer patterns.

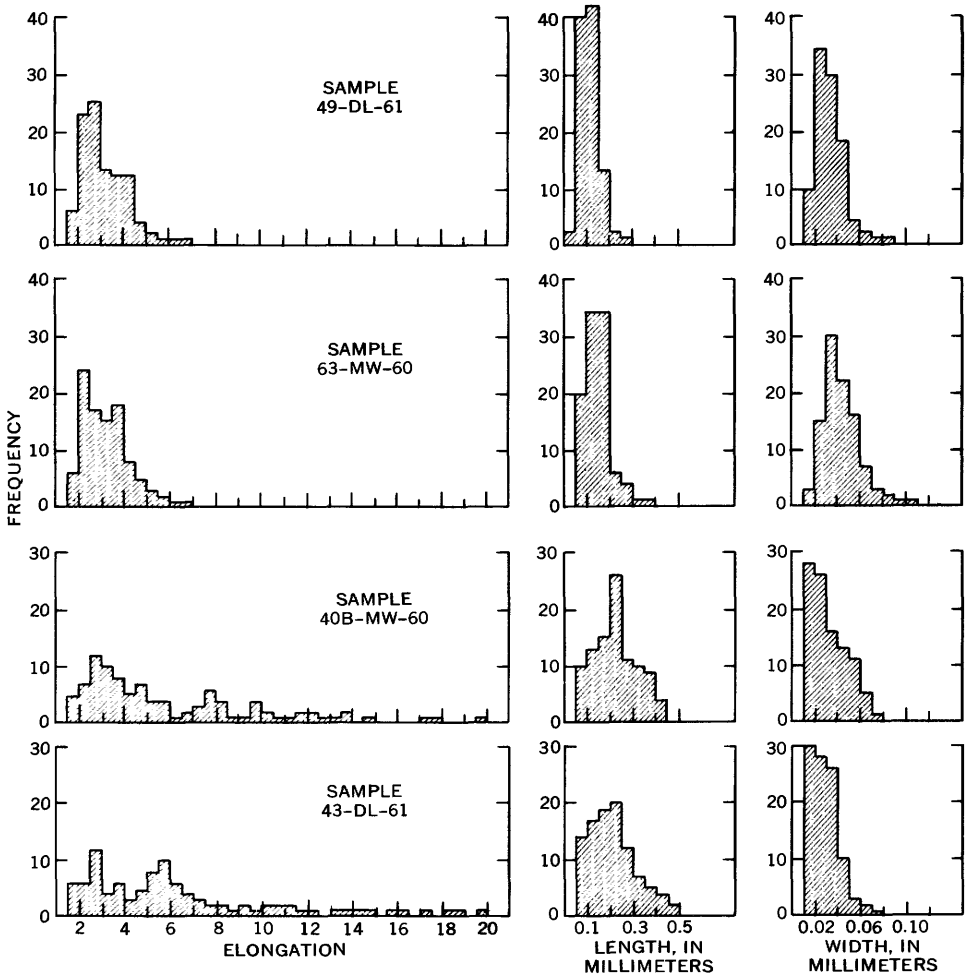

FIGURE 3.—Elongation- and size-frequency histograms of four representative zircon fractions (table 1). Upper two samples are from CaO-poor rocks, lower two samples from CaO-rich rocks. Note that size scales for length- and width-frequency histograms are not the same. Plots are based on counts of 200 zircons from each rock.

Spectrographic analyses

Semiquantitative spectrographic analyses of the zircons are listed in table 1. Amounts of elements like Ca and Ti probably are a measure of contamination by such closely associated minerals as sphene and apatite. The contamination may have resulted from inclusions or compound grains. Some of the CaO-poor rocks contain tiny amounts of blue anatase, and because of its high specific gravity and low paramagnetic susceptibility this mineral was especially difficult to separate quantitatively from the zircon.

If it is correct that the uranium content of the granitoid rocks is nearly uniform throughout the area under study and that the uranium in these rocks is mostly in the zircon lattice, then the trend shown in figure 4 could be attributed to the sparsity of zircons in the CaO-poor rocks (fig. 1); the sparsely distributed zircons in the CaO-poor rocks contain more uranium in their crystal lattices than do the more abundant zircons in the CaO-rich rocks.

From the standpoint of igneous processes, one of the most studied and interesting aspects of accessory zircon is its content of hafnium. It has been shown (Lyakhovich and Shevaleyevskii, 1962; Gottfried and Waring, 1964) that hafnium content is higher in zircon from early-formed gabbroic rocks than in zircon from late siliceous differentiates. Hevesy (1925), Hevesy and Jantzen (1923), Fleischer (1955), and several more recent investigators have shown that accessory zircon from alkalic rocks is characterized by low hafnium content. Hafnium-poor zircon also has been described from hybrid granites, and this is of particular interest to us here. Lyakovich and Shevaleyevskii (1962, p. 522) stated, "A higher than average ZrO_2/HfO_2 ratio would indicate that assimilation must have occurred on a large scale during emplacement of the igneous body." The

TABLE 1.—*Analytical data and physical properties for*

[Samples arranged in order of increasing CaO content.
CaO analyses by Paul Elmore, Samuel Botts, H. Smith, and Gillison Chloe.
Indices of refraction determined in sodium light by the immersion method.
Cell parameters were obtained by least-squares refinement of powder diffractometer data, using a self-indexing computer program developed by Evans, Appleman, and Handwerker (1963). The internal standard was CaF_2. Margin of error for both a and c is ±0.001A, except as noted.

Sample No.	49-DL-61	63-MW-60	229-MW-61	230-MW-61	238-MW-61	190-MW-61	205-MW-61	147-MW-61	234-MW-61	190-DL-62	71-MW-60	14-MW-60
CaO in rock (weight percent)	0.47	0.55	0.68	0.75	0.78	1.2	1.4	1.5	1.6	2.0	2.1	2.2
Indices of refraction												
1 ϵ±0.005		1.977–1.985				1.978–1.987				1.980–1.990		1.987–1.990
		1.981 (avg)				1.983 (avg)				1.985 (avg)		1.989 (avg)
2 ω± 0.005		1.922–1.930				1.922–1.928				1.920–1.930		1.928–1.931
		1.926 (avg)				1.925 (avg)				1.925 (avg)		1.930 (avg)
3 $\epsilon-\omega$		0.055				0.058				0.060		0.059
Cell parameters												
4 a (A)	6.624 (±.004)	6.621						6.605		6.607	6.605	
5 c (A)	6.015 (±.009)	6.002 (±.003)						5.988		5.989	5.984	
6 c/a	.9082	.9065						.9066		.9064	.9068	
7 Volume (A^3)	263.92 (±.35)	263.15 (±.11)						261.27 (±.06)		261.44 (±.05)	261.09 (±.07)	
Semiquantitative spectrographic analyses (weight percent)												
8 Al	0.2	0.15	0.3	0.1	0.07	0.7	0.15	0.15	0.015	1.5	3	0.05
9 Fe	.1	.02	.1	.15	.02	.07	.07	.1	.05	.05	.1	.015
10 Mg	.005	.002	.003	.01	.0015	.005	.007	.015	.005	.0015	.002	.0015
11 Ca	.15	.07	.3	.15	.03	.5	.7	.7	.1	1.5	3	.1
12 Ti	.2	.3	.03	.02	1.5	.03	.3	.1	.03	.01	.02	.015
13 Mn	.003	.0007	.003	.003	.001	.003	.007	.007	.002	.003	.007	0
14 B	.005	0	.001	.003	.001	0	.003	.0015	0	0	0	0
15 Hf	.5	.5	.3	.5	.3	.5	.7	.2	.5	.15	.15	.5
16 Nb	.01	.005	.003	.005	.015	.003	.007	.007	.003	0	0	.003
17 Ni	0	0	.0015	.001	.0007	0	0	0	0	0	0	0
18 Pb	.007	.015	.007	.005	.007	.003	.02	.01	0	.005	(2)	0
19 Sb	.07	0	0	.015	.015	0	0	0	0	0	0	0
20 Sc	.07	.07	.07	.1	.07	.05	.07	.03	.05	.02	.015	.03
21 Sn	.1	.003	.1	.15	.0015	.003	.07	.03	.01	.007	0	0
22 Sr	0	0	.0015	0	0	.003	0	.002	0	.007	.05	0
23 Th	.1	.15	.1	.1	.07	.07	.07	.07	.1	0	0	.05
24 U	.5	.5	.3	.5	.5	.5	.5	.3	.3	0	0	.15
25 V	0	.003	0	0	0	0	0	0	.003	0	.002	.003
26 Y	.5	.5	.2	.7	.7	.5	.3	.7	.5	.3	.2	.3
27 Yb	.15	.1	.1	.1	.1	.1	.15	.1	.1	.05	.05	.05
28 Gd	.03	0	.02	.05	.02	.02	.015	.02	0	0	0	0
29 Dy	.05	0	.03	.05	.05	.03	.03	.05	0	0	0	0
30 Other	None	(Be) .0005	(W) .02	(Hg)[4]	None	None	None	(La) .02	None	None	None	None
Lead-alpha age determinations												
31 α/mg-hr											647	
32 Pb ppm											57.5	
33 Pb/α age, m.y.											220±25	

[1] Xenolith.
[2] See quantitative lead value below.

hafnium values (0.15–0.7 percent) listed in table 1 are even lower than the results given in the papers just cited, and thus agree with the idea that assimilation has been important in the history of these rocks. The small range in hafnium values shows no obvious correlation with the geology.

Zircons from the CaO-poor rocks tend to contain more thorium than those from CaO-rich rocks (fig. 4*B*), but the thorium trend is not as steep as for uranium (fig. 4*A*), and the reason for the trend is probably different. Study of monazite from these same rocks (Lee and Bastron, 1967) showed that there is a relative dearth of thorium where CaO is abundant. The relation shown in figure 4*B* is consistent with this observation. Regarding the thorium contents of these zircons, about 100 micrograms of a green mineral identified as metamict thorite or huttonite was recovered from 1,000 grams of sample 126–MW–61. This mineral has a specific gravity above 3.32 and is optically isotropic with an index of refraction near 1.80; the small fraction analyzed spectrographically showed lines only for silicon and thorium. The thorium content of the zircon coexisting with this mineral is 0.07 percent, not notably high.

The allanites and monazites that coexist with these 25 zircons show an appreciable range of composition in terms of the rare-earth elements (Lee and Bastron,

accessory zircons from the Mount Wheeler mine area, Nevada

Semiquantitative spectrographic analyses by R. E. Mays. Results are based on their identity with geometric brackets whose boundaries are 1.2, 0.83, 0.56, 0.38, 0.26, 0.18 0.12, and so forth, and are reported arbitrarily as midpoints of these brackets, 1., 0.7, 0.5, 0.3, 0.2, 0.15, 0.1, respectively. The precision of a reported value is approximately plus or minus one bracket at 68-percent, or two brackets at 95-percent confidence. 0, below limit of detection; leaders, (---), not determined.
Age values determined by T. W. Stern from lead determinations by Harold Westley. All lead values are averages of duplicate determinations. Basis of calculations given in table 3]

36-DL-61	8-DL-61	31-DL-60	38-MW-61	40A-MW-60	25-DL-61	152-MW-61	40B-MW-60 [1]	126-MW-61 [1]	43-DL-61	27-DL-61 [1]	16-MW-60	98-DL-62 [1]	
2.2	2.3	2.4	2.4	2.4	3.1	3.2	3.5	3.5	3.9	4.1	4.3	4.5	
Indices of refraction—Continued													
---	---	1.980–1.983	---	1.985–1.993	1.982–1.990	1.989–1.991	1.983–1.990	1.985–1.992	---	---	---	1.989–1.991	1
		1.982 (avg)		1.989 (avg)	1.986 (avg)	1.990 (avg)	1.987 (avg)	1.989 (avg)				1.990 (avg)	
---	---	1.920–1.924	---	1.921–1.930	1.923–1.930	1.929–1.931	1.922–1.928	1.925–1.930	---	---	---	1.929–1.932	2
		1.922 (avg)		1.926 (avg)	1.927 (avg)	1.930 (avg)	1.925 (avg)	1.928 (avg)				1.931 (avg)	
---	---	0.060	---	0.063	0.059	0.060	0.062	0.061	---	---	---	0.059	3
Cell parameters—Continued													
---	---	---	6.604	6.605	---	---	6.608	---	---	---	---	6.603	4
---	---	---	5.984	5.986	---	---	5.984	---	---	---	---	5.980	5
---	---	---	.9061	.9063	---	---	.9056	---	---	---	---	.9056	6
---	---	---	261.01 (±.05)	261.13 (±.04)	---	---	261.25 (±.05)	---	---	---	---	260.75 (±.04)	7
Semiquantitative spectrographic analyses (weight percent)—Continued													
0.03	0.07	0.05	0.05	1.5	0.3	0.05	0.1	0.1	0.05	0.05	0.02	0.15	8
.05	.07	.03	.1	.2	.07	.015	.05	.05	.015	.07	.03	.15	9
.005	.005	.005	.01	.005	.005	.0007	.005	.01	.0007	.005	.002	.02	10
.15	.3	.2	.15	1	1	.2	.2	.2	.05	.02	.1	.2	11
.015	.1	.07	.07	1.5	1.5	.1	.015	.015	.02	.02	.07	.015	12
.0005	.001	.0002	.005	.007	.003	0	.0015	.0015	0	.0015	0	.0015	13
0	0	0	0	0	0	0	0	0	0	0	0	0	14
.5	.3	.3	.7	.5	.15	.5	.5	.5	.3	.3	.5	.5	15
.005	.003	0	0	0	.005	0	0	0	0	0	0	0	16
0	0	0	0	0	0	0	0	0	0	0	0	0	17
(2)	.005	0	.015	(3)	.005	0	(2)	(2)	0	(2)	(2)	(2)	18
0	0	0	0	0	0	0	0	0	0	0	0	0	19
.03	.03	.03	.03	.02	.015	.03	.02	.02	.02	.03	.03	.015	20
0	0	0	0	0	.007	.02	0	0	0	0	0	0	21
0	0	0	0	.01	.003	0	0	0	0	0	0	0	22
.05	.05	.05	.07	.1	0	.05	.07	.07	0	.05	0	.07	23
.05	0	.05	.3	0	0	.05	0	0	0	0	0	0	24
.003	0	0	0	.0015	.003	0	.0015	.0015	0	.002	.002	0	25
.3	.3	.3	.15	.15	.3	.3	.15	.15	.3	.3	.2	.1	26
.05	.05	.05	.07	.07	.05	.05	.07	.07	.05	.05	.05	.05	27
0	0	0	0	0	0	0	0	0	0	0	0	0	28
0	0	0	0	0	0	0	0	0	0	0	0	0	29
None	None	None	None	None	None	None	None	None	None	None	(Au) .003 (W) .02 (Hg) [4]	None	30
Lead-alpha age determinations—Continued													
584	---	---	---	---	---	---	283	443	---	428	302	405	31
43.0	---	---	---	---	---	---	2.0	6.8	---	29.0	20.5	6.7	32
180±20	---	---	---	---	---	---	20±10	40±10	---	170±30	170±20	40±10	33

[3] Lead value for 40A-MW-60 given in table 2.
[4] Present in less than measurable amount.

1967). Yttrium and the heavier lanthanides are present in largest amounts in minerals from the more felsic rocks, whereas the lighter or more basic lanthanides increase in abundance directly with CaO content of the rocks. Though rare-earth contents of the 25 zircons are much smaller, the same trend is apparent from the higher amounts of Y in zircons from the rocks poor in CaO (fig. 4*C*) and also from the fact that detectable amounts of Gd and Dy are found only in these same zircons (table 1). Scandium shows a trend (fig. 4D) very similar to that of Y, with which it is closely related chemically.

Small amounts of Nb, Sn, Sb, and B are present in some of the zircons from the rocks low in CaO (table 1). Deer, Howie, and Zussman (1962, p. 61) stated that such elements are more probably present as inclusions in zircon than in the zircon lattice; and this is a likely explanation for the small amounts of Nb, Sn, Sb, and B shown in table 1, for the same zircons contain the greatest number and variety of inclusions.

As shown in table 1, small amounts of other elements such as Hg, W, and Au were detected in some samples, and are present either as inclusions or as part of the zircon lattice.

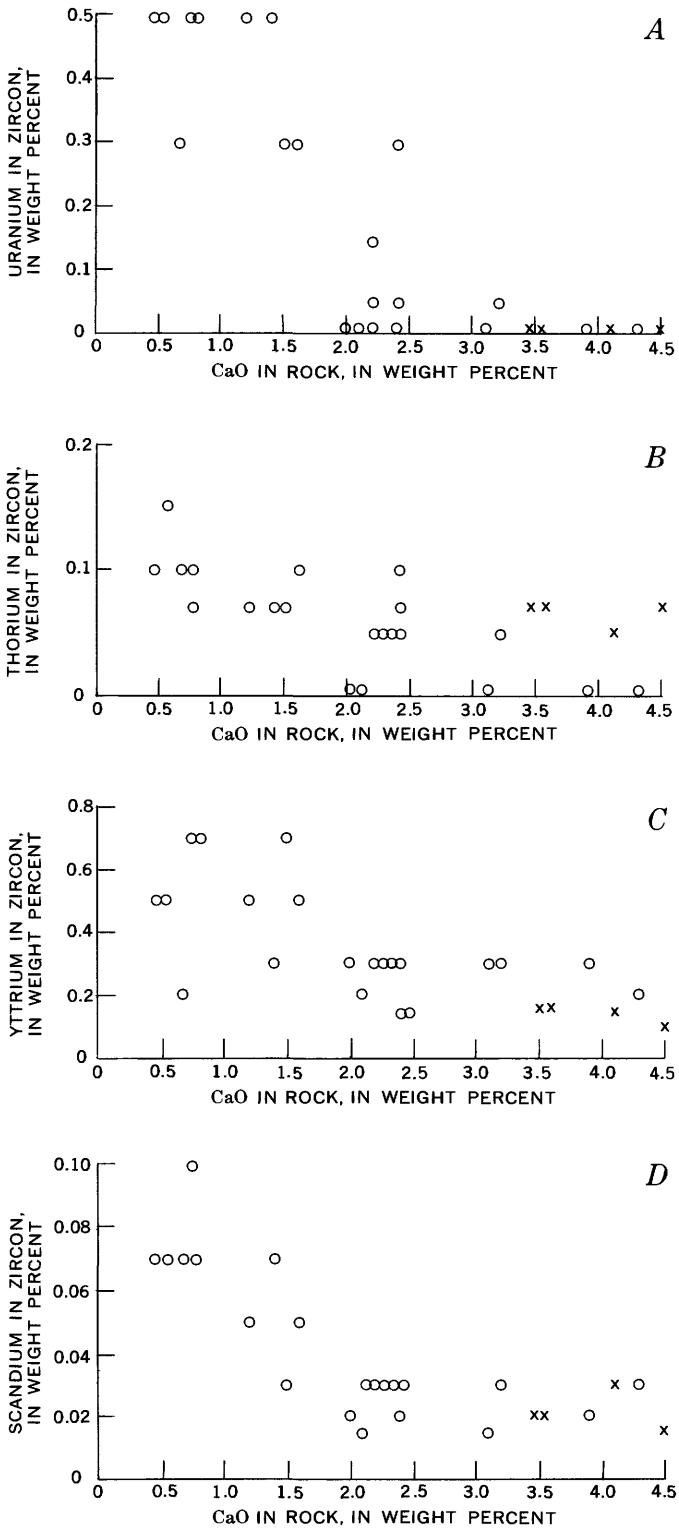

FIGURE 4.—Weight percentage of CaO in rock versus weight percentage of uranium (*A*), thorium (*B*), yttrium (*C*), and scandium (*D*) in constituent zircon. o, sample from main intrusive phase; x, xenolith.

Radiometric age determinations

Pb/α ages were determined for seven of the zircon fractions (table 1). Four of the ages are in the range 170 ± 20–220 ± 25 million years and three are in the range 20 ± 10–40 ± 10 m.y. Each of the three lower ages was determined on zircons recovered from a xenolith about the size and shape of a coconut. Ordinarily one would expect xenolithic zircons to show an age older, not younger, than zircons from the host intrusive phase, and so we were very surprised by the three young ages listed in table 1.

There is a general decrease in radioactivity (α/mg-hr) of the zircons as the CaO content of the rocks decreases, as one would expect from the uranium and thorium values already discussed. The most striking aspect of these age data, however, is the very small amounts of lead found in the three zircon fractions recovered from small xenoliths. Probably there has been loss of lead from these zircons through diffusion, but it is obvious that this explanation meets with difficulties, for two reasons. First, as already described, the zircons recovered from these small xenoliths are fresh and so would not be as readily susceptible to diffusion as the Precambrian, somewhat metamict zircon described by Tilton and others (1964). Second, in the case of our zircons there is a relatively short period of time ($180\pm$ m.y.) available for diffusion of lead to take place.

Table 2 presents uranium-thorium-lead isotope ages for zircon 40A–MW–60; the data show that the age of this zircon is Middle Jurassic. The processes that resulted in the very low lead values and consequent mid-Tertiary Pb/α ages may be related in some way to assimilation of the xenolithic masses from which the zircons in question were recovered. Whatever the nature of these processes, it is clear that sharply lowered Pb/α ages are not always found in zircons from similar environments. For comparative purposes, table 3 gives Pb/α ages for two zircon fractions recovered from rocks collected in the House Range, Millard County, Utah. Zircon 298–DL–64 is from the main intrusive phase, a porphyritic quartz monzonite (Gehman, 1958), whereas 299–DL–64 is from a coconut-size xenolith about 10 feet away. The Pb/α ages determined from these two zircon fractions are about the same, although the zircon from the xenolith actually has a higher lead content.

SUMMARY AND CONCLUSIONS

The results of this study support the idea that assimilation of country rock has played a significant role

TABLE 2.—*Uranium-thorium-lead isotopic ages of sample 40A–MW–60 zircon from Mount Wheeler mine area, Nevada*

[T. W. Stern and M. F. Newell, analysts]

Concentration (ppm)			Atom percent abundance				Ages (m.y.)		
U	Th	Pb	Pb^{204}	Pb^{206}	Pb^{207}	Pb^{208}	$\frac{Pb^{206}}{U^{238}}$	$\frac{Pb^{207}}{U^{235}}$	$\frac{Pb^{208}}{Th^{232}}$
411. 5	203. 9	12. 84	0. 215	73. 82	7. 10	18. 86	162	175	153

Decay constants: $U^{238} = 1.54 \times 10^{-10}\ yr^{-1}$
$U^{235} = 9.72 \times 10^{-10}\ yr^{-1}$
$Th^{232} = 4.88 \times 10^{-11} yr^{-1}$

Atomic ratios: $U^{238}/U^{235} = 137.7$
$Pb^{204}, Pb^{206}, Pb^{207}, Pb^{208} = 1.000, 18.51, 15.72, 38.44$

TABLE 3.—*Lead-alpha ages of two zircons from the House Range, Millard County, Utah*

[T. W. Stern, analyst. See text for exact locations and descriptions of samples]

Sample No.	Alpha/mg-hr	Pb (ppm)[1]	Age (m.y.)[2]
298–DL–64	854	69	200±40
299–DL–64	1, 510	111. 5	180±20

[1] Lead determination by Harold Westley. Single determination made for 298–DL–64; value for 299–DL–64 is average of two determinations.
[2] Ages were calculated using the following equations:
(a) $t = c$ lead/alpha, and
(b) $t_o = t - \frac{1}{2}Kt^2$,
where c=constant (based upon an assumed Th/U ratio of 1) equal to 2,485,
K=constant equal to 1.56×10^{-4},
t=approximate age in millions of years,
t_o=age in millions of years, corrected for decay of parents,
lead=lead content in parts per million, and
alpha=alpha activity in alpha/mg-hr.

in the history of these granitoid rocks of the Mount Wheeler mine area, Nevada. These results include:

1. The crystal morphology of zircons from the CaO-rich rocks is almost identical to that of zircons taken from hybrid rocks in other areas. Distinctive features include large elongation ratios and rather simple crystal habits.
2. The very low Hf content of these zircons is consistent with the idea that assimilation has taken place.
3. Zircons from the more CaO-poor rocks tend to concentrate more of the heavier, less basic rare earths. Though not as well defined as the evidence provided by the allanites and monazites described previously, this still agrees with that evidence and favors assimilation over differentiation as an explanation for the chemical gradients observed.

Uranium-thorium-lead isotope ages date the crystallization of these rocks as Middle Jurassic. Mid-Tertiary Pb/α ages for three zircon fractions recovered from rather small xenoliths alert us to the apparent loss of lead, which may have resulted from diffusion in the solid state. Speculation on possible defects in the crystal structure of these zircons must await single-crystal study.

REFERENCES

Deer, W. A., Howie, R. A., and Zussman, J., 1962, Rock-forming minerals, v. 3, Sheet silicates: New York, John Wiley & Sons, Inc., 270 p.

Drewes, H. D., 1958, Structural geology of the southern Snake Range, Nevada: Geol. Soc. America Bull., v. 69, no. 2, p. 221–239.

Evans, H. T., Jr., Appleman, D. E., and Handwerker, D. S., 1963, The least squares refinement of crystal unit cells with powder diffraction data by an automatic computer indexing method [abs.]: Am. Cryst. Assoc. Ann. Mtg., 1963, Program and Abs., no. E–10, p. 42.

Fleischer, M. B., 1955, Hafnium content and hafnium-zirconium ratio in minerals and rocks: U.S. Geol. Survey Bull. 1021–A, p. 1–13.

Gehman, H. M., Jr., 1958, Notch Peak intrusive, Millard County, Utah—Geology, petrogenesis, and economic deposits: Utah Geol. and Mineralog. Survey Bull. 62, 50 p.

Gottfried, David, and Waring, C. L., 1964, Hafnium content and Hf/Zr ratio in zircon from the southern California batholith, *in* Geological Survey Research 1964: U.S. Geol. Survey Prof. Paper 501–B, p. B88–B91.

Hevesy, G. von, 1925, The discovery and properties of hafnium: Chem. Reviews, v. 2, p. 1–41.

Hevesy, G. von, and Jantzen, V. T., 1923, The hafnium content of zirconium ores: Jour. Chem. Soc., v. 123, p. 3218–3223.

Huang, W. W. T., 1958, Zircons in the Precambrian igneous rocks, Wichita Mountains, Oklahoma [abs.]: Geol. Soc. America Bull., v. 69, no. 12, pt. 2, p. 1589.

Lee, D. E., and Bastron, Harry, 1962, Allanite from the Mount Wheeler area, White Pine County, Nevada: Am. Mineralogist, v. 47, nos. 11–12, p. 1327–1331.

——— 1967, Fractionation of rare-earth elements in allanite and monazite as related to geology of the Mount Wheeler mine area, Nevada: Geochim. et Cosmochim. Acta, v. 31, no. 3, p. 339–356.

Lee, D. E., and Dodge, F. C. W., 1964, Accessory minerals in some granitic rocks in California and Nevada as a function of calcium content: Am. Mineralogist, v. 49, nos. 11–12, p. 1660–1669.

Lyakhovich, V. V., and Shevaleyevskii, I. D., 1962, Zr: Hf ratio in the accessory zircon of granitoids: Geochemistry (Geokhimiya), no. 5, p. 508–524.

Poldervaart, Arie, 1956, Zircons in rocks—pt. 2, Igneous rocks: Am. Jour. Sci., v. 254, no. 9, p. 521–554.

Taubeneck, W. H., 1957, Zircons in the metamorphic aureole of the Bald Mountain batholith, Elkhorn Mountains, northeastern Oregon [abs.]: Geol. Soc. America Bull., v. 68, no. 12, pt. 2, p. 1803–1804.

Tilton, G. R., Davis, G. L., Hart, S. R., Aldrich L. T., Steiger, R. H., and Gast, P. W., 1964, Geochronology and isotope geochemistry: Carnegie Inst. Washington Year Book 63, 1963–64, p. 240–256.

Whitebread, D. H., Griggs, A. B., Rogers, W. B., and Mytton, J. W., 1962, Preliminary geologic map and sections of the Wheeler Peak quadrangle, White Pine County, Nev.: U.S. Geol. Survey Mineral Inv. Field Studies Map MF–244.

Wyatt, Michael, 1954, Zircons as provenance indicators: Am. Mineralogist, v. 39, nos. 11–12, p. 983–990.

SOLVING PROBLEMS IN PHOSPHATE MINERALOGY WITH THE ELECTRON PROBE

By CYNTHIA W. MEAD and MARY E. MROSE,
Washington, D.C.

Abstract.—Qualitative and quantitative electron-probe analyses of nonconducting minerals, in conjunction with single-crystal and powder diffraction X-ray data, have been used successfully to solve several problems in phosphate mineralogy. The formulas of calcioferrite from Battenburg, Bavaria, and montgomeryite from Fairfield, Utah—minerals inferred to be isostructural on the basis of powder patterns—have been established by quantitative electron-probe analysis. Type zincian rockbridgeite from Maxedo, Portugal, has been shown to be a mixture of zincian lipscombite and zincian rockbridgeite. Electron-probe spectrometer traces, together with quantitative determinations of P and S, led to the identification of a mineral from Butte, Mont., as hinsdalite. Qualitative analysis of a white mineral from Västanå (Westanå), Sweden, confirmed that it has a composition similar to pink orthorhombic attakolite from the same locality and therefore is its monoclinic dimorph.

Qualitative and quantitative electron-probe analyses have been used in conjunction with single-crystal and powder diffraction X-ray data to solve several problems in phosphate mineralogy. Four such problems, presented in part at the First National Conference on Electron Probe Microanalysis, at College Park, Md., in 1966, are discussed in detail here.

SAMPLE PREPARATION AND OPERATING CONDITIONS

All the samples were prepared by mounting tiny fragments of the minerals in epoxy resin. Rough polishing of the samples was done manually on a series of silicon carbide papers down to 600 grit. Final polishing was done on vibratory polishers using Linde A (0.3 micron Al_2O_3) and Linde B (0.05μ Al_2O_3) as polishing compounds. The surfaces of the samples were coated with a layer of carbon to make them electrically conducting. The carbon coating was somewhat heavier than usual in order that the sample surfaces would not be damaged by bombardment with the electron beam. In order to insure further that the sample surface would not be damaged, operating voltages not greater than 20 kilovolts and specimen currents not greater than 0.02 microamperes were used. A commercially built electron-probe having an effective take-off angle of 41° was used for the analyses.

PROBLEMS AND THEIR SOLUTION

Problem 1.—The first problem involved the analysis of two extremely rare minerals: (1) type calcioferrite, a hydrated calcium ferric phosphate of uncertain formula, from Battenberg, Bavaria, and (2) montgomeryite, a hydrated calcium aluminum phosphate with questionable formula, from Fairfield, Utah. X-ray powder patterns indicated the minerals to be isostructural, but the quantities available were not large enough to permit even partial chemical analyses by conventional methods. The following mineral standards used in the analyses were selected on the basis of qualitative determinations by electron-probe spectrometer traces on the unknowns.

Mineral standard	Chemical analyses (ir percent)			
	Fe	Al	Ca	P
Pyroxene	2. 3	------	17. 6	-------
Väyrynenite	4. 6	------	------	17. 4
Albite	------	11. 0	1. 9	-------

For the analyses of the unknowns, a LiF crystal was used for the determination of Fe, a KAP (potassium acid phthalate) crystal was used for the determination of Al and P, and a PET (pentaerythritol) crystal was used for the determination of Ca. The data are corrected for background and absorption. Results of the quantiminations by electron-probe spectrometer traces on the unknowns.

Specimens	Electron-probe analyses (in percent)			
	Fe	Al	Ca	P
Calcioferrite	19. 0	--------	10. 0	14. 8
Montgomeryite	--------	11. 1	13. 0	16. 5

U.S. GEOL. SURVEY PROF. PAPER 600-D, PAGES D204-D206

These data, together with crystallographic considerations, led to the following formulas for the two minerals: $Ca_2Fe_2(PO_4)_3(OH)\cdot 7H_2O$, for calcioferrite; and $Ca_2Al_2(PO_4)_3(OH)\cdot 7H_2O$, for montgomeryite. These satisfied the space-group criteria established by single-crystal X-ray work. The advantage of the electron probe for analyzing small samples is immediately evident.

Problem 2.—The second problem related to the use of the electron probe as the only means of conclusively determining the homogeneity and chemical composition of zincian rockbridgeite. X-ray powder diffraction patterns of type material from Viana do Castelo, Maxedo, Portugal, taken for the X-ray powder diffraction film files at the U.S. Geological Survey, suggested that the material represented a mixture of two minerals, rockbridgeite and lipscombite. Čech, Padera, and Povondra (1961) called attention to the fact that their X-ray powder data for a mixture of lipscombite and rockbridgeite from Otov I, near Domažlice (Bohemia, Czechoslovakia), are very similar to those published for zincian rockbridgeite by Lindberg and Frondel (1950). Therefore, the amount of ZnO reported in the chemical analysis for zincian rockbridgeite (Lindberg and Frondel, 1950) was considered attributable to the rockbridgeite phase, and (or) the lipscombite phase, or possibly to the associated sphalerite. Electron-probe analyses of carefully selected fragments, followed by supporting X-ray identification of these same fragments, seemed the most reliable approach to resolving this problem. Qualitative spectrometer traces were made first of two deep-blue-green microcrystalline aggregates. The traces showed that zinc was present in each fragment. These fragments were removed from the epoxy, and X-ray powder diffraction patterns taken of each proved to be identical with those of lipscombite, a hydrated ferrous-ferric phosphate. Lipscombite had not been reported previously from the Maxedo locality nor, to our knowledge, has a zinc-bearing lipscombite been recorded in the literature. Individual, very thin, greenish-brown laths, found sparingly in the type material, were selected for electron-probe analysis. Spectrometer traces showed that zinc was also present in these laths, in amounts comparable to that found in the deep-blue-green lipscombite fragments; a single-crystal X-ray study made of one of these zinc-bearing laths confirmed its structural identity to rockbridgeite. Electron-probe and X-ray diffraction studies proved beyond question that the material described as zincian rockbridgeite actually represents a mixture of zincian lipscombite and zincian rockbridgeite, both containing approximately equal amounts of zinc.

Problem 3.—The third study required a partial quantitative electron-probe analysis to permit positive identification of minute, colorless to pale-yellow, hexagonal crystals that were found sparingly distributed on ore specimens from Butte, Mont. Single-crystal and powder diffraction X-ray study indicated that the mineral was either plumbogummite, a hydrated basic phosphate of lead and aluminum, or hinsdalite, a basic sulfate-phosphate of lead and aluminum. A spectrometer trace of the unknown compared with that for type hinsdalite showed them to be virtually identical and strongly suggested that the Butte mineral was hinsdalite. The following standards were used for the quantitative work:

Standard	Chemical analyses (in percent)	
	P	S
Type hinsdalite (Colorado)	6.4	5.7
Indium phosphide (InP)	21.2	----
Pyrite	----	53.1
Plumbogummite (Cumberland, England)	8.2	----

Four analyses were done on the Butte unknown, each using a different standard for the determination of P and S. A KAP crystal was used for the determination of P, and an ADP (ammonium dihydrogen phosphate) crystal was used for the determination of S. All data are corrected for background. The value for P obtained when indium phosphide was used as the standard is corrected for absorption, and the values for S and P obtained when pyrite and plumbogummite, respectively, were used as standards are corrected for atomic number. The results of the analyses are shown in table 1.

TABLE 1.—*Electron-probe analyses of* P *and* S *in the Butte mineral*

[Quantities are in percent]

	Analysis and standard used			
	1 (type hinsdalite)	2 (indium phosphide)	3 (pyrite)	4 (plumbogummite)
P	6.4	6.2	----	6.3
S	6.2	----	6.2	----

The electron-probe data verified that the Butte mineral contains appreciable sulfur and therefore is hinsdalite, $(Pb, Sr)Al_3(PO_4)(SO_4)(OH)_6$.

Problem 4.—In the fourth problem, spectrometer traces were used to show the relationship between pink orthorhombic attakolite from Västanå (Westanå), Sweden, described by Gabrielson and Geijer (1964) as a hydrous silicophosphate of Al, Ca, and Mn, and an adjacent white monoclinic attakolite-like mineral. The specimen bearing these two minerals is in the U.S. National Museum (USNM R5615). Single-crystal X-ray study of these two minerals show them to have closely agreeing cell parameters (table 2). Electron-probe spectrometer traces for the two minerals are vir-

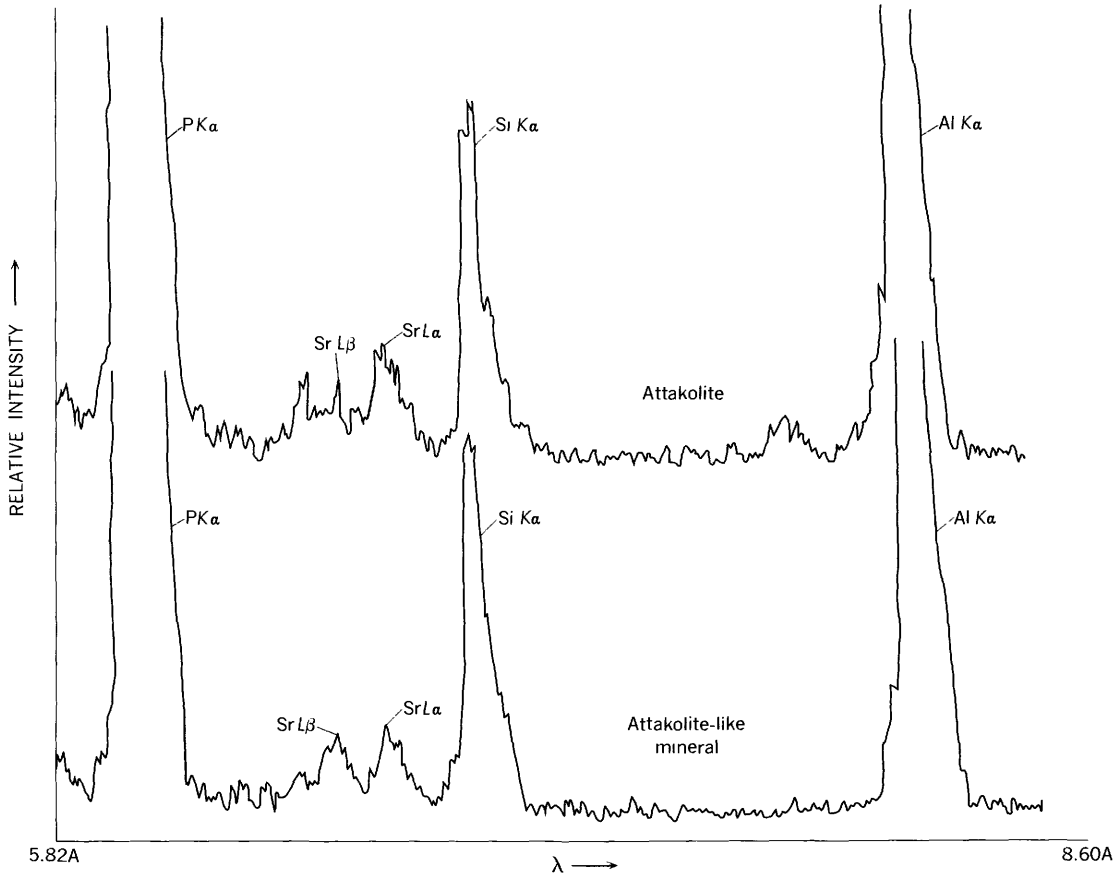

FIGURE 1.—Spectrometer traces (λ, 5.82–8.60A) of attakolite and the attak olite-like mineral from Västanå (Westanå), Sweden. A KAP crystal was used.

TABLE 2.—*Comparison of attakolite and an attakolite-like mineral from Västanå (Westanå), Sweden*

[U.S. National Museum specimen R5615]

Crystallographic data	Attakolite [1] (pink)	Attakolite-like mineral [2] (white)
Symmetry	Orthorhombic	Monoclinic
Space group	*I****	*I**/*
Cell dimensions		
a	11.46±0.01A	11.45±0.01A
b	15.71±0.02A	15.69±0.02A
c	7.28±0.01A	7.30±0.01A
β		91°30′±05′

[1] Data from von Knorring and Mrose (1967).
[2] Data from present report.

tually identical, as may be seen in figure 1, which shows the peaks for P, Sr, Si, and Al obtained with a KAP crystal. Traces made with a LiF crystal show peaks for Fe, Mn, and Ca. These traces, later supplemented by quantitative electron-probe analyses, verified that the pink and white minerals have approximately the same composition; that they differ crystallographically indicates that the monoclinic attakolite-like mineral is dimorphous with orthorhombic attakolite and therefore is a new mineral species.

REFERENCES

Cech, Frantisek, Padera, Karel, and Povondra, Pavel, 1961, Lipscombite from pegmatites at Otov near Domažlice (Bohemia, Czechoslovakia): Carolinae Univ. Acta Geologica, No. 3, p. 171–190 [Czech with English summary].

Gabrielson, Olof, and Geijer, Per, 1964, The mineral attakolite: Arkiv Mineralogi och Geologi, v. 3, no. 30, p. 537–543.

Knorring, Oleg von, and Mrose, M. E., 1966, Bertossaite, $(Li,Na)_2(Ca,Fe,Mn)Al_4(PO_4)_4(OH,F)_4$, a new mineral from Rwanda (Africa) [abs.]: Canadian Mineralogist, v. 8, pt. 5, p. 668.

Lindberg, M. L., and Frondel, Clifford, 1950, Zincian rockbridgeite: Am. Mineralogist, v. 35, p. 1028–1035.

ATOMIC ABSORPTION DETERMINATION OF CADMIUM IN GEOLOGIC MATERIALS

By H. M. NAKAGAWA and T. F. HARMS, Denver, Colo.

Abstract.—A simple, rapid, and sensitive atomic absorption method for the determination of cadmium in rocks and soils has been developed. The sample is digested with nitric acid and the supernatant liquid atomized in an atomic absorption spectrophotometer. The method has been used to determine cadmium in soils and rocks and in minerals, such as sphalerite and zincite, with no observed interference. The results obtained compare favorably with those from colorimetric and spectrographic methods. As little as 0.2 ppm in the sample can be satisfactorily determined.

The crustal abundance of cadmium is reported to be from 0.1 to 0.2 part per million (Turekian and Wedepohl, 1961). Very little is known of the geochemistry of cadmium and only a meager amount of information has been published concerning the distribution of this element in various magmatic rocks and minerals. Very little is known about the role of cadmium in the process of soil formation or about its occurrence in sedimentary rocks (Goldschmidt, 1954). Trace amounts of cadmium are generally associated with zinc and zinc minerals, but have also been observed in chalcopyrite and galena (Vlasov, 1964). The cadmium content in rocks and weathered products, especially soils, could be useful as a guide in locating primary or secondary zones of enrichment that are related to hidden ore bodies of economic importance. Thus the determination of trace amounts of cadmium in geologic materials may be useful in mineral exploration.

Conventional methods of analysis for cadmium are spectrographic, polarographic, colorimetric, and gravimetric methods. Each of these has its disadvantages in that sensitivity is limited, and tedious separations by chelation, precipitation, or ion exchange are necessary to isolate cadmium from other elements, especially zinc. The relative ease and simplicity of separations by the proposed method offer a distinct advantage for determining trace quantities of this metal in diverse materials. The procedure described has also simplified the atomic absorption methods of Fixman and Boughton (1966) and Farrar (1966), who used a combination of acids and precipitations and evaporations.

REAGENTS AND APPARATUS

Reagents

Standard cadmium solution (0.1 percent): Dissolve exactly 0.2031 gram of $CdCl_2.2\frac{1}{2}H_2O$ in 100 milliliters of $8N$ HNO_3.

Dilute standard cadmium solution (0.01 percent): Dilute 10.0 ml of 0.1 percent Cd solution to 100 ml with $8N$ HNO_3.

Dilute standard cadmium solution (0.001 percent): Dilute 10.0 ml of 0.01 percent Cd solution to 100 ml with $8N$ HNO_3.

Nitric acid, concentrated, reagent grade.

Nitric acid $8N$ (1+1): Add 500 ml of concentrated HNO_3 to 500 ml of water.

Apparatus

Electric hotplate with magnetic stirrer.

Aluminum block, drilled to accommodate 16-millimeter culture tubes. Hotplate, magnetic stirrer, and block with capacity of 13 tubes are available commercially.

Magnets, Teflon-coated bars, 0.5 inch long.

Culture tubes, 16×150 mm.

Atomic absorption spectrophotometer.

Instrumental parameters

The instrumental parameters used are those as suggested in "Analytical Methods for Atomic Absorption Spectrophotometry," by Perkin-Elmer Corp (1966).

PROCEDURE

Solution of sample

Transfer a pulverized sample of rock or soil, up to 1 g in weight, to a 16- ×150-mm culture tube that contains a Teflon-coated magnet. Add 5 ml of concentrated nitric acid, place the tube and contents in the heating block on top of the hotplate which has the magnetic stirrer, and boil for 30 minutes. Remove the tube from the hotplate, allow to cool slightly, add 5 ml of demineralized water, and heat the tube and its contents again to its boiling point. Remove the tube from the hotplate and allow the sample solution to cool to room temperature. Adjust the volume of the cool sample solution to 10 ml with demineralized water, mix thoroughly, and centrifuge.

Estimation

Aspirate the clear acidic solution into the atomic absorption spectrophotometer and record the percent-

U.S. GEOL. SURVEY PROF. PAPER 600-D, PAGES D207-D209

age of absorption. Repeat and calculate an average of two readings. Convert to parts per million from a standard curve previously prepared in a similar manner. Alternately, a digital concentration readout or a recorder readout may be used for the estimation of the element.

Preparation of standards

Pipet 0.1 and 0.5 ml of 0.001 percent and 0.5 and 1.5 ml of 0.01 percent standard cadmium solution into four 50-ml volumetric flasks. Dilute to 50-ml mark with 8*N* nitric acid and shake the flasks thoroughly. These standard solutions contain 0.02, 0.05, 1.0, and 3.0 ppm of cadmium. Atomize each of the prepared solutions at least three times, average these readings, and plot a standard curve from which the concentrations of the unknown samples are calculated. The standard solutions may be used to calibrate the digital concentration readout and the recorder readout, either of which may also be used for determining the concentrations of the sample solutions. The optimum working range for cadmium is 0.05–3 ppm.

DISCUSSION

Cadmium is usually associated with zinc in minerals, such as sphalerite and zincite, that are readily attacked by a mineral acid. The results obtained after a simple nitric acid digestion compare favorably with those obtained by a more rigorous method of sample dissolution. The method described is applicable particularly to the needs found in geochemical exploration, which requires the analysis of a large number of samples.

Although interferences in atomic-absorption spectrophotometry are seldom encountered, several elements that have resonance lines close to the resonance line of cadmium were checked for possible interference. These elements were added individually to solutions of nitric acid containing 1 ppm of cadmium as shown in table 1. No serious interference was observed. Only one element, nickel, slightly enhanced the recovery of cadmium and should therefore be classified as an interference. The estimation of cadmium was made by means of the digital concentration readout, and more accurate determinations can be obtained by a finer calibration of this instrument.

TABLE 1.—*Effect of various metals on the recovery of 1 part per million of cadmium in nitric acid*

[In parts per million]

Sample No.	Metal added		Cadmium recovered
	Name	Concentration	
1	None	----------	1. 08
2	None	----------	1. 09
3	Ca	4, 000	1. 06
4	Na	1, 000	1. 06
5	K	4, 000	1. 10
6	Sr	1, 000	1. 07
7	Co	2, 500	1. 08
8	Ni	1, 000	1. 18
9	Fe(III)	2, 000	1. 10
10	Pb	6, 000	1. 07
11	Zn	4, 500	1. 11
12	Sn	4, 000	1. 07
13	Sb	2, 000	1. 11

PRECISION AND ACCURACY

The repeatability of the technique was evaluated by repeat determinations on five samples of various composition (table 2). Precision of the method is indicated by the relative standard deviation.

TABLE 2.—*Replicate determinations of cadmium*

[Five determinations for each sample]

Sample No.	Description	Cadmium content (ppm)			Relative standard deviation (percent)
		Maximum	Minimum	Average	
63-898	Lead-silver ore	62	47	52	12. 4
63-979	Quartz monzonite	1. 8	1. 4	1. 6	26. 0
64-327	Lead-silver-zinc ore	153	138	148	4. 0
CR-14-56-173	Hemimorphite	12, 500	11, 900	12, 200	2. 3
CR-14-56-174	Hydrozincite	1, 040	950	990	3. 6

The cadmium content of several different types of samples including soils, rocks, and minerals was determined, and the results were compared with those obtained by other methods (table 3). In view of the fact that no special precautions were taken during the analysis of these samples, the comparison of the results indicates that this method is useful for geochemical exploration purposes.

TABLE 3.—*Comparison of cadmium recovery by atomic absorption spectrophotometry and by other methods*

[Maurice De Valliere, analyst. Results in parts per million]

Sample No.	Description	Method	
		Atomic absorption	Spectrographic
63-898	Lead-silver ore	56	50
63-976	Lead-zinc baritic breccia.	70	20
63-979	Quartz monzonite	2	<20
64-320	Copper-gold ore	153	100
64-327	Lead-silver-zinc ore	147	150
CR-14-56-173	Hydrozincite	1, 000	1, 500
CR-14-56-174	Hemimorphite	12, 000	15, 000
	Sphalerite	2, 100	[1] 1, 500
NBS-113	Zinc ore	4, 750	[2] 4, 200
G-1	Granite	0. 6	[1] <0. 3
W-1	Diabase	. 6	[1] <0. 3

[1] Colorimetric analysis by C. J. Huffman, Jr.
[2] Uncertified value.

REFERENCES

Farrar, B., 1966, Determination of cadmium in ore and magnesium in rock samples: Atomic Absorption Newsletter (Perkin-Elmer Corp.), v. 5, no. 3, p. 62.

Fixman, M., and Boughton, L., 1966, Mineral assay for silver, zinc, and cadmium by atomic absorption: Atomic Absorption Newsletter (Perkin-Elmer Corp.), v. 5, no. 2, p. 33.

Goldschmidt, V. M., 1954, Geochemistry: Oxford, Clarendon Press, 730 p.

Perkin-Elmer Corp., 1966, Standard conditions for cadmium, sheet Cd 1, *in* Analytical methods for atomic absorption spectrophotometry 990–9366: Perkin-Elmer Corp.

Turekian, K. K., and Wedepohl, K. H., 1961, Distribution of the elements in some major units of the Earth's crust: Geol. Soc. America Bull., v. 72, no. 2, p. 175–192.

Vlasov, K. A., ed., 1964, Mineralogy of rare elements, v. 2 *of* Geochemistry and mineralogy of rare elements and genetic types of their deposits: Moscow, Akad. Nauk SSSR Inst. Mineralogii, 949 p., [in Russian]: translation by Israel Program for Scientific Translations, Jerusalem, 1966, 945 p.

DETERMINATION OF RHODIUM IN ROCKS

By MARIAN M. SCHNEPFE and F. S. GRIMALDI, Washington, D.C.

Abstract.—The precious metals are concentrated by coprecipitation with tellurium formed by the reduction of tellurite with stannous chloride. A fraction containing rhodium and part of the iridium is isolated after separating tellurium, gold, palladium, and platinum. Rhodium is determined in this fraction spectrophotometrically with stannous bromide in a perchloric-hydrobromic acid medium. Approximately 0.01 ppm Rh can be detected as a lower limit on a 10-g sample. Detailed data are given on the behavior of other elements in the spectrophotometric method.

In the sequential method for determining minute amounts of palladium and platinum in rocks, previously described by Grimaldi and Schnepfe (1968), a fraction containing the rhodium and part of the iridium originally present in the sample is isolated. The steps involved are (1) concentration of the precious metals by coprecipitation with tellurium formed by reduction of tellurite with stannous chloride, (2) separation of tellurium and gold by methyl isobutyl ketone extraction of their chlorides, and (3) separation of palladium and platinum by chloroform extraction of their diethyldithiocarbamates formed in the presence of iodide. The final aqueous phase thus obtained contains the rhodium and iridium. After organic matter is destroyed, rhodium and iridium are converted to complex chlorides and the rhodium is determined spectrophotometrically in perchloric-hydrobromic acid medium with stannous bromide, following in part the method of Tertipis and Beamish (1962). Separation of iridium is not necessary as it reacts very slowly with the stannous bromide under the conditions used. Approximately 0.01 part per million of rhodium can be detected as a lower limit on a 10-gram sample.

EXPERIMENTAL METHOD

Reagents

Required reagents described in the previous paper of Grimaldi and Schnepfe (1968) are: solutions of platinum metals, tellurium, stannous chloride (for the precipitation of tellurium), sodium diethyldithiocarbamate, and sodium chloride (5 milligrams of NaCl per milliliter), as well as chloroform and methyl isobutyl ketone. For the determination of rhodium described in the present article, the following are needed:

Sodium iodide, 13.5 percent (w/v) aqueous solution: Prepare fresh solution daily.

Sodium chloride, 4 percent (w/v) aqueous solution.

Perchloric acid, 1.8*M*.

Stannous bromide solution, 6 percent (w/v) in Sn^{+2} and 4 molar in HBr. Treat 11.4 g of $SnCl_2 \cdot 2H_2O$ with 20 ml of HBr and evaporate the solution to dryness on the steam bath. Treat the residue with an additional 2 ml of HBr and evaporate the solution to dryness. Place in an oven at approximately 100°C to eliminate most of the remaining HCl. Dissolve the residue in 45 ml of distilled HBr, and dilute the solution to 100 ml with water. Prepare fresh solution weekly.

Procedure

1. Follow the procedure of Grimaldi and Schnepfe (1968, p. B100) through the chloroform extraction of the diethyldithiocarbamates (steps 1–15), but substitute sodium iodide, 13.5 percent, for the 15-percent KI (step 12). Collect the aqueous phase from this extraction in a 30-ml beaker. Evaporate the solution to dryness.
2. Add approximately 5 ml of water, followed by HNO_3 dropwise until elemental iodine is formed, and then add a slight excess of HNO_3.
3. Evaporate the solution to dryness to remove I_2 and place the beaker in a cold furnace. Heat the residue at 225°–250° C for 30 minutes. The organic matter is made more amenable to chemical destruction by this procedure.
4. After cooling the beaker, add 1 ml of fuming HNO_3 and 0.5 ml of $HClO_4$. Evaporate the HNO_3 and bring to fumes of $HClO_4$ on a hotplate not exceeding 250° C. Cover the beaker until the solution is colorless. After the $HClO_4$ has been fumed off, place the beaker in a furnace for 30 minutes at 225°–250° C.
5. Repeat step 4. If there is any evidence of organic matter, repeat step 4 again.
6. Treat the residue with 20 drops of (1+1) HNO_3 and 3 ml of HCl. Cover and heat on a steam bath until the reaction subsides. Evaporate the solution to dryness.
7. Add a small volume of water and 3 ml of HCl to dissolve salts. Evaporate to dryness to remove HNO_3.
8. Repeat step 7.
9. Add 0.72 ml of 4 percent NaCl solution, 2 ml of water, and a few drops of HCl. (A total of 100 mg of NaCl are now present in the solution. This includes the NaCl formed from the sodium diethyldithiocarbamate and the NaI, as well as the NaCl added to the aqueous phase of the methyl isobutyl ketone extraction.)

U.S. GEOL. SURVEY PROF. PAPER 600-D, PAGES D210-D213

10. Prepare standards by taking different amounts of rhodium up to 30 micrograms, adding 2.5 ml of 4-percent NaCl solution and a few drops of HCl, and evaporating the solutions to dryness.
11. Add 10 ml of 1.8*M* $HClO_4$ to samples and standards, stir, and let stand for a few minutes to dissolve salts.
12. Add 5 ml of $SnBr_2$ solution, and mix.
13. After 30 minutes, determine the absorbances in 2-centimeter cells at 427mμ (millimicrons) against water. To eliminate differences in cells, the same cell should be used for standards and samples. Correct absorbances of samples for the procedural blank.

RESULTS AND DISCUSSION

Coprecipitation of rhodium and iridium with tellurium

Sandell (1959, p. 722), reporting on the separation of noble metals by coprecipitation with tellurium formed with stannous chloride as the reductant, states that the tellurium precipitate carries down rhodium "incompletely but in large amount" and iridium "very incompletely." With titanous chloride as the reductant, Sandell (1959, p. 767) cites data which indicate that 95 percent of the rhodium is collected by tellurium when from 8 to 16 μg of rhodium are present. There seems to be no theoretical reason for titanous chloride being better than stannous chloride in the recovery of rhodium and accordingly tests were made to clarify the meaning of "large amount."

With stannous chloride we recovered more than 95 percent of the rhodium from test solutions containing from 2 to 30 μg of rhodium. Similarly, we recovered approximately 25 percent of the iridium from test solutions containing from 5 to 50 μg of iridium.

Copper tends to accompany tellurium in the precipitate. For example, 0.65 mg of copper was coprecipitated when 50 mg were taken. This amount of copper did not noticeably affect the recovery of 20 μg of rhodium, but drastically reduced that of 20 and 50 μg of iridium to only 2 percent. It seems that iridium must compete with copper to be incorporated in the tellurium precipitate as a telluride.

Stannous bromide method for the determination of rhodium

Reagent concentrations.—The procedure used here differs from that of Tertipis and Beamish (1962) in that the extraction of rhodium into isoamyl alcohol and its determination in this phase is avoided; rhodium is determined directly in the aqueous phase. The extraction of the colored rhodium complex does not facilitate its determination inasmuch as any colored iridium complex that develops is also extracted. The extraction is recommended by Tertipis and Beamish (1962) when it is desirable to separate rhodium from iridium.

The final reagent concentrations selected differ only slightly from those of Tertipis and Beamish (1962) and are as follows: $SnBr_2$, 0.17*M*; HBr, 1.35*M*; and $HClO_4$, 1.25*M*. These conditions are easily determined because lower HBr concentrations produce unstable reagent blanks, and higher concentrations increase the absorbancy of the blank solutions. Higher concentrations of perchloric acid (up to 2.0*N*) increase the absorbancy of both the reagent blanks and the rhodium solutions without significantly affecting the stability of the system.

Dependence of the reactivity of iridium on its initial state.—The basic problem in determining rhodium is interference from iridium. Only part of the iridium is precipitated with tellurium and its interference is further minimized if iridium is converted to a complex chloride prior to the addition of stannous bromide. In the absence of this conversion, for example, starting with bromides, iridium reacts rapidly and would interfere to the extent that 10 μg of Ir would produce a color intensity equivalent to 1 μg of Rh after a 30-minute wait. With irridium initially present as chloride, 325 μg of iridium produce the same effect.

Spectral characteristics of the rhodium-stannous bromide color system.—A plot of the absorbance difference between rhodium and reagent blank solutions as a function of wavelength results in a fairly smooth curve with its peak at approximately 427 mμ. The same curve is obtained whether the stannous bromide is prepared by transforming stannous chloride with HBr or by dissolving metallic tin in HBr. Beer's law is followed for rhodium concentrations up to 2 ppm with absorbances taken after 30 minutes and up to 3.33 ppm after 60 minutes, the maximum concentration tested (fig. 1). The sensitivity according to Sandell's notation is 0.0039 μg/cm² at 427 mμ.

Reproducibility of absorbances.—Excellent reproducibility of absorbances of reagent blanks and rhodium solutions is obtainable if measurements are made by some standardized procedure. With a 2-cm light path, 0.1 μg of rhodium in a 15-ml volume yields a net absorbance of 0.003. This is readily distinguishable from a blank so that on a 10-g sample approximately 0.01 ppm of rhodium is determinable as a lower limit.

Effect of sodium chloride.—The effect of sodium chloride on the color development was investigated by evaporating blanks, 10 μg of Rh, and 500 μg of Ir, separately, with different amounts of NaCl prior to the addition of the $SnBr_2$ reagent. With increase in NaCl the reaction rates of both the rhodium and iridium decreased slightly; the reagent blanks are not affected. In the range of 40 to 100 mg of NaCl, the reaction of 10 μg of Rh is practically complete in 30 minutes.

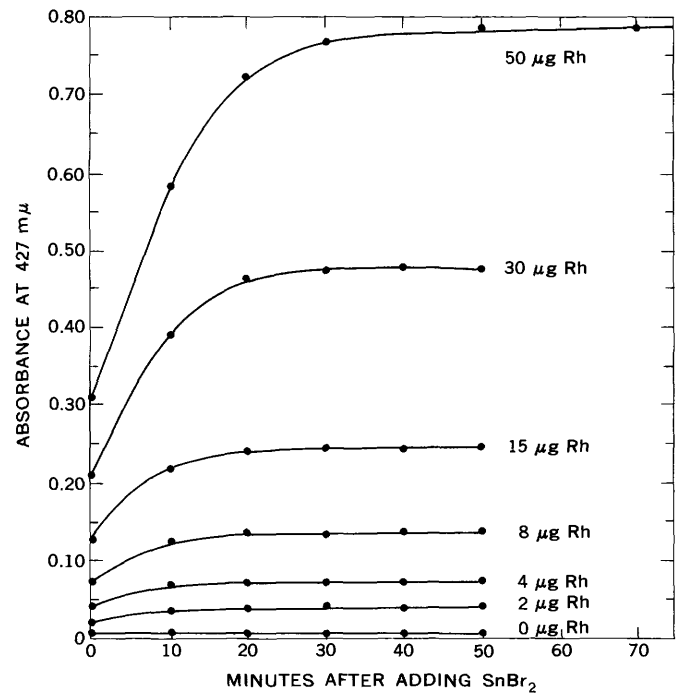

FIGURE 1.—Absorbance of rhodium solutions as a function of time. All solutions had a total volume of 15 ml. Absorbances were measured in 1-cm cells using water as reference.

Effect of other elements.—Tolerances for various elements expressed in micrograms of element giving a net absorbance equivalent to 1 μg of rhodium are given in table 1. Osmium, palladium, ruthenium, and gold when present alone yield positive errors. In the presence of rhodium, however, these elements decrease the rate at which the rhodium color develops. The extent and sign of the errors are thus determined by the concentration of rhodium, the concentration of the interfering element, time, and temperature. The interplay of these factors sometimes results in no apparent error.

TABLE 1.—*Tolerances for various elements, and the effect of time in the stannous bromide procedure for the determination of rhodium*

[Directions of error are (+) positive, (−) negative]

Element	Concentration (ppm)		Micrograms of element equivalent to 1 μg of Rh	
	Element	Rhodium	In 30 minutes	In 60 minutes
Os(IV)	6.67	------	130 (+)	120 (+)
	33.3	------	130 (+)	120 (+)
	0.33	0.13	5.4 (−)	20 (−)
	0.33	0.67	1.3 (−)	12 (−)
	0.33	2	.5 (−)	4 (−)
	1.33	0.13	20 (−)	37 (−)
	1.33	0.67	3.2 (−)	5 (−)
	1.33	2	1.5 (−)	2.5 (−)
	33.3	0.67	500 (+)	150 (+)
Pd(II)	0.67 to 6.67	------	5.3 (+)	5.3 (+)
	0.13	0.13	7 (+)	5.3 (+)
	0.13	0.67	2 (−)	5 (+)
	0.13	2	0.5 (−)	3 (+)
	0.33	0.13	5 (+)	5 (+)
	0.33	0.67	5 (−)	6 (+)
	0.33	2	2 (−)	7 (+)
	0.67	0.13	6 (+)	5 (+)
	0.67	0.67	10 (−)	8 (+)
	0.67	2	6 (−)	3 (+)
	3.33	0.67	8 (+)	7 (+)

TABLE 1.—*Tolerances for various elements, and the effect of time in the stannous bromide procedure for the determination of rhodium*—Continued

[Directions of error are (+) positive, (−) negative]

Element	Concentration (ppm)		Micrograms of element equivalent to 1 μg of Rh	
	Element	Rhodium	In 30 minutes	In 60 minutes
Ru(IV)	1.33	------	16 (+)	16 (+)
	0.13	0.13	14 (+)	14 (+)
	0.13	0.67	No apparent interference	16 (+)
	0.13	2	17 (+)	14 (+)
	0.33	0.13	17 (+)	14 (+)
	0.33	0.67	No apparent interference	14 (+)
	0.33	2	7 (−)	7 (+)
	1.33	0.13	40 (+)	12 (+)
	1.33	0.67	6 (−)	15 (+)
	1.33	2	1.2 (−)	12 (+)
Pt(IV)	1.33 to 6.67	------	10 (+)	10 (+)
	6.67	0.67	10 (+)	10 (+)
Au(III)	1.67	------	156 (+)	156 (+)
	3.33	------	110 (+)	60 (+)
	0.067	0.13	8 (−)	15 (−)
	0.067	0.67	4 (−)	15 (−)
	0.067	2	No apparent interference	10 (+)
	0.33	0.13	5 (−)	7 (−)
	0.33	0.67	5 (−)	8 (−)
	0.33	2	5 (−)	5 (−)
	1.67	0.67	5 (−)	5 (−)
Te(IV)	0.67	--------	5 (+)	5 (+)
	2	--------	5 (+)	5 (+)
	0.67	0.13	5 (+)	5 (+)
	1	0.67	5 (+)	5 (+)
Ir(IV)	1.67	33.3	325 (+)	240 (+)
	3.33	0.13	325 (+)	240 (+)
	3.33	0.67	325 (+)	240 (+)
	3.33	3.33	325 (+)	240 (+)
	33.3	0.13	325 (+)	240 (+)
	33.3	0.67	325 (+)	240 (+)
	33.3	3.33	325 (+)	240 (+)
Cr(III)	67	--------	560 (+)	560 (+)
	67	0.67	560 (+)	560 (+)
Fe(III)	333	--------	No interference.	No interference.
	333	0.13	12,500 (+)	12,500 (+)
	333	0.67	4,200 (+)	4,200 (+)
	333	2	4,000 (+)	4,000 (+)
	3333	0.67	16,000 (+)	16,000 (+)
Ni	667	--------	10,000 (+)	10,000 (+)
	667	0.67	10,000 (+)	10,000 (+)
Co	667	--------	20,000 (+)	20,000 (+)
	667	0.67	20,000 (+)	20,000 (+)
Ag	80	--------	No interference.	No interference.
	80	0.67	-----do-------	Do.
Cu	667	----------	-----do-------	Do.
	667	0.67	-----do-------	Do.
Pb	133	----------	-----do-------	Do.
	133	0.67	-----do-------	Do.
	667	----------	-----do-------	Do.
	667	0.67	-----do-------	Do.
Zn	667	----------	-----do-------	Do.
	667	0.67	-----do-------	Do.
S as SO_4^{-2}	667	----------	-----do-------	Do.
	667	0.67	-----do-------	Do.

Destruction of organic matter

The aqueous phase from the diethyldithiocarbamate (DTC) extraction contains the separated rhodium and iridium along with sodium iodide and sodium diethyldithiocarbamate. Destruction of the organic matter and the elimination of iodine is facilitated by initially evaporating the aqueous phase to dryness, during which process the DTC decomposes and some of the iodide is lost as HI. Residual iodide is removed with nitric acid, and organic matter is destroyed by alternating nitric-perchloric acid evaporations to dryness and by baking the resulting residues at 225°–250° C. The baking was found to be necessary as wet oxidation alone did not remove the last traces of organic matter.

Test of the total procedure

Synthesized solutions containing 10 μg of each of Rh(III), Ir(IV), Pd(II), Pt(IV), Ru(IV), and Os(IV) were carried through the entire procedure starting with the tellurium precipitation both in the presence and absence of 50 mg of Cu. Recoveries of Rh were better than 96 percent. Recoveries of the separated Pd and Pt were each better than 94 percent.

The procedure was also tested on a pentlandite concentrate. Both aqua-regia-soluble rhodium and total rhodium were determined on sample weights ranging from 1 to 10 g. The average for acid-soluble rhodium resulting from five determinations was 0.40 with a standard deviation of ±0.03. Complete decomposition of duplicate samples yielded values of 0.47 and 0.50 ppm of Rh. These values compare with 0.37 and 0.41 obtained on duplicate samples by a fire-assay solution spectrochemical technique by Haffty and Riley (1968).

REFERENCES

Grimaldi, F. S., and Schnepfe, M. M., 1968, Determination of palladium and platinum in rocks, *in* Geological Survey Research 1968: U.S. Geol. Survey Prof. Paper 600–B, p. B99–B103.

Haffty, Joseph, and Riley, L. B., 1968, Determination of palladium, platinum, and rhodium in geologic materials by fire assay and emission spectrography: Talanta, v. 15, p. 111–117.

Sandell, E. B., 1959, Colorimetric determination of traces of metals, 3d ed.: New York-London, Interscience, 1032 p.

Tertipis, G. G., and Beamish, F. E., 1962, Solvent extraction separation and spectrophotometric determination of rhodium and iridium: Anal. Chemistry, v. 34, no. 6, p. 623–625.

DETERMINATION OF BROMINE AND IODINE BY X-RAY FLUORESCENCE

By J. S. WAHLBERG and A. T. MYERS, Denver, Colo.

Abstract.—Iodide and (or) bromide are concentrated on an oleic-stearic acid disk, and amounts are then determined by X-ray fluorescence. No interferences have been encountered from several salts tested. The sensitivity is about 1 μg for iodine or 0.1 ppm on a 10-g sample, and about 2 μg for bromine or 0.2 ppm on a 10-g sample.

Bromine in concentrations greater than 50 parts per million can be determined by direct X-ray fluorescence; however, unless rather complex corrections for interelement effects are made, or standards which approximate the composition of the unknown samples are used, the results may be questionable. In most samples that we have analyzed the iodide or bromide content is too low to be detected by direct X-ray fluorescence. It is thus necessary to concentrate the halogens and preferably isolate them in order to eliminate interelement effects. This separation has been accomplished by an adaptation of the iodine number determination technique (Scott, 1939).

The halogens are adsorbed on a filter disk that has been saturated with a 1–1 mixture of oleic and stearic acids. For bromide and iodide to be adsorbed by the oleic acid, they must be in the form of free halogens. Oxidation to iodine presented a minor problem because most agents will oxidize iodide to iodate. Of the apparently possible choices of oxidizing agents for iodide (Lundell and Hoffman, 1938, p. 151–162), only sodium nitrite in acid solution was found to be suitable. For bromide the choice is not as critical as that for iodide.

EXPERIMENTAL METHOD

Apparatus and reagents

X-ray spectrometer, single-channel, vacuum; equipped with a pulse-height analyzer, a tungsten-target X-ray tube, a lithium fluoride analyzing crystal, a gas-flow proportional detector, and a scintillation detector.

Caplugs, No. EC–16 1-inch size, available from Protective Closures Co., Buffalo, N.Y.

1-inch inside-diameter steel curtain rings.

Mylar film, 0.25 mil thick.

Oleic and stearic acids.

Ball mill that has a rotation rate of about 56 revolutions per minute.

PROCEDURE

Preparation of the oleic-stearic acid adsorption disk

Detailed instructions for the preparation of the adsorption disks are given, because large variations in background rates were observed if the disks were not uniformly prepared. Variation in counting backgrounds probably arises from varying scatter radiation caused by unequal amounts or distribution of the oleic-stearic acid on the filter disk.

Place a disk approximately ⅞ inch in diameter (the disk should be cut from Whatman No. 541 filter paper) into a beaker containing a 1–1 mixture of oleic and stearic acids that has a temperature slightly above the melting point of the mixture (≈40°C). Remove the disk from the acid by means of a pair of pointed tweezers whose points have been warmed by flame to ≈60°C. Shake the disk to remove the excess oleic-stearic acid. When only the area around the warmed tweezers is liquid, grasp the opposite edge of the disk with a pair of cool tweezers. Release the warm tweezers and allow the liquid spot to solidify. The disk is then ready for use or storage. If disks are kept in a closed container at a cool temperature (<30°C), they can be stored for an indefinite length of time.

Determination of bromide

Leach or dissolve a 10-gram sample, ground to pass a 100-mesh sieve, in approximately 25 milliliters of 10-percent v/v H_2SO_4 and transfer into a 2-ounce wide-mouth screwcap bottle. Insoluble material that is too coarse or too sharp will cause excessive abrasion on the oleic-stearic acid adsorption disk, and it may be necessary to filter the sample. If the sample is filtered, wash with a 10-percent v/v H_2SO_4 solution, and dilute the solution with 10-percent H_2SO_4 to a final volume of approximately 40 ml. Add 1 ml of 30-percent H_2O_2 and an oleic-stearic acid adsorption disk. Cap the bottle and place it in a rotating mixer (ball mill) for 16 hours.

U.S. GEOL. SURVEY PROF. PAPER 600-D, PAGES D214-D216

A rotating mixer causes less abrading of the oleic-stearic acid adsorption disk than does a shaking mixer. Remove the disk from the solution and wash with distilled water. Place the disk on a 0.25-mil Mylar film that is stretched over a 1-inch Caplug and is held in place by a 1-inch curtain ring. Allow the disk to air-dry. Center the disk on the Mylar and stretch another piece of 0.25 mil film over it. Secure in place by a 1-inch curtain ring.

Place the disk in a fluorescence X-ray spectrometer and take three 1-minute counts using the following parameters: tungsten target X-ray tube operated at 30 kilovolts and 30 milliamperes; bromine $K\alpha$ radiation diffracted with a lithium fluoride analyzing crystal at a 2θ angle of 29.92°. Background corrections can be made at a 2θ angle of 29°; if the adsorption disks are prepared properly, however, backgrounds are uniform and such a correction is not required. Use a scintillation detector along with a pulse-height analyzer. The amount of bromine in the sample is read from a standard curve prepared by taking 0–1,000 micrograms of bromine through the procedure and determining the count rates of the disks. A straight-line curve is obtained.

Determination of iodide

Dissolve the sample in approximately 25 ml of 10-percent v/v H_2SO_4 and transfer (filter if necessary) into a 2-ounce screwcap bottle. Use water for the wash solution, and make up the final volume to approximately 40 ml. Add approximately 0.1 g of $NaHSO_3$, swirl and allow to react for 2–3 minutes. Place the oleic–stearic acid adsorption disk in the bottle, rapidly add approximately 0.3 g of $NaNO_2$ and place the screwcap on the bottle to prevent loss of nitrous oxide. Place bottle on a rotating mixer for 16 hours. Prepare the disk for counting as in the bromine procedure. Place the disk in a vacuum-type fluorescence X-ray spectrometer and take three 1-minute counts at the following parameters: vacuum path; tungsten-target X-ray tube, operated at 30 kv and 30 ma, and iodine $L\alpha$ radiation diffracted with a lithium fluoride analyzing crystal at a 2θ angle of 102.87°. Background corrections can be made at a 2θ angle of 104°; however, if adsorption disks are prepared properly, a background correction is not required. A flow-proportional detector is used. The amount of iodine in the sample is read from a standard curve prepared by adding 0–500 μg of iodide to 40 ml of 6-percent H_2SO_4 and extracting the iodide with an oleic-stearic acid disk as described in the iodide procedure. A straight-line curve is obtained.

RESULTS AND DISCUSSION

One gram each of various salts was added to solutions containing 25 μg of iodide or bromide in 40 ml of acid solution, and the iodide or bromide content was determined (table 1). It was found that of the salts tested only sodium chloride gave significantly high results for bromide; however, this result was undoubtedly due to the known (as indicated by the analysis given for reagent-grade sodium chloride) impurity of bromide in the sodium chloride. Table 1 also shows that 1 milligram of bromide had no effect on the iodide results.

The catalytic decomposition of the H_2O_2 by the ferric ion caused the bottle to either explode or leak when 2 ml of H_2O_2 was used. It was found that if only 1 ml of 30-percent H_2O_2 was used, this problem was avoided and the 1 ml of H_2O_2 was enough to cause complete adsorption of the bromide. It was also found that if appreciably more than 0.3 g of $NaNO_2$ was used, the nitrous oxide liberated would cause the bottle to explode.

To test the effect of acid concentration on the adsorption of iodide and bromide, iodine and bromine were adsorbed from solutions containing 0–10 percent H_2SO_4. It was found that approximately 6-percent v/v H_2SO_4 was the optimum for iodine adsorption; however, for bromine a H_2SO_4 concentration of approximately 10-percent v/v gave the best results.

Since iodine in nature may occur as iodate (Goldschmidt, 1954, p. 602–620), the effectiveness of this method for iodate determination and also for bromate was tested. Table 2 shows that bromate was just as effectively adsorbed as bromide. Table 2 also shows that iodate was adsorbed if $NaHSO_3$ and nitrite were added to a neutral or acid solution of the iodate. Nitrite alone works well only in neutral solutions. Experience has shown the $NaHSO_3$–$NaNO_2$ 6-percent acid procedure to be the most convenient to use in the iodide determination.

In X-ray analysis, the detection limit is normally taken as three standard deviations of the background count. A 3-minute count will give a detection limit of 0.65 μg for bromide and 0.40 μg for iodide; however, experience has shown 1 μg for iodide and 2 μg for bromide to be more practical lower limits of detection.

It occurred to us that there might be a slow diffusion of the iodine and bromine from the surface of the oleic-stearic acid adsorption disk to the interior, a diffusion

TABLE 1.—*Effect of various salts on the adsorption of 25 μg of iodide or bromide*

[One-gram quantities of salts were used, except where otherwise indicated. Leaders (---), not determined]

Salt	Quantity detected (μg)	
	Iodide	Bromide
NaCl	25.1	31.5
$Fe(NO_3)_3$	25.0	24.6
$CuSO_4$	23.4	---
$Ca(NO_3)_2$	25.0	25.0
$Mg(NO_3)_2$	24.8	24.9
$Al_2(SO_4)_3$	24.5	25.0
Br 1 mg	25.2	---

TABLE 2.—*Effect of various salts in acid and neutral solutions on the adsorption of 100 μg of iodide as* IO_3 *and of bromide as* BrO_3

[0.3-gram quantities of salts were used, except where otherwise indicated. (.....) not determined]

Salt	Quantity detected (μg)	
	Iodide	Bromide
$NaHSO_3$ (neutral)	101	.....
$NaHSO_3$ (acid)	99	.....
$NaNO_2$ (neutral)	96	.....
$NaNO_2$ (acid)	10	.....
H_2O_2 (acid)—1 ml	.....	101

which would cause a progressive lowering of the count rate. However, even after several weeks, no apparent lowering of the count rate was observed. This stability makes it possible to use the same set of standards for many determinations.

This method obviously is applicable only to materials in which the bromide and iodide are soluble in dilute H_2SO_4 (brines or evaporites). If bromide and iodide determinations are to be run on other materials, the iodide and bromide are distilled from concentrated H_2SO_4 and dissolved in dilute NaOH. If the halogens are in a silicate matrix, the silicates can be decomposed on a steam bath with an $HF–H_2SO_4–Ag^{+1}$ solution. The bromide and iodide can be liberated from the resulting silver halide by distillation with concentrated H_2SO_4. More simply, the halides can be dissolved by reducing the silver halide with zinc. The iodide and bromide can be separated from the reduced silver by filtration and are then adsorbed on the oleic-stearic acid disk.

REFERENCES

Goldschmidt, V. M., 1954, Geochemistry: Oxford, Clarendon Press, 730 p.

Lundell, G. E. F., and Hoffman, J. I., 1938, Outlines of methods of chemical analysis: New York, John Wiley & Sons, Inc., 250 p.

Scott, W. W., 1939, Standard methods of chemical analysis; a manual of analytical methods and general reference for the analytical chemist and for the advanced student (5th ed., N. H. Furman ed.): New York, D. Van Nostrand Co., Inc., 2v., 2667 p.

A TEMPERATURE-CONTROLLED WATER BATH FOR MINERAL SOLUBILITY STUDIES

By P. B. HOSTETLER and C. L. CHRIST,
Menlo Park, Calif.

Abstract.—The design of a temperature-controlled water bath for study of mineral phase equilibria in aqueous media is described. The bath consists of a polypropylene cylinder in which five polypropylene reaction vessels, providing a silica-free environment, are suspended. Temperatures ranging from 0°C to 95°C (at 1 atmosphere total pressure) can be maintained at approximately ±0.4°C for periods of months. Provision is made for sweeping a selected gas through the contents of any of the reaction vessels.

The apparatus described in this paper was designed and developed in order to carry out phase studies of minerals in the presence of aqueous solution at constant temperatures ranging from 0°C to 95°C, at 1 atmosphere total pressure, and in a silica-free environment.

It consists of a cylindrical polypropylene water bath in which are suspended 5 polypropylene reaction vessels, 3 with a 1,500-milliliter capacity and 2 with a 400-ml capacity, and auxiliary vessels. Water is used as the bath-filling medium, and constant temperature is maintained through an automatic regulating system. Provision is made for bubbling a selected gas through the aqueous system in a reaction vessel, for removing samples for chemical analysis, and for making in situ electrode measurements. An apparatus of the kind described here was successfully used for the determination of the activity-product constant of chrysotile at 90°C (Hostetler and Christ, 1968), and a number of these baths are presently in operation in connection with our continuing studies of the system MgO–SiO_2–CO_2–H_2O.

Acknowledgments.—The water baths were fabricated to our specifications by Precision Laboratory Products, Mountain View, Calif. We are indebted to Mr. Robert Runge of Precision Laboratory Products, and to Mr. S. A. Russo, Jr., formerly of that firm, for many valuable suggestions concerning the design and construction of the baths.

DESCRIPTION

The overall assembly of bath and control equipment is shown in figure 1. Gases are led to the coarse-valve assembly (1*A*)[1] through three ⅜-inch outside-diameter copper-tubing lines (1*B*). A selected gas then proceeds through the fine-valve system (1*C*) into a presaturation vessel (1*D*) containing pure water at bath temperature, where the gas becomes saturated with water vapor, thence to a reaction vessel (1*E*). After sweeping through the aqueous system in (1*E*), the gas is led to a water-bubbler tube (1*F*), and then escapes to the atmosphere.

Temperature control is achieved through the use of a Sargent Thermonitor unit, model ST (1*G*). A temperature-sensing device (1*H*) operates in conjunction with the temperative controller (1*G*) to control the heat input into the water of the bath. The top of the circulating and heating unit (1*I*) (Sargent P–6495), is surmounted by a (water-cooled) stirring motor (1*J*). The unit (1*I*) consists of a hollow metal cylinder, perforated to permit circulation of the bath water, and contains three immersion heaters. The lower portion of the cylinder is shown in figure 3 (3*J*). A propeller-type stirrer, used to circulate the water of the bath, passes along the central axis of the cylinder and is driven by the motor. It is important to note that the vertical dimensions of this circulating and heating unit control the vertical dimensions of the bath, and, in part, the diameter of the bath, as well. The temperature of the bath water is measured with a thermometer (1*K*).

Stirring of the aqueous system within the reaction vessel is carried out with a Teflon-coated magnetic bar rotated by a magnetic stirrer (1*L*). The whole bath rests on five Sargent magnetic stirrers, which are positioned under the five reaction vessels of the bath

[1] In the text, "1*A*" designates item A in figure 1, "2*A*" designates item A in figure 2, and so forth.

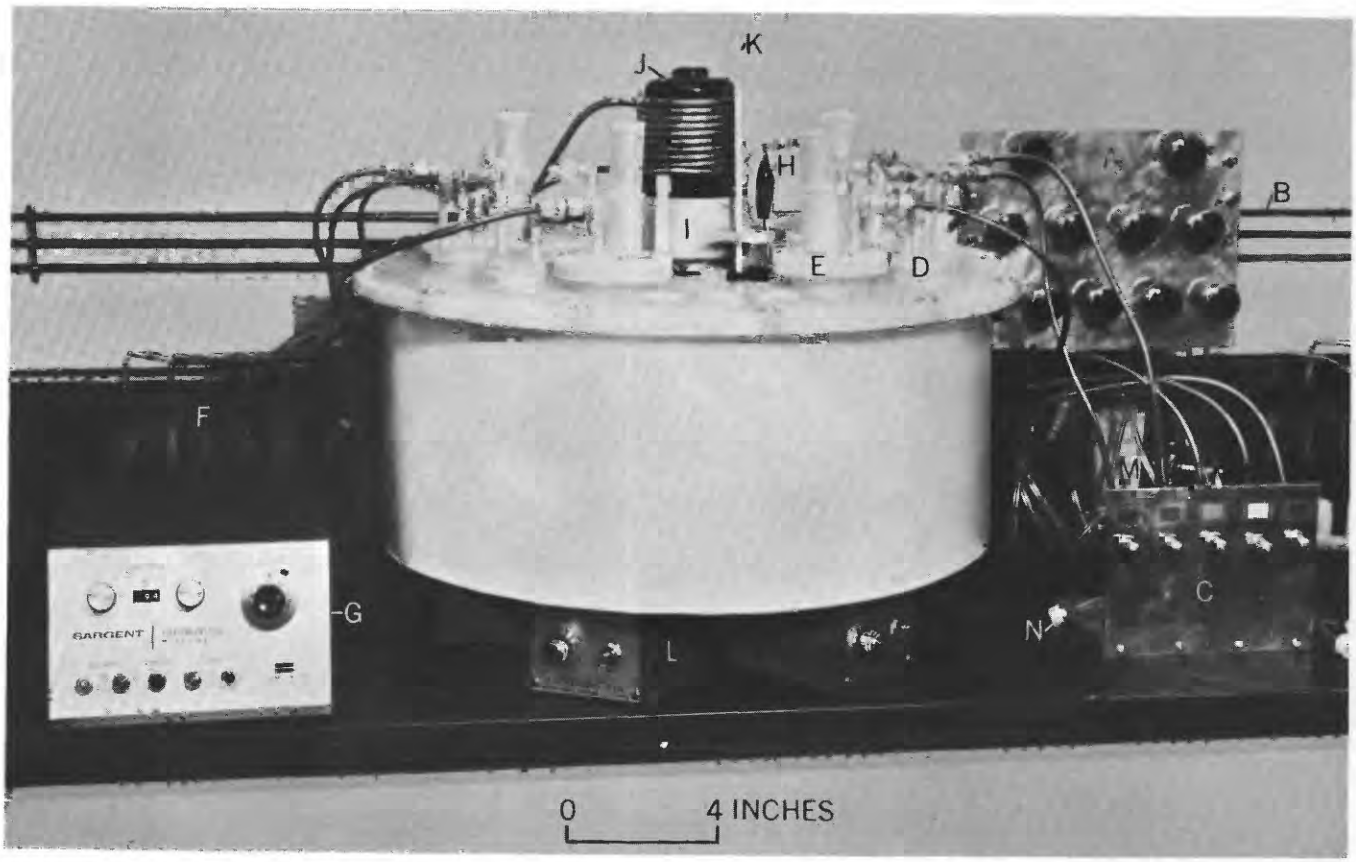

FIGURE 1.—Overall assembly of bath and control equipment. *A*, coarse-valve assembly; *B*, gas lines; *C*, fine-valve assembly; *D*, presaturation vessel; *E*, reaction vessel; *F*, water bubblers; *G*, temperature controller; *H*, temperature sensor; *I*, heating and circulating unit; *J*, stirring motor; *K*, thermometer; *L*, magnetic stirrer; *M*, CO_2 scrubber; *N*, capped gas outlet tube.

through accurately placed polypropylene strips, in square array, welded to the bottom of the bath.

The coarse-valve assembly (1*A*) consists of eleven Whitey Micro-Regulating valves (1RS4–A ¼ in.) mounted on a sheet of aluminum (9 in. × 12 in. × ¼ in.). The valves are arranged in tiers of five, four, and two; the valves in each tier are connected by a manifold made of ¼-inch O.D. Tygon tubing connected with Swagelok tube fittings (rear of panel). Each tier corresponds to a different gas; in our work, nitrogen is led into the five-valve tier, carbon dioxide into the four-valve tier, and nitrogen–carbon dioxide mixture into the two-valve tier. Carbon dioxide and nitrogen–carbon dioxide are led directly into the manifolds of the coarse valve assembly from the main gas lines (1*B*). Nitrogen, however, is bled off the main gas line by a Whitey Vee Stem valve (1VS6–A ¼ in.) (not visible in fig. 1), through a CO_2 scrubber containing Mallcosorb (1*M*), and then to the manifold of the coarse-valve assembly.

The fine-valve assembly (1*C*) is composed of five Nupro needle valves (B–4M ¼ in.) attached to a sheet of aluminum (6 in. × 8 in. × ⅛ in.), which in turn is fastened to a base of cast iron (6 in. × 8 in. × ½ in.). Any of 11 Tygon tubes from the coarse-valve assembly can be connected, by means of Swagelok nuts, to any of 5 needle valves. The unused outlets, bearing Swagelok nuts, are conveniently capped (1*N*) with the lids from standard 2-ounce Nalgen polyethylene bottles to prevent contamination. The needle valves are cadmium-plated brass; all other valves and the Swagelok fittings are brass. Copper tubing, ¼ inch O.D., is used to connect the needle valves with the presaturators, and the reaction vessels with the bubblers. Tygon tubing is used to connect the presaturators with the reaction vessels; all connections are made with Swagelok tube fittings. The system is color coded; small rectangles of paper, of five distinctive colors, are attached to the five-valve assembly and to corresponding reaction vessels; the water in the five bubblers is colored with vegetable dyes. The rate of gas flow is observed at the bubblers and adjusted with the needle valves.

Details of the bath are shown in figures 2 and 3. The cylindrical bath is 22 inches O.D., 9¾ inches high (including lid), with walls ¼ inch thick, and bottom ⅜ inch thick; the free-volume capacity is 40 liters. It is

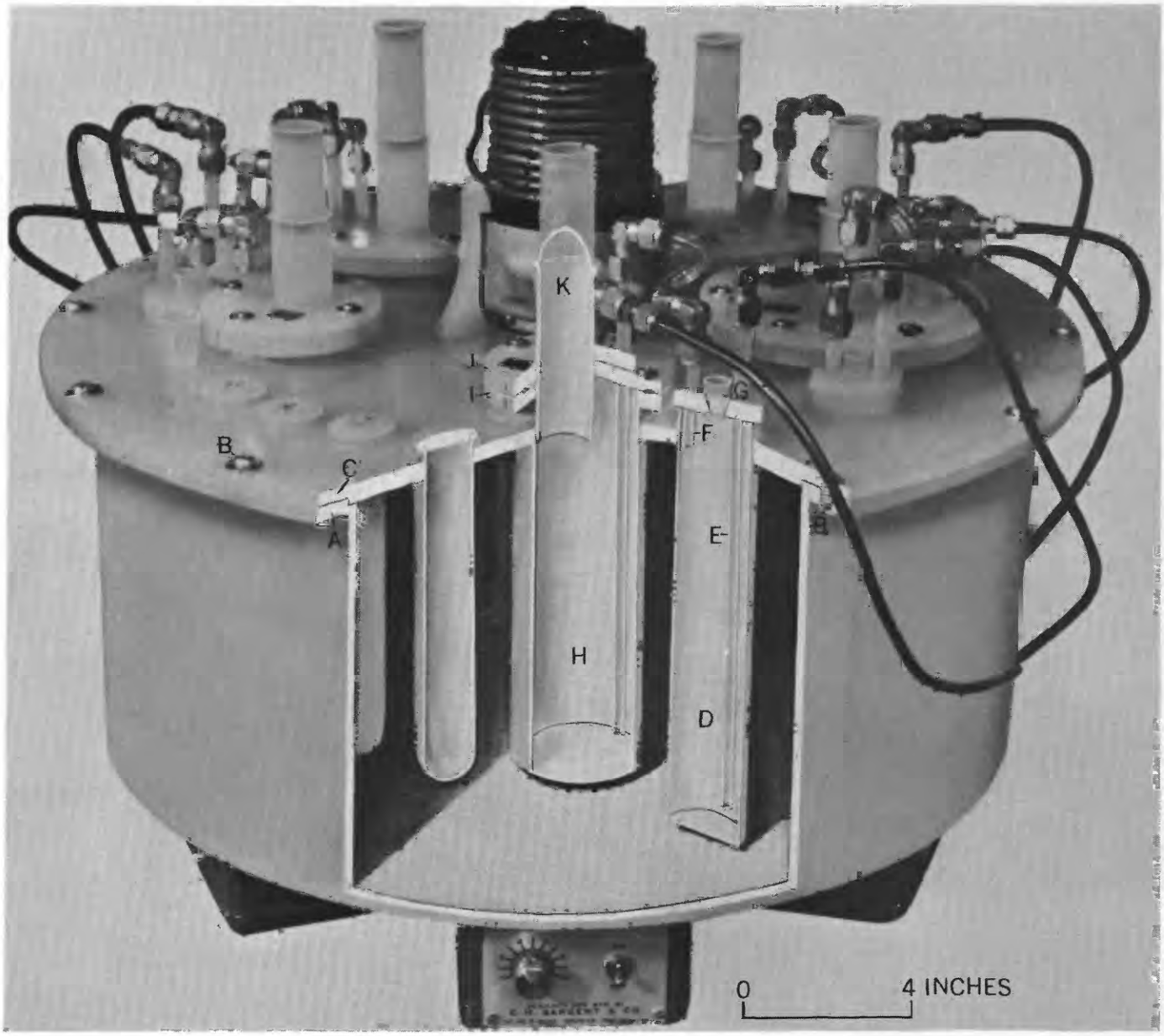

FIGURE 2.—Some details of construction of the water bath. *A*, rim; *B*, nut and bolt fastening rim to lid; *C*, details of lid and rim fit; *D*, presaturator; *E*, gas inlet tube; *F*, gas outlet tube; *G*, presaturator filling hole; *H*, small reaction vessel; *I*, rim; *J*, lid; *K*, sampling aperture.

constructed entirely of welded polypropylene. A rim (2*A*), ⅜ inch thick and 1 inch wide, is welded to the top of main body. A lid, ⅜ inch thick, is fastened to the rim by twelve ¼-20 Phillips-head machine bolts (*B*2) and T-nuts. Where the lid contacts the rim, the thickness of the lid is reduced to ¼ inch (2*C*). This design insures a snug fit of the lid to the wall and rim of the bath at higher temperatures where differential thermal expansion is pronounced. The ¼-inch-diameter machine bolts are inserted through $\frac{5}{16}$-inch-diameter holes, again to allow for thermal expansion.

All the vessels, which extend through the lid, are welded in place on both the topside and underside of the lid. The 5 presaturation vessels (3*A*), the 2 small reaction vessels (3*B*), and the 3 large reaction vessels (3*C*), all extend 8 inches into the bath, ending 1 inch from the bottom. The circulating and heating unit (3*D*) is pressed against a neoprene O-ring, recessed into the lid, through the combination of the weight of the motor, and two polypropylene clamps (3*E*) that exert a spring action. A virtually vapor-tight seal results.

313-005 O—68——15

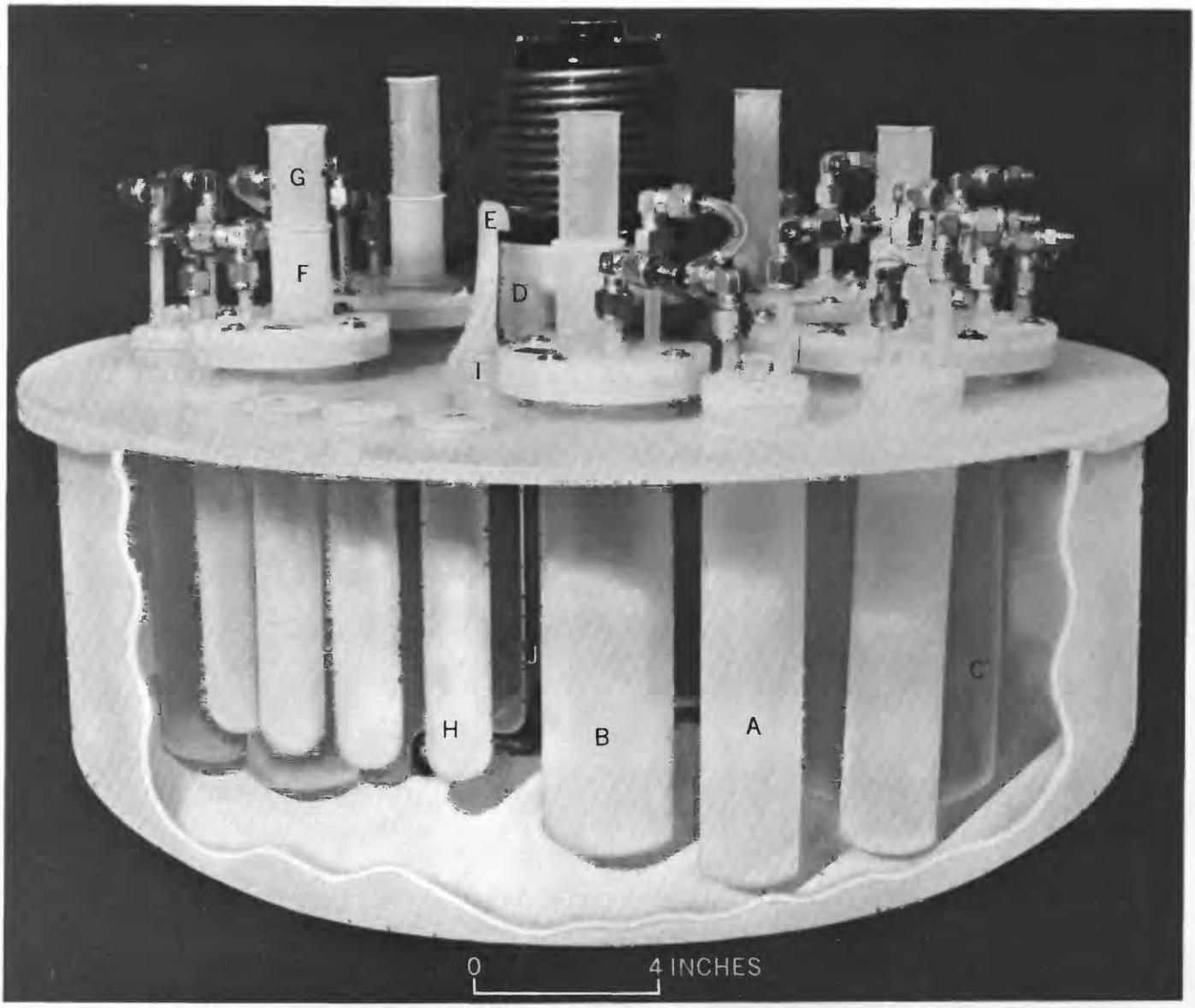

FIGURE 3.—Additional details of construction of the water bath. *A*, presaturation vessel; *B*, small reaction vessel; *C*, large reaction vessel; *D*, circulating and heating unit; *E*, clamp; *F*, sampling aperture; *G*, stopper tube; *H*, buffer vessel; *I*, stoppered bath-filling hole; *J*, lower end of heating and circulating unit.

The bath, all vessels, and the gas inlet and outlet tubes are fabricated from polypropylene. The presaturation vessels, one of which is shown in cutaway view in figure 2 (2*D*), are made of standard[1] 1.9-inch O.D. tubing having 0.2-inch walls, and have a capacity of 230 ml. The lids of these vessels are ¼ inch thick and are permanently welded to the vessels. Gas inlet (2*E*) and outlet (2*F*) tubes, welded to the lids, are made from standard ¼-inch O.D. tubing. The inlet tube extends nearly to the bottom of the vessel, is sealed at its bottom, and is perforated at 1 inch from the bottom with approximately fifty 1/32-inch holes to provide better saturation of the aqueous phase by the gas. The gas outlet tube extends approximately 1 inch below the lid. In both presaturator and the reaction vessel, the inlet tube extends 2 inches above the lid, and the outlet tube 1 inch above. By having the inlet tube of the reaction vessel higher than that of the outlet tube of the presaturator any water from the presaturator condensing in the connector can drip back into the presaturator. The staggered arrangement is also necessary to allow manipulation of the Swagelok fittings. Water is added to the presaturator through a hole in the lid of the vessel. This hole is cut on a taper, and a standard hollow polypropylene stopper of the same taper (0.6-in. top O.D.), with

[1] By "standard" here and elsewhere in the text is meant a stock item listed in the catalogs of laboratory supply houses.

bottom removed, is welded into the hole (2*G*). Sealing is effected by inserting a similar stopper into the sleeve thus provided.

A cutway view of one of the two small reaction vessels is shown in figure 2 (2*H*). The vessel is made from a standard 500-ml graduated cylinder, from which the top ¾ inch was removed. A rim ¾ inch wide and ⅜ inch thick is welded to the top of the cylinder (2*I*). A removable lid, ¼ inch thick (2*J*), is fastened to the rim by four 8–32 Phillips-head machine bolts and T-nuts. A vapor-tight seal is made between rim and lid by means of a Teflon gasket (Zip Joint), placed in matching recesses cut approximately ⅛ inch wide and 1/16 inch deep in the lid and rim.

The contents of a reaction vessel are sampled through a hollow tube extending above and below the lid of the vessel (2*K*, 3*F*). The tube is made from a standard 100-ml round-bottomed polypropylene centrifuge tube with the bottom cut off. The resulting tube is welded into the lid so that it extends 2 inches above the lid, and 1 inch into this reaction vessel. This tube is stoppered by inserting a standard 50-ml round-bottomed polypropylene centrifuge tube (3*G*). At 90°C, this assembly provides such an effective seal that care must be taken not to insert the smaller tube too tightly.

The three large reaction vessels are identical with the smaller vessels in emplacement detail and positioning of ancillary equipment, except that six instead of four machine bolts and T-nuts are used to secure the lid to the rim. The vessels themselves are standard 2-quart polypropylene jars with a length of 9 inches and an O.D. of 4¾ inches. The rim welded around the top of these vessles is ⅜ inch thick and 0.85 inch wide.

In addition to the reaction and presaturation vessels, four standard 100-ml round-bottom polypropylene centrifuge tubes (3*H*), are welded into the lid of the water bath so that the tops of the tubes barely extend above the bath lid. These tubes are used for buffer solutions. The tubes are fitted with the standard caps customarily supplied with the tubes.

Water in the bath itself is replenished, at bath temperature, through a tapered hole fitted with a standard 1-inch top O.D. tapered hollow polypropylene stopper with the bottom removed, welded into the bath lid (3*I*). This arrangement is then sealed with an identically sized stopper.

The bath is provided with a ¼-inch O.D. copper coil placed on the floor of the bath, and connected to two ¼-inch O.D. polypropylene tubes welded into the lid of the bath, by means of ¼-inch Swagelok unions. Cold water is circulated through the coil when it is desired to maintain the bath at or below room temperature.

OPERATION OF THE BATHS

Three of these baths have been operated continually for periods of several months at temperatures of 90° C to 95° C, and show fluctuations in temperature of bath water of approximately ±0.2° C. Temperature fluctuations in the small reaction vessels do not exceed ±0.4° C (normal solution volume, 400 ml), and are ±0.3° C in the large reaction vessels (normal solution volume, 1,500 ml). The small vessels have thinner walls (1/16 in.) than the large vessels (0.2 in.) and hence show smaller thermal lag. Temperature of solution in the large vessels is about 4° C lower than that of the bath water, whereas that in the small vessels is about 2.5° C lower. Loss of water vapor from the reaction vessels is irregular but slight. Most of the loss is in the form of water carryover to the bubbler tubes. The bath itself loses 1 to 2 liters of water per week, from a total of 40 liters, mostly by vapor escaping between the lid and the rim.

For making measurements, the pH electrode and thermometer used in the reaction vessels are fitted with No. 6 rubber stoppers, which ensure a tight fit to the sampling tube. The magnetic stirrers are turned off during pH measurements to eliminate erratic readings due to current fluctuations. Liquid or slurry for chemical analyses and (or) X-ray diffraction examination are removed through the sampling tube with a polypropylene syringe pipet (meat-baster type).

REFERENCE

Hostetler, P. B., and Christ, C. L., 1968, Studies in the system MgO–SiO_2–CO_2–H_2O—(I) The activity-product constant of chrysotile: Geochim. et Cosmochim. Acta, v. 32, no. 5, p. 485–498.

FOSSILIFEROUS ROCKS FROM SUBMARINE CANYONS[1] OFF THE NORTHEASTERN UNITED STATES

By THOMAS G. GIBSON, JOSEPH E. HAZEL, and JAMES F. MELLO, Washington, D.C.

Abstract.—Ages, based on Foraminifera and Ostracoda, are assigned to 74 rock samples collected from 13 Atlantic coast submarine canyons between 37° and 42° north latitude. Strata of Paleocene, middle Eocene, Oligocene, and early Miocene age are recorded for the first time in this offshore area, representing a considerable northward extension of deposits of these ages. Strata of Late Cretaceous, early Eocene, late Eocene, late Miocene, and Pleistocene age were also found. Station location, collecting equipment, litholgy, and age-diagnostic species are given for each of the 74 samples.

As part of the U.S. Geological Survey–Woods Hole Oceanographic Institution program to study the Atlantic continental margin of the United States (Emery, 1966), many rock samples were collected from Atlantic coast submarine canyons (fig. 1). Sixty-eight datable samples were secured from dredge hauls of the R/V *Gosnold*, of which 63 were collected by chain-bag dredge and five by pipe dredge. In addition, six samples were collected using the DSRV *Alvin*. Table 1 gives the ages assigned to the 74 datable samples and table 2 lists the diagnostic species of Foraminifera and Ostracoda on which the age assignments are based.

The Cretaceous Foraminifera were identified by Mello and Gibson, the Cenozoic Foraminifera by Gibson (with the exception of the assemblage in sample 53 from Oceanographer Canyon which was identified by M. Ruth Todd, U.S. Geological Survey), and the Cretaceous and Cenozoic Ostracoda by Hazel. We are grateful to scientists of the U.S. Geological Survey and Woods Hole Oceanographic Institution, particularly J. C. Hathaway and John Schlee, who collected the materials used in this study.

PREVIOUS WORK

The first firmly dated rocks from the study area, dredged off Nova Scotia, are of Late Cretaceous and Miocene or Pliocene ages on the basis of molluscan assemblages (Dall, 1925). Cruises made under the direction of H. C. Stetson (1936) collected considerable fossiliferous material in the area south of Georges Bank. Cushman (1936) described one foraminiferal assemblage of Late Cretaceous age and many assemblages of late Tertiary age from tows and cores in the submarine canyons. Stephenson (1936) described a molluscan assemblage of Late Cretaceous age dredged from the continental slope south of Georges Bank, and Bassler (1936) reported on the Bryozoa from the same area. Phleger (1939, 1942) reported on the foraminiferal faunas of Pleistocene age found in many cores from the shelf and slope from Georges Bank to Virginia. Cushman (1939) found Foraminifera of late Eocene age in two cores on the continental slope south and southeast of Long Island. A summary of the stratigraphic studies on the shelf and slope was published by Stetson (1949). Northrop and Heezen (1951) found an outcropping rock ledge of probable late Eocene age on the continental slope southeast of Long Island. Richards and Ruhle (1955) and Richards and Werner (1964) identified the macroinvertebrates of probable Pleistocene age found in cores from Hudson Canyon and from the shelf off Long Island and New Jersey. Gibson (1965) reported Foraminifera of early Eocene age from a grab sample on the continental slope south of Cape Cod and late Miocene Mollusca from four dredge hauls on the north side of Georges Bank. Schlee and Cheetham (1967) report a middle or late Eocene age for Bryozoa found in rocks dredged from the central Gulf of Maine.

SAMPLE DISTRIBUTION

Samples containing microfossils were recovered from 13 Atlantic coast submarine canyons from Norfolk Canyon on the south to Corsair Canyon on the north (fig. 1). More than half of the samples came from three canyons—Oceanographer, Wilmington, and Hudson. The depths from which the samples were dredged range from 324 to 1,820 meters.

[1] Contribution No. 2155 of the Woods Hole Oceanographic Institution.

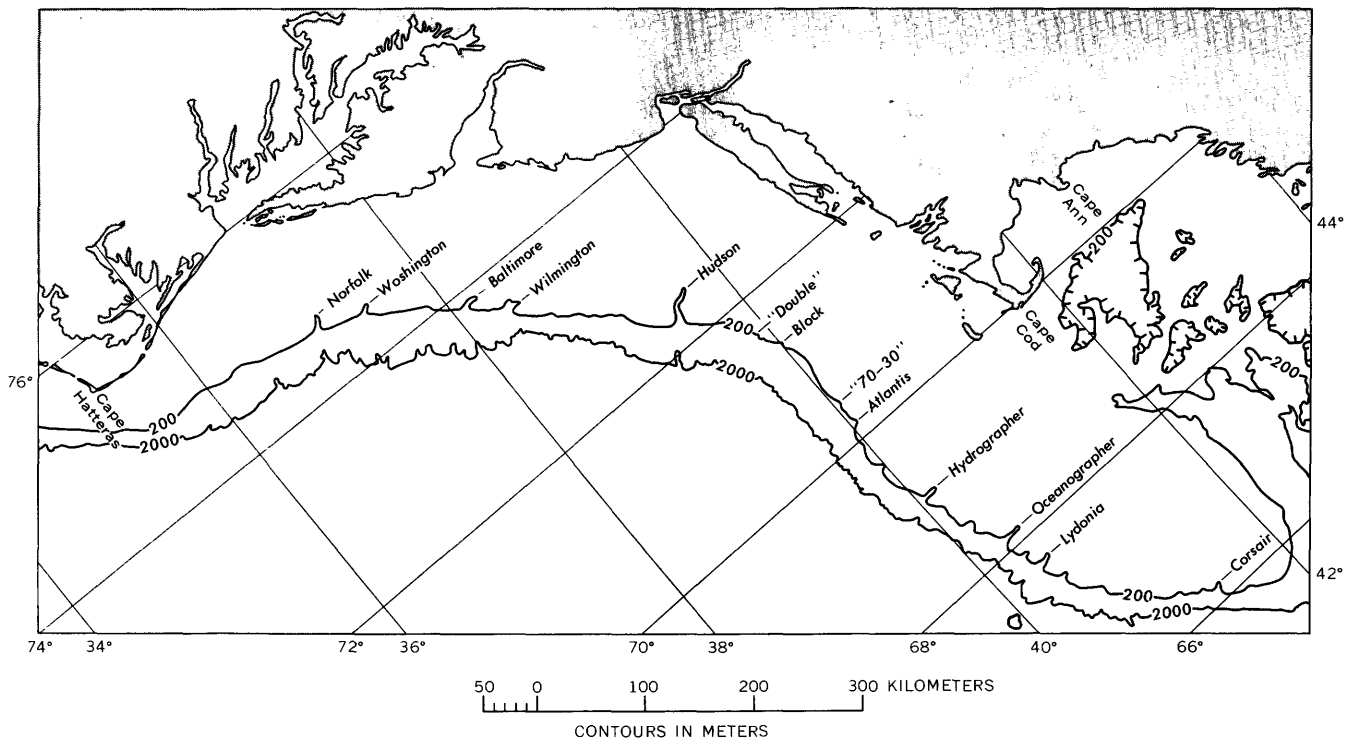

FIGURE 1.—Map showing location of submarine canyons from which samples were obtained. (Modified from Uchupi, 1965.)

Most of the assemblages suggest original sites of deposition in relatively deep waters, in many instances similar to present depths. Some, however, particularly the Cretaceous assemblages from Oceanographer Canyon and many Pleistocene assemblages, suggest original depositions at considerably shallower depths than those at which the assemblages are presently found. In the Cretaceous and older Cenozoic samples, there is little or no evidence for mixing of shallow- and deep-water assemblages by transportation of shallow-water specimens into deeper water environments. In several of the younger Cenozoic samples, the foraminiferal assemblages indicate considerable movement of shallow-water material into deeper water. Slumping of material is indicated because rocks containing geologically younger assemblages were dredged from the same depth as, or greater depths than, older assemblages in the same canyon.

Many of the indurated and partly indurated sediments are extensively bored by organisms. Although care was used in obtaining those parts of the samples processed for age determination, it is possible that some unfossiliferous samples or those such as the dolomitic claystones (samples 43 and 44), which are difficult to break down, could have been erroneously dated as late Cenozoic because of contamination by younger assemblages filling the borings.

CRETACEOUS SAMPLES

Samples containing Cretaceous microfossils were collected in Lydonia, Oceanographer, "70–30", and Hudson Canyons (samples 23, 36, 45–50, 66, and 67, tables 1 and 2). These samples yield assemblages indicative of late Campanian age to early Maestrichtian age, thus suggesting equivalence with deposits of Navarro and perhaps Taylor age in the Gulf and Atlantic Coastal Plains. The planktonic Foraminifera were placed in the zonal scheme proposed by Pessagno (1967).

The ostracode and (or) foraminiferal assemblages in Oceanographer and Lydonia Canyons suggest original sites of deposition in the sublittoral zone. However, sample 36 from "70–30" canyon contains a high percentage of planktonic Foraminifera and the ostracode genera *Argilloecia*, *Bythocytheremorpha*, and *Phacorhabdotus*, thus suggesting deposition at bathyal depths. Sample 23 from Hudson Canyon contains an entirely planktonic foraminiferal assemblage, also suggesting deposition in the bathyal zone.

TABLE 1.—*Fossiliferous rocks from submarine canyons off the northeastern United States—sample location, depth, age, and lithology, and equipment used for collecting*

Sample	Station	Canyon	Coordinates		Dredge depth (meters)	Collecting equipment	Age	Lithology
			Lat (N.)	Long (W.)				
1	2577A	Norfolk	37°03.0′	74°36.4′	400	Chain bag	Pleistocene–Recent	Gray silty clay.
2	2571	do	37°05.8′	74°38.8′	408	Pipe dredge	Pleistocene	Green sandy clay.
3	2499B	do	37°04.0′	74°39.0′	610	do	Pleistocene–Recent	Black clay.
4	2573	Washington	37°23.5′	74°20.3′	910	Chain bag	Pliocene–Recent	Green clay.
5	2572B	do	37°25.6′	74°29.9′	410	Pipe dredge	do	Brown clay.
6	2572A	do	37°25.6′	74°29.9′	410	do	Pleistocene	Gray silty clay.
7	2492B	Baltimore	38°06′	73°46.6′	497	Chain bag	Pliocene–Recent	Do.
8	2596B	do	38°09.7′	73°51.2′	566	do	do	Glauconitic sandstone.
9	2593A	do	38°07.6′	73°50.6′	580	do	Pleistocene	Gray clay.
10	2593C	do	38°07.6′	73°50.6′	580	do	do	Gray silty clay.
11	2594	do	38°06.6′	73°50.5′	715	do	do	Gray clay.
12	2580C	Wilmington	38°23.8′	73°31.2′	530	do	Pliocene–Recent	Gray silty clay.
13	2582B	do	38°22.4′	73°29.0′	435	do	do	Gray clay.
14	2580B	do	38°23.8′	73°31.2′	530	do	Pleistocene	Do.
15	2583B	do	38°22.9′	73°29.4′	443	do	do	Do.
16	2586B	do	38°21.0′	73°26.5′	520	do	do	Do.
17	2590B	do	38°18.8′	73°29.4′	1,165	do	do	Gray sandy clay.
18	2591	do	38°28.2′	73°30.6′	390	do	do	Green silty sand.
19	2583A	do	38°22.9′	73°29.4′	443	do	?Pleistocene	Green silty clay.
20	2584	do	38°28.4′	73°30.6′	324	do	Pleistocene–Recent	Green sandy clay.
21	2585B	do	38°19.8′	73°26.5′	1,010	do	?Pleistocene	Gray clay.
22	2589B	do	38°20.9′	73°31.9′	817	do	Pleistocene–Recent	Do.
23	2608F	Hudson	39°20.7′	72°04.2′	1,820	do	Late Campanian–early Maestrichtian	Gray siltstone.
24	2608G	do	39°20.7′	72°04.2′	1,820	do	Early Eocene	Yellow calcareous clay.
25	2608H	do	39°20.7′	72°04.2′	1,820	do	do	White chalk.
26	2608D	do	39°20.7′	72°04.2′	1,820	do	Middle Eocene	Yellow calcareous clay.
27	2609	do	39°22.0′	72°04.1′	1,450	do	Late Eocene	Buff calcareous clay.
28	2606	do	39°29.1′	72°13.3′	680	do	Pliocene–Recent	Gray clay.
29	2610D	do	39°22.8′	72°03.6′	1,165	do	do	Gray silty clay.
30	2602B	do	39°32.6′	72°23.5′	403	do	Pleistocene–Recent	Gray clay.
31	2604B	do	39°30.7′	72°19.0′	700	do	Pleistocene	Do.
32	2612B	do	39°15.8′	71°54.0′	1,810	do	Pleistocene–Recent	Do.
33	2619	"Double"	39°44.6′	71°39.9′	847	do	Early Miocene	Brown silty clay.
34	2621C	Block	39°49′	71°12′	1,070	do	Middle Eocene	Yellow calcareous clay.
35	2620A	do	40°00.4′	71°19.3′	333	do	Pleistocene	Gray clay.
36	2625C	"70–30"	39°46.2′	70°30.5′	1,775	do	Late Campanian–early Maestrichtian	Gray silty clay.
37	2625B	do	39°46.2′	70°30.5′	1,775	do	Early Eocene	Yellow calcareous clay.
38	2625A	do	39°46.2′	70°30.5′	1,775	do	do	Yellow chalk.
39	2626B	Atlantis	39°46.8′	70°13.5′	1,880	do	Pleistocene	Gray clay.
40	2662C	Hydrographer	40°00.0′	68°59.5′	1,250	do	Miocene–Recent	Yellow silty claystone.
41	2663F	do	40°03.8′	69°01.1′	820	do	Late Miocene–Recent	Gray clay.
42	2662B	do	40°00′	68°59.5′	1,250	do	Pliocene–Recent	Green clayey silt.
43	2663D	do	40°03.8′	69°01.1′	820	do	do	Gray dolomitic claystone.
44	2665A	do	40°01.3′	69°01.3′	1,140	Pipe dredge	Pleistocene–Recent	Do.
45	2652A	Oceanographer	40°15.1′	68°07.2′	1,500	Chain bag	Maestrichtian	Gray silty clay.
46	2652B	do	40°15.1′	68°07.2′	1,500	do	do	Glauconitic sandstone.
47	2652C	do	40°15.1′	68°07.2′	1,500	do	do	Buff calcareous clayey sand.
48	2697	do	40°15.0′	68°06.0′	940	DSRV *Alvin*	do	Gray glauconitic clayey sand.
49	2693	do	40°15.0′	68°06.0′	1,230	do	do	Gray silty clay.
50	2696	do	40°15.0′	68°06.0′	1,039	do	do	Brown silty clay.

51	2656B	----do----------	40°16.0′	68°08.3′	950	Chain bag----------	Late Paleocene----------	Do.
52	2695	----do----------	40°15.0′	68°06.0′	1,046	DSRV *Alvin*--------	Oligocene----------	Brown glauconitic sandy clay.
53	2698	----do----------	40°15.0′	68°06.0′	886	----do----------	----do----------	Buff calcareous clay.
54	2656F	----do----------	40°16.0′	68°08.3′	950	Chain bag----------	Late Miocene–Recent----------	Gray silty clay.
55	2659D	----do----------	40°19.3′	68°07.2′	1,050	----do----------	----do----------	Buff dolomitic sand.
56	2660B	----do----------	40°20.2′	68°08.6′	840	----do----------	Pliocene–Recent----------	Gray calcareous silty clay.
57	2659C	----do----------	40°19.3′	68°07.2′	1,050	----do----------	----do----------	Brown micaceous silty clay.
58	2652F	----do----------	40°15.1′	68°07.2′	1,500	----do----------	Pleistocene–Recent----------	Green silty clay.
59	2694	----do----------	40°15.0′	68°06.0′	1,292	DSRV *Alvin*----------	----do----------	Brown clayey silt.
60	2651C	----do----------	40°14.7′	68°06.2′	1,620	Chain bag----------	Pleistocene----------	Gray silty clay.
61	2654B	----do----------	40°14.3′	68°06.2′	1,270	----do----------	----do----------	Green silty clay.
62	2655A	----do----------	40°14.3′	68°06.2′	1,080	----do----------	----do----------	Do.
63	2655C	----do----------	40°15.2′	68°07.2′	1,080	----do----------	----do----------	Do.
64	2659A	----do----------	40°19.3′	68°07.2′	1,050	----do----------	----do----------	Do.
65	2659B	----do----------	40°19.3′	68°07.2′	1,050	----do----------	----do----------	Gray clayey silt.
66	2646B	Lydonia----------	40°20.5′	67°41.0′	1,175	----do----------	Late Campanian–early Maestrichtian----	Gray micaceous silty clay.
67	2646D	----do----------	40°20.5′	67°41.0′	1,175	----do----------	Late Campanian–early Maestrichtian----	Brown silty mudstone.
68	2642A	----do----------	40°28.2′	67°39.8′	403	----do----------	Late Miocene----------	Green clayey silt.
69	2644	----do----------	40°22.0′	67°41.0′	795	----do----------	Pleistocene----------	Do.
70	2637B	Corsair----------	41°22.6′	66°09.6′	522	----do----------	Pliocene–Recent----------	Brown silty clay.
71	2638C	----do----------	41°22.5′	66°11.5′	462	----do----------	Pleistocene–Recent----------	Brown clayey sand.
72	2632C	----do----------	41°23.9′	66°13.4′	360	----do----------	Pleistocene----------	Gray silty clay.
73	2632B	----do----------	41°23.9′	66°13.9′	360	----do----------	----do----------	Brown clayey sand.
74	2632A	----do----------	41°23.9′	66°13.4′	360	----do----------	----do----------	Red sandy clay.

TABLE 2.—*Distribution of age-diagnostic Foraminifera and Ostracoda*

[See table 1 for location

	Age-diagnostic Foraminifera and Ostracoda	Canyon	Norfolk			Washington			Baltimore					Wilmington										
		R/V *Gosnold* station	2577A	2571	2499B	2573	2572B	2572A	2492B	2596B	2593A	2593C	2594	2580C	2582B	2580B	2583B	2586B	2590B	2591	2583A	2584	2585B	2589B
		Sample No.	1	2	3	4	5	6	7	8	9	10	11	12	13	14	15	16	17	18	19	20	21	22
	Ostracoda																							
1	*Acanthocythereis? dunelmensis* (Norman) s.l.										X					X	X	X						
2	*Actinocythereis dawsoni* (Brady)			X																X				
3	*Amphicytherura curta* (Jennings)																							
4	*Antibythocypris gooberi* Jennings																							
5	*Baffinicythere emarginata* (Sars)																X							
6	*Bythocytheremorpha biloba* (Schmidt)																							
7	*marssonitina* (Coryell)																							
8	*"Cythere" huntensis* Alexander																							
9	*Cythereis communis* Israelsky																							
10	*Cytherelloidea navesinkensis* Jennings																							
11	*spiralia* Jennings																							
12	*Cytheropteron angulatum* Brady and Robertson																							
13	*fossatum* Skinner																							
14	*inflatum* Brady, Crosskey, and Robertson																							
15	*testudo* Sars																	X						
16	*Echinocythereis planibasalis procteri* (Blake)																							
17	*Elofsonella concinna* (Jones)																X							
18	*Eucytheridea bradii* (Norman)																	X	X					
19	*punctillata* (Brady)																X							
20	*Finmarchinella angulata* (Sars)																							
21	*finmarchica* (Sars)			X				X				X						X						
22	*Haplocytheridea puncti'ifera* (Jennings)																							
23	*Henryhowella* aff. *H. echinata* (Reuss)																							
24	*Hermanites* aff. *H. claibornensis* (Gooch)																							
25	*Heterocyprideis fascis* (Brady and Norman)																X	X						
26	*Lozoconcha? prava* Alexander																							
27	*Muellerina abyssicola* (Sars)																							
28	*canadensis* (Brady)			X	X			X				X	X			X	X	X	X	X	X		X	
29	*Normanicythere leioderma* (Norman)																							
30	*Palmenella limicola* (Norman)																X		X					
31	*Patagonacythere dubia* (Brady)																							
32	*Phacorhabdotus* aff. *P. furcatus* Pietrzeniuk																							
33	aff. *P. venodus* Crane																							
34	*Pterygocythereis* aff. *P. fimbriata fimbriata* (von Münster)																							
35	*Sphaeroleberis* cf. *S. pseudoconcentrica* (Butler and Jones)																							
36	*Thaerocythere crenulata* (Sars)																							
37	*Trachyleberidea goochi* (Swain)																							
38	aff. *T. goochi* (Swain)																							
39	*Xestoleberis opina* Schmidt																							
40	*seminulata* Crane																							
41	Other ostracode species			X	X			X			X	X	X			X	X	X	X	X	X		X	
	Foraminifera																							
42	*Bifarina vicksburgensis* (Cushman)																							
43	*Caucasina* sp.																							
44	*Elphidium clavatum* Cushman		X		X		X	X	X	X			X		X									
45	*Globigerina ampliapertura* Bolli																							
46	*ciperoensis* Bolli																							
47	*dutertrei* d'Orbigny			X							X					X	X		X			X	X	
48	*frontosa* Subbotina																							
49	*inaequispira* Subbotina																							
50	*incompta* Cifelli																							
51	*inflata* d'Orbigny			X	X	X	X	X	X	X	X	X	X	X	X	X	X	X	X	X	X	X	X	X
52	*mckannai* White																							
53	*ouachitaensis* Howe and Wallace																							
54	*primitiva* Finlay																							
55	*sellii* (Borsetti)																							
56	*soldadoensis angulosa* Bolli																							
57	*spiralis* Bolli																							
58	*tripartita tripartita* Koch																							
59	*yeguaensis pseudovenezuelana* Blow and Banner																							
60	*Globigerinelloides messinae messinae* (Bronnimann)																							
61	*Globigerinita dissimillis* (Cushman and Bermudez)																							
62	*stainforthi* (Bolli, Loeblich, and Tappan)																							
63	*unicava* (Bolli, Loeblich, and Tappan)																							
64	*Globigerinoides conglobatus* (Brady)			X	X												X				X			X
65	*ruber* (d'Orbigny)			X	X		X	X						X	X	X	X	X	X	X	X		X	X
66	*trilobus* (Reuss)			X				X										X	X	X	X	X			X
67	*Globoquadrina altispira* Cushman and Jarvis																							
68	Globorotalia *angulata* (White)																							
69	*aragonensis* Nuttall																							
70	*aspensis* (Colom)																							
71	*bullbrooki* Bolli																							
72	*centralis* Cushman and Bermudez																							
73	*ehrenbergi* Bolli																							
74	*elongata* Glaessner																							
75	*hirsuta* (d'Orbigny)			X															X		X	X		
76	*imitata* Subbotina																							
77	*lehneri* Cushman and Jarvis																							
78	*menardii* (d'Orbigny)			X	X		X	X			X				X	X	X	X	X	X	X	X		X
79	*permicra* Blow and Banner																							
80	*postcretacea* (Mjatliuk)																							
81	*punctulata* (d'Orbigny)												X											
82	*pusilla laevigata* Bolli																							

in rocks from submarine canyons off northeastern United States

and age of samples]

Hudson										"D"[1]	Block		"70–30"			At.[2]	Hydrographer					
2608F	2608G	2608H	2608D	2609	2606	2610D	2602B	2604B	2612B	2619	2621C	2620A	2625C	2625B	2625A	2626B	2662C	2663F	2662B	2663D	2665A	
23	24	25	26	27	28	29	30	31	32	33	34	35	36	37	38	39	40	41	42	43	44	
																X						1
												X										2
																						3
																						4
																X						5
																						6
													X									7
																						8
																						9
																						10
																						11
																						12
																						13
																X						14
																						15
												X										16
																X						17
																X						18
																X						19
																						20
																						21
																						22
																						23
			X																			24
																X						25
																						26
																X						27
								X				X				X						28
																						29
																X						30
																						31
														X								32
													X									33
																						34
													X									35
																X						36
											X											37
									X	X												38
																						39
																						40
			X				X	X			X	X	X	X	X	X						41
																						42
																						43
					X							X				X		X	X			44
				X																		45
																						46
									X			X							X	X	X	47
											X											48
															X							49
																	X	X				50
					X	X	X	X	X			X				X			X	X	X	51
														X	X							52
																						53
	X	X																				54
																						55
														X	X							56
																						57
																						58
				X																		59
X													X									60
																						61
										X												62
										X												63
									X			X										64
					X			X	X			X				X						65
										X		X				X						66
										X												67
																						68
		X												X								69
														X								70
			X								X											71
			X																			72
																						73
																						74
																						75
																						76
			X																			77
							X		X			X				X						78
										X												79
																						80
																						81
																						82

Oceanographer																					Lydonia				Corsair					
2652A	2652B	2652C	2697	2693	2696	2656B	2695	2698	2656F	2659D	2660B	2659C	2652F	2694	2651C	2654B	2655A	2655C	2659A	2659B	2646B	2646D	2642A	2644	2637B	2638C	2632C	2632B	2632A	
45	46	47	48	49	50	51	52	53	54	55	56	57	58	59	60	61	62	63	64	65	66	67	68	69	70	71	72	73	74	
																	X	X	X	X									X	1
																														2
X																														3
X		X	X																											4
																	X													5
X																														6
																														7
X		X																												8
X																														9
			X																											10
X																														11
																	X													12
		X																												13
																														14
																														15
																														16
																	X													17
																	X													18
																	X	X												19
																	X	?X												20
																	X	X	X	X							X			21
		X																												22
								X																						23
																														24
															X	X	X	X	X					X				X		25
						X																								26
																	X	X		X										27
																	X	X		X				X		X			X	28
																	X													29
																	X	X												30
																				X										31
																														32
																														33
								X																						34
																														35
																		X						X						36
																														37
																														38
X		X																												39
X																														40
X		X	X			X		X							X	X	X	X	X	X	X			X		X	X	X	X	41
								X																						42
								X																						43
									X	X	X		X	X	X			X	X					X	X		X	X		44
							X	X																						45
								X																						46
													X		X	X	X	X	X					X				X	X	47
																														48
																														49
									X	X															X					50
											X	X	X	X	X	X	X	X	X	X				X	X	X	X	X	X	51
																														52
							X	X																						53
																														54
							X																							55
																														56
						X																								57
							X																							58
							X																							59
X		X	X	X																	X									60
							X																							61
																														62
																														63
											X																			64
											X				X		X	X						X		X		X	X	65
											X																			66
																														67
						X																								68
																														69
																														70
																														71
																														72
						X																								73
						X																								74
																														75
						X																								76
																														77
											X				X		X	X	X	X				X		X			X	78
																														79
								X																						80
																										X				81
						X																								82

TABLE 2.—*Distribution of age-diagnostic Foraminifera and Ostracoda*

[See table 1 for location

	Age-diagnostic Foraminifera and Ostracoda	Canyon	Norfolk			Washington			Baltimore					Wilmington										
		R/V *Gosnold* station	2577A	2571	2499B	2573	2572B	2572A	2492B	2596B	2593A	2593C	2594	2580C	2582B	2580B	2583B	2586B	2590B	2591	2583A	2584	2585B	2589B
		Sample No.	1	2	3	4	5	6	7	8	9	10	11	12	13	14	15	16	17	18	19	20	21	22
83	cf. *G. rugosoaculeata* (Subbotina)																							
84	*scitula* (Brady)																							
85	*truncatulinoides* (d'Orbigny)			X	X			X			X					X	X	X	X	X	X	X	X	X
86	*tumida* (Brady)										X			X			X					X		X
87	*wilcoxensis* Cushman and Ponton																							
88	*Globorotaloides suteri* Bolli																							
89	*Globotruncana arca* (Cushman)																							
90	*duwi* Nakkady																							
91	*fornicata* Plummer																							
92	*lapparenti* Brotzen																							
93	*linneiana linneiana* (d'Orbigny)																							
94	*mariei* Banner and Blow																							
95	*stuarti stuarti* (de Lapparent)																							
96	*stuarti stuartiformis* Dalbiez																							
97	*subcircumnodifer* Gandolfi																							
98	*ventricosa* White																							
99	*Guembelitria cretacea* Cushman																							
100	*Heterohelix glabrans* Cushman																							
101	*Loxostoma wilsoni* McLean																							
102	*Nonion pizarrense* Berry																							
103	*Orbulina universa* d'Orbigny			X	X			X				X	X		X	X	X	X	X	X	X	X		X
104	*Planulina renzi* Cushman and Stainforth																							
105	*Plectofrondicularia vaughani* Cushman																							
106	*Praeglobotruncana havanensis havanensis* (Voorwijk)																							
107	*Pseudoguembelina costulata* (Cushman)																							
108	*Pseudohastigerina micra* (Cole)																							
109	*wilcoxensis* (Cushman and Ponton)																							
110	*Pseudotextularia elegans elegans* (Rzehak)																							
111	*elegans fructicosa* (Egger)																							
112	*Pulleniatina obliquiloculata* (Parker and Jones)			X	X										X					X				
113	*Robulus americanus* (Cushman)																							
114	*Rugoglobigerina rugosa macrocephala* Bronnimann																							
115	*rugosa rugosa* (Plummer)																							
116	*rugosa subrugosa* (Gandolfi)																							
117	*Siphogenerina seriata* (Cushman and Jarvis)																							
118	*Sphaerodinella dehiscens dehiscens* (Parker and Jones)																							
119	*Truncorotaloides rohri* Bronnimann and Bermudez																							
120	*topilensis* (Cushman)																							
121	*Turrilina robertsi* (Howe and Ellis)																							
122	*Virgulina vicksburgensis* Cushman																							

[1] Abbreviation, "D", "Double Canyon."
[2] Abbreviation, At., Atlantic Canyon.

LOWER TERTIARY SAMPLES

Samples containing microfossils of early Tertiary age were found in Hudson, Block, "70–30", and Oceanographer Canyons. A late Paleocene assemblage was found in sample 51 from Oceanographer Canyon. Early Eocene assemblages were found in samples 24 and 25 from Hudson Canyon. Middle Eocene was found in Hudson Canyon (sample 26) and in Block Canyon (sample 34). A late Eocene age was assigned to sample 27 from Hudson Canyon. Oligocene assemblages were found in samples 52 and 53 from Oceanographer Canyon. Rocks of late Paleocene, middle Eocene, and Oligocene ages have not previously been reported from areas offshore of the northeastern United States. Paleocene and middle Eocene deposits crop out in New Jersey; however, rocks of Oligocene age are not known from outcrops north of North Carolina.

The dating of these samples is based almost entirely on the Foraminifera, mainly planktonic species. Although ostracodes are common in some of the early Tertiary samples, all the species seem to be new except for *Loxoconcha? prava* Alexander in sample 51 and *Trachyleberidea goochi* (Swain) in sample 34. Both the foraminiferal and ostracode assemblages suggest original deposition in relatively deep waters; this no doubt accounts in part for the variety of new species of Ostracoda because early Tertiary bathyal ostracode assemblages are poorly known.

UPPER TERTIARY SAMPLES

Only two samples could be dated unequivocally as late Tertiary. Based upon the Foraminifera, sample 33 from "Double Canyon" is considered early Miocene in age, and sample 68 from Lydonia Canyon is of late Miocene age. Several other samples (table 1) could possibly be of late Tertiary age; however, the assemblages contained only species which are also known to be living today. This is the first report of rocks of early Miocene age in this area.

QUATERNARY SAMPLES

Twenty-five samples, two questionably, are dated as Pleistocene (probably late Pleistocene) on the basis of the Ostracoda. Twenty-eight of the identifiable species

in rocks from submarine canyons off northeastern United States—Continued

and age of samples]

Hudson										"D"[1]	Block		"70–30"			At.[2]	Hydrographer					Oceanographer																					Lydonia				Corsair					
2608F	2608G	2608H	2608D	2609	2606	2610D	2602B	2604B	2612B	2619	2621C	2620A	2625C	2625B	2625A	2626B	2662C	2663F	2662B	2663D	2665A	2652A	2652B	2652C	2697	2693	2696	2656B	2695	2698	2656F	2659D	2660B	2659C	2652F	2694	2651C	2654B	2655A	2655C	2659A	2659B	2646B	2646D	2642A	2644	2637B	2638C	2632C	2632B	2632A	
23	24	25	26	27	28	29	30	31	32	33	34	35	36	37	38	39	40	41	42	43	44	45	46	47	48	49	50	51	52	53	54	55	56	57	58	59	60	61	62	63	64	65	66	67	68	69	70	71	72	73	74	
				X																																																83
										X																																										84
							X	X	X							X						X														X			X	X	X	X	X				X						X	85
						X	X		X																												X	X															86
	X	X												X	X																																					87
																													X																						88
X													X																														X									89
													X												X																										90
X													X																														X									91
X													X										X																				X									92
X													X																														X									93
X													X																															X								94
X													X										X																													95
X													X												X																										96
																									X																									97
													X												X																										98
													X										X		X	X	X																								99
																						X	X	X	X	X	X																	X									00
																																													X							101
																																													X							102
							X	X	X			X				X																	X						X	X	X	X												103
																													X																						104
																													X																						105
													X										X																				X									106
X													X									X	X	X	X	X	X																										107
				X																																															108
	X	X												X																																					109
X													X									X	X		X	X																	X									110
																							X																												111
							X					X																				X		X		X									X						X	112
																																												X							113
																						X	X		X																		X									114
													X										X		X	X	X																	X									115
																																											X									116
																													X																						117
																			X																																118
			X								X																																								119
			X																																																120
																													X																						121
																													X																						122

of Ostracoda in these samples have been recorded only from Pleistocene or Recent sediments. Of these, only six species are known to occur in pre-Pleistocene rocks, and three of these seem to represent new subspecies. The above data, coupled with the presence of the planktonic foraminifer *Globorotalia truncatulinoides* in several samples, indicate that these samples are post-Pliocene. The 23 samples dated unequivocally as Pleistocene contain ostracode species whose modern southern limits are north of the northernmost canyons. The zoogeographic data indicate considerably colder conditions than are now present at the latitudes of the canyons; the conclusion is that these assemblages represent a glacial Pleistocene interval or intervals (see Hazel, 1968, for a more detailed account of the Pleistocene ostracode assemblages).

The samples dated by Foraminifera as late Miocene to Recent, Pliocene to Recent, and Pleistocene to Recent contain the same dominant cool-water species of planktonic Foraminifera in a similar state of preservation. However, the critical species of planktonic Foraminifera that are used to define the base of the Pliocene and the base of the Pleistocene are warm-water forms which are rare in samples from the temperate northern Atlantic coast, and occur in this region only as a result of eddying of the Gulf Stream (Gibson, 1967, p. 644). Thus, the absence of the warm-water species critical for dating, which may only reflect slight ecological differences or insufficient sampling rather than age, prohibits further refinement of the age range. All the samples dated as late Miocene or Pliocene to Recent are probably of Pleistocene or Recent age.

All the upper Cenozoic samples contain species of *Globigerina*, including *G. bulloides* and *G. pachyderma*, in abundance; these species are not listed on the faunal chart of characteristic species.

REFERENCES

Bassler, R. S., 1936, Geology and paleontology of the Georges Bank canyons; pt. 3, Cretaceous bryozoan from Georges Bank: Geol. Soc. America Bull., v. 47, p. 411–412.

Cushman, J. A., 1936, Geology and paleontology of the Georges Bank canyons; pt. 4, Cretaceous and late Tertiary Foraminifera: Geol. Soc. America Bull., v. 47, p. 413–440.

——— 1939, Eocene Foraminifera from submarine cores off the eastern coast of North America: Cushman Found. Foram. Research Contr., v. 15, p. 49–76.

Dall, W. H., 1925, Tertiary fossils dredged off the northeastern coast of North America: Am. Jour. Sci., 5th series, v. 10, p. 213–218.

Emery, K. O., 1966, Atlantic continental shelf and slope of the United States—Geologic background: U.S. Geol. Survey Prof. Paper 529–A, 23 p.

Gibson, T. G., 1965, Eocene and Miocene rocks off the northeastern coast of the United States: Deep-Sea Research, v. 12, p. 975–981.

——— 1967, Stratigraphy and paleoenvironment of the phosphatic Miocene strata of North Carolina: Geol. Soc. America Bull., v. 78, p. 631–650.

Hazel, J. E., 1968, Pleistocene ostracode zoogeography in Atlantic coast submarine canyons: Jour. Paleontology, v. 42, no. 5, p. 1264–1271.

Northrop, John, and Heezen, B. C., 1951, An outcrop of Eocene sediment on the continental slope: Jour. Geology, v. 59, p. 396–399.

Pessagno, E. A., Jr., 1967, Upper Cretaceous planktonic Foraminifera from the Western Gulf Coastal Plain: Palaeontographica Americana, v. 5, no. 37, p. 245–445.

Phleger, F. B., Jr., 1939, Foraminifera of submarine cores from the continental slope: Geol. Soc. America Bull., v. 50, p. 1395–1422.

——— 1942, Foraminifera of submarine cores from the continental slope, pt. 2: Geol. Soc. America Bull., v. 53, p. 1073–1098.

Richards, H. G., and Ruhle, J. L., 1955, Mollusks from a sediment core from the Hudson submarine canyon: Pennsylvania Acad. Sci. Proc., v. 29, p. 106–190.

Richards, H. G., and Werner, Eberhard, 1964, Invertebrate fossils from cores from the continental shelf off New Jersey: Acad. Nat. Sci. Philadelphia Notulae Naturae, no. 372, 7 p.

Schlee, John, and Cheetham, A. H., 1967, Rocks of Eocene age on Fippennies Ledge, Gulf of Maine: Geol. Soc. America Bull., v. 78, p. 681–684.

Stephenson, L. W., 1936, Geology and paleontology of the Georges Bank canyons; pt. 2, Upper Cretaceous fossils from Georges Bank (including species from Banquereau, Nova Scotia): Geol. Soc. America Bull., v. 47, p. 367–410.

Stetson, H. C., 1936, Geology and paleontology of the Georges Bank canyons; pt. 1, Geology: Geol. Soc. America Bull., v. 47, p. 339–366.

——— 1949, The sediments and stratigraphy of the east coast continental margin, Georges Bank to Norfolk Canyon: Massachusetts Inst. Technology and Woods Hole Oceanog. Inst., Papers in Physical Oceanography and Meterology, v. 11, no. 2, 60 p.

Uchupi, Elazar, 1965, Map showing relation of land and submarine topography, Nova Scotia to Florida: U.S. Geol. Survey Misc. Geol. Inv. Map I–451, 3 sheets, scale 1:1,000,000.

TORTUGAS TERRACE, A SLIP SURFACE? [1]

By ELAZAR UCHUPI, Woods Hole, Mass.

Abstract.—In November 1966, three seismic profiles were recorded on Tortugas Terrace and vicinity, west of Dry Tortugas, Fla., to determine whether the terrace is a structural feature. The study suggests that the terrace is a slump-slip surface, not a fault block.

During the last few years, the wide application of continuous seismic profilers has added new impetus to submarine physiographic studies. Structures of continental margins and other submarine topographic features, and variations in sediment thickness within the oceanic basin can be determined from data obtained by this relatively new technique. Such information has proven useful in reconstructing the geologic history of oceanic basins. The present report describes the structure of Tortugas Terrace, off southern Florida, as revealed by a seismic profiler.

Tortugas Terrace is about 80 kilometers west of Dry Tortugas, Fla. (fig. 1). It is a rectangular block 6 km wide by 11 km long, oriented northeastward almost at right angles to the trend of the Florida-Hatteras Slope (fig. 2). The terrace is bordered on the northwest by a 200-meter-high slope that falls away at an angle

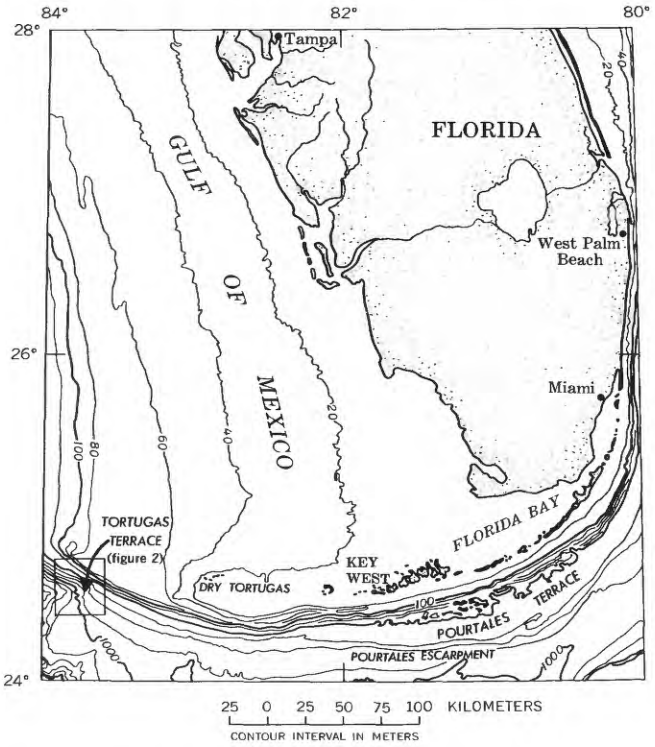

FIGURE 1.—Chart of the Straits of Florida, showing the location of Tortugas Terrace. The slope south of the Florida Keys and east of the Florida peninsula is known as the Florida-Hatteras Slope.

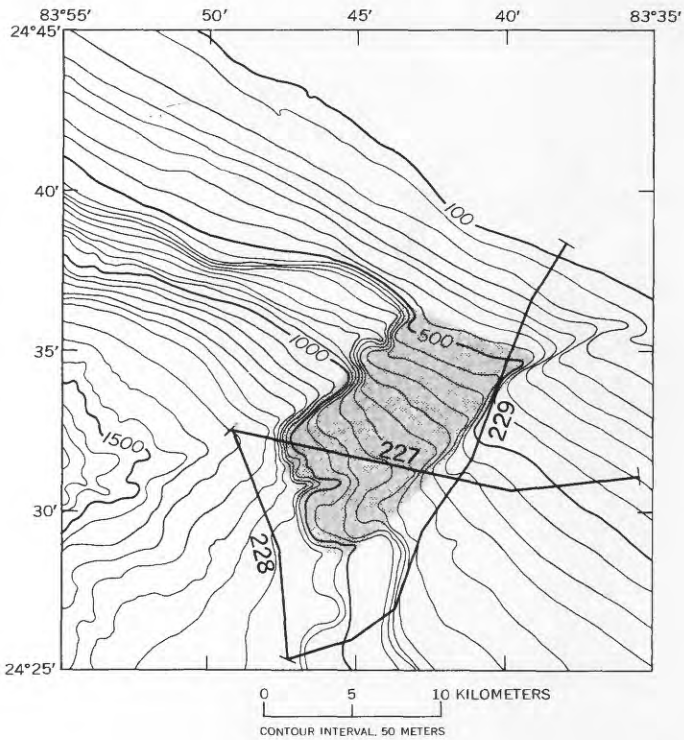

FIGURE 2.—Bathymetric chart showing Tortugas Terrace (shaded area) and location of seismic profiles 227, 228, and 229 (figs. 3, 4). Bathymetry based on soundings from U.S. Coast and Geodetic Survey hydrographic surveys.

[1] Contribution No. 1989 of the Woods Hole Oceanographic Institution.

U.S. GEOL. SURVEY PROF. PAPER 600-D, PAGES D231-D234

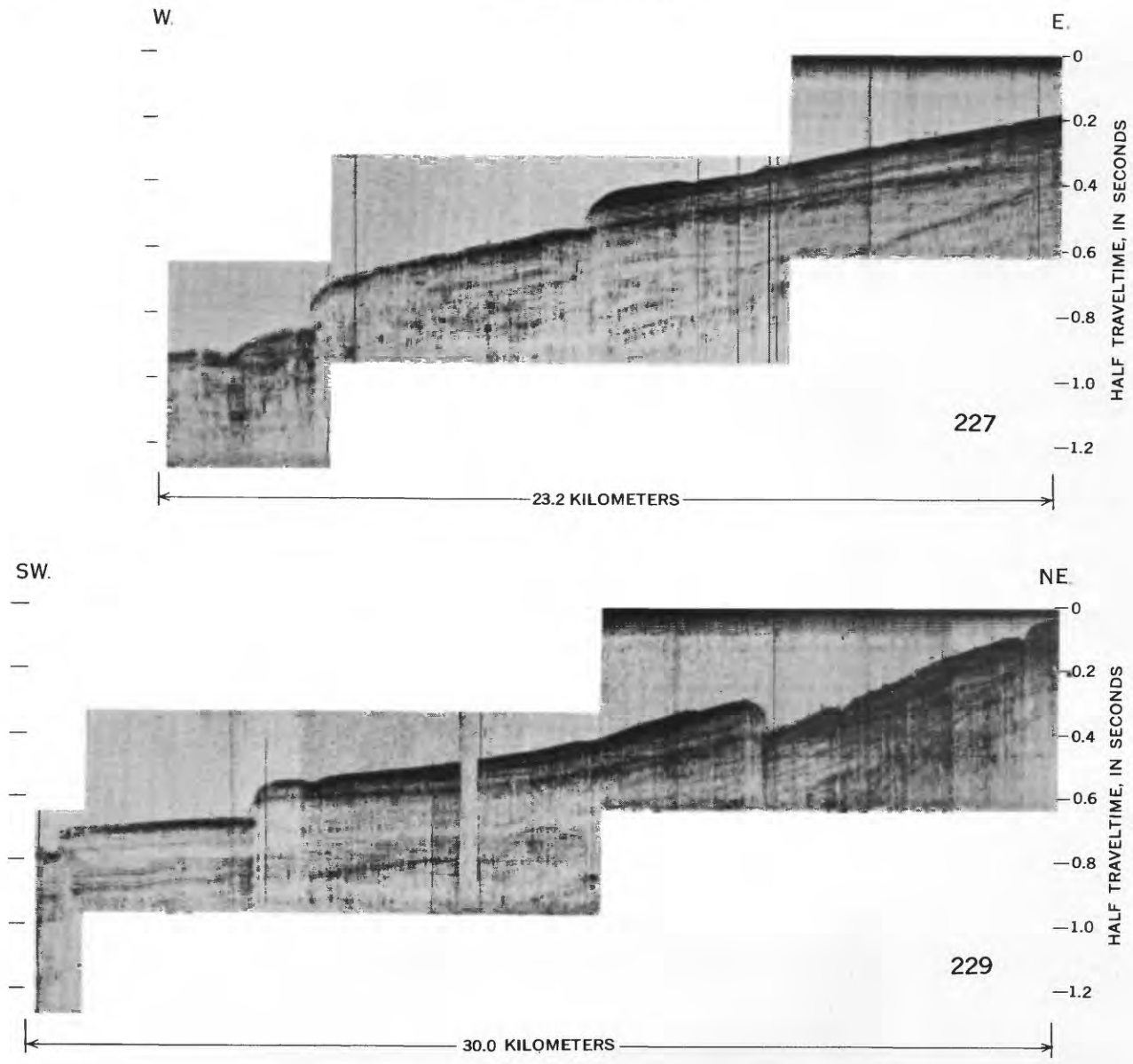

FIGURE 3.—Seismic profiles 227 and 229 across Tortugas Terrace. Profiles were recorded at a frequency interval of 75–150 cycles per second. See figure 2 for location of profiles.

of about 16°. A 100-m slope with a gradient of 6° to 14° rises above the terrace on the southeast; the southwest slope flanking the terrace has a relief of about 100 m and a declivity of about 6°. The surface of Tortugas Terrace itself is rather smooth and ranges in depth from 500 m on the northeast to 1,000 m on the southwest. Kofoed and Jordan (1964), who first described and named the feature, suggested that side slopes of Tortugas Terrace are fault scarps and that movement along them formed the terrace. Their interpretation was based solely on bathymetry.

In November 1966, three seismic profiles were recorded on Tortugas Terrace and vicinity to determine whether the terrace is a structural feature. The seismic profiles were obtained by use of a 15,000-joule sparker as a sound source. Profile 227 (fig. 3) crosses the terrace in a westerly direction, profile 228 (fig. 4) is immediately southwest of the terrace, and profile 229 (fig. 3) is along the southeastern edge of the terrace.

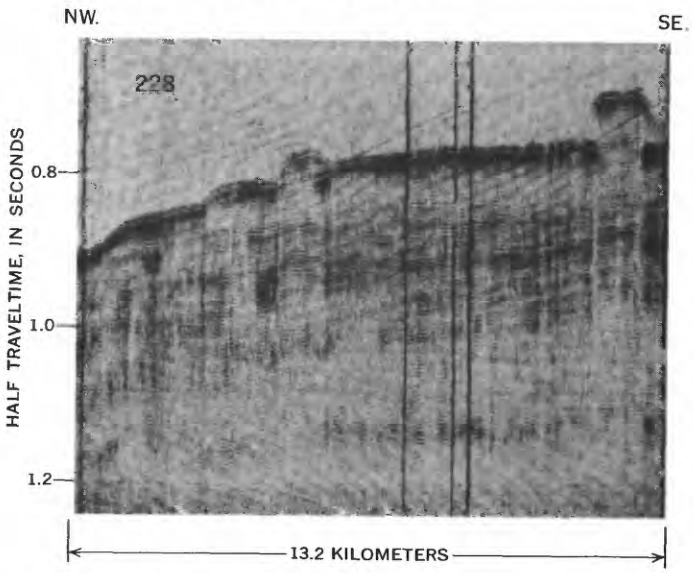

FIGURE 4.—Seismic profile 228 southwest of Tortugas Terrace. Profile was recorded at frequencies of 75–150 cycles per second. See figure 2 for location of profile.

In profiles 227 and 229 (fig. 3), the subbottom reflectors continue beneath the terrace's side slopes without any displacement, thus indicating that the steep slopes southeast and northwest of the terrace are not normal fault scarps. The only structure revealed by the three profiles is the slight warping of the deeper reflectors. The apparent warping along profile 228 (fig. 4) is restricted to the area immediately beneath the surface knolls, an indication that the warping is due to differences in compressive wave velocity between the water and sediments. This phenomenon is analogous to the apparent bending of subbottom horizons when they intersect steep slopes such as the sides of submarine canyons. It will be noted that some of the reflectors in profiles 227 and 229 also have a similar but more subdued apparent warping as they extend beneath the steep side slopes. As the warping beneath the steep slopes is a small fraction of the surface relief shown by the slopes, this warping is also due to differences in velocity between the sediments and water and not to vertical displacement.

As faulting does not seem to be the cause of the terrace formation, it is suggested that Tortugas Terrace and the embayment to the west were formed by slumping. The topographic features shown in figure 2 are analogous to slump-slip surfaces. Before slumping took place, the area was probably characterized by a smooth slope having a gradient of about 2°; similar dips occur east of the terrace. This slope probably had an outbuilding or prograding type structure; that is, the internal reflectors were parallel to the bottom. The embayment west of the terrace was formed by the downslope displacement or slumping of the upper several hundred meters of sediment. Farther east, the sediments were displaced in two segments, the first being composed of the sediments south of Tortugas Terrace. This removed the support from the sediments farther up the slope, causing them also to slump. Displacement of the upper slope sediments led to the formation of Tortugas Terrace. Differences in depth between the terrace and

the embayment to the west are due to the different thicknesses of material displaced from the slope by slumping. Sediment removed from the slope by slumping came to rest at the base of the slope. Unfortunately, profile 229 does not extend far enough southward to cross the slump mass.

Available data do not indicate when slumping occurred but the state of preservation of the slip surfaces on the upper slope suggests that slumping probably took place during the Pleistocene. The terrace region is one of relative crustal stability, and slumping was probably not initiated by an earthquake. Consequently, it is suggested that mass movement was probably due to strength failure caused by sediment loading.

This and other studies of the structure of the Straits of Florida indicate that faulting along the side slopes of the straits is not very common. Only along Pourtales Escarpment and Pourtales Terrace has any indication of folding and faulting been found (Uchupi, 1966). Evidence to date suggests that the side slopes of the Straits of Florida have been formed by a combination of carbonate accretion or reef buildup and outbuilding by carbonate sediments that has mostly buried the reef structures. In segments of the side slopes, slumping has modified the original structures.

REFERENCES

Kofoed, J. W., and Jordan, G. F., 1964, Isolated fault scarps on the continental slope off southwest Florida: Southeastern Geology, v. 5, no. 2, p. 69–77.

Uchupi, Elazar, 1966, Shallow structure of the Straits of Florida: Science, v. 153, no. 3735, p. 529–531.

THE CARTER MOUNTAIN LANDSLIDE AREA, NORTHWEST WYOMING

By WILLIAM G. PIERCE, Menlo Park, Calif.

Abstract.—Coalesced landslides, mostly earthflows but partly slumps in their headward parts, cover an area 5 miles wide and more than 20 miles long on the flanks of Carter Mountain. Two periods of movement are indicated by topographic and stratigraphic relationships. The older landslides, which extended over most of the area, are subdued and extensively eroded. The younger landslides, about half as widespread, lie mostly within the older and cut it with sharp borders. Of the 100 ponds and lakes in the area, 95 are in the younger slides. An end moraine of Wisconsin age rests in places on an older slide. The moraine is also believed to overlie the Cody terrace, but a bench 30 feet below the terrace is glaciofluvial. The landslides probably are related to times of greater precipitation, and may be associated with glacial-pluvial periods.

The Carter Mountain landslides are located on the north and east sides of Carter Mountain, about 15 miles southwest of Cody, Wyo., and 30 miles east of Yellowstone National Park. This exceptionally large landslide area formed in two separate periods of movement, as indicated by differences in degree of erosion of the deposits and by crosscutting relations.

After the first major movements of the Carter Mountain landslides, and before the second, a terminal moraine of Wisconsin age was deposited within the same valley. The lower part of the valley also contains well-formed stream terraces. The relation of moraines and terraces to the landslides will be discussed following a description of the landslides.

DESCRIPTION OF LANDSLIDES

The Carter Mountain landslide area is more than 20 miles long and about 5 miles wide (fig. 1). It covers about 85 square miles, and is one of the largest landslide masses that has been mapped.

The older landslides cover about 35 square miles, and the younger ones about 50 square miles (fig. 1). However, the older landslides originally extended over the entire landslide area of roughly 85 square miles, whereas the younger landslides are mostly reactivated older landslides. Thus the older landslides were nearly twice as extensive as the younger ones.

The landslide deposits range in altitude from about 6,000 to 9,000 feet. The ratio of height to length of the slope on which the masses moved ranges between 1 to 7 and 1 to 11, or between 5° and 8°. The upper part of the slope is steeper, and the lower part is flatter, probably only 2° or 3°.

Carter Mountain, which is the source area for the landslide debris, consists of more than 3,000 feet of cliff-forming volcanic sediments and flows overlying roughly 1,000 feet of shale, siltstone, and sandstone of the Willwood Formation of early Eocene age. The Willwood Formation is primarily involved in the initiation of the landsliding, for it gave way beneath the high, steep cliffs formed by the volcanic rocks. Concomitantly, the weight of the overlying volcanic rocks undoubtedly contributed to the failure by overloading the unstable rocks below. Both the Willwood and overlying rocks are flat lying. The general relation of Carter Mountain to the landslides is shown in figure 1.

The difference in sharpness of topographic form between older and younger landslides is strikingly shown by the distribution of lakes and ponds. Of about 100 lakes and ponds in the landslide area, all but 5 are in younger landslides (fig. 1). Figure 2 shows the topographic contrast between the older and younger landslides in the Bull Creek-Marquette Creek area. The ponds, lakes, and sharp topography of the younger landslides contrast markedly with the rounded topography of the older landslides. The borders of the younger landslides, moreover, are well defined, whereas the contact between the older landslides and bedrock is less well defined.

The areal distribution of some of the older landslides also indicates considerable erosion. For example, the several small masses of older landslide shown on the left side of figure 3 were at one time connected to the main mass of older landslide, but they have since been

U.S. GEOL. SURVEY PROF. PAPER 600-D, PAGES D235-D241

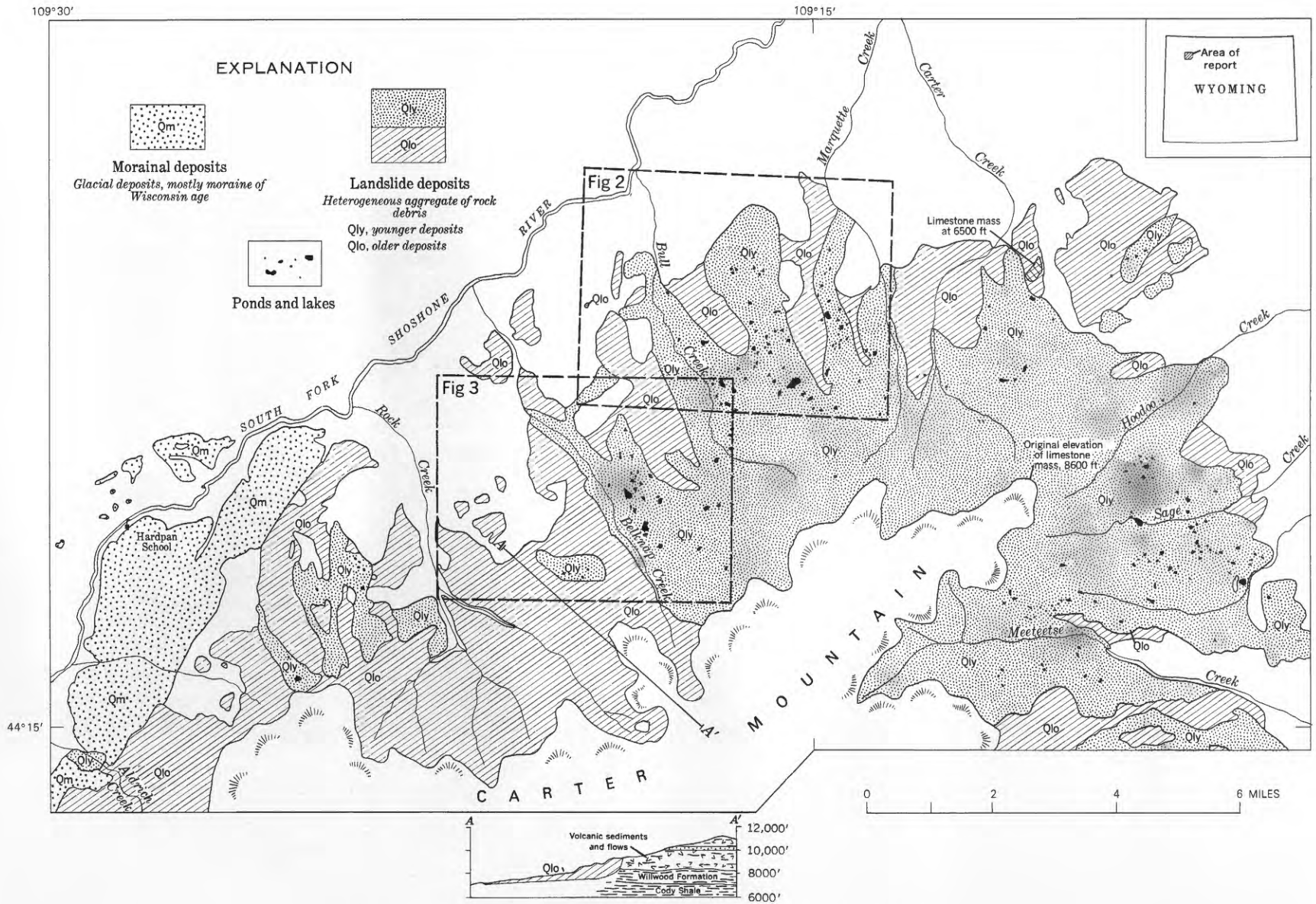

FIGURE 1.—Map showing distribution of the Carter Mountain landslides.

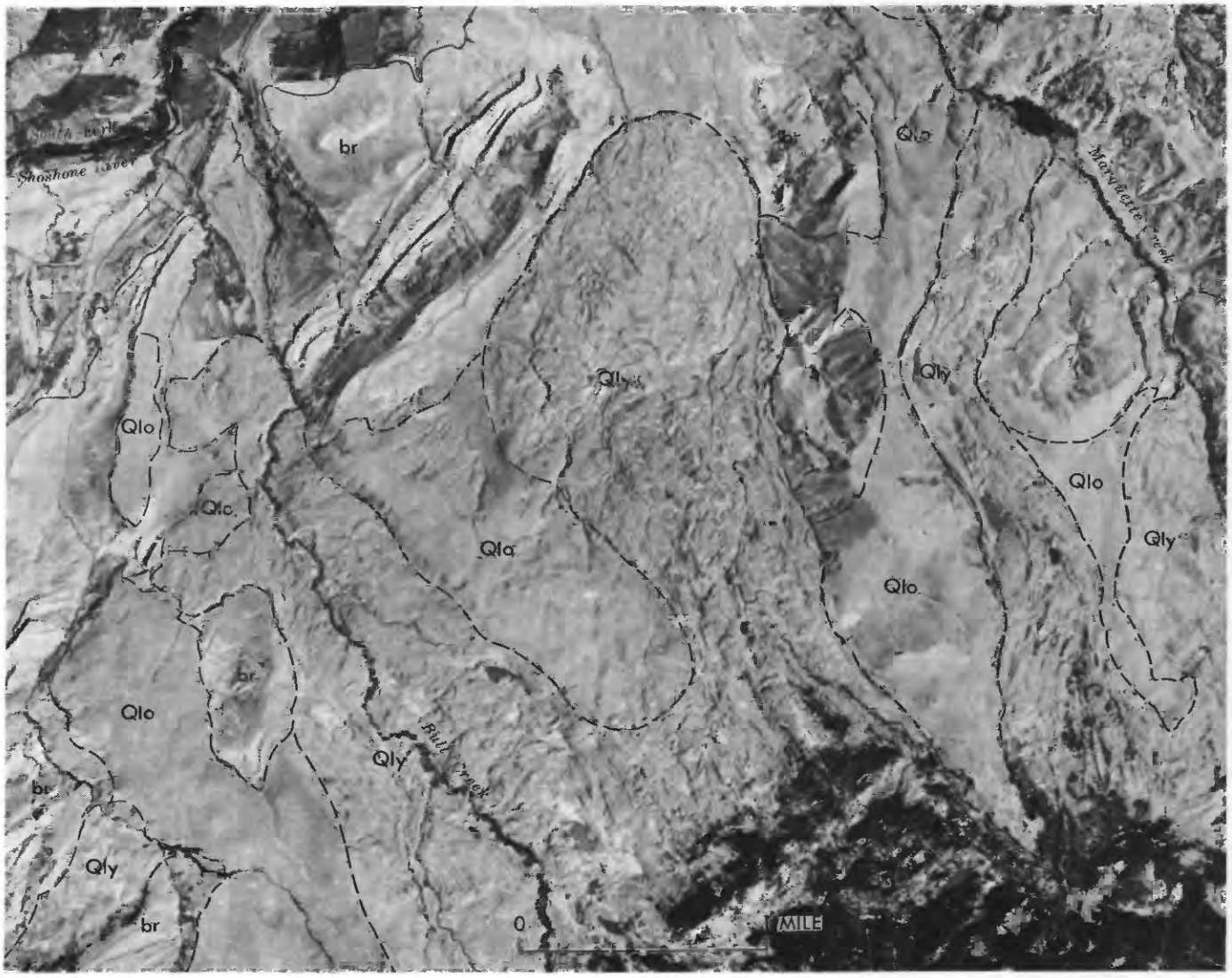

FIGURE 2.—Aerial photograph of the Bull Creek–Marquette Creek area. Rounded topography of older landslides (Qlo) contrasts with sharp topography of younger landslides (Qly) containing ponds and lakes. Note also the well-defined contact of younger landslides with older landslides and bedrock (br). Location of area shown on figure 1.

isolated by erosion. A ground view of the rounding and smoothing of the older landslide surface is shown in figure 4*A*. The much sharper topography of the younger landslides is illustrated in figure 4*B*. The contrast in topographic form, where the two are adjacent, is shown in figure 4*C*.

The younger, or second, period of landsliding extended in varying degree over the area of previous movement. Instability was not uniform, however, as is shown by the distribution of the younger landslides on the map. West of Belknap Creek, the younger landsliding was much less extensive, and for the most part did not extend southward up the side of Carter Mountain far enough to reach the upper limit of the older landsliding. East of Belknap Creek, however, and extending eastward around the point of Carter Mountain, the younger landsliding involved all of the older landslide and probably some material previously not involved. The difference in distribution is not due to differences in the bedrock or its attitude, for these are about the same in both areas. Perhaps such things as a somewhat drier second pluvial cycle, slightly greater precipitation at the northeast tip of Carter Mountain, and greater solar insolation on the northwest exposure (Hansen, 1961) combined in varying degree to account for the distribution of the younger landsliding.

In the northeast part of the map area at an altitude of 6,500 feet a jumbled mass of Paleozoic limestone and dolomite ¾ of a mile long and as much as 150 feet thick rests on landslide debris derived from the

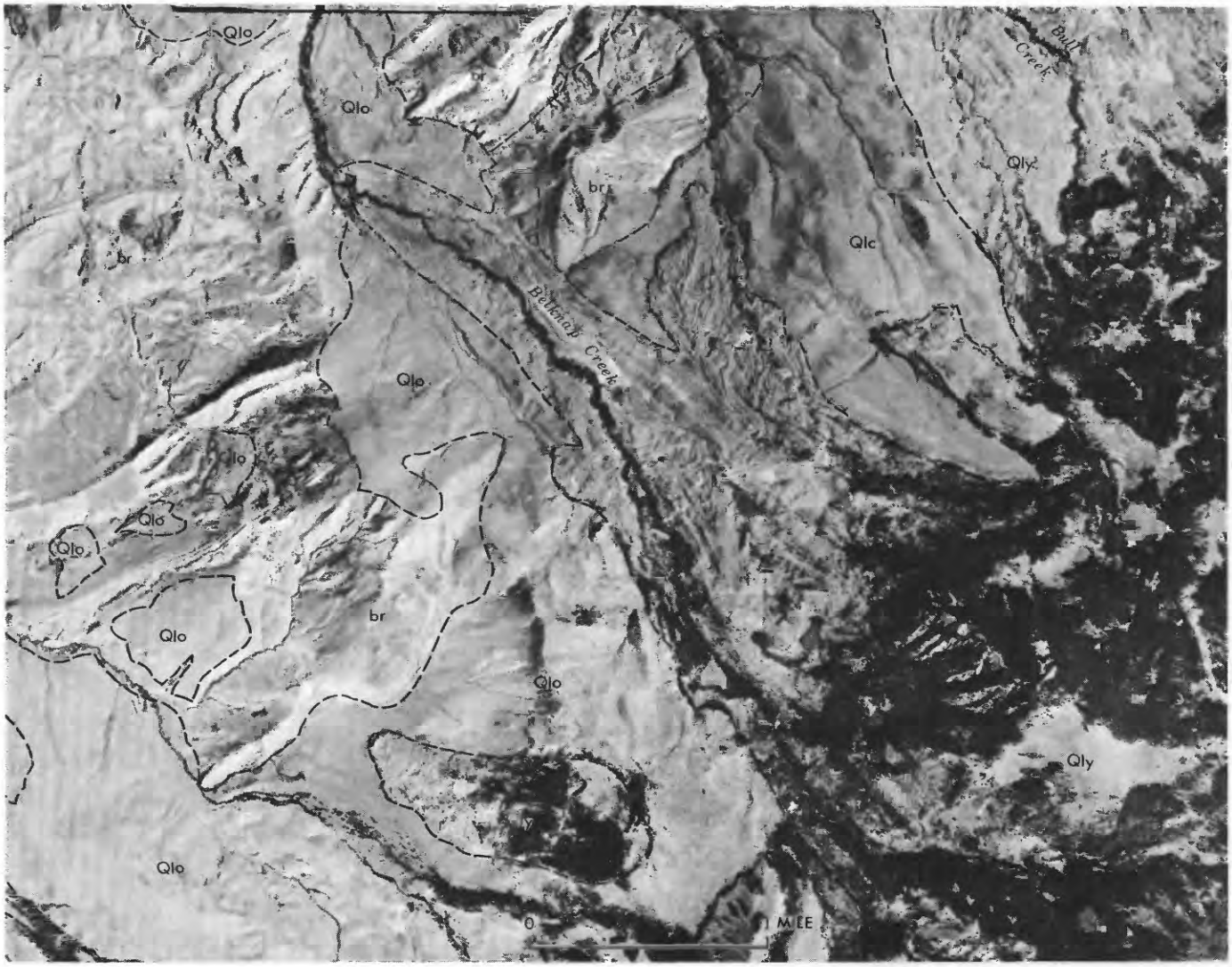

FIGURE 3.—Aerial photograph of the Belknap Creek area. The small areas of older landslide (Qlo) which at one time were connected to the larger masses have been isolated by erosion. Note fingerlike penetration of the main mass of younger landslide (Qly) through the older landslide along Belknap Creek and branching to the north and northeast. A local mass of younger landslide lies in the south-central part of the photograph. br, bedrock. Location of area shown on figure 1.

Willwood Formation of Eocene age (fig. 4*D*). These Paleozoic rocks are a remnant of the upper plate of the Heart Mountain detachment fault. Similar but smaller remnants occur in Carter Mountain, between the Willwood Formation and the overlying volcanic sediments. Regional studies (Pierce, 1957) show that when the Heart Mountain fault blocks were originally emplaced in this area in Eocene time, they came to rest on the Willwood Formation and were buried soon afterward by volcanic sediments and flows. This horizon between the Willwood and volcanic sediments is at an altitude of about 8,600 feet in the northeast part of Carter Mountain, and the Paleozoic carbonate rocks in the landslide originally were at that altitude. They slid to their present position 2,100 feet lower during the earlier time of landsliding. Furthermore, they seem to have slid as a unit, for no Willwood or younger rocks are mixed with them.

MOVEMENT

The Carter Mountain landslides are mostly earthflows and mudflows, but they also include slump, especially in their upper reaches. Movement probably extended over a considerable span of time, and no doubt local conditions caused many variations. It is unlikely that all the deposits grouped in a landslide event moved at exactly the same time. Movement probably was slow and intermittent. Although the older and younger landslides behaved similarly, the periods of movement for each were separated by a span of time sufficiently long for erosion to significantly

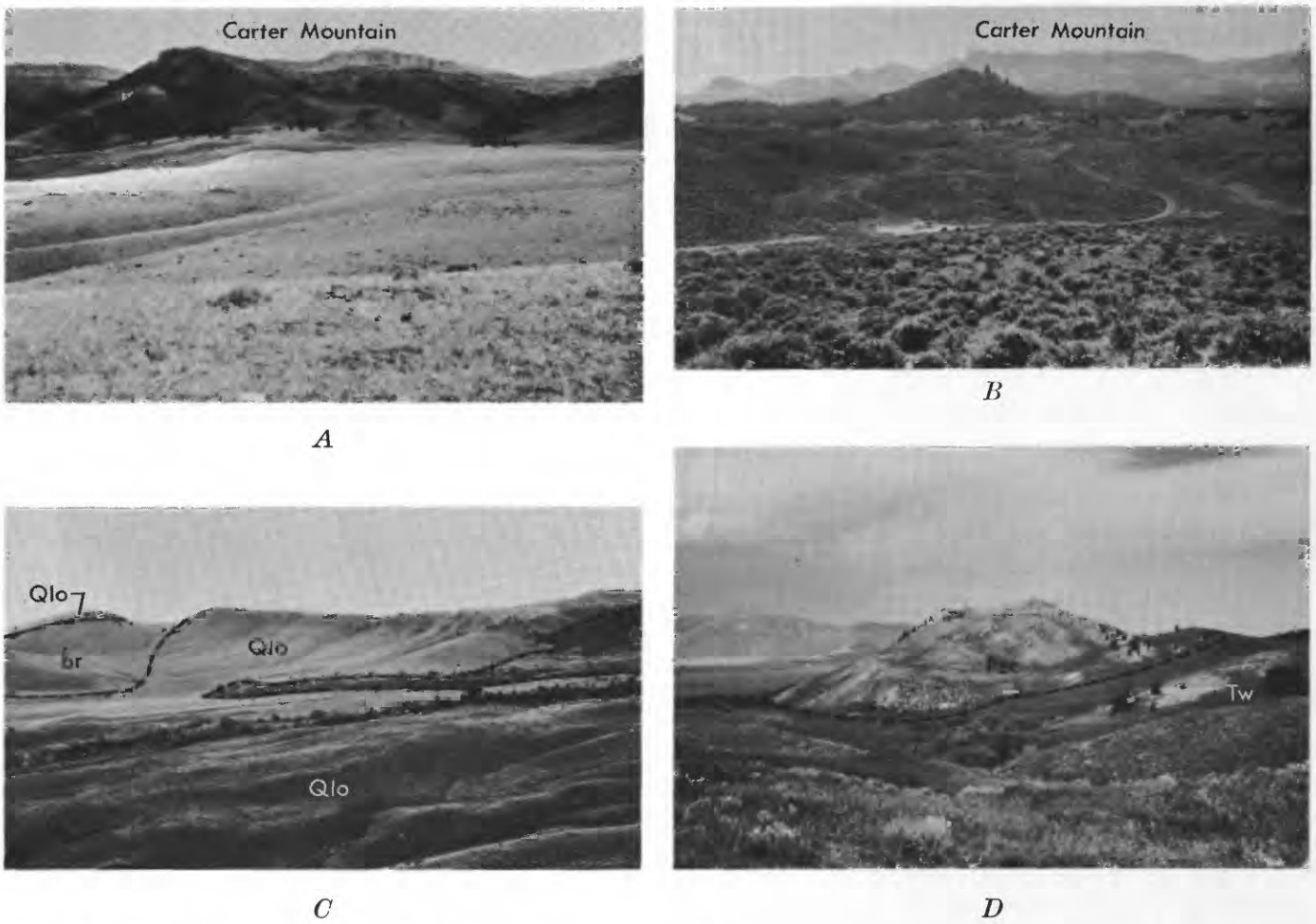

FIGURE 4.—Views of terrain of older and younger landslide.
A, View southeast up Rock Creek valley. Older landslide extends from foreground to base of Carter Mountain cliffs.
B, View southeast up Belknap Creek valley. Younger landslide extends from foreground to base of Carter Mountain cliffs.
C, View northeast toward divide between Rock and Belknap Creeks. The divide on the middle skyline is covered by older landslide (Qlo). A tongue of younger landslide (Qly) lies in the valley in the middle distance. The bedrock (br) on the left is the Cody Shale.
D, Remnant of Heart Mountain detachment fault in older landslide. The mass of Paleozoic carbonate rock (Pzc) rests on landslid Willwood Formation (Tw). The Paleozoic rock has slid northward down the flank of Carter Mountain about 2,100 feet vertically and about 3 miles horizontally. Location indicated on figure 1 as "limestone mass."

smooth the older deposits. The older landslides in particular might have had several distinct periods of movement. Obviously, if the last movement was as extensive as the preceding ones, evidence of earlier movement would be obliterated.

The bulk of the younger landslides also appear to be stable even though they look fresh. Trees growing on them stand erect. Although there are local areas of active landsliding on both the younger and older landslides, the larger masses as a whole are not moving.

RELATION OF LANDSLIDES TO MORAINE AND STREAM TERRACES

Moraine

A glacier of Wisconsin age (Alden, 1932, pl. 1; Rouse, 1934) extended down the South Fork of Shoshone River and left the large end moraine west of Rock Creek (fig. 1; fig. 5*A*). Along its southeast border the moraine overlies part of an older landslide, thus indicating that the moraine at that locality is younger than the landslide. Border relations between the moraine and the older landslide also indicate that the moraine is younger (fig. 5*B*). The age of the moraine is, therefore, of interest for, if known, it would establish a minimum age for the older landslide.

Moss and Bonini (1961, fig. 2) show two moraines in their terrace profile along the South Fork of Shoshone River, a higher one which they assign to the Bull Lake Glaciation and a lower one which they assign to the Pinedale. The deposits which they called Bull Lake moraine, however, are here regarded as older landslide deposits, and the moraine which they assign to the

A

B

FIGURE 5.—Glacial moraine and contact between moraine and older landslide. Photographs by K. E. Lohman.
A, Glacial moraine bordering the southeast side of South Fork of Shoshone River. View northeast.
B, View along contact between moraine (Qm) and older landslide (Qlo), looking northeast between South Fork of Shoshone River and Rock Creek.

Pinedale Glaciation therefore, could be of Bull Lake age.

Since the end moraine was deposited, the South Fork of Shoshone River has lowered its channel 200 feet, which is much more than most comparable streams have cut down since Pinedale time. A few younger morainal deposits are within the main end moraine. These younger moraines may be Pinedale in age, but a definite correlation cannot yet be made. In any event, the writer tentatively correlates the main end moraine with the Bull Lake Glaciation, and if it is eventually shown definitely to be of Bull Lake age, the older landslide is at least 30,000 years old, according to age assignments used by Richmond (1965, table 2).

Terraces

Three sets of stream terraces, the Powell, the Cody, and the lower Cody, are well developed along the South Fork of the Shoshone River. The oldest is the Powell terrace, which is between 250 and 450 feet above the river and has a minor bench above its main level. The intermediate Cody terrace, which is particularly well formed in the area covered by figure 1, is between 160 and 200 feet above the river. A series of smaller terraces, which are grouped and mapped as the lower Cody terraces, extend downward from about 30 feet below the Cody terrace (Pierce and Andrews, 1941, p. 156; Pierce, 1966).

The older landslides rest in places on the Powell terrace, thus indicating that they are younger than the Powell terrace. In the vicinity of Rock Creek, the Cody terrace truncates and is cut below some older landslide deposits, thus indicating that the Cody terrace is younger than the older landslide. The relations between the older landslide, the terraces, and the moraine are illustrated diagrammatically in figure 6. The sequence of events as thus illustrated, from older to younger, is Powell terrace, older landslide, Cody terrace, moraine, and lower Cody terraces. The age of the younger landslides relative to these events cannot be determined directly, but the much sharper topographic form of the younger landslides strongly suggests that they are younger than the moraine.

RELATION OF MORAINE TO CODY TERRACE

Two interpretations have been made of the relation of the moraine to the Cody terrace. Rouse (1934), Mackin (1937), and Pierce and Andrews (1941) concluded that the moraine rests on the Cody terrace, hence that the moraine is younger than the terrace. Moss and Bonini (1961, p. 551) agree that the moraine overlies the bedrock surface of the Cody terrace, but do not believe that the moraine rests on the Cody terrace gravel. They conclude "that the gravel in front of the moraine extending downstream to form part or

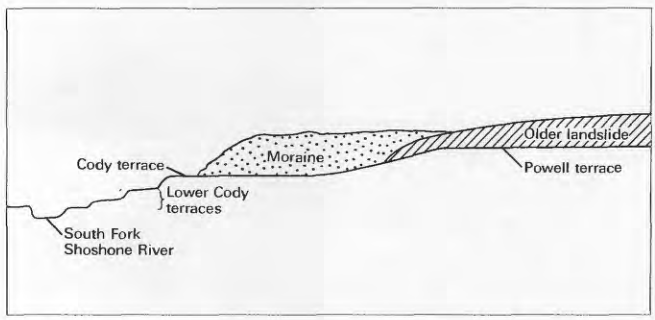

FIGURE 6.—Diagrammatic sketch showing depositional sequence, from older to younger, of Powell terrace, older landslide, Cody terrace, moraine, and lower Cody terraces.

all of the Cody gravel in the basin is genetically associated with the building of the moraine system and should be classified as glaciofluvial in origin." This difference of interpretation may be due primarily to a difference in the number of benches or levels that are included in the Cody terrace, and becomes of importance in determining the extent to which a glaciofluvial origin is applicable.

When Rouse (1934, p. 746 and fig. 5) concluded that the moraine was deposited on the Cody terrace, he was referring to the Cody terrace proper; the terrace 30 feet below it he considered a separate terrace, formed after the deposition of the moraine. This lower bench is uppermost of the "inner flight" of Mackin (1937) and uppermost of the "lower Cody terraces" of Pierce and Andrews (1941). Moss and Bonini (1961, p. 548), however, describe the Cody terrace as "not a single bench but rather a series of broad steps ranging from 120 to 190 feet above present river level." It thus appears from that statement and from their cross section (1961, fig. 2) that they include in their Cody terrace, the lower terraces as well. The principal question, therefore, is whether the particular moraine-terrace relationships which Moss and Bonini considered indicative of a glaciofluvial origin pertain to the highest terrace, here called the Cody terrace, or to the terrace 30 feet below the Cody terrace proper.

Additional evidence that the moraine rests on the gravel of the Cody terrace is provided by a spring line or line of seeps from 1 to 1¼ miles east of the Hardpan School. There, the moraine either adjoins or overlies the highest Cody terrace. The presence of a spring line, which begins a short distance below the contact between the moraine and the terrace, suggests that the Cody terrace gravel extends beneath the moraine.

From the data now available, Rouse's conclusion seems valid, namely, that the moraine rests on the Cody terrace and hence is younger, and the next lower terrace—which I include in the "lower Cody" group—was formed after deposition of the moraine. Although the difference in elevation between the Cody terrace proper and the first bench below it is only about 30 feet, differentiating them is desirable, for if Rouse's conclusion is correct, the time interval between their formation included the time of maximum glacial advance down the South Fork of the Shoshone River.

RELATION OF LANDSLIDE EVENTS TO CLIMATE

It seems reasonable to assume that the Carter Mountain landslides were caused by failure following an increase in the water content of the soil and underlying rock, brought about by increased precipitation. Periods of increased precipitation commonly are associated with glaciation, so a correlation between landslide events and glacial periods seems reasonable. This is not a new idea. Nearly 60 years ago, Howe (1909, p. 30–31) described Pleistocene landslides in the San Juan Mountains, Colo., in which the landslide material was emplaced "during or immediately after the first recognized stage of glaciation." Near Gardiner, Mont., which is about 90 miles northwest of the Carter Mountain area, Waldrop and Hyden (1963) have differentiated and mapped interglacial and postglacial earthflows. However, until the age of the moraine in the Carter Mountain landslide area is more accurately known, it is hazardous to attempt to correlate landslide events with specific glacial stages of Wisconsin time. When a more specific age for the moraine is established, some correlative speculation may be in order.

It has been shown that the older landslide was emplaced after the Powell terrace was formed and before the Cody terrace. A discussion of the possible causes of downcutting between the times that these two terraces were formed is beyond the scope of this paper, except to note that downcutting might have been associated with a climatic change involving greater precipitation. If so, the climatic change thus indicated would be in keeping with the moister climate needed for the older landsliding event.

REFERENCES

Alden, W. C., 1932, Physiography and glacial geology of eastern Montana and adjacent areas: U.S. Geol. Survey Prof. Paper 174, 133 p.

Hansen, W. R., 1961, Landslides along the Uinta fault east of Flaming Gorge, Utah: Art. 132 *in* U.S. Geol. Survey Prof. Paper 424–B, p. B306–B307.

Howe, Ernest, 1909, Landslides in the San Juan Mountains, Colorado, including a consideration of their causes and their classification: U.S. Geol. Survey Prof. Paper 67, 58 p.

Mackin, J. H., 1937, Erosional history of the Big Horn Basin, Wyoming: Geol. Soc. America Bull., v. 48, no. 6, p. 813–893.

Moss, J. H., and Bonini, W. E., 1961, Seismic evidence supporting a new interpretation of the Cody terrace near Cody, Wyoming: Geol. Soc. America Bull., v. 72, no. 4, p. 547–555.

Pierce, W. G., 1957, Heart Mountain and South Fork detachment thrusts of Wyoming: Am. Assoc. Petroleum Geologists Bull., v. 41, no. 4, p. 591–626.

———1966, Geologic map of the Cody quadrangle, Park County, Wyoming: U.S. Geol. Survey Geol. Quad. Map GQ–542, scale 1:62,500.

Pierce, W. G., and Andrews, D. A., 1941, Geology and oil and coal resources of the region south of Cody, Park County, Wyoming: U.S. Geol. Survey Bull. 921–B, p. 99–180.

Richmond, G. M., 1965, Glaciation of the Rocky Mountains, *in* Wright, H. E., Jr., and Frey, D. G., eds., The Quaternary of the United States—A review volume for the VII Congress of the International Association for Quaternary Research: Princeton, N.J., Princeton Univ. Press., p. 217–230.

Rouse, J. T., 1934, The physiography and glacial geology of the Valley region, Park County, Wyoming: Jour. Geology, v. 42, no. 7, p. 738–752.

Waldrop, H. A., and Hyden, H. J., 1963, Landslides near Gardiner, Montana: Art. 182 *in* U.S. Geol. Survey Prof. Paper 450–E, p. E11–E14.

POTASSIUM-ARGON AGES OF SOME IGNEOUS ROCKS IN NORTHERN STEVENS COUNTY, WASHINGTON

By ROBERT G. YATES and JOAN C. ENGELS,
Menlo Park, Calif.

Abstract.—Isotopic dating of igneous rocks from northern Stevens County, Wash., leads to the conclusion that there were two separate and distinct post-Jurassic igneous events—one about 100 m.y. ago in Cretaceous time, and the other about 50 m.y. ago in middle Eocene time. The rocks recording the Cretaceous event are plutonic; those recording the Eocene event are both plutonic and volcanic. The Cretaceous rocks are calc-alkaline and include the Spirit pluton and Kaniksu batholith. The Eocene rocks are alkaline and include satellitic dikes of the Coryell batholith as well as hypabyssal dikes and sills of shonkinite and lamprophyre.

Northeastern Washington, northern Idaho, and adjacent southeastern British Columbia constitute a province of igneous rocks of diverse ages, compositions, and modes of occurrence. The rocks range in age from late Precambrian to Miocene, in composition from dunite to alkali granite, and in mode of occurrence from lava flow to batholith.

Northern Stevens County, Wash., or, more specifically, the northern half of the Colville 30-minute quadrangle (fig. 1), lies in the heart of the province, and although not representative of the entire region, does record at least four major igneous events. The two earlier events in the Precambrian and Jurassic, which produced marine basaltic rocks, have not yet been isotopically dated and therefore are not discussed; the two later events, Cretaceous and Eocene, have been dated by the potassium-argon method, and the ages assigned to them are reported here.

Prior to the isotopic dating, the rocks now considered to be Cretaceous were believed to have been no older than Middle Jurassic and no younger than Miocene. Those determined to be Eocene include some rocks that were believed to have been possibly as old as Jurassic and others as young as Miocene.

GEOLOGIC SETTING

Figure 1 is an index map showing the general distribution of the post-Jurassic igneous rocks discussed in this report. The larger masses are shown as they would appear if the extensive glacial debris were removed. The smaller masses, mostly lamprophyre and genetically related felsic dikes and sills, are shown diagrammatically as dike swarms.

These intrusive and extrusive igneous rocks are intruded into, or deposited on, marine sedimentary and volcanic rocks ranging in age from late Precambrian to Middle Jurassic. Many different rock types are present. Included in one assemblage is quartzite, limestone, and dolomite; and in another, marine basaltic lavas, argillite, and graywacke. The structural relations between these assemblages are complex, being the product of intense late Mesozoic folding and faulting. At least two periods of folds can be distinguished—one a very strong deformation that produced northeast-trending folds, and the other a later much weaker deformation that produced east-west-trending folds and faults.

One of these east-west structures probably controlled the emplacement of the Spirit pluton, a postkinematic intrusion that dominates the southern half of the area (fig. 1). The Spirit pluton is surrounded by a metamorphic aureole in which the regional metamorphic background is raised from the chlorite-muscovite facies to high in the amphibolite facies.

The Eocene igneous rocks were extruded and emplaced during a period when tectonic movements were confined to block faulting and tilting. These movements had largely ceased by the Miocene.

ANALYTICAL PROCEDURES

Potassium determinations were made in duplicate on a Baird flame photometer using a lithium internal standard. Argon analyses were made using standard techniques of isotope dilution, and a 6′ 60° sector mass spectrometer. Constants used in the age calculation are as follows:

U.S. GEOL. SURVEY PROF. PAPER 600-D, PAGES D242-D247

K^{40} decay constants:

$\lambda\epsilon = 0.585 \times 10^{-10}$ yr^{-1}

$\lambda\beta = 4.72 \times 10^{-10}$ yr^{-1}

$K^{40}/K = 1.19 \times 10^{-2}$ atom present.

Errors ($\pm$ values) have been assigned on the basis of experience with duplicate analyses and uncertainties in the individual runs.

Analytical data are summarized in table 1.

IGNEOUS ROCK UNITS

The Cretaceous igneous rocks, a calc-alkaline suite, are represented by the Spirit pluton and the Kaniksu batholith. In contrast, the Tertiary igneous rocks are alkaline and include both intrusive and extrusive rocks. The intrusive Tertiary rocks include the Sheppard Granite and apophyses of the Coryell batholith, as well as hypabyssal dikes and sills of lamprophyre monzonite, and shonkinite. The extrusive rocks include tuffaceous sedimentary rocks, rhyodacite, and olivine-augite andesite.

Intrusive rocks

Spirit pluton.—The southern part of the area (fig. 1) is dominated by the Spirit pluton (Yates and Ford, 1960), a composite intrusion, that is predominantly granodiorite. It is elongate in an east-west direction discordantly across northeast-trending folds. The pluton is a magmatic differentiate that consists of two phases—a (1) central mass of porphyritic biotite granodiorite locally bordered by a (2) nonporphyritic granodiorite. Both phases contain inclusions and selvage remnants of quartz diorite and hornblende gabbro that represent the composition of the pluton in its early stage of emplacement. In addition, both phases are cut by dikes and by small elongate intrusions of genetically related medium-grained quartz monzonite and alaskite. Contacts between the pluton and the intruded argillites, dolomites, limestones, and greenstones are sharp. Within 100 feet of the contact, the intruded rocks of appropriate compositions are metamorphosed to sillimanite-, cordierite-, or wollastonite-bearing rocks; whereas as much as 3 miles from the contact, biotite- and andalusite-bearing rocks were formed.

Samples collected from the early quartz diorite phase and from the late quartz monzonite dike at the Smackout Pass locality in the eastern end of the pluton were dated by R. W. Kistler. Hornblende from the quartz diorite, sample 12H, gave an age of 94 ± 3.0 million years. Biotite and muscovite from the late dike, samples 13B and 13M, gave ages of 91 ± 3.0 and 96 ± 3.0 m.y., respectively. The Smackout Pass locality is more than 5 miles from the nearest known Tertiary dike—a lamprophyre just south of Deep Lake. It seems probable therefore that the rocks had been little influenced by the heat of the Eocene event. Nevertheless, it was thought desirable to check this assumption by measuring the age of biotite from the west end of the batholith near the Williams Lake area (see fig. 1), a center of strong Eocene intrusive and extrusive activity. Biotite (sample 11B) from nonporphyritic granodiorite was found to have an age of 100 ± 2.8 m.y. This biotite occurred as large (avg 2–4 mm) fresh crystals and was apparently unaffected by the Eocene activity. The biotite from the eastern end of the batholith, while concordant with the hornblende and muscovite, may have suffered a small amount of argon loss owing to later heating or weathering. The sample was lower in potassium content than is usual for fresh biotites, which may reflect some type of alteration, such as incipient chloritization. Biotite from the Kaniksu batholith,

TABLE 1.—*Analytical data on some igneous rocks in northern Stevens County, Wash.*

Sample number	Rock type	Mineral	K_2O (percent)	Radiogenic Ar^{40} (moles/gram)	Atmospheric Ar^{40} (percent)	Age (m.y.) $\pm 2\sigma$
2H	Hornblende andesite	Hornblende	1.02	7.68×10^{-11}	20.8	50.5 ± 1.5
6B	"Minette"	Biotite	8.04	6.00×10^{-10}	20.7	49.9 ± 1.5
7B	Shonkinite	do	6.30	4.69×10^{-10}	11.6	49.7 ± 1.5
1B	Biotite-andesite	do	8.76	6.61×10^{-10}	7.8	50.4 ± 1.5
4B	Coryell batholith, monzonite satellite dike	do	8.66	6.53×10^{-10}	10.4	50.4 ± 1.5
5H	Lamprophyre dike	Hornblende	1.50	1.17×10^{-10}	16.2	51.7 ± 1.5
10H	Rhyodacite flow	do	.639	4.77×10^{-11}	36.7	49.8 ± 1.5
3B	Coryell batholith, monzonite satellite dike	Biotite	8.60	6.53×10^{-10}	6.8	50.7 ± 1.5
8B	O'Brien Creek Formation, tuffaceous sandstone	do	6.78	4.22×10^{-10}	42.4	41.6 ± 1.2
8B	do	do	6.78	4.16×10^{-10}	51.6	41.1 ± 1.2
9B	do	do	5.92	3.56×10^{-10}	44.4	40.2 ± 1.3
12H[1]	Spirit pluton, quartz diorite	Hornblende	.944	1.34×10^{-10}	24.0	94.0 ± 3.0
13B [1]	Spirit pluton, quartz monzonite dike	Biotite	5.76	7.91×10^{-10}	8.0	91.0 ± 3.0
13M [1]	do	Muscovite	9.73	1.42×10^{-9}	8.0	96.0 ± 3.0
11B	Spirit pluton, nonprophyritic granodiorite	Biotite	9.14	1.39×10^{-9}	25.3	100.0 ± 2.8
14B	Kaniksu batholith, quartz monzonite	do	8.72	1.22×10^{-9}	7.1	92.2 ± 3.0
14M	Kaniksu batholith, pegmatite	Muscovite	10.6	1.60×10^{-9}	11.2	99.1 ± 3.2

[1] Samples dated by R. W. Kistler, U.S. Geological Survey.

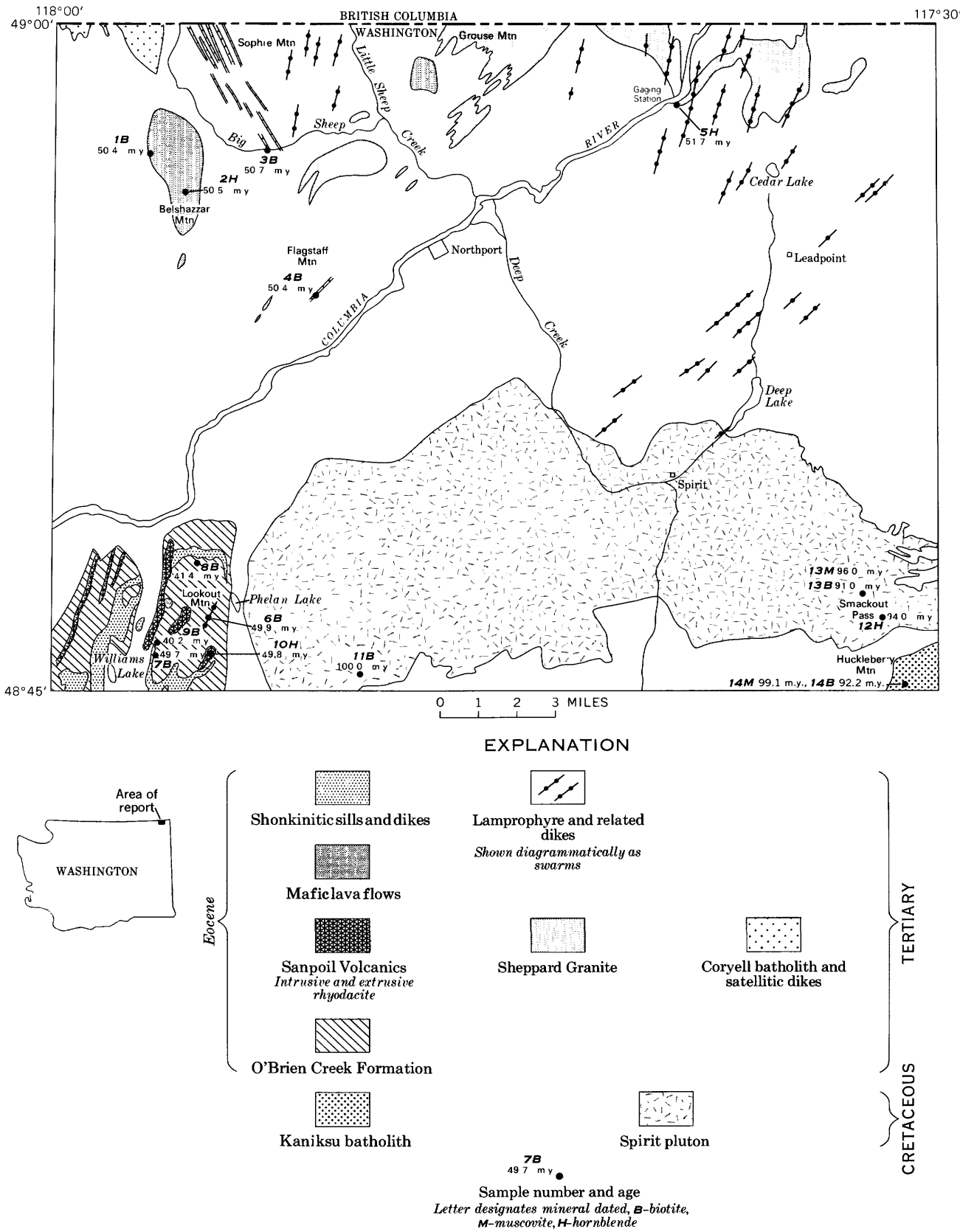

FIGURE 1.—Index map of the northern half of the Colville 30-minute quadrangle, Washington, showing generalized distribution of post-Jurassic igneous rocks.

which is described below, has an almost identical pattern.

Kaniksu batholith.—The Kaniksu batholith, roughly 2,500 square miles in area, covers much of the "panhandle" of Idaho and extends westward into Washington, occupying most of southern Pend Oreille County. Only a small portion of the batholith extends into the map area; it occupies approximately 1 square mile in the southeast corner, near Huckleberry Mountain. No intrusive contacts between the Spirit pluton and the Kaniksu batholith were found in the map area. To the east, in the adjoining Metaline quadrangle, Park and Cannon (1943, p. 24) recognized three facies in the batholith—a biotite quartz monzonite, a porphyritic quartz monzonite, and a muscovite quartz monzonite. Only the muscovite facies occurs in the map area; here it is a coarse-grained, foliated, two-mica quartz monzonite. In many places the quartz monzonite contains small irregular dikelets, or autointrusions, of muscovite-feldspar pegmatite. In thin section the quartz monzonite shows a strong gneissic fabric, strained quartz, and bent micas. The zoned plagioclase is accompanied by anhedral microcline, biotite and spatially associated muscovite, and small amounts of epidote and clinozoisite. The feldspars are altered, and the biotite is considerably chloritized. Biotite from the foliated quartz monzonite (sample 14B) and muscovite from the pegmatite (sample 14M) yielded ages of 92.2 ± 3.0 and 99.1 ± 3.2 m.y., respectively. The younger age of the biotite suggests partial argon loss, a pattern remarkably similar to that in the Spirit pluton. It is probable then that the Spirit pluton is indeed part of the Kaniksu batholith and that the time of emplacement was about 100 m.y. ago.

Coryell batholith.—The main mass of the Coryell batholith lies in British Columbia (Little, 1960, map 1090A). Little (1960, p. 90–93) describes the Coryell batholith as "dominantly of syenite, but with some granite, shonkinite, and apparently related monzonite." The predominance of potassium feldspar, the low quartz content, and the presence of augite and olivine in some phases, sets the Coryell suite apart from other batholiths in the province.

There have been two potassium-argon age determinations reported on biotites from Coryell syenites about 3 miles north of the international boundary in British Columbia. These ages are 54 and 58 m.y. (Baadsgaard and others, 1961, p. 697). Tongues of syenitic rocks extend into the northwest corner of the map area, but no material suitable for age determinations was collected. However, in this general area satellitic dikes are common, and one that crops out on the south bank of Big Sheep Creek was sampled (sample 3B). It is a porphyritic monzonite that has phenocrysts of orthoclase, plagioclase, and augite in a fine-grained matrix of feldspar, augite, and biotite. The age of the biotite was determined to be 50.7 ± 1.5 m.y. Biotite from another dike, similar both mineralogically and chemically (sample 4B), collected from the eastern slope of Flagstaff Mountain, had an age of 50.4 ± 1.5 m.y.

Sheppard Granite.—The Sheppard Granite occurs in the northern part of the map area as peneconcordant intrusions of medium-grained, albite-microcline leucogranite. The granite extends into British Columbia where it was first described by Daly (1912, p. 354–356). It cuts Late Cretaceous or early Tertiary rocks and is believed to be genetically related to the Coryell batholith (Little, 1960, p. 94–95). Lamprophyre and alkali rhyolite dikes cut the granite. Isotopic dating of this rock would be highly desirable as it plays an important part in the petrogenic history. However, the rock is not suitable for potassium-argon dating because a late magmatic alteration has destroyed the mafic minerals.

Eocene volcanic rocks

The Eocene event, in addition to producing the Coryell batholith, produced both volcanic rocks and hypabyssal intrusive rocks. Volcanic rocks are found in the following three areas: (1) on the southwest slope of Grouse Mountain, (2) on Belshazzar Mountain, and (3) in the Williams Lake area. The minerals in the volcanic rocks on Grouse Mountain are too badly altered for age determinations; for example, biotite is completely pseudomorphed by chlorite. The rocks on Belshazzar Mountain are largely flat-lying flows of olivine-augite andesite, but include at least one hornblende-bearing flow (sample 2H), as well as a biotite-bearing rock (sample 1B) at the base of the mountain just above the talus. This biotite andesite is believed to be a basal flow, but the possibility that it intrudes the volcanic pile cannot be eliminated. The hornblende had an age of 50.5 ± 1.5 m.y.; the biotite, 50.4 ± 1.5 m.y.

The Williams Lake area contains, in general, volcanic rocks that are quite unlike those of Grouse and Belshazzar Mountains. The predominant volcanic unit is an "arkosic sandstone," which is believed to be a crystal tuff that, in part, fell directly into a lake, but was mainly washed into the lake from neighboring highlands during and after the volcanic eruptions. The rock is composed largely of angular clasts of plagioclase and quartz, which are unquestionably of volcanic origin. In addition, it contains euhedral biotite crystals considered to be contemporaneous. This unit is correlative with the tuffs of the O'Brien Creek Formation (Muessig, 1967, p. 45–50) in the Republic quadrangle,

30 miles to the west. These rocks are assigned to the O'Brien Creek Formation.

Two samples of the biotite from the tuff were dated (samples 8B and 9B). The average age of 41.4±1.2 m.y. obtained for two runs of sample 8B is too young for the O'Brien Creek Formation, which is cut by a dike and a sill giving ages of 49.9±1.5 m.y. and 49.7±1.5 m.y. and is overlain by a flow giving an age of 49.8±1.5 m.y. (see fig. 1). In an attempt to resolve this anomaly the O'Brien Creek Formation was resampled 2 miles south of the 8B locality. This sample, 9B, yielded an age of 40.2±1.3 m.y., which agrees with the earlier measurement.

These anomalously young ages provide an interesting commentary on the potassium-argon dating of water-laid tuffs. These dates, combined with a relatively low potassium content and a high atmospheric argon content on duplicate runs, cast suspicion on the freshness of pyroclastic biotite. Even though the biotite appears unaltered, it has lost argon and apparently some of its potassium as well. It may have been converted during diagenesis into some form of biotite that was more susceptible to argon leakage than the dike and sill biotites. The porous character of the rock suggests that the biotite clasts may have been exposed to circulating ground waters since their burial, a condition which also could have aided this postulated argon leakage (Kulp and Engels, 1963).

In the Republic quadrangle, the O'Brien Creek Formation is overlain by the Sanpoil Volcanics (Muessig, 1967, p. 50–54; Pearson, 1967), which are rhyodacite flows; in the Williams Lake area, the O'Brien Creek Formation is overlain by rocks so similar to the Sanpoil Volcanics that the name is extended to this area. An intrusive phase of the Sanpoil occurs in both areas and is so like the extrusive phase that, in many places, it is difficult, if not impossible, to separate the two. The rock is a medium-gray porphyritic rhyodacite with phenocrysts of hornblende and plagioclase in a fine-grained groundmass. Chemical analysis confirms the rhyodacite classification. Hornblende from an extrusive phase was collected (sample 10H) and had an age of 49.8±1.5 m.y.

The youngest volcanic rock in the Williams Lake area, a biotite andesite, overlies a conglomerate that contains cobbles of Sanpoil rhyodacite. This rock was not dated but is similar to the biotite-augite andesite in the Belshazzar and Grouse Mountain areas.

Eocene hypabyssal intrusive rocks

The O'Brien Creek Formation is intruded by sills of leucocratic shonkinite—a rock closely related to the monzonite dikes of the Coryell batholith, only more mafic and having a lower ratio of sodium to potassium. Because contacts between the rhyodacite of the Sanpoil Volcanics and the shonkinite are not exposed, the relative age of the two rocks is in doubt. The mineral ages of 49.7±1.5 m.y. for biotite in the shonkinite (sample 7B) and 49.8±1.5 m.y. for hornblende in the rhyodacite (sample 10H) are identical within the limits of analytical error.

Lamprophyre dikes containing phenocrystic biotite, monoclinic pyroxene, olivine, or hornblende are common. They occur in the dike swarms shown diagrammatically in figure 1. The dikes cut the Spirit pluton, the Sheppard Granite, and the rocks of the O'Brien Creek Formation. Mineralogically and chemically they are consanguineous with the Coryell batholith and the leucoshonkinite of the Williams Lake area.

The lamprophyres were sampled for radiometric dating. One age was measured on large phenocrysts of kaersutite, a titanium-rich hornblende, collected from a large dike (sample 5H) near the gaging station on the Columbia River, 2 miles south of the international boundary. The other age was measured from biotite collected from a "minette" (sample 6B) about 1 mile southwest of Phelan Lake. The age of the hornblende was determined to be 51.7±1.5 m.y. and that of the biotite 49.9±1.5 m.y.

SUMMARY AND CONCLUSIONS

Potassium-argon dating of the post-Jurassic igneous rocks in northern Stevens County, Wash., establishes the age of the two latest igneous events as Late Cretaceous and middle Eocene. The Spirit pluton and the much larger Kaniksu batholith appear to be contemporaneous and emplaced approximately 100 m.y. ago. The more recent event, about 50 m.y. ago, resulted in the accumulation of large volumes of volcanic rock in a relatively short period of time. If the dated flows and dikes are correctly correlated with the Coryell batholith to the north in British Columbia, there must have been penecontemporaneous plutonism and volcanism. It was found that the age of biotite from the water-laid tuffs was not representative of the age of the tuff and that such samples should be used with caution and interpreted with care.

REFERENCES

Baadsgaard, Halfdan, Folinsbee, R. E., and Lipson, J. I., 1961, Potassium-argon dates of biotites from Cordilleran granites: Geol. Soc. America Bull., v. 72, no. 5, p. 689–701.

Daly, R. A., 1912, Geology of the North American Cordillera at the forty-ninth parallel: Canada Geol. Survey Mem. 38, pts. 1–3, 857 p.

Kulp, J. L., and Engels, Joan, 1963, Discordances in K-Ar and Rb-Sr isotopic ages, *in* Symposium on radioactive dating, Athens, 1962, Proceedings: Vienna, Internat. Atomic Energy Agency, p. 219–238.

Little, H. W., 1960, Nelson map-area, west half, British Columbia: Canada Geol. Survey Mem. 308, 205 p.

Muessig, Siegfried, 1967, Geology of the Republic quadrangle and a part of the Aeneas quadrangle, Ferry County, Washington: U.S. Geol. Survey Bull. 1216, 135 p.

Park, C. F., Jr., and Cannon, R. S., Jr., 1943, Geology and ore deposits of the Metaline quadrangle, Washington: U.S. Geol. Survey Prof. Paper 202, 81 p.

Pearson, R. C., 1967, Geologic map of the Bodie Mountain quadrangle, Ferry and Okanogan Counties, Washington: U.S. Geol. Survey Geol. Quad. Map GQ–636, scale 1:62,500, 4 p. text.

Yates, R. G., and Ford, A. E., 1960, Preliminary geologic map of the Deep Lake quadrangle, Stevens and Pend Oreille Counties, Washington: U.S. Geol. Survey Mineral Inv. Field Studies Map MF–237, scale 1:24,000.

MAGNETIZATION OF THE LOWERMOST KEWEENAWAN LAVA FLOWS IN THE LAKE SUPERIOR AREA

By KENNETH G. BOOKS, Silver Spring, Md.

Abstract.—The average direction of remanent magnetization for the lowermost Keweenawan lava flows in the Lake Superior region is significantly different in direction and opposite in polarity from that of the middle Keweenawan Portage Lake Lava Series and the upper Keweenawan Copper Harbor Conglomerate. This same general direction and apparent reversal in the earth's geomagnetic fields is present in other geologic units of Precambrian age around the periphery of Lake Superior, suggesting a similar time interval for all, and providing a datum that can be utilized in further paleomagnetic studies in the region.

Directions of remanent magnetization recently have been applied to problems of geologic structure and correlation for Keweenawan rocks (Precambrian) in the Lake Superior region by DuBois (1962) and by Books, White, and Beck (1966). The pioneering paleomagnetic geochronology developed by DuBois for Keweenawan units provides a background for the present study, which is part of a broader program of geophysical investigation in the region. The lowermost Keweenawan lava flows on opposite sides of the Lake Superior basin have a similar direction of remanent magnetization, and this direction differs significantly from that of succeeding middle Keweenawan lava flows. The new paleomagnetic data presented here thus provide a useful tool for stratigraphic correlation in the region.

GEOLOGIC SETTING

The general sequence and structure of Keweenawan stratified rocks in the Lake Superior region have been known for many years, due largely to the detailed studies carried out in the search for copper and iron deposits. Figure 1 is a generalized geologic map of the western Lake Superior region, showing the major features of the Keweenawan strata and adjoining rocks. The map is chiefly a generalization of the geologic map of the Lake Superior region by Leith, Lund, and Leith (1935, pl. 1) with modifications in the area east of Mellen and south of the Keweenaw fault(?) taken from a more recent map by White (1966, fig. 1). White (1966, fig. 1) suggested that a sedimentary rock unit separates the two belts of Keweenawan lava flows.

Three areas have furnished samples for this investigation. They include the middle Keweenawan Portage Lake Lava Series near Kearsarge, Mich. (collection area 1, fig. 1), and two sample-collection areas in the lowermost Keweenawan lava flows on opposite sides of Lake Superior. On the south side of the lake these lowermost flows are exposed in the so-called South Trap Range, near Ironwood, Mich. (collection area 2, fig. 1), where they dip steeply (70°–85°) toward the lake. They directly overlie pre-Keweenawan rocks and are separated from the main sequence of middle Keweenawan lava flows to the north by a drift-covered area 2 miles wide. Lava flows in this area strike approximately N. 80° E. On the northwest side of the lake, near Grand Portage, Minn. (collection area 3, fig. 1), the lowermost Keweenawan lava flows dip gently (10°–15° SW.) toward the lake. The strike of the flows in this area ranges from N. 54° W. to N. 76° W.

FIELD AND LABORATORY METHODS

A total of 145 drill-core samples were collected from the Kearsarge area, Michigan, 70 drill-core samples from the so-called South Trap Range in the Ironwood area, Michigan, and 55 drill-core samples from the Grand Portage area, Minnesota. The cores were drilled in bedrock by using a water-cooled diamond-impregnated bit powered by a modified chain-saw motor. Local declination anomalies made it necessary to use a sun compass for orientation.

Remanent magnetic moments were measured on a motor-driven "spinner" magnetometer (Doell and Cox, 1965). To eliminate the effects of unstable magnetic moments, all samples were magnetically "washed" in alternating fields in steps as high as 200 oersteds. No marked effect was observed.

U.S. GEOL. SURVEY PROF. PAPER 600-D, PAGES D248–D254

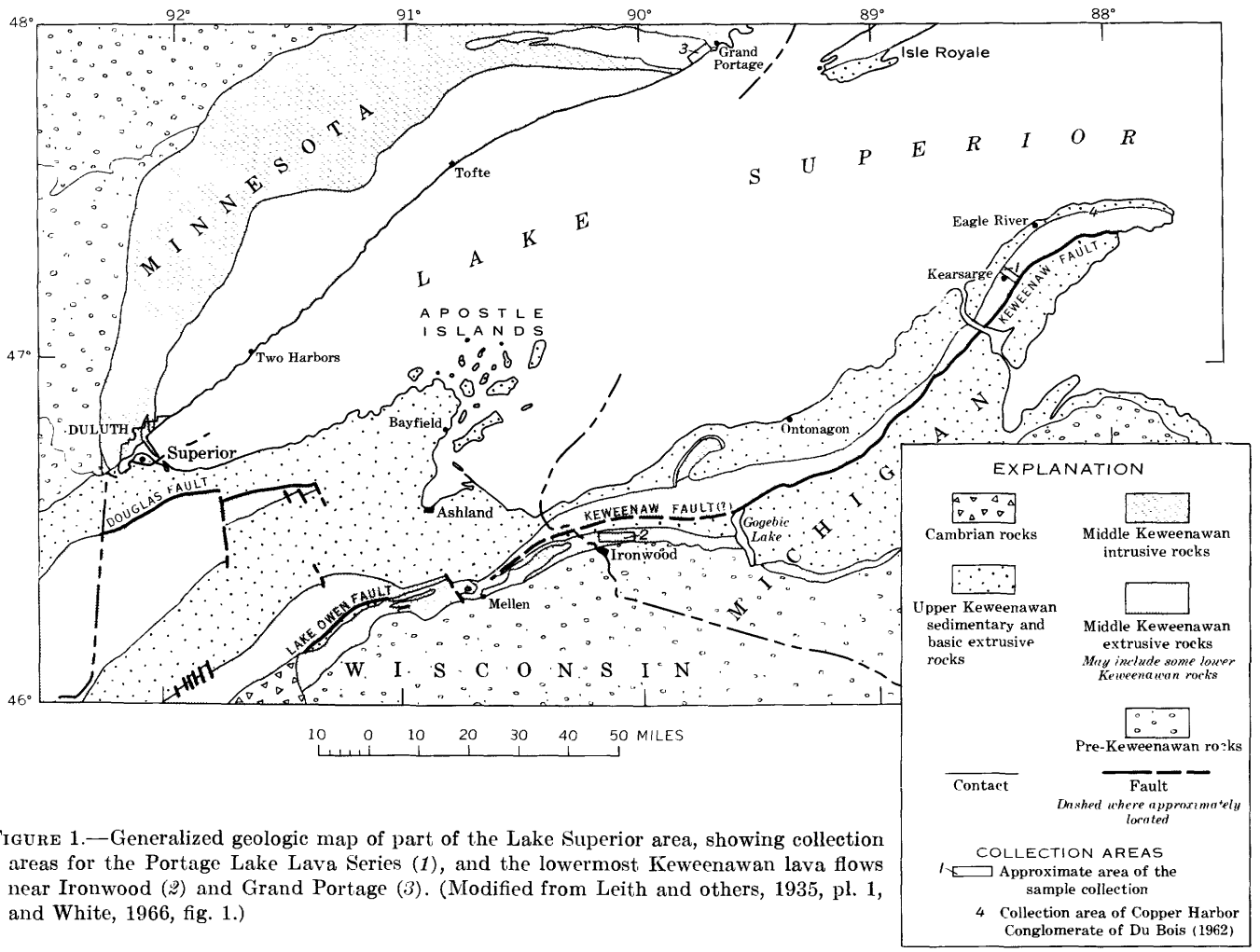

FIGURE 1.—Generalized geologic map of part of the Lake Superior area, showing collection areas for the Portage Lake Lava Series (*1*), and the lowermost Keweenawan lava flows near Ironwood (*2*) and Grand Portage (*3*). (Modified from Leith and others, 1935, pl. 1, and White, 1966, fig. 1.)

Data are presented in terms of declination, D, measured in degrees east of geographic north, and inclination, I, plotted in the lower hemisphere of an equal-area net to permit direct comparison of directions. Conventional statistical analyses (Fisher, 1953) at the 95-percent level of confidence were applied to the directions derived from the laboratory procedures. Mean directions were compiled for individual sampling sites, as well as a mean of site means (D' and I') for both the Portage Lake lavas and the lowermost Keweenawan lava flows at Ironwood, Mich., and Grand Portage, Minn. These, together with pertinent statistical data, are presented in table 1. All have been recomputed to an equivalent direction, lat. 45° N., long. 90° W., in conformity with the practice established in the area by DuBois (1962) to permit direction comparison of directions of magnetization from sampling sites located some distance from each other. Means for the recomputed data, with circles of 95-percent confidence, are shown in figure 3. The new data are corrected for the estimated geologic dip at each sample site; the corrections fall within the following ranges: Kearsarge, 35°–49° NW.; lava flows near Ironwood, 70°–85° NW.; and lava flows near Grand Portage, 10°–15° SW.

DISCUSSION OF RESULTS

It is important in paleomagnetic studies to demonstrate that the paleomagnetic field direction measured for the rocks is an original magnetization and represents the direction of the earth's field at the time the rocks were deposited. DuBois (1962, p. 26) has demonstrated the stability of magnetization for a large number of flows in the Portage Lake Lava Series, and the present results agree.

The lowermost Keweenawan lava flows near Iron-

TABLE 1.—*Summary of paleomagnetic data for lowermost Keweenawan lava flows*

Site No.	Location of collecting site		Mean direction of magnetization at collecting site		Type polarity (R, reversed; N, normal)	Radius of confidence circle α_{95}	Precision parameter (K)	No. of samples (N)	Mean direction at lat 45° N., long 90° W.	
	North lat (degrees)	West long (degrees)	Azimuth, D (degrees)	Inclination, I (degrees)					Azimuth, D' (degrees)	Inclination, I' (degrees)
Ironwood area, Michigan										
K01	46.5	90.0	277.0	77.5	R	14.0	43.8	4	278.0	77.0
K02	46.5	90.0	238.0	79.0	R	20.4	37.6	3	239.0	79.0
K06	46.5	90.0	237.0	64.0	R	8.4	84.1	5	238.5	64.5
K07	46.5	90.0	235.0	74.5	R	14.4	29.2	5	236.5	75.0
K98	46.5	90.1	253.0	80.0	R	8.2	88.4	5	254.5	80.0
K09	46.5	90.1	252.0	67.5	R	12.5	38.3	5	253.5	68.0
K12	46.5	90.1	270.5	71.5	R	23.7	16.0	4	272.0	71.5
K13	46.5	90.1	264.0	54.0	R	11.4	46.0	5	265.5	55.5
K20	46.5	90.1	249.9	63.5	R	12.1	58.9	4	250.5	64.0
K21	46.5	90.1	303.0	69.0	R	6.3	150.4	5	304.0	68.5
K86	46.5	90.1	214.0	75.5	R	5.5	281.0	4	215.0	76.0
K87	46.5	90.1	229.0	65.5	R	20.8	20.4	4	230.5	66.0
K46	46.5	90.2	249.5	75.5	R	19.3	23.7	4	251.0	75.5
K48	46.5	90.2	259.0	64.5	R	15.7	35.4	4	260.5	65.0
Grand Portage area, Minnesota										
K30	47.9	89.7	293.6	63.3	R	12.5	55.2	4	296.6	62.5
K31	47.9	89.7	296.6	62.8	R	4.6	393.1	4	299.7	62.0
K33	47.9	89.7	285.5	55.6	R	11.9	42.4	5	288.6	55.1
K34	47.9	89.7	296.5	55.3	R	14.0	44.0	4	299.7	54.2
K35	47.9	89.7	308.1	66.7	R	4.3	323.5	5	312.1	65.4
K36	47.9	89.7	297.9	54.6	R	8.3	85.2	5	301.0	53.6
K37	47.9	89.7	294.7	64.3	R	3.3	542.8	5	298.2	63.6
K38	47.9	89.7	276.6	49.9	R	13.7	32.3	5	279.6	49.9
K39	47.9	89.7	307.1	64.9	R	5.0	235.8	5	309.8	63.8
K40	47.9	89.7	304.4	59.2	R	5.6	188.6	5	307.2	58.0
K42	47.9	89.7	256.2	71.9	R	4.8	255.0	5	259.2	72.5
Mean of site means for Ironwood data (C) [1]					R	4.8	71.1	14	254.0	71.5
Mean of site means for Grand Portage data (E) [1]					R	4.0	129.4	11	297.0	59.2
Mean of site means for Portage Lake lavas (A) [1]					N	2.6	105.8	29	289.3	35.3

[1] Refers to localities shown on figure 1.

wood are lithologically distinct (R. G. Schmidt and H. A. Hubbard, oral commun. 1967) and are geographically separated from the main belt of the Portage Lake Lava Series; they may represent a separate, older group of flows. Hubbard (1967) believes that the oldest flows of the lowermost rocks in the "South Trap Range" might better be considered lower Keweenawan. Because they are probably of different age than the Portage Lake lavas, stability of magnetization should be demonstrated for them as well. Some evidence for magnetic stability is indicated by the consistency of site mean directions of magnetization (fig. 2) within the two areas (Ironwood and Grand Portage) and their divergence from the direction of the earth's present magnetic field. Another method of testing the magnetic stability for the lowermost Keweenawan flows is to determine whether the directions of magnetization are more or less scattered after correction for geologic dip (fig. 2*B*). If the rocks are magnetically stable, the dispersion before correction for dip should be greater than dispersion after correction. The precision factor at Ironwood before and after correction for dip is 45.9 and 64.7, respectively, and at Grand Portage 106.9 and 125.0, respectively. Both suggest magnetic stability, but because the dip and strike of the lava flows for all sites in each area are fairly uniform the reduction in dispersion is not expected to be great. Magnetic stability is also suggested by the fact that a correction for geologic dip brings the site mean directions for Ironwood and Grand Portage close together.

Portage Lake Lava Series

The direction of magnetization shown at A in figure 3 is the mean of 29 site mean directions computed from 145 samples, collected across the strike of the Portage Lake Lava Series in the vicinity of Kearsarge, Mich. The suite of samples represents 29 lava flows from all parts of the stratigraphic section in this area; the direction of magnetization agrees with that from other middle Keweenawan flows on the south side of Lake Superior as well as that from middle Keweenawan flows (K. G. Books, unpub. data) on the Minnesota shore of Lake Superior and Isle Royale. In addition (fig. 3), the direction of magnetization is not significantly different from that of the upper Keweenawan Copper

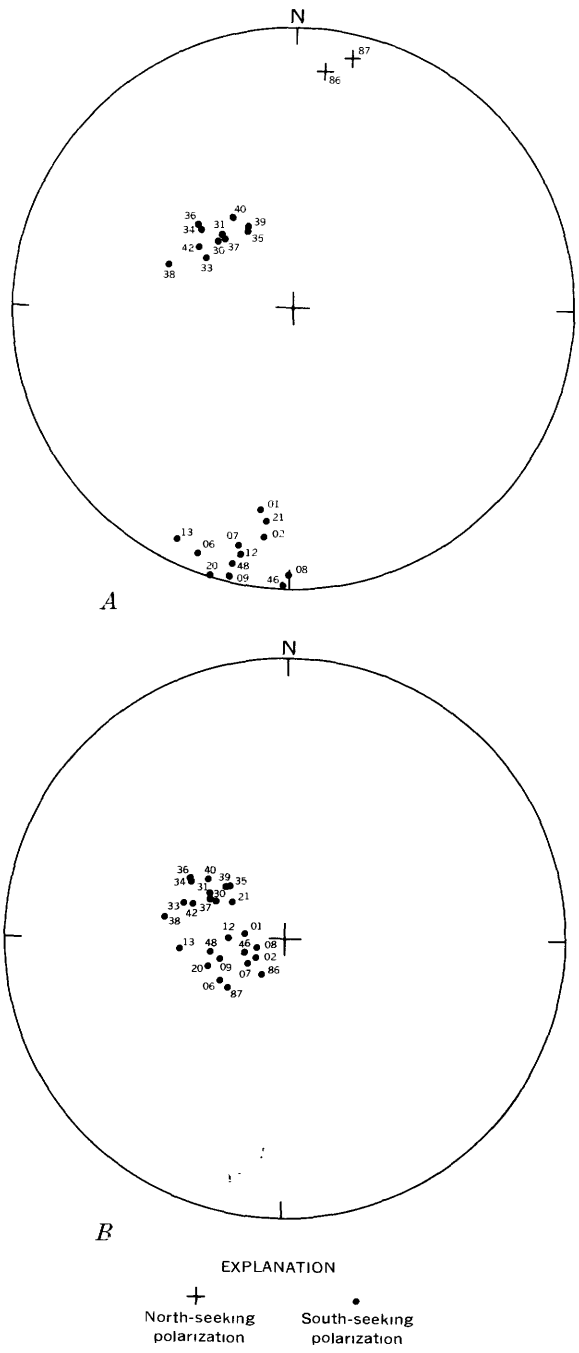

FIGURE 2.—Site mean directions of magnetization for the lower sequence of Keweenawan lava flows before (*A*), and after (*B*), correction for geologic dip. Numbers correspond to site numbers given in table 1. Equal-area projection, lower hemisphere.

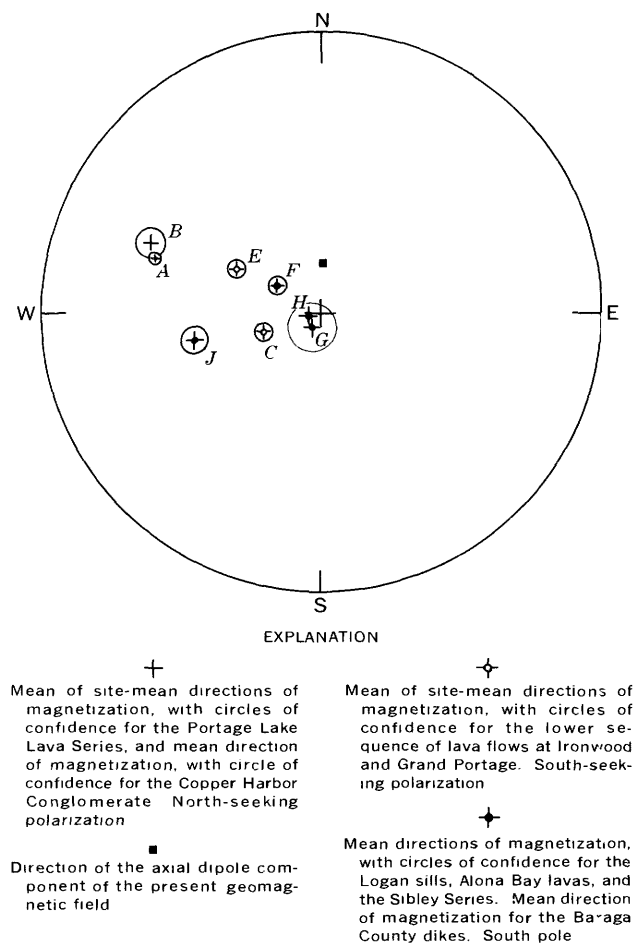

FIGURE 3.—Mean directions of magnetization for Keweenawan rocks, Lake Superior region. Geologic units are: *A*, Portage Lake Lava Series; *B*, Copper Harbor Conglomerate; *C*, lower sequence of Keweenawan lava flows at Ironwood, Mich.; *E*, lower sequence of Keweenawan lava flows at Grand Portage, Minn.; *F*, Logan sills of Lawson (1893); *G*, lavas at Alona Bay; *H*, mafic dikes in Baraga County; and *J*, the Sibley Series of Tanton (1927). The data from the Portage Lake and the lower sequence of lava flows are new; other data are from DuBois (1962, table 18). Directions are recalculated to values that the equivalent dipole would produce at lat 45° N.; long 90° W. Equal-area projection, lower hemisphere.

Harbor Conglomerate as given by DuBois (1962, table 18), indicating a uniform magnetic field direction for this part of Keweenawan time (during deposition of the Portage Lake lavas and extending through deposition of the Copper Harbor Conglomerate). The Portage Lake lava paleomagnetic results of Books (unpub. data) are presented here rather than the results of DuBois (1962, table 18) because they represent a more complete sampling of the lava flows. The two directions are just significantly different.

Lowermost Keweenawan lava flows

The average direction of remanent magnetization for the lowermost Keweenawan lava flows in the Ironwood area (fig. 3, point *C*) and in the Grand Portage area (fig. 3, point *E*) is significantly different in direction and opposite in polarity from the middle Keweenawan direction represented by the Portage Lake Lava Series at Kearsarge (fig. 3, point *A*), and the upper Keweenawan field direction represented by the Copper Harbor Conglomerate (fig. 3, point *B*).

In the Ironwood area, the direction of magnetization shown in figure 3 (point C) is the mean of 14 site-mean directions for 14 lava flows. A total of 70 samples were collected at intervals across the steeply dipping flows, beginning about 1,300 feet above the lowermost flows exposed in the area, and continuing to the top of the "South Trap Range" section. The samples represent about 6,700 feet of the estimated 8,000-foot section of lava flows in the "South Trap Range." Samples were also collected from the basal lava flows just above the Animikie Series at three sites in this area; data from these samples are not shown in the figures or table. The low precision of the results for these samples, even after "washing" in alternating magnetic fields, precluded their use in this paper. Their polarity, however, is worthy of note. The estimated direction is $I=36°$, $D=258°$, which is a normal polarization, and indicates a change in the character of the magnetic field between the time of extrusion of the basal flows and those higher in the "South Trap Range" section.

In the Grand Portage area, the direction of magnetization shown in figure 3 (point E) is the mean of 11 site mean directions. A total of 55 samples were collected across the more gently dipping lava flows along the north shore of Lake Superior. Sample collections from 11 flows represent about 4,550 feet of strata and extend from flow 3 of Grout, Sharp, and Schwartz (1959, p. 37 and pl. 4) near the base of the lava flows in sec. 17, T. 62 N., R. 4 E., to flow 19 in sec. 26, T. 26 N., R. 4 E. The collection-site location of flow 19 is approximately 2,000 feet northwest of a large diabase instrusion (Grout and others 1959, pl. 4) which is exposed for a distance of about 4⅓ miles along the lakeshore, separating the Keweenawan lava flows into two groups. Beyond the diabase intrusion to the southwest, and as far as Tofte, Minn., the lava flows above the diabase have a direction of magnetization (Books, unpub. data) similar to that of the middle Keweenawan Portage Lake lavas.

Although it is evident that the site mean directions (fig. 2B) representing the lowermost flows from both Ironwood and Grand Portage have the same polarity, it is a matter for concern that the mean of the two distributions (fig. 3, points C and E) are significantly different even after corrections for geologic dip. Assuming that the rocks collected became magnetized over a sufficient interval of time to average out secular variations, there are several possible factors that may contribute to this difference. The contributing factors fall into two broad categories, presented as follows:

(A) The difference in direction between points C and E (fig. 3) represents an initial difference, dating from the time the lavas cooled. This would mean that the lava flows at Ironwood and at Grand Portage were extruded at different times between which the direction of the geomagnetic field had changed significantly. This explanation is not attractive from a geologic point of view because it complicates an otherwise simple stratigraphy, but it is the only probable explanation if those that follow prove inadequate.

(B) The difference in direction between points C and E (fig. 3) does not represent an initial difference, and the rocks originally had the same virtual geomagnetic pole.

Two possibilities follow:

(1) The present difference is not real, but is due to an inadequate correction for structural rotations since the rocks were extruded.

(a) It is possible that the geologic dips estimated for the lava flows in one or both areas may be too small. Dips of lava flows are not easily measured in the field; it is conceivable that some dips in the Ironwood area may have been underestimated by 15°–20° and some dips in the Grand Portage area by 5°–10°, but many errors of this magnitude would affect the regional dip and be difficult to explain. The mean directions at C and E (fig. 3) are approximately 22° apart, and added corrections would bring C and E closer together.

(b) It is possible that field measurements of dip are correct on a regional scale where the measurements are made on prominent hills at some distance from the outcrop, but numerous small step faults make the dip on a regional scale gentler than the actual dip of the rocks within individual fault blocks. This phenomenon may effect a few measurements, but is probably inadequate to fully explain the consistent difference in magnetic directions between the two areas.

(c) It is possible that there has been structural movement around vertical axes in the two areas, resulting in declination changes in magnetic field directions. Both the Ironwood and Grand Portage collection locations are in areas of post-extrusion structural movement where such rotations are possible. Because this component of structural movement is not diminished by geologic-dip corrections, it would remain in the data and be reflected in the declination of observed field directions. If there have been significant rotations around a vertical axis, the geologic map suggests that these have been clockwise in both areas. A correction for such rotation would move points C and E (fig. 3) in the same

direction (counterclockwise) with the probability of an even greater difference than at present because of the greater deformation at Ironwood.

(2) It is possible that the present difference in magnetic directions in the two areas is real, but that the stable magnetic direction of one or both groups was imposed at some time following cooling of the lavas, when their attitude was no longer horizontal. The lavas at Ironwood have a number of secondary minerals, such as chlorite, that may represent products of low-grade metamorphism; thus the magnetic direction in the rocks may conceivably be a chemical remanent magnetization (Irving, 1964, p. 28–29) acquired during this low-grade metamorphism. Such an explanation would be attractive if the correction for geologic dip were too large to make points *C'* and *E* coincide, because the metamorphism presumably would have occurred after some of the tilting had already taken place. The correction for geologic dip is too small, however, so that imposition of a later chemical remanent magnetization does not explain the difference.

In summary, it is possible that two or more factors contribute to divergence of paleomagnetic field directions in the rocks at Ironwood (fig. 3, point *C'*) and Grand Portage (fig. 3, point *E*). If the divergence does not represent an initial difference, the most likely contributor is underestimation of geologic dip due to structural rotation. If the divergence represents an initial difference, the lava flows in the two areas must have been extruded at different times.

In view of the above uncertainties, the field directions shown at *C'* and *E* in figure 3 cannot be considered precise, but are the best available estimation of geomagnetic field directions during extrusion of the lava flows in the two areas. The most significant result of the present work is discovery of the near reversal (135°–155° rather than 180°) between the magnetic fields in the lowermost Keweenawan lava flows and those that are typical of the middle Keweenawan lava flows. This distinctive polarity in the lowermost lava flows at Ironwood and Grand Portage suggests a common general time interval for both and provides a useful paleomagnetic datum.

COMPARISON WITH PREVIOUS INVESTIGATIONS

Figure 3 shows the paleomagnetic field directions for the lowermost Keweenawan lava flows near Ironwood (*C'*), the lowermost flows near Grand Portage (*E*), the Logan sills of Lawson (1893) (*F*), lavas at Alona Bay (*G*), mafic dikes in Baraga County (*H*), and the Sibley Series of Tanton (1927) (*J*). All characteristically exhibit the same reversed polarity and the same general direction of magnetization. The extrusive rocks and the Sibley Series are all in the lowermost part of the Keweenawan sequence. The Sibley Series is lower Keweenawan according to the generally accepted classification of the Keweenawan rocks (Leith and others, 1935). The Logan sills and Baraga County dikes intrude the pre-Keweenawan basement. As DuBois (1962, p. 60–63 and table 19) has indicated, the similar magnetic field direction for certain units noted above (*F*, *G*, *H*, *J*) suggests a similarity in their age. Since one member of the group, the Sibley Series, is lower Keweenawan, he suggests that all should be so classified.

The present investigation shows that the rocks of the so-called South Trap Range near Ironwood, Mich., and the lowermost part of the Keweenawan lava flows near Grand Portage, Minn., have a magnetic direction and polarity similar to that of rocks of early Keweenawan age, and unlike that in the Portage Lake Lava Series of middle Keweenawan age. In view of the consistency of remanence data for localities on all sides of Lake Superior (fig. 4), it may well be that the surface separating the rocks with reversed polarity from those with normal polarity would make the best possible datum for

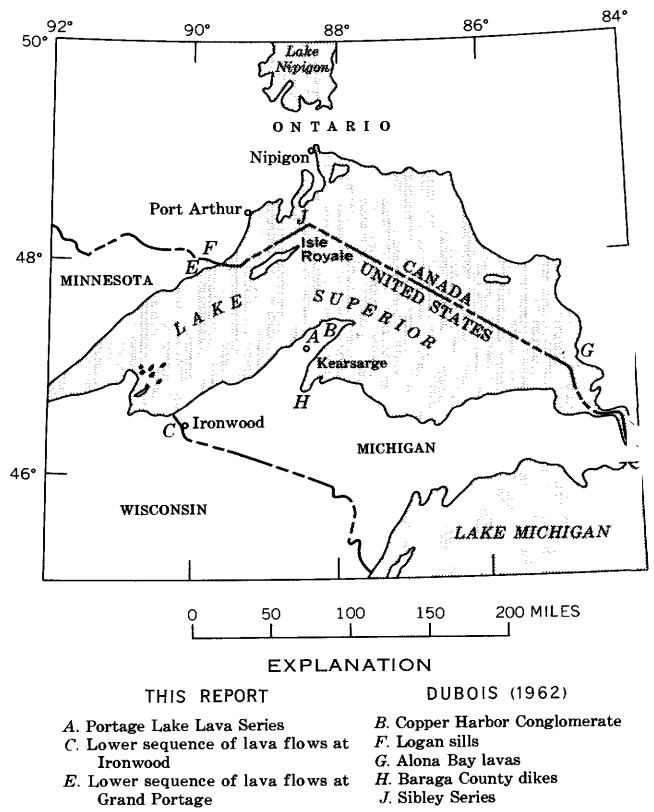

FIGURE 4.—Index map showing collection localities for this report and for DuBois (1962).

the arbitrary separation of lower and middle Keweenawan rocks throughout the Lake Superior region.

REFERENCES

Books, K. G., White, W. S., and Beck, M. E., Jr., 1966, Magnetization of Keweenawan gabbro in northern Wisconsin and its relation to time of intrusion, *in* Geological Survey Research 1966: U.S. Geol. Survey Prof. Paper 550–D, p. D117–D124.

Doell, R. R., and Cox, Allan, 1965, Measurement of the remanent magnetization of igneous rocks: U.S. Geol. Survey Bull. 1203–A, 32 p.

DuBois, P. M., 1962, Paleomagnetism and correlation of Keweenawan rocks: Canada Geol. Survey Bull. 71, 75 p.

Fisher, R. A., 1953, Dispersion on a sphere: Royal Soc. London Proc., ser. A, v. 217, p. 295–305.

Grout, F. F., Sharp, R. P., and Schwartz, G. M., 1959, Geology of Cook County, Minnesota: Minnesota Geol. Survey Bull. 39, 163 p.

Hubbard, H. A., 1967, Keweenawan volcanic rocks near Ironwood, Michigan [abs.]: East Lansing, Mich., Inst. Lake Superior Geology, 13th, 1967, p. 20–21.

Irving, E., 1964, Paleomagnetism and its application to geological and geophysical problems: New York, John Wiley and Sons, Inc., 399 p.

Lawson, A. C., 1893, The laccolithic sills of the northwest coast of Lake Superior: Minnesota Geol. and Nat. History Survey Bull. 8, p. 24–48.

Leith, C. K., Lund, R. J., and Leith, Andrew, 1935, Precambrian rocks of the Lake Superior Region: U.S. Geol. Survey Prof. Paper 184, 34 p.

Tanton, T. L., 1927, Stratigraphy of the northern subprovince of the Lake Superior region [abs.]: Geol. Soc. America Bull., v. 38, p. 114–115.

White, W. S., 1966, Tectonics of the Keweenawan basin, western Lake Superior region: U.S. Geol. Survey Prof. Paper 524–E, 23 p.

SEISMIC-REFRACTION PROFILES ACROSS SIX CANYONS IN THE WASATCH RANGE NEAR SALT LAKE CITY, UTAH

By ROBERT E. MATTICK, Denver, Colo.

Work done in cooperation with the Utah State Engineer

Abstract.—Thickness of fill in six narrow canyons east of Salt Lake City, Utah, was determined by seismic-refraction profiling. The reciprocal method of shallow seismic-refraction interpretation proved a simple and reliable technique for depth computations where conventional seismic interpretation techniques were not applicable. A maximum fill thickness of about 250 feet and a minimum of about 5 feet were determined in Little Cottonwood and Big Cottonwood Canyons, respectively.

Investigation of the water resources of Salt Lake County, Utah, by the U.S. Geological Survey in cooperation with the Utah State Engineer involved the determination of the amount of ground water that is discharged through the unconsolidated fill material in several narrow canyons of the Wasatch Range east of Salt Lake City. To determine the thickness of the fill, seismic-refraction profiles were made across six canyons during the summer of 1965. The locations of these profiles are shown in figure 1. The steeply sloping ground surface in these narrow canyons, together with a small thickness of fill material, provides an unusual shallow seismic-refraction problem.

Figure 2 (City Creek Canyon) shows a typical seismic-refraction time-distance plot together with the computed cross section. This canyon is about 200 feet wide, and the ground surface is steeply sloping with sharp changes in slope. The unconsolidated fill material consists of boulders and stream debris. Bedrock is exposed on the northwest canyon slope and in the stream at the base of the steep southeast canyon wall.

In shooting the profile, 11 vertical seismometers were spaced between the bedrock outcrops and 1-pound dynamite charges were exploded in the stream and on the rock outcrop at the northwest end of the profile. The placement of charges directly on bedrock reasonably assures that the recorded seismic waves are refracted along the high-velocity interface and elimi-

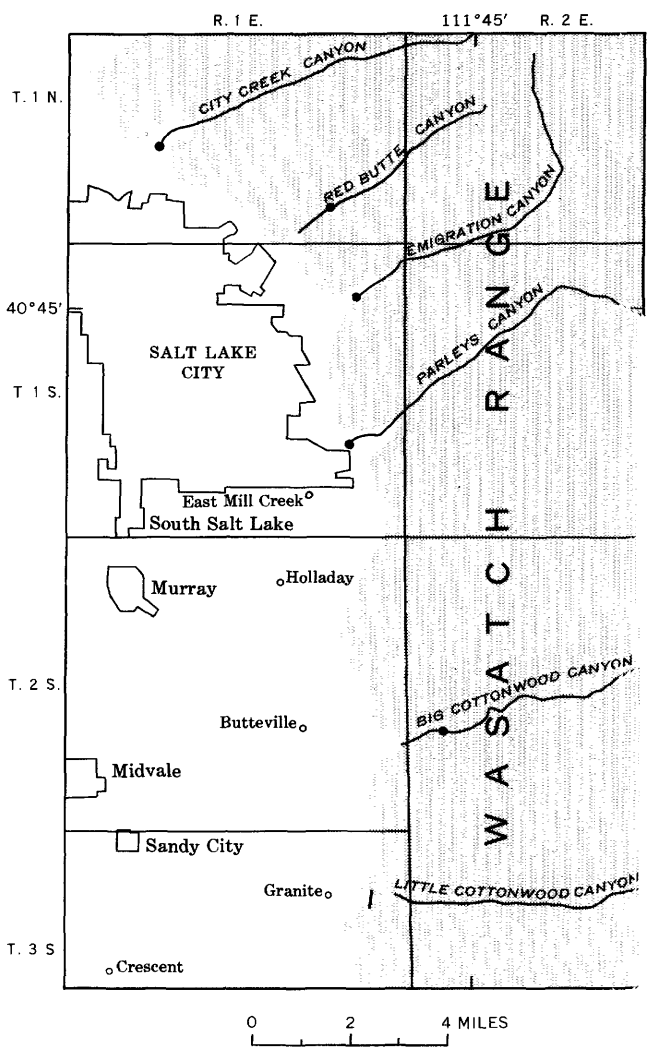

FIGURE 1.—Index map showing locations of the seismic profiles. Solid circles show the locations of seismic profiles in the five northern canyons, and a solid line shows the location of a seismic profile near the mouth of Little Cottonwood Canyon.

U.S. GEOL. SURVEY PROF. PAPER 600-D, PAGES D255-D257

313-005 O—68——18

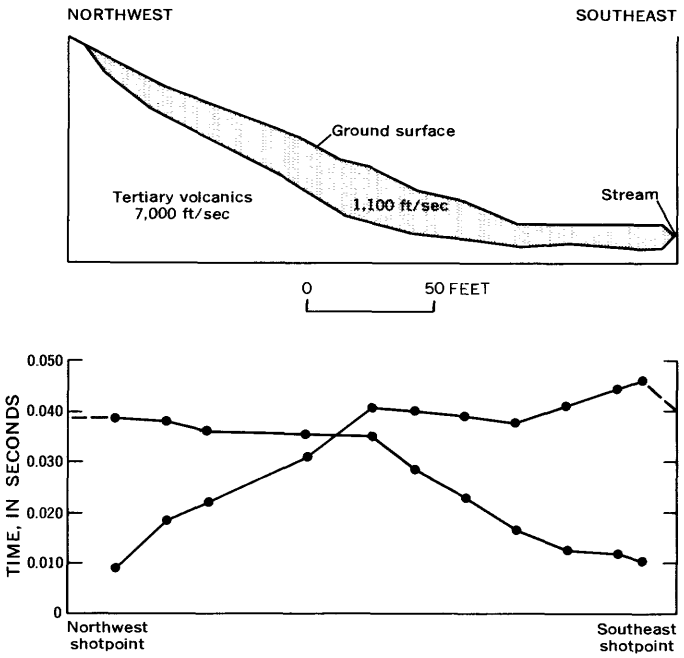

FIGURE 2.—Computed section across City Creek Canyon (above) together with corresponding time-distance plot (below). Horizontal and vertical scales are equal. Shaded area indicates unconsolidated fill material.

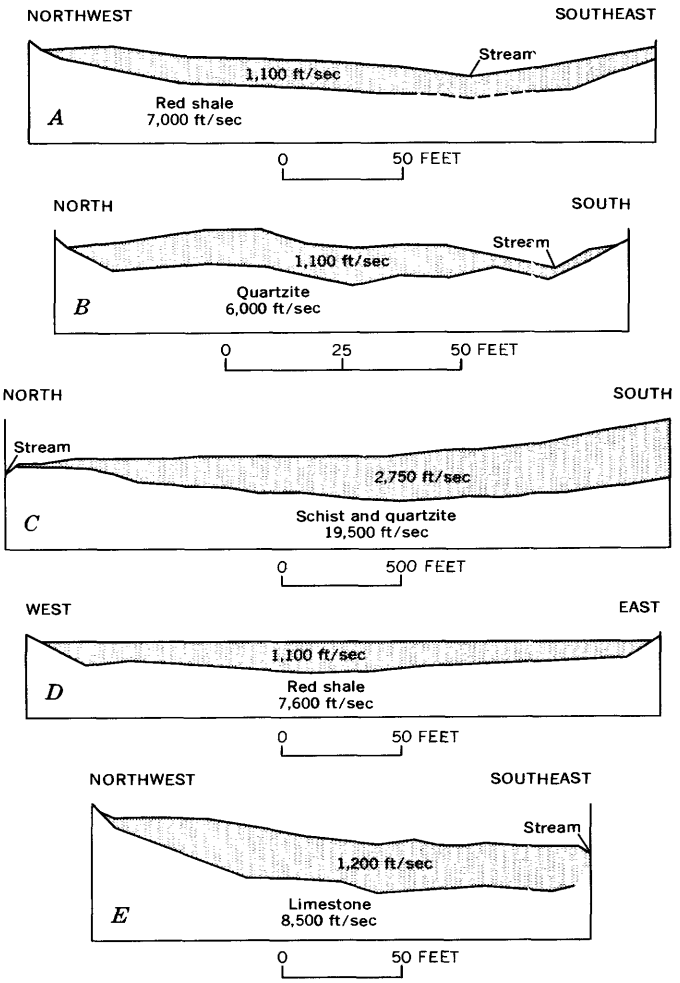

FIGURE 3.—Computed sections across Red Butte Canyon (*A*), Big Cottonwood Canyon (*B*), Little Cottonwood Canyon (*C*), Parleys Canyon (*D*), and Emigration Canyon (*E*). The scale below each section refers to both horizontal and vertical distances. Shaded area indicates unconsolidated fill material.

nates the computing of shotpoint correction times. However, little or no information as to the velocity of the unconsolidated fill material and bedrock can be obtained; consequently, the velocities were measured independently. Measurement of the velocity of the thin unconsolidated debris is difficult, and where the debris is less than about 5 feet thick velocity determinations cannot be made. Where the fill was sufficiently thick to allow measurement of the velocity, the resulting measurements were consistently between 1,000 and 1,200 feet per second. Therefore, an average velocity of about 1,100 fps was assumed for the low-velocity material consisting of boulders and stream debris in all of the canyons except Little Cottonwood, where a velocity of 2,750 fps was measured.

The bedrock velocity was determined by placing several geophones on an outcrop and exploding a small charge on its surface. The author noted that the recorded velocity is dependent upon the shot-to-geophone distance (for distances less than approximately 2,000 ft). This indicates that the velocity of the bedrock increases with depth, probably because of weathering of the near-surface rock. Therefore, in measuring velocities on bedrock outcrops, the shot-to-geophone distance was kept equal to the length of the corresponding profile over the unconsolidated fill. Using this technique, where the profile lengths were about 200 feet, measured bedrock velocities (for shale, limestone, quartzite, and volcanic rock) ranged from 6,000 to 8,500 fps, which is 50–60 percent lower than the results contained in typical published velocity tables, but at least 5.5 times greater than the measured fill velocity.

The calculation of fill thickness is based on the reciprocal method presented by Hawkins (1961). This procedure results in calculated depths at each geophone along a line, normal to the bedrock surface, which passes through the geophone; but, if it is assumed that the bedrock surface roughly parallels the ground surface, the resulting depths will be along a line normal to the average ground slope at each geophone. Elevation corrections are unnecessary because the topographic surface is taken as the datum.

The determination of depths is based on a function termed the "time depth." Where a geophone spread is bracketed by shotpoints, the time depth at a geophone is obtained by adding the traveltimes from both shotpoints, subtracting the shotpoint-to-shotpoint time,

and dividing the total by 2. It can be shown (Hawkins, 1961) that at a geophone the depth (Z) to the refracting interface, along the normal to the plane of the refractor, is given by

$$Z=tV_0/\cos i, \quad (1)$$

where t is the time depth, V_0 is the velocity of the fill material, and i (the critical angle) is a function of V_0 and V_1 (bedrock velocity).

If the velocity of the bedrock is greater than the velocity of the fill by a factor of 5 or more, cos i will be approximately equal to 1 (error <2) and equation 1 reduces to

$$Z=t\,V_0. \quad (2)$$

In such cases the true velocity of the bedrock is of little importance, and the uncertainty in depth estimation is directly related to the accuracy with which the velocity (V_0) through the fill is measured. If a representative average velocity $\overline{V}_0$ is used in equation 2, the depth at a given point may be in error due to local velocity changes within the fill material, but the computed overall volume of fill will be relatively accurate.

Figure 3 shows computed sections across five additional narrow canyons in the Wasatch Range near Salt Lake City, Utah, The recording of relatively higher velocities for the fill in Little Cottonwood Caryon (fig. 3*C*) is attributed to its greater thickness. The higher bedrock velocity probably reflects the much greater width of this canyon, which allowed longer profiles (about 1,000 ft) and hence a deeper penetration of the seismic waves.

REFERENCE

Hawkins, L. V., 1961, The reciprocal method of routine shallow seismic refraction investigations: Geophysics, v. 26, no. 6, p. 806–819.

THE EFFECT OF CURRENT LEAKAGE AND ELECTRODE SPACING ERRORS ON RESISTIVITY MEASUREMENTS

By ADEL A. R. ZOHDY, Denver, Colo.

Abstract.—Distortion of vertical electrical sounding curves often results from errors in the measurement of the apparent resistivity. The most important source of error is leakage of electric current from damaged insulation on the current cables. The effect of leakage on resistivity sounding curves can be mathematically analyzed in regard to the dependence of that effect on the unreeling procedure of the cables in the field. If the leakage does not take place through the current reels themselves, it is best to maintain the reels at the center of the array instead of advancing the reels at each current electrode spacing. When the leakage takes place near the center of the array it is possible to measure negative apparent resistivities. A formula is derived for computing errors arising from inaccuracies in the measurement of electrode spacing distances. Calculations based on this formula indicate that errors in current electrode spacings result in larger errors in the apparent resistivity than corresponding errors in the potential electrode spacings.

Vertical electrical sounding (VES) curves obtained in the field are sometimes distorted and cannot be interpreted by means of theoretically computed curves for horizontally stratified media. The distortions may be caused either by geologic factors or by erroneous measurements. When the distortions are geologic in origin it is not always possible to interpret correctly all the information contained in a single curve, and, in general, it is necessary to obtain at least one pair of "crossed" soundings before a satisfactory interpretation of the geologic section can be obtained. Errors in measurements may be related to instrumental factors—such as damaged insulation that permits current leakage, or instruments of inferior quality—or they may be attributed to human frailties—such as misreading or miscalculating any of the parameters used in the evaluation of the apparent resistivity, $\bar{\rho}$. Instrumental or human sources of error other than current leakage and electrode spacing errors will not be considered here. Furthermore, the discussion will be limited to the symmetric quadripole AMNB electrode arrays (Schlumberger and Wenner).

CURRENT LEAKAGE

Leakage of electric current caused by damaged insulation of the current and (or) potential cables can cause gross errors in the measurement of the apparent resistivity. The probability for leakage effects increases tremendously under wet conditions. It also increases wherever the contact grounding resistance at the electrodes is high. Leakage from the current line is also enhanced when high impressed voltages are used to drive the current into the ground. When metallic reels are used, the current leakage often takes place through the reels themselves rather than through the cable laid on the ground. The value of the current, i, leaking into the ground is usually a hundredth or a thousandth of the total current, I, put into the ground. Nevertheless, the effect of leakage on the measured potential difference, ΔV, can be very significant.

EFFECT OF LEAKAGE ON VES CURVES

A formula (Dakhnov, 1953, p. 263–265) for computing the percentage of relative error in resistivity $\left(\frac{\Delta\rho}{\rho}\right)$ caused by a current leakage, i, in the positive current line at a point, F (fig. 1), is given by:

$$\frac{\Delta\rho}{\rho}=\frac{\rho'-\rho}{\rho}=50\eta\left[\frac{K}{\pi}\left(\frac{1}{FM}-\frac{1}{FN}\right)-1\right]\text{percent}, \quad (1)$$

where ρ' and ρ=erroneous and correct values of resistivity, respectively;

$\eta=\frac{i}{I}$=ratio of current, i, leaking at point F, to total current, I;

$K=\pi\frac{(AB/2)^2-(MN/2)^2}{MN}$=geometric factor of the electrode array; and $\frac{AB}{2}$ and $\frac{MN}{2}$ are half the distance between the current elec-

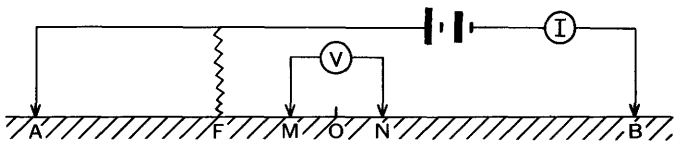

FIGURE 1.—Leakage from the positive current line at point F. A and B are current electrodes, M and N are potential electrodes, and O is center of array.

trodes and half the distance between the potential electrodes, respectively;

FM and FN=distances of the point of leakage, F, from the potential electrodes M and N, respectively.

It can be shown that if the leakage occurs in the negative current line at a point, F', symmetrically opposed to the point, F, with respect to the center of the array, then the same error (with the same sign) will be obtained. In general the sign of the percentage of relative error is positive, but it can be negative if, in equation 1, the distance FM is larger than FN. The magnitude of the percentage of relative error is illustrated by the following example. If $\frac{AB}{2}$=1,000 feet, $\frac{MN}{2}$=100 feet, FM=5 feet, FN=205 feet, and η=0.01, then $\frac{\Delta\rho}{\rho}$=482 percent, which is a very large error indeed.

In practice, the effect of current leakage on the form of a VES curve depends primarily on the procedure used for unreeling the cable in the field. The reels carrying the current lines may be left stationary at the center of the electrode array or they may be carried away while the outer end of the cable remains at the center.

In the first procedure (stationary reels) if the current leakage is through one of the reels, then, depending on the position of the reels on the ground, one of two possible effects on the VES curve may take place. When the current reels are placed in the same order as the current electrodes (electrode A, reel A, reel B, electrode B), the sign of $\frac{\Delta\rho}{\rho}$ in equation 1 will be positive and $\frac{\rho'}{\rho}>1$ (fig. 2A), but when the order of the reels is reversed with respect to the current electrodes (electrode A, reel B, reel A, electrode B), the sign of $\frac{\Delta\rho}{\rho}$ will be negative and $\frac{\rho'}{\rho}<1$ (fig. 2B). The curves in figure 2A and B were computed under the assumptions that the leaking reel is a point source placed 1 foot from the center of the array and that η=0.01=constant. A practical example of a reduction in apparent resistivity

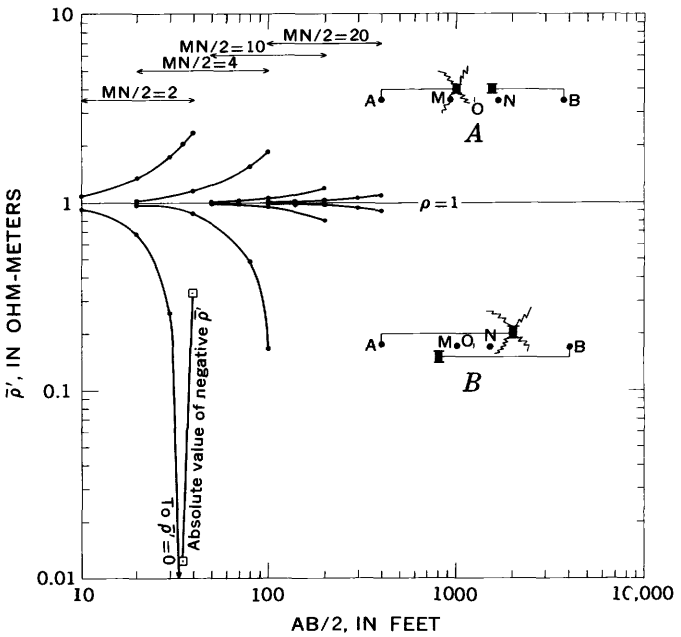

FIGURE 2.—Leakage from reel at a distance of 1 foot from center of array. A, effect of leakage from reel in ordered position. B, effect of leakage from reel in reversed position. Negative values of apparent resistivity are possible. Symbols are explained in figure 1.

caused by leakage from a reel placed in reversed position is shown in figure 3. The VES curve shown was obtained on the island of Hawaii, Hawaii.

If the leakage does not take place at either of the stationary reels but takes place at a point on the reeled-out current cable, then the effect of leakage will have a substantially different influence on the shape of the VES curve (fig. 4A).

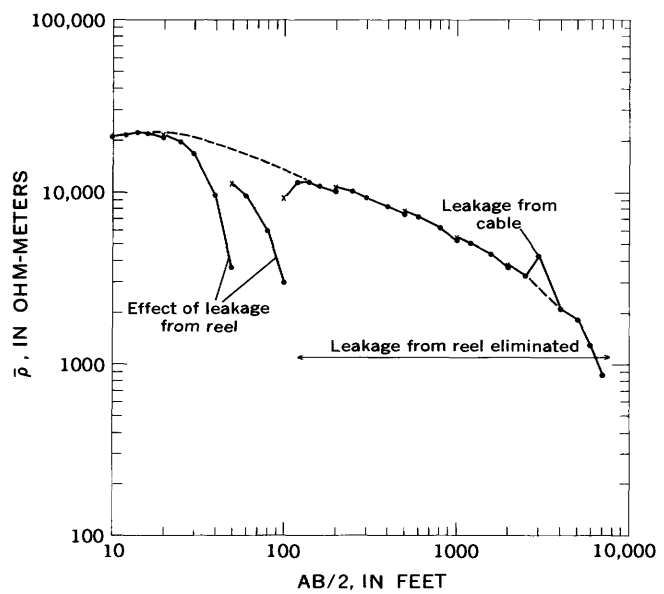

FIGURE 3.—Practical example (Hawaii, VES 10) of the effect of leakage from a reel placed in a reversed position.

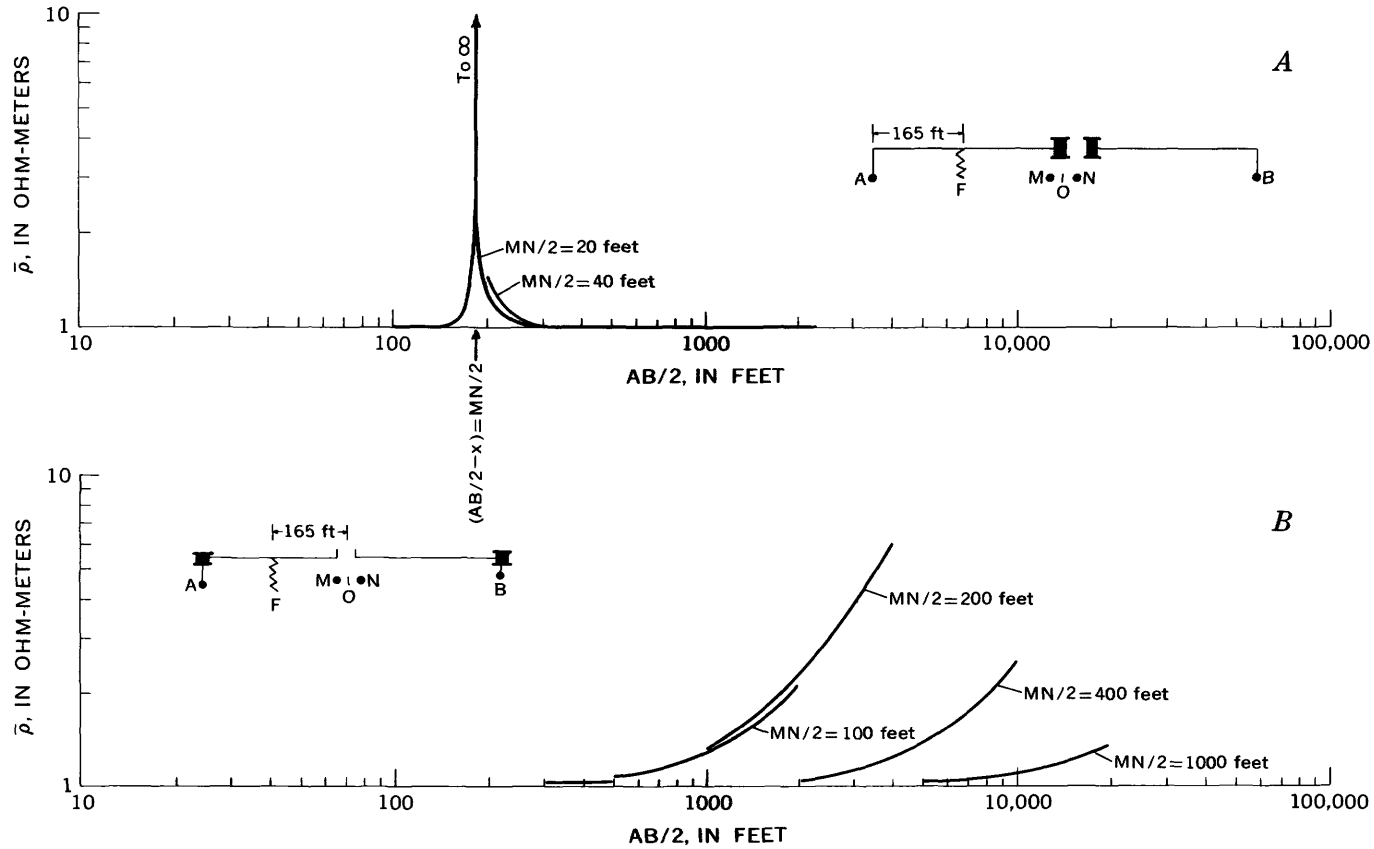

FIGURE 4.—Effect on VES curves ($\rho=1$) when leakage is 165 feet from end of cable. *A*, reels at center of array; *B*, reels at electrodes *A* and *B*. Symbols are explained in figure 1.

In the second procedure (reels carried away from center), the effect of leakage from the reels on the VES curve is negligible because of the proximity of the reels to the current electrodes. However, a current leakage at a point on the reeled-out portion of the cable may have a significant effect on the VES curve (fig. 4*B*). The nature of the distortions of the VES curves shown in figure 4*A* and *B* indicates that in practice it is advisable to maintain the reels, rather than the cable terminals, at the center of the array. When the reels are placed at the center of the array, the distances between a leakage source and the potential electrodes will be different for each electrode spacing, $\frac{AB}{2}$, and the result will be the formation of a cusp on the VES curve which is similar to that indicating the presence of a small near-surface lateral heterogeneity of high resistivity. This type of distortion can be corrected by graphical smoothing. On the other hand, when the cable terminals are maintained at the center of the array, a leakage point source on a current cable will remain at fixed distances from the potential electrodes for several successive $\frac{AB}{2}$ spacings, and its influence may thus distort a large segment of the VES curve.

The two VES curves shown in figure 4 were computed for a current leakage from one of the current cables at a distance of 165 feet from its terminal end, and it was assumed that $\eta=0.01=$constant.

To generalize, equation 1 may be written in the more useful forms

$$\frac{\rho'}{\rho}=1+\frac{\eta}{2}\left\{\frac{MN}{4x}\left[\left(\frac{AB}{MN}\right)^2-1\right]\left[\frac{1}{\left|\frac{MN}{2x}-1\right|}-\frac{1}{\frac{MN}{2x}+1}\right]-1\right\}, \quad (2)$$

and

$$\frac{\rho'}{\rho}=1+\frac{\eta}{2}\left\{\frac{MN}{4x}\left[\left(\frac{AB}{MN}\right)^2-1\right]\left[\frac{1}{\frac{MN}{2x}+1}-\frac{1}{\left|\frac{MN}{2x}-1\right|}\right]-1\right\}. \quad (3)$$

Equation 2 is applicable whenever the leakage is from the positive line at a point, F, located at the center of the electrode array, O, or between the center, O, and the positive electrode A; whereas equation 3 applies when the leakage is also from the positive line but at a point located at the center, 0, or between the center, 0, and the negative electrode B. In 2 and 3, x is the distance, $0F$, from the center, 0, to the leakage point, F.

A plot of the values of $\frac{\rho'}{\rho}$ for $3 \leq \frac{AB}{MN} \leq 25$, $\infty \geq \frac{MN}{2x} \geq 0$, and $\eta = 0.01 = \text{constant}$ is shown in figure 5. It can be shown from equations 2 and 3 that as $\frac{MN}{2x}$ tends to 1 (that is, the leakage occurs at a potential electrode) the values of $\frac{\rho'}{\rho}$ tend to $+\infty$ and $-\infty$, respectively. Conversely as $\frac{MN}{2x}$ tends to ∞ (that is, the leakage occurs at the center, 0,) the value of $\frac{\rho'}{\rho}$ tends to $1-\frac{\eta}{2} \simeq 1$.

It is interesting to note that when equation 5 applies, the apparent resistivity value may be negative $\left(\frac{\rho'}{\rho} < 0\right)$. The maximum values of $\frac{AB}{MN}$ for which the value of $\frac{\rho'}{\rho}$ is positive are obtained by setting equation 3 equal to zero and solving for $\frac{AB}{MN}$. The expression thus obtained is

$$\frac{AB}{MN} = \left\{ 2\left[1-\frac{2}{\eta}\right] \times \left[\frac{MN}{2x}\left(\frac{1}{\frac{MN}{2x}+1} - \frac{1}{\left|\frac{MN}{2x}-1\right|}\right)\right]^{-1} + 1 \right\}^{\frac{1}{2}} \quad (4)$$

The curves shown in figure 6 were obtained from equation 4 for $0.1 \leq \frac{MN}{2x} \leq 10$ and $\eta = 0.01 = \text{constant}$. The curves separate the domain in which $\frac{\rho'}{\rho}$ is negative from that in which it is positive. In practice, a negative apparent resistivity is represented by a reversal in the polarity of the measured potential difference. If the absolute value of $\frac{\rho'}{\rho}$ is used in plotting the VES curve, then a discontinuity and an abrupt change in the slope (from negative to positive) of the VES curve will be observed (see VES curve for $\frac{MN}{2}=2$ in fig. 2B).

The effect of current leakage on the potential line MN generally has a very minor effect (<1 percent) on the form of a Schlumberger curve except when the reciprocal array $MABN$ is used. The formulas (Dakhnov, 1953) for computing the relative error in resistivity caused by leakage into the potential line MN at a point, f, are

$$\frac{\rho'-\rho}{\rho} = \frac{R_M}{2R_f}\left[\frac{K}{\pi}\left(\frac{1}{Af}-\frac{1}{Bf}\right)-1\right], \quad (5)$$

and

$$\frac{\rho'-\rho}{\rho} = \frac{R_N}{2R_f}\left[\frac{K}{\pi}\left(\frac{1}{Af}-\frac{1}{Bf}\right)-1\right], \quad (6)$$

where R_M, R_N, and R_f are the ground resistances at the electrodes M, N, and at the leakage point f. Equations 5 and 6 apply when point f is on the lines OM and ON, respectively.

DETECTION OF LEAKAGE IN THE FIELD

The detection of leakage in the current line AP is generally achieved by noting the form of the sounding curve as it is plotted in the field. The following characteristics are generally indicative of leakage:

1. The VES curve, plotted on a set of bilogarithmic coordinates, rises at an angle greater than 45° with respect to the abscissa axis.
2. The VES curve is distorted by the formation of cusps.
3. A large displacement occurs on the VES curve upon changes in the electrode spacing MN.
4. The magnitude of the measured potential difference varies as a function of the current, I, for a given electrode setup (owing to variation in the value of η as a function of the current density in the cables and the contact resistance at the leakage point).
5. A sudden large increase occurs in the value of apparent resistivity.

The first three characteristics mentioned above can be caused by laterally inhomogeneous geologic structures. However, it is advisable to examine their origin in the field as soon as they are observed on the sounding curve. In order to determine, in the field, the branch of the electrode array (OA or OB) in which the leakage occurs, the following procedure is recommended. One of the current electrodes (A or B) should be disconnected, and the cable end should be lifted above the

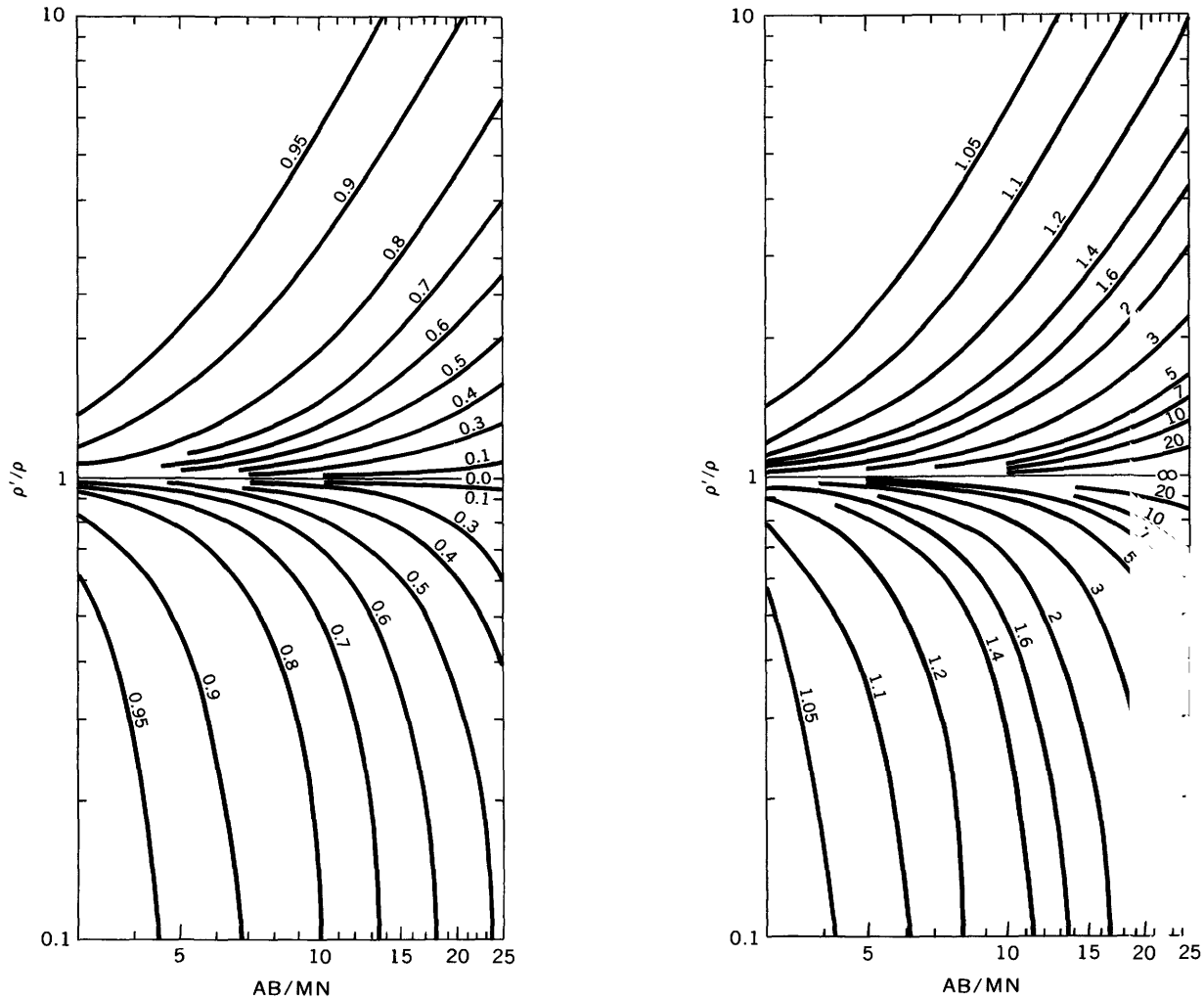

FIGURE 5.—Variation of $\frac{\rho'}{\rho}$ as a function of $\frac{AB}{MN}$, for $\eta=0.01$. Values on curves$=\frac{MN}{2x}$.

ground. The current is then turned on, and the impressed voltage is increased until it approximates the value to be used in the reading. An indication of any current flow on the most sensitive scale of the instrument ammeter, or, more important, any recording of a potential difference between the potential electrodes at that time is definite indication of leakage. The leakage source must be found and eliminated, then the test is repeated. If there is no indication of leakage during the second test, the cable is reconnected to the electrode and the second branch of the line is tested in the same manner. A leakage in the current line of less than 1 percent can be tolerated if there is no indication of a measurable potential difference between the electrodes M and N. It is recommended to test for leakage at the outset of each sounding, especially when metallic reels are used.

ELECTRODE SPACING ERRORS

Errors in the value of the apparent resistivity, $\bar{\rho}$, can be related to errors in the measured distances between the four electrodes A, M, N, and B. A formula for the evaluation of such errors may be derived as follows: The potential difference between the electrodes M and N caused by a current, I, is given by

$$\Delta V=\frac{I\rho}{2\pi}\left(\frac{1}{AM}-\frac{1}{AN}-\frac{1}{BM}+\frac{1}{BN}\right)$$
$$=\frac{I\rho}{2\pi}\left(\frac{1}{AO-MO}-\frac{1}{AO+NO}-\frac{1}{BO+MO}+\frac{1}{BO-NO}\right), \quad (7)$$

where AO, MO, NO, and BO are the distances of the electrodes A, M, N, and B from the chosen center of the array, O,

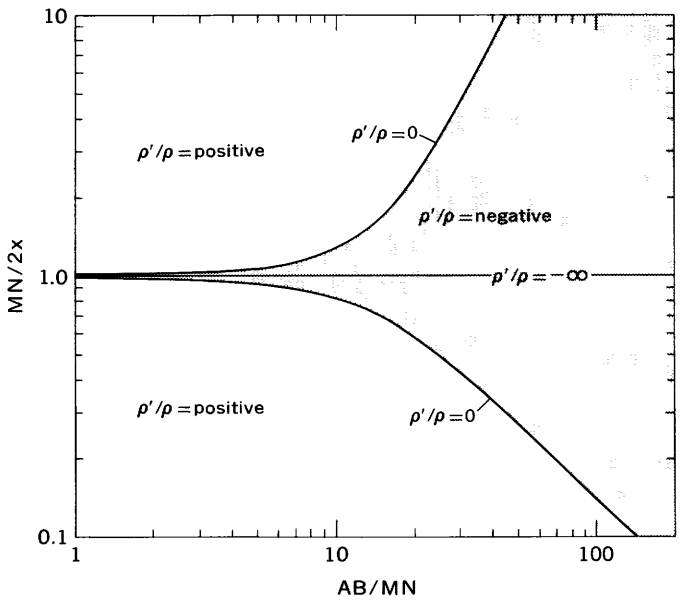

FIGURE 6.—Curves defining domains of $\frac{\rho'}{\rho}$ positive, zero, and negative for $0.1 \leq \frac{MN}{2x} \leq 10$, $1 \leq \frac{AB}{MN} \leq 200$.

Let $AO=\lambda_1 a$, $BO=\lambda_2 a$, $MO=\epsilon_1 b$, $NO=\epsilon_2 b$,

where a and b are the correct values of the symmetric electrode spacings $\frac{AB}{2}$ and $\frac{MN}{2}$ assumed in the computation of the geometric factor K and λ_1, λ_2, ϵ_1, and ϵ_2 are error coefficients. If the electrodes A, M, N, and B are symmetrically placed with respect to the chosen center, O, and $\lambda_1=\lambda_2=\epsilon_1=\epsilon_2=1$, then equation 7 reduces to

$$\Delta V=\frac{\rho I}{\pi}\left(\frac{2b}{a^2-b^2}\right). \tag{8}$$

If however, $\lambda_1 \neq \lambda_2 \neq \epsilon_1 \neq \epsilon_2 \neq 1$, then equation 7 may be written in the form

$$\Delta V'=\frac{I\rho}{2\pi}\left(\frac{1}{\lambda_1 a-\epsilon_1 b}-\frac{1}{\lambda_1 a+\epsilon_2 b}-\frac{1}{\lambda_2 a+\epsilon_1 b}+\frac{1}{\lambda_2 a-\epsilon_2 b}\right), \tag{9}$$

where $\Delta V'$ is the erroneous potential difference. Consequently, an erroneous apparent resistivity, ρ', will be computed from the formula

$$\rho'=K\frac{\Delta V'}{I}=\pi\left(\frac{a^2-b^2}{2b}\right)\frac{\Delta V'}{I}. \tag{10}$$

Substituting equation 9 in equation 10 and rearranging we get

$$\frac{\rho'}{\rho}=\frac{(a/b)^2-1}{4}\left[\frac{1}{\lambda_1\left(\frac{a}{b}\right)-\epsilon_1}-\frac{1}{\lambda_1\left(\frac{a}{b}\right)+\epsilon_2}-\frac{1}{\lambda_2\left(\frac{a}{b}\right)+\epsilon_1}+\frac{1}{\lambda_2\left(\frac{a}{b}\right)-\epsilon_2}\right]. \tag{11}$$

Equation 11 indicates that the error in the apparent resistivity is not only a function of the error in any of the electrode spacings, but it is also a function of the ratio $a/b=AB/MN$. Calculations based on equation 11 indicate that when the value of $\frac{AB}{MN}$ is small $\left(\frac{AB}{MN}=3,\right.$ as in the Wenner array$\left.\right)$ the errors in the measured apparent resistivity are greater than when $\frac{AB}{MN}$ is large $\left(\frac{AB}{MN}\geq 5,\right.$ as in the Schlumberger array$\left.\right)$. Furthermore, errors in the current electrode spacing, $\lambda_1 \neq 1$, or $\lambda_2 \neq 1$, cause larger errors in the value of ρ than corresponding errors in the potential electrode spacings, $\epsilon_1 \neq 1$ or $\epsilon_2 \neq 1$. For example, if λ_1 or $\lambda_2=0.9$, then at $\frac{AB}{MN}=3$ (Wenner array), $\frac{\rho'}{\rho}=1.135\left(\right.$or $\frac{\Delta\rho}{\rho}=+13.5$ percent$\left.\right)$; and at $\frac{AB}{MN}=10$ (Schlumberger array), $\frac{\rho'}{\rho}=1.1187$ $\left(\right.$or $\frac{\Delta\rho}{\rho}=+11.9$ percent$\left.\right)$. On the other hand, if ϵ_1 or $\epsilon_2=0.9$, then at $\frac{AB}{MN}=3$, $\frac{\rho'}{\rho}=0.939\left(\right.$or $\frac{\Delta\rho}{\rho}=-6.1$ percent$\left.\right)$, and for $\frac{AB}{MN}=10$, $\frac{\rho'}{\rho}=0.949\left(\right.$or $\frac{\Delta\rho}{\rho}=-5.1$ percent$\left.\right)$.

It should be noted that, in practice, when errors are made in the spacing distance of the potential electrodes the magnitude of the error obtained by equation 11 may be only a part of the difference between the observed erroneous apparent resistivity and its true value. This is explained by the fact that, over horizontally stratified media, the probing depth and therefore the value of the apparent resistivity is a function of the spacing ratio $\frac{AB}{MN}$ (Deppermann, 1954), especially when the spacing error occurs at a point on a steeply descending portion of a VES curve.

SUMMARY AND CONCLUSIONS

Current leakage and errors in spacing distances constitute two primary sources of error in resistivity measurements. The effect of current leakage on a VES

curve depends on the method used for unreeling the cables in the field. The percentage of relative error in the measured apparent resistivity, caused by leakage from the current lines, may reach plus or minus several hundred percent. Leakage into the cables of the potential electrodes, however, has a much smaller effect except when the reciprocal *MABN* array is used.

Errors in apparent resistivity caused by errors in the electrode spacing distances were evaluated and found to be significant, especially if the error in distance measurement is made in the current electrode spacing.

REFERENCES

Dakhnov, V. N., 1953, Electrical prospecting for petroleum and natural gas: Gostoptekhizdat, 497 p. [in Russian].

Deppermann, K., 1954, Die Abhängigkeit des scheinbaren Widerstandes vom Sondenabstand bei der Vierpunkt-Methode: Geophys. Prosp. [Netherlands], v. 2, no. 4, p. 262–273.

SUBJECT INDEX

[For major headings such as "Economic geology," "Geophysics," "Paleontology," see under State names or refer to table of contents]

AUTHOR INDEX

U.S. GOVERNMENT PRINTING OFFICE : 1968—O-313-005